Number/
Numéro

1

TRACK/TRAIN DYNAMICS

VOLUME I, 1978

editors,
Hamouda Ghonem
and
Alan E. Bethune

A Publication of
TECHNICAL AND OPERATIONS RESEARCH
Canadian Pacific
MONTREAL, CANADA

FORMULE DE DOCUMENTATION POUR RAPPORT

1 Nº du rapport Transports Canada
TP 4756E

2 Nº de l'étude — CDT
5028

3 Nº de catalogue du destinataire

4. Titre et sous-titre
Track/Train Dynamics, Volume 1, 1978

5 Date du rapport
1978

6 Nº du rapport de l'organisme exécutant

7 Auteur(s)
H. Ghonem, A.E. Bethune (Editeurs)

8 Nº de dossier Transports Canada
D1465-108-7-2

9 Nom et adresse de l'organisme exécutant
Canadien Pacifique Limitée
Recherche technique et opérationnelle
Gare Windsor, Montréal, Québec
H3C 3E4

10 Nº de dossier — ASC
14ST.T8200-4-4515

11 Nº de contrat — ASC ou Transports Canada
OST5-00042

12 Nom et adresse de l'organisme parrain
Centre de développement des transports (CDT)
1000 ouest, rue Sherbrooke
Suite 2421
Montréal, Québec H3A 2R3

13. Genre de rapport et période visée
Final; 1975 - 1978

14 Code de l'organisme parrain
CDT 5028

15 Remarques additionnelles

16 Agent de projet — CDT
W.S.C. McLaren

17 Résumé

Cet ouvrage renferme huit mémoires sur le résultat des recherches portant sur l'interaction dynamique roue-rail, conduites par le bureau de recherche du Canadien Pacifique entre mars 1975 et septembre 1978. Voici la liste des mémoires publiés et des auteurs:

Study of Crack Initiation in 100-Ton Coal Car Truck Bolsters	- H. Ghonem
Rail Metallurgy	- J. Kalousek, G. Beynton
Development of High-Strength Weldable Chromium Molybdenum Rail	- H. Ghonem, J. Kalousek
Measurement of Angle-of-Attack with Laser	- J. Kalousek, L.M. Lee
Comparative Performance of Type II Trucks	- H. Ghonem, R. Gonsalves
Effect of Unsprung Weight on Vertical Track Dynamics	- J. Robert
Design of Lockable Draw Gear	- H. Ghonem, W. Pak
Stringer Stress Measurements on Bridge, Mile 51.5, Windermere Subdivision	- J. Kalousek, A.E. Bethune

18. Mots-clés
Interaction dynamique roue-rail, Métallurgie des rails, Fissuration, Bogies de wagons, Angle d'inscription, Masse non suspendue, Attelage, Calcul de ponts-rails

19 Diffusion
Le CDT dispose d'un nombre limité d'exemplaires

20. Classification de sécurité (de ce rapport)
Non-classifié

21. Classification de sécurité (de cette page)
Non-classifiée

22 Nombre de pages

23 Prix

REPORT DOCUMENTATION FORM

1. Transport Canada Report No
TP 4756E

2. TDC Project No
5028

3. Recipient's Catalogue No

4. Title and Subtitle
Track/Train Dynamics, Volume 1, 1978

5. Report Date
1978

6. Performing Organization Report No

7. Author(s)
H. Ghonem, A.E. Bethune (Editors)

8. Transport Canada File No
D1465-108-7-2

9. Performing Organization Name and Address
Canadian Pacific Limited
Technical and Operations Research
Windsor Station, Montreal, Quebec
H3C 3E4

10. DSS File No
14ST.T8200-4-4515

11. DSS or Transport Canada Contract No
OST5-00042

12. Sponsoring Agency Name and Address
Transportation Development Centre (TDC)
1000 Sherbrooke Street West
Suite 2421
Montreal, Quebec H3A 2R3

13. Type of Report and Period Covered
Final; 1975 - 1978

14. Sponsoring Agency Code
TDC 5028

15. Supplementary Notes

16. TDC Project Officer
W.S.C. McLaren

17. Abstract

This publication consists of eight papers on track/train dynamics investigations undertaken by the Research Department of Canadian Pacific Limited from March 1975 to September 1978. The following papers are included:

Study of Crack Initiation in 100-Ton Coal Car Truck Bolsters	- H. Ghonem
Rail Metallurgy	- J. Kalousek, G. Beynton
Development of High-Strength Weldable Chromium Molybdenum Rail	- H. Ghonem, J. Kalousek
Measurement of Angle-of-Attack with Laser	- J. Kalousek, L.M. Yee
Comparative Performance of Type II Trucks	- H. Ghonem, R. Gonsalves
Effect of Unsprung Weight on Vertical Track Dynamics	- J. Robert
Design of Lockable Draw Gear	- H. Ghonem, W. Pak
Stringer Stress Measurement on Bridge, Mile 51.5, Windermere Subdivision	- J. Kalousek, A.E. Bethune

18. Key Words
Track/train dynamics, Rail metallurgy, Crack initiation, Freight car trucks, Wheelset angle-of-attack, Unsprung weight, Draw gear, Bridge stresses

19. Distribution Statement
Copies available from sponsoring agency

20. Security Classification (of this report)
Unclassified

21. Security Classification (of this page)
Unclassified

22. No of Pages
398

23. Price

TRACK/TRAIN DYNAMICS

VOLUME I, 1978

editors,
Hamouda Ghonem
and
Alan E. Bethune

A Publication of:
TECHNICAL AND OPERATIONS RESEARCH
Canadian Pacific
MONTREAL, CANADA

Contents

Preface - R. Klein

Study of Crack Initiation in 100-Ton Coal Car Truck Bolsters - H. Ghonem 1

Rail Metallurgy - J. Kalousek and G. Beynon 64

Development of High-Strength Weldable Chromium-Molybdenum Rail - H. Ghonem and J. Kalousek 110

Measurement of Angle-of-Attack with Laser - J. Kalousek and L M Yee 157

Comparative Performance of Type II Trucks - H. Ghonem and R. Gonsalves 184

Effect of Unsprung Weight on Vertical Track Dynamics - J. Robert 309

Design of Lockable Draw Gear - H. Ghonem and W. Pak 323

Stringer Stress Measurements on Bridge, Mile. 51.5, Windermere Subdivision - J. Kalousek and A.E. Bethune 362

PREFACE

The purpose of this publication is to set forth and explain a series of investigations conducted by the Research Department (Technical and Operations Research section) of Canadian Pacific Ltd. related to Track/Train Dynamics.

In recent years there has been a concerted industry-wide effort in Canada and the United States to obtain a fundamental understanding of the dynamic interaction between rail vehicles and between these vehicles and the supporting track structure in order to improve safety and reduce operating and maintenance expenses. Canadian Pacific Ltd. has actively participated in these industry-wide programs and has vigorously pursued research in areas of particular concern to CP Rail and in areas where we possessed specialized expertise and skills.

The following chapters of this work explain the methodology, results and recommendations of several track/train dynamics investigations undertaken by the Research Department between March 1st, 1975 and September 30th, 1978. This volume is the first of a series of similar reports to be issued on a regular basis.

It is a pleasure to acknowledge the suggestions and help of many railway personnel and industry colleagues. It is our privilege to acknowledge our indebtedness to the Technical Research and Development Centre (MOT) for their shared cost financial support (Contract OST5-0042), and to the references which are given in the text as they make the work of this type possible.

R Klein

R. Klein
Manager, Research
Montreal, Quebec

H. Ghonem

Study of Crack Initiation in 100-Ton Coal Car Truck Bolsters

ABSTRACT: CP Rail has recently experienced an increase in the number of 100-ton coal car truck bolsters suffering from cracks in the vicinity of the snubber pocket location. In order to determine the reasons for the initiation of these cracks, the Research Department has carried out the following studies: i) a dynamic field test to determine the actual level of stresses acting on the snubber pocket of a truck bolster; ii) nondestructive tests using gamma-rays to study the effect of the presence of casting shrinkage cavities at critical cross-sections of the bolsters in the initiation of fatigue cracks at these locations; iii) metallurgical analyses of the welded areas in the snubber pocket to determine the microstructural changes occurring as a result of the welding process.

INTRODUCTION

In the early 1960's, the loading capacity of the freight car increased from 50-70 tons to 100 tons. To accommodate this level of additional loading and yet not exceed the permitted axle load limit, car designers tended to minimize the tare weight of the car(1)*: truck parts were lightened, car bodies built to size, centre of gravities were raised and truck centre distances lengthened. All these changes tended to affect the life of the truck bolster, the component that supports the car body.

CP has recently been observing cracks on a large number of 100-ton coal-car bolsters in the vicinity of the snubber pocket location. At the request of the Office of the Chief Mechanical Officer, the Research Department has carried out an investigation to determine the possible causes leading to the initiation of these cracks.

---

* The number in parenthesis refers to the references at the end of this report.

An inspection of several cracked bolsters has shown that the cracks in these bolsters can be classified into two groups. The first is service fatigue cracks initiated in the bolster from sites of higher stress concentration which then propagated further into the bolster. These cracks are characterized by the existence of fatigue striations on the fracture surface, see Figure 1. The second group is associated with weld repairs on worn bolster surfaces which were in contact with the snubbers; an example of these cracks is shown in Figure 2.

This report, which describes the investigation carried out on fatigue cracks in the bolsters of 100-ton cars is divided into three parts. The first part describes a dynamic test designed to determine the actual stress levels acting on the snubber pocket of a truck bolster. From this, the service life of the bolster can be estimated. In the second part, several factors affecting the bolster's fatigue life were analyzed and correlated to the design of the bolster and the technique employed in manufacturing them. The last part of this study involved metallurgical examinations of the welded area, the heat-affected zone and the original metal of the bolster to determine the microstructural changes that occur in the vicinity of the weld deposit as a result of the welding process. Each part of this report ends with recommendations that are designed to inhibit the initiation of cracks and increase the life of the snubber pocket area of the bolster.

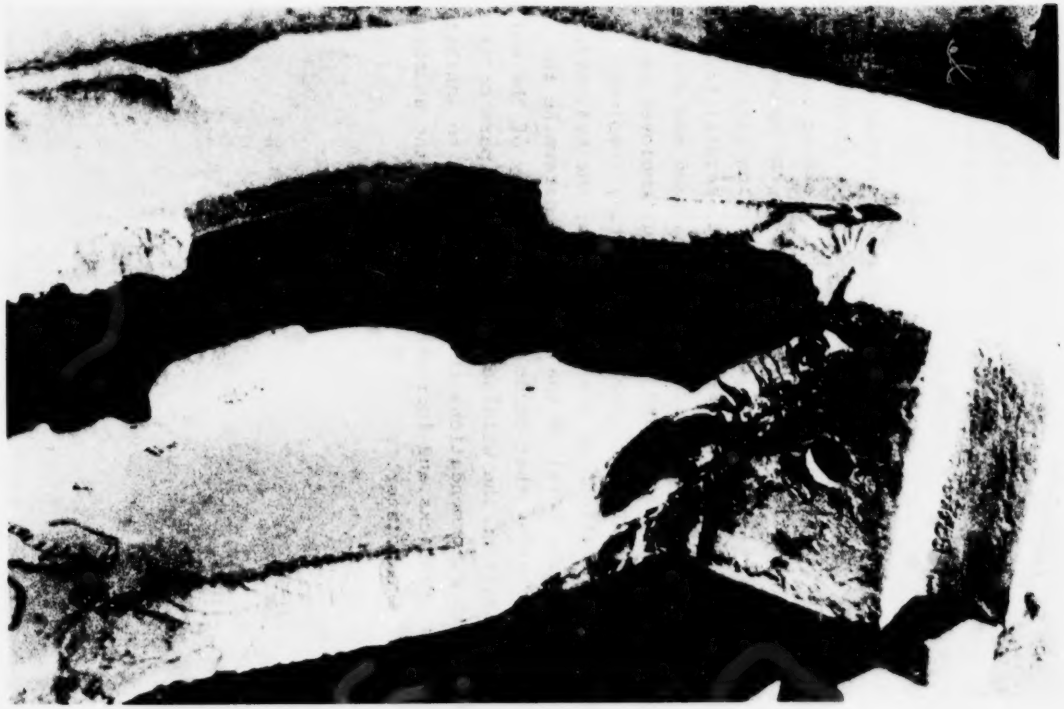

Figure 1: Fracture Surface of a Service Fatigue Crack

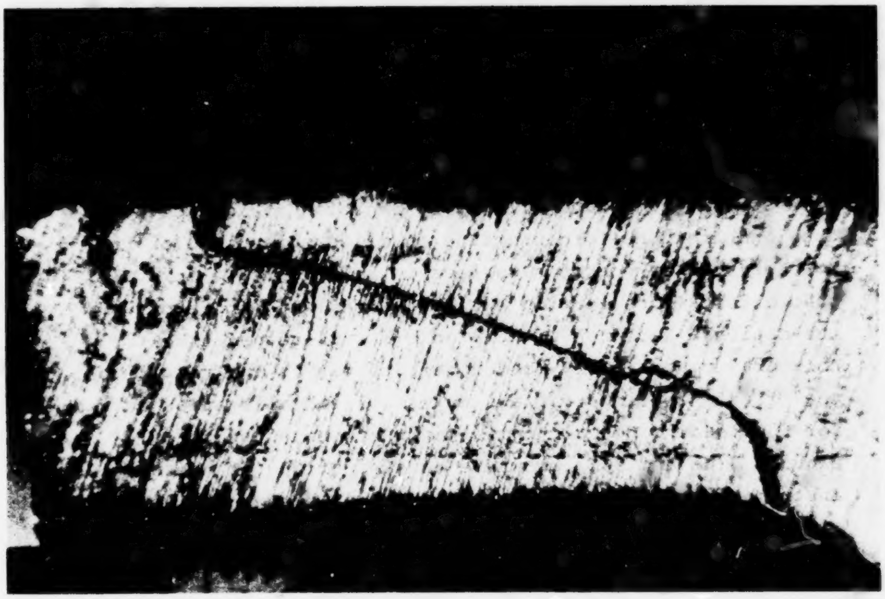

Figure 2: Section Through Crack Initiated at the Welded Side

I DYNAMIC TEST AND STRESS ANALYSIS

I.1 Test Description

A dynamic field test was carried out, between Kamloops and North Bend on the Thompson Subdivision, on the truck bolster of a 100-ton laden car whose snubber pocket was not welded. The aim of this test was to measure the dynamic stress values acting on the bolster snubber pocket. This was done by installing a number of strain gauges at pre-selected locations on the surface and in the vicinity of this pocket. These locations, which were chosen areas of highly concentrated stresses, were determined by using a brittle coating technique. The details of this technique can be found in references 2-4. Furthermore, two snubbers were instrumented with strain gauges and allowed to function as load cells, thus enabling the forces acting on different points of the bolster snubber pocket's surface to be measured. Several static tests were carried out at the railway laboratory of the National Research Council on a strain-gauged truck bolster, using a fully-loaded car, to verify the results of the brittle coating test and to establish calibration curves for the loading behaviour of the instrumented snubbers. Figures 3(a) and 3(b) show the details of one of these instrumented snubbers; their calibration curves are shown in Figures 4 and 5, and the gauge locations are indicated in Figures 6(a), 6(b) and 6(c).

In addition, two extensometers were installed by linking the two edges of the instrumented side of the bolster end to two fixed references (the side frame) to record the vertical displacements of the two edges during the test and to thus evaluate the twisting of the bolster (if any) around its lateral axis. These extensometers are shown in Figure 7.

In general, there were no problems in the placement of the strain gauges except for gauges 3 and 4. However, difficulties arose from the large diameter of the grinding disk. After several trials it was possible to position them; nevertheless, gauge 3 failed during the test while the operation of gauge 4 was without failure during the entire test. Another problem was encountered during the reading of the snubber-gauges output as a result of the change in their reference points due to the vibration associated with the test. With the help of N.R.C. personnel(5), a method was devised for using the output of channel 9 on both recorders 1 and 2 (the output of the extensometers) as a guide in reading with sufficient accuracy the output of the snubber gauges. There was no problem in reading the output of the remaining strain gauges.

I.2 Instrumentation

The instrumentation used in this test was provided by the Division of Mechanical Engineering of the National Research Council of Canada. The instruments were shipped in an N.R.C. instrument van via CP Rail to Kamloops. The van contained three 18-channel CEC paper recorders and the necessary electronic hardware to connect installed gauges to appropriate Wheatstone bridge circuits. The gauges were calibrated by placing a resistor of known resistance on the gauge and measuring the resulting gauge output, from which the amount of strain per 1" of trace deflection on the CEC recorder could be calculated. The calibrating procedure is described in detail in N.R.C. Report No. INS-46(6). The "proper" calibrated values for each gauge are presented in Tables 1 and 2 while sample traces of recorders 1, 2 and 3 are shown in Graphs 1, 2 and 3.

I.3 Test Procedure

During the run from Kamloops to North Bend, the instrumented bolster was in the lead position and the stress levels were recorded on a total 15 miles of track. Additional recordings covering six miles of operation were taken on the return from North Bend to Kamloops in order to assess the effect on the stress levels while the bolster was trailing. The exact locations of the readings are shown in Table 3. The test sections were selected in such a way as to obtain a representative sample of track speeds, jointed and welded rail, as well as curved and tangent track so as to assess the individual effect of these factors on stress levels acting on the bolster. The highest recorded speed in the test was 48 m/h and the lowest was 27 m/h, while the largest degree of curvature was 5^o and the smallest 3^o.

I.4 Data Analysis

The stresses acting on the gauges of the instrumented snubbers were obtained by measuring the deflection of the appropriate trace and multiplying it by the corresponding calibrated strain equivalent taken from Table 2. These strain values were then averaged at each corner of the snubber and, by using the calibration curves shown in Figures 4 and 5, the corresponding force values were obtained. By knowing the value of these forces and the area of the snubber-bolster surface, which is estimated 25 in.^2, it was possible to calculate the stresses acting on the corners of this surface on the two sides of the instrumented end of the bolster. The values of these stresses are shown in Table 4.

Each rectangular rossette, R_a and R_b shown in Figure 6, measured strains in three directions, 45^o apart, and gave three traces on the CEC records, namely, traces 7-12 on record 3. In order to determine the stresses located at these rossettes, each trace reading was multiplied by the proper calibration value; the results, which represent the values of the strains, were then used as input for the formulas described in several references, see references 7 and 8, for example, to evaluate the principle stresses and strains and the direction in which the maximum stresses and strains were acting. These calculations were carried out in two locations and the results are shown in Table 5. The output deflection in the traces of the other single-strain gauges located on the inside surface of the upper and lower bolster snubber pocket were multiplied by the appropriate stress equivalent taken from Table 1 and the values of the stresses at these locations determined.

Reviewing the magnitude of the stresses as calculated from all these strain gauges, it was decided that the stress analysis of the fatigue behaviour of the bolster snubber pocket would be based on the data of gauge no. 4, for two reasons. First, the output of all other gauges was found, generally, to be smaller in terms of static and dynamic stress values as compared to the results of gauge no. 4. The second reason is that the location of gauge no. 4 is, in the next part of this report, identified as the main source of observed fatigue cracks.

Now, in order to determine the fatigue life of the bolster snubber pocket, the following steps were carried out:

1. The dynamic stresses acting on this pocket are attributed to the existence of surface defects on the rails. In order to quantify this relationship, the output of gauge no. 4, taken while running on four chosen rails - two welded and two jointed - was analyzed by using the Filter Signal Technique to obtain a histogram of the number of occurrences of fatigue cycles per mile

for different stress amplitudes. Such histograms and their curve-fitted distributions are shown in Figures 8-11.

2. These distributions were then correlated to the surface defect distribution, shown also in Figures 8-11, obtained from data collected by the track recording car at the same locations analyzed in step 1. From such a correlation, we arrived at Figure 12 which shows an increasing linear relationship between the stresses acting on the snubber pocket area, specifically at the location of gauge no. 4, and the depth of surface defects on the rail.

   The number of cycles per mile corresponding to any stress level occurring on the bolster snubber pocket area can now be determined by combining this figure, 12, with the distribution of the surface irregularities obtained from the entire Pacific region, shown in Figure 13.

3. Once the values of the stresses acting on the snubber pocket area are known, then, using the "S-N" curve for the bolster metal alloy (0.35%C normalized cast steel), the number of cycles that such an area can tolerate before failure can be determined. The "S-N" curve for the bolster alloy is not, to the author's knowledge, available in material fatigue data, thus the "S-N" curve for normalized 0.27%C cast steel was used instead. Such an approximation is valid because of the similarity in contents and microstructure in the two alloys.

As this curve, shown in Figure 14, was obtained on the basis of a sinusoidal loading application with R = -1, i.e., the mean stress is zero, the endurance limit in this figure (20 Ksi) was modified by using the Soderberg law(9) to accommodate the condition in the present case in which the mean stress acting on the location of gauge 4 is 5.4 Ksi. The new endurance limit is, therefore, equal to 17.5 Ksi.

Realizing that the maximum amplitude of fatigue stress cycles acting on the snubber pocket area is 2.8 Ksi, leads to the conclusion, using Figure 14, that the life of this pocket is infinity.

Due to the existence of the "knee" in the "S-N" diagram of this normalized steel, we thus may interprete the infinity here to be 10^6-10^8 cycles as is customary in fatigue studies. Then, the life of the bolster snubber pocket area in terms of mileage is calculated by using Figures 12 and 13 to be 3.5 x 10^6 miles. Projecting that a bolster travels 127,750 miles(10) every year, the minimum number of years that the bolster can survive this type of loading is calculated to be an average of 26 years.

One conclusion drawn from this analysis is that the dynamic stresses acting on the bolster snubber pocket area are not the "only" reason for the early failure experienced in CP 100-ton truck bolsters. However, when these stresses are combined with other internal and external parameters, they can result in such early failures. In the next part, some of these parameters are discussed.

Finally, from the analysis of dynamic test results, some noteworthy conclusions were obtained. These are:

1. From the results of the two extensometers shown in Figure 7, it was difficult to determine whether or not the bolster twists along its lateral or vertical axis. However, it was clear from these results that the vertical movements of the two edges of the instrumented ride of the snubber were not even; thus facilitating the concentrations of acting forces on one of these edges.

2. The vertical forces acting on the bolster were, in general, larger when the bolster was in a trailing position than when it was in a leading position. This, to a certain extent, is in agreement with the findings of reference(17).

3. The range of the speed between 25 and 45 mph has no observable effect on the amplitude of the stresses on the bolster. This is in agreement with the findings of reference(18).

Figure 3: Details of an Instrumented Snubber

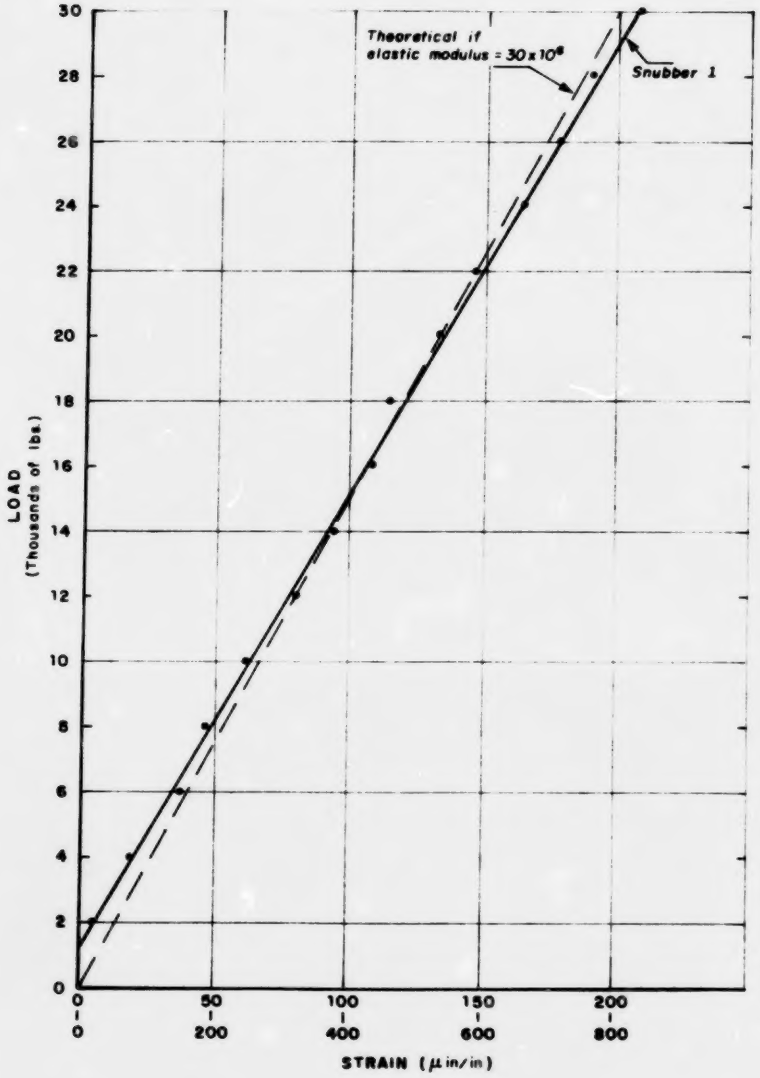

Figure 4: Calibration Curves for Instrumented Snubber #1

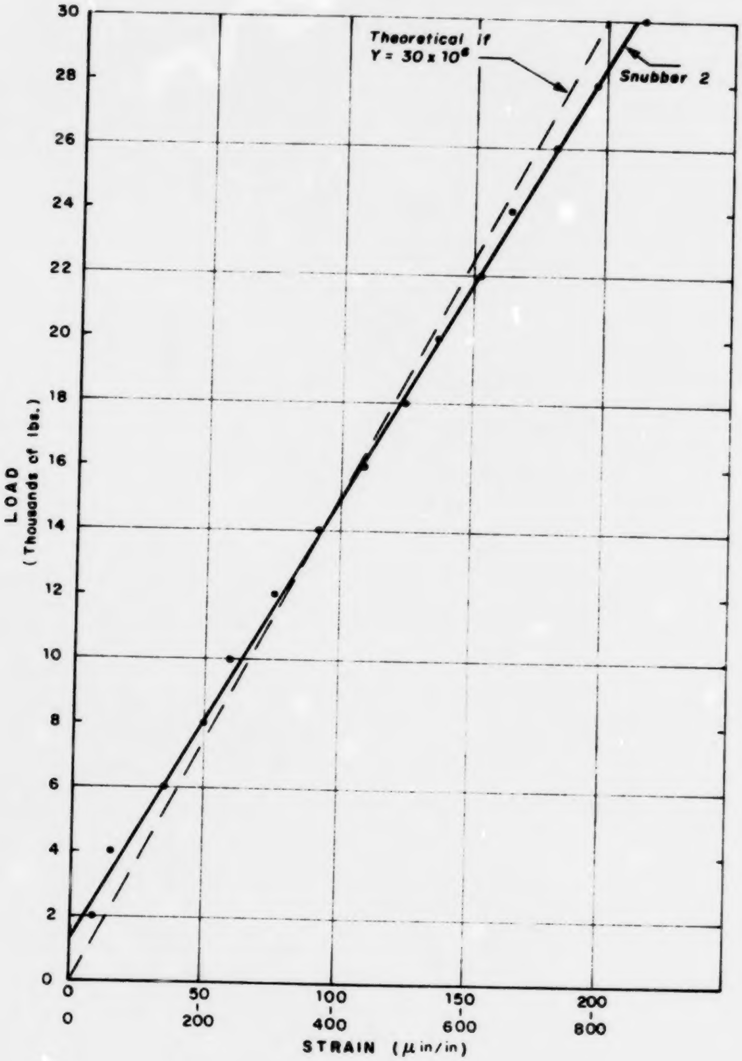

Figure 5: Calibration Curves for Instrumented Snubber #2

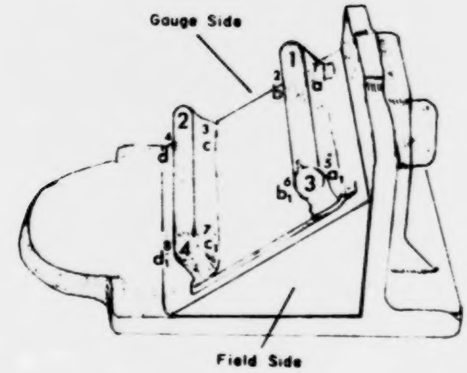
Gauge Side
1
2
3
4
a
b
c
d
a_1
b_1
c_1
d_1
Field Side

Gauge Locations on instrumented Snubber.

(6a)

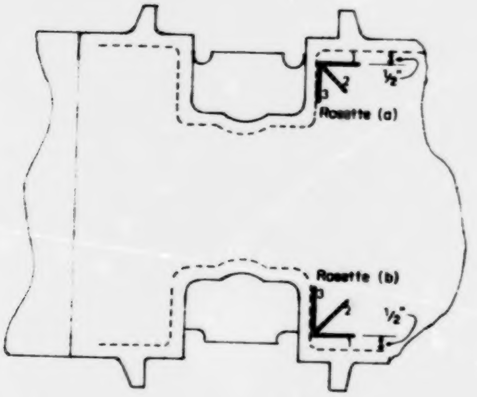
Rosette (a)
Rosette (b)
1
2
3
1/2"

Locations of rosettes 'a' and 'b'

(6b)

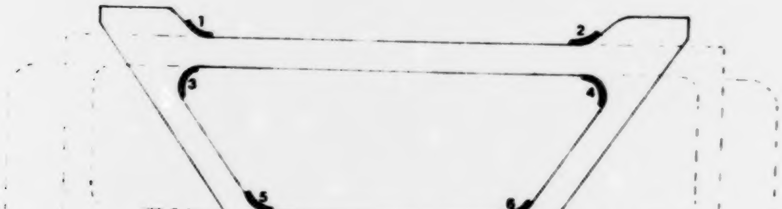

Locations of gauges on the bolster

(6c)

Figure 6 - Gauge Locations

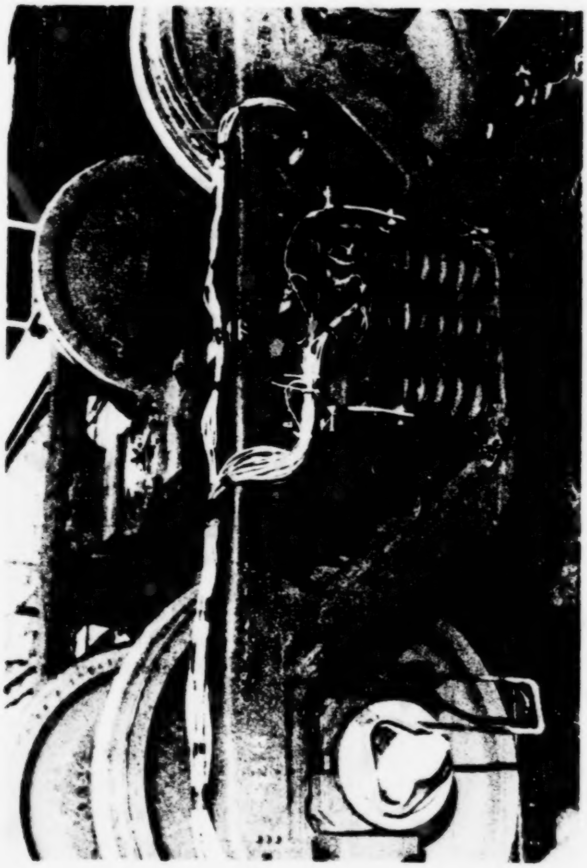

Figure 7: Gauged Test Truck

Figure 8

Thompson Sub. - Mile. 28.45 to 28.98
(welded rail)

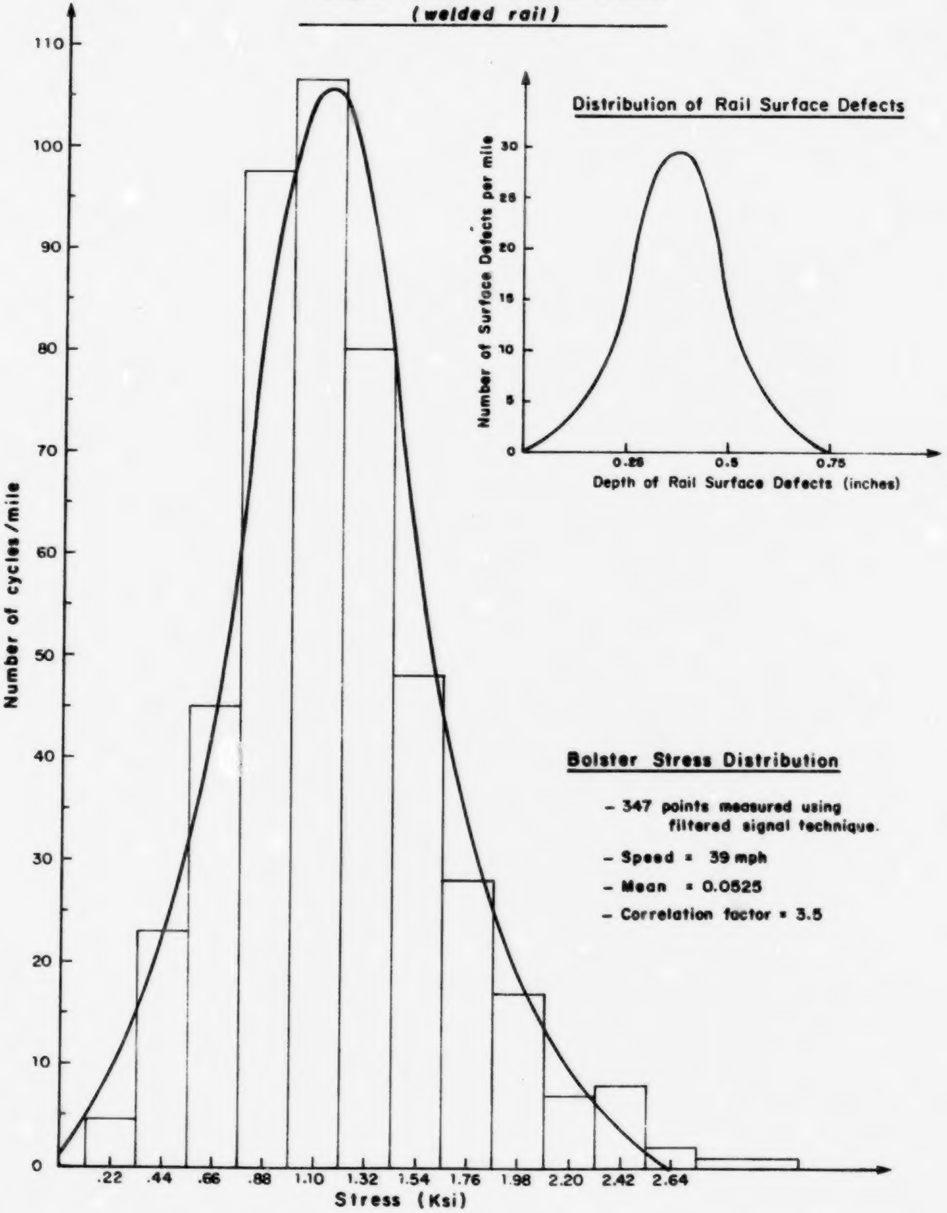

Figure 9

Thompson Sub. – Mile. 70.00 to 70.75
(welded rail)

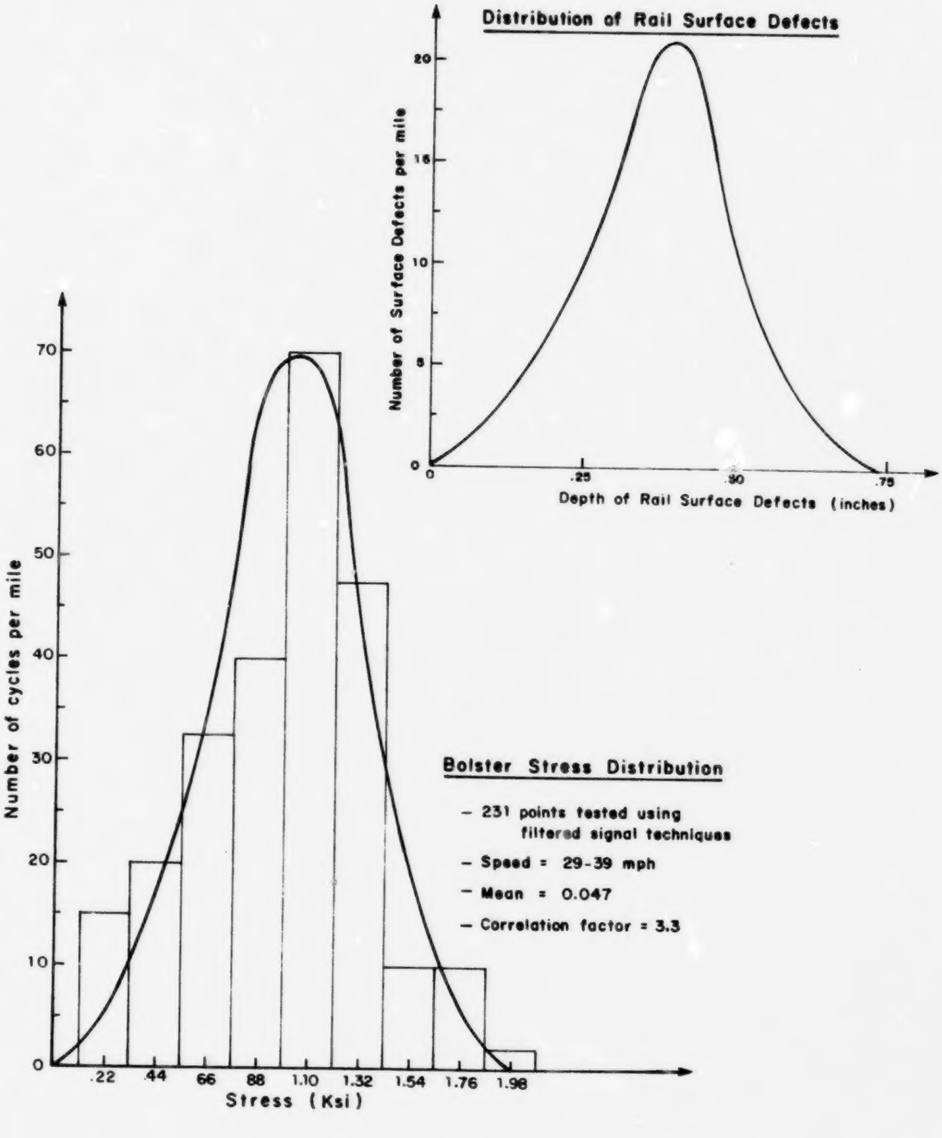

Bolster Stress Distribution

- 231 points tested using filtered signal techniques
- Speed = 29-39 mph
- Mean = 0.047
- Correlation factor = 3.3

Figure 10

Thompson Subdivision - Mile. 52.47 - 52.97

(Jointed Rail)

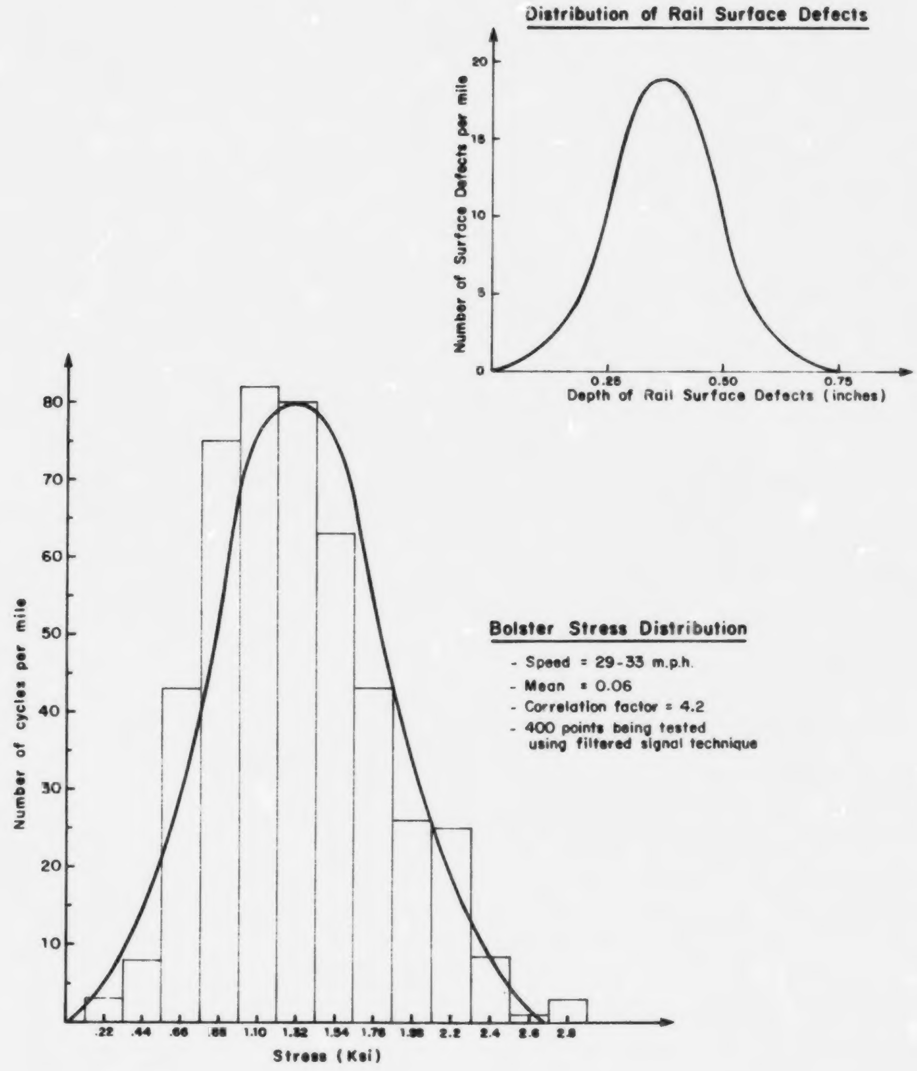

Figure 11

Thompson Subdivision - Mile. 20.50 - 21.00

(Jointed Rail)

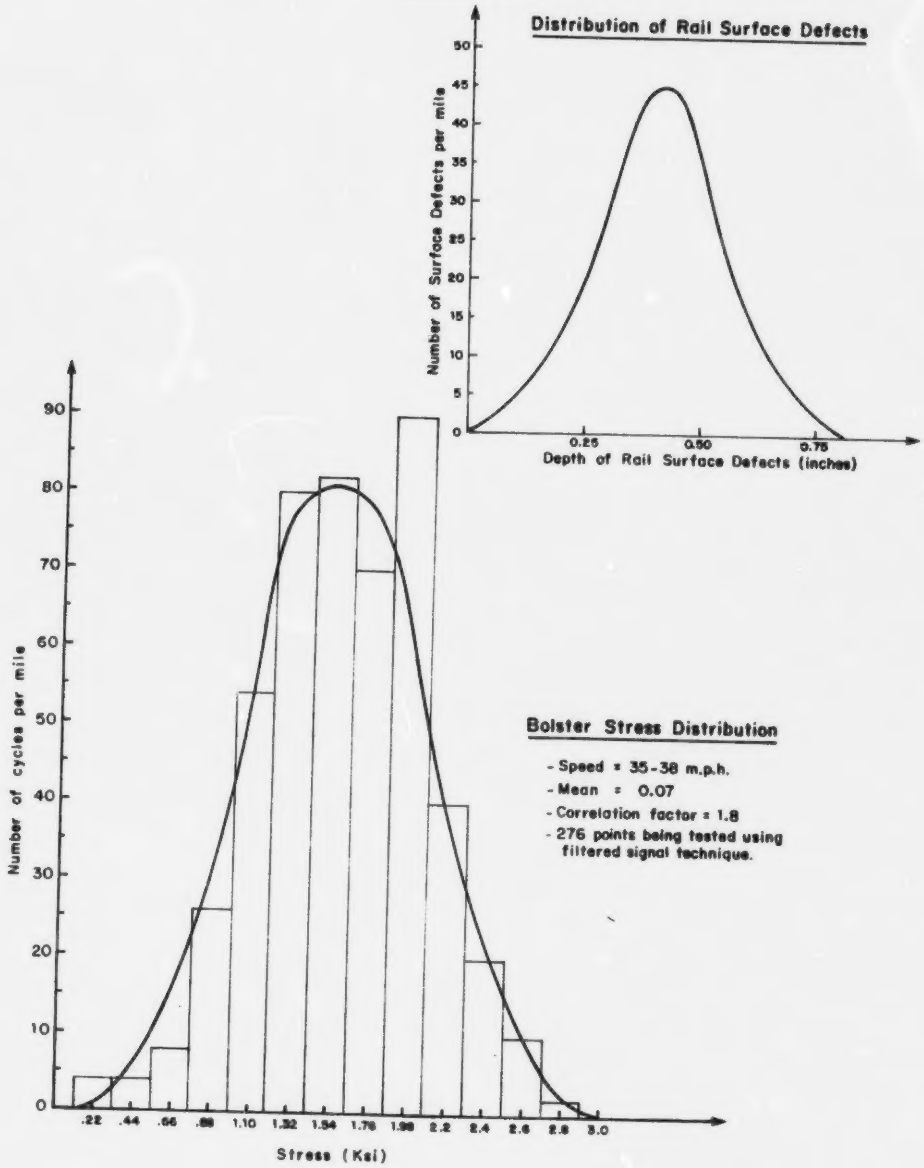

Distribution of Rail Surface Defects

Bolster Stress Distribution

- Speed = 35-38 m.p.h.
- Mean = 0.07
- Correlation factor = 1.8
- 276 points being tested using filtered signal technique.

Figure 12

STRESS VS DEPTH OF DEFECT

Thompson Subdivision

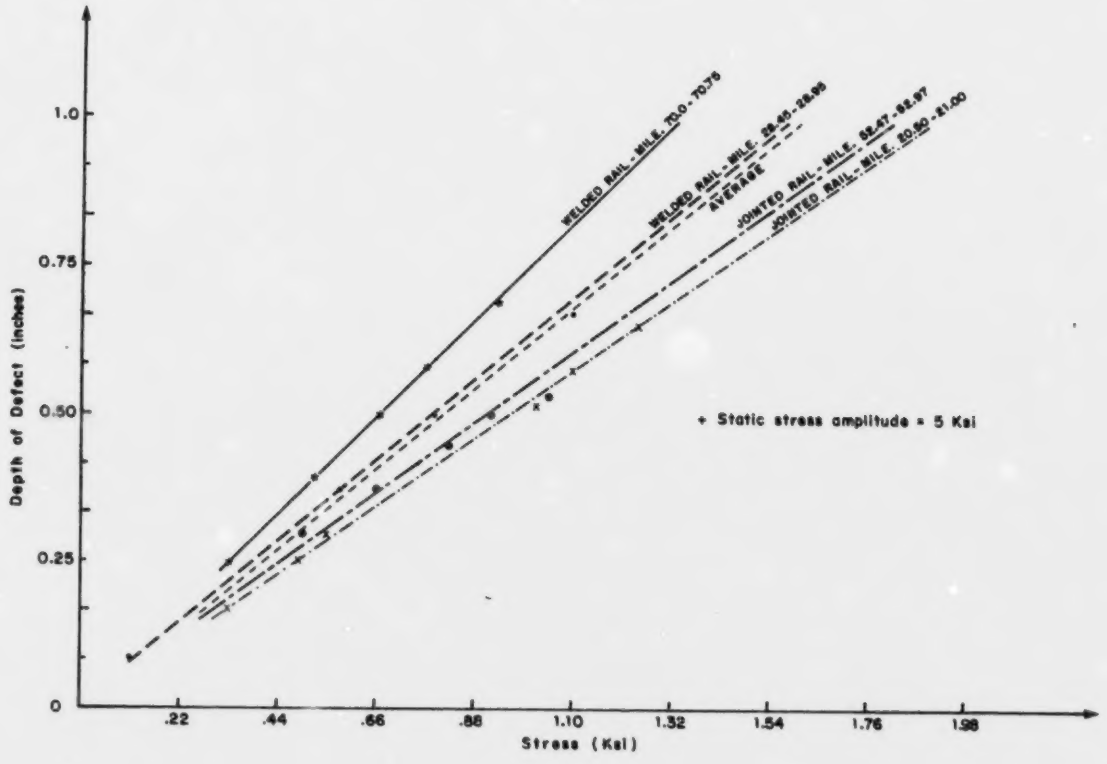

Figure 13

DISTRIBUTION OF RAIL SURFACE DEFECTS FOR THE ENTIRE PACIFIC REGION

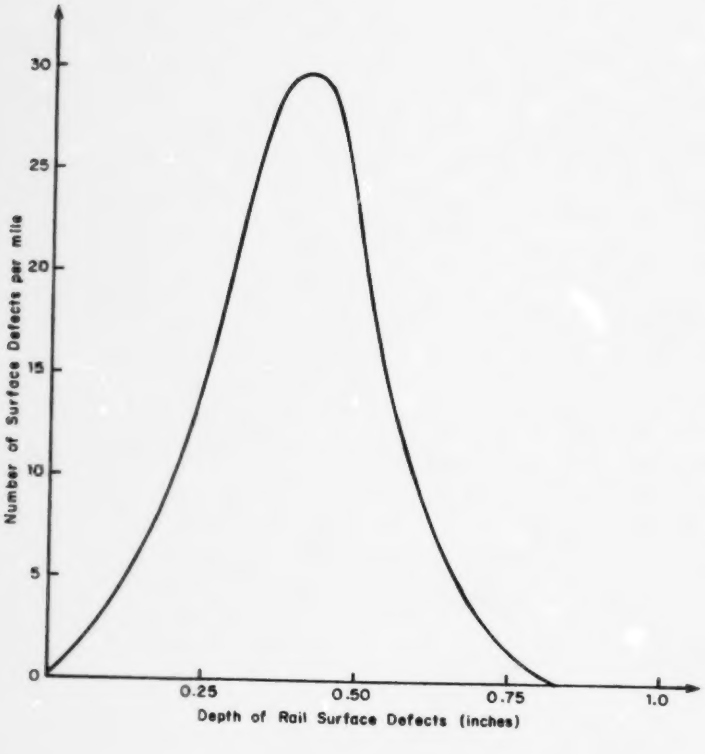

Figure 14

S-N Curves for Normalized 0.27 percent Carbon Cast Steel

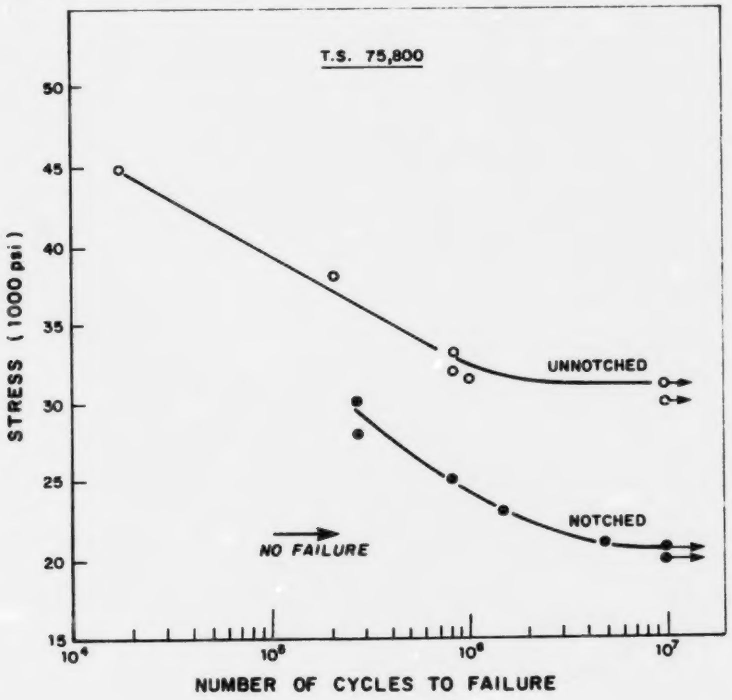

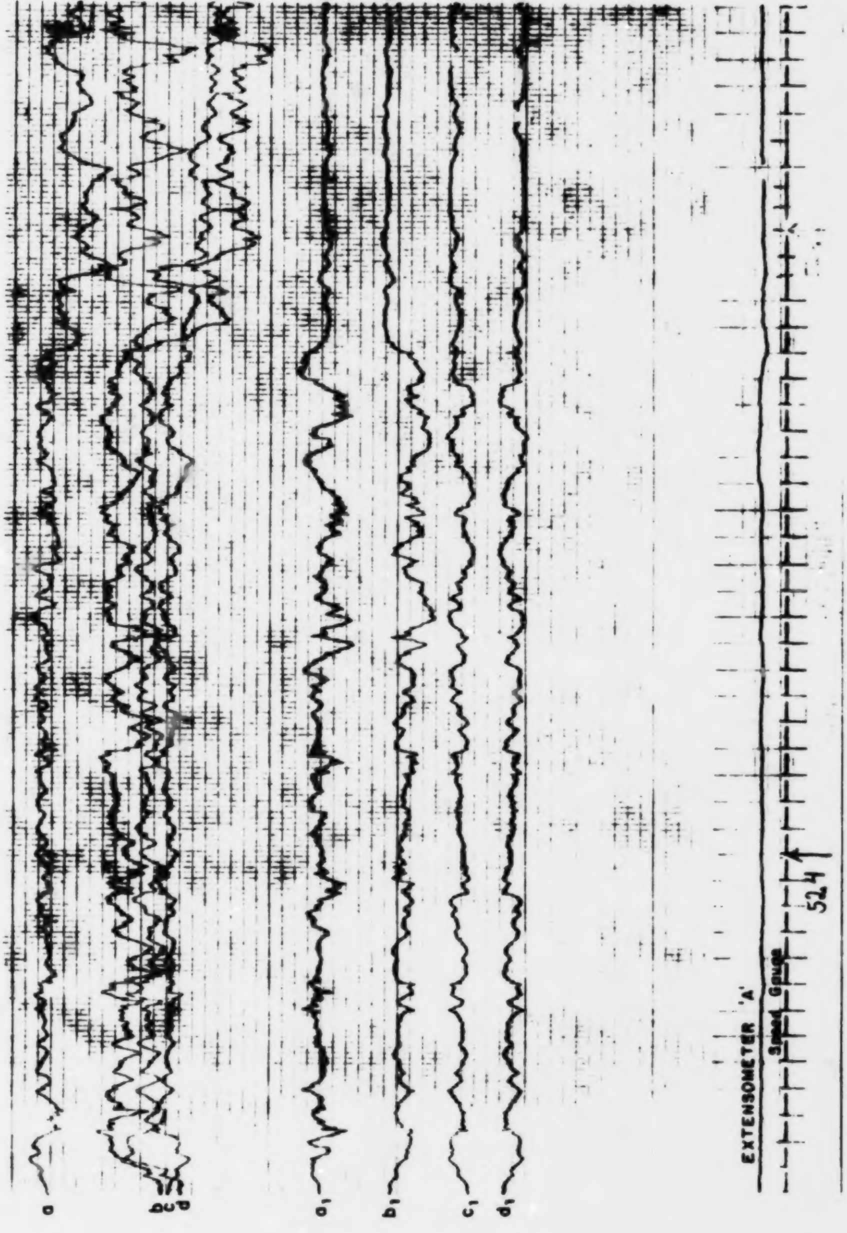

Graph No. 1 – Trace Sample of Recorder No. 1

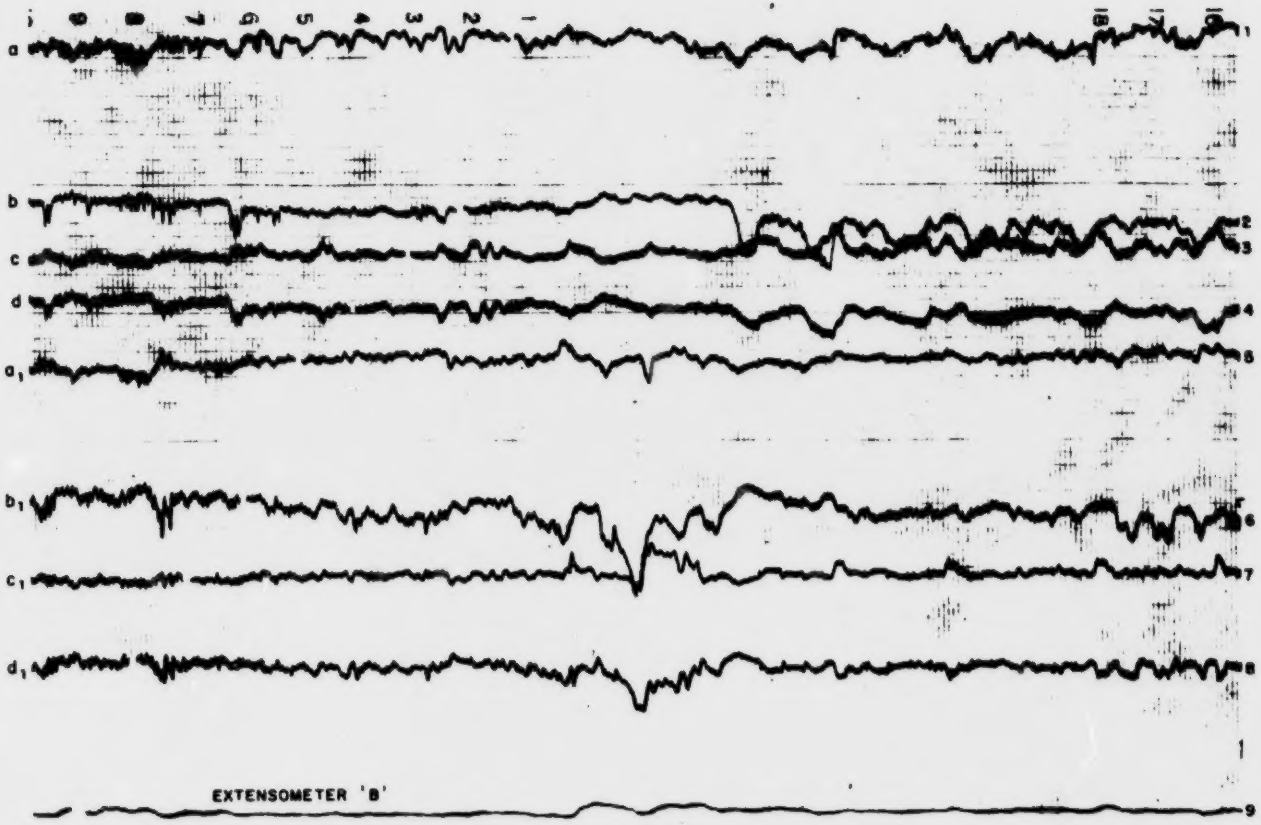

Graph No. 2 - Trace Sample of Recorder No. 2

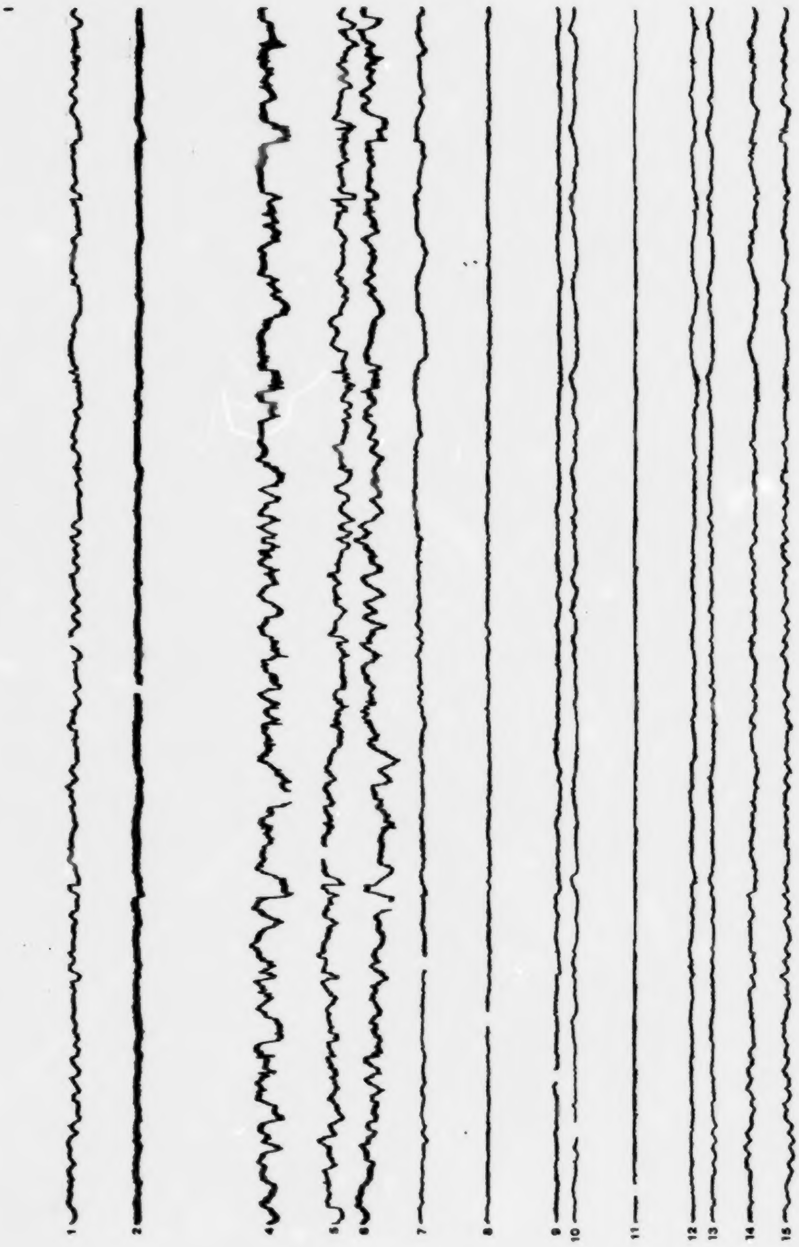

Graph No. 3- Trace Sample of Recorder No. 3

TABLE 1

"PROPER" CALIBRATED VALUES FOR VARIOUS GAUGES

All traces are recorded by recorder no. 3.

Gauge Position	Gauge Factor	Trace No.	Proper Stress psi/x1"T.D.*	Proper Strain μin./in./1"T.D.*
Top A		1	20,000	686
Inside Upper A		3	24,300	809
Inside Lower A		5	21,400	711
Rossette R_a	2.10	7	21,700	723
	2.10	8	42,700	1423
	2.10	9	43,400	1445
Top B		2	20,300	676
Inside Upper B		4	21,900	729
Inside Lower B		6	20,600	686
Rossette R_b	2.10	10	43,400	1445
	2.10	11	68,300	2276
	2.10	12	44,500	1482

---

* T.D. -- Trace Deflection.

TABLE 2

"PROPER" CALIBRATED VALUES FOR SNUBBER GAUGES

Snubber A

Traces are recorded by Recorder No. 1
Gauge factor for all strain gauges is 2.09 ±0.5%.

Gauge Position	Trace No.	Proper Strain µin./in./1"T.D.*
a	1	669
b	2	661
c	3	612
d	4	710
a_1	5	684
b_1	6	676
c_1	7	669
d_1	8	661

Snubber B

Traces are recorded by Recorder No. 2
Gauge factor for all strain gauges is 2.09 ±0.5%.

Gauge Position	Trace No.	Proper Strain µin./in./1"T.D.*
a	1	661
b	2	701
c	3	676
d	4	676
a_1	5	684
b_1	6	669
c_1	7	646
d_1	8	661

* T.D. -- Trace Deflection.

TABLE 3

TEST LOCATIONS

A. Kamloops → North Bend
(The gauged bolster was in leading position)

No. of The Test	Mile Post	Length of Data Recordings in Miles	Average Speed Miles/Hr.
1	19-22	3	27
2	33-36	3	38
3	38-40	2	48
4	50-53	3	27
5	70-71	1	27

B. North Bend → Kamloops
(The gauged bolster was in trailing position)

No. of The Test	Mile Post	Length of Data Recordings in Miles	Average Speed Miles/Hr.
1	73-70	3	27
2	29-28	1	38
3	21-19	2	38

TABLE 4

MAXIMUM STRESS VALUES ACTING ON THE BOLSTER-SNUBBER CONTACT SURFACE

	Side A	Side B
Maximum static stress (Ksi)	-0.34	0.29
Maximum stress at 1 (Ksi)	-0.96	0.96
Maximum stress at 2 (Ksi)	0.58	0.19
Maximum stress at 3 (Ksi)	2.40	1.04
Maximum stress at 4 (Ksi)	0.58	0.89

TABLE 5

SOME RESULTS OBTAINED FROM R_a AND R_b

	Static Load	M.P.79	M.P.70
Rosette R_a			
Max. Stress (Ksi)	1.084	1.665	- .761
Min. Stress (Ksi)	-3.876	-4.451	-5.110
Max. Shear Stress (Ksi)	2.477	3.058	2.174
Principal Axis (degree)	- 83.4	- 71	- 75.6
Max. Strain (μ in./in.)	75	100	26
Min. Strain (μ in./in.)	-140	-105	-136
Max. Shear Strain (μ in./in.)	215	265	188
Rosette R_b			
Max. Stress (Ksi)	2.160	2.160	-.199
Min. Stress (Ksi)	-3.274	-3.274	-5.929
Max. Shear Stress (Ksi)	2.717	2.717	2.865
Principal Axis (degree)	- 86.8	- 86.8	72.4
Max. Strain (μ in./in.)	105	105	53
Min. Strain (μ in./in.)	131	-131	-196
Max. Shear Strain (μ in./in.)	235	235	248

II VARIABLES AFFECTING THE FATIGUE LIMIT OF A BOLSTER

In addition to the dynamic and static stresses acting on the bolster, many other factors contribute in decreasing the fatigue endurance limit of the alloy of the bolster. The main factors are:

1. Casting defects
2. Fretting fatigue
3. Corrosion fatigue

Following is a discussion of each of these factors.

II.1 Casting Defects

Discontinuities of some form are always present in any type of casting. When the cast is loaded, these discontinuities can result in the development of a non-uniform and complex stress field adjacent to the discontinuity, with local peak stresses in such regions much greater than the average or nominal stress across the section. These discontinuities are usually the preferred sites for originating fatigue cracks.

Bearing this in mind, several fractured bolsters were inspected at the Test Department of Angus Shop. It was observed in the majority of cases that casting defects were present in the cross-section immediately below the snubber pocket extension. By tracing these defects in a sample, shown in Figure 15, taken from a randomly chosen bolster, it was observed that shrinkage cavities of the size shown in Figure 16 exist in the casting. By judicious choice of a sectioning path, the sample was cut into several portions so as to expose the pertinent areas of the shrinkage cavity and fatigue crack surfaces. It was clear that this cavity penetrated the entire length of the original specimen and that, in fact, it increased in severity. The two sides of one such section are illustrated in Figures 17(a) and 17(b).

In order to avoid the possibility of the existence of this shrinkage cavity having been a rare case, a non-destructive gamma-ray radioisotope test was carried out on a bolster that had not been fractured and which showed no surface defects. Again, the test revealed the existence of the same type of cavities in the same locations.

In general, shrinkage cavities are likely to occur at points in a case where hot spots occur, i.e. where the solidification rate (and thus the contraction rate) is different than the rest. If such a difference is not compensated for by adequate feeding, shrinkage of the casting will produce finely dispersed porosity or localized internal voids. The risk of defects attributable to variation in thickness increases with the massiveness of the part concerned with respect to the casting as a whole.

A simple means of assessing the mass is the "inscribed circle"(11) method which enables the mass effect in any particular section of a casting to be represented by the surface of the inscribed circle in this section. Carrying out this comparison for the sections indicated in Figure 15, it is found that the ratio of the square of the maximum and minimum radii is approximately:

$$\left(\frac{3}{4}\right)^2 / \left(\frac{11}{32}\right)^2 = 4.7 \qquad (1)$$

This represents a mass increase in the neighbourhood of the shrinkage cavity of almost 370% over that in the rest of the cross bolster. This is, in the author's opinion, a major design error.

A measure of severity of a stress concentration at the location of this shrinkage cavity is given by the stress concentration factor K_t which is defined as the ratio of the maximum local stresses in the region of the cavity to the nominal local stresses acting on the rest of the bolster-snubber surface. From the data obtained in the previous part, this factor should be:

$$K_t = \frac{\sigma'\ \text{max.}}{\sigma\ \text{nom.}} = 2.9 \text{ to } 3.5$$

Furthermore, the appearance of these shrinkage defects on the surface can be considered a case of severe notch which results in the decrease of the fatigue limit of the bolster alloy to the range of 7-9 Ksi (the notch sensitivity factor for this alloy is 0.433).

Turning attention to some of the conclusions which may be drawn from the careful scrutiny of the exposed crack surfaces in the sample shown in Figure 16, it is the opinion of the author that, cracks were initiated in the snubber pocket area of the bolster where the presence of the shrinkage cavity was most detrimental to its load carrying capacity. Although some of the surface details were obliterated due to subsequent corrosion, the corresponding views, on each exposed surface, of the crack initiation zone are shown in Figure 18. The crack initiated at the shrinkage cavity, progressed along several facets toward the inner and outer surfaces of the bolster and then propagated in two opposite directions. These paths were not always unique since branching was observed to have occurred at several locations, one of which is illustrated in Figure 19. It also shows that rather large amplitudes of relative motion have taken place since the surface has been rubbed smooth in several locations.

In conclusion, the shrinkage cavity present in this specimen and present in others, contributed in a most significant manner to the fatigue crack initiation and hence to its subsequent crack propagation. Due to the shrinkage cavity, with the size discussed, the crack was, in all probability, initiated prior to the first in-service loading of the cross bolster. Steps should be taken to eliminate the likelihood of its presence in all future cross bolsters and a close inspection program should be instigated to routinely examine existing bolsters for cracks in this location.

My recommendations pertain to the future manufacture of cross bolsters and not to those presently in service. In order of preference they are:

1. the casting design should be altered so as to have a more uniform cross-sectional area throughout this area of the bolster,
2. if this is deemed unadvisable, then external chills should be incorporated into the casting molds, as in Figure 16(a), so as to substantially increase the rate of heat removal from this location of the bolster.

II.2 Fretting Fatigue

Another factor involved in the failure occuring at the interaction surfaces between the bolster and snubber can be associated with fretting fatigue. This phenomenon, which is discussed in several references, see for example reference (12-15), is a particular type of fatigue damage which occurs when two unlubricated surfaces, under moderate or heavy pressures, experience relative vibrational movement of small amplitude. The process of fretting damage is a form of mechanical wear which occurs without oxidation but can be greatly aggrevated if corrosion occurs simultaneously.

Due to the vibration accompanying the dynamic movement of the car truck, the two surfaces of the bolster and snubber - which contact one another only at surface asperotoes - are subjected to a transverse cyclic loading so that one contacting surface is relatively displaced cyclically parallel to the other face. During this process, a few points of direct metallic contact are ruptured, forming oxide particles which are harder than the metal of the snubber or the bolster itself. The appearance of oxide particles is usually accompanied by localized pitting of the surface in the fretted region and this can result in a serious reduction of the fatigue endurance limit. It is known that soft metals are generally more susceptible to fretting corrosion than hard metals. This indicates that the bolster surface will be the one more seriously affected since its hardness is 175 BHN while the snubber surface hardness is 340 BHN.

It is observed that the fretting process is limited not only to the contact surface between the snubber and bolster, but that it also acts on the fracture surface of existing cracks in the bolster. Example of these cases are shown in Figures 19 and 20. Figure 19 shows a fracture surface which was polished as a result of continuous rubbing against the opposite surface while in Figure 20, chipping away of the brittle corrosion-prevention coating is a sign of the relative movement of both sides of the crack.

One of the characteristic features of the fretting process is the small amplitude of the relative motion required to damage contacting surfaces. It was shown(16) that an amplitude in the order of 0.0001 inches was often sufficient. The damage at the bolster surface increases with the amount of slip on the snubber surface, but an upper limit may be reached when the movement is sufficient to allow the oxidation particles to escape. Fretting damage on the bolster surface also increases as the temperature decreases and shows sudden increase at temperatures below freezing. During winter the bolster surface is subjected to temperatures as low as -40°F.

There is no quantitative formula that can predict the reduction in the fatigue limit of the bolster surface material due to this fretting damage. However, it was found experimentally(9) that the fatigue limits of carbon steel specimens, whose surfaces have been fretted prior to fatigue testing, were 13% lower than the corresponding fatigue limit of the unfretted samples.

There are many measures which can be taken to reduce the effect of the fretting process between moving surfaces. These measures are amply reported in numerous references, for example, see 9 and 19. However, the most valid measure in the present situation is the placement of anti-fretting, high strength, steel alloy plates, such as ASTM 516, between the cast surface of the bolster and the snubber surface.

II.3 Corrosion Fatigue

Surface conditions are exceptionally important in the fatigue behaviour of metals since the initiation of microcracks is associated, in general, with a free surface. Corrosion due to the environment can result in the roughening and forming of pits or crevices at certain points on the unprotected surface of the bolster snubber pocket, as shown in Figures 22(a) and 22(b). The effects of this corrosion damage are analogous to those resulting from small stress concentrators or other mechanically-formed surface discontinuities; they act as initiation sites for cracks, resulting in a considerable loss of fatigue resistance when the bolster is subjected to fluctuating stresses. One of the most significant features of corrosion-fatigue results from the progressive and time-dependent nature of the corrosion process. This means that the microcracks in the bolster, originally from the "as-cast" surface irregularities, will continue to propagate while the corrosion-fatigue condition persists. Thus, the carbon steel alloy of the bolster which exhibits a definite fatigue limit (20 Ksi) under normal laboratory conditions, gives no indication of such a limiting stress under corrosion-fatigue conditions and will eventually fracture even under low alternating stresses such as the obtained value in Tables 3, 4, and 5.

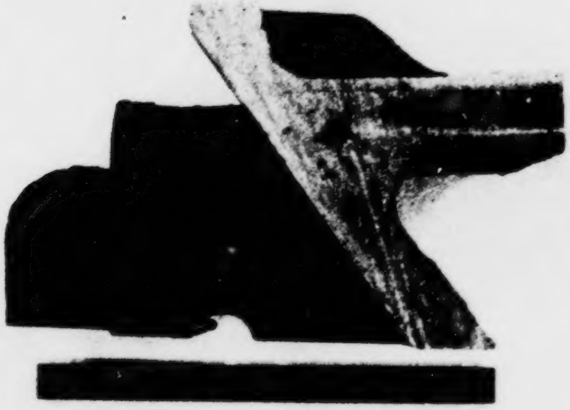

Figure 15: Shrinkage Cavity at one End of Original Sample

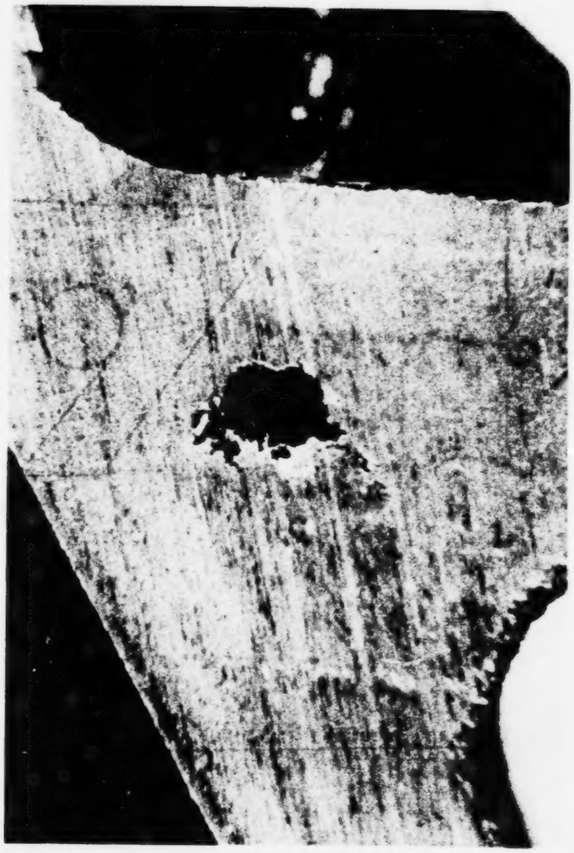

Figure 16: Close-up of Previous View

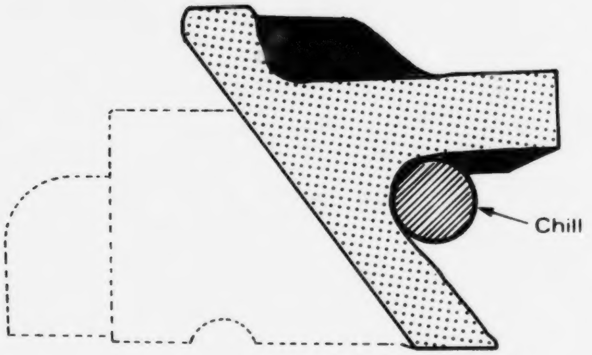

Figure 16(a): External Chill in Web Intersection

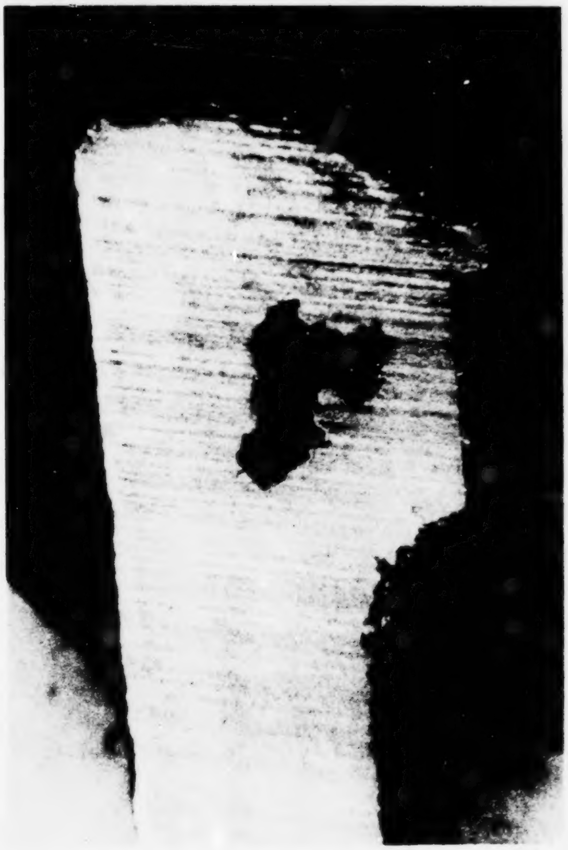

Figure 17(a): Shrinkage Cavity Close-up

Figure 17(b): The Shrinkage Cavity on the Other Side of the Section Shown in the Previous Figure

Figure 18(a): Detail of Fatigue Crack Initiation Zone

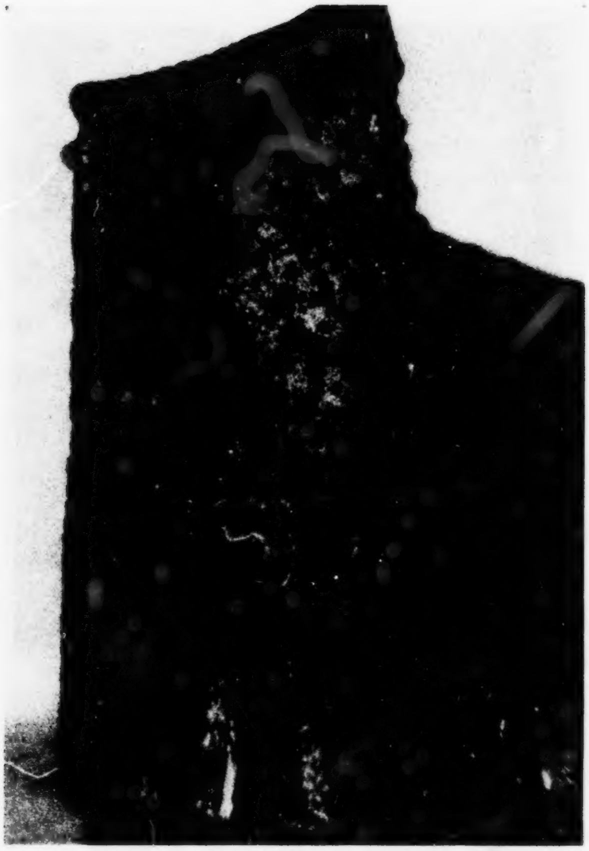

Figure 18(b): Corresponding View of Fatigue Crack Initiation Zone

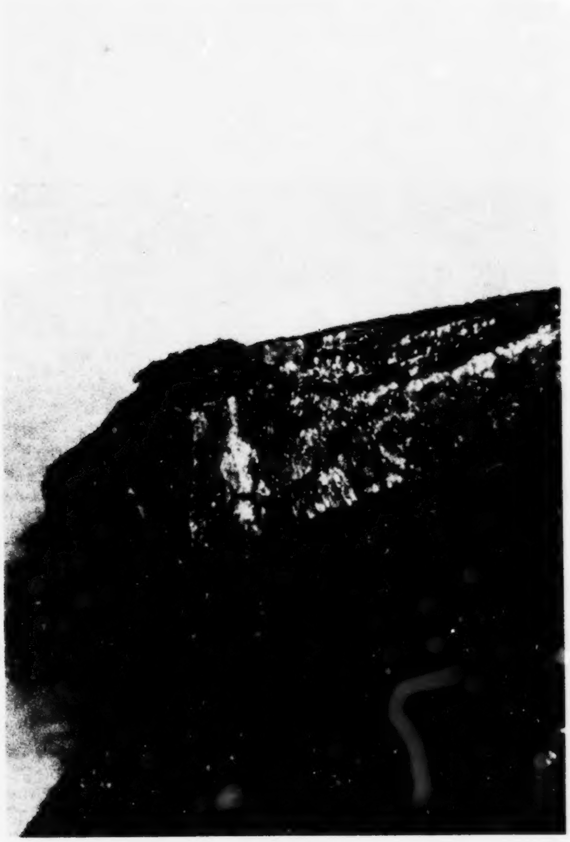

Figure 19: Detail of fatigue Crack Branching and Crack Surface Polishing

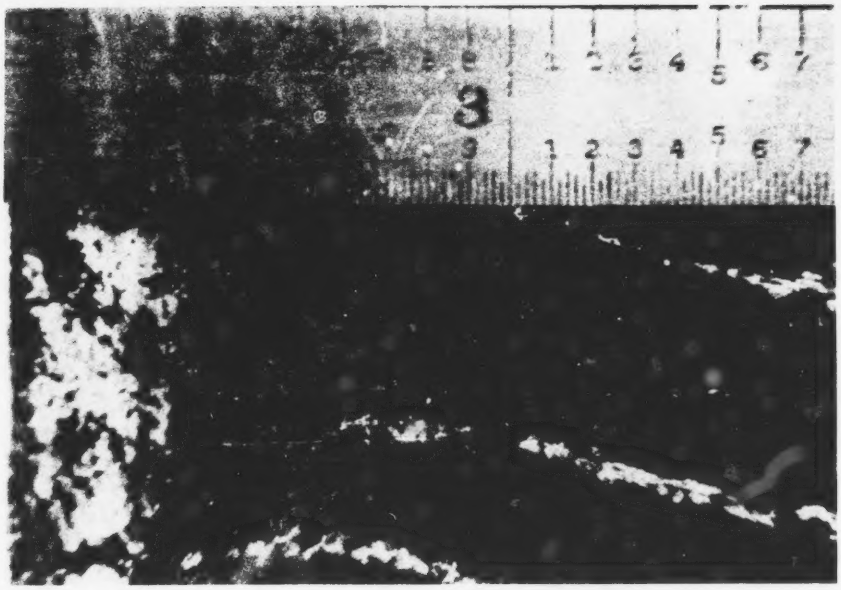
3
1 2 3 4 5 6 7
1 2 3 4 5 6 7

Figure 20: Close-up of Crack Tip

III. THE WELD INVESTIGATION

III.1 Micrographic Analysis

The second group of cracks that has been observed on the bolster is the one associated with previous weld repair on the bolster surfaces, which was in contact with the snubbers. The repairs were made by using Arctec 30, a low-alloy steel-welding electrode. To investigate the role of this weld in initiating cracks, the weld deposit, the heat affected zone and the original bolster material were examined metallurgically. Several sections of these areas were polished, etched in 4% Nitral for 5 seconds and microscopically examined. All sections showed the characteristics depicted in the series of micrographs 22-29. Their relative positions are indicated in Figure 21 with the estimation of grain size and temperature resulting from welding operation. The average hardness and the approximate tensile strength of the material indicated in the figure is shown in the caption of each micrograph. Following is the metallurgical analysis of these micrographs.

Figure 22:
The as-cast weld deposit is illustrated in this figure. This deposit has solidified with coarse ferrite dendrites, an intermediate transformation product, and fine pearlite (dark areas). A "normalizing" heat treatment (air cooling from $165^{\circ}F$) is necessary to achieve refinement of this "as-welded" coarse grained structure.

Figure 23:
This figure illustrates the cladding (deposit) interface. The upper zone is the coarse dendritic deposit shown in Figure 22, while the lower region shows the base metal after

heating and austenite grain growth below the fusion temperature. This coarse weld structure would be greatly refined by "normalizing" after welding.

Figure 24:
This is a close-up of the microstructure and deposit zone illustrated in Figure 23. The deposit appears well-bonded and diffused; however, this coarse grained microstructure and transition zone can be susceptible to brittle fracture and fatigue cracking. The weld transition zone constitutes a metallurgical notch unless welding is followed by normalizing to obtain a fine-grained microstructure similar to the one in Figure 29.

Figure 25:
This photomicrograph shows the most severely altered original microstructure when austenite grain growth has produced a coarse-grained microstructure. The relatively slow cooling rate has allowed formation of pre-eutectoid ferrite and fine pearlite with traces of wedmonstatten ferrite on slip planes within the austenite grains.

Figure 26:
This microstructure results from heating slightly above Ar_3 followed by air cooling, which produces equi-axed ferrite and fine pearlite by recrystallization without austenite grain growth. (Austenite grain growth is visible in Figures 23 and 24 in high temperature regions adjacent to the weld deposit.) Slight seggregation of carbon in the original as-cast dendrite regions is also visible.

Figure 27:
This region has been heated to 1100-1250°F, resulting in spheroidization of the pearlite. It is incomplete at the bottom of the picture and more advanced at the top of the picture. (A similar microstructure to that visible at the bottom of this picture would be obtained if the original

microstructure, Figure 28, were heated to 1100°F and air cooled, as occurs during stress relief.)

Figure 28:
Pearlite areas have started to coalesce in the process of becoming spheoidized. The ferrite grain size may be slightly larger than that of the original cast - normalized structure due to subcritical growth at about 1300°F. Some seggregation of carbon is visible. This is a close-up of the second transition zone shown in Figure 26.

Figure 29:
This is the original cast (normalized) microstructure comprising pllygonal ferrite and fine pearlite. Its carbon content is approximately 0.30% and it is most likely an ASTM A27 cast steel. It shows approximately 65% ferrite and is the microstructure desired after heat treatment of welds by normalizing or normalizing and tempering, thus effecting recrystallization of coarse grained weld zones. This relief treatment at 1000-1250°F is concerned mainly with relief of stress and elimination of hard zones but does not affect recrystallization.

From this analysis, while the weld deposit appears to be well-bonded to the parent metal and does not have areas harder than 200 BHN, the "as-welded" coarse-grained condition as illustrated by Figures 26-29, inclusive, can be susceptible to brittle fracture and fatigue depending on the design, nominal and impact stresses, service temperature and on the presence of stress raisers, arc strikes or microcracks capable of providing a critical flaw size. Furthermore, the wide difference between the microstructure of the weld deposit and that of the base metal is considered a metallurgical notch.

Based on this micrographic study, the following are recommendations designed to improve the microstructure of the weld deposit and increase the efficacy of the weld in general.

III.2 Recommendations

1. The recommended (AAR) procedure for minimizing the effect of the coarse microstructure of a weld is to normalize after welding by heating at 1600 to 1650°F for 15-30 minutes per inch of section thickness followed by cooling in still air. This procedure will result in the microstructure shown in Figure 29, Grain Size No. 27, of polygonal ferrite and fine pearlite. Such material offers better resistance to fatigue and has a lower impact transition temperature than the weld-repair microstructure shown in Figures 22-29, inclusive.

2. If normalizing heat treatment is not done, a less effective substitute is to stress relieve at 1100°F to 1200°F for 1 hour per inch of section followed by air cooling. This type of treatment, although it does not refine the coarse grain of the microstructure, ensures that hard areas (martensite), such as arc strikes, will not enter service and provide initiation sites for brittle fractures (which is frequently started within hard spots, HAZ zones which were not stress relieved and contained more than 0.20% C).

3. Welded areas which are not normalized and stress relieved, should be strengthened by use of notch-tough reinforcement and arrester plates. Steel plates, ASTM 516, tested for conformity to specified Charpy V notch properties may be suitable for this use.

4. Chemical analysis should be made prior to welding to estimate the carbon equivalent for production of sound welds with correct pre-heat/post-heat procedure, especially at carbon content greater than .2% C. (Grade C casting steel has 0.35% C.)

5. Non-destructive inspection after welding is important to minimize the hazard of a flow of critical size entering service. (One of the bolsters, which had previously been welded and gave no indication of surface cracks, was examined by the author using gamma-rays. This test revealed the existence of incomplete fusion, slag inclusion and gas bubbles, although it showed a good degree of weld bonding with the parent metal.)

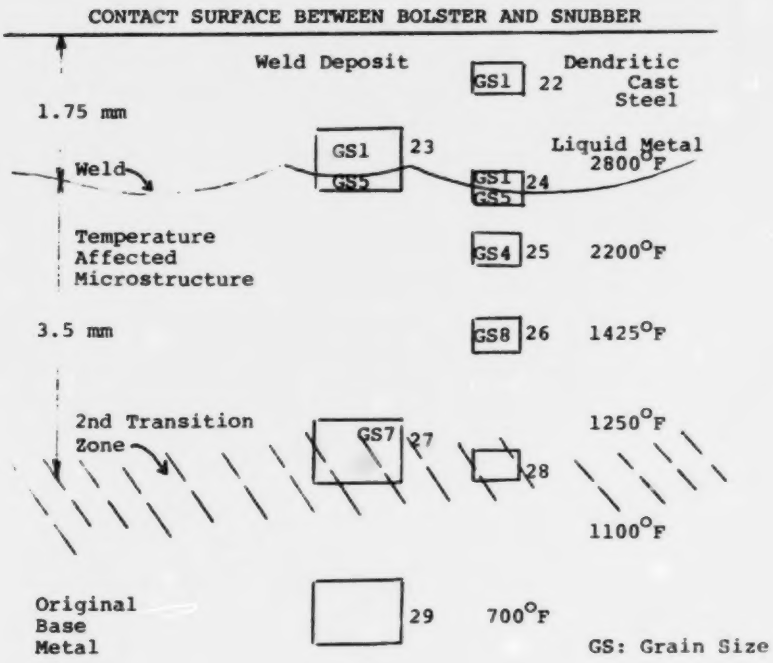
CONTACT SURFACE BETWEEN BOLSTER AND SNUBBER
Weld Deposit
GS1
22
Dendritic Cast Steel
1.75 mm
GS1
23
Liquid Metal 2800°F
Weld
GS5
GS1
24
GS5
Temperature Affected Microstructure
GS4
25
2200°F
3.5 mm
GS8
26
1425°F
2nd Transition Zone
GS7
27
1250°F
28
1100°F
Original Base Metal
29
700°F
GS: Grain Size

Figure 21: Positions of Following Micrographs

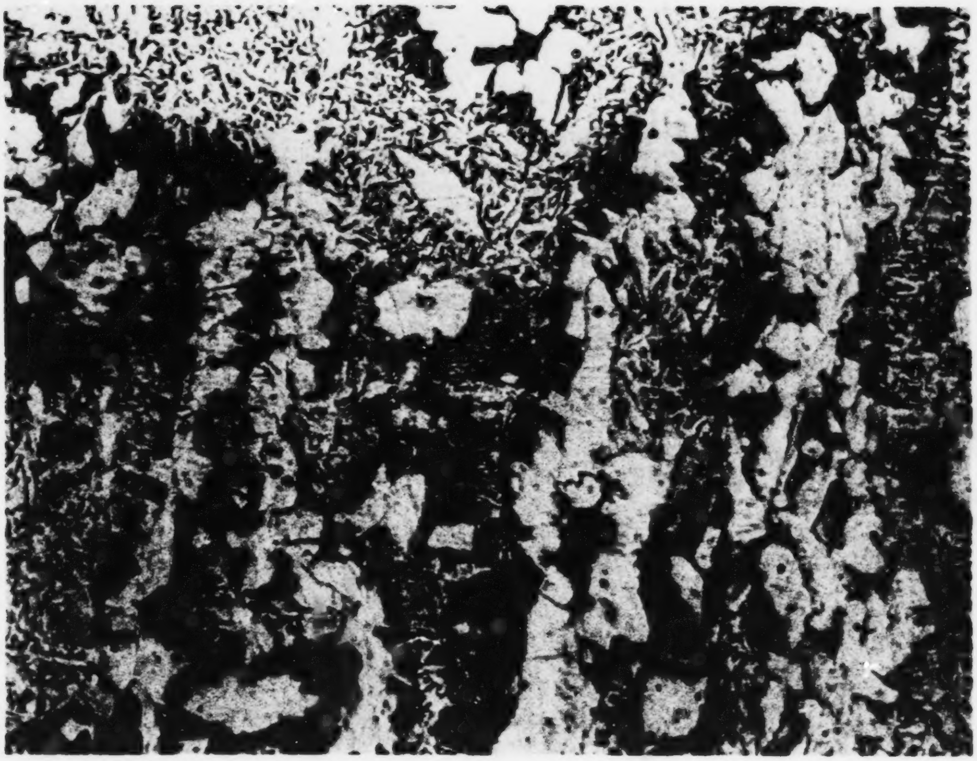

Figure 22: X500, 179 BHN, 103 Ksi Approximate Tensile Strength

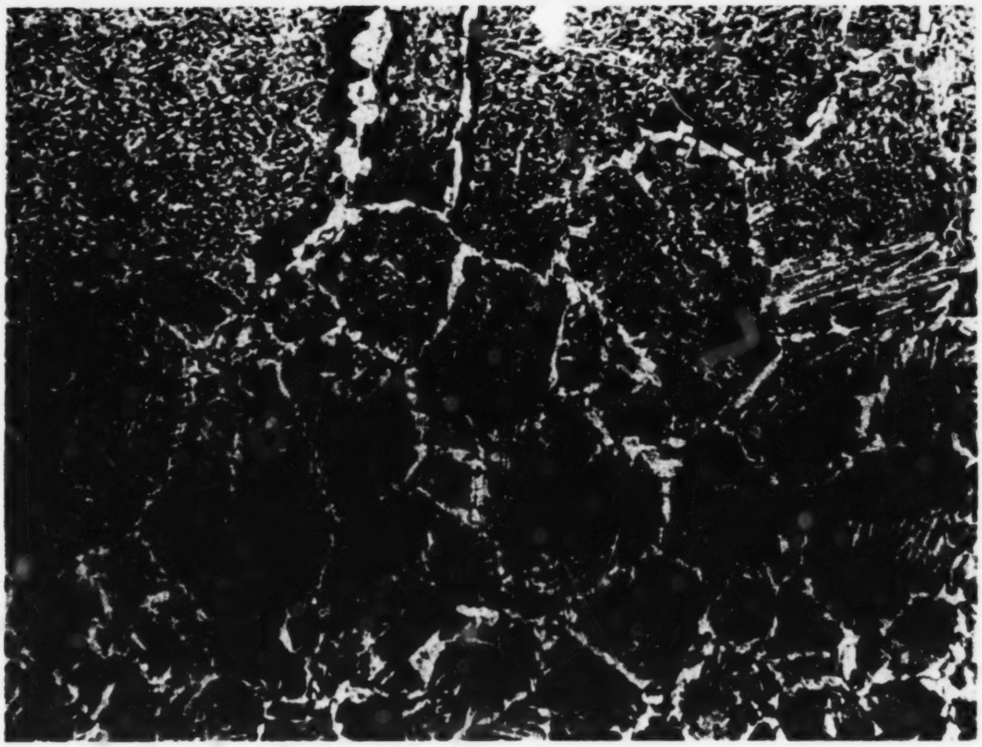

Figure 23: X200, 167 BHN, 96 Ksi Approximate Tensile Strength

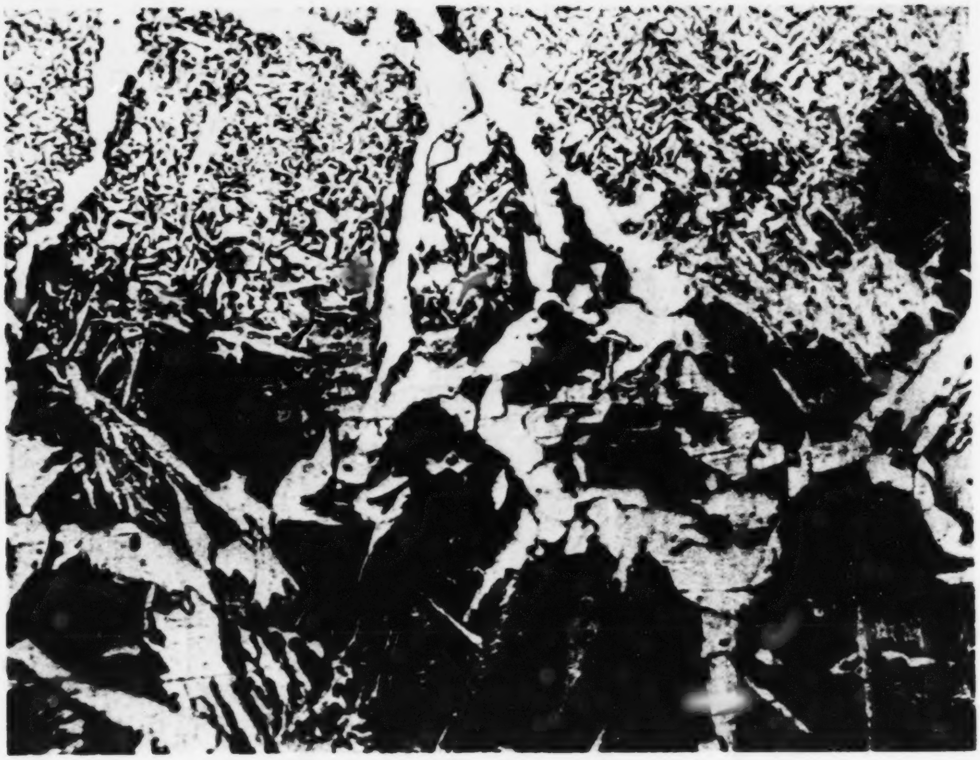

Figure 24: X500, 167 BHN, 96 Ksi Approximate Tensile Strength

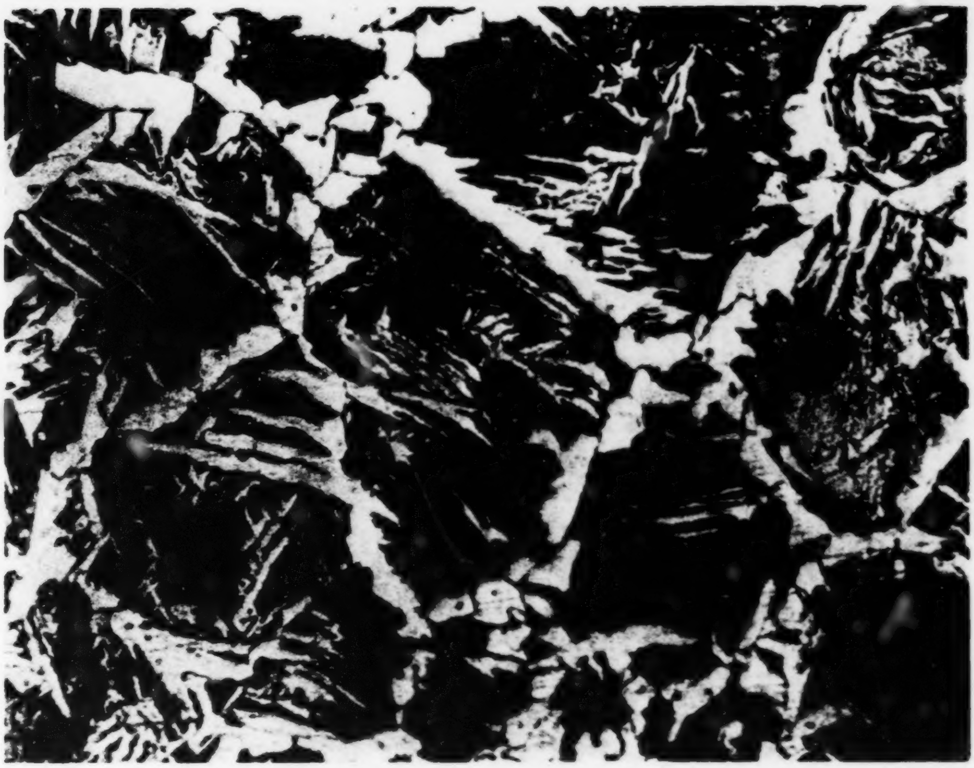

Figure 25: X500, 167 BHN, 96 Ksi Approximate Tensile Strength

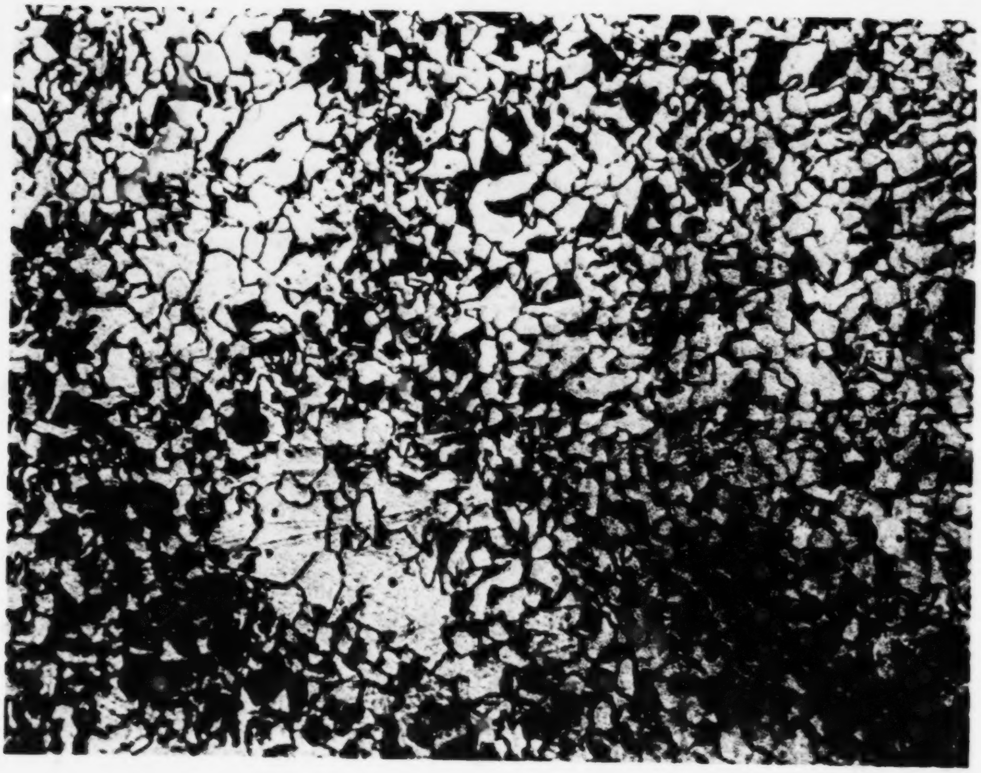

Figure 26: X500

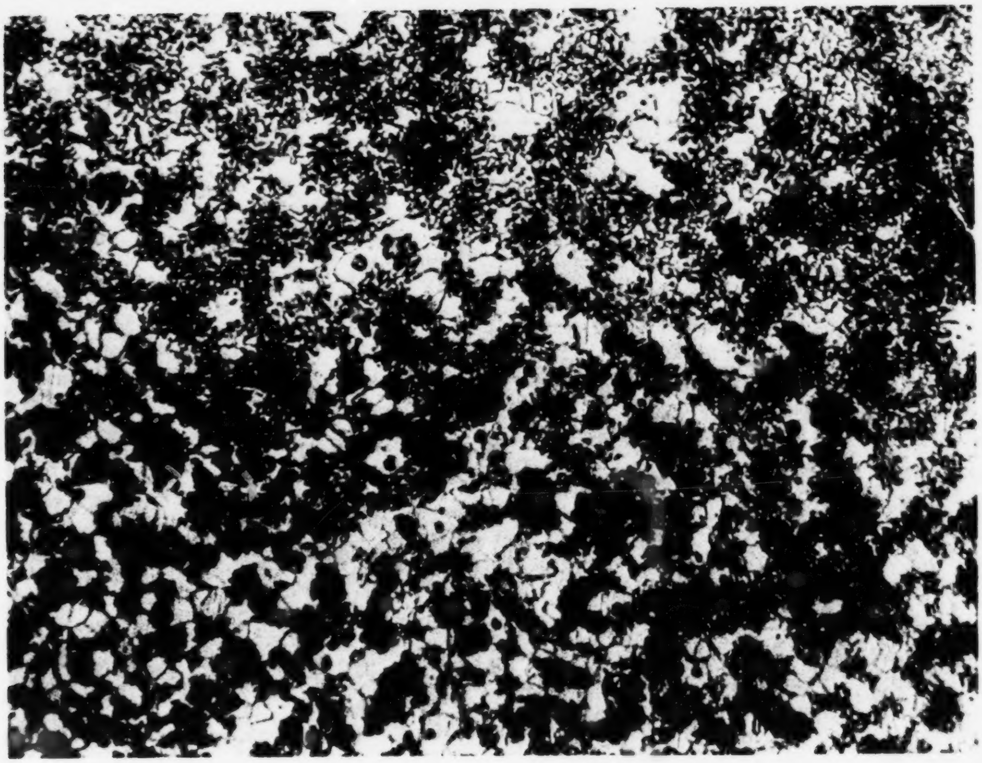

Figure 27: X200, 142 BHN, 80 Ksi Approximate Tensile Strength

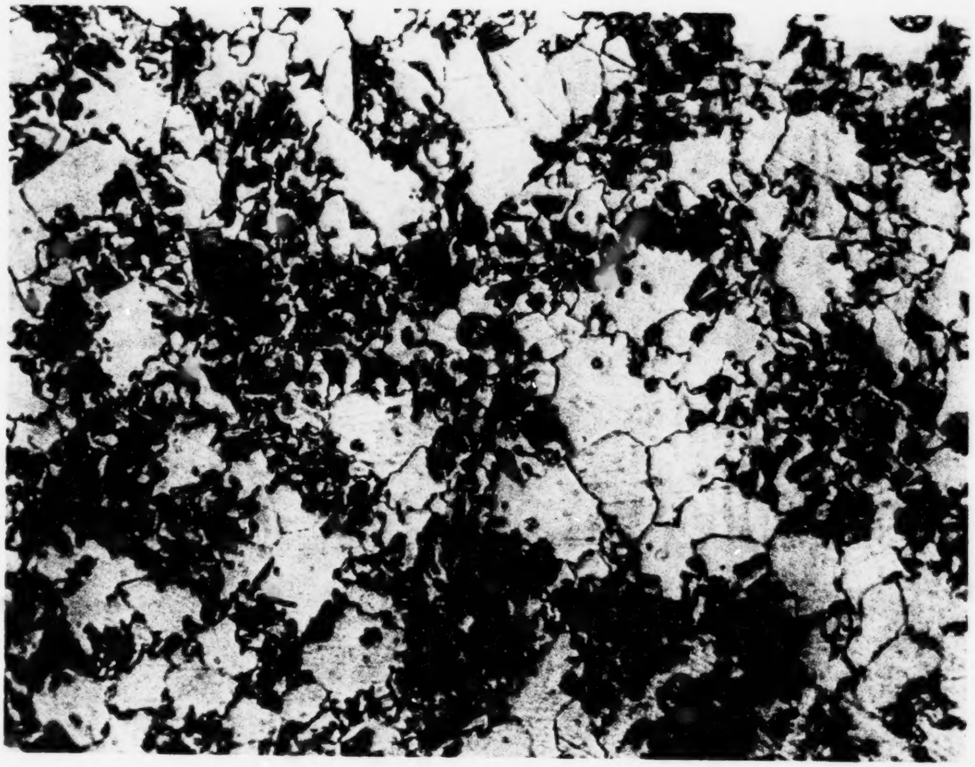

Figure 28: X500, 142 BHN, 80 Ksi Approximate Tensile Strength

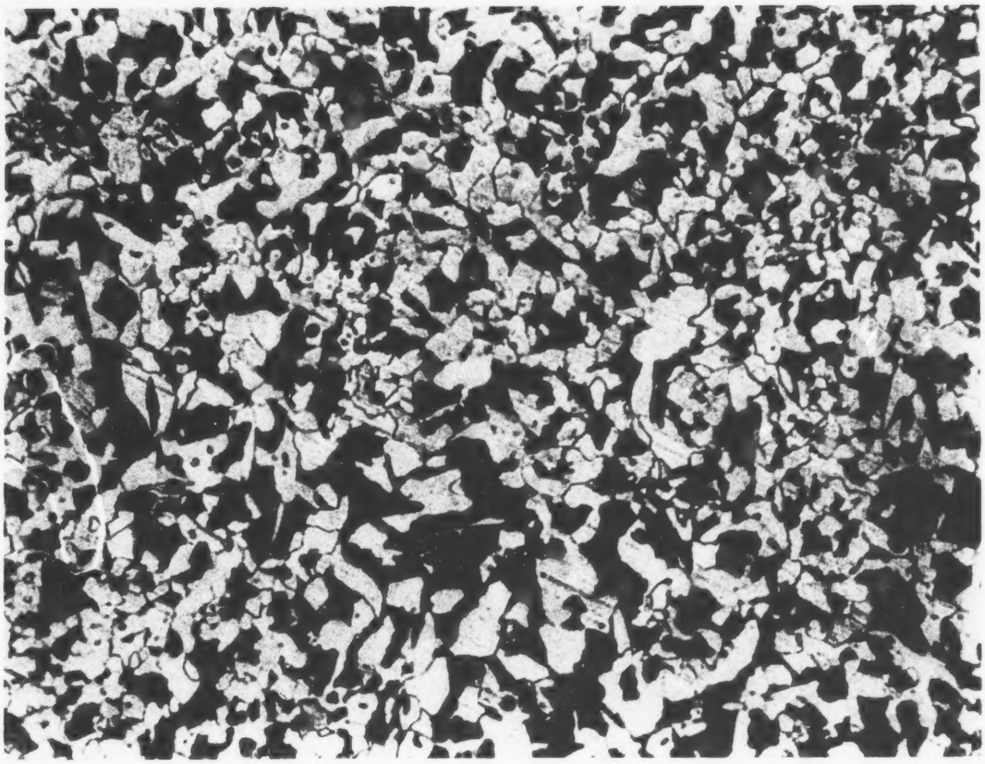

Figure 29: X200, 133 BHN, 74 Ksi Approximate Tensile Strength

REFERENCES

1.	H.G. TENNIKAIT	American Steel Foundaries Dynamic Test Facility for Railway Truck Components, Closed Loop, 4, (1974)
2.	M. HETENYI W.E. YOUNG	Applications of the Brittle Lacquer Method in the Stress Analysis of Machine Parts, Proc. Soc. Exptl. Stress Anal., 1, No. 2, (1943)
3.	G. ELLIS F.B. STERN	Dynamic Stress Analysis with Brittle Coatings, Proc. Soc. Exptl. Stress Anal., 3, No. 1, (1945)
4.	A.J. DURELLI E.A. PHILLIPS C.H. TSOO	Introduction to the Theoretical and Experimental Analysis of Stress and Strain, McGraw Hill Book Company, Inc., (1958)
5.	C.A.M. SMITH W.J. WATSON	Private Communication
6.	W.J. WATSON L.A. WEATHERSTON	Measurement Systems & Reduction Techniques Used in Railway Engineering, NRC Report, No. INS-46.
7.	PARRY & LISSNER	The Strain Gauge Primer, McGraw Hill, (1962)
8.	J.W. DALLY W.F. RILEY	Experimental Stress Analysis, McGraw Hill Book Company, Inc., (1965)
9.	N.E. FROST K.J. MARCH L.P. POOK	Metal Fatigue, Clarendon Press, Oxford, (1974)
10.	R. YU	Private Communication

11. T. LYMAN, ed. Properties and Selection of Metals, Metals Handbook, Eigthth Edition, (1961)

12. H.F. MOORE, S.W. LYON, N.J. ALLEMAN A Study of Fatigue Cracks in Car Axles, Univ. Ill. Eng. Exp. Sta. Bull, 197, Part II, (1929)

13. K.GUENTHER The Effect of Surface Defects on the Bending Fatigue Strength, Veroffent. Woehler Inst., Braunschweig, No. 2, (1929)

14. N.A. SCARLETT Greases to Prevent Fretting Corrosion, Engineering, Mar. 25, 1960

15. F.P. BOWDEN, K.W.W. RIDLER Physical Properties of Surfaces, Proc. Roy. Soc. (London), 154, (1935)

16. R.B. HEYWOOD Designing Against Fatigue, Chapman and Hall, London, (1962)

17. P. MARCOTTE et al Ride of Empty 100-Ton Hopper Car Aluminium and Steel, Technical Research Centre, CNR, (1970)

18. R. EVANS, M. JOHNSON Analysis of Environmental Truck Component Load and Bolster Fatigue Test Data, AAR, Interim Report No. R-246, (1976)

19. P.J.E. FORSYTH The Physical Basis of Metal Fatigue, Blackie & Son Limited, London, (1969)

J. Kalousek and G. Beynon

Rail Metallurgy

ABSTRACT: Rail wear has accelerated and changed in nature on a number of Canadian Pacific lines within the past five years. These changes have coincided with the introduction of heavier axle loads and more intensive utilization of the fixed plant.

Because of anticipated, continuously rising freight traffic volumes and the difficulties of obtaining sufficient track occupancy time to perform maintenance and rail replacement programs, there is an increasing need to obtain improved rail steel. It has been estimated that potential annual savings to Canadian Pacific alone of at least $2 million could be realized if rail life in curves could be doubled.

Recently completed studies on rail corrugations, which are one manifestation of the "new" wear phenomenon reveal that rail life is governed by a complex interrelationship between wheel/rail contact geometry, lubrication, surface fatigue endurance of rail steel and rail metallurgy.

The nature of the accelerated curve wear currently being experienced suggests that significant improvements in rail life might be attained by introducing rail with improved mechanical properties.

A review of the current state-of-the-art of rail metallurgy and techniques to improve mechanical properties of rail steels was initiated.

The results of the study are presented in this report. Data was obtained from laboratory testing and literature surveys and from numerous discussions with researchers working in this field, rail manufacturers and railway operating personnel.

Our efforts to explore the degree to which rail life might be extended by introducing steels with improved mechanical properties have led to the preparation of a specification for mechanical properties and a series of recommendations to achieve an improved rail steel.

INTRODUCTION

Railroad maintenance of way personnel have, in the last five years, encountered an unexpected increase in maintenance cost on lines with very heavy annual traffic densities. The causes for such increased costs are difficult to analyse as they result from many variables. Increased traffic density and heavy axle loads certainly have a most pronounced effect on the deterioration and life of the rail.

The basic mechanism of rail deterioration has qualitatively changed within this period from rail deterioration attributed predominantly to fretting wear to rail deterioration attributed to plastic flow and surface fatigue of the rail head material. (1, 2, 3, 4)* Previously rail life in curves could be predicted using AREA formulae (5). It is the opinion of the authors, that the basic physical mechanism of rail deterioration which the formulae reflects is that of fretting wear. However, on present high traffic density lines rail life in curves is controlled largely by surface fatigue defects such as spalling flaking, shelling, plastic flow of the rail head metal and formation of long wage-length corrugations.

A schematic illustration of two different modes of rail deterioration is given in Figure 1. It may be said with a high degree of certainty that the rail on lines with 20 MGT/annum or less are replaced primarily because of wear and abrasion (excluding rail failures), while rails on lines above 40 MGT/annum are replaced primarily due to surface fatigue deterioration. In the intermediate traffic density range (i.e. transition zone) there exists a wide region, between 20-40 MGT/annum, in which both abrasion and surface fatigue phenomena occur simultaneously. The 30 MGT/annum figure in the middle of the transition zone will be taken as the dividing point between the two modes of rail deterioration in curves.

---

* The numbers in parenthesis refers to the references at the end of this report.

This report is concerned with the development of high strength rails needed to provide longer life and greater reliability in curved territories with traffic density of 30 MGT/annum or greater. To increase rail life, the rail material must have increased resistance to surface fatigue, plastic flow and brittle fracture.

Plastic flow in the rail head is a function of the axle load, the geometry of the wheel and rail contact zone, and the rail strength characteristics (3). For a constant wheel and rail contact geometry, the load required to produce yield in the rail head is proportional to the cube of the material yield strength (6). Hence, increasing the material yield strength provides a very effective way of reducing the incidence of rail head plastic flow failures.

The resistance of rail material to surface fatigue is a function of many factors associated with the vertical and lateral forces, geometry of wheel and rail contact zone, lubrication (7) and microstructural properties (8) of rail material. Depending on the inter-relationship of the above mentioned factors, the resistance of steel to surface fatigue increases in proportion to the rail hardness raised to between the second and fourth power.

Hence the benefits associated with improved mechanical properties of rail material are self-evident.

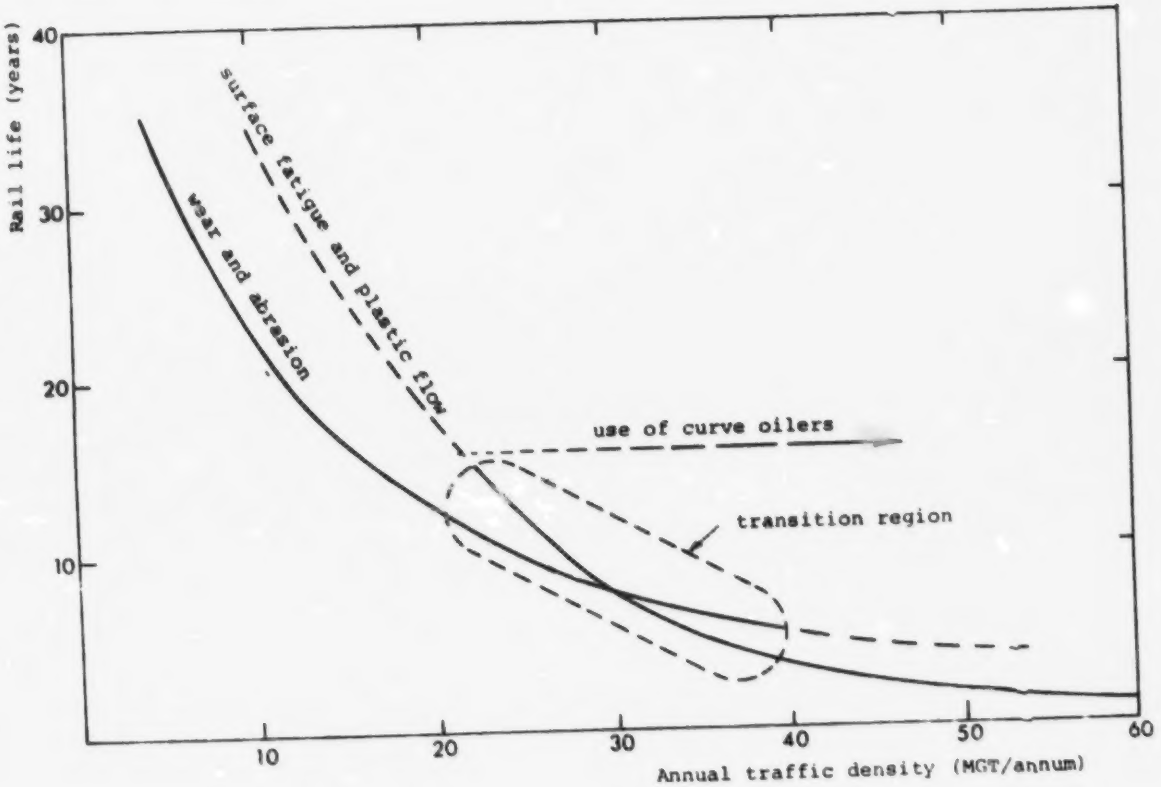

Figure 1: Rail life vs annual traffic density

between 20-40 MGT/annum, in which both abrasion and surface fatigue phenomena occur simultaneously. The 30 MGT/annum figure in the middle of the transition zone will be taken as the dividing point between the two modes of rail deterioration in curves.

This report is concerned with the development of high strength rails needed to provide longer life and greater reliability in curved territories with traffic density of 30 MGT/annum or greater. To increase rail life, the rail material must have increased resistance to surface fatigue, plastic flow and brittle fracture.

Plastic flow in the rail head is a function of the axle load, the geometry of the wheel and rail contact zone, and the rail strength characteristics.(3) For a constant wheel and rail contact geometry, the load required to produce yield in the rail head is proportional to the cube of the material yield strength (6). Hence, increasing the material yield strength provides a very effective way of reducing the incidence of rail head plastic flow failures.

The resistance of rail material to surface fatigue is a function of many factors associated with the vertical and lateral forces, geometry of wheel and rail contact zone, lubrication (7) and microstructural properties (8) of rail material. Depending on the inter-relationship of the above mentioned factors, the resistance of steel to surface fatigue increases in proportion to the rail hardness raised to between the second and fourth power.

Hence the benefits associated with improved mechanical properties of rail material are self-evident.

Type of rail	Carbon	Chromium	Proposed
Hardness range (BHN)	250 - 270	310 - 330	380 - 400
Replacement factor for 6 year period	3	1.715	1
1976 posted price for rail steel (dollars/ton)	300	390	480
Cost of rail for 195 track miles in 6 year period (millions of dollars)	40.8	30.2	21.8
Cost of labour to relay 195 miles of track (millions of dollars)	5.8	3.4	1.9
Total cost (material and labour)	46.6	33.6	23.7

Table 1: Material and labour cost of rail replacement.

It is beyond the scope of this technical study to accurately evaluate the full economic benefits of an improved rail, but for the purpose of illustration, the following order of magnitude analysis may be considered. In 1974 the annual traffic volume exceeded 30 MGT/annum on 394 miles of CP lines (9). The total curvature length on these lines is approximately 195 miles. The average rail life in these curves is approximately 2 years for carbon rail, 3.5 years for chromium rail and is forecast to be 6 years for a rail, the metallurgy of which is proposed in this report. The projected 6 year life is thought to be reasonable in view of the non-linear increase in rail life with respect to improved mechanical properties of rail.

The 1976 posted price of 132 RE rail is $300/ton for carbon rail $390/ton for chromium rail, and is estimated at $480/ton for the proposed rail. To relay 195 miles of track requires 45,300 tons of steel. The cost of rail steel and labour in a 6 year period at 1976 prices is presented in Table 1. The cost of labour to relay 1 mile of track is estimated at $10,000/mile.

It is shown in Table 1 that chromium rail presents a potential savings of 13 million dollars and the proposed rail will save 23 million dollars compared to plain carbon rail. Additional savings may be realized if the proposed rail is used for special track work such as switch points, frogs, diamond crossings and guard rails.

As traffic density increases in the latter half of this decade an increasingly greater percentage of total main line rail life will be governed by plastic flow and surface fatigue. The 1983 traffic forecast compiled by CPR indicates that the traffic density will in all probability exceed [illegible]0 MGT/annum on 2,880 miles of CP trackage. This means that premium rail will be needed on 580 miles of curved track requiring either 38,700 tons of chromium rail or 22,500 tons of newly developed rail annually.

Hence, increasing traffic densities will reinforce the need for improved rail steel. The potential savings are a significant incentive to advance a metallurgical research program.

The need for improved rail was recognized in the 1940's, when the first "wear resistant" rails were introduced. Typical examples of such rails are the Hi-Si and Hi-Mn rail. It was not until the 60's that "special" types of rail were available for use in areas of high traffic density. A typical requirement for these "special" rails is a tensile strength of 155-175,000 psi (10,11). The best performing rail in this category, conditionally available on North American market, is Bethlehem Steel's fully heat-treated rail. U.S. Steel's Curvemaster rail also falls into this category. The mechanical properties, microstructure and service performance of these rails and three alloy rails, Algoma Steel chromium rail, Sydney Steel wear resistant rail and a Cr-Mo rail developed by the Climax Molybdenum Company are reviewed in the following chapter. On the basis of the analysis carried out in Chapter II, the mechanical properties of a better rail material are proposed.

The ultimate tensile strength of the proposed rail is 200,000 psi with a corresponding hardness of 400 BHN. It is interesting to note that such a rail is produced in the USSR for use on lines with very high traffic densities (12). Unfortunately, the Russian literature does not specify the metallurgical nature of this rail.

Chapter III deals with the fundamental aspects of alloying and heat treatment and the ways in which these practices can be used to enhance the mechanical properties of rail steels. On the basis of the material provided in Chapter III, Chapter IV contains recommendations on how to achieve 400 BHN hardness in the rail head of the proposed high strength rail. For future use on high traffic density lines the authors foresee a need for a rail with the hardness of 450 BHN. Development of such a rail will require extensive experimental work by the rail producers and consumers.

II. REVIEW OF COMMERCIALLY PRODUCED RAIL STEELS

2.1 Mechanical Properties and Microstructure

There are at present six basic commercially produced rail steels in North America. Due to the high demand for premium rails and limited production capacities, not all of these are available but they must none the less be discussed from the viewpoint of future production of rail steels in Canada. The chemical composition of these rails is given in Table 2, and the mechanical properties in Table 3. The basic rail is the AREA Control Cooled Carbon Rail (C) which accounts for the bulk of rail production in North America. The next three rails, Chromium (Cr), Manganese-Chromium-Vanadium (Mn-Cr-V), and the Chromium-Molybdenum (Cr-Mo) are alloy rails in which the mechanical properties have been enhanced by the addition of varying amounts of alloying elements. The average hardness in the alloy rail heads has been increased from 250 BHN in the C rail to anywhere from 310 to 360 BHN. Except for the Cr rail, the fracture toughness is significantly higher than that of C rail with the result that these rails can withstand larger size crack defects without fracturing in a brittle manner. Because the fracture toughness of Cr rail is lower than that of C rail, its defect tolerance is lower, an undesirable property. The last two rails, Fully Heat-Treated (H.T.) and Induction Hardened (I.H.) rail are made by heat-treating carbon rail. The techniques employed in the heat-treating processes will be discussed in Chapter III, but at this point it is obvious that heat-treatment produces a very substantial improvement in the mechanical properties. The H.T. rail has the highest

	C	Mn	P	S	Si	Cr	Mo	V
AREA Control Cooled Carbon	.69-.82	.7-1.0	.040 max.	.055 max.	.1-.25	-	-	-
Chromium (Algoma Canada)	.65-.7	.45-.55	.040 max.	.055 max.	.1-.25	1.2-1.3	-	-
Manganeese-Chromium -Vanadium (ladle analysis) (Sydney Steel Corp.)	.62	1.61	.010	.027	.234	.27	-	.12
Chromium-Molybdenum (Climax Corp.)	.70-.80	.80-1.0	.030 max.	.030 max.	.25 max.	.7-.9	.19-23	-
Fully Heat treated (Bethlehem Steel)	Same as AREA Carbon Rail							
Induction Hardened Head (USS-"curvemaster")	Same as AREA Carbon Rail							

Table 2: Chemical composition of commercial rail steels.

	.2% yield strength (ksi)	ultimate tensile strength (ksi)	elongation %	reduction area %	hardness BHN	fracture toughness K_{ID} at 75°F (ksi)$\sqrt{\text{inch}}$	weldability-carbon equivalent
AREA Control Cooled Carbon	66-88	100-138	9-20	15	235-260	26	.99
Chromium (Algoma Canada)	100	160	12	15	295-325	18	1.05
Manganeese-Chromium -Vanadium (Sydney Steel Corp.)	95	155	12	20	250-310	30	.97
Chromium-Molybdenum (Climax Corp.)	109-125	172-184	6-11	8-25	340-360	33	1.22
Fully Heat-treated (Bethlehem Steel)	114	172	13	35	315-370	36	.99
Induction Hardened Head (USS-"Curvemaster")	115	173	13	40	370-395	34	.99

Table 3: Mechanical properties and weldability of commercial rail steels.

fracture toughness of all the rails being considered. On the other hand, the I.H. rail has a high fracture toughness in the head but service experience on CP lines indicates that the fracture toughness in the transition zone is inadequate.

Weldability of rail steels is an important consideration. A quantitative assessment of weldability can be found from the carbon equivalent of the alloy. The formula for carbon equivalent is:

$$\text{C.E.} = \%\ \text{C} + \frac{\%\ \text{Mn}}{6} + \frac{\%\ \text{Cr}}{5} + \frac{\%\ \text{Mo}}{4} + \frac{\%\ \text{V}}{5}$$

and shows, for example, that chromium reduces the weldability of an alloy only 1/5 as much as the weight percent of carbon. As is expected, the alloy rail steels have a higher carbon equivalent, and therefore, poorer weldability than carbon rail, (and also poorer weldability than the heat-treated rails). The matter of weldability is only one of degree; the carbon rail has poor weldability while the alloy rails have poorer weldability and therefore may, depending on the carbon equivalent, require both pre-heating and post-heating to be successfully joined or repaired.

The microstructures of the six rails were examined in two ways. Firstly, cross-sectional slices were cut from the five sample rails, then polished and macro-etched. Unfortunately we were unable to obtain a sample of the Cr-Mo rail. A Vickers hardness survey was taken on each section and the results are shown directly on the macrographs in Figures 2 and 7. Because the Cr-Mo rail sample was not

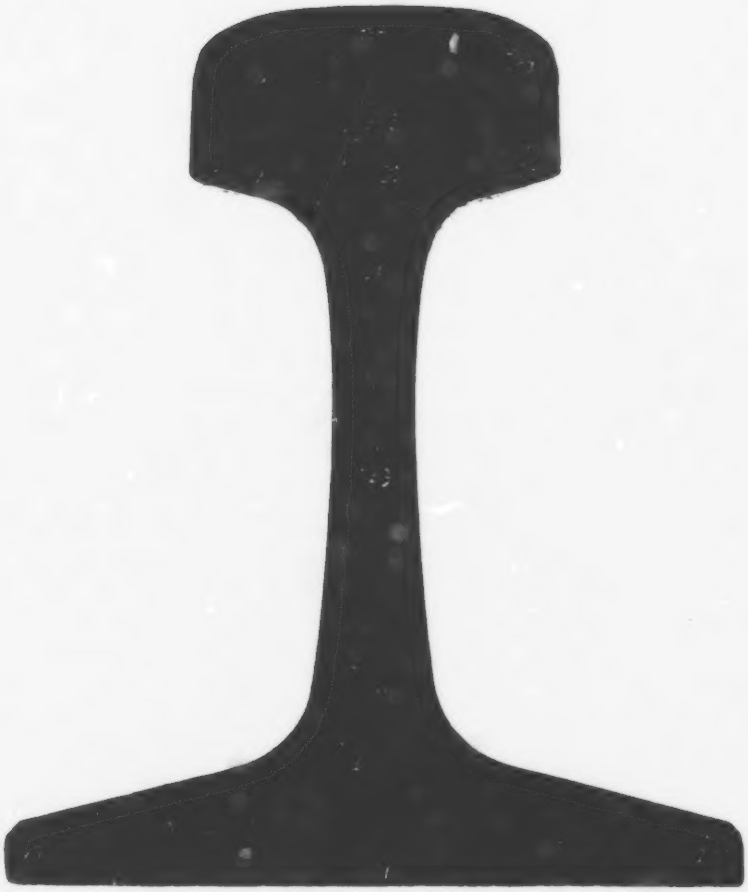

Figure 2: Macrograph of AREA Control Cooled Carbon Rail.

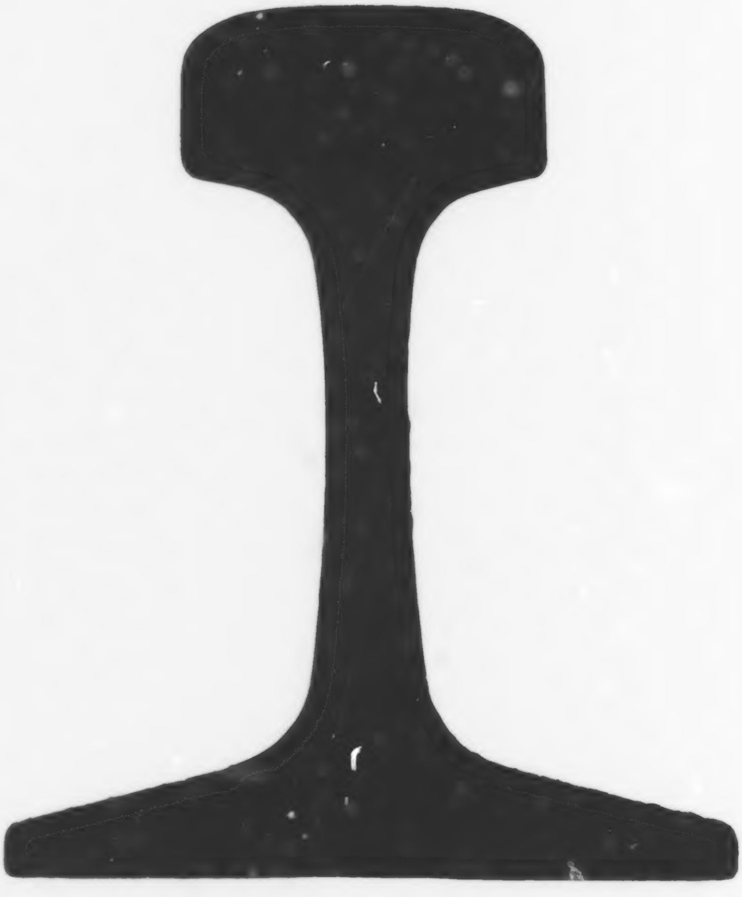

Figure 3: Macrograph of Manganese-Chromium-Vanadium Rail.

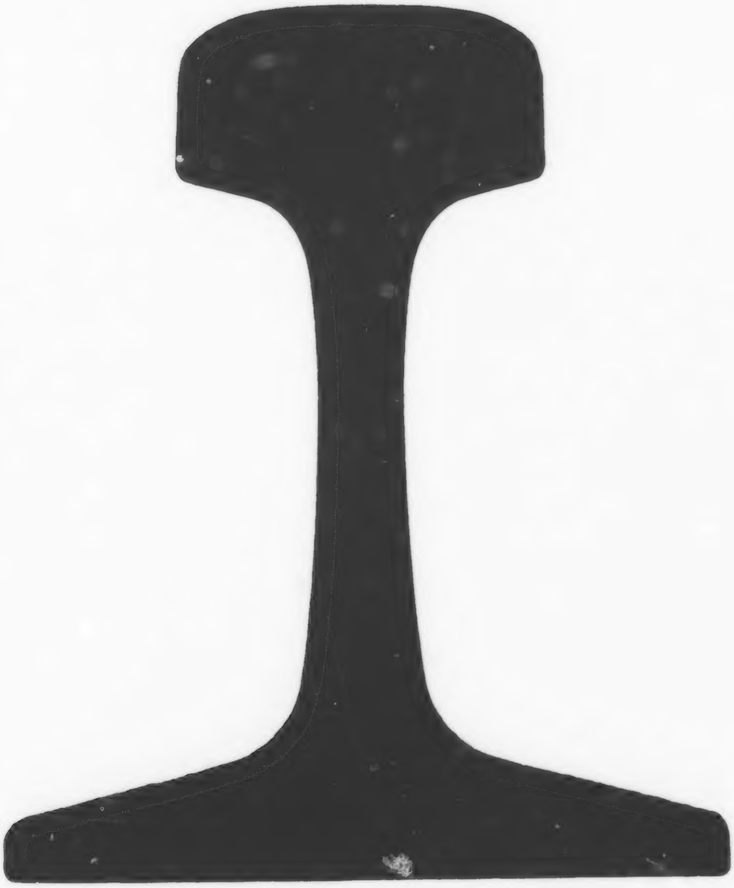

Figure 4: Macrograph of Chromium Rail.

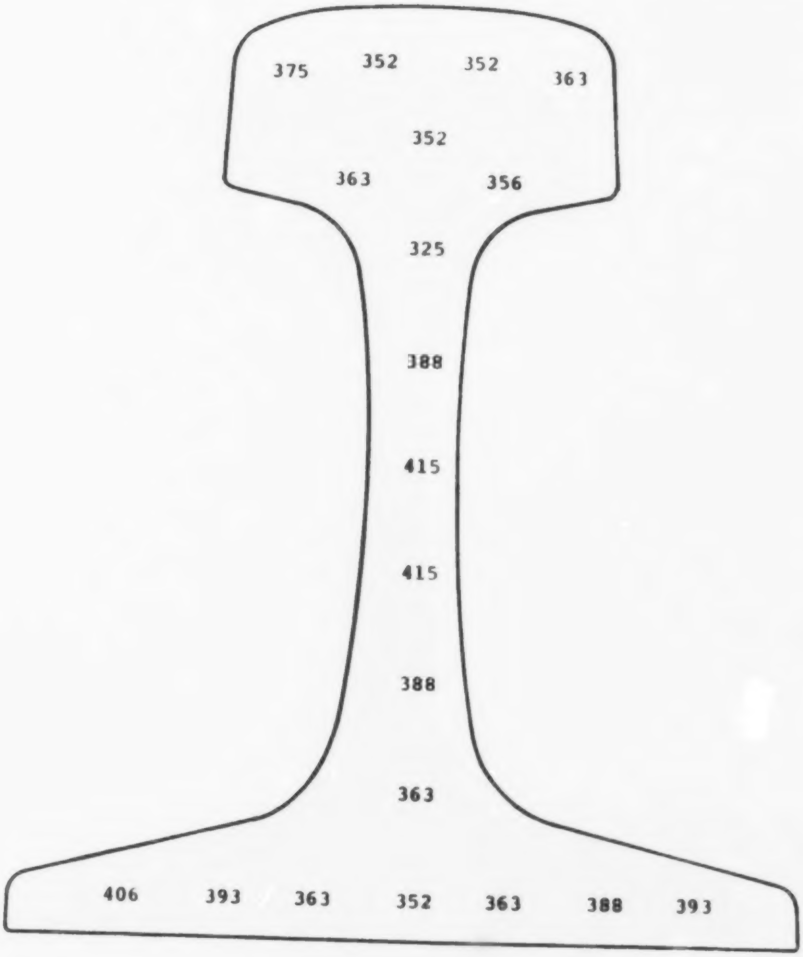
375
352
352
363
352
363
356
325
388
415
415
388
363
406
393
363
352
363
388
393

Figure 5: Brinell hardness survey of Chromium - Molybdenum Rail.

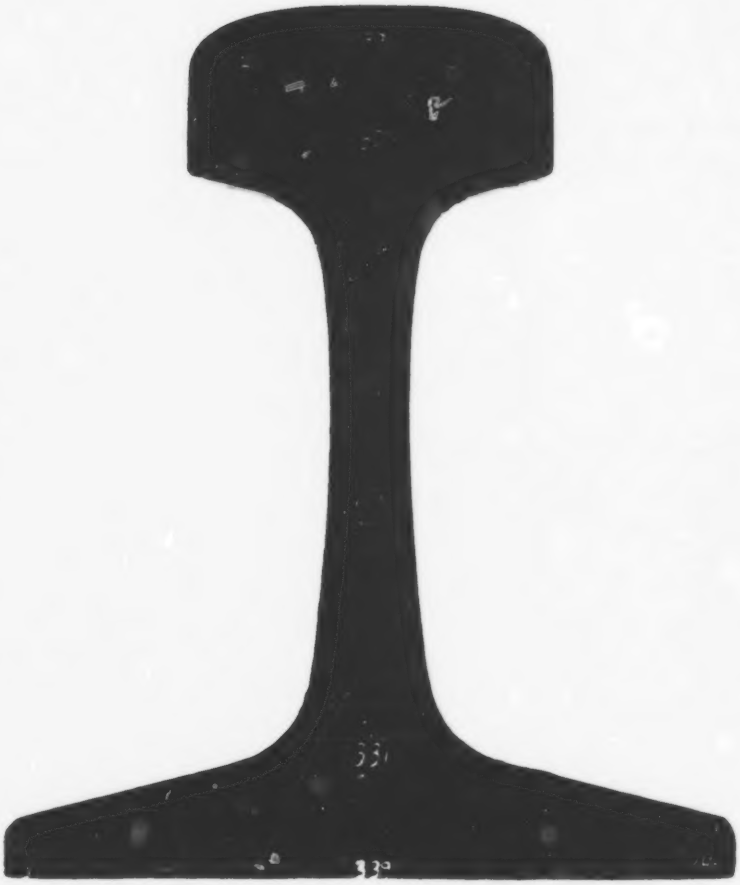

Figure 6: Macrograph of Fully Heat-Treated Rail.

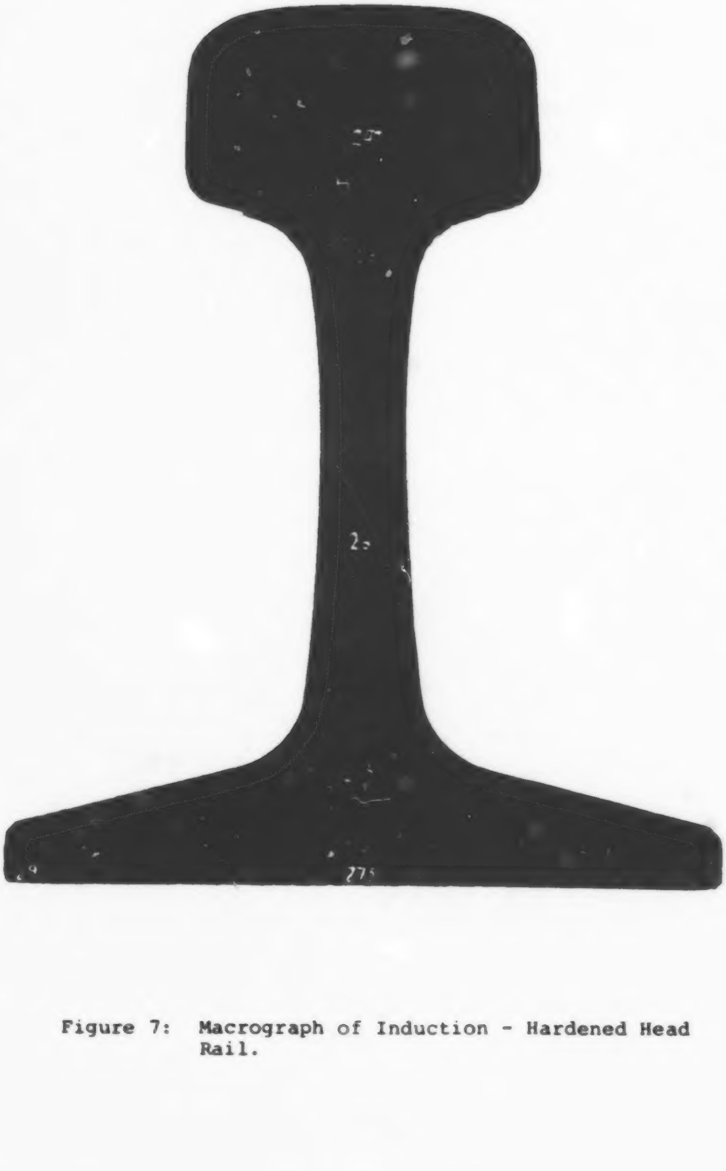

Figure 7: Macrograph of Induction - Hardened Head Rail.

available, Figure 5 shows only the hardness values. All hardness figures can be converted to BHN values by multiplying by 0.95.

Small samples were cut from the heads of the five rail sections and prepared for micro-examination by polishing and etching. Also a micrograph of the Cr-Mo rail alloy was obtained from the Climax Molybdenum Company of Michigan. The six micrographs are shown in Figures 8 to 13.

Examination of Figures 2 to 7 reveals striking differences in the macro-structure of the rails. The C rail is relatively coarse-grained compared to the darker appearing fine-grained structure of the H.T. rail. The Mn-Cr-V rail has a finer grain size than the C rail, and the Cr rail slightly finer yet. The Cr-Mo rail (not shown) has a grain size almost as fine as that of the H.T. rail. The I.H. rail is perhaps the most striking specimen because of the large difference in grain size between the head and the unheat-treated base and web.

The differences in grain size of the rail steels is also evident in the micrographs, Figures 8 to 13. Comparing first the C rail and the H.T. Rail one can see the fine-grained character and the smaller interlamellae spacing in the H.T. steel. These two factors account for the higher hardness, fracture toughness, etc. found in the H.T. rail. The grain size in the head of the I.H. rail is somewhat greater than in the H.T. rail but the pearlite lamellae spacing is approximately the same. In fact the interlamellar spacing in the pearlite of the H.T. and I.H. rails is so fine

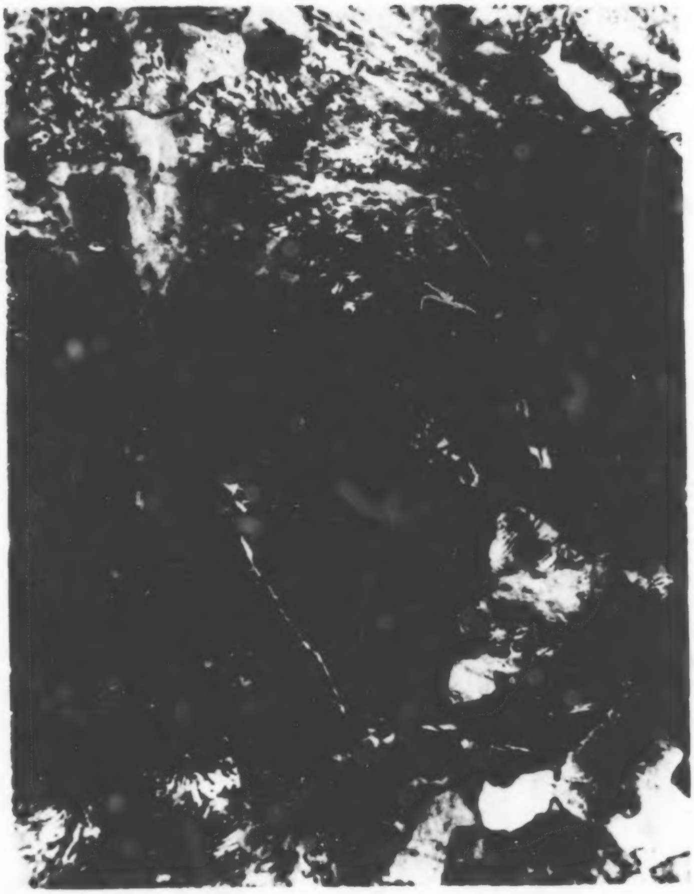

Figure 8: Micrograph of AREA Control Cooled Carbon Rail.

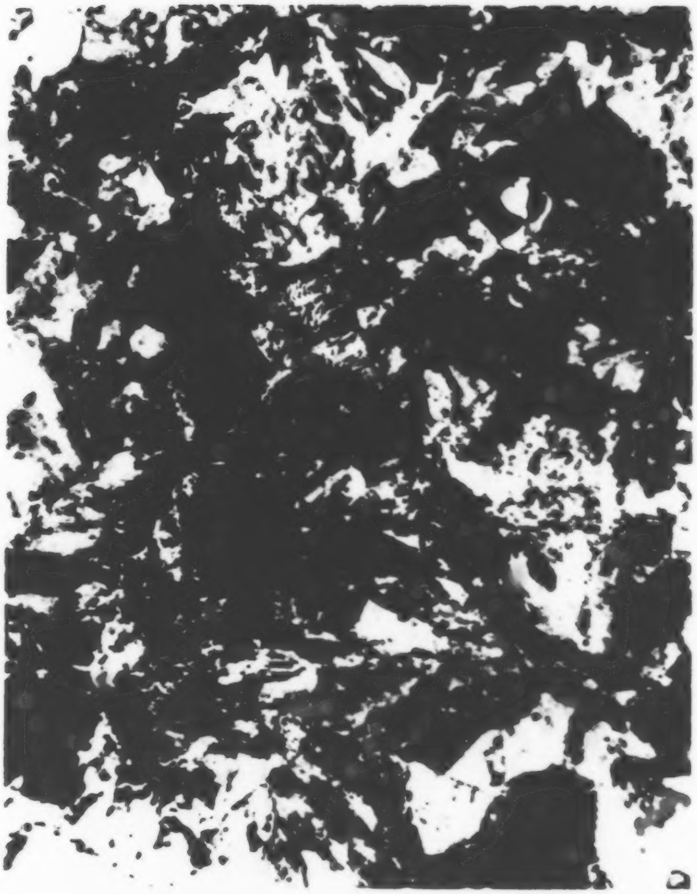

Figure 9: Micrograph of Manganese-Chromium-Vanadium Rail.

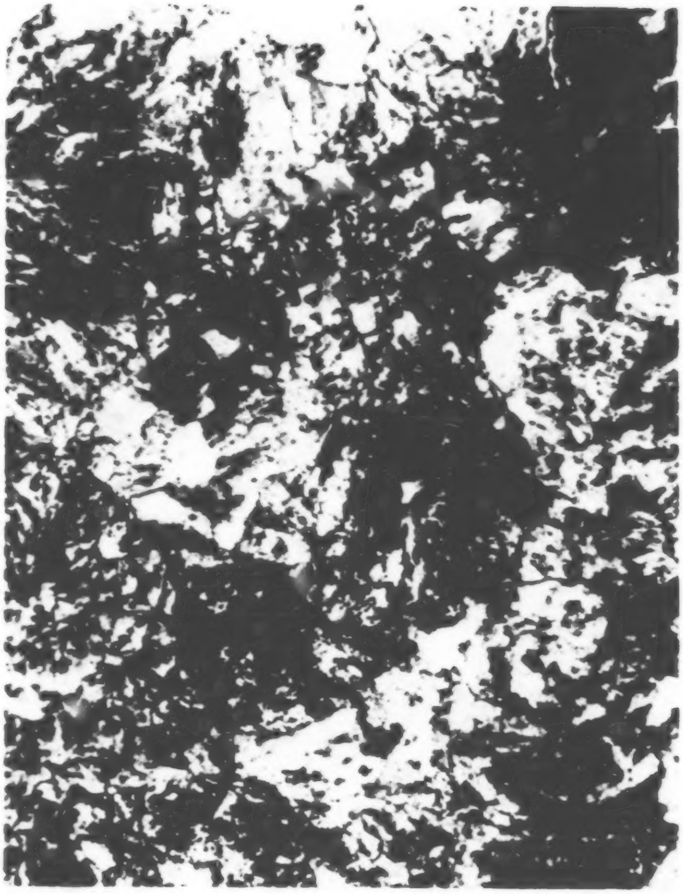

Figure 10: Micrograph of Chromium Rail.

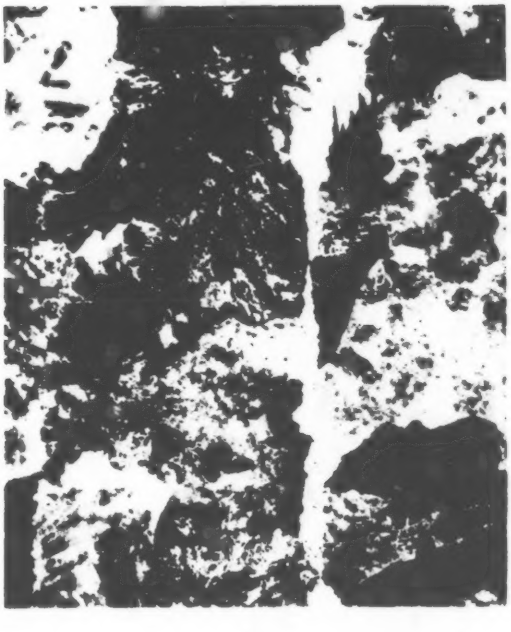

Figure 11: Micrograph of Chromium - Molybdenum Rail.

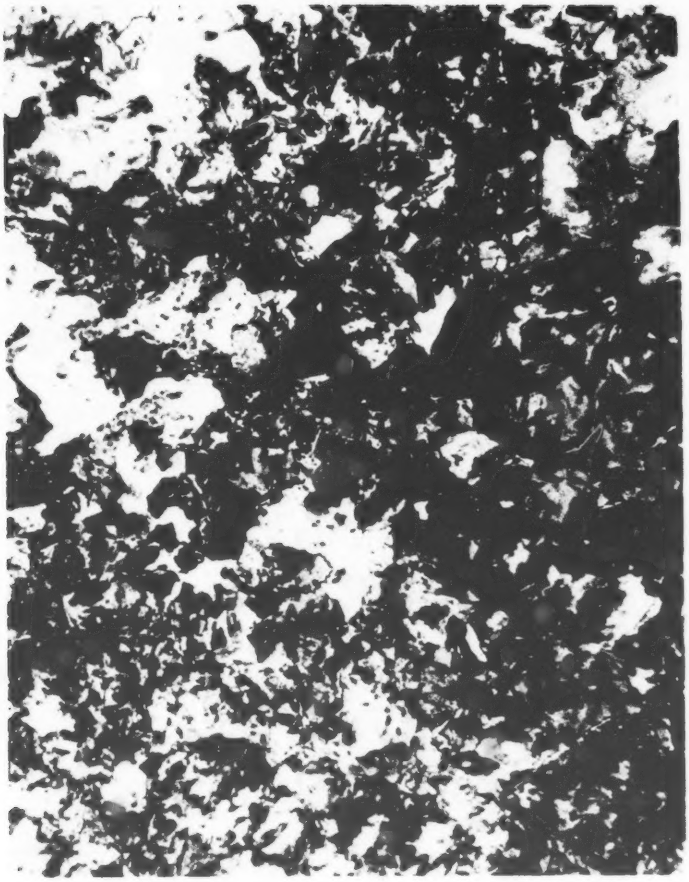

Figure 12: Micrograph of Fully Heat-Treated Rail.

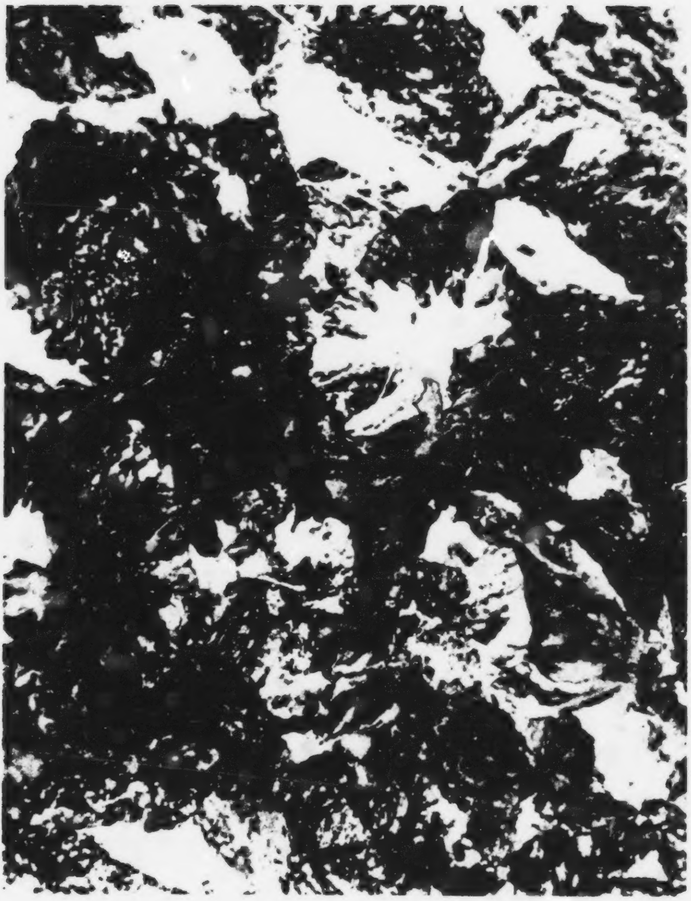

Figure 13: Micrograph of Induction - Hardened Head Rail.

that it cannot be resolved at this magnification. As mentioned previously, the three alloy steels have progressively finer grain sizes. This is shown in Figures 9 to 11. Also, the pearlite lamellae spacing decreases in the same order. In these steels, then, the effect of the alloying elements is to refine the grain size and the pearlite interlamellar spacing. In addition, the chemical effects of solid solution hardening and carbide formation improve the mechanical properties of the steel. These effects will be discussed in greater detail in Chapter III.

2.2 Proposal for Mechanical Properties of Future Rail Materials

The previous section has presented and discussed the mechanical and metallurgical properties of the various types of commercially produced rails. The question is, are these materials adequate for today's needs and those of the future. The premium rails available today represent a major step forward in terms of rail life, but there is a need to make even further progress towards new, higher strength rail materials. At present, the best materials available have hardnesses in the range of 315 to 395 BHN. However, in view of the potential savings, there is a strong case for improving the mechanical properties even more, and the major recommendation of this report is to produce pearlite rails with the following properties:

Ultimate Tensile Strength (KSI)	190-210
0.2% Yield Strength (KSI)	120-130
% Elongation (2 in.)	10-12
Reduction of Area - %	20-25
Hardness (BHN)	380-420
Fracture Toughness, K_{ID} (KSI $\sqrt{\text{in.}}$)	30-35

These properties are not significantly higher than those of the presently available better rail materials and, in fact, the lower end of the range is probably attainable by making minor modifications to the chemistry of the Cr-Mo alloy rail shown in Table 3. The desirable microstructure for this rail is fine grained pearlite with very small lamellae spacing.

The ultimate goal for higher mechanical properties is to produce a rail steel with an average hardness of 450 BHN. In general when the hardness of an alloy is increased, the fracture toughness decreases. Such an alloy would therefore require modification of the chemical composition to maintain an adequate level of fracture toughness. The hardness level of 450 BHN is probably not attainable with pearlitic microstructure and therefore either bainitic or martensitic microstructures will be required. It is generally recognized that for a given alloy, the microstructure with the highest fracture toughness is tempered martensite. Therefore, the use of tempered martensite might be the best choice for the future high hardness rail steels.

The use of high strength rails will require improvements in the techniques and equipment used for rail straightening drilling, cutting, bending, and welding. Technology currently exist to cope with these requirements, but it will have to be introduced to the rail maintenance people at the same time as new rail materials become available.

III. METHODS OF IMPROVING MECHANICAL PROPERTIES OF RAIL STEELS

AREA Standard Carbon Rail has a carbon content range of 0.69 to 0.82 weight percent. For the purposes of this discussion we shall deal with steel of eutectoid composition (0.8% C), as shown on the iron-cementite phase diagram in Figure 14. There are two methods of improving the mechanical properties of steel. These are heat-treatment and alloying and they can be used individually or together.

3.1 Heat Treatment

All heat-treating operations consist of subjecting a metal to a definite time-temperature cycle to produce a desired microstructure. The first stage of heat-treatment is the heating stage, in which the steel is transformed into austenite.* In the case of a eutectoid steel this will occur above a temperature of 1330°F, (see Figure 14).

The next stage of heat-treating is holding at temperature in the austenite range. A typical holding temperature for a eutectoid steel is 1550°F. The steel must be held in the austenite range sufficiently long to ensure complete uniformity of temperature and adequate chemical homogeneity.

The third stage of heat-treating is cooling. In this stage the metal is cooled, usually in a quenching medium, at a rate which will produce a particular microstructure. The actual cooling rate is determined by the mass of the metal

---

* Austensite is a high temperature phase of steel.

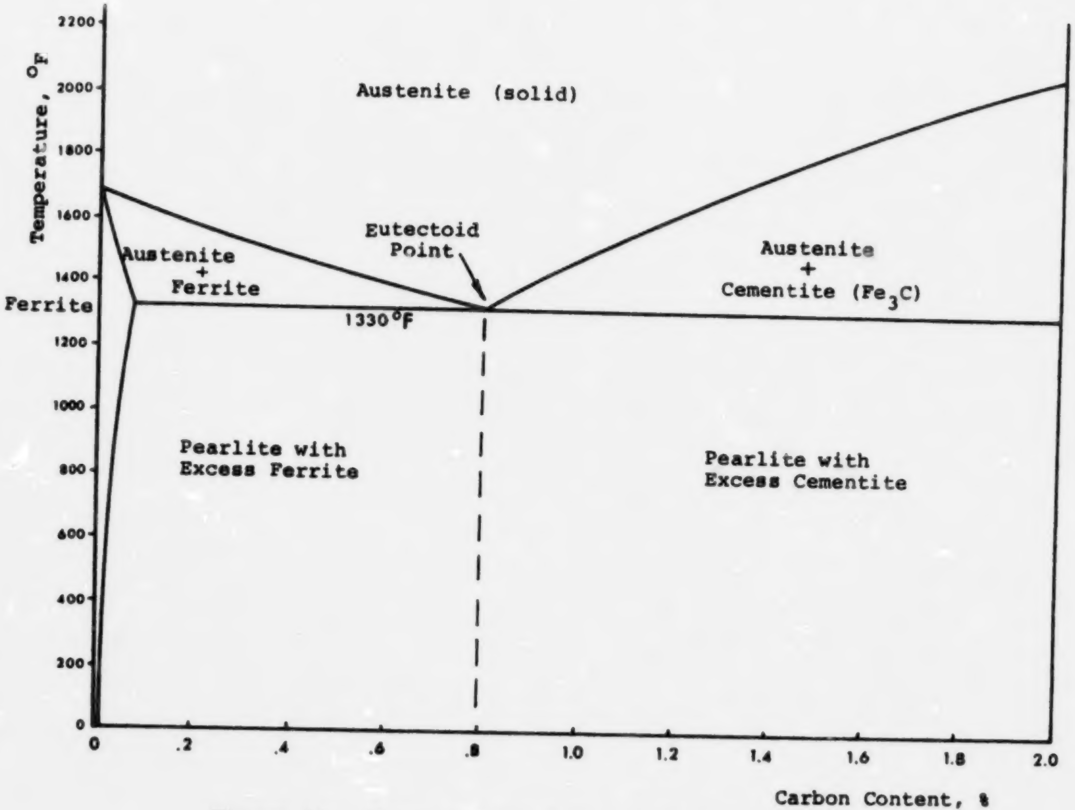
Temperature, °F
2200
2000
1800
1600
1400
1200
1000
800
600
400
200
0
Austenite (solid)
Austenite + Ferrite
Ferrite
Eutectoid Point
1330°F
Austenite + Cementite (Fe3C)
Pearlite with Excess Ferrite
Pearlite with Excess Cementite
0
.2
.4
.6
.8
1.0
1.2
1.4
1.6
1.8
2.0
Carbon Content, %

Figure 14: Phase diagram for carbon steels.

being cooled and the quenching medium employed. The effect of cooling rate on the microstructure of small samples of eutectoid steel can best be demonstrated by the continuous cooling curve diagram shown in Figure 15. The vertical axis is temperature and the horizontal axis time. Curves A to E represent successively slower rates of cooling, as would be obtained by cooling in iced brine (A), water (B), oil (C), air (D), and furance (F), respectively. The two solid curved lines, P_s and P_f, represent the start and the finish of the pearlite reaction while the two lower dashed straight lines, M_s and M_f, represent the start and the finish of the martensite transformation. Pearlite is a relatively soft two phase aggregate having a lamellar structure as shown in Figure 16. Martensite is a hard single phase structure with a typical feather-like appearance, as shown in Figure 17.

The slowest cooling rate is that according to curve E. In this case, the austenite starts to form pearlite at temperature t_1, and completes transformation at t_2. The final product is coarse pearlite with relatively low hardness. When cooled according to curve D, pearlite formation begins at t_3 and is completed at t_4; the final product is fine pearlite and its hardness is greater than the steel cooled according to curve E. When cooled according to curve C, transformation begins at t_5 and is only partially complete when t_6 is reached; the product of this partial transformation is very fine pearlite. The remainder of the austenite does not decompose until the M_s temperature is reached, when it begins to transform to martensite, completing this transformation at the M_f temperature. The final structure is then a mixture of

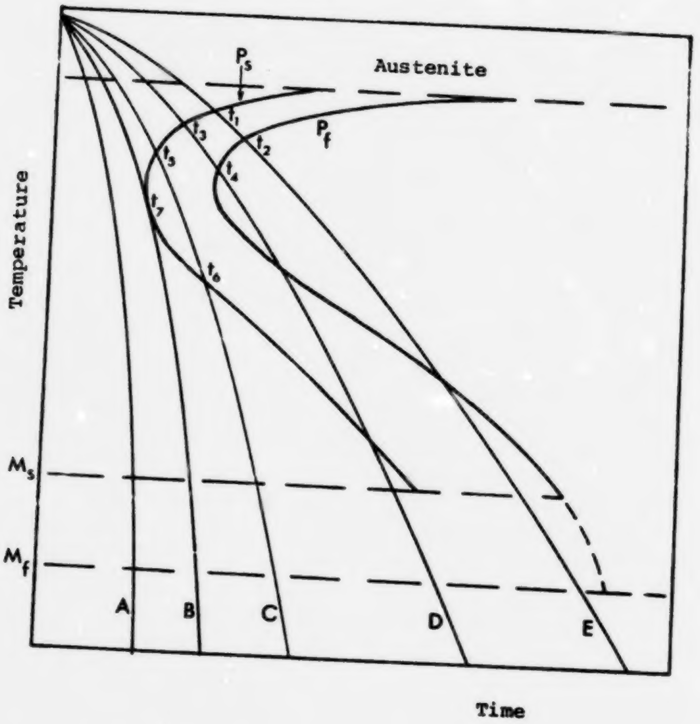

P_s
Austenite
t_1
t_2
t_3
t_4
t_5
t_6
t_7
P_f
Temperature
M_s
M_f
A
B
C
D
E
Time

Figure 15: Continuous cooling curve diagram of an eutectoid steel.

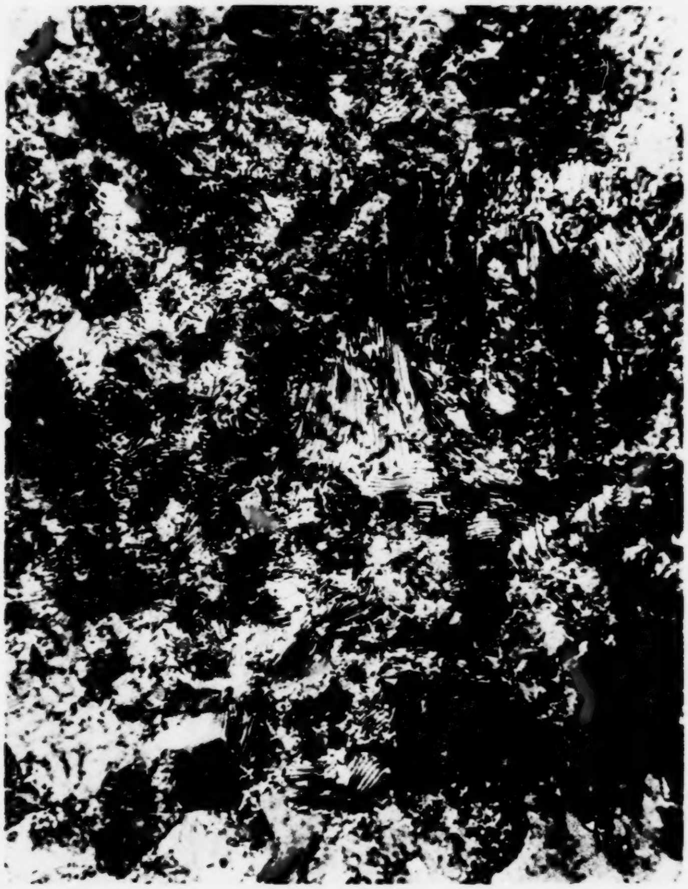

Figure 16: Typical Example of Pearlite.

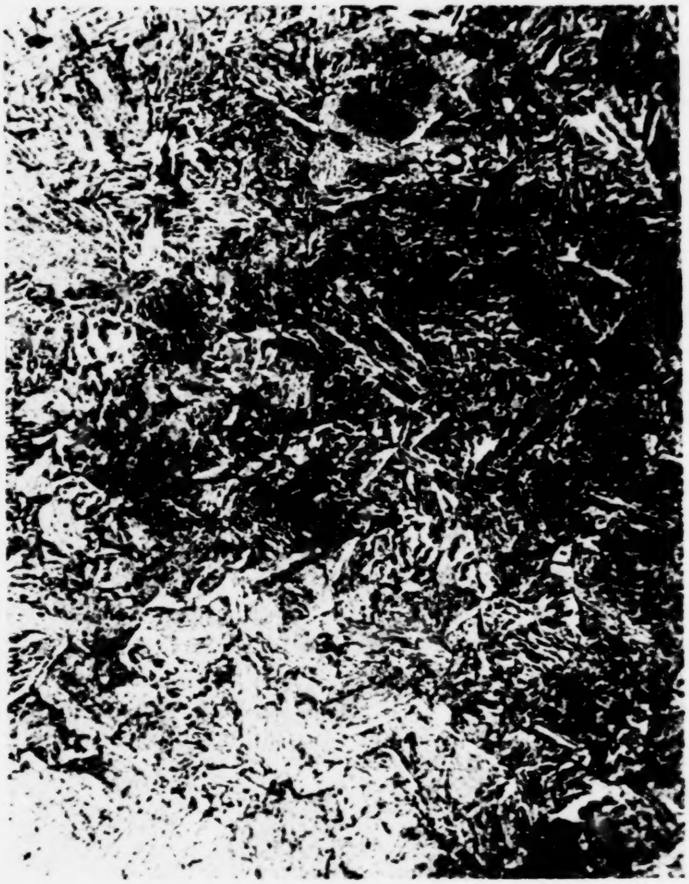

Figure 17: Typical Example of Martensite.

fine pearlite and martensite with a higher hardness than was obtained with the steel cooled according to curve D. The rate of cooling represented by curve B is just sufficient to intersect the nose of the P_s curve. Consequently only a minute amount of the austenite decomposes into fine pearlite at temperature t_7; the remainder of the austenite is unchanged until the martensite transformation range is reached. If the steel is cooled at a slightly faster rate, so that no transformation takes place at the nose of the pearlite formation curve, the steel is completely transformed to martensite and is completely hardened ($\approx$ 750 BHN). This particular rate is termed the critical cooling rate and is the slowest rate at which the steel can be cooled and yet be completely hardened. In fact, a sample cooled on curve A is also completely martensitic but no harder than the sample cooled at the critical cooling rate.

How does the continuous cooling curve diagram relate to rail production? In the case of standard carbon rail, hot rolling starts at a metal temperature of approximately 2000°F and is completed at a temperature of about 1600°F. The rails are then air cooled to 1000°F on the cooling bed. By this time the steel is completely transformed to pearlite, and the following controlled cooling to 500°F has almost no effect on the microstructure. The microstructure is relatively coarse pearlite with an average hardness of 260 BHN.

Bethlehem fully heat-treated rail is made from standard carbon rail as follows: the material is austenetized at 1550°F, oil quenched for 15 minutes, and tempered at 750°F. The cooling rate of the rail during the oil quench is intermediate between curves C and D in Figure 15, and the resulting microstructure is fully pearlitic. Because this cooling rate is considerably faster than that of the air cooled hot rolled rails, the lamellar spacing in the pearlite is extremely small, and the hardness substantially higher (360 BHN). The purpose of the tempering operation, which is carried out immediately after the oil quench is to relieve internal stresses as well as slightly reduce the hardness and improve the fracture toughness of the steel.

U.S. Steel also produce a heat-treated plain carbon rail, ("Curvemaster"). Their technique is to harden only the head of the rail by induction hardening. In this process, a high-frequency current is passed through a coil enclosing the head of the rail, the surface of which is heated by electromagnetic induction. The depth to which the heated zone extends depends on the frequency of the current (the lower frequencies giving greater depths) and on the duration of the heating cycle. Selective heating (and therefore hardening) is accomplished by suitable design of the induction coils. At the end of the heating cycle most of the head of the rail has been transformed into austenite, and the steel is quenched by air jets passing through the induction coils. Precise methods for controlling the operation, that is, rate of energy input, duration of heating, and rate of cooling, are necessary. The cooling rate of the rail head is very close to that obtained by the oil quenching technique used by Bethlehem Steel and the microstructure is fine pearlite with an average hardness of 370 BHN.

Hardness greater than 360 BHN can be produced by heat-treating standard carbon rail but as the hardness increases the fracture toughness decreases. Also, the higher hardness values can only be obtained by faster quenching rates which, for the complex shape of a rail, may produce unacceptable distortion. If this is the case, the only alternative is to increase the alloy content of the steel to produce higher hardness with the same heat-treatment. Before discussing this possibility, we shall first consider what can be accomplished by alloying alone.

3.2 Alloying

The use of alloying is another method of improving the mechanical properties of standard carbon rail. When alloying elements are added to steel, both solid-solution and compound formation usually occur. Solid solution is the dissolution of the alloying element atoms within the iron atomic matrix, whereas compound formation is the formation of metal carbides within the continuous ferrite phase. Qualitative information on the tendency of the individual alloying elements in steel to form a solid solution or a carbide phase is given in Table 4(13).A given alloying element (manganese, for example) will typically form both a solid-solution and a carbide. The position of the X in Table 4 with respect to the lines representing (complete) solid solution or carbide formation roughly denotes the proportion of the alloying element that enters each of these phases. The X for manganese indicates that about three-quarters of the manganese in a typical steel is in solid solution in the ferrite, while the remaining one-quarter is in the carbide phase. A number of

Alloying Element	Tends to Form	
	Solid Solution	Carbide
Silicon	X	
Aluminum	X	
Nickel	X	
Cobalt	X	
Manganese	X	
Chromium	X	
Molybdenum		X
Tungsten		X
Vanadium		X
Niobium		X
Titanium		X

Table 4: Distribution of alloying elements in steels.

Alloying Element	Approximate increase in yield strength of ferrite per 1% alloying element, ksi
Silicon	16
Manganese	15
Nickel	12
Titanium	10
Aluminum	6
Molybdenum	4
Tungsten	3
Vanadium	3
Cobalt	3
Chromium	2

Table 5: Effect of alloying elements in strengthening ferrite.

elements, such as silicon, dissolve entirely in the solid solution. Others, like titanium, are almost completely combined in carbide phases.

Each alloying element in steel produces specific effects. However, a number of general properties are associated with the formation of any carbide phase or of any solid solution. Since the carbide particles are hard, they increase wear resistance, decrease machinability, and slightly increase the hardness of the alloy. Some hard carbides may act as microscopic stress raisers under conditions of surface fatigue. On the other hand, when an alloying element is present in solid solution, it actively influences most of the properties of the steel. Not only does it appreciably increase hardness and strength, as shown in Table 5, but it also affects corrosion resistance, electrical properties, and that most important quality, hardenability.

The term hardenability normally refers to the ability of an alloy to be transformed into martensite upon being cooled from the austenitic range. A steel with good hardenability will, under a given cooling rate, form martensite at a greater depth from the surface than a steel with poor hardenability. In the case of pearlitic rail steels, hardenability refers specifically to pearlite hardenability. That is, the ability of an alloy to transform to a desired pearlitic microstructure at a given depth when cooled from the austenitic range. The pearlite hardenability for the common alloying elements is shown in Figure 18(14). It can be seen that molybdenum shows the greatest pearlite hardenability effect. Although the effect of vanadium is small and goes through a maximum at a low alloy content, it has the next greatest effect. Chromium is next, then manganese, then silicon, and then nickel. Using information of this type it is possible to produce experimental alloys with a desired microstructure and mechanical properties.

The three commercially available alloy rails were discussed in Chapter II. These rails have significantly better mechanical properties than carbon rail because of the effects of the alloying elements. The practical hardness limit for alloy rail steel is probably 420-430 BHN, but this can only be determined accurately by a metallurgical investigation.

So far, we have discussed the possibility of either heat-treating standard carbon rails or adding alloying elements. Both routes are being followed in today's commercial rail production. A third route is to combine the two methods to produce heat-treated alloy rails.

3.3 Heat-Treating plus Alloying

The fully heat-treated rail made by Bethlehem Steel may represent the optimum hardness that can be obtained from plain carbon steel. If this is the case, then in order to produce rails in the hardness range 400 - 450 BHN it may be necessary to resort to both alloying and heat-treating. This will involve making the appropriate alloy addition to the carbon rail chemistry to produce a material which upon quenching and tempering will produce the desired microstructure and mechanical properties. Development of such an alloy will require extensive laboratory work with a variety of alloys and heat treatments as well as extensive assessment of the mechanical properties so produced. It is probable that the microstructure required to produce the higher hardnesses will be tempered martensite rather than pearlite, but this can only be determined by experimental studies.

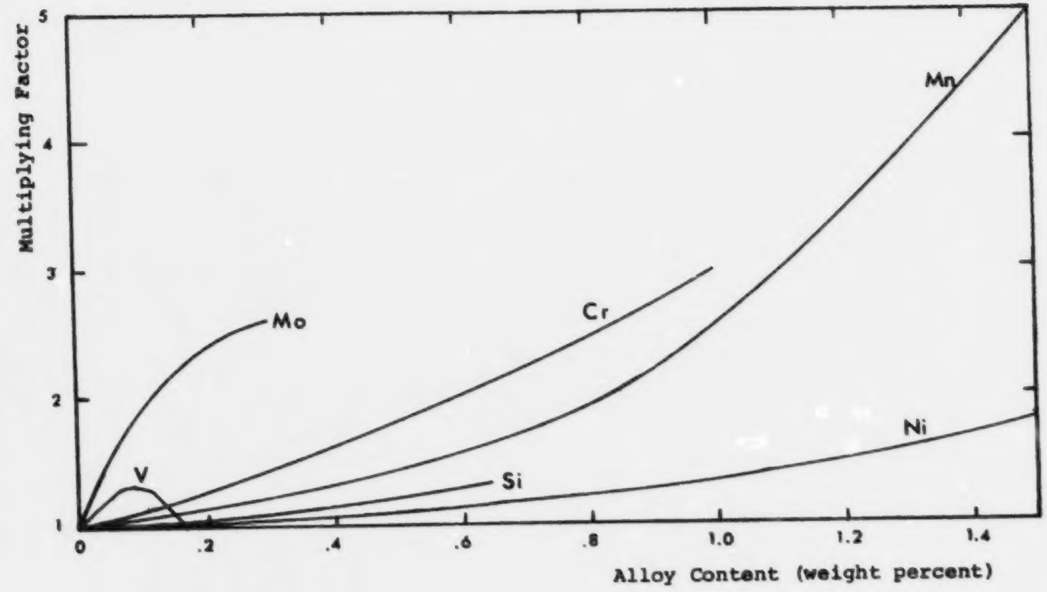

Figure 18: Pearlite - hardenability factors for several alloying elements.

IV. RECOMMENDATIONS OF RAIL METALLURGY

The introduction presented the arguments in favour of high strength rail steels. As the hardness and yield strength of rails increase, so do the savings on track maintenance and rail replacement. It is therefore desirable to be able to obtain rails with hardnesses above the 360 BHN range.

The commercially available rails with mechanical properties in the 360 BHN range are the Fully Heat-Treated rail, the Induction-Hardened rail, and the Chromium-Molybdenum rail. These all have approximately the same hardness (360 BHN) and the same mechanical properties. The Fully Heat-Treated rail is presently unavailable due to the production limitations of Bethlehem Steel's heat-treating facilities. The Induction-Hardneed rail is, in our opinion, prone to longitudinal fractures similar to shelling in the railhead and therefore not suitable for service on our lines. The chromium-molybdenum alloy rail, although not presently produced in Canada, can be manufactured following procedures commonly used for the production of standard AREA carbon rail. This alloy rail was developed specifically because of the lack of facilities for the production of heat-treated rail. The Cr-Mo rail does have a slightly lower fracture toughness than the H.T. rail, but is still tougher than C rail. The ductolity of Cr-Mo rail, although lower than that of the H.T. rail, is comparable to that of C rail and therefore adequate.

The recommendations of this report may be summarized as follows:

1. The fully heat-treated rail steel has the best mechanical properties. For this reason, we recommend that a study be made to establish what type of heat-treating process will best meet the needs of rail producers and their customers.

2. The alloying route offers the best immediate solution to the need for higher strength rails. We therefore recommend that the Cr-Mo rail in its maximum hardness range be produced in Canada.

   Initial evaluation of this rail will require the production and laying of a few 100 ton heats of the rail in a region of high traffic density. Prior to the laying of this rail, samples from each heat would be studied in the laboratory to confirm that the mechanical properties of the rail meet those expected of this alloy.

3. We also recommend that the alloying route be explored as a mean to produce rail with a hardness range of 390-410 BHN. This can be done in a relatively short period of time at minimal cost.

4. The ever growing traffic density will require the development of a rail with an average hardness of 450 BHN. We therefore recommend that further research be undertaken to develop this rail. Combination of heat treatment and alloying is the most likely route toward this end. The development of such a rail would require a concerted effort on the part of both the rail producers and railroads.

REFERENCES

1. R.E. Ahlf,
"Heavy Four-Axle Cars and Their Maintenance of Way Cost." (Personal Communication).

2. I.A. Reiner,
"An Approach of Determining Economical Wheel Loads." (Personal Communication).

3. J. Kalousek,
"Rail Corrugations", Canadian Pacific, Department of Research No. S488-75, February, 1975.

4. R.G. Read,
"The Rail for High Intensity Mineral Traffic", AREA Bulletin No. 639.

5. H.B. Christianson - et. all,
"Determination of Maintenance of Way Expense Variation with Various Traffic Volumes and Effect of Using Such Variations in Terms of Equated Mileage or Other Derived Factors, for Allocation of Available Funds to Maintenance of Way" AREA Bulletin No. 614.

6. R.I. Meir,
"Material Aspects of Rail Design", Rail Track Material Seminar, BHP Melbourne Research Laboratories, October, 1971.

7. T.E. Tallian,
"Rolling Contact Failure Control Through Lubrication" Proceedings Institute of Mechanical Engineers, Vol. 182, Pt. 3A, 1967-68.

8. R.J. Henry,
"Development of Rail Steel to Resist Shelling" (Personal Communication).

9. CP Rail,
"1974 Statement of Cars and Tonnage Moved".

10. J.D. Young,
"The Manufacture of Improved Rail Steels" Rail Steels, Iron and Steel Institute Meeting, London, November 23, 1972.

11. W. Heller,
"The Development and Further Development of the Quality and Service Properties of Modern Rail Steels" ETR - Eisenbahntechnische Rundschau No. 1 and 2, 1971.

12. V.G. Albrecht and L.P. Melentiev,
"The Main Methods of Increasing Efficiency of Utilization of Rails on the Soviet Railroads. Rail International, Vol. 47, 351-358, May 1974.

13. A.G. Guy and J.J. Hren,
"Elements of Physical Metallurgy" 3rd Ed. Addison-Wesley, 1974.

14. R.D. Manning, H.M. Reichhold and J.M. Hodge:
"A Pearlite Hardenability Concept as a Basis for Alloy Development". Transformation and Hardenability in Steels, Symposium,February, 1967.

H. Ghonem and J. Kalousek

Development of High-Strength Weldable Chromium-Molybdenum Rail

ABSTRACT: This paper summarizes the Canadian Pacific effort in producing a high-strength Chromium-Molybdenum rail. The experimental work and the results are detailed and compared with those of alloyed and heat treated rails.

1. Introduction

Recent innovations in the railway industry leading to higher operating speeds and increasing axle loads were designed to improve productivity and reduce transportation costs. Accompanying these trends were new problems for railway engineers relating to life of rolling stock and track structure components. A complete understanding of the effects of higher speeds and heavy axle loads is difficult because of the complexity of the problem and the large number of variables involved. If studies are focussed on improving rail and the wheel life only, the two most basic railroad components which appear to suffer most, the problem becomes less complex.

Previous studies on potential improvements in rail life have indicated that increased service life may be achieved through any combination of the following measures:

i) reduction in axle loading
ii) increase in wheel diameter
iii) improvements in wheel/rail lubrication
iv) reduction of forces in wheel flanges/rail contact by improved car truck design
v) improvements in rail metallurgy

In view of the very large number of cars now designed for 65,000 lb./axle loading, it is very unlikely that axle loading reductions will occur except perhaps for high capacity cars with six axles designed for branch line service. As far as the second measure is concerned, further increases in wheel diameter are deemed impractical crom a car design point of view.

While significant R & D advances have been made in the remaining three areas iii - v), further research is vital to improve performance and reduce costs. The "optimization" process should be individually tailored to the need of every major railway line. Practical observation has shown that certain premium rails perform quite differently when used by different railroads. Reports on the performance of Hi-Si rail are an example. The variability in performance of a specific rail type is understandable since each major railway line carries a unique blend of rolling stock, is operated under different climatic conditions, has unique topographical characteristics and often uses a different type of rail lubricant to alleviate gauge face wear in curves.

Rail life, if all variables remain constant, is dependent upon the composition and microstructure of rail material. The resistance of pearlite* to wear, plastic flow, shelly spots, flaking and corrugations can be increased by refinement of both grain size and interlamellar spacing. This leads to higher hardness, yield and ultimate tensile strength with the capability of maintaining or outperforming coarse pearlite in ductility and fracture toughness characteristics.

Refinement of grain size and interlamellar spacing can be achieved by the following methods:

---

* Pearlite is a name of microstructure common to most rails presently produced. It has a coarse to fine lamellar structure consisting of alternate plates of ferrite (pure iron) and cementite (FeC_3).

i) heat-treating
ii) alloying
iii) combination of heat-treating and alloying

During heat-treating, rapid cooling of austenitized** rail material with the chemistry of standard carbon rail, is used to obtain the necessary refinement of grain size and interlamellar spacing. The initial cost of a facility for heat-treating an entire rail is substantial due to the high installation costs of oil quench bath, tempering furnaces, etc. Some reduction in first costs for such a facility can be achieved by limiting the heat treatment to the rail head alone.

The second method, i.e., the alloying route, achieves an improved rail product by adding different metallic elements to lower the transformation temperature of the steel developing a finer pearlite at the characteristic cooling rate of any particular steel mill hot bed. This m ethod has the advantage of not requiring any immediate investment in existing rail production facilities. The premium paid is primarily attributed to the cost of alloying elements. A good summary of available premium rails produced by the above two methods, heat treatment and alloying, may be found in references 1 and 2.

The third method combines heat-treating and alloying. In this method a certain degree of refinement of pearlite is achieved by "higher hot bed" cooling rates, while further refinement is achieved by adding specific amounts of alloying elements, usually less than would be required in case of full alloying.

** Austenitizing is a process of forming austenite in a steel by heating it either into or above its critical temperature (approx. 720°C for most rail steels). Austenite is an interstitial solid solution of carbon and often other alloying elements dissolved in gamma iron.

From an economic point of view, while the relationship between the method of producing a rail and the production quantity can only be determined by a detailed cost study, it may appear that the production of fully heat-treated rails is preferable for very large quantities while the alloying method is preferable for the production of "small" quantities.

CP Rail requires approximately 16,000 tons of premium rail annually. It was considered that such a requirement is rather modest in terms of annual steel mill capacity. Hence, preference has been given to the alloying route as a means to achieve increased rail life under heavy traffic conditions.

Out of a large number of commercially available alloyed rails or those being experimentally investigated in the U.S., Europe and Japan, the Cr-Mo rail composition proposed by Climax Molybdenum Co. of Michigan appeared to be the most desirable for future premium alloyed rails. Field tests carried out on Mt. Newman Co. Railway in Australia, and more recent preliminary data from FAST* indicate that this type of alloy rail metallurgy gives superior performance in the areas of plastic flow, abrasive and fatigue forms of wear and is paralleled in performance by the head hardened rail (curvemaster rail). Further tests on Cr-Mo rail are underway in Southern Pacific and Sante Fe. These tests showed that the performance of the fully heat treated rail and Cr-Mo rail are comparable.

Two experimental 100-ton heats of Cr-Mo rail have been produced by Algoma Steel Ltd., heat No. C5599 which was ingot cast in October 1975 and rolled into 132 lb. RE rails, heat No. 9273B was continuously cast in early 1977 and rolled into rails in two stages - with narrow and wide spacing on the hot-bed. The following chapter summarizes the laboratory findings and industrial testing performed on these products.

---

* Facility for Accelerated Service Testing, Pueblo, Colorado, U.S.A.

2. PROPERTIES OF HEATS NOS. C5599 AND 9273B

A brief summary of the participating organizations may help to clarify the origin of quoted data in this chapter and outline the contribution of each organization to this project in the period of 1975-78.

CP Rail or CP - The Engineering Department (CP Rail) and the Research Department of Canadian Pacific Ltd. have been instrumental in initiating this project. Through the series of "rail metallurgy" meetings, to which the various parties mentioned below have been invited, CP served as the focal point(3)*.

Algoma - Algoma Steel Corporation of Sault Ste. Marie produced and subsequently rolled approximately 200 tons of Cr-Mo rail in two heats and carried out metallurgical investigations of both heats(4,5). Two representatives from Algoma Steel together with a representative from Sydney Steel went to Europe on a state-of-the-art mission to assess premium rail production at various European steel manufacturers(6).

EMR - The metallurgy section of CANMET (Canada Centre for Mineral and Energy Technology) of the Canadian Government Department of Energy, Mines and Resources (EMR) carried out comprehensive and meticulous testing of both Cr-Mo heats. The testing of Cr-Mo rail was a portion of their broader interest in rail metallurgy, welding of rails and development of a new rail manufacturing process(7,10).

TDC - Transport Canada - Research and Development Centre of the Canadian Government Ministry of Transport provided financial assistance to support the production of both Cr-Mo rail heats and the fact finding tour of Algoma and Sysco representatives to Europe. They also supported the rail metallurgy development program at CP through CP/TDC Train/Track Dynamic program by partially financing studies of rail wear.

---

* The number in parenthesis refers to the references at the end of this report.

CN Rail & Sysco - Representatives of CN Rail and Sydney Steel Corporation participated in the discussions and offered advice in the rail metallurgy meetings. It should be noted, that CN & Sysco have an advanced rail metallurgy program of their own.

Climax - Climax Molybdenum Corporation of Michigan, U.S.A., conceived and developed Cr-Mo rail alloy and vigorously promoted its industrial production(11-18). They also generously tested a number of Cr-Mo rail samples and assisted in Cr-Mo rail welding tests.

Abbreviations shown above will be used throughout the report to indicate the source of data. As in any kind of summary, some of the data may appear to be incomplete and sometimes not fully reflecting the views of reporting organizations. Should this be noticed by any reader, an original source of information should be consulted.

2.1 Chemical Composition

Ladle and spectroscopic analyses were carried out by participating organizations, to determine the chemical composition of the two Cr-Mo heats. Table 1 shows the average percentage, as well as the highest and lowest reported value, of each alloy component for both heats.

The chemical composition of heat C5599 was on the low side of the specified Climax limits but within recheck limits for carbon, chromium and molybdenum(19). On the other hand, the steel composition of heat 9273B was out of the recommended range of 0.15 to 0.20% Mo.

For readers not acquainted with metallurgical composition of various types of rail, Table 2 shows the typical chemical composition of several heat-treated and alloyed rails.

2.2 Mechanical Properties

Table 3 shows the average value of different mechanical properties of both Cr-Mo heats as determined by various investigators while Table 4 compares the typical mechanical properties of rail materials for which the chemical composition is shown in Table 2.

From Table 3 one can observe that the continuous cast heat 9273B has a higher yield, higher ultimate tensile strength and higher level of hardness than the ingot cast heat C5599. This significant increase in the mechanical properties of heat 9273B can be attributed to both its predominantly bainitic* microstructure (described in Section 2.6) which is caused by a higher molybdenum content and the different type of deoxidation practice. However, the values of El% and RA% reflect the reduction in the ductility of heat 9273B as compared to heat C5599.

2.3 Hardness Surveys

Figure 1a and 1b show typical hardness surveys performed on rail samples of heat C5599 and 9273B, respectively. The average hardness on rail head samples of heat C5599 of eight readings conducted by Climax(20) was 347 HBN. This was within the anticipated hardness range of 340-360 HB, i.e. Phase I Cr-Mo rail. The average hardness of the web was 372 HB and of the flanges was 383 HB. For heat 9273B, the hardness of the centre of the rail head was 427 HBN which is higher than any Cr-Mo rail previously tested. Web and flange hardness are 410 and 356 HB, respectively. Here, it should be mentioned that the hardness characteristics of rail flanges and web sections of Cr-Mo alloy rail make cutting and drilling of this material with conventional tools currently used by the railway industry very difficult. This will be discussed in Section 11 of this chapter.

---

* Bainite is a name of steel microstructure consisting of carbide particles finely dispersed in ferrite matrix.

2.4 Inclusion Content

The nonmetallic inclusions, such as sulfides, alumina, silicates, etc., if too large, can act as nucleation sites for fatigue cracks leading to various types of rail failures such as transverse fracture, detail fracture, vertical split heads, shells, etc. It is, therefore, desirable to check the distribution, size and volumetric content of the inclusions on several cross-sectional samples of the rail.

A normal distribution of inclusions containing sulphur was observed on all sulphur prints made by EMR(21,22) on samples of both heats, examples of which are shown in Figure 2. However, a minor segregation of sulphur was visible at the center of the web on some of these prints.

A moderate amount of another type of inclusion, Al_2O_3, was reported by Algoma to have occured on samples taken from heat C5599. The concast heat was not aluminium deoxidized and thus the tests for Al_2O_3 inclusions were not carried out. Deoxidation practice should ensure that inclusions are spheroidal rather than angular.

The total content of all types of inclusions can be assessed on automatized quantitative metallographic equipment. Such an investigation was carried out by Climax(20) and it was found that .11 and .3 volume percent inclusions, respectively, occured in the web and in the flange of samples taken from Heat C5599.

All these findings are within the normal range of inclusion content in rail steels, except that modification of Al_2O_3 inclusions to duplexed form may be desirable in future Al-killed heats.

2.5 Impact Properties & Fracture Toughness

Rail materials have to resist a suddenly applied load caused by rail joints, wheel flats, etc. The impact resistance of materials is established on standard notched specimens fractured by an impact blow. The energy required to propagate the crack from the bottom of the notch across the specimen is termed "energy to fracture" and is measured in ft-lb. In these tests, the size and acuity of the notch is important since very minor variations in either of them will cause large variations in the test results. Variation in test results might be reduced if all test specimens were "identically" manufactured by the same machine shop.

The results of "notched" and "unnotched" Charpy impact tests carried out by EMR(21,22) on both Cr-Mo heats and other types of rail steels are illustrated in Figures 3 and 4. The "unnotched" specimens were tested in the transition temperature range. The notched specimens in this range do not show any appreciable difference in test values. Figures 3 and 4 indicate that the Charpy "energy to fracture" values of Heat C5599 Cr-Mo rail are close to those obtained from fully heat-treated rail samples. The Charpy values of Heat 9273B Cr-Mo rail, which is a predominantly bainitic microstructure, are in a lower range. However, the latter are comparable to the values for plain carbon rail steel.

Fracture toughness, represented by the stress intensity factor K_{IC}, is indicative of the material's resistance to fracture in the presence of a pre-existing fatigue crack(22,28). It can be simply said that increase of the K_{IC} value increases the allowable critical crack length and the opportunity for detection of the crack prior to brittle fracture.

The specification for fracture toughness testing ASTM E399, requires several factors to be within certain limits for a test to provide a valid K_{IC} value. One of these factors is that the ratio of the maximum stress intensity factor (K_{max}) to the stress intensity factor associated with the cleavage burst or pop in (K_Q) must be less than 1.10, for the relation between K_{max} and K_Q, see Figure 5. It is common for rail steels of all types to violate this validity criteria because of short cleavage bursts which occur well below the breaking load.

The results of fracture toughness tests carried out by CMR and Climax on specimens made from both heats according to ASTM Specifications E399-74 are shown in Table 6. In this table, the K_{IC} (K_Q) values for Cr-Mo heat C5599 are higher than those of fully heat-treated and plain carbon rails, while the K_{IC} (K_Q) values for the second heat 9273B are close to those of plain carbon rail steel.

The relation between K_{IC} and the critical defect size d_c is shown in equation 1 in Table 6. In this equation, the critical defect size in the rail head can be calculated by knowing the K_{IC} for any specific rail material and stress level acting on the head. For a typical value of applied stress 28.6 ksi, the critical crack length in rail samples from heat C5599 was found to be greater than one inch while it was about ½ inch in the case of heat 9273B. It should be mentioned here, that in these calculations it was assumed that the stress field across the rail head is uniformally distributed. This is not necessarily the real situation since the rail head in service is subjected to a complex stress field resulting from a dynamic combination of Hertzian, bending, lateral and thermal stresses(29-32).

2.6 Microstructure

Metallographic examination of the heads and the flanges of samples taken from heat C5599 showed that their microstructure consists of fine pearlite without evidence of bainite or martensite. The web of each of those samples was also completely pearlite except for the presence of white streaks resembling retained austenite which was transformed completely or partially to bainite. According to ASTM standard E112, see Figure 6, the typical grain size of the microstructure of the heads of these samples is no. 8 while their pearlite interlamellar spacing, see Figure 7, is in the range of 850-1800A^0 with an average of 1100^{0}A(22,23). As shown in Table 7, the interlamellar spacing compares favourably with that for other rail steels. Minimum interlamellar spacing was observed in the fast-cooled web-centre and flange-tip regions of each rail.

Unlike heat C5599, the microstructure of the rail heads of samples taken from heat 9273B was found to be of a bainitic nature(34). In the centre of these heads a mixture of 50% bainite and 50% transitional pearlite was observed, see Figure 8. The interlamellar spacing measurement is not applicable to bainite microstructures, however, the interlamellar spacing of the transitional 9273B pearlite was evaluated to range between 500 to 800^{0}A(22).

While EMR findings are similar to those of Climax, they also tested one rail from heat 9273B having a mainly pearlitic head microstructure resulting from rolling and camber trials when a lower rate of cooling was obtained by close spacing of rails on the hot bed.

2.7 "White" Streaks in the Rail Web

Figure 9a shows a section through an irregularly-shaped area of web segregation and is an example of a "white" streak as observed, using an optical microscope, in the continuously cast heat 9273B. The origin of web streaks is related to cooling rate and to microsegregation of alloying elements. In Table 8, the concentration of alloying constituents in the streak areas is listed demonstrating that the streaks are alloyed to a degree higher than the matrix itself(19). This indicates that during the cooling process, the streak's material may transform to a different type of microstructure with a hardness different than that of the neighbouring material. The hardness of the streaks in both heats is measured as 55 Rc (or 520 BHN) while their volumetric content varies from two to five percent. The streak microstructure and hardness is unchanged by retempering or by subzero quenching.

Initially it was thought that the streaks were untempered martensite, however, subzero cooling and electron microscopy indicate this phase to be lower bainite with traces of martensite. Later, studies carried out by Scanning Electron Microscopy confirmed that the "white" streaks are predominantly bainite (Figure 9b) with occasional traces of martensite or stable austenite. In order to determine the effect of these streaks on the fatigue characteristics of Cr-Mo rail, a sample of rail containing streaks was tested by AAR Metallurgical Laboratory using a cradle machine and wheel loading of 52,000 lbs.(35). It was found that this sample can withstand three million cycles without failure. It should be noted that an AREA plain carbon rail fails on the average of one million cycles under the same test conditions. The results of AAR laboratory test is supported by the current experiences in both Australia (Mt. Newman Railway Co.) and the U.S.A. which indicate that bainitic streaks in the rail web are not conducive to an early catastrophic failure of the Cr-Mo rails.

The continuously cast heat (9273B) was made as an attempt to reduce the segregation of alloying elements on the basis that a volume of solidifying metal in concast cooling mold is smaller than that of 10t ingot mold. It was then expected that the reduction of the segregation would result in reduced amount of smaller size streaks(36). The reduction in the segregation was achieved, however, due to the increased hardenability and rapid cooling of the concast heat on the hot bed, the volumetric amount and size of the streaks in both heats (C5599 and 9273B) were about the same.

It is the belief of the authors that in order to resolve the controversy over the effect of bainitic streaks on the fatigue life of Cr-Mo rail, further testing of this rail should be carried out under controlled service conditions (such as in FAST) complimented with a laboratory investigation aimed at the study of crack propagation in the plane of the rail web.

2.8 Hardenability

In order to achieve better control over the mechanical properties of any Cr-Mo heats, the hardenability of the steel should be specified in addition to the chemical composition.

The hardenability of the steel, in addition to other methods, can be expressed by the Grossmann ideal diameter D_i which is defined as the diameter of round bar that when cooled at infinitly rapid rate, will, at the centre of the bar, result in a microstructure containing 50% martensite. (In the case of alloy rail steel we are concerned instead with microstructure which contains pearlite or bainite but no martensite.) The value of D_i is considered a measure of the hardenability of the steel independent of the cooling medium.

A steel with a higher D_i value will have a higher hardness microstructure than a steel with a lower D_i value if cooled at the same cooling rate. As shown in Figure 10, D_i values for any type of steel can be calculated from the knowledge of its chemical composition and the austenitic grain size number which in turn is affected by the steel deoxydation process. Adjustment of D_i value and grain size control depends, in individual plants, on the temperature and length of time for soak prior to rolling and on the initial and final rolling temperatures as these affect the steel's tendency for grain coarsening with subsequent change of D_i hardenability. A procedure analogous to Grossman's but specifically developed for pearlite microstructure was reported by Manning and others in 1976(37).

Neither Grossman factors nor R.D. Manning method is the final answer for describing the hardenability of alloy rail steel(38). However, it was found(39) that available Grossman's D_i data is useful in sorting different rail composition where hot bed cooling rate of 60°F/min. is constant.

The ingot cast heat (C5599) was aluminium deoxidized with an austenite grain size No. 8 and a calculated D_i of 4.5 while the concast heat (9273B) was silicon deoxidized with an austenitic grain size No. 5 and a D_i of 7.2. Both, the higher content of molybdenum and the silicon-deoxidation practice were responsible for heat 9273B having harder bainite-pearlite rail head microstructure developed at normal hot-bed cooling rates, (60°F/min. at 1300°F).

2.9 Wear Properties

Cr-Mo rail resistance to wear and plastic flow to date according to the experience accumulated at FAST and Mt. Newman Railway Co., is superior to any other type of commercially available alloy rail paralleled only by some heat treated brands of rail. Table 9 shows some data obtained at FAST(40).

It should be pointed out, that the microstructure of test Cr-Mo rails at FAST and Mt. Newman Railway Co. is fine pearlite - comparable with the microstructure of Algoma heat C5599. However, large portions of the rails from heat No. 9273B have a bainitic microstructure in the rail head. Up till now no reliable data is available on the wear behaviour and the resistance of bainitic rail materials to plastic flow under unlubricated or lubricated curve or tangent track conditions. The experience of grinding balls in ore processing plants suggests, that the gauge face wear resistance of bainitic rail may be reduced in comparison with pearlitic rails of the same hardness range. However, no experience is available which would reflect on plastic flow and rolling fatigue behaviour of bainitic rail materials in the 390-410 BHN hardness range. Laboratory wear tests together with the results from FAST on service performance of heat 9273B are needed to evaluate the behaviour of bainitic rails under lubricated conditions. Early results suggest superior wear resistance for bainitic steel in tangent track and/or pearlitic (tougher) steel in curved track service.

2.10 Weldability

The flash-butt welding characteristics of any type of rail are very important to its acceptance.

Modified flash-butt welding procedures for the conventional Cr-Mo rails (0.80% Mn, 0.75% Cr, 0.18% Mo) were established in the U.S.A.(41-43) and Australia(44,45) and all the rails which are in service now have been successfully welded using these procedures.

Recent development of the Cr-Mo composition for improved welding characteristics indicate that the square composition (0.60% Mn, 0.60% Cr, 0.22% Mn) offers better transformation characteristics than conventional Cr-Mo and permits welding with much less preheating and post-heating cycles(46).

Heat C5599 was not tested for flash-butt welding. However, no special problems should be anticipated in welding this heat since it has a microstructure similar to any weldable, conventional Cr-Mo rail.

Heat 9273B, which is different than any known Cr-Mo rail, was subjected to several welding tests to develop its valid welding procedure(41,45). A total of 13 welds with different procedures, shown in Table 10, were made at CP Transcona welding plant using AI welder. Based on metallurgical analysis done by EMR and Climax on samples of these welds, a specific welding procedure was selected as the valid procedure to weld bainitic rails produced from concast heat 9273B. This procedure, see Figures 11 and 12, comprises the following cycles:

- Flash off
- 7 preheats (2.5 sec. on, 1 sec. off)
- Forging
- 10 post-heats (3 sec. on, 2 sec. off)
- Shear.

The resulting weld (49,50) will be very wide, particularly on the top of the rail head. Hardness in the centre 2.5 inches of the weld will be uniform, between 30 and 42 RC(49,51), see Figure 13. Two soft zones, one on each side of the weld, will have a minimum hardness of 27 RC and each soft zone will be about 1 inch wide. The microstructure of the welded zone will be mainly pearlitic in the head(49) or mixture of bainite and pearlite in the web and the base(5) with traces of martensite.

2.11 Machinability

Machinability of Cr-Mo rail material is reduced due to the increase in the hardness values in the web area. A web drilling experiment has been carried out by CPR Test Department on Racine Portable Model "AIC" drilling machine with 1-1/8" diameter double and single ended "Republic" type drills. Each end of Republic-double-ended drill drilled 2 and 6 holes at webs having hardness of 418 and 387 BHN respectively. A Republic-single-ended drill made 10 holes in a web of 387 BHN hardness. In all of the tests a SAE 30 Motor Oil was used as a lubricant and the drilling time per hole was approximately 2-1/2 minutes. However, in a previous evaluation using Algoma Chrome rail, an average of 25 holes was drilled with each end of Republic-double-ended and 26 holes with single ended drills under the same lubricating conditions and the drilling time per hole was approximately 2 minutes.

This experience indicates that special tools such as those containing carbide tips are required to make machining of Cr-Mo rail more productive.

3. DISCUSSION

At the beginning of this program, it had been proposed by one of the authors (J. Kalousek) that the alloying approach to refine rail microstructure to its finest pearlitic state be explored in three phases leading to rails of various head hardness: Phase I: 340-360 BHN, Phase II: 360-380 BHN, and Phase III: 380-400 BHN.

In October 1975, an ingot casting heat (C5599) of Cr-Mo rail steel was produced by Algoma and rolled into 132 lb./yd. Phase I rail. Metallurgical evaluations of this rail, described in the previous chapters, showed that the Phase I objective had been achieved. However, streaks of martensite and bainite were observed in segregated regions at the centre of the web of this rail. In an effort to reduce such segregation to eliminate web streaks, a second heat (9273B) of continuously cast Cr-Mo rail was made in early 1977. It was intended that this heat also fall in the Phase I Cr-Mo rail category. Metallurgical examination of this heat showed, however, that the average head hardness of this heat was over 380 BH, and it could not even be categorized as Phase III rail because of its dominant bainitic nature.

This outcome can be understood in view of a lack of previous industrial experience with the Cr-Mo steel-making and rail production processes and it suggests that better-than-average control of chemical composition and hardenability of steel is needed to achieve the desired mechanical properties and hardness range.

During the early stages of the steelmaking process of these two heats, no difficulties were experienced in melting the heats, ingot pouring (C5599) and concasting (9273B), rolling of ingots into blooms and rolling of both heats into 132 lb. section rail.

However, major production difficulty was encountered due to abnormal behaviour of the rails during cooling on the hot bed. Some of the rails developed excessive curvatures in the vertical or the lateral planes, resulting in excessive camber or sweep limits, and some bent in both directions giving a twisted rail. Subsequent straightening using "gag" press technology was very difficult and most of the rails produced from heat C5599 could not be satisfactorily straightened.

Excluding the bainitic heat 9273B as a special case, the following has been learned from the Cr-Mo alloying approach.

- In comparison to other types of alloy rails, Cr-Mo rails have high .2% yield stress and hardness values. This offers increased resistance to:
  a) gauge face wear;
  b) rolling contact fatigue (typically manifested by shelly spots on high rails and flaking on low rail);
  c) plastic flow of railhead material.

- Good ductility and high fracture toughness values increase the Cr-Mo rail endurance life and offer a better opportunity for critical crack detection prior to fracture.

- The "harmful" effect of white etching streaks in the rail webs has not been substantiated by actual service testing. Further field experience and laboratory data are needed to resolve the question of whether the streaks may have an effect on the longevity of Cr-Mo rails.

- Reduction of machinability in the web of Cr-Mo rails was caused by their high hardness. This can only be overcome by using special tools for drilling and cutting operations.

- Cr-Mo rail requires a special flash-butt welding cycle which consist of extra numbers of preheat and postheat cycles. This makes the welding cycle longer and more expensive than for carbon steels.

4. RECOMMENDATIONS

- It is recommended that studies be initiated to assess whether heat C5599 can be salvaged, and possibly subsequently tested in actual service.

- A third experimental concast or ingot-cast Cr-Mo steel heat aimed at producing pearlitic microstructure in the railhead, is strongly recommended. This heat, following the recommendations of EMR, should have a target chemistry composition similar to that of heat C5599, restricting the Mo. content to 0.16% and having 0.053% total Al and an austenite grain size No. 8. This may result in a pearlitic rail competitive in properties with oil-quenched, tempered carbon steel suitable for curved track service.

- Testing of both heats, C5599 and 9273B, should continue. Additional quantitative data should be collected, such as determining the effect segregation-caused streaks may have on railhead or web splitting. Determination of the fracture characteristics, wear and contact fatigue resistance of bainitic microstructure is desirable. This can be done utilizing the service of the FAST track.

- The fact that heat C5599 is pearlitic while heat 9273B, which is produced by the same technique, is bainitic, suggests that the refinement of pearlite into the Phase III hardness range may be difficult to achieve by the alloying route alone. Therefore, in parallel with the above recommendations, the need to establish a Canadian facility for partially or fully heat-treated rail should be investigated.

- All high-strength rails require special straightening; this fact was particularly brought out by the Canadian delegation to the European rail mills in 1975. Based on the experience with both Cr-Mo heats, additional capital investment will be required in Canada to obtain straightening equipment that can handle high-strength rails.

5. REFERENCES

1.	J. Kalousek G. Beynon	Rail Metallurgy; Canadian Pacific, Department of Research Report No. S497-75, July 1975.
2.	S. Marich	Research on Rail Metallurgy; American Railway Association - Bulletin, Vol. 78, No. 663, pp. 594-610, 1977.
3.	Canadian Pacific Ltd. (Research Department)	Proposal to TDA, File Q9-2-4.
4.	Algoma Steel Corp. Ltd.	Evaluation of a Cr-Mo Rail Heat that was produced at request of CP Rail. Rail Heat C5599, Investigation 5R322, Nov. 1975.
5.	Algoma Steel Corp. Ltd.	Evaluation of Algoma Cr-Mo Rails - Interim Experimental Results, December 1975.
6.	G.F. Morris H. Jaeger L. Trask	Report of Visit to European Rail Producers, Algoma Steel Corporation, Ltd., March 1976.
7.	L.P. Trudeau D.W.G. White W.J. Craigen	Premium Rails: A Review of Options; Energy, Mines and Resources Canada, CANMET Program Report MRP75-14 (ACT) (TR) (CF), July 1975.
8.	D.E. Parsons	Visit to Algoma Steel Corporation, Ltd., Sault Ste. Marie; Energy, Mines and Resources Canada, CANMET Report MRP/PMRL-77-4(FT), March 1977.
9.	D.E. Parsons D.M. Fegredo Z. Paley	Visit to Sydney Steel Corp., Sydney, Nova Scotia, concerning the premium rail program; Energy, Mines and Resources Canada, CANMET Report MRP/PMRL(CF)77-9(F), April 1977.
10.	D.M. Fregredo	Current R&D Activity at Railway Technical Centre, British Rail, Derby, England - Notes and Appendix; Energy, Mines and Resources Canada, CANMET Report MPR/PMRL-77-3(R).
11.	J.W. Hallock	High Strength Rail Steels; Climax Report ISJ-768, April 1973.
12.	J.W. Hallock Y.E. Smith	High Strength Pearlitic Rail Steels; Climax Report ISJ-768-03, May 1973.
13.	W.W. Cias	Effects of Temperature on the Magnetic Saturation of Experimental Low-Alloy Steels Containing 0.60 and 0.75%C; Climax Report ISJ-768-02, April 1973.
14.	W.W. Cias	Evaluation of a Flash-Weld Joint of the Trial Cr-Mo Fine Pearlitic Steel Rails; Climax Report ISJ-768-10.

15.	Y.E. Smith F.B. Fletcher	Alloy Steels for High-Strength As-Rolled Rails; ASTM Symposium on Rail Steels, Denver, November 1976.
16.	Climax Molybdenum Co.	Heavy Duty Cr-Mo Steel Rails, June 1975.
17.	Climax Molybdenum Co.	High Strength Cr-Mo Rail Steels - A Summary of of Data, November 1975.
18.	Y.E. Smith J.M. Sawhill, Jr. W.W. Cias G.T. Eldis	High Strength Chromium-Molybdenum Rails; Climax Molybdenum Report, April 15, 1976 - AREA Bulletin 658, June-July 1976.
19.	D.E. Parsons D.A. Munro	Examination of Three High Strength Cr-Mo Alloy Steel Rail Samples; Energy, Mines and Resources of Canada, CANMET, Report MRP/PMRL(CF)-76-2(IR), February 1976.
20.	F.B. Fletcher	Evaluation of Algoma Cr-Mo Rail Steel for Canadian Pacific Railroad; Climax Molybdenum Report J-4183, January 1976.
21.	D.E. Parsons	Some Properties of Mn-Nb-Cr, Cr-Mo and Aluminum-Deoxidized Carbon Steel Rails; Energy, Mines and Resources Canada, CANMET, Report MPR/PMRL-76-19(R), February 1977.
22.	D.E. Parsons Z. Paley J. Ng-Yelim D.A. Munro	Metallurgical Examination of As-Rolled Rail Samples from Strand-Cast "Cr-Mo" Heat 9273B; Energy, Mines and Resources Canada, CANMET, Report MRP/PMRL-77-78(TR), July 1977.
23.	D.E. Parsons	Chemical Composition and Impact Transition Temperatures of Carbon and Alloy Rail Steels (1951-1977); Energy, Mines and Resources Canada, CANMET, Report MRP/PMRL-77-4(R),
24.	G.R. Irwin	Analysis of Stresses and Strains Near the End of Crack Traversing A Plate; J. of Applied Mechanics, Vol. 24, pp. 361, 1957.
25.	H. Ghonem	Stochastic Fatigue Crack Initiation and Propagation in Polycrystalline Solids, Ph.D. Thesis; Micromechanics Laboratory, McGill University, March 1978.
26.	D. Broek R.C. Rice	Fatigue Crack Growth Properties of Rail Steels; DOT-TSC-1076, July 1977.
27.	D.F. Cannon R.J. Allen	The Application of Fracture Mechanics to Railway Failures; REJ, pp. 6-23, July 1974.
28.	D.H. Stone	The Fracture Toughness of Carbon Steel, Alloy-Steel and Heat-Treated Railway Rails; AAR Report No. R-163, September 1974.

29. J. Kalousek Rail Corrugations; Track/Train Dynamics Report #4, Canadian Pacific, Department of Research Report No. S488-75, February 1975.

30. S. Timoshenko, B.F. Langer Stresses in Railroad Track; Transactions of ASME #54-302, pp. 277, 1932.

31. V.V. Lempitskii, D.S. Kazarnovskii Effect of the Strength of Railroad Rails on the Formation of Contact Fatigue Damage During Use; Strength of Material, Vol. 9, pp. 13-17, 1975.

32. R.I. Mair, R. Groenhout Prediction of Rail-Steel Strength Requirements - A Reliability Approach; ASTM Symposium on Rail Steels, Denver, November 14-16, 1976; ASTM Pub. No. STP 644, June 1978.

33. F.B. Fletcher Algoma Chromium Rail Microstructure; Climax Molybdenum Co., Report J-4208, June 1976.

34. F.B. Fletcher Evaluation of Algoma Continuously Cast Chromium-Molybdenum Rail Steel; Climax Molybdenum Co., Report L-311-13, February 1978.

35. D.H. Stone Correspondence with Canadian Pacific Research Department, File Q9-2-4, September 1977.

36. J.D. Young The U.K. Development of Rails Rolled from Continuously Cast Blooms; ASTM Symposium on Rail Steels, Denver, November 14-16, 1976; ASTM Pub. No. STP 644, June 1978.

37. R.D. Manning, H.M. Reichhold, J.M. Hodge A Pearlite Hardenability Concepts as a Basis for Alloy Development; Symposium - Transformation and Hardenability in Steels, pp. 177, February 1967.

38. F.B. Fletcher Correspondence with EMR, June 26th, 1978.

39. D.E. Parsons Correspondence with Climax Molybdenum Co., July 1978.

40. R.K. Steele Private Communication, July 1978.

41. J.M. Sawhill, Jr. Flash-Butt Welds in Cr-Mo Rail Steels; Climax Molybdenum Co., Report ISJ-768-11, June 1974.

42. J.M. Sawhill, Jr. Induction Heating of Flash-Butt Welds in Cr-Mo Rail Steel; Climax Molybdenum Co., Report ISJ-768-13, March 1977.

43. F.B. Fletcher Lower Alloy Chromium-Molybdenum High Strength Rail Steels for Improved Weldability; Climax Molybdenum Co., Report No. L-311-07, August 1977.

44.	S. Marich P. Curcio	An Investigation of Flash-Butt Welded High Strength Rail Steels; BHP Melbourne Research Laboratories, Report No. MRL/083/75/008, August, 1975.
45.	B. Watson A. Marks I. Wray	Assessment of Production Tyre Flash-Butt Welds in High Strength Rail - Port Holland Welder; BHP Newcastle Works Research Report No. BHP/MNM/RWC/76/023, April, 1976.
46.	F.B. Fletcher	Development of a Weldable High-Strength Chromium-Molybdenum Rail Steel; Climax Molybdenum Co., Report No. L-311-12, August 1977.
47.	J. Kalousek	Experimental Welding of Cr-Mo Rail; Canadian Pacific, Research Department File Q9-2-4, August 1977.
48.	H. Ghonem	Experimental Welding of Cr-Mo Rail; Canadian Pacific, Research Department File Q9-2-4, March 1978.
49.	Z. Paley	Preliminary Results (Private Communication), July 1978.
50.	F.B. Fletcher	Correspondence with Canadian Pacific Ltd. Research Department, File Q9-2-4, June 26th, 1978.
51.	S. Pittelli	Investigation 8M632, Evaluation of Welding Chromium-Molybdenum Rails; Algoma Steel Corp., June 1978.

		C	Mn	P	S	Si	Cr	Mo	Al
AIM COMPOSITION		.7-.8	.8-1.0	.030 max.	.030 max.	.25	.7-.9	.15-.20	-
	RE-FER-ENCE	HEAT NO. C5599 (INGOT CAST)							
ALGOMA - LADLE		.70	.94	.012	.022	.24	.83	.15	.051
ALGOMA (9 RAILS AVERAGE		.69	.98	.007	.021	.25	.80	.15	.047
CLIMAX (RAIL 4G)		.70	.86	.010	.022	.24	.80	.17	.05
EMR (3 RAIL AVERAGE)		.67	.95	.007	.32	.29	.65	.16	.053
LOWEST AND HIGHEST REPORTED VALUES		.65-.73	.89-1.00	.006-.010	.20-.34	.24-.29	.65-.80	.15-.17	.042-.053
		HEAT NO. 2973B (CONTINUOUSLY CAST)							
ALGOMA - LADLE		.72	.79	.009	.023	.23	.78	.21	-
CLIMAX (RAIL 2-2D)		.74	.82	.012	.023	.26	.84	.22	
EMR (6 RAIL AVERAGE)		.725	.84	.013	.023	.27	.83	.22	.005
LOWEST AND HIGHEST REPORTED VALUES		.72-.74	.79-.84	.009-.013		.23-.27	.78-.84	.21-.22	

TABLE 1: Ladle and Spectrochemical analysis of Cr-Mo Rail Heats No. C5599 and 9273B

MANUFACTURER	RAIL TYPE		C	Mn	Si	Cr	Mo	V	Nb
		STANDARD AREA	.80	.90	.20	-	-	-	-
BETHLEHEM STEEL	HEAT TREATED	FULLY HEAT TREATED	.80	.90	.20	-	-	-	-
U.S. STEEL		HEAD HARDENED	.80	.90	.20	-	-	-	-
NIPPON STEEL		HEAD HARDENED	.65	.90	.20	-	-	-	-
NIPPON KOKAN		HEAD HARDENED	.65	.90	.20	-	-	-	-
RUSSIAN		FULLY HEAT TREATED	.75	.90	.30	-	-	-	-
CF&I	ALLOYED	Hi Si	.75	.80	.65	-	-	-	-
BRITISH STEEL		Cr	.75	1.25	.35	1.15	-	-	-
ALGOMA		Cr	.75	.65	.25	1.15	-	-	-
CF&I & ALGOMA (EXPERIMENTAL)		Cr-Mo	.75	.90	.25	.8	.18	-	-
KLOCKNER		Cr-Mo-V	.65	.80	.30	1.00	.10	.10	-
SYDNEY		Mn-Cr-V	.70	1.65	.20	.30	-	.10	-
SYDNEY		Cr-Si-Nb	.70	1.10	.55	.80	-	-	.06
KRUPP		Cr-Si	.70	1.05	.75	1.00	-	-	-
AUG. THYSSEN		Cr-Si-V	.65	1.05	.60	1.15	-	.20	-

TABLE 2: Typical Chemical Composition of Several Types of Rails

	U.T.S.		.2% Y.S.		El	R.A.	HEAD HARDNESS	
	ksi	MPa	ksi	MPa	%	%	BHN	Rc
	HEAT NO. C5599 (INGOT CAST)							
Algoma	173	1191.97	112	771.7	12	31	331*	36
Climax	168	1157.5	111	764.8	14	30	348	37.5
EMR	171	1178.2	113	778.6	12	33	331*	36
CPR	169	1164.4	121	833.7	12	28		
Highest and Lowest Reported Value	168 175	1157.7 1212.6	94.9 121	653.9 833.7	12 14	28 37	293* 363	31 39
	HEAT NO. 9273B (CONTINUOUSLY CAST)							
Algoma	201	1384.9	154	1061.1	6			
Climax	181	1247.1	136	937	8	14		
EMR	201	1384.9	163	1123.1	14	23		41
Highest and Lowest Reported Value	180 218	1240.2	136 176	937 1212.6	3 18	N.A.	N.A.	N.A.

* Converted either from Rc or BHN

N.A. - Not Available

TABLE 3: Tensile Properties and Hardness of Cr-Mo Rail Heats No. C5599 and 9273B

MANUFACTURER		RAIL TYPE	U.T.S.		0.2% Y.S.		El	R.A.	HARDNESS
			ksi	MPa	ksi	MPa	%	%	BHN
		STANDARD AREA	134	924	74	510	11	30	255
BETHLEHEM STEEL	HEAT TREATED	FULLY HEAT TREATED	177	1,220	126	870	13	30	365
U.S. STEEL		HEAD HARDENED	183	1,260	132	910	12	33	380
NIPPON STEEL		HEAD HARDENED	165	1,140	120	830	17	50	360
NIPPON KOKAN		HEAD HARDENED	165	1,140	120	830	17	50	360
RUSSIAN		FULLY HEAT TREATED	181	1,250	119	820	14	40	380
CF&I	ALLOYED	Hi Si	142	980	75	520	11	14	285
BRITISH STEEL		Cr	164	1,130	100	690	11	17	325
ALGOMA		Cr	150	1,035	95	655	9	17	320
CF&I & ALGOMA (EXPERIMENTAL)		Cr-Mo	181	1,250	124	855	12	20	365
KLOCKNER		Cr-Mo-V	166	1,145	102	703	12	20	325
SYDNEY		Mn-Cr-V	150	1,035	102	703	12	18	325
SYDNEY		Cr-Si-Nb	165	1,140	102	703	10	15	340
KRUPP		Cr-Si	165	1,140	98	676	12	20	315
THYSSEN		Cr-Si-V	164	1,130	99	683	12	20	320

TABLE 4: Typical Tensile Properties and Hardness of Several Types of Rail

HEAT NO.	ORGANIZATION	UNITS	HEAD			WEB			BASE		
			Max.	Min.	Ave.	Max.	Min.	Ave.	Max.	Min.	Ave.
C5599	Climax (3 samples)	BHN**	363	337	344	415	347	375	417	345	381
		Rc*	39	36	37	45	37	40	45	37	41
	EMR (3 samples)	BHN*	360	293	331	388	321	352	401	311	363
		Rc**	38.5	31	36	42	34	38	43	33	39
9273B	Climax	BHN**	432	366	403	432	388	410	370	345	356
		Rc*	46	39	43	46	42	44	40	37	38
	EMR (6 samples)	BHN*	429	341	382	444	375	388	429	326	382
		Rc**	46	37	41	47	40	42	46	35	41

* Converted Values
** Reported Values

TABLE 5: Summary of Hardness Surveys of Transverse Rail Sections

TYPE OF RAIL	TEST PERFORMED BY	TEST TEMPERATURE	AVERAGE K_{IC}		NUMBER OF SPECIMENS TESTED	dc	
			ksi $\sqrt{\text{inch}}$	MPa$\sqrt{\text{m}}$		INCH	mm
Cr-Mo (C5599)	EMR	$75^{\circ}F$	39.2	43.4	12	1.22	31
Cr-Mo (C5599)	Climax	Room Temp.	46.3	51.3	4	1.67	42
Cr-Mo (9273B)	EMR	$75^{\circ}F$	29.0	32.0	30	.65	17
Cr-Mo (9273B)	Climax	Room Temp.	30.9	34.0	2	.74	19
Fully heat treated	EMR	$75^{\circ}F$	36.0	39.9	n.a.	1.02	26
Plain Carbon	EMR	$75^{\circ}F$	30.3	33.5	n.a.	.71	18

$$d_c = \frac{2}{\pi}(K_{IC}/\sigma_{app})^2 \qquad (1)$$

TABLE 6: Average Fracture Toughness K_{IC} Values for Cr-Mo, Fully Heat Treated and Plain Carbon Rail Steels.

TYPE OF RAIL	PEARLITE INTERLAMMELLAR SPACING IN THE RAIL HEAD		
	max. A^o	min. A^o	ave. A^o
Cr-Mo - ingot cast	2500	900	1100
Cr-Mo - concast (applies to transitional pearlite only)	1000	500	800
Standard carbon	4000	900	1500
Fully heat treated	2400	900	1000

TABLE 7: Pearlite Interlamellar Spacing in the Rail Head of Different Alloys

Segregation Ratio, (White Area: Matrix)		Nominal Composition (%)	
		Segregate	Matrix
Mo	6 : 1	0.96	0.16
Cr	2.6 : 1	1.69	0.65
Mn	1.6 : 1	1.52	0.95

TABLE 8: Microprobe Analysis of White Areas in the Web of Rail Sample from Heat C5599

Tie Plate Cant	Average Wear of Cr-Mo inch/MGT	Average Wear of Standard Rail inch/MGT
1:30	0.0040	0.00823
1:40	0.0039	0.0092

TABLE 9: Cr-Mo Rail Wear Vs. Standard Rail Wear ($<$ 40MGT)

WELD NO.	TYPE OF ENDS	TYPE OF WELD	TYPE OF WELDING CYCLE
1 2 3	hot saw cut flame cut flame cut	Carbon & Cr-Mo Cr-Mo & Cr-Mo Cr-Mo & Cr-Mo	Flash off - 7 PH (2.5 sec. on, 1 sec. off) - forging - no delay - 10 Post H (2 sec. on, 1 sec. off) - Shear
4 5 6	flame cut flame cut flame cut	Cr-Mo & Cr-Mo Cr-Mo & Cr-Mo Cr-Mo & Cr-Mo	Flash off - 11 PH (3 sec. on, 1 sec. off) - forging - no delay - 10 Post H (2.5 sec. on, 1 sec. off) - Shear
7	hot saw cut	Cr-Mo & Cr-Mo	7 PH (2.5 sec. on, 1 sec. off) - forging - 185 sec. delay (Shear) - 2 Post H - 110 sec. delay - 2 Post H
8	machine cut	Cr-Mo & Cr-Mo	7 PH (2.5 sec. on, 1 sec. off) - forging - 250 sec. delay (Shear) - 2 Post H* - 50 sec. delay - 2 Post H* - 50 sec. delay - 2 Post H*
9	machine cut	Cr-Mo & Cr-Mo	9 PH (2.5 sec. on, 1 sec. off) - forging - 160 sec. delay (Shear) - 2 Post H* - 100 sec. delay - 2 Post H* - 120 sec. delay - 2 Post H*
10 11 12 13	machine cut machine cut machine cut hot saw cut	Cr-Mo & Cr-Mo Cr-Mo & Cr-Mo Cr-Mo & Cr-Mo Cr-Mo & Carbon	9 PH (2.5 sec. on, 1 sec. off) - forging - 150 sec. delay (Shear) - 2 Post H* - 140 sec. delay - 2 Post H*

PH - Preheat; Post H - Post Heat, *(5 sec. on, 2 sec. off)

TABLE 10: Experimental Welding of Cr-Mo Rail, Transcona, Manitoba, Aguust 23, 1977

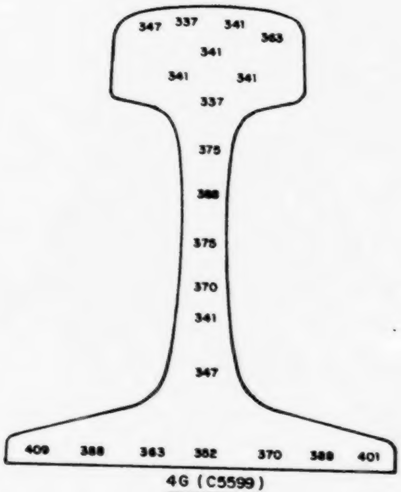
347
337
341
363
341
341
341
337
375
388
375
370
341
347
409
388
363
382
370
388
401

4G (C5599)

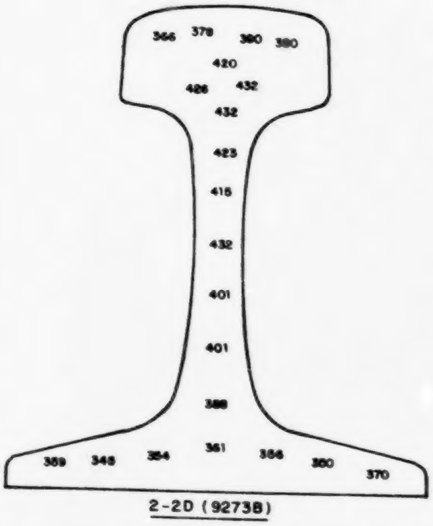
366
379
390
380
420
426
432
432
423
416
432
401
401
388
369
348
354
361
386
380
370

2-2D (92738)

Figure 1 - BRINELL HARDNESS PATTERNS OF ALGOMA Cr-Mo RAIL SAMPLES NO. 4G AND 2-2D.

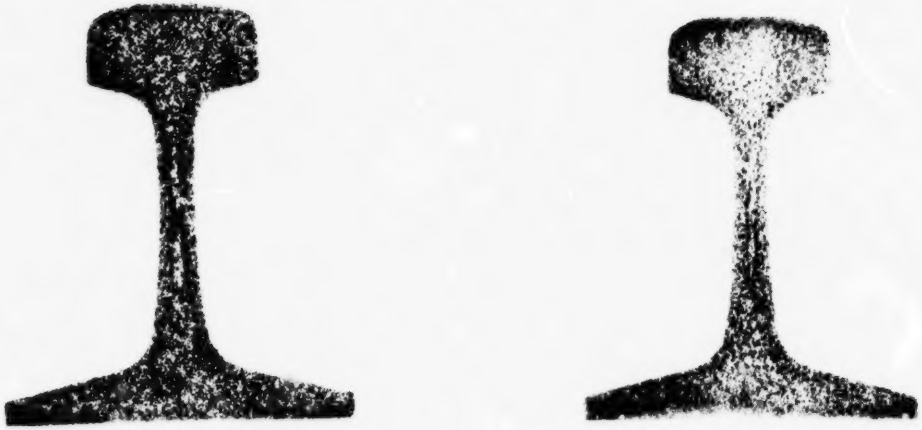

Rail No. 20

Rail No. 17

FIGURE 2a: Sulphur Prints of Samples from Heat C5599

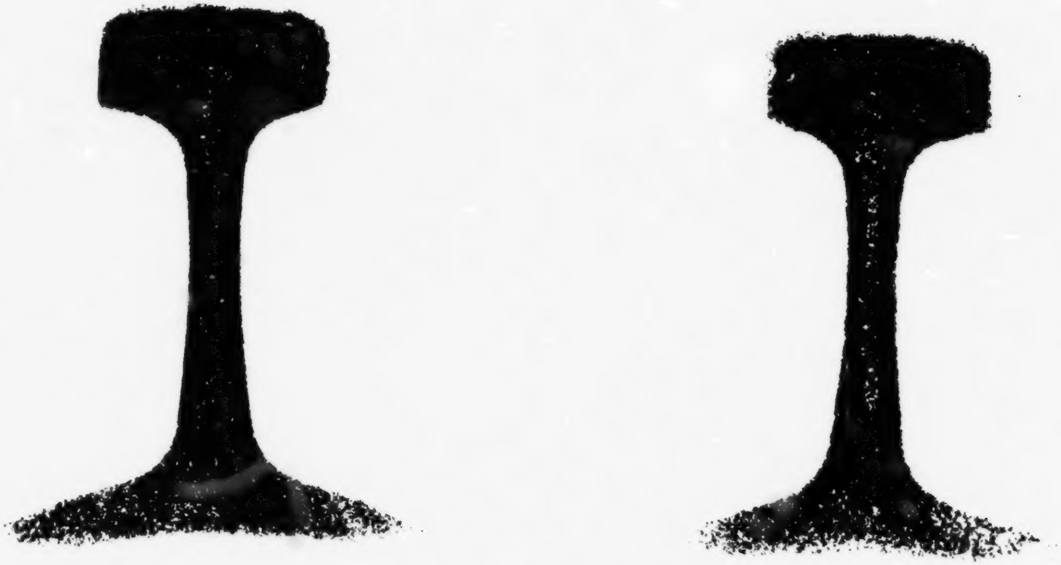

Rail No. 2-2-D

Rail No. 4-6-D

FIGURE 2b: Sulphur Prints of Samples from Heat 9273B

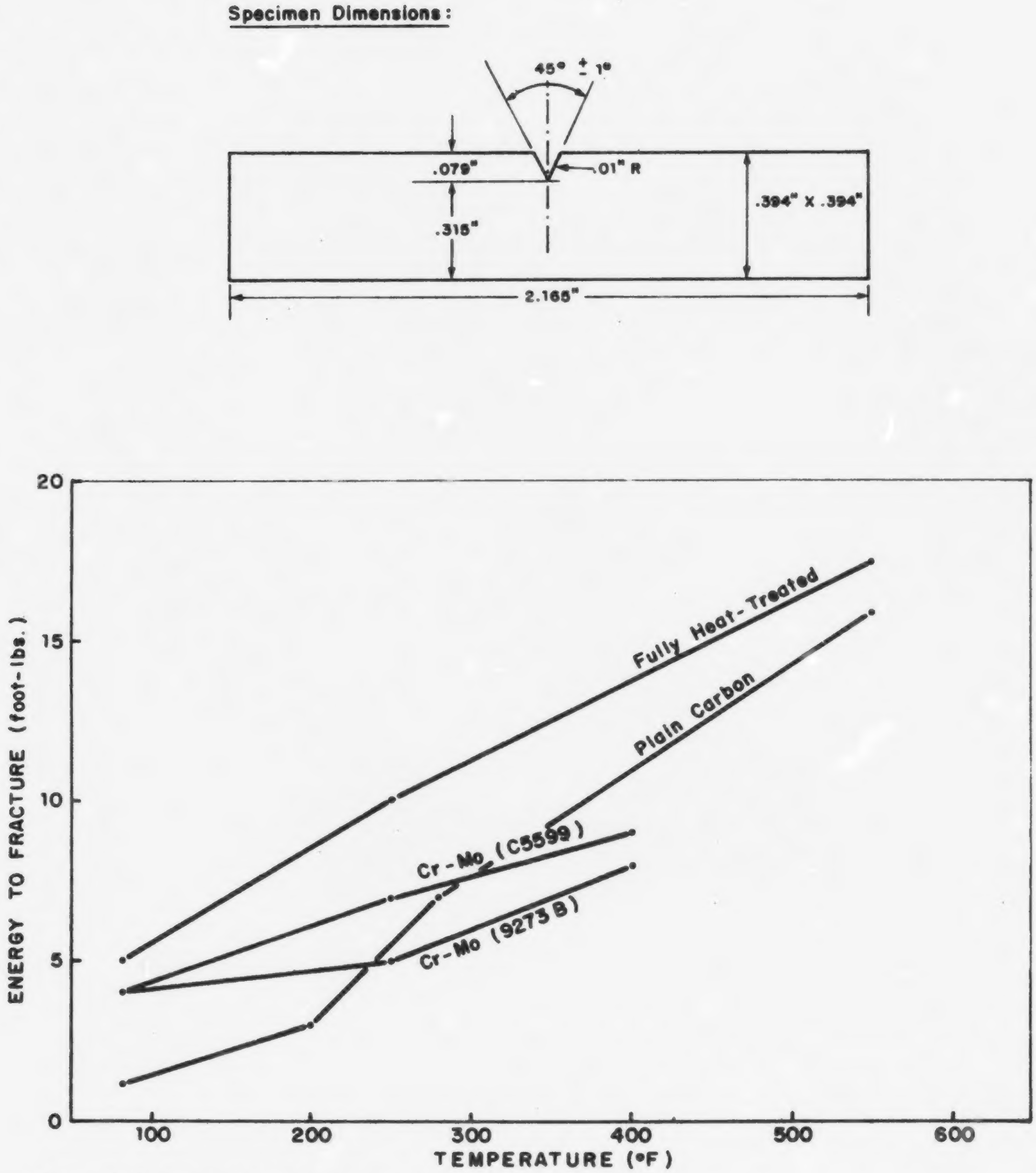

Note: Each data point is an average of at least four specimens.

Figure 3- CHARPY V-NOTCH IMPACT ENERGY VS TEMPERATURE OF FULLY HEAT-TREATED PLAIN CARBON AND Cr-Mo RAIL SPECIMENS.

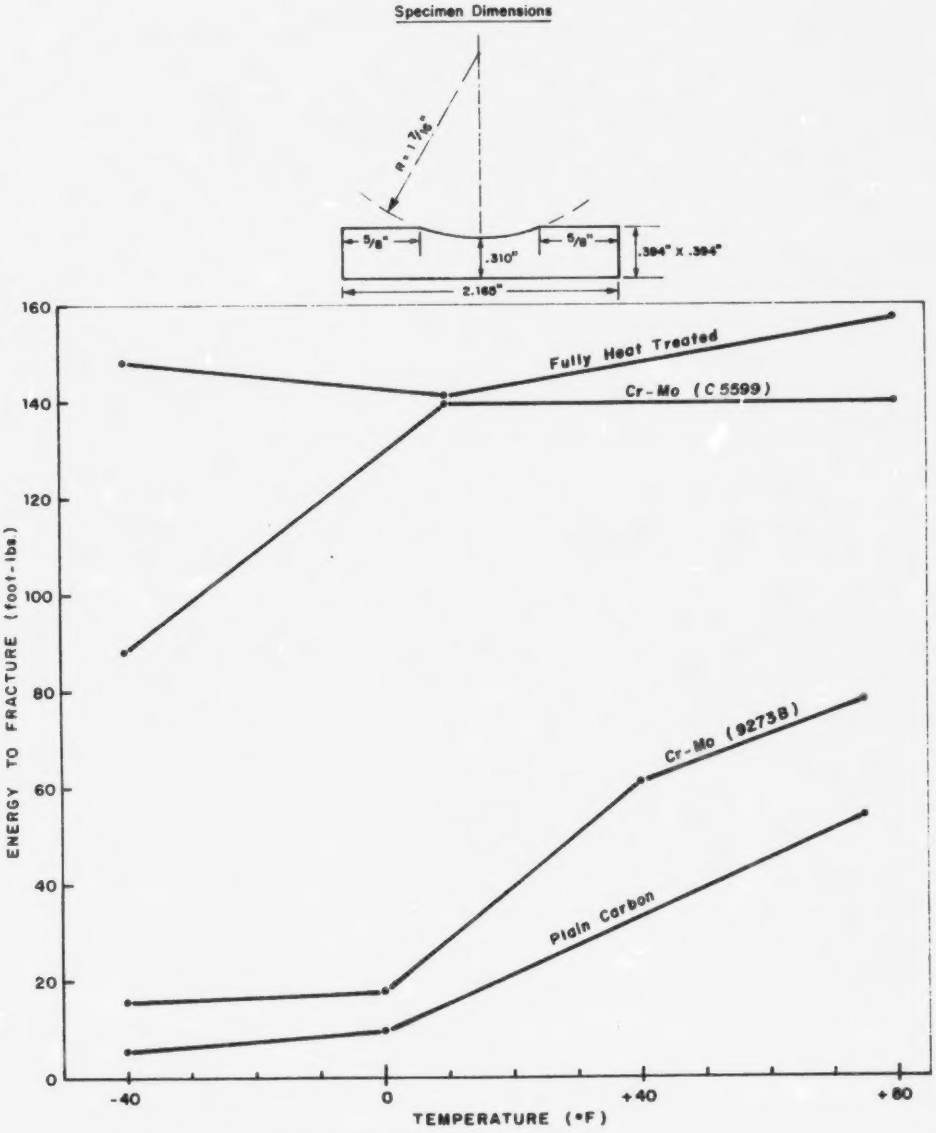

Note: Each data point is an average of at least four specimens.

Figure 4 - CHARPY UNNOTCHED IMPACT ENERGY VS TEMPERATURE OF FULLY HEAT TREATED, PLAIN CARBON AND Cr-Mo RAIL SPECIMENS.

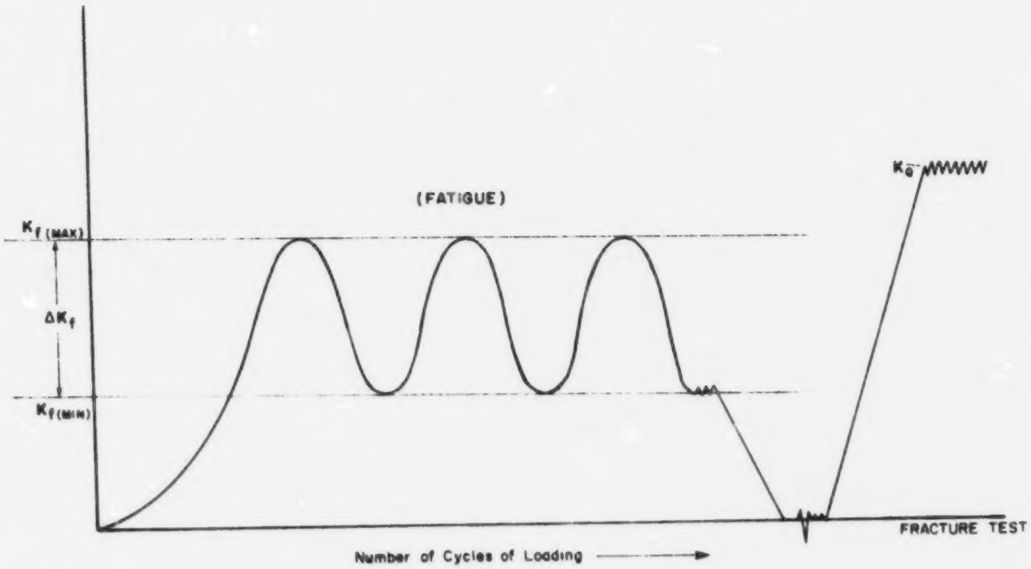
(FATIGUE)
$K_{f(MAX)}$
ΔK_f
$K_{f(MIN)}$
K_Q
FRACTURE TEST
Number of Cycles of Loading

Figure 5- RELATION BETWEEN $K_{(MAX)}$, ΔK FATIGUE AND K_Q

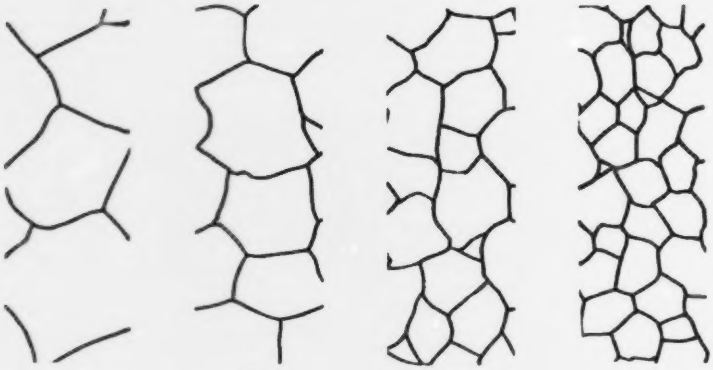

No. 1
Up to 1½ Grains

No. 2
1½ to 3 Grains

No. 3
3 to 6 Grains

No. 4
6 to 12 Grains

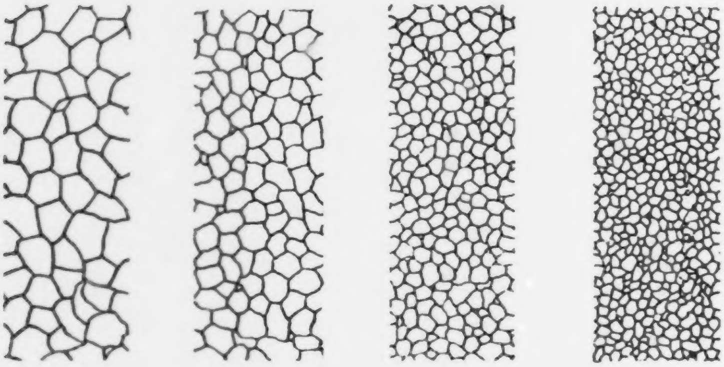

No. 5
12 to 24 Grains

No. 6
24 to 48 Grains

No. 7
48 to 96 Grains

No. 8
96 Grains and more

Figure 6 - ASTM GRAIN SIZE CHART. GRAIN SIZE MEASURED AT 100 MAGNIFICATIONS.

Source: Johnson & Weeks Metallurgy American Tech Soc. 1977 (5TH Edition)

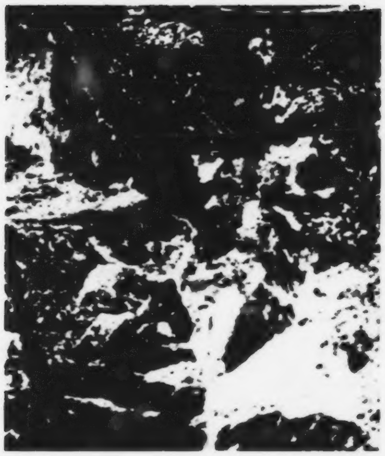

75-2075 4% Picral X500

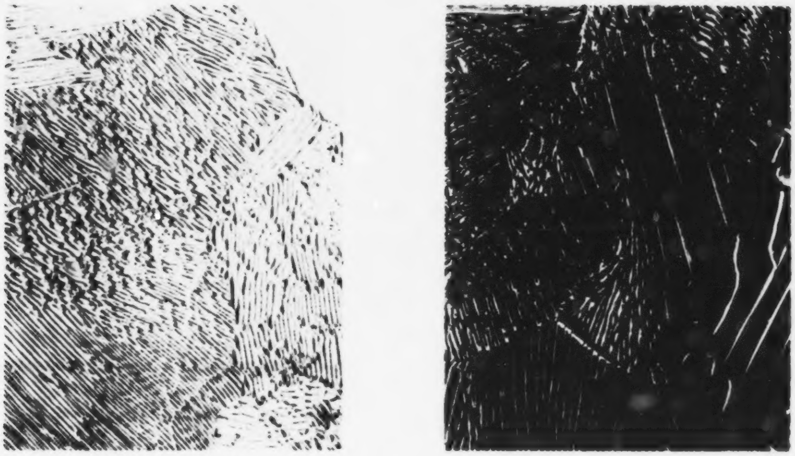

G3982 4% Picric Acid and 1% Nitric Acid in Ethanol X5000

G3983 4% Picric Acid and 1% Nitric Acid in Ethanol X5000

FIGURE 7: Optical and Replica Electron Micrographs of the Longitudinal Head Section of Algoma Cr-Mo Rail 4G (Heat C5599). Hardness at location of metallographic Sample 341 HB.

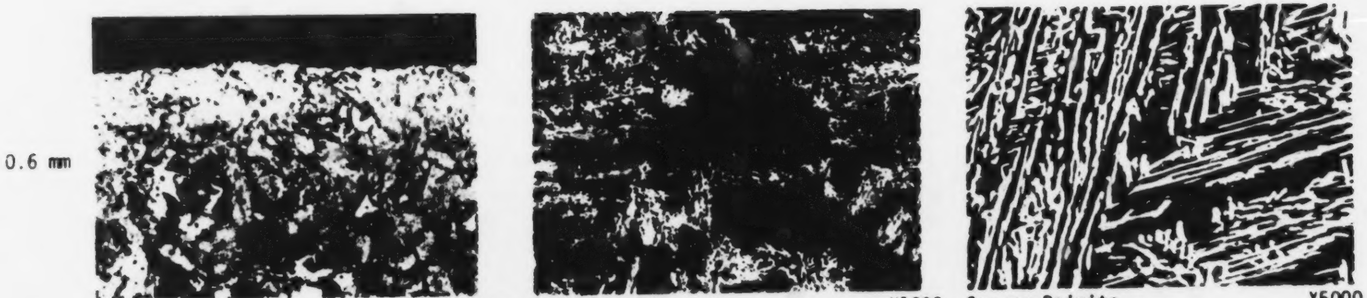

0.6 mm Below Surface-100% Bainite X500 100% Bainite X1000 Coarse Bainite X5000

5 mm Below Surface-50% Bainite X500 Bainite & Transitional Pearlite X1000 Transitional Pearlite X5000

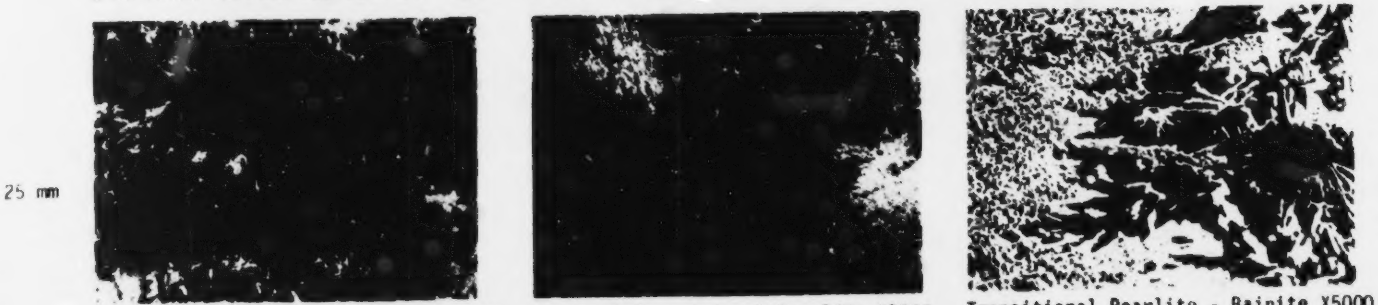

25 mm Below Surface-50% Bainite X500 Bainite & Transitional Pearlite X1000 Transitional Pearlite - Bainite X5000

FIGURE 8: Micrographs of Rail Head Sample of Heat 9273B

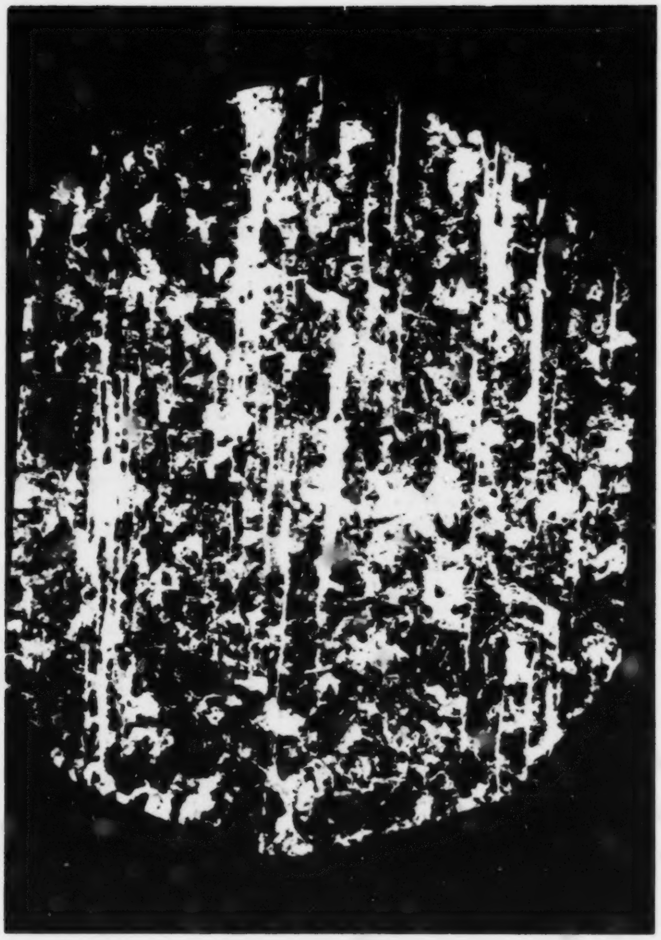

FIGURE 9a: Optical Micrograph (X100) of White Streaks Observed in the Web of a Rail Sample from Heat 9273B

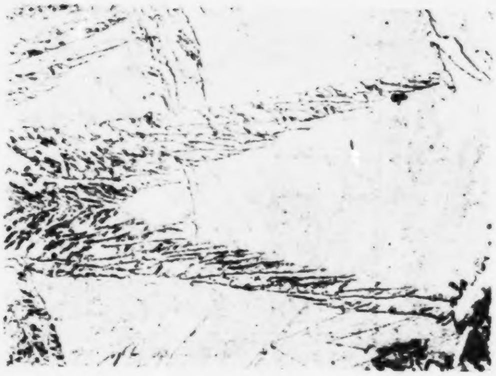

X11200

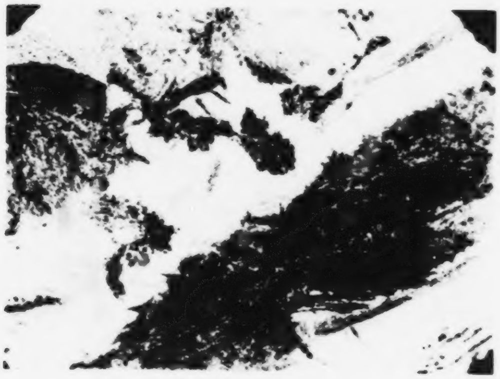

X950

FIGURE 9b: SEM Micrographs of White Streaks Observed in the Web of a Rail Sample from Heat 92738

Ref: Karl-Erik Thelming: Steel and It's Heat Treatment. Bofors Handbook, Butterworths, 1975 pp 134-5.

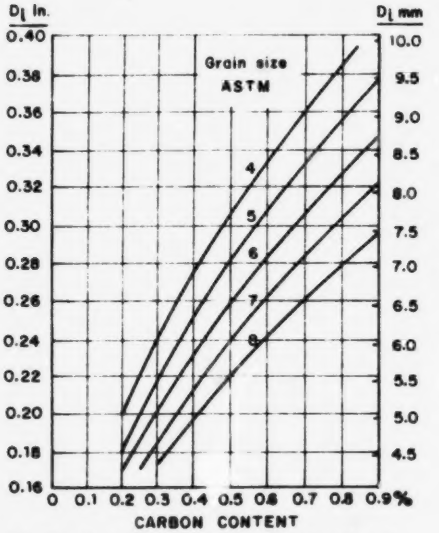

(a) The ideal critical diameter as a function of the carbon content and austenite grain size for plain carbon steels (after Grossman)

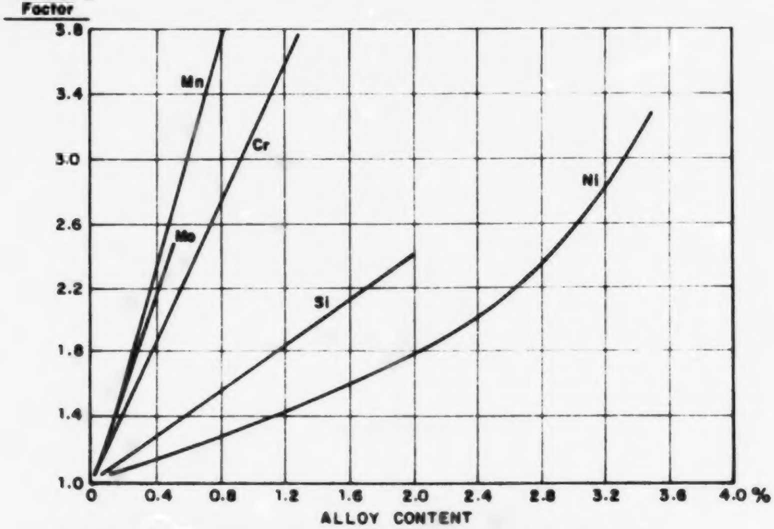

(b) Multiplying factors for different alloying elements for hardenability calculations (after AISI)

Figure 10- GRAPHS USED FOR CALCULATION OF D_I Values

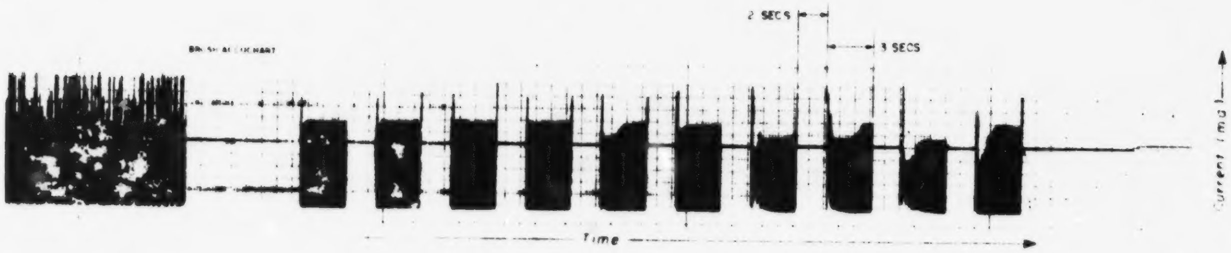

FIGURE 11: Current Records for Experimental Weld of Heat 9273B (Each Vertical Line Represents 0.2 second)

Figure 12- FLASH-BUTT WELD COOLING CURVES

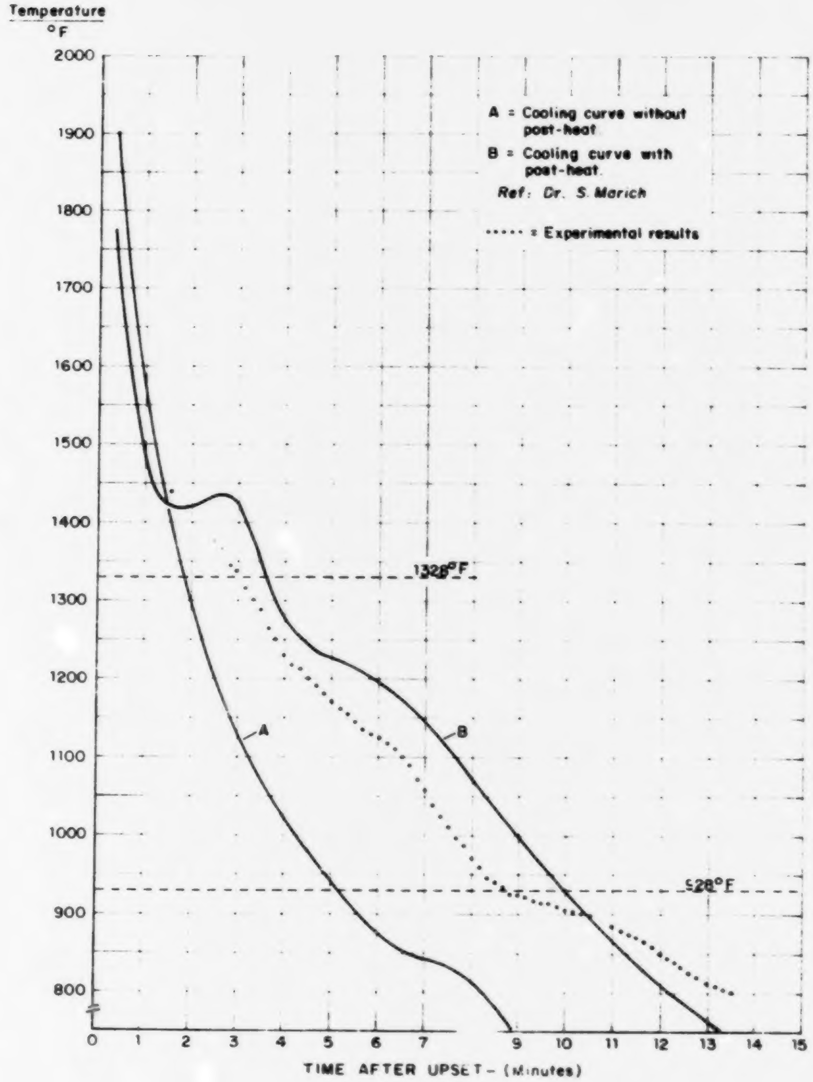

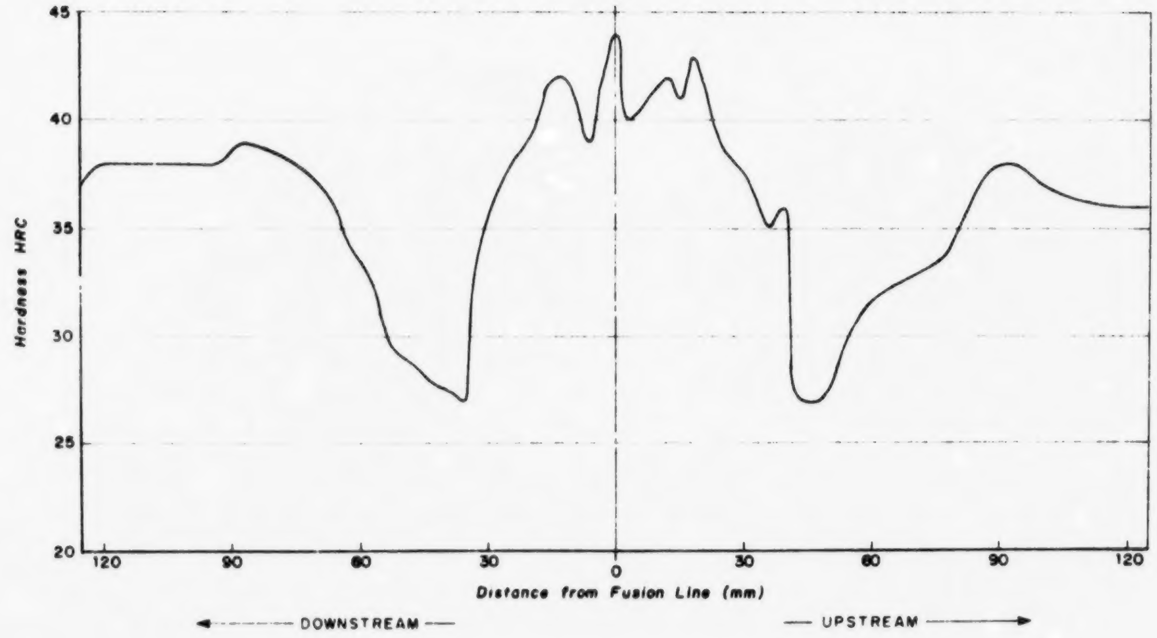

Figure 13- HARDNESS PATTERN FROM THE RAIL HEAD OF WELD 1 (49)

J Kalousek and L M Yee

Measurement of Angle-of-Attack With Laser

ABSTRACT: An angle-of-attack is formed when a wheelset of a truck deviates from the radial position whilst negotiating a curve. The angle-of-attack is defined as the enclosed angle between the vertical plane of the wheel and the vertical plane of the rail. When a critical angle-of-attack is exceeded, contact occurs between the flange (s) of the wheel (s) and the gauge side of the rail (s). Wear on the outside flange of the wheel (s) and the gauge side of the rail (s) is a function of lateral force, hardness of rail and wheel, lubrication and relative sliding velocity. Relative sliding velocity is greatly influenced by the magnitude of the angle-of-attack.

Wear of both wheels and rails has prompted development of new designs of trucks for rail vehicles. Curving characteristics of old and new truck designs can be best established in curving performance tests, in which the lateral forces are usually determined by either instrumented rail, instrumented tie plate, instrumented wheel or any combination of these. To supplement data for such a test, a method of measuring the angle-of-attack of wheelsets on curves was developed.

The method of measuring angle-of-attack utilizes low-powered, low-cost lasers with photo-electric sensing circuitry. The lasers and detectors are carefully aligned perpendicular to the rails. Figure 1 (a) shows the alignment of the lasers and detectors. Interruption of each laser beam causes a change of state in the signal of each detector and the signals are recorded on separate channels on an analogue magnetic tape recorder. The angle-of-attack is derived according to the formulae and signal traces presented in Figure 1 (b).

The experimental design involves the use of an analogue tape recorder for recording the signals from the photocells. These signals trigger time counters measuring the time interruption intervals from which the angles can be calculated manually. This experimental design will be modified to include a micro-computer for calculating the angles-of-attack instantaneously and a printer to print the results in real time.

The angle-of-attack measuring system should prove invaluable in the study of wheelsets of trucks negotiating curves and also provide a means of comparison between various truck designs. The measuring system can also be used as a maintenance tool to detect cars that have wheelset(s) with large angles-of-attack and are acting as "bad performers" in a fleet.

Preliminary results from tests are very encouraging. The apparatus is capable of measuring angles-of-attack up to several degrees with accuracy of 2.5 minutes.

1.0 INTRODUCTION

Wear of both wheels and rails have prompted development of new designs of trucks for rail vehicles. Curving characteristics of old and new truck designs can be best established in curving performance tests, in which the lateral forces are usually determined by either instrumented rail, instrumented tie plate, instrumented wheel or any combination of these. To supplement data for such a test, a method of measuring angle-of-attack was developed. Angle-of-attack is formed when the axis of the wheel-set do not align radially to the curve while negotiating the curvature.

Various methods of measuring angle-of-attack have been exploited by other researchers. One method utilized strain gauges applied to the rails evaluating the time difference between the shear strain records caused by each wheel of a wheel-set. The major drawback of such a system can be attributed to the longitudinal shifting of the rails due to traction, braking or rolling friction forces acting along the rail. The quantitative measurement of such a rail shifting is difficult, particularly on curves.

Another method employed collimated beam incandescent lamps with photo-electric sensors. The method has been under development for several years. The apparatus proved difficult to align and may be modified in the future to permit easier alignment.

The method developed by the CP Research Department in collaboration with NRC utilizes three low-powered lasers and three photo-diode sensors and is described in the next section.

2.0 DESCRIPTION OF THE METHOD

The method developed to measure the angle-of attack utilizes the small diameter of laser beam (.04") to achieve high accuracy of the measurement.

The equipment set-up and information it yields are illustrated in Figure 1(a) and (b). Lasers 1 and 2 (Figure 1(a)) are placed next to the track structure so that their beams are aligned radially to the curve and are used to assess the actual value of angle-of-attack. The detectors are placed in the middle of a track structure and collect the light from lasers. Providing the flange, which blocks off the light and forms a "pulse" in a trace of the detector, is round, the axis of that wheel is in the center of the pulse it causes.

The third laser is needed to evaluate the instantaneous speed of the wheel-set, the knowledge of which is necessary to convert the time signals received by detectors into distances. The calculations of the angle-of-attack are then performed according to formulae presented in Figure 1(b). The time interval for "d" corresponds to a time delay between the passing of the centre of one wheel disc to the other wheel disc of a wheel-set. The period "T" is the time required to travel one inch providing the lasers 2 and 3 are 2.5" apart. The formula for "T" is written for the direction of travel as shown in Figure 1(a). For the opposite direction of travel, subscripts 2 and 3 must be interchanged.

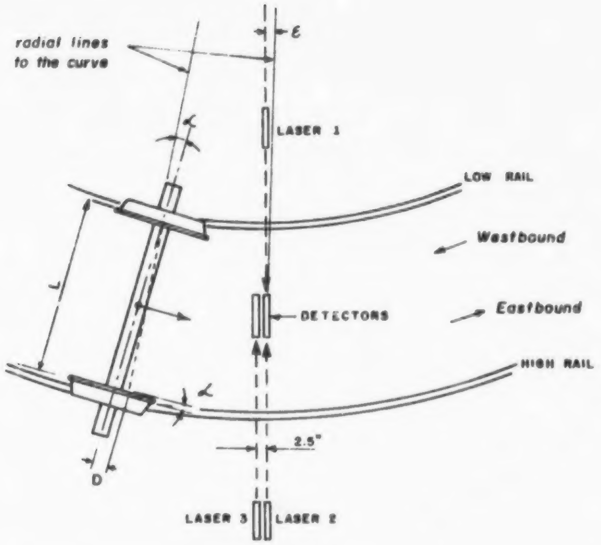
radial lines
to the curve
ε
∠
LASER 1
LOW RAIL
Westbound
L
DETECTORS
Eastbound
HIGH RAIL
∠
2.5"
D
LASER 3
LASER 2

(a) Sketch showing alignment of Lasers and Detectors

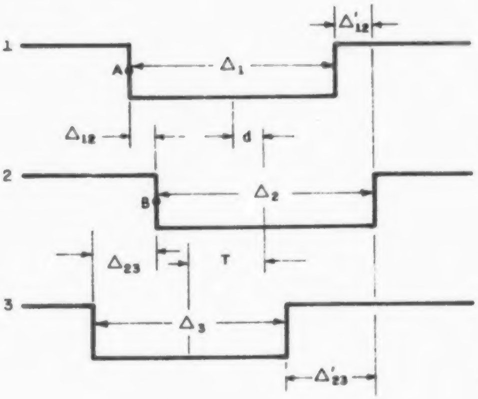
Δ'_{12}
1
A
Δ_1
Δ_{12}
d
2
B
Δ_2
Δ_{23}
T
3
Δ_3
Δ'_{23}

d = time interval corresponding to angle-of-attack

$$= \frac{\Delta_2}{2} + \Delta_{12} - \frac{\Delta_1}{2} \text{ [msec]}$$

T = time for 1" of travel

$$\frac{\left[\left(\frac{\Delta_2}{2} + \Delta_{23}\right) - \frac{\Delta_3}{2}\right]}{2.5} \left[\frac{\text{msec}}{\text{in}}\right]$$

$$D = \frac{d}{T} \text{ [inch]}, \quad \tan\angle = \frac{D}{L} \text{ [rad]}$$

$$\angle = \text{Angle-of-Attack} = \left(\tan^{-1}\left(\frac{d}{LT}\right)\right) \times 60 \text{ [min]}$$

(b) Signal Traces and calculation of Angle-of-Attack

Figure 1

3.0 DESCRIPTION OF TEST EQUIPMENT AND TEST SITE

The test equipment consisted of three Spectra-Physics model 136 helium-neon lasers complete with individual power supplies. Each laser had precision slots for mounting.

The detector tubes were designed to be of similar shape as the lasers. This permitted the lasers and detectors to be mounted on similar mounting apparatus. Each detector tube had a 3 mm. hole at the center of a cap fitted at each end. Discs can be inserted behind the caps to change the diameter of the holes.

The lasers and detectors were mounted on machined mounts which permitted vertical and lateral adjustment as shown in Figure 2(a) and 2(b).

A low voltage dc power supply was used to supply power to the sensing circuitry. A Philips multi-channel analogue recorder was used to record the signals from the photodiodes.

The above described equipment has been used to measure the angle-of-attack for the first time at the CN's Montreal yard. The general layout of the test site is shown in Figure 3. The north leg of the "WYE" with a curvature of 5 degrees was instrumented for the test. An instrument trailer near the test site was used to house data recording and power supply equipment.

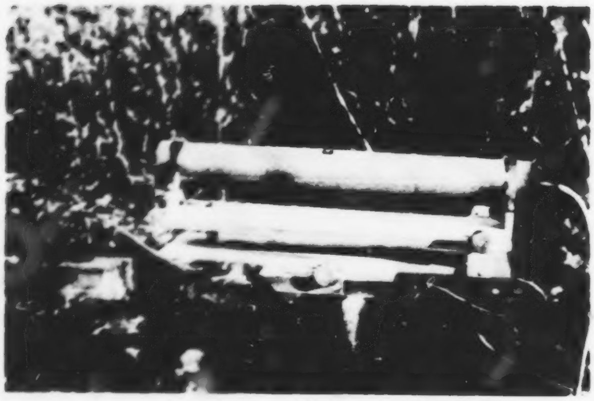

FIGURE 2(a).   LASER WITH MOUNT

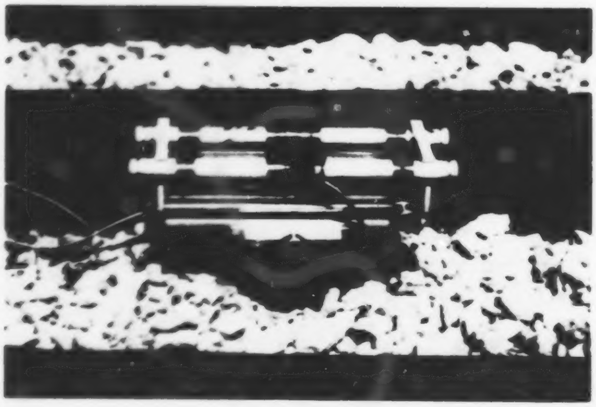

FIGURE 2(b).   DETECTORS WITH MOUNT

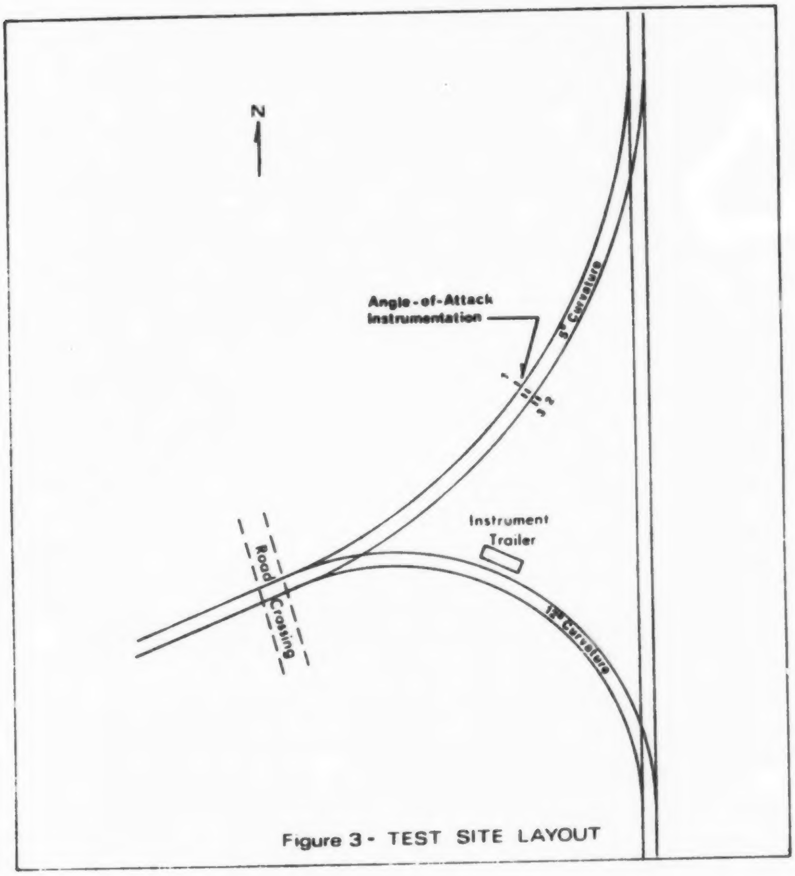
N
Angle-of-Attack Instrumentation
8° Curvature
1
2
3
Instrument Trailer
Road Crossing
12° Curvature

Figure 3 - TEST SITE LAYOUT

4.0 TEST PROCEDURE

The procedure to establish a radial line in a curve utilized a CN test rig for plotting two points of this line on rail running surfaces. The rig consisted of two square aluminum rods with a peg at one end of each rod, and attached together by a stranded steel wire with the center of the wire marked. The pegs to which the wire was attached insured contact at the gauge side of the rail at points B and C shown in Figure 4. Point D was determined by the intersection of two equidistant lines from points B and C. Another rod was used to connect points D and A together to mark point E on the gauge side of the rail. This particular procedure was used for this test but there are a number of variations which may be adopted.

A two-foot long 2 1/4 inch diameter steel pipe was driven into each of the locations F, G and H, shown in Figure 4, to permit mounting of the lasers and detectors. Alignment of the lasers must be such that the beams emanating from both lasers F and H, simultaneously intersect points D and E. This can be best accomplished by first aligning one of the lasers so that the beam is actually "touching" the surfaces of both rails at points D and E. The second laser is positioned in such a way, that the beam of the first laser illuminates its orifice and the same alignment procedure is then repeated for this laser. After the alignment of two main lasers, the light beams are then raised one millimeter above the running surface of the rails by means of vertical adjustment screws. Finally, the detector unit is placed into the center of the track and aligned to receive the beams from all three lasers. The detectors are then connected to a tape recorder, which records the signal of each detector on a separate channel.

The test train consist is illustrated in Figure 5. It contained a van, a locomotive, a standard reference car and a test car which had retro-fit self-steering trucks.

Runs No. 1 to 20 were done with car no. 330077 leading in eastward direction. The train was then wyed for the test Runs No. 21 to 40. Runs 41 to 46 were performed after grease was applied manually to the rail running surfaces. Grease is commonly applied to curves in Western Canada. Therefore, a large quantity of grease was applied manually to both high and low rail heads, and gauge faces to determine its effects on angle-of-attack. In all the runs, odd numbers denote eastward bound and even numbers denote westward bound. The consecutive test runs alternated between eastward and westward bound movements.

Acquisition of the data from the tape recorder is normally obtained via Hewlett-Packard frequency counters. These counters, in the time interval measure mode, allow the accurate assessment of time pulses $\Delta 1$, $\Delta 2$, $\Delta 3$, $\Delta 12$ and $\Delta 23$. However, the counters were under repair and a method utilizing a dual-trace Tektronix oscilloscope with a time interval counter was used. An electronic piece of equipment called "micro-viewer" was connected between the tape recorder and oscilloscope. This "micro-viewer" enabled one to view a small section of the tape recording on the oscilloscope at a speed reduced by the factor of 16. The two signals originating from the main lasers were displayed simultaneously on the oscilloscope as shown in Figure 1(b) as signal traces 1 and 2. An intensified spot on each signal trace identified a particular instant of time on both signals. With the intensified spot set at position A, the LED (Light Emitting Diode) display time counter on the scope was reset by pushing the reset button. The intensified spot was then moved to position B and, the reading of the measured time interval (in milli-seconds) was taken. This procedure was used to measure the pulse widths and difference between start of pulses.

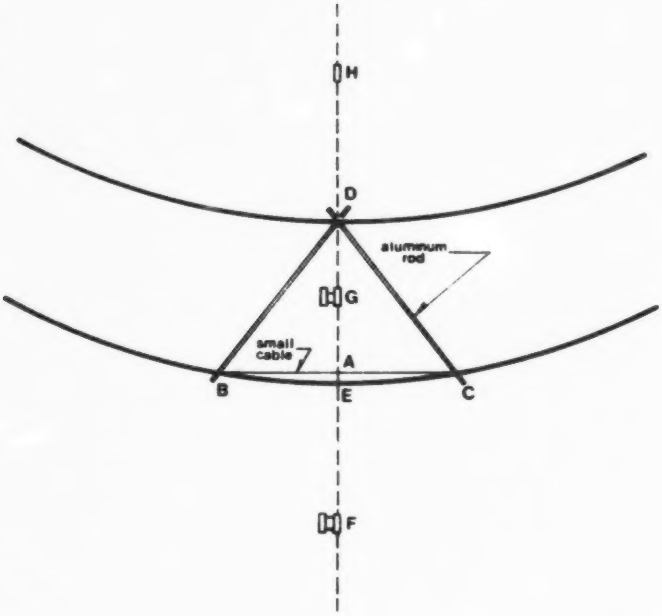
H
D
aluminum rod
G
small cable
A
B
E
C
F

FIGURE 4: ALIGNMENT PROCEDURE OF LASERS AND DETECTORS

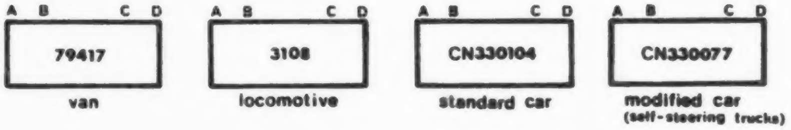
A B C D
79417
van
A B C D
3108
locomotive
A B C D
CN330104
standard car
A B C D
CN330077
modified car
(self-steering trucks)

NOTE: TRUCK CD OF CN330077 LEADING FOR EASTWARD MOVEMENT BEFORE WYEING OF TRAIN

FIGURE 5: TRAIN CONSIST

5.0 ANALYSIS OF TEST RESULTS

The experimental data obtained from the test runs are tabulated in Table 1. Average values of angle-of-attack are given in Table 2. The measured angles-of-attack varied in intervals of -16 to +38 minutes of arc for a standard car like CN 330104 and -16 to +14 minutes of arc for a modified car (CN 330077).

It should be realized that the measured values of angle-of-attack are not the actual values of angle-of-attack since several unavoidable effects influence the values of angle-of-attack measured in the field.

The most pronounced of these possible effects are:

a) offset angle "ε",
b) effects of track irregularities,
c) effects of acceleration.

5.1 Offset Angle

The presence of the offset angle "ε" is due to practical limitations imposed in the field alignment procedures described in Section 4.0. The offset angle may be defined as a deviation between the line to which the lasers are aligned and the true radial line of the curves. Taking into consideration Figure 1(a), the offset angle "ε" is additive to the true angle-of-attack for runs in one direction and subtractive for runs in the opposite direction.

Assuming, then, in Figure 1(a) the wheelset runs with a positive angle-of-attack with respect to the radial line, the measured angle-of-attack can be expressed as:

$\alpha_E' = \alpha_E + \varepsilon$ for eastbound runs
$\alpha_W' = \alpha_W - \varepsilon$ for westbound runs

where α_E', α_W' - measured angles-of-attack for eastbound and westbound runs respectively.

α_E, α_W - true angles-of-attack

ε - offset angle.

The average offset angles for the leading and trailing axles of each truck as given in Table 3 may be calculated by the formula:

$$\varepsilon_{av_{axle}} = \frac{\alpha_{E_{1_{av}}}' - \alpha_{W_{1_{av}}}' + \alpha_{E_{2_{av}}}' - \alpha_{W_{2_{av}}}'}{4}$$

It may be difficult to assess the offset angle "ε" and measured angle-of-attack values of wheelsets from trains running in one direction only. The most accurate evaluation of the offset angle can be achieved by wyeing of the same test consist. Then, the average offset angle may be calculated according to the following formula:

$$\varepsilon_{av} = \frac{\sum_{i=1}^{n/2} \alpha_{E_i}' - \sum_{i=1}^{n/2} \alpha_{W_i}'}{n}$$

It may be possible to statistically evaluate the value of offset angle by assuming the large number of wheelsets travelling in both directions, however, the accuracy of such method would be subjected to statistical error. The asymmetrical properties in a truck may cause a skew running of the whole truck. This assymmetry of trucks remains constant within certain limits and usually cancels in the computation of angle "ε" due to the fact that the train was wyed. Table 3 gives the values of offset angle "ε" for the leading and trailing axles of each truck. It should also be noted that each truck was treated as a separate entity in the computation of "ε".

The offset angles were within a narrow tolerance for the standard truck indicating the permanency of the asymmetrical characteristics in the truck. The offset angles for the self-steering trucks varied and thus could not be used in determining "ε". A possible explanation of the behaviour of the self-steering trucks is that it may be caused by the profiled A wheels which results in increased vertical movement of wheelsets due to the inherently high effective conicity of profile A. Vertical movement induces errors in the measured angle-of-attack as will be explained in the latter part of this section.

Average corrected values of angle-of-attack are given in Table 4. Average differences in angle-of-attack between leading and trailing axles are given in Table 5.

The results indicate that the angles-of-attack are larger for the standard trucks than the self-steering trucks both before and after manual lubrication of the rails by the method described on page 8. On standard trucks the angle-of-attack differential between the leading and trailing axles is greater than that of the self-steering trucks. The application of grease to the rails increased the angle-of-attack on both types of trucks. Also, after lubrication of the rails, the difference in angles-of-attack between the two types of trucks are not as pronounced. Greasing the rail also increased the difference in angle-of-attack between the leading and trailing axles of the self-steering trucks substantially.

5.2 Effect of Track Irregularities on the Angle-of-Attack

The measuring method used is based on the principle that the angle-of-attack is formed by the offset distance between the centre of the wheel discs of a wheelset. This offset distance was taken as the displacement between the centre of the signal pulses of the two wheel discs. Where differential slope exists on rails due to track irregularities, an angle-of-attack will appear when in actuality no angle-of-attack exists. The amount of error this phenomena would introduce into the measurement of angle-of-attack depends on the degree of differential slope. For example, an 0.87 percent differential slope introduces the error of 10.3 minutes. Results from track recorder car measurements indicate that the occurrence of a differential slope of 0.8 percent is quite common, and therefore the alignment of the actual test site must be carefully considered prior to installation of the angle-of-attack equipment.

It should be also noted, that the method used for measuring angle-of-attack is sensitive to the vertical motion of the wheel over track irregularities. The error results when both wheel discs block the respective lasers but one wheel disc is raised or lowered due to track irregularities before wheel discs are clear of the lasers. This situation is somewhat similar to that of track twist described above and for practical purposes should be considered as an integral part of track irregularities.

5.3 Effect of Acceleration

The angle-of-attack measurement method is also sensitive to acceleration. Vertical acceleration sustained over a distance will have an effect of changing the height at which the lasers are blocked by the wheel discs. This phenomena is very much similar to the vertical motion discussed above. An acceleration of 0.1G sustained for an interval of one foot at 10 mph will induce a change of 8.4 minute angle of the angle-of-attack.

6.0 OUTLINE OF MODIFICATIONS TO TEST EQUIPMENT AND TEST PROCEDURE

Detectors

It was felt that the photo-diode used for detection was sufficiently fast in response for the speed range of this test. However, the photo-diodes will be changed to permit increased speed level.

Data Acquisition Equipment

The data compiled for this test was done manually. A micro-computer such as the Intel 8080 or 8085 may be interfaced with the counters and recorder to determine the angle-of-attack. A printer may be attached to the micro-computer for hard copy output. Buffer memory may be utilized where necessary to store data either before or after computation by the micro-computer.

It was felt that commercial counters may be the solution for counting time interval. Original design counters may require troubleshooting and debugging.

Possible Data Acquisition Equipment

3 - counters
1 - micro-computer
1 - printer - eight digit or less
1 - oscilloscope

Modifications to Test Procedure

Future tests should utilize counters, and storage of the data in digital form either on magnetic tape or in a computer memory to increase accuracy and reduce error introduced by recording equipment.

Better accuracy may be attained by measuring $\Delta 12$ and $\Delta 12'$ (Figure 1 (b)) and using the following formula in determining "d" (Figure 1 (b)).

$$\text{"d"} = \frac{\Delta 12 + \Delta 12'}{2}$$

Similarly, "T" could be determined by measuring $\Delta 23$ and $\Delta 23'$ (Figure 1 (b)) and using the following formula.

$$\text{"T"} = \frac{\Delta 23 + \Delta 23'}{2}$$

7.0 CONCLUSIONS

The technique utilizing the lasers and detectors appears to be a viable method for measuring angle-of-attack.

The equipment may be further modified to calculate the angle-of-attack at a measurement location as a permanent installation, for rolling stock maintenance management by pointing out the bad truck performers in a fleet.

The instrument suitably modified to include a microcomputer may be used as a scientific instrument for truck evaluation.

Further work is required to determine the practical resolution to which the angle-of-attack may be measured.

TABLE 1

MEASURED ANGLES-OF-ATTACK

TEST SERIES NO. 1

		EASTWARD		WESTWARD	
		RUN NO. 1		RUN NO. 2	
	Axle	Speed (mph.)	α'_E (min.)	Speed (mph.)	α'_W (min.)
CN 330104 STANDARD	A	14.7	3.9	12.5	5.8
	B	14.3	37.6	12.2	- 9.9
	C	14.0	9.9	11.7	12.7
	D	14.1	32.4	11.7	-10.4
CN 330077 MODIFIED	A	13.0	8.1	11.5	- 4.5
	B	13.5	13.2	11.5	-10.4
	C	13.1	- 3.5	11.1	3.9
	D	12.8	5.7	10.9	-15.5
		RUN NO. 5		RUN NO. 6	
CN 330104	A	15.4	10.9	10.9	4.8
	B	15.2	22.9	11.1	-11.8
	C	14.8	7.9	10.4	12.9
	D	14.6	33.6	10.5	-11.6
CN 330077	A	14.6	6.5	10.7	- 2.5
	B	14.7	7.8	10.7	- 6.1
	C	14.5	6.4	10.6	0.2
	D	14.7	7.8	10.4	-13.9
		RUN NO. 9		RUN NO. 10	
CN 330104	A	13.7	4.9	10.3	1.6
	B	13.5	25.1	10.1	-14.0
	C	13.3	8.2	10.0	13.9
	D	13.6	32.0	10.0	-10.8
CN 330077	A	13.3	9.5	9.8	- 5.0
	B	12.7	11.2	10.1	- 8.9
	C	13.6	5.5	9.7	- 0.3
	D	13.3	9.4	9.7	-15.9

		EASTWARD		WESTWARD	
		RUN NO. 13		RUN NO. 14	
	Axle	Speed (mph.)	α'_E(min.)	Speed (mph.)	α'_W(min.)
CN 330104	A	13.3	3.5	10.7	1.9
	B	13.4	22.9	10.7	-13.7
	C	13.4	5.9	10.5	14.4
	D	13.1	35.0	10.2	- 9.7
CN 330077	A	13.0	5.3	9.9	- 4.6
	B	13.0	8.1	10.0	- 7.1
	C	12.8	4.8	10.2	0.0
	D	12.7	7.9	10.0	-13.6
		RUN NO. 17		RUN NO. 18	
CN 330104	A	13.2	8.2	11.4	5.1
	B	13.4	21.7	11.3	-16.0
	C	13.0	5.8	11.2	6.0
	D	12.9	31.2	11.3	-16.0
CN 330077	A	13.1	6.0	11.4	- 8.3
	B	13.2	8.2	11.4	- 7.9
	C	12.8	7.9	11.3	0.4
	D	13.1	8.1	11.3	-15.6

SERIES NO. 2

		RUN NO. 21		RUN NO. 22	
CN 330104	A	14.3	25.5	11.2	-12.7
	B	14.2	7.3	11.2	5.4
	C	14.5	19.6	11.1	- 8.4
	D	14.7	12.2	11.2	1.4
CN 330077	A	14.7	11.7	11.0	-12.6
	B	14.8	5.3	11.5	7.7
	C	15.3	6.8	11.2	- 8.6
	D	14.9	6.9	11.3	- 1.8

		EASTWARD		WESTWARD	
		RUN NO. 25		RUN NO. 26	
	Axle	Speed (mph.)	α'_E (min.)	Speed (mph.)	α'_W (min.)
CN 330104	A	13.3	24.8	11.4	-14.2
	B	13.4	8.3	11.6	8.6
	C	13.8	22.8	11.6	- 9.4
	D	13.7	11.0	11.6	- 1.9
CN 330077	A	14.1	9.0	11.7	-11.4
	B	14.1	7.5	11.3	11.6
	C	14.3	8.9	12.0	- 9.8
	D	14.3	10.2	12.3	- 2.2
		RUN NO. 29		RUN NO. 30	
CN 330104	A	14.6	24.1	11.4	-15.8
	B	14.9	7.2	11.7	9.6
	C	15.3	20.6	11.5	- 5.3
	D	14.8	11.8	11.7	- 3.5
CN 330077	A	15.2	8.4	11.4	- 8.5
	B	15.0	7.2	11.7	1.9
	C	15.4	5.5	11.6	- 5.7
	D	15.2	10.8	11.7	- 1.5
		RUN NO. 33		RUN NO. 34	
CN 330104	A	14.6	28.5	12.4	-12.3
	B	14.5	5.9	12.2	6.0
	C	14.0	18.2	12.3	-10.9
	D	13.7	8.5	12.8	- 5.2
CN 330077	A	14.0	8.9	12.5	-12.1
	B	14.1	6.0	12.4	8.8
	C	14.1	6.7	12.9	- 8.7
	D	14.6	7.8	13.3	2.4

		EASTWARD		WESTWARD	
		RUN NO. 37		RUN NO. 38	
	Axle	Speed (mph.)	α'_E (min.)	Speed (mph.)	α'_W (min.)
CN 330104	A	14.4	23.3	10.6	-12.8
	B	14.2	7.5	10.4	1.7
	C	14.5	17.0	10.7	- 6.1
	D	14.3	11.4	10.7	- 2.5
CN 330077	A	14.6	9.3	10.8	-12.3
	B	14.8	7.4	10.5	- 0.9
	C	14.6	7.8	10.7	- 4.9
	D	14.8	10.5	10.6	- 1.9

FOLLOWING RUNS WITH RAILS LUBRICATED

		RUN NO. 41		RUN NO. 42	
CN 330104	A	14.5	30.5	9.8	- 3.7
	B	14.6	11.1	9.6	14.7
	C	14.9	24.8	10.1	- 3.2
	D	14.8	17.4	9.6	4.6
CN 330077	A	14.6	26.6	10.1	- 9.9
	B	14.9	10.0	10.1	10.8
	C	15.1	13.7	10.4	- 1.8
	D	15.1	9.6	10.1	8.1

		RUN NO. 43		RUN NO. 44	
CN 330104	A	13.4	41.8	10.5	- 2.8
	B	14.3	24.0	10.0	12.1
	C	13.3	32.2	10.4	- 1.8
	D	13.4	24.2	10.8	12.1
CN 330077	A	13.5	25.1	10.5	- 4.5
	B	13.5	11.9	10.6	10.9
	C	13.4	20.8	10.8	0.0
	D	13.6	10.9	10.8	6.7

		EASTWARD		WESTWARD	
		RUN NO. 45		RUN NO. 46	
	Axle	Speed (mph.)	α'_E(min.)	Speed (mph.)	α'_W(min.)
CN 330104	A	13.0	40.6	11.4	3.4
	B	13.4	20.9	10.7	13.4
	C	13.5	26.9	11.0	- 4.9
	D	13.3	22.6	10.7	8.2
CN 330077	A	13.6	22.5	11.1	- 6.5
	B	13.6	10.9	10.8	6.7
	C	13.9	13.8	11.0	- 2.5
	D	13.5	14.4	11.2	6.0

TABLE 2

AVERAGE VALUES OF ANGLE-OF-ATTACK

SERIES NO. 1

		EASTWARD		WESTWARD	
	Axle	Average Angle-of-Attack (min.)		Average Angle-of-Attack (min.)	
CN 330104 STANDARD	A	6.28	(- 3.87)	3.84	(13.99)
	B	26.04	(15.89)	-13.08	(- 2.93)
	C	7.54	(- 2.61)	11.98	(22.13)
	D	32.84	(22.69)	-11.7	(- 1.55)
CN 330077 MODIFIED	A	7.08	(- 3.07)	- 4.98	(5.17)
	B	9.7	(- 0.45)	- 8.08	(2.07)
	C	4.22	(- 5.93)	0.84	(10.99)
	D	7.78	(- 2.37)	-14.9	(- 4.75)

SERIES NO. 2

		EASTWARD		WESTWARD	
CN 330104 STANDARD	A	25.24	(15.09)	-13.56	(- 3.41)
	B	7.24	(- 2.91)	6.26	(16.41)
	C	19.64	(9.49)	- 8.02	(2.13)
	D	10.98	(0.83)	- 2.34	(7.81)
CN 330077 MODIFIED	A	9.46	(- 0.69)	-11.38	(- 1.23)
	B	6.68	(- 3.47)	5.82	(15.97)
	C	7.14	(- 3.01)	- 7.54	(2.61)
	D	9.24	(- 0.91)	- 1.0	(9.15)

SERIES NO. 2
(Rails Lubricated)

	Axle	EASTWARD		WESTWARD	
CN 330104 STANDARD	A	37.63	(27.48)	- 1.03	(11.15)
	B	18.67	(8.52)	13.4	(23.55)
	C	27.97	(17.82)	- 3.3	(6.85)
	D	21.40	(11.25)	8.3	(18.45)
CN 330077 MODIFIED	A	24.73	(14.58)	- 6.97	(3.18)
	B	10.93	(0.78)	9.47	(19.62)
	C	16.10	(5.95)	- 1.43	(8.72)
	D	11.63	(1.48)	6.93	(17.08)

NOTE: Values in parentheses are corrected for misalignment of lasers and detectors.

TABLE 3

OFFSET ANGLE

			Offset Angle (min.)	Average Offset Angle av. (min.)
CN 330104 STANDARD	Truck AB	Leading Axle	10.30	10.15
		Trailing Axle	10.04	
	Truck CD	Leading Axle	10.71	
		Trailing Axle	9.56	
CN 330077 MODIFIED	Truck AB	Leading Axle	4.58	6.41
		Trailing Axle	8.31	
	Truck CD	Leading Axle	3.77	
		Trailing Axle	8.98	

TABLE 4

AVERAGE CORRECTED VALUES OF ANGLE-OF-ATTACK

		Average Corrected Angle-of-Attack	
		Truck AB	Truck CD
CN 330104 STANDARD	Leading Axle	15.4 (min.)	15.5 (min.)
	Trailing Axle	-3.3	-0.3
CN 330077 MODIFIED	Leading Axle	5.0	3.7
	Trailing Axle	-1.4	-2.3

With Lubricated Rails

		Average Corrected Angle-of-Attack	
		Truck AB	Truck CD
CN 330104 STANDARD	Leading Axle	25.5 (min.)	18.1 (min.)
	Trailing Axle	9.8	9.1
CN 330077 MODIFIED	Leading Axle	17.1	11.5
	Trailing Axle	2.0	5.1

TABLE 5

AVERAGE DIFFERENCE IN ANGLE-OF-ATTACK BETWEEN LEADING AND TRAILING AXLES OF TRUCKS

	Difference in Angle-of-Attack	
	Truck AB (min.)	Truck CD (min.)
CN 330104 STANDARD	18.7	15.8
CN 330077 MODIFIED	6.4	6.0

With Lubricated Rails

	Difference in Angle-of-Attack	
	Truck AB (min.)	Truck CD (min.)
CN 330104 STANDARD	15.7	9.0
CN 330077 MODIFIED	15.1	6.4

H Ghonem and R Gonsalves

Comparative Performance of Type II Trucks

ABSTRACT: Freight car truck evaluation tests were conducted at two locations near Calgary, Alberta, in June 1978, by Canadian Pacific to determine the curving performance and high speed tracking ability of 5 "new generation" trucks.

Truck assemblies used in the program were:-

DR-1 with 'A' profile* wheels
Barber-Scheffel with 'A' profile wheels
Devine-Scales with 'A' profile wheels
Swing Motion truck with 'A' profile wheels
A3 Ride Control truck with 'A' profile wheels
Barber S-2 truck with C-PEP and 'A' profile wheels
Barber S-2 truck with Stucki Constant Contact Side Bearings and 'A' profile wheels
Barber S-2 truck with AAR profile wheels
Barber S-2 truck with 'A' profile wheels as reference base.

Curving performance tests were carried out on a 5 degree mainline track curve equipped with 78 ft. 132 lb. rail section. The test curve was instrumented with strain-gauges circuits and CN base plates at various locations to measure lateral and vertical forces during curve negotiation. The angle-of-attack a wheelset makes with the rail during curve negotiation was measured using a laser beam technique that had previously been developed by the Research Department.

The curving tests were carried out with fully loaded 100-ton "bathtub" coal cars at the curve equilibrium speed and also above and below the equilibrium speed to determine the variation of forces and the angle-of-attack measurements with speed. Each test consisted of a series of passes through the instrumented curve in each direction.

High speed stability tests were carried out on a two mile section of continuously welded 115 lb. mainline tangent track. Instrumentation applied to the test vehicle consisted of accelerometers mounted on both the axle and the body of the test cars. Video tape cameras were mounted on the test cars to obtain a visual record of truck performance.

All truck pairs were tested under 100-ton empty bathtub coal cars in 5 mph increments from 45 mph to 75 mph. During each test run the speed was held constant over the two mile test zone to record accelerometer output data and to observe the trucks through T.V. monitors.

---

* 'A' profile is a worn wheel profile developed by CN Rail Research based on an average of typical worn profiles in the running zone of the tread.

The DR-1 and Barber-Scheffel trucks were most effective in reducing lateral curving forces. The Ride Control, Devine-Scales and Barber S-2 truck with C-PEP also reduced lateral curving forces but to a lesser extent. A marginal reduction in lateral curving forces was obtained with Stucki Constant Contact Side Bearings on the standard truck. The Swing Motion truck with 'A' profile wheels and the Barber S-2 truck with 'AAR' wheel profile showed an increase in the lateral curving forces.

The DR-1, Barber-Scheffel and Devine-Scales trucks were found to have a much reduced Wear Index* in comparison to the reference truck**. The Barber S-2 trucks equipped with C-PEP was the next effective truck in reducing the Wear Index while a marginal reduction in the Wear Index was found with the Ride Control, Barber S-2 with Stucki Constant Contact Side Bearings and Barber S-2 truck with AAR profile wheelsets. The Swing Motion truck showed an increase in the Wear Index in relation to the reference Barber S-2 truck.

The reference Barber S-2 truck whick formed part of the test consist during each lateral stability test showed a wide variation in "hunting" performance. However, up to 55 mph performance was comparable to all other test trucks. Intermittent hunting of the reference Barber S-2 truck commenced at 60 mph to 65 mph. C-PEP and Stucki Constant Contact Side Bearings were both effective in raising the threshold speed of hunting of speed of the Barber S-2 truck to above 75 mph, the maximum test speed.

The Barber-Scheffel and Swing Motion trucks were dynamically stable throughout the range of test speeds to 75 mph. Intermittent hunting occurred at 65 mph on the Ride Control truck, and on the DR-1 and Devine-Scales trucks with 'A' profile wheels, and Barber S-2 truck with AAR wheels hunted intermittently from 70 mph.

In summary, results of the test program clearly show that the "self steering" trucks DR-1 and Scheffel, are the most effective of the "new generation" truck designs in reducing lateral curving forces, and lower-in the Wear Index while maintaining stability at higher operating speeds.

C-PEP and Stucki C.C.S.B. devices applied to current generation truck designs appreciably increase stability at higher operating speeds without being detrimental to curving performance.

The test data also conclusively shows that a modification of the AAR standard profile to the 'A' profile, or equivalent, significantly reduces lateral curving force.

---

* Wear Index is proportional to the product of the wheel flange force and angle-of-attack.

** The reference truck is the Barber S-2 truck with 'A' profile wheels.

PART I
INTRODUCTION

Truck manufacturers and designers have recently developed "new" truck designs aimed at alleviating the two most prevalent current generation truck problems; high lateral wheel/rail forces during curve negotiation and lateral instability at higher operating speeds. Each of these "new" truck designs contain features or characteristics that are claimed to improve one or both of the two major operating deficiencies. However, no comprehensive test or service information is available.

In order to obtain quantitative data on the performance of various "improved" truck designs, the Mechanical Department of CP Rail requested Research Department to develop and implement a test program that could provide such data. A two-phase plan was then formulated. The first phase consisted of short-term field tests which were designed to obtain quantitative data on curving performance and high speed stability in order to identify the most effective truck designs. The second phase of the program would be long-term in-service testing of the most promising candidate trucks under carefully controlled and monitored conditions to provide data on truck and car body maintenance.

In the first phase of the test program, five candidate trucks were selected for testing and comparison. These trucks included the Barber S-2 truck which was used as the reference truck, the Barber-Scheffel, DR-1 Radial, Devine-Scales Radial, Swing Motion, and the Ride Control. All the test trucks were equipped with CN 'A' profile wheelsets. In addition, the Barber S-2 truck was tested with AAR profile* wheels. Also an evaluation was made to assess the effect of C-PEP and Stucki Constant Contact Side Bearings on the performance of the Barber S-2 truck with 'A' profile wheels.

This report describes the first phase of the test plan which was carried out at two pre-selected sites near Calgary, Alberta, in June 1978. The second part of the report briefly discusses the design and features of the test trucks. The third part describes curving performance tests that were designed to evaluate lateral and vertical track forces and measure wheelset to rail angle-of-attack. The fourth part describes the high speed stability characteristic tests. The report ends with conclusions of the overall results.

---

* All the wheels which have been used in these tests were new.

PART II
TEST TRUCKS

II.1 Introduction

The evolution of railroad technology toward increased axle loads and higher operating speeds has placed the performance of the conventional roller-bearing, three-piece truck design under much closer scrutiny. Two major deficiencies exist with this truck in the area of vehicle guidance. The first is the need for excessive flange guidance force during curve negotiation. The resulting high force accelerates rail and wheel wear and is responsible for many maintenance problems encountered in today's operations. The second deficiency is truck lateral instability, commonly known as "hunting", which places major constraints on the maximum speed that can safely be attained by trains. Wheel/rail forces that develop from hunting oscillations lead to deterioration of truck and track components at an accelerated rate and result in increased maintenance costs to assure safe operations.

A considerable amount of research has been carried out on the static and dynamic behaviour of conventional and improved truck designs running on a curved track. The desirability of avoiding flange contact, either as a result of large rolling displacement of the wheelset in a curve or as a result of sliding, has been emphasized in recent studies of high speed rail technology(1-3)*. Uebelacker(4), Heumann(5,6) and Baseler(7) have developed various methods to define and explain geometric and kinematic forces acting between curved rail and vehicle under equilibrium static conditions. Muller and others(8,9) have built up a theoretical framework describing curve negotiation for vehicles with stiff primary suspension whose axles are forced to remain parallel to each other in the presence of slip.

Extensive studies were made on the dynamic stability of the conventional truck to analyze the influence of axle loads, track gauge and wheel contour on the truck's hunting behaviour. Studies(10) were also carried out to evaluate the ability of the wheel flange and tread contour to limit hunting oscillations. The nature of conventional truck motion at the critical speed was also investigated and the energy conversion between the forward motion of the vehicle and the lateral motion of the truck or wheelset was explained in the work of Wickens(11).

---

* Number in parenthesis refers to reference(s) listed at the end of the report.

All these theoretical and experimental studies have established conditions under which a new generation of two-axle trucks can be designed to reduce flange contact and increase dynamic stability.

This Chapter gives a summary description of several of these new trucks as well as other specific components designed to improve existing truck performance, see Table 1. Some of the data and features of the trucks and components discussed are not fully described and the original source of information, which is listed with each description, should be consulted.

II.2 Self-Steering Trucks

II.2.1 Barber-Scheffel Truck*

The Barber-Scheffel truck is the result of a joint development between South African Railways and Standard Car Truck Co.*, see reference 12 and 13.

The truck consists of cast-steel sideframes and a bolster arranged as shown in Figure 1. Diagonally placed anchors connect special adapters of diagonally opposite axle boxes. These anchors pass through openings in the cast-steel bolster. An additional adapter is provided which supports the sideframes on two elastomer pads and provides a connection to the anchors. A controlled lateral motion of ±½ inch is obtained by the elastomer pads in shear.

---

* Standard Car Truck Co., Chicago, Ill., U.S.A.

The diagonally placed anchors, while constraining the wheelsets to each other to control lateral instability, do not interfere with the natural tendency of profiled wheels to align themselves radially on curved track. The steering capacity is obtained entirely by the natural ability of the profiled wheelsets to align themselves in curves. Sufficient clearance is provided in the longitudinal direction between special adaptors and the pedestal opening of the side frame to allow the axles to assume a radial position on curves. The dual requirement of improved steering and high speed stability is achieved by having a low yaw constraint on each wheelset for curving and cross anchors connecting opposite wheelsets for high speed stability. The low yaw constraint between wheelset and sideframes is obtained by mounting the sideframe axle box on rubber sandwiches of low shear stiffness.

II.2.2 DR-1 Radial Truck

The DR-1 radial truck is a joint development of CN Rail Research, the Dresser Transportation Equipment Division in the U.S. and Dominion Foundries in Canada based on conceptual and investigative work performed by H.A. List of Railway Engineering Associates, Inc., References 14 and 15.

It consists of a "steering device" which can be retrofitted to a standard three-piece truck sideframe and bolster assembly with conventional suspension components. The "steering device" consists of two similar C-shaped cast-steel arms, one on each side of the bolster as illustrated in Figure 2. The two C-shaped arms are attached to the wheelsets at the bearing adaptors. An elastomeric pad is provided between the roller bearing adaptor and roof of the sideframe pedestal with adequate clearance longitudinally to allow the wheelset to move in seeking a radial position.

---

* Railway Engineering Associates, Inc.,
38 West University Avenue, Bethlehem, Pennsylvania 18015, U.S.A.

Interaxle lateral stiffness is achieved through the cast-steel steering arms which in turn has an upgrading effect on the hunting stability. Interaxle yaw stiffness is achieved by elastically coupling the wheelsets to each other through the truck side frames. This allows longitudinal movement of the axles under resilient control of the elastomeric pads which in turn permits the radial positioning of the wheelset in the frame.

II.3 Forced Steering Trucks

II.3.1 Devine-Scales Radial Truck

The Devine-Scales radial truck is manufactured by J.P. Devine Mfg. Co.*. This truck is of a primary suspension type similar to the trucks now being introduced on British Railways, see References 16 and 17.

The truck frame is an 'H' shaped design as illustrated in Figure 3. Its suspension consists of four sub-frames which are located in pockets at the corners of the truck frame. The sub-frames are able to slide longitudinally on low friction slides. Each sub-frame contains a saddle which is located in vertical guides. Standard coil springs are fitted between the top of the saddle and the underside of the top of the sub-frame. Load sensitive friction damping is obtained with barber friction shoes positioned on either side of the saddle which bear against the vertical guides of the sub-frame. The two sub-frames on each side of the truck are connected by tie bars to the opposite ends of a control link located on the transverse centre line of the truck. The midpoints of the control links on each side of the truck are attached to vertical spindles which pass through the truck frame and are connected to outwardly projecting lever arms. The outer ends of the lever arms are coupled by radius rods to anchor points on the car body.

---

* J.P. Devine Mfg. Co., 100-49th Street, Pittsburgh, Pa. 15201, U.S.A.

The leverage is designed so that the sub-frames on the outside of the curve are moved further apart whereas the sub-frames on the inside are moved closer together during curve negotiation. These movements are in proportion to the "swivelling" of the truck which is proportional to the degree of curvature.

II.4 Premium Trucks

II.4.1 Swing Motion Truck

The "Swing Motion" truck is a development of National Castings Division of Midland Ross Corporation*, see Reference 18.

The truck consists of two cast steel sideframes and a cast-steel truck bolster which are arranged as in a conventional truck, see Reference 18. The truck is rigidized and thus prevented from "parallelogramming" by use of a transom which connects the two sideframes through special rocker seats. In addition, the transom also provides for controlled lateral motion. This is accomplished by the transom connecting the two sideframes and supporting the load springs by a rocker connection between the sideframe and transom as illustrated in Figure 4. This type of arrangement allows the sideframes to swing laterally in unison. Swinging of the sideframe (3^{o} maximum) is stopped by the contact between the sideframe member and underside of the rocker seat, with a 5/8" lateral motion to each side. The resistance to lateral motion is dependent upon the weight and varies in proportion to the vertical load.

Increased stability against car roll is accomplished by eliminating the conventional gibs on the truck bolster and providing lateral stops between the bolster and the transom at the height of the sideframe spring seat.

---

* National Casting Division, Midland-Ross Corporation,
700 South Dock Street, Sharon, Penn. 16146, U.S.A.

The truck is provided with long travel springs. Other truck components such as wheels and axles, roller bearings, roller bearing adaptors, truck centre plates and side bearings are as on conventional trucks.

II.4.2 Ride Control Truck

The Ride Control truck is manufactured by American Steel Foundries* and is of 100-ton capacity. It was developed to provide a greater reserve capacity in the suspension system.

The truck is a three-piece arrangement with cast-steel sideframes and bolster with conventional wheels, coils, bearings, brake rigging and adaptors and equipped with special winged Friction Shoes as shown in Figure 4(b). The D-7 longer travel springs are used in the suspension system with nine outer and five inner D-7 coils.

II.5 Components

II.5.1 Stucki Constant Contact Side Bearing

The Stucki resilient side bearings are a development of A. Stucki Company** and are designed to provide rotational control of the car body and limit its rock and roll. The Stucki model 688-BR, as shown in Figure 5, consists of three polyurethane blocks (4" x 3" x 1") interspaced with 2 metal blocks which fit into the standard pocket of the double roller side bearing.

Application of this bearing to the truck is simple, but requires that the car be allowed to settle on the polyurethane blocks for a period of 12-24 hours prior to use for the relaxation of the blocks and for the required clearance to be met.

These bearings are developed for application to conventional or new truck designs.

---

* American Steel Foundries, Granite City, Ill., U.S.A.

**A. Stucki Company, 2600 Nevile Road, Pittsburgh, Pa. 15225, U.S.A.

II.5.2 C-PEP

C-PEP is a development of Standard Car Truck Co., and is an acronym for Centre Plate Extension Pad(19). It consists of elastometric pads located between the car centre plate and the side bearings of the car, as illustrated in Figure 6. The shear characteristics of the pad act as a yaw spring/damper providing rotational control between the truck and car body.

Vertically, the pad's high spring rate gives an effective static and dynamic couple between the car body mass and the truck suspension system. The pads are preloaded by the use of shims under them at assembly which results in pressure being applied immediately as the car reacts to an irregular truck action. Control of "rock and roll" is accomplished by the car sway compressing the C-PEP pads which activate the friction snubbers of the truck immediately rather than after the normal side bearing clearance is taken up when a dynamic force has been developed.

PART III
CURVING PERFORMANCE TESTS

III.1 Introduction

It has been shown(8,20,21) that flange contact and associated high lateral forces can produce track shifts, gauge widening and rail roll-over. These forces, when coupled with a large angle-of-attack between the vertical plane of the wheel and rail direction, cause wear of wheel treads, flanges and rails and increase the risk of derailment due to flange climbing.

Recently proposed truck designs to improve curving performance have been based on a concept to accommodate the difference between the length of the outer rail and the inner rail on a curve. The wheelset and wheel path length can, therefore, match the rail length permitting the wheelset to steer through the curve freely without sharp flange contact. This can be achieved by an appropriate combination of lateral and yaw stiffness between the two axles of a truck which will permit the wheelsets to take up approximate radial alignment with the rail.

Evaluation of existing and new truck configurations requires quantitative estimates of curving performances. This Chapter describes in detail the curving tests that were carried out on selected trucks and devices which have been described in the previous chapter. The first part of this chapter deals with the technique and results of lateral and vertical load measurement while the second part is concerned with the angle-of-attack measurement. Both of these measurements were combined to evaluate the curving performance of the trucks.

III.2 Test Curve

In order to evaluate curving forces in a field test, the test curve selected should be long and have minimum variation in curvature, superelevation and gauge. This will ensure that lower limits of dynamic effects are encountered and avoid unnecessary scatter in the test results. The curve chosen should be within the 4 to 8 degree range. This range is responsible for the most frequent rail replacement on Canadian Pacific, see Figure 7. Curves of less than 4 degrees generally have less maintenance requirements while curves exceeding 8 degrees represent a small percentage of existing curves, see Table 2.

With the above consideration in mind, the curve chosen for the test was near Calgary at Mileage 12.4 on the Laggan Subdivision. Curvature and static gauge measurements are shown in Figure 8. The rail in this curve is Algoma 1971 RE 132 lb., 78' jointed with a superelevation of 4.5" with an equilibrium speed of 37 mph. Typical rail head profiles of the test curve taken by Seiki rail profile gauge are shown in Figure 9.

III.3 Lateral and Vertical Load Measurement

In the curving tests, the vertical and lateral loads of test trucks were measured by applying strain gauges to the test curve rail's web and base(22). The following sections give details of the strain gauge circuits and calibration techniques.

III.3.1 Strain Gauge Circuit

Various strain gauge circuits have been designed and applied to measure wheel loads on rails. Some of these circuits are reviewed in Reference 22. The circuits used to measure the vertical and lateral loads of the test trucks are shown in Figures 10, 11 and 12 respectively.

The vertical load measurement circuit is the one adapted from the strain gauge patterns designed by ORE(23) and used by several railroads. In this circuit the gauge pattern is designed to measure the shear force differential between the two gauged regions, i.e., a-b and c-d, as shown in Figure 10. The concept of this circuit is based on there being no direct support under the rail within the gauged region. The output of this circuit is thus proportional to vertical load, P. Gauges are oriented about the neutral axis to measure the principal strains which are 45^0 from the vertical shear force line of action. This circuit's zone of influence is confined to the crib distance.

The lateral load measurement circuit, Figure 11, is the one developed by Battelle and described briefly in the amendment to Reference 22. This circuit was tested by CP Research at the NRC Uplands Railway Laboratory prior to being employed in the actual test. As for the vertical circuit, the lateral circuit was designed to measure the shear force differential at the base of the rail resulting from the wheel lateral load, as shown in Figure 11. The influence zone of this circuit is also confined to the crib where there is no direct support under the rail. This circuit considers no attenuation of lateral forces in the rail head, and the cross talk error resulting from the offset of the vertical load from the centre line of the head surface is assumed to be minimal.

III.3.2 Application

Six locations on the test curve were chosen to be gauged by the previously described circuit in order to record lateral and vertical forces. Five of these locations were on the high rail and one on the low rail. These locations were approximately equi-distant from one another and had the same characteristics of track gauge and curvature. The position of the strain-gauge locations and the rail joints are shown in Figure 13.

Prior to installing the strain-gauges, location sites on the web and base of the rail were ground and prepared to accommodate the gauges and their weather-proof straps. A specially developed fixture was used to accurately mark the neutral axis which was previously determined from the rail head profile and a mathematically derived formula. This fixture was also used to accurately index the locations of the gauges on opposite sides of the rail. Each of the strain-gauges used in the vertical and lateral circuits had a resistance of 120 ohms, a gauge factor of 2.10 and accuracy of 0.55%. Weldable gauges having a resistance of 350 ohms, a gauge factor of 2.05 and accuracy of 1% were used at location no. 4.

In addition to the strain-gauged locations, two of Canadian National Railway's base plates were installed as supplementary instrumentation on the high rail, as shown in Figure 13, to measure lateral and vertical forces. A description and application of these base plates can be found in References 24 and 25.

III.3.3 Calibration

A modified technique based on the one described in Reference 22 was used to calibrate the vertical and lateral load strain-gauge circuit in the field. The lateral circuit was calibrated by applying a known lateral load between the heads of outer and inner rails using a hydraulic jack. A laboratory-calibrated load cell in series with a hydraulic jack was used to drive the indicator of a calibrated load-measuring instrument, while the output of the strain-gauge was recorded on a 32 channel FM tape recorder displayed on an 8 channel Gould brush chart.

Simultaneous with the lateral circuit calibration, the vertical load-measuring strain-gauge circuit was calibrated by applying a vertical load on the railhead through the use of a specially designed frame fixture, see Figure 14. In this fixture, another laboratory calibrated load cell was employed in series with a hydraulic jack pressing against the underframe of a stationary locomotive. Similarly to the calibration of the lateral circuit, the load cell was used to indicate the actual vertical load, while the output from the vertical strain-gauge was recorded on an FM tape and displayed on a brush chart.

During these calibrations, the vertical load was set each time at a certain load value over a range from 0-30 Kips while the lateral load was allowed to vary from 0-20 Kips and back to zero in incremental steps. This procedure permits monitoring of the linearity and hysteresis loop of the vertical and lateral circuits. Cross-talk error between vertical and lateral loads was determined by repeating the previous procedure at each strain-gauged location, varying the vertical load position laterally across the rail head, i.e. at the centre, gauge and field side. This was done by inserting a small flat steel pad between the rail head and the vertical load cell. Varying the position of this steel pad changes the vertical loading contact point across the railhead.

The data obtained from the vertical and lateral calibration procedure were plotted as chart deflection versus force (lb.). Results of the vertical calibration are shown in Figures 15 to 18, while results of lateral calibration are shown in Figures 19 to 22.

Calibration curves of vertical loads showed no cross talk effect from the lateral loads and all were found to have perfect linearity up to 25 Kips. The lateral calibration curves also showed good linearity. For each lateral circuit the scatter in the results due to the cross talk effect resulting from the position and magnitude of the vertical load was bounded by an upper and lower level as shown in Figures 21 and 22. The upper level is due to the highest vertical load acting on the rail field side (30 Kips) while the lower one is due to the highest vertical load acting on the rail gauge side (20 Kips). The maximum cross-talk was 17 lbs. for every 1,000 of vertical load as shown in Figures 19-21. There was no cross-talk effect between the vertical load and the lateral load circuit for lateral calibration curves of strain-gauge circuit no. 5 as shown in Figure 22.

III.4 Angle-of-Attack Measurements

Angle-of-attack or incidence ι of a wheel running up against a rail is the angle between its instantaneous direction of motion and the tangent in the horizontal plane at the point of contact between the flange and the rail. It is formed when a wheelset of a truck deviates from the radial position while negotiating a curve.

The method used to measure the angle-of-attack in the present test was developed by the Research Department of Canadian Pacific in cooperation with the Railway Laboratory of NRC and is described in Reference 26.

III.4.1 Instrumentation

The test equipment consisted of 3 low-power laser tubes, each having a 0.04" diameter laser beam, three photo diode detectors and the necessary electronic recording systems. This system included a Philips 7-channel analogue tape recorder, a brush chart recorder, Tektronix 475 Oscilloscope, and a DC power supply.

The lasers and detectors were positioned on machined mounts permitting fine vertical adjustment of beam height above the rail and lateral adjustment for radial alignment. These mounts were placed longitudinally on an aluminum channel firmly installed between two ties, Figure 23, at the centre of the instrumented test curve as shown in Figure 13.

III.4.2 Alignment

Alignment of the measuring equipment required the laser beams 1 and 2, see Figure 23, to intersect each other in the horizontal plane radially to the curve. This was done by a special alignment jig equipped with an optical flat placed longitudinally on the rail. After aligning the laser beams, they were raised about 0.25" vertically above the running surface of the rails. The detectors were then placed in the centre of the track and laterally aligned to receive the laser beams.

III.4.3 Measurements

The angle-of-attack is evaluated as the arctangent of the ratio of the distance between the centres of wheel discs of one wheelset and the distance between their flange centres, see Figure 24. The displacement between the centres of the two wheels was obtained by measuring the difference between the time they interrupted and cleared the pulses of laser 1 and 2. To convert this time signal into displacement, the speed of the wheelset was calculated from the instantaneous velocity of the wheel to travel from laser 1 to laser 3, which are 2.5" apart. Formulae presented in Figure 25 are used to calculate the angle-of-attack from data supplied by the laser pulses. It should be noted that these calculations depend on the running direction of the test truck, i.e., which of the laser beams will be cut off first. These calculations will also be affected by misalignment of the lasers which could provide an offset angle to be added or subtracted from the angle-of-attack depending on the truck's running direction.

III.5 Test Procedure

Four test series were carried out with 100-ton laden bathtub coal cars. Each test series consisted of 5 runs eastward and westward on the test curve at both the equilibrium speed of 37 mph and 25 mph. In addition, 3 runs were carried out in each direction at a speed of 45 mph. On completion of each test series, the test consist was returned to Calgary to be wyed and the aforementioned tests were repeated. Tests were designed in this manner of direction/orientation to take into account the offset angle-of-attack and the unsymmetric features and misalignment due to truck/wheelsets assembly tolerance. Through the entire test, the consists were left to coast freely through the curve. All tests were carried out on dry rail in order to minimize the change in the adhesion factor and thus avoid further scatter in the test results. Test consists are shown in Table 3.

III.6 Data Analysis

All signals from both vertical and lateral strain-gauge circuits were recorded on 16-channels of an FM tape recorder. Six channels were used for the lateral and six channels for the vertical signals. In addition, four channels were used to record the CN base plate output signal: two for the vertical and two for the lateral. The recorder signals were subsequently displayed through a brush recorder. A typical output of the vertical and lateral signals at one of the test speeds is shown in Figure 26.

There was no problem in reading the recorded signals of any of the gauges with the exception of those of gauge circuits 1 and 4. Their reference lines were observed to be unstable during the running test period. This defect may have occurred as a result of poor bonding between the strain-gauges and the rail as the test proceeded.

The output recorded from CN base plates generally followed the trend of signals from the strain-gauge circuits, however, because of the noise accompanying the base plate signals, no analysis was carried out on them.

The analysis of the vertical and lateral response of the tested trucks was based on the output of strain gauge circuits 2, 3A, 3B and 5.

To evaluate the signal of any of the vertical strain-gauge circuits, the corresponding chart divisions were counted and, by utilizing the vertical calibration curve, converted to a load value. Consideration was given to the difference between the recording sensitivity of the test output signal and the sensitivity used to plot its calibration curve in the calculation.

To evaluate the signal of any lateral strain gauge circuit, the corresponding vertical load was first evaluated as described above and then plotted on the corresponding lateral circuit calibration curve as two lines representing the cross-talk effect of this (vertical) load on the lateral circuit when acting on the railhead in two extreme cases: the gauge side and the field side. The mid-line between these two lines is the value then used to transfer the counted division of the corresponding lateral signal into the lateral load.

The lateral load results for all test trucks are tabulated by axles for each consist at three test speeds in Table 4. These results were then reduced in Tables 5 and 6 for the leading and trailing axles of each truck in both directions. All the results are shown in the form of algebraic average, absolute average and the maximum values recorded.

For the angle-of-attack measurements, difficulties were encountered in processing the data in the field using an analog processor during the tests. All the data was then analyzed using a Phillips Tape Recorder and an oscilloscope with an attached microviewer. In a form similar to Tables 4 and 5, the results of the angle-of-attack measurement are shown in Tables 7 to 9.

From these results shown in the above mentioned tables, the test trucks can be compared only within their own test consist. For comparison of all the trucks simultaneously, a normalizing technique was applied to their values utilizing the fact that a reference truck (Barber S-2 with 'A' profile wheel) was always included in each test consist and remained unmodified throughout the test series. The normalized lateral force for the outer leading wheel of each truck was calculated by using a formula, similar to that used in Reference (27), which can be written as:

$$\text{Normalized average value of lateral force of outer leading wheel of a test truck} = \text{Average lateral force of this wheel measured in its test consist} \times \frac{\text{Average lateral force of the corresponding wheel of the reference truck for all test consists}}{\text{Average lateral force of the corresponding wheel of the reference truck measured in the test consist}}$$

This method of normalization assumes that the change in external parameters would produce proportionally similar effects on both the test and reference truck. Utilizing this method, the normalized lateral forces for the outer leading wheels of all test trucks are as shown in Table 10 while the normalized angle-of-attack values are shown in Table 11.

From the results of lateral forces and angles-of-attack, the following observations can be made:

- The lateral forces appear low in general where their measured value varied from less than 1 Kips to 11 Kips. However, knowing that the measured value of a lateral force is a result of a tread creep force and a flange force acting in opposite directions, see Appendix I, the actual flange force may have been as high as 22 Kips.

- Lateral forces were found to be dependent upon the travelling direction on the test curve. This effect could be related to the location of the rail joint with regard to the strain-gauge circuit position.

- The offset angle due to laser misalignment was calculated as 5 minutes. This angle was found to be equal to the misalignment of the radial trucks in both test directions while, for the other trucks, their misalignment angles are shown in Table 12.

III.7 Discussion

1. The first important parameter to be discussed is the flange force or the side thrust of the outer leading wheel of each test truck. On the basis of Appendix I and Tables 6 and 10, this force* and its normalized value for each truck in each test consist are plotted against speed in Figures 27(a) and 27(b), respectively. The ratio of flange force of each truck to the reference truck** at the three test speeds is shown in Table 13. In Figures 27(a) and 27(b), a linear relationship between the speed and the force is assumed.

2. The lateral force distribution between the outer leading and trailing wheels for each truck is an important parameter in comparing the curving performance of the trucks. These forces, in addition to being an indication of the relative position of the axles with respect to the rail, have a sum*** which represents a fatigue bending or twisting cycle acting on the rail. The average sum of these lateral forces for each test truck is plotted as a ratio to that of the reference truck as shown in Figure 28.

3. The angle-of-attack is the second important parameter obtained from this series of curving tests. It is an indication of the wheel position on the rail and subsequently of the amount of sliding area between the rail and the wheel which is a main factor in the rail/wheel wear process. Table 14 lists the ratio of the angle-of-attack of the outer leading wheel of each truck to that of the reference truck in each test consist while Figure 29(a) shows the angle-of-attack of each truck in each test consist versus speed.

   Utilizing the normalized data for the angle-of-attack shown in Table 11, the results of the leading axles of all test trucks are plotted versus speed in Figure 29(a), assuming a linear relationship between the speed and the angle-of-attack.

---

* The flange force is calculated here as 2X the measured lateral force.

** Barber S-2 truck with 'A' profile wheels.

*** This is valid assuming that the induced force in the rail will produce a stress field of wide distribution and the time difference between two outer wheels of a truck with respect to one point on the rail is very small (0.2 seconds for 25 mph).

4. From Appendix III and the work of Heumann(28), it can be shown that the wear of wheel tread and flange, as well as the rail gauge side and head can be represented by a Wear Index which is proportional to the product of the wheel flange force and angle-of-attack. The Wear Index of the test trucks in each test consist are shown in Table 15, while the ratio to that of the reference truck is plotted versus speed in Figure 30.

   From the foregoing figures and tables, the following conclusions can be made.

   - Based on the values of flange force and angle-of-attack, the curving performance of the test trucks can be categorized into three groups. The first group includes the Swing Motion truck with 'A' profile wheels which is designed as a rigid truck and the Barber S-2 with AAR profile wheels. On the Swing Motion truck, the wheel base is made longer in order to decrease the flange forces needed to supply the required turning moments to the truck frame. However, results show that this truck exerts flange forces higher than those of the conventional truck while having a reduced angle-of-attack at all test speeds. The Barber S-2 truck with the AAR profile wheels produced the highest level of flange forces. The value is more than 1.75 times that of the Barber S-2 truck with 'A' profile wheels. However, while it is understood that a low conicity profile such as the AAR profile wheel, see Figure 30(b), imposes high contact stresses on the rail due to lack of conformity with worn curve rail, this truck produced an angle-of-attack smaller than that of the Barber S-2 with 'A' profile wheels at all test speeds. It should be mentioned that while the 'A' profile wheel with a conicity of 1:10 is a wear worn profile developed for rail having a tie cant of 1:40, rail in the test curve has a tie cant of 1:20.

The second group of trucks includes the Barber S-2 with 'A' profile wheels, Barber S-2 with Stucki Constant Contact Side Bearings, Barber S-2 with the Centre Plate Extension Pads and Ride Control. Centre Plate Extension Pads and Stucki Constant Contact Side Bearings are anti-hunting components which would increase the torque required to swivel a truck, however, the measured lateral forces (or the flange forces) and angle-of-attack for this group were found to be comparable in general, with the exception of Ride Control which shows a higher angle-of-attack at the equilibrium speed. This may be due to the squaring characteristics of this truck.

The third group consists of the radial trucks, DR-1, Barber-Scheffel and Devine-Scales. They have, in general, a lower level of flange forces and a smaller angle-of-attack than the rest of the test trucks. In this group, which has a comparable angle-of-attack values, Devine-Scales produced flange forces higher than those of DR-1 and Scheffel.

- With the exception of Barber S-2 with the AAR profile wheels, the flange force of the outer leading wheel of all test trucks showed an increase with the speed*. In the conventional trucks the rate of increase of this flange force after the equilibrium speed is ~ 2.5 times higher than before this speed, while for the radial trucks (the third group) this ratio is ~ 0.3.

---

* The flange force due to the centrifugal force becomes larger as the running speed increases. However, the flange of the trailing outer wheel gradually approaches the outer rail as the speed increases and the angle-of-attack of the leading wheelset becomes smaller. As the influence of decrease of the angle-of-attack on the flange force is larger than the influence of increase of centrifugal force(29), the flange force eventually becomes smaller or increases with a very low rate. This tendency of a limited increase of flange force with running speed comes to an end after the equilibrium speed when the trailing outer wheel flanges. Under this condition, angle-of-attack of the truck being determined geometrically, the flange force of the leading wheel caused by the centrifugal force becomes larger with a high increase rate as the speed increases above the equilibrium speed.

- The curving performance tests were carried out at, as well as above and below, the equilibrium speed of the test curve in order to determine the variation in the flange force, angle-of-attack and Wear Index as related to change in the speed. Emphasis should however be placed on the test results obtained at the equilibrium speed for the test curve. At this speed, a reduction (or increase) in flange force, angle-of-attack and Wear Index of the different test trucks, as compared to the reference truck, is as in the table which follows.

- Another factor in comparing the test trucks is their rolling resistance* in the curves. The work of Marcotte(30) showed that both formulations of Wear Index and rolling resistance in curves are proportional to each other since they depend on the same parameters, namely, the flange force and angle-of-attack of the wheelset in relation to the rail. Therefore, all the results obtained in Table 15 and Figure 31 are valid to describe the rolling resistance of the test trucks.

---

* Curve resistance or "drag" represents the energy dissipated in overcoming friction at the wheel-rail interface, and is an indication of fuel and power requirement necessary for a truck to traverse a curve, see Reference (30).

Truck	Reduction in Flange Force in Relation to the Reference Truck+	Reduction in Angle-of-Attack in Relation to the Reference Truck	Reduction in Wear Index in Relation to the Reference Truck
DR-1	29%	62%	74%
Barber-Scheffel	22%	52%	67%
Devine-Scales	8%	56%	62%
Swing Motion	- 53%*	14%	- 40%
Ride Control	11%	- 15%*	9%
Barber S-2 with C-PEP	6%	1%	19%
Barber S-2 with C.C.S.B.	1%	1%	9%
Barber S-2 with the 'AAR' Profile Wheels	- 72%*	20%	3%

* Negative values refer to an increase in the specified parameter in relation to the reference truck.

+ The reference truck is the Barber S-2 with 'A' profile wheels.

CURVING PERFORMANCE RESULTS OF THE TEST TRUCKS IN RELATION TO THE REFERENCE TRUCK AT 37 MPH

PART IV
HIGH SPEED STABILITY TESTS

IV.1 INTRODUCTION

Lateral instability, commonly known as "hunting", is a complex self-excited oscillation in which a periodical movement of the wheelsets occur back and forth between the two rails.

Two types of hunting are generally encountered on a rail vehicle. Car or body hunting, which is termed primary hunting, takes place at relatively low speeds, whereas wheelset or truck hunting called secondary hunting occurs at relatively higher speeds. Car body hunting has a resonant frequency in a narrow speed range, above or below which it may not be a problem. However, with truck hunting there is a critical speed above which the wheel/rail forces increase with speed while the frequency remains relatively constant. Body hunting can be eliminated by adding reasonable damping to the body suspension, but truck hunting once it occurs, becomes more severe with increasing speed resulting in deterioration of both the track and truck components with a possibility of derailment.

During hunting a coupled lateral and yaw motion of the wheelsets and sideframes occurs as a result of the combined interaction of creep forces and rail/ wheel contact geometry. A small lateral displacement of the axle causes a difference in the rolling radii between the two wheels on the same axle resulting in a change in the geometry of the wheel/rail contact area. Thus equilibrium between the two wheels of an axle is disturbed resulting in a net lateral force trying to steer the wheelsets back to equilibrium position. During this phase the wheelsets make an angle with the rails. Creep forces which are related to loading on the rail and the relative velocity between the wheel and rail, tend to restore the wheelset to its original equilibrium position.

Wheel tread profile or conicity plays a large part in determining the stability characteristics of a truck. Low values of conicity reduce hunting. Cylindrical wheels are regarded as one cure for hunting as there would be no restoring moment associated with a displacement from the track centre line. With new wheels, conventional trucks under a light car have a higher critical speed as compared to a car with worn wheels. As wheel treads wear, there is a tendency for a common worn wheel profile to develop regardless of the initial profile on the wheel. A change in the coning angle increases the effective conicity. Higher conicity increases the turning moment and results in more energy available to drive an oscillation.

When hunting occurs a certain amount of energy is dissipated during each impact of the wheel flange against the rail. The magnitude of energy loss depends on various factors such as wheel/rail geometry, truck condition and speed. Hunting will stop only if the forward speed of the wheel is sufficiently low that the energy dissipated during an impact is greater than the lateral energy being added to the system. Hunting can occur on perfectly good track and continue for miles if the forward speed of the vehicle is high enough and a track irregularity causes an initial flange contact.

This part of the report is related to the high speed tests conducted with various trucks to determine stability characteristics at different speeds.

The trucks evaluated were the same as those used for the curving performance tests previously described in Part II.

IV.2 Test Site

High speed stability tests were carried out on the Brooks Subdivision east of Calgary between Mileage 160 and 158. The rail on this section of tangent track consists of 115 lbs. continuous welded rail in 1440 foot lengths which were laid in 1977.

The Track Recorder Car Summary Report of the surface defects, cross-level and gauge in the two mile test zone measured prior to the test is shown in Table 16. There were two turnouts and several road crossings in the two mile test zone.

IV.3 Instrumentation

The leading axle of each trailing truck on the test cars was instrumented with three accelerometers, one mounted in the lateral direction and two in the longitudinal direction, one on each side of the axle. The accelerometers on the axle were mounted on specially adapted bearing end caps as illustrated in Figure 31(a). In addition, one accelerometer was mounted in the lateral direction on the stub sill of the cars near the centre plate, at the same end of the car with the instrumented axle.

Video cameras were mounted on each of the test cars and directed at the instrumented trailing truck of each car to obtain a visual record of truck performance. The video camera was mounted on the side of the tub of the car and "angled" to observe the truck and in particular one wheel. It was not possible to mount the camera under the tub of the car due to inadequate clearances.

Test speed was monitored by a proximity pickup on the axle of the caboose. All the data was recorded on a Sangamo 32-channel FM recorder. During the test run, the output of three lateral accelerometers on the car body and three longitudinal accelerometers on the axles of the test cars were displayed on an 8-channel Gould brush chart recorder to determine if any truck or car body instability developed during the test.

IV.4 Test Procedure

The consist for each of the tests is illustrated in Figure 31(b). It was comprised of three empty 100-ton bathtub coal cars, two 1750 HP passenger locomotives, an instrument caboose for recording data and a crew caboose. The three empty 100-ton bathtub coal cars CP 349537 (scaled weight 57,700 lbs.), CP 349157 (scaled weight 55,800 lbs.) and

CP 351668 (scaled weight 56,600 lbs.) were tested with the various trucks, each car being equipped with two similar trucks. Car CP 349537 with Barber S-2 trucks was used as the reference car throughout the test program.

Data on the bathtub coal cars and the various trucks tested can be found in Tables 17 and 18. As in the curving test, all three test cars were equipped with profile 'A' wheels except for Test 4. In Test 4, a Barber S-2 truck was tested with new AAR wheels for comparison with the reference Barber S-2 truck with 'A' profile wheels.

Five tests were conducted with the consist as illustrated in Figure 31(b). A gradual in-step increase in the test car consist speed in 5 mph increments from 45 to 75 mph was carried out for each of the tests. Initially the first test was started at 35 mph but as there was no evidence of instability it was decided to begin all the other tests at 45 mph. The required speed was attained prior to reaching the test zone between Mileage 160 and 158. The speed was held constant throughout the two mile test zone to visually observe the trucks through the TV monitors and record the accelerometer output data on a Sangamo 32-channel FM tape recorder.

On completion of each test run at a given speed the consist was backed up to an initial starting point. The tests were all run in the same direction over the same section of track.

IV.5 Results and Discussions

The lateral accelerometer data was analyzed by a power spectral density method, details of which can be found in Appendix II. Although the frequency range 0 to 30 Hz was analyzed, only the frequency range 0 to 15 Hz, which is of interest, is illustrated. The wheel frequency is predominant in the analyses of the lateral accelerometer on the axle of the trucks possibly due to an eccentricity of the wheel. This is indicated by peaks occurring in the range of 7 to 11.7 Hz for test speeds of 45 to 75 mph. When truck hunting did occur, the frequency remained relatively constant at approximately 2.8 Hz while the amplitude increased with increasing speed. The R.M.S. 'g' which is an average of the root mean square acceleration as seen by the accelerometer was then calculated for the frequency range 1 to 5 Hz. This frequency range of 1 to 5 Hz was selected so as to include the hunting frequency and avoid the wheel frequency which showed up predominantly in the P.S.D. analysis of the lateral accelerometer mounted on the axle. If hunting did occur at a certain speed, it should be indicated by a sharp increase in the R.M.S. 'g' value from one test speed to the next. However, it must be kept in mind that the R.M.S. 'g' value is an average value and if hunting was intermittent which was the case in several of the tests, the increase in the R.M.S. 'g' from one test speed to the next will not be pronounced. The R.M.S. 'g' values for the lateral accelerometer on the axle and car body are tabulated in Tables 20 to 21 and plots of this data can be found in Figures 32 to 37. As hunting was intermittent for some of the trucks in the speed range 45 to 75 mph, Table 19 was prepared from the longitudinal accelerometers output on the axle to give the approximate percent of time the trucks were hunting in the two mile test zone.

Consideration was given to normalizing the data with respect to the reference car with Barber S-2 trucks as our tests were conducted over a one week period. However, there was a wide variation in performance of the reference car with Barber S-2 trucks over the test period as illustrated in Figures 32 and 33. In addition, a change produced in the reference car truck would not necessarily produce a corresponding change in another type of truck. For a comparison of the reference car with Barber S-2 trucks with the other test trucks, an envelope which includes the results of all tests with the reference car has been included in Figures 34 to 37.

As we were testing complete trucks as well as devices such as C-PEP and Stucki Constant Contact Side Bearings to control hunting, and also the effect of AAR wheels on truck performance the test results have been grouped as follows:

A. Performance of Test Trucks

i) Barber S-2 Truck (Reference Car Truck With 'A' Profile Wheels)

A wide variation in performance of the Barber S-2 truck was observed during the entire test period as illustrated in Figures 32 and 33 even though weather conditions were similar with dry rail and the tests were conducted over the same section of track. The truck was stable to a test speed of 55 mph except for one test when there was a short burst of intermittent hunting at 55 mph. In general, the lateral ride on the Barber S-2 truck was comparable to the other trucks to a test speed of 55 mph. No large torsional oscillations of the car body were observed throughout the test. The speed at which lateral instability did develop varied between 60 and 65 mph during the tests and is indicated by the R.M.S. 'g' plots in Figures 32 and 33 and the P.S.D. Analysis in Appendix II where the frequency remains relatively constant (2.8 Hz) and the amplitude increases with increasing speed.

The 'A' profile used in the test program is a worn wheel profile. It was anticipated that the reference car with Barber S-2 trucks would commence hunting in the speed range of 45 to 50 mph. One probable cause, see Reference 32, for the higher speed at which truck hunting occurred on the Barber S-2 truck could be the fact that the 'A' profile was developed from service worn wheels on tracks laid with 1:40 tie cant plates. Our tests were conducted on track laid with 1:20 tie plates. As the worn wheel tread conforms closely to the rail head profile, a small increase in rail angle causes a large outward shift in the location of the wheel/rail contact area. Running on a reduced effective conicity may result. In addition, the two rate spring which is standard on our 100-ton cars offers a less stiff suspension for the light car. In addition to improving the vertical ride for a light car, it may also have a bearing on the lateral motion.

ii) Barber-Scheffel Truck ('A' Profile Wheels)

The Barber-Scheffel truck was dynamically stable throughout the speed range to a maximum test speed of 75 mph. The Barber-Scheffel truck was tested twice and on both occasions the lateral ride of the truck and on the car body was comparable. Figures 34 and 35 illustrate the lateral ride and the P.S.D. Analysis are in Figures 39 and 42 of Appendix II.

iii) DR-1 Radial Truck (Retrofitted to Barber S-2 Truck With 'A' Profile Wheels)

The DR-I radial retrofit applied to the Barber S-2 truck was tested twice, once inadvertently with conventional springs and again with the two rate springs which are standard on Canadian Pacific's 100-ton* cars. Considerable improvement in the ride was observed with the DR-1 with two rate springs as compared to conventional springs. With the conventional spring arrangement lateral car body 'jolts' were observed to develop as low as 55 mph. However, when the test was repeated with dual rate springs the lateral car body 'jolts' were reduced. The P.S.D. Analysis and R.M.S. 'g' values for different speeds illustrated in Figures 40 and 46 of Appendix II and Figures 34 and 35 respectively indicate the difference in ride with the conventional and two rate springs.

The ride with the DR-I (with the two rate springs on the Barber S-2 truck) was comparable to the reference truck to a test speed of 55 mph after which there was an improvement in the lateral ride compared to the Barber S-2 truck as seen in Figures 34 and 35. However, at 70 mph the DR-1 hunted intermittently for approximately 11% of the time in the two mile test zone. This intermittent lateral motion was observed during the test and appeared as an increase in the R.M.S. 'g' value at 70 mph as illustrated in Figure 34 and an input at 2.8 Hz on the P.S.D. Analysis in Figure 46. In comparison, the reference car with Barber S-2 trucks was hunting quite steadily at 70 mph which is indicated by a larger amplitude at 2.8 Hz at 70 mph.

---

* "Bathtub" coal cars.

iv) Devine-Scales Truck ('A' Profile Wheels)

The Devine-Scales truck was dynamically stable to a speed of 65 mph. At 70 mph the trucks hunted intermittently for approximately 39% of the time in the test zone. This intermittent hunting of the trucks (2.6 Hz) was observed visually during the tests and is illustrated by the P.S.D. plots in Figures 51 and 54 of Appendix II and R.M.S. 'g' in plots in Figures 34 and 35 respectively.

v) Swing Motion Truck ('A' Profile Wheels)

The Swing Motion truck was dynamically stable throughout the speed range and showed no tendency toward hunting at speeds to 75 mph. This was confirmed visually during the test and is also illustrated by the P.S.D. Analysis in Figures 52 and 55 of Appendix II and R.M.S. 'g' plots in Figures 34 and 35 respectively.

vi) Ride Control Truck

The Ride Control truck was stable to 60 mph and started to hunt intermittently at 65 mph for approximately 12% of the time in the two mile test zone. The performance of the ride control truck was comparable to the Barber S-2 reference truck to 55 mph. At 75 mph hunting was intermittent for approximately 74% of the time in the two mile test zone. The P.S.D. Analysis and R.M.S. 'g' plots are illustrated in Figures 64 and 67 of Appendix II and Figures 34 and 35 respectively.

B. Effect of C-PEP and Stucki Constant Contact Side Bearings on the Cars with Barber S-2 Trucks (With 'A' Profile Wheels)

C-Pep as well as Stucki constant contact side bearings stabilized the Barber S-2 truck to a maximum test speed of 75 mph by increasing the torque required to swivel the truck. In comparison the Barber S-2 truck on the reference car hunted intermittently at 60 mph and was hunting for approximately 50% of the time at 75 mph in the test zone during the test. Figures 36 and 37 illustrate the lateral truck and car body ride which indicate the improvement in stability of the truck and car body with C-PEP and Stucki Constant Contact Side Bearings. The P.S.D. Analysis for the test as compared to the Barber S-2 reference truck at various speeds is illustrated in Figures 57 to 61 of Appendix II.

C. Comparison of Barber S-2 Truck With 'A' Profile Wheels and AAR Wheels

The ride with 'A' profile wheels and AAR wheels on the Barber S-2 truck (with two rate springs) were comparable to a speed of 60 mph after which there was an improvement with new AAR wheels as illustrated in Figure 36. With AAR wheels intermittent truck hunting commenced at 70 mph whereas with the reference Barber S-2 truck intermittent hunting occurred at 60 and 65 mph during the test. The P.S.D. Analysis of the lateral ride of the truck and car can be found in Figures 63 and 66 of Appendix II.

With AAR wheels it was expected that the truck would not hunt in the range of our test speeds to 75 mph. The AAR wheels used in the test were the same wheels as used previously for the curving tests. This could have had an effect of changing the flange root area of the wheel as this area is known to wear very rapidly on AAR wheels resulting in a lower critical speed for the onset of hunting.

PART V

CONCLUSIONS

Test results have shown that a number of the "new generation" truck designs improve both curving and tracking performance whereas others only achieve improvement in one area and hence only partially meet the performance objectives of future truck designs. The performance of each experimental truck with regard to tracking and curving performance is individually summarized as follows:

1. DR-1 Radial (Retrofit Barber S-2 Truck with Two Rate Springs and 'A' Profile Wheels)

   The DR-1 truck reduced lateral curving forces by 29% and reduced the Wear Index by 74% in comparison to the Barber S-2 reference truck. Intermittent hunting occurred at 11% and 20% of the transit time in the two mile test zone at 70 mph and 75 mph respectively. Increased stability was obtained with the DR-1 retrofit Barber S-2 truck equipped with two rate springs as compared with conventional single rate springs.

2. Barber-Scheffel Truck ('A' Profile Wheels)

   The Barber-Scheffel design reduced lateral curving forces by 22% and reduced the Wear Index by 67%. The truck was dynamically stable to a maximum test speed of 75 mph.

3. Devine-Scales Truck ('A' Profile Wheels)

   The Devine-Scales truck reduced lateral curving forces by 8% and reduced the Wear Index by 62%. The truck hunted intermittently at 70 and 75 mph for approximately 40% of the transit time in the two-mile test zone.

4. Ride Control Truck ('A' Profile Wheels)

The Ride Control Truck reduced lateral curving forces by 11% and improved the wear index by 9%. Intermittent hunting occurred at 65 mph and hunting was sustained for approximately 74% of the 75 mph run.

5. Swing Motion Truck ('A' Profile Wheels)

The Swing Motion Truck increased lateral curving forces by 53% and increased the wear index by 40%. The truck was dynamically stable to the maximum test speed of 75 mph.

6. Barber S-2 Truck (Reference Truck 'A' Profile Wheels)

There was a wide variation in the tracking performance of the Barber S-2 reference truck over the period of testing. In general lateral ride was comparable to the "new generation" trucks up to a speed of 55 mph. The Barber S-2 truck started to hunt intermittently at 60 mph.

7. C-PEP on the Barber S-2 Truck ('A' Profile Wheels)

C-PEP reduced lateral curving forces by 6% and reduced the Wear Index by 19%. C-PEP was effective in stabilizing the Barber S-2 truck to a maximum test speed of 75 mph.

8. Stucki Constant Contact Side Bearings on the Barber S-2 Truck ('A' Profile Wheels)

A marginal improvement of 1% in lateral curving forces and a 9% reduction in the Wear Index was obtained. Stucki C.C.S.B. were effective in stabilizing the Barber S-2 truck to a maximum test speed of 75 mph.

9. Barber S-2 Truck with AAR Profile Wheels

These wheels had the effect of increasing lateral curving forces by 72% and marginally reducing the Wear Index by 3%. For this truck, intermittent hunting was observed from 70 mph.

REFERENCES

1. Newland, D.E. "Steering a Flexible Railway Truck on Curved Track", Transaction of the ASME, 908, August 1969.

2. Koci, L.F.
Marta, H.A. "Lateral Loading Between Locomotive Truck Wheels and Rail Due to Curve Negotiation", ASME, Paper No. 05-WA/RR-4.

3. Wickens, A.H. "Recent Developments in the Lateral Dynamics of High Speed Railway Vehicles", monthly Bulletin of the International Railway Congress Association, Vol. XLIV, No. 12, 781, Dec. 1967.

4. Uebelacker "Untersuchungen uber dic Bewegung von Lokomotiven mit Drehgestellen in Bahnkrummungen" Organ Fortschr, Eisenbwes, 1903.

5. Heumann, H. "Das Verhalten von Eisenbahnfahrzengen in Gleisbogen", Organ Fortschr, des Eisenbwes, 1913.

6. Heumann, H. "Grundzuge der Fuhrung der Schienenfahrzeuge", Sonderdruck aus Elektrische Bahnew.

7. Baseler "Das Geheimnis der freien Lenkachsen - wie weit sind sie eine Losung der Kurrenfrage?", Z. Ver. Deutsch Eisenbahnverwalt, 1929.

8. Muller, C.Th. "Dynamics of Railway Vehicles on Curved Track", Proceedings Institution of Mechanical Engineers, London Vol. 180, 1965.

9. Boocock, D. "Steady State Motion of Railway Vehicles on Curved Track", J. Mech. Eng. Science, Vol. II, 6, 1969.

10. Hannebrink, D.N. et al "Influence of Axle Load, Track, Gauge, and Wheel Profile on Rail Vehicle Hunting", ASME, Paper No. 76-WA/RT-3.

11. Wickens, A.H. "Steering and Dynamic Stability of Railway Vehicles", Vehicle System Dynamics, 5, 15, 1975/76.

12. Scheffel, H. "A New Design Approach for Railway Vehicle Suspension", Rail International, Vol. 5, 638, 1974.

13. Scheffel, H. "The Hunting Stability and Curving Ability of Railway Vehicles", Rail International, Vol. 5, 154, 1974.

14. Bailey, E.C., Caldwell, W.N., Marcotte, P.P. "The DR-1 Truck, A Significant Advance in Freight Car Truck Technology", Engineering Conference, Pub. Col., 1978.

15. Marcotte, P.P., Caldwell, W.N. "Articulated Truck Development", CN Rail Research, June 1978.

16. Scales, B.T. "Behaviour of Bogies on Curves", Railway Eng. Nournal, Vol. 1, 19, 1972.

17. Scales B.T. Private Communication with C.R. Pike, August 4, 1978.

18. Weber, H.B. "Trucks for 100 MPH Freight Service", National Castings Division, Midland-Ross Corporation.

19. Southern Pacific Transportation Co. "Freight Car Truck Design Optimization", Report No. FRA-OR&D 76-133.

20. Perlman, A.B. "Computational Methods for the Prediction of Truck Performance in Curves", ASME Paper No. 76-WA/RT-15.

21. Anon "Northeast Corridor High Speed Rail Passenger Improvement Study", Task a....Technical and Economic Analysis of Vehicle/Right-of-Way Systems", Vol. 1, FRA-ONECD-75-9, 1975.

22. Ahlbeck, D.R., Harrison, H.D. "Techniques for Measuring Wheel/Rail Forces with Trackside Instrumentation", ASME publications, 77-WA/RT-9.

23. Anon "Stresses in the Rails, the Ballast and the Formation Resulting from Traffic Loads", Interim Report No. 1, Stresses in Rails, ORE, UIC, Utrecht, Netherlands (D71/RRI/E(ee900)), 1965.

24. Lundgren, J.R. et al "Measurement of Curving Forces of Railway Vehicles with Instrumented Baseplates" CN Rail Research, Report No. 113, 1973.

25. Scott, J.F. "Measurement of Tieplate Loads in Track, Mile 33.3 Lac St. John Subdivision", CN Rail Research, Report 107, August 1972.

26. Kalousek, J., Yee, L. "Measurement of Angle-of-Attack with Lasers" Canadian Pacific Ltd., Research Report No. S552-77, 1977.

27. Marcotte, P.P. "Test Report on the Comparative Curving Performance of Freight Car Trucks on Special Wheel Profiles", CN Rail Research, Report No. 122, 1975.

28. Heumann H. "Grundzuge der Fuhrung der Schienenfahrzeuge", R. Oldenburg, Munich, 1954.

29. Kunieda, M. "Theoretical Study on the Side Thrust of Truck Wheels Running on Curves", Quarterly Reports, 105, 1970.

30. Marcotte, P.P. "Theoretical Study Concerning the Use of Profiled Wheels on Freight Car Trucks", CN Rail Research, Report 115, 1973.

31. Hay, W.W. "Railroad Engineering", John Wiley & Sons, Inc., 1953.

32. List, H. Private Communication with C.R. Pike, August 1978, Canadian Pacific, Research Department, File Q9-2-4.

APPENDIX I

WHEEL AND RAIL WEAR

With reference to Figure 68, the lateral force equilibrium of a leading wheelset on a curve can be written as:

(Creep Force of Outer Wheel, $\mu Q \cos\xi$) + (Creep Force of Inner Wheel, $\mu Q \cos\xi$) + (Flange Force of Outer Wheel, P_f) + (Force Transmitted to the Wheelset from the Truck Frame Through the Suspension System) = 0.

Even in the case of the wheel having a profile that ensures a one-point contact condition on the straight track, it is usual that there are two wheel contact points when the flange touches the curved rail with a certain angle-of-attack. The above equation can, therefore, be applied in almost all cases.

The wheel load of the outer and inner wheels can be considered equal, especially in the case of balance speed, and their coefficient of sliding friction would, accordingly, be equal. The force transmitted to the wheelset from the truck frame can be disregarded as it is rather small compared to the creep and flange forces. With these approximations, the above equation can be written as:

Creep Force of Outer Leading wheel = $\frac{1}{2} \times$ (Flange Force of Outer Leading Wheel)

The side thrust or the guiding lateral force, Y_f (which was measured by the lateral strain gauge circuit), can be described as:

$$Y_f = \text{Flange Force} - \text{Creep Force}$$

Thus,

$$Y_f = \tfrac{1}{2} \text{ Flange Force } (P_f)$$

or

$$P_f = 2\,Y_f$$

The wear of the wheel tread and the flange, as well as of the rail top and gauge side, can be described as follows:

i. The wear of the wheel flange is proportional to $P_f\ \alpha/r$, see Reference 28, where r is the wheel rolling circle radii. The value of r cannot be evaluated with instrumentation used in this test. For simplicity, r can be considered a constant factor for all tested trucks and can then be calculated as proportional to:

$$P_f\,\alpha = 2\,Y_f\,\alpha$$

ii. The wear of the rail gauge, see Reference 28, is proportional to:

$$P_f\,\alpha = 2\,Y_f\,\alpha$$

iii. The wear of the rail top and wheel tread is proportional to:

$$\mu\,Q\cos\xi = \tfrac{1}{2}\,P_f\,\alpha = Y_f\,\alpha$$

From the above, it can be shown that the wear of the wheel tread and flange as well as of the rail gauge side and head is proportional to the product of the lateral force, Y_f, and the angle-of-attack, α.

APPENDIX II

HIGH SPEED TEST DATA ANALYSIS

Several methods exist for describing mechanical or electrical vibrational phenomena. If the vibration is periodic, all the information necessary for a complete description is contained in one period of the signal. However, if the signal is non-periodic, an infinitely long record of the signal is theoretically necessary for a complete description of the signal. Furthermore, if the time record of the signal is too long it becomes a very inconvenient form of signal description and other methods are used.

The accelerometer data recorded during the test and presented in the report was analyzed by Hewlett-Packard, Model 5420A Digital Signal Analyzer with an analog/digital converter at the National Research Council of Canada, Railway Laboratory.

In the high speed stability tests the output signal, in volts, from the accelerometers which was recorded on analog tape formed an input to the Analyzer. In the case of the lateral accelerometers located on the axle and the car body, the accelerometer signal outputs were first suitably filtered at 30 Hz using a Krohn-Hite filter with a 24 db octave attenuation slope and any DC offset was removed by filtering below 0.1 Hz.

The power spectral density analysis technique consists of analyzing an electrical signal into its component frequencies and calculating the normalized signal power of each of its component frequencies. In the Digital Signal Analyzer, the range of frequencies looked for in the Fourier Analysis of the signal is not infinite nor is its resolution. By reducing the analyzer bandwidth the resolution can be increased. In our analysis of the lateral accelerometer data the bandwidth of 0-30 Hz gave a resolution of .125 Hz. By considering the frequency range of 0 to 30 Hz, most of the recorded data at the maximum test speed of 75 mph was analyzed. At lower speeds, below 75 mph, as the length of recorded data increased the number of samples accepted by the analyzer remained constant, thus a shorter sample of recorded data was analyzed. For uniformity and to avoid the variable of track input to various test trucks, the data at different test speeds was analyzed over the same section of track for all the trucks. The output of the analysis is in the form of a plot of signal power normalized to a 1 Hz bandwidth against frequency, i.e., in our particular case mean square acceleration in units g^2/Hz (g - 32.2 ft./sec.^{2}) as the amplitude versus frequency.

The shape of the plot then defines the distribution of the mean square acceleration per unit bandwidth as a function of the frequency over the frequency range that has been selected. Signal power is not generally equivalent to physical power but the concept of signal power is nonetheless useful in analyzing the signal. The most readily available result of the power spectral density analysis is the square root under the P.S.D. curve which is the root mean square of the signal, which corresponds to the root mean square acceleration level as seen by the accelerometers.

The data from the two longitudinal accelerometers mounted on an axle of the test trucks is not presented in the report. Part of the data was analyzed to determine the yaw angle of the axle. When the trucks were hunting, the two ends of the axle of the instrumented truck were 180^0 out of phase and the hunting component frequency was the dominant frequency. However, when the trucks were not hunting, the wheel frequency was the dominant frequency and the displacement spectrum did not have any component of sufficient magnitude to make it meaningful and consequently further analysis of the signals were meaningless.

APPENDIX III

LIST OF OBSERVERS PRESENT AT THE TRUCK EVALUATION TESTS IN CALGARY

Name	Title	Company
R.A. Bardwell	Engineer of Tests	Southern Pacific Transportation Company, Technical Research and Development, San Francisco, Ca.
Joseph Brown	Senior Product Engineer	Midland Ross, National Castings Division, Cleveland, Ohio
Harold A. Mork	Sales Engineer	Griffin Steel Foundries Ltd., Quebec
W.J. Kucera	Senior Engineer	Griffin Wheel Company, Chicago, Ill.
Gerald A. Musolf	Project Engineer	Standard Car Truck Co., Chicago, Ill.
Erwin R. Perc	Sales Representative	Canadian Steel Wheel Division, Hawker Siddeley Canada Ltd., Quebec
R.E. Waring	Manager, Marketing	I.E.C. - Holden Ltd., Montreal, Quebec
Don Wiebe	Vice President, Research & Engineering	A. Stucki Co.
Norman A. Morella	Manager, Engineering & Development	Midland Ross, National Castings Division, Cleveland, Ohio
G. Tennikait	Manager, Test Engineering	American Steel Foundries, Granite City, Illinois
Dennis L. Rhen	Project Engineer	A. Stucki Co., Pittsburgh, Ohio
Dave W. Falconi	Railroad Service Representative	Dominion Foundries and Steel Limited, Hamilton, Ontario
Harold A. List		Railway Engineering Associates Inc.
Nelson Caldwell	Senior Research Engineer	Canadian National Railways
P. Marcotte	Research Engineer	Canadian National Railways
B.T. Scales		J.P. Devine Mfg. Co.
R. Dukkipati	Associate Research Officer	National Research Council Railway Laboratory

TRUCK	BARBER S-2 (REFERENCE TRUCK)	DR-I RADIAL RETROFITTED TO BARBER STANDARD TRUCK	BARBER-SCHEFFEL TRUCK	DEVINE-SCALE TRUCK	SWING MOTION TRUCK	RIDE CONTROL TRUCK
Capacity	100-ton	100-ton	100-ton	100-ton	100-ton	100-ton
Wheels 36" Diameter	'A' Profile	'A' Profile	'A' Profile	'A' Profile	'A' Profile	'A' Profile
Axle Type	Standard AAR	Standard AAR	Standard AAR	Standard AAR	Standard AAR	Standard AAR
Roller Bearings	6½" x 12"	6½" x 12"	6½" x 12"	6½" x 12"	6½" x 12"	6½" x 12"
Wheel Base	70"	70"	75"	70"	72"	70"
Bolster Centre Plate Diameter	14"	14"	16"	14"	16"	14"

TABLE 1: TESTED TRUCK DATA

Curvature Range Degrees	Percent of Mileage							
	Total Route	Laggan Sd	Mountain Sd	Shuswap Sd	Thompson Sd	Cascade Sd	Lake Windermere Sd	Cranbrook Sd
Tangent	62.16	69.53	59.64	63.95	51.43	64.87	61.68	63.74
1- 2	5.62	6.93	3.46	9.31	4.56	5.95	4.15	4.91
2- 3	7.27	8.62	2.63	5.26	6.86	9.12	8.74	10.38
3- 4	5.54	4.85	4.64	3.24	7.87	7.18	6.33	3.75
4- 5	5.34	3.59	4.63	3.69	8.55	4.98	6.83	4.56
5- 6	3.30	2.85	3.40	2.91	4.86	2.99	3.52	2.01
6- 7	3.84	0.95	5.99	3.52	6.38	1.84	4.80	3.21
7- 8	1.59	0.04	1.68	1.72	3.05	0.95	1.72	2.48
8- 9	2.76	0.62	6.56	4.41	3.97	1.52	1.16	1.15
9-10	0.86	0.33	1.45	1.55	0.76	0.56	0.39	1.42
10-11	1.44	1.70	5.51	0.19	1.01	0.00	0.69	1.05
11-12	0.16	0.00	0.33	0.14	0.50	0.00	0.00	0.33
12-13	0.12	0.00	0.00	0.08	0.21	0.00	0.00	1.01
13-14	0.00	0.00	0.00	0.00	0.00	0.00	0.00	0.00
14-15	0.02	0.00	0.09	0.00	0.00	0.02	0.00	0.00

TABLE 2: CURVATURE ON CANADIAN PACIFIC LINES BETWEEN CALGARY-VANCOUVER

TABLE 3: CURVING PERFORMANCE TEST CONSISTS

Consist I

SD-40 locomotive (CP 5774)

1	50 ton box (loaded with grain)
1	Bathtub coal car (CP 351478 - wt. 259,200 lbs.) with 2 Barber S-2 Trucks.
1	Bathtub coal car (CP 351397 - wt. 260,500 lbs.) with 2 DR-1 Trucks.
1	Bathtub coal car (CP 351393 - wt. 259,300 lbs.) with 2 Barber-Scheffel Trucks.
1	Caboose.

Consist II

SD-40 locomotive (CP 5682)

2	50 ton box (loaded with grain) (CP 112250 and CP 118584).
1	Bathtub coal car (CP 351478 - wt. 259,200 lbs.) with 2 Barber S-2 Trucks.
1	Bathtub coal car (CP 351397 - wt. 260,500 lbs.) with 2 Devine-Scale Radial Trucks.
1	Bathtub coal car (CP 351393 - wt. 259,300 lbs.) with 2 Swing Motion Trucks.
1	Caboose.

Consist III

SD-40 locomotive (CP 5825)

1	50 ton box (loaded with grain) (CP 111466)
1	Bathtub coal car (CP 351478 - wt. 259,200 lbs.) with 2 Barber S-2 Trucks.
1	Bathtub coal car (CP 351393 - wt. 259,300 lbs.) with 2 Barber S-2 Trucks equipped with C-PEP.
1	Bathtub coal car (CP 351397 - wt. 260,500 lbs.) with 2 Barber S-2 Trucks equipped with Stucki Constant Contact Side Bearings.
1	Caboose.

Consist IV

SD-40 locomotive (CP 5640)

1 50 ton box (loaded with grain) (CP 111466)

1 Bathtub coal car (CP 351478 - wt. 259,200 lbs.) with 2 Barber S-2 Trucks.

1 Bathtub coal car (CP 351393 - wt. 259,300 lbs.) with 2 Ride Control Trucks.

1 Bathtub coal car (CP 351397 - wt. 260,500 lbs.) with 2 Barber S-2 Trucks.

With each of these consists, except Consist IV, all three test cars were equipped with CN 'A' profile wheelsets which is a worn wheel profile approximating an average service-worn wheel pattern, see Reference 30. In Consist IV, the Standard Barber trucks were equipped with AAR profile wheels for comparison with the reference Barber S-2 truck with 'A' profile wheels.

TABLE 4 - LATERAL FORCE RESULTS TABULATED BY AXLES FOR EACH CONSIST AT THREE TEST SPEEDS

SPEED = 25 MPH, CONSIST NO.1, GAUGE 2L

			ABSOLUTE AVERAGE (KIPS)			ALGEBRAIC AVERAGE (KIPS)			MAXIMUM VALUE (KIPS)		
ORIENT.	DIR.	AXLE	BARBER	LIST	SCHEFFEL	BARBER	LIST	SCHEFFEL	BARBER	LIST	SCHEFFEL
UNMVED	WEST	1	1.90	1.50	1.90	1.90	1.50	1.90	2.00	1.00	2.00
		2	0.45	3.65	1.45	0.15	-3.65	1.45	0.00	-4.00	2.60
		3	0.75	2.15	2.00	-0.45	2.15	2.00	-1.20	2.30	2.20
		4	1.05	1.30	4.85	-1.05	-1.30	-4.85	-1.20	-2.30	-5.00
UNMVED	EAST	4	8.60	7.05	5.60	8.60	7.05	5.60	10.20	7.30	6.50
		3	3.90	1.15	3.00	6.90	-1.15	3.00	1.90	-1.00	3.70
		2	9.20	4.20	5.30	5.20	4.20	5.30	10.50	4.70	6.10
		1	2.30	0.60	2.90	2.30	-0.60	-2.90	2.60	-0.90	-3.20
MVED	WEST	4	2.40	0.45	2.05	2.40	-0.45	2.05	3.20	-0.00	2.60
		3	2.45	1.80	3.60	2.45	-1.00	-3.00	2.90	-1.00	-4.10
		2	1.75	1.65	0.45	1.75	1.65	0.45	2.30	1.00	6.60
		1	1.75	1.80	0.45	-1.75	-1.80	-0.45	-2.00	-1.00	-0.66
MVED	EAST	1	5.00	4.55	3.50	5.00	4.55	3.50	5.00	4.70	3.00
		2	2.75	0.60	2.30	2.75	0.60	-2.30	3.50	1.20	-2.30
		3	0.75	2.00	2.30	0.75	2.00	2.30	9.30	2.00	2.60
		4	1.00	2.60	1.75	-1.00	-2.60	1.75	-2.00	-2.40	2.00

SPEED = 25 MPH, CONSIST NO.1, GAUGE 3L

			ABSOLUTE AVERAGE (KIPS)			ALGEBRAIC AVERAGE (KIPS)			MAXIMUM VALUE (KIPS)		
ORIENT.	DIR.	AXLE	BARBER	LIST	SCHEFFEL	BARBER	LIST	SCHEFFEL	BARBER	LIST	SCHEFFEL
UNMVED	WEST	1	2.10	4.25	3.55	2.10	4.25	3.55	3.10	4.50	4.50
		2	3.30	3.30	2.10	6.30	-3.30	2.10	0.00	-3.70	3.10
		3	3.90	3.25	3.55	6.90	3.25	3.55	6.90	3.40	4.30
		4	3.55	2.70	4.55	6.55	-2.70	-4.55	1.10	-3.10	-5.10
UNMVED	EAST	4	4.25	4.00	2.55	4.25	4.00	2.55	5.70	4.00	3.10
		3	3.70	3.70	1.40	-3.70	-3.70	1.40	-4.00	-3.70	1.70
		2	5.00	3.10	4.40	5.00	3.10	4.40	0.00	3.10	4.66
		1	1.15	0.15	3.70	-1.15	0.15	-3.70	-2.30	0.30	-4.00
MVED	WEST	4	4.70	1.05	3.30	4.70	1.05	3.30	7.40	3.10	4.30
		3	2.45	0.00	3.55	2.45	0.00	-3.55	3.70	0.00	-4.00
		2	4.55	4.00	2.55	4.55	4.00	2.55	6.06	5.10	3.10
		1	1.15	1.75	0.60	-1.15	-1.75	0.00	-2.30	-2.60	-0.60
MVED	EAST	1	2.45	2.45	2.45	2.45	2.45	2.05	3.40	2.60	2.00
		2	2.15	1.30	4.40	-2.15	-3.70	-4.40	-2.00	-2.00	-4.50
		3	5.00	2.75	1.05	5.00	2.75	1.05	5.70	2.50	2.00
		4	2.70	1.55	1.05	-2.70	-1.55	1.05	-3.10	-1.70	2.60

SPEED = 25 MPH, CONSIST NO.1, GAUGE 5L

			ABSOLUTE AVERAGE (KIPS)			ALGEBRAIC AVERAGE (KIPS)			MAXIMUM VALUE (KIPS)		
ORIENT.	DIR.	AXLE	BARBER	LIST	SCHEFFEL	BARBER	LIST	SCHEFFEL	BARBER	LIST	SCHEFFEL
UNMVED	WEST	1	2.30	1.05	1.45	2.00	1.05	1.45	2.60	2.30	2.00
		2	2.60	4.45	0.45	-2.60	-4.45	-0.45	-2.90	-4.90	-0.60
		3	0.75	1.10	1.70	0.15	1.10	1.76	0.90	1.20	1.70
		4	2.90	4.60	4.90	-2.90	-4.60	-4.90	-3.20	-5.20	-5.20
UNMVED	EAST	4	0.95	0.30	1.60	0.55	0.30	-1.60	1.20	0.00	-2.30
		3	2.75	3.05	1.30	-2.75	-3.05	-1.30	-2.90	-4.00	-1.40
		2	0.75	1.15	3.45	0.75	-1.15	-3.45	0.90	-1.40	-3.70
		1	3.75	4.15	4.90	-3.75	-4.15	-4.90	-4.00	-4.30	-5.20
MVED	WEST	4	2.30	0.15	0.45	2.30	-0.15	0.45	3.70	-0.30	6.00
		3	0.45	2.00	3.75	-0.45	-2.00	-3.75	-0.60	-2.60	-4.00
		2	1.95	0.30	0.15	1.95	0.30	0.15	3.50	0.30	0.30
		1	3.85	4.60	1.15	-3.85	-4.60	-1.15	-4.00	-5.20	-1.40
MVED	EAST	1	0.55	1.20	1.05	-0.55	-1.20	-1.05	-0.60	-1.20	-2.30
		2	3.20	3.60	3.60	-3.20	-3.60	-3.60	-3.50	-3.70	-3.70
		3	0.30	2.30	0.90	0.00	-2.30	-0.90	-0.30	-2.30	-1.20
		4	2.75	4.00	2.60	-2.75	-4.00	-2.60	-2.90	-4.00	-2.60

SPEED = 25 MPH, CONSIST NO.2, GAUGE 2L

			ABSOLUTE AVERAGE (KIPS)			ALGEBRAIC AVERAGE (KIPS)			MAXIMUM VALUE (KIPS)		
ORIENT.	DIR.	AXLE	BARBER	SCALE	SWING	BARBER	SCALE	SWING	BARBER	SCALE	SWING
UNMVED	WEST	1	2.35	2.05	5.05	2.35	2.05	5.05	3.20	2.20	5.70
		2	3.65	0.90	0.50	3.65	-0.93	0.60	5.00	-1.00	1.50
		3	2.50	0.80	3.50	2.50	-3.50	3.50	3.50	-1.30	4.40
		4	1.35	2.05	2.45	-1.35	-2.05	-2.45	-1.50	-2.90	-2.50
UNMVED	EAST	4	6.70	5.30	8.40	6.70	5.30	8.90	6.70	5.30	8.60
		3	5.20	3.20	0.00	5.20	3.20	0.00	5.20	3.20	0.00
		2	9.90	4.40	0.90	9.90	4.40	0.50	9.90	4.40	0.50
		1	0.90	1.20	3.90	0.90	1.20	-3.50	0.90	1.20	-3.80
MVED	WEST	4	2.00	3.35	2.30	2.00	3.35	2.30	2.90	3.50	2.60
		3	0.25	3.95	2.45	0.25	-3.95	-2.45	0.30	-4.40	-2.90
		2	1.40	0.90	1.75	-1.40	0.90	1.75	-1.50	1.20	2.30
		1	2.45	0.55	2.05	-2.45	-0.55	-2.05	-2.00	-0.00	-2.30
MVED	EAST	1	4.70	4.70	7.00	4.70	4.70	7.00	4.70	4.70	7.00
		2	1.20	0.93	5.00	1.20	0.93	-5.00	1.20	0.93	-5.00
		3	6.10	3.20	7.60	6.10	3.20	7.00	6.10	3.20	7.60
		4	1.90	1.20	2.90	1.90	1.20	-2.90	1.90	1.20	-2.56

SPEED = 25 MPH, CONSIST NO.2, GAUGE 3L

			ABSOLUTE AVERAGE (KIPS)			ALGEBRAIC AVERAGE (KIPS)			MAXIMUM VALUE (KIPS)		
ORIENT.	DIR.	AXLE	BARBER	SCALE	SWING	BARBER	SCALE	SWING	BARBER	SCALE	SWING
UNMVED	WEST	1	2.80	2.30	10.80	2.80	2.30	10.00	2.80	2.30	10.00
		2	2.30	2.00	1.40	2.30	2.00	-1.00	2.30	2.00	-1.46
		3	5.70	4.30	11.10	5.70	4.30	11.10	5.70	4.30	11.10
		4	2.00	1.30	0.00	2.00	-1.30	0.00	2.00	-1.30	0.00
UNMVED	EAST	4	3.95	2.05	4.85	3.95	2.05	4.85	4.00	3.40	5.00
		3	0.55	1.30	3.65	-0.55	-1.30	-3.65	-1.10	-1.70	-4.36
		2	5.55	2.55	5.65	5.55	2.55	5.65	7.10	3.10	6.50
		1	2.40	2.00	3.15	-2.40	-2.00	-3.15	-3.10	-2.30	-3.40
MVED	WEST	4	3.25	5.70	3.55	3.25	5.70	3.60	3.60	5.70	3.76
		3	1.55	4.25	3.70	1.55	-4.25	-3.70	1.70	-4.00	-3.76
		2	0.45	2.00	5.70	0.45	2.00	5.70	0.60	2.00	6.00
		1	1.60	2.80	3.65	-1.60	-2.66	-3.65	-2.30	-2.30	-4.30
MVED	EAST	1	1.40	2.70	3.40	1.40	2.70	3.00	1.40	2.70	3.40
		2	4.90	3.10	4.20	-4.00	-3.10	-4.00	-4.00	-3.10	-4.06
		3	2.30	2.60	6.00	2.30	2.00	6.00	2.30	2.00	0.00
		4	2.10	2.30	4.06	-2.30	-2.30	-4.00	-2.30	-2.30	-4.00

SPEED = 25 MPH, CONSIST NO.2, GAUGE 5L

			ABSOLUTE AVERAGE (KIPS)			ALGEBRAIC AVERAGE (KIPS)			MAXIMUM VALUE (KIPS)		
ORIENT.	DIR.	AXLE	BARBER	SCALE	SWING	BARBER	SCALE	SWING	BARBER	SCALE	SWING
UNMVED	WEST	1	3.20	2.90	0.00	3.20	2.90	6.00	3.20	2.90	0.00
		2	0.60	2.60	0.60	4.60	-2.66	0.00	4.60	-2.00	0.60
		3	4.30	0.90	4.30	4.30	0.96	4.30	4.30	6.90	4.30
		4	3.50	3.20	4.60	-3.50	-3.20	-4.60	-3.50	-3.20	-4.66
UNMVED	EAST	4	2.30	1.40	0.30	2.30	-1.46	-0.30	2.30	-1.40	-0.30
		3	1.70	0.06	0.30	-1.70	0.06	0.30	-1.70	6.00	0.36
		2	1.70	3.20	4.50	1.70	-3.20	0.90	1.70	-3.20	4.56
		1	3.70	4.30	4.00	-3.70	-4.36	-4.00	-3.70	-4.30	-4.00
MVED	WEST	4	3.90	3.45	2.15	6.90	3.45	2.15	1.90	3.70	2.00
		3	2.15	5.20	5.05	-2.15	-5.20	-5.05	-2.00	-5.50	-5.26
		2	2.00	0.90	1.30	-2.60	0.90	1.30	-2.00	6.90	1.40
		1	3.90	5.65	3.75	-3.36	-5.65	-3.75	-3.70	-5.00	-4.36
MVED	EAST	1	0.30	0.30	0.00	-0.30	0.30	0.00	-0.30	0.30	0.66
		2	4.30	5.00	3.40	-4.30	-5.00	-3.40	-4.30	-5.00	-3.46
		3	2.60	3.70	1.40	-2.60	-3.70	1.00	-2.00	-3.70	1.00
		4	4.90	4.60	4.50	-4.90	-4.60	-4.50	-4.90	-4.00	-4.50

SPEED = 25 MPH, CONSIST NO.3, GAUGE 2L

ORIENT.	DIR.	AXLE	ABSOLUTE AVERAGE (KIPS) BARBER	C-PEP	STUCKI	ALGEBRAIC AVERAGE (KIPS) BARBER	C-PEP	STUCKI	MAXIMUM VALUE (KIPS) BARBER	C-PEP	STUCKI
UNWYED	WEST	1	[illegible]	[illegible]	[illegible]	[illegible]	[illegible]	[illegible]	[illegible]	[illegible]	[illegible]
		2	[illegible]	[illegible]	[illegible]	[illegible]	[illegible]	[illegible]	[illegible]	[illegible]	[illegible]
		3	[illegible]	[illegible]	[illegible]	[illegible]	[illegible]	[illegible]	[illegible]	[illegible]	[illegible]
		4	[illegible]	[illegible]	[illegible]	[illegible]	[illegible]	[illegible]	[illegible]	[illegible]	[illegible]
UNWYED	EAST	4	[illegible]	[illegible]	[illegible]	[illegible]	[illegible]	[illegible]	[illegible]	[illegible]	[illegible]
		3	[illegible]	[illegible]	[illegible]	[illegible]	[illegible]	[illegible]	[illegible]	[illegible]	[illegible]
		2	[illegible]	[illegible]	[illegible]	[illegible]	[illegible]	[illegible]	[illegible]	[illegible]	[illegible]
		1	[illegible]	[illegible]	[illegible]	[illegible]	[illegible]	[illegible]	[illegible]	[illegible]	[illegible]
WYED	WEST	4	[illegible]	[illegible]	[illegible]	[illegible]	[illegible]	[illegible]	[illegible]	[illegible]	[illegible]
		3	[illegible]	[illegible]	[illegible]	[illegible]	[illegible]	[illegible]	[illegible]	[illegible]	[illegible]
		2	[illegible]	[illegible]	[illegible]	[illegible]	[illegible]	[illegible]	[illegible]	[illegible]	[illegible]
		1	[illegible]	[illegible]	[illegible]	[illegible]	[illegible]	[illegible]	[illegible]	[illegible]	[illegible]
WYED	EAST	1	[illegible]	[illegible]	[illegible]	[illegible]	[illegible]	[illegible]	[illegible]	[illegible]	[illegible]
		2	[illegible]	[illegible]	[illegible]	[illegible]	[illegible]	[illegible]	[illegible]	[illegible]	[illegible]
		3	[illegible]	[illegible]	[illegible]	[illegible]	[illegible]	[illegible]	[illegible]	[illegible]	[illegible]
		4	[illegible]	[illegible]	[illegible]	[illegible]	[illegible]	[illegible]	[illegible]	[illegible]	[illegible]

SPEED = 25 MPH, CONSIST NO.3, GAUGE 3L

ORIENT.	DIR.	AXLE	ABSOLUTE AVERAGE (KIPS) BARBER	C-PEP	STUCKI	ALGEBRAIC AVERAGE (KIPS) BARBER	C-PEP	STUCKI	MAXIMUM VALUE (KIPS) BARBER	C-PEP	STUCKI
UNWYED	WEST	1	[illegible]	[illegible]	[illegible]	[illegible]	[illegible]	[illegible]	[illegible]	[illegible]	[illegible]
		2	[illegible]	[illegible]	[illegible]	[illegible]	[illegible]	[illegible]	[illegible]	[illegible]	[illegible]
		3	[illegible]	[illegible]	[illegible]	[illegible]	[illegible]	[illegible]	[illegible]	[illegible]	[illegible]
		4	[illegible]	[illegible]	[illegible]	[illegible]	[illegible]	[illegible]	[illegible]	[illegible]	[illegible]
UNWYED	EAST	4	[illegible]	[illegible]	[illegible]	[illegible]	[illegible]	[illegible]	[illegible]	[illegible]	[illegible]
		3	[illegible]	[illegible]	[illegible]	[illegible]	[illegible]	[illegible]	[illegible]	[illegible]	[illegible]
		2	[illegible]	[illegible]	[illegible]	[illegible]	[illegible]	[illegible]	[illegible]	[illegible]	[illegible]
		1	[illegible]	[illegible]	[illegible]	[illegible]	[illegible]	[illegible]	[illegible]	[illegible]	[illegible]
WYED	WEST	4	[illegible]	[illegible]	[illegible]	[illegible]	[illegible]	[illegible]	[illegible]	[illegible]	[illegible]
		3	[illegible]	[illegible]	[illegible]	[illegible]	[illegible]	[illegible]	[illegible]	[illegible]	[illegible]
		2	[illegible]	[illegible]	[illegible]	[illegible]	[illegible]	[illegible]	[illegible]	[illegible]	[illegible]
		1	[illegible]	[illegible]	[illegible]	[illegible]	[illegible]	[illegible]	[illegible]	[illegible]	[illegible]
WYED	EAST	1	[illegible]	[illegible]	[illegible]	[illegible]	[illegible]	[illegible]	[illegible]	[illegible]	[illegible]
		2	[illegible]	[illegible]	[illegible]	[illegible]	[illegible]	[illegible]	[illegible]	[illegible]	[illegible]
		3	[illegible]	[illegible]	[illegible]	[illegible]	[illegible]	[illegible]	[illegible]	[illegible]	[illegible]
		4	[illegible]	[illegible]	[illegible]	[illegible]	[illegible]	[illegible]	[illegible]	[illegible]	[illegible]

SPEED = 25 MPH, CONSIST NO.3, GAUGE 5L

ORIENT.	DIR.	AXLE	ABSOLUTE AVERAGE (KIPS) BARBER	C-PEP	STUCKI	ALGEBRAIC AVERAGE (KIPS) BARBER	C-PEP	STUCKI	MAXIMUM VALUE (KIPS) BARBER	C-PEP	STUCKI
UNWYED	WEST	1	[illegible]	[illegible]	[illegible]	[illegible]	[illegible]	[illegible]	[illegible]	[illegible]	[illegible]
		2	[illegible]	[illegible]	[illegible]	[illegible]	[illegible]	[illegible]	[illegible]	[illegible]	[illegible]
		3	[illegible]	[illegible]	[illegible]	[illegible]	[illegible]	[illegible]	[illegible]	[illegible]	[illegible]
		4	[illegible]	[illegible]	[illegible]	[illegible]	[illegible]	[illegible]	[illegible]	[illegible]	[illegible]
UNWYED	EAST	4	[illegible]	[illegible]	[illegible]	[illegible]	[illegible]	[illegible]	[illegible]	[illegible]	[illegible]
		3	[illegible]	[illegible]	[illegible]	[illegible]	[illegible]	[illegible]	[illegible]	[illegible]	[illegible]
		2	[illegible]	[illegible]	[illegible]	[illegible]	[illegible]	[illegible]	[illegible]	[illegible]	[illegible]
		1	[illegible]	[illegible]	[illegible]	[illegible]	[illegible]	[illegible]	[illegible]	[illegible]	[illegible]
WYED	WEST	4	[illegible]	[illegible]	[illegible]	[illegible]	[illegible]	[illegible]	[illegible]	[illegible]	[illegible]
		3	[illegible]	[illegible]	[illegible]	[illegible]	[illegible]	[illegible]	[illegible]	[illegible]	[illegible]
		2	[illegible]	[illegible]	[illegible]	[illegible]	[illegible]	[illegible]	[illegible]	[illegible]	[illegible]
		1	[illegible]	[illegible]	[illegible]	[illegible]	[illegible]	[illegible]	[illegible]	[illegible]	[illegible]
WYED	EAST	1	[illegible]	[illegible]	[illegible]	[illegible]	[illegible]	[illegible]	[illegible]	[illegible]	[illegible]
		2	[illegible]	[illegible]	[illegible]	[illegible]	[illegible]	[illegible]	[illegible]	[illegible]	[illegible]
		3	[illegible]	[illegible]	[illegible]	[illegible]	[illegible]	[illegible]	[illegible]	[illegible]	[illegible]
		4	[illegible]	[illegible]	[illegible]	[illegible]	[illegible]	[illegible]	[illegible]	[illegible]	[illegible]

SPEED = 25 MPH, CONSIST NO.4, GAUGE 2L

ORIENT.	DIR.	AXLE	ABSOLUTE AVERAGE (KIPS) BARBER	RIDE	NEW AAR	ALGEBRAIC AVERAGE (KIPS) BARBER	RIDE	NEW AAR	MAXIMUM VALUE (KIPS) BARBER	RIDE	NEW AAR
UNWYED	WEST	1	[illegible]	[illegible]	[illegible]	[illegible]	[illegible]	[illegible]	[illegible]	[illegible]	[illegible]
		2	[illegible]	[illegible]	[illegible]	[illegible]	[illegible]	[illegible]	[illegible]	[illegible]	[illegible]
		3	[illegible]	[illegible]	[illegible]	[illegible]	[illegible]	[illegible]	[illegible]	[illegible]	[illegible]
		4	[illegible]	[illegible]	[illegible]	[illegible]	[illegible]	[illegible]	[illegible]	[illegible]	[illegible]
UNWYED	EAST	4	[illegible]	[illegible]	[illegible]	[illegible]	[illegible]	[illegible]	[illegible]	[illegible]	[illegible]
		3	[illegible]	[illegible]	[illegible]	[illegible]	[illegible]	[illegible]	[illegible]	[illegible]	[illegible]
		2	[illegible]	[illegible]	[illegible]	[illegible]	[illegible]	[illegible]	[illegible]	[illegible]	[illegible]
		1	[illegible]	[illegible]	[illegible]	[illegible]	[illegible]	[illegible]	[illegible]	[illegible]	[illegible]
WYED	WEST	4	[illegible]	[illegible]	[illegible]	[illegible]	[illegible]	[illegible]	[illegible]	[illegible]	[illegible]
		3	[illegible]	[illegible]	[illegible]	[illegible]	[illegible]	[illegible]	[illegible]	[illegible]	[illegible]
		2	[illegible]	[illegible]	[illegible]	[illegible]	[illegible]	[illegible]	[illegible]	[illegible]	[illegible]
		1	[illegible]	[illegible]	[illegible]	[illegible]	[illegible]	[illegible]	[illegible]	[illegible]	[illegible]
WYED	EAST	1	[illegible]	[illegible]	[illegible]	[illegible]	[illegible]	[illegible]	[illegible]	[illegible]	[illegible]
		2	[illegible]	[illegible]	[illegible]	[illegible]	[illegible]	[illegible]	[illegible]	[illegible]	[illegible]
		3	[illegible]	[illegible]	[illegible]	[illegible]	[illegible]	[illegible]	[illegible]	[illegible]	[illegible]
		4	[illegible]	[illegible]	[illegible]	[illegible]	[illegible]	[illegible]	[illegible]	[illegible]	[illegible]

SPEED = 25 MPH, CONSIST NO.4, GAUGE 3L

ORIENT.	DIR.	AXLE	ABSOLUTE AVERAGE (KIPS) BARBER	RIDE	NEW AAR	ALGEBRAIC AVERAGE (KIPS) BARBER	RIDE	NEW AAR	MAXIMUM VALUE (KIPS) BARBER	RIDE	NEW AAR
UNWYED	WEST	1	[illegible]	[illegible]	[illegible]	[illegible]	[illegible]	[illegible]	[illegible]	[illegible]	[illegible]
		2	[illegible]	[illegible]	[illegible]	[illegible]	[illegible]	[illegible]	[illegible]	[illegible]	[illegible]
		3	[illegible]	[illegible]	[illegible]	[illegible]	[illegible]	[illegible]	[illegible]	[illegible]	[illegible]
		4	[illegible]	[illegible]	[illegible]	[illegible]	[illegible]	[illegible]	[illegible]	[illegible]	[illegible]
UNWYED	EAST	4	[illegible]	[illegible]	[illegible]	[illegible]	[illegible]	[illegible]	[illegible]	[illegible]	[illegible]
		3	[illegible]	[illegible]	[illegible]	[illegible]	[illegible]	[illegible]	[illegible]	[illegible]	[illegible]
		2	[illegible]	[illegible]	[illegible]	[illegible]	[illegible]	[illegible]	[illegible]	[illegible]	[illegible]
		1	[illegible]	[illegible]	[illegible]	[illegible]	[illegible]	[illegible]	[illegible]	[illegible]	[illegible]
WYED	WEST	4	[illegible]	[illegible]	[illegible]	[illegible]	[illegible]	[illegible]	[illegible]	[illegible]	[illegible]
		3	[illegible]	[illegible]	[illegible]	[illegible]	[illegible]	[illegible]	[illegible]	[illegible]	[illegible]
		2	[illegible]	[illegible]	[illegible]	[illegible]	[illegible]	[illegible]	[illegible]	[illegible]	[illegible]
		1	[illegible]	[illegible]	[illegible]	[illegible]	[illegible]	[illegible]	[illegible]	[illegible]	[illegible]
WYED	EAST	1	[illegible]	[illegible]	[illegible]	[illegible]	[illegible]	[illegible]	[illegible]	[illegible]	[illegible]
		2	[illegible]	[illegible]	[illegible]	[illegible]	[illegible]	[illegible]	[illegible]	[illegible]	[illegible]
		3	[illegible]	[illegible]	[illegible]	[illegible]	[illegible]	[illegible]	[illegible]	[illegible]	[illegible]
		4	[illegible]	[illegible]	[illegible]	[illegible]	[illegible]	[illegible]	[illegible]	[illegible]	[illegible]

SPEED = 25 MPH, CONSIST NO.4, GAUGE 5L

ORIENT.	DIR.	AXLE	ABSOLUTE AVERAGE (KIPS) BARBER	RIDE	NEW AAR	ALGEBRAIC AVERAGE (KIPS) BARBER	RIDE	NEW AAR	MAXIMUM VALUE (KIPS) BARBER	RIDE	NEW AAR
UNWYED	WEST	1	[illegible]	[illegible]	[illegible]	[illegible]	[illegible]	[illegible]	[illegible]	[illegible]	[illegible]
		2	[illegible]	[illegible]	[illegible]	[illegible]	[illegible]	[illegible]	[illegible]	[illegible]	[illegible]
		3	[illegible]	[illegible]	[illegible]	[illegible]	[illegible]	[illegible]	[illegible]	[illegible]	[illegible]
		4	[illegible]	[illegible]	[illegible]	[illegible]	[illegible]	[illegible]	[illegible]	[illegible]	[illegible]
UNWYED	EAST	4	[illegible]	[illegible]	[illegible]	[illegible]	[illegible]	[illegible]	[illegible]	[illegible]	[illegible]
		3	[illegible]	[illegible]	[illegible]	[illegible]	[illegible]	[illegible]	[illegible]	[illegible]	[illegible]
		2	[illegible]	[illegible]	[illegible]	[illegible]	[illegible]	[illegible]	[illegible]	[illegible]	[illegible]
		1	[illegible]	[illegible]	[illegible]	[illegible]	[illegible]	[illegible]	[illegible]	[illegible]	[illegible]
WYED	WEST	4	[illegible]	[illegible]	[illegible]	[illegible]	[illegible]	[illegible]	[illegible]	[illegible]	[illegible]
		3	[illegible]	[illegible]	[illegible]	[illegible]	[illegible]	[illegible]	[illegible]	[illegible]	[illegible]
		2	[illegible]	[illegible]	[illegible]	[illegible]	[illegible]	[illegible]	[illegible]	[illegible]	[illegible]
		1	[illegible]	[illegible]	[illegible]	[illegible]	[illegible]	[illegible]	[illegible]	[illegible]	[illegible]
WYED	EAST	1	[illegible]	[illegible]	[illegible]	[illegible]	[illegible]	[illegible]	[illegible]	[illegible]	[illegible]
		2	[illegible]	[illegible]	[illegible]	[illegible]	[illegible]	[illegible]	[illegible]	[illegible]	[illegible]
		3	[illegible]	[illegible]	[illegible]	[illegible]	[illegible]	[illegible]	[illegible]	[illegible]	[illegible]
		4	[illegible]	[illegible]	[illegible]	[illegible]	[illegible]	[illegible]	[illegible]	[illegible]	[illegible]

TABLE 4 - Continued

SPEED = 37 MPH. CONSIST NO.1. GAUGE 2L

ORIENT.	DIR.	AXLE	ABSOLUTE AVERAGE (KIPS)			ALGEBRAIC AVERAGE (KIPS)			MAXIMUM VALUE (KIPS)		
			BARBER	LIST	SCHEFFEL	BARBER	LIST	SCHEFFEL	BARBER	LIST	SCHEFFEL
UNWYED	WEST	1	7.35	3.00	3.50	7.35	3.00	3.50	7.50	4.40	3.00
		2	1.65	3.05	2.20	1.65	-3.05	2.20	2.30	-3.20	2.40
		3	2.45	2.30	2.10	2.45	2.30	2.10	2.70	3.00	2.50
		4	1.20	1.20	2.90	-1.20	-3.20	-2.90	-1.40	-1.40	-3.00
UNWYED	EAST	4	8.00	7.20	6.40	8.00	7.20	6.40	8.00	7.20	6.40
		3	1.50	0.50	2.50	-1.50	0.50	2.50	-1.50	0.50	2.50
		2	8.00	5.00	7.00	8.00	5.00	7.00	8.00	5.00	7.00
		1	1.00	0.60	2.00	1.00	0.60	-2.00	1.00	0.60	-2.00
WYED	WEST	4	3.10	2.40	3.90	3.10	2.40	3.90	3.00	2.00	4.40
		3	1.75	0.45	3.00	1.75	-0.45	-3.00	1.80	-0.90	-3.40
		2	2.05	1.05	1.75	2.05	1.05	1.75	3.00	2.30	2.60
		1	0.85	1.30	1.70	-0.85	-1.30	1.70	-1.70	-1.90	2.30
WYED	EAST	1	8.15	5.25	6.40	8.15	5.25	6.40	8.20	5.40	7.10
		2	4.65	2.25	1.40	4.65	2.25	-1.40	4.40	2.30	-1.40
		3	8.65	4.15	4.90	8.65	4.15	4.90	8.80	4.30	5.10
		4	1.35	1.50	3.05	1.35	-1.50	3.05	1.60	-1.90	3.60

SPEED = 37 MPH. CONSIST NO.1. GAUGE 3L

ORIENT.	DIR.	AXLE	ABSOLUTE AVERAGE (KIPS)			ALGEBRAIC AVERAGE (KIPS)			MAXIMUM VALUE (KIPS)		
			BARBER	LIST	SCHEFFEL	BARBER	LIST	SCHEFFEL	BARBER	LIST	SCHEFFEL
UNWYED	WEST	1	8.10	5.35	7.00	8.10	5.35	7.00	8.40	6.00	7.30
		2	3.70	2.30	2.05	3.70	-2.30	2.05	4.20	-2.00	2.20
		3	6.60	4.40	3.50	6.60	4.40	3.50	7.20	4.00	4.00
		4	1.35	1.75	3.00	1.35	-1.75	-3.00	1.40	-1.90	-4.00
UNWYED	EAST	4	4.80	3.70	1.75	4.80	3.70	1.75	5.00	4.00	1.90
		3	2.45	2.40	1.70	-2.45	-2.40	1.70	-2.70	-2.60	1.80
		2	3.90	2.05	3.10	3.90	2.05	3.10	4.20	3.00	3.20
		1	1.25	0.60	4.40	1.25	0.60	-4.40	1.50	0.80	-4.40
WYED	WEST	4	3.40	0.30	4.30	3.40	0.30	4.30	3.40	0.80	4.30
		3	2.30	2.60	3.70	2.30	-2.60	-3.70	2.30	-2.80	-3.70
		2	3.70	2.00	3.40	3.70	2.00	3.40	3.70	2.00	3.40
		1	0.90	3.10	0.00	0.90	-3.10	0.00	0.90	-3.10	0.00
WYED	EAST	1	4.15	3.90	3.25	4.15	3.90	3.25	4.20	4.50	3.60
		2	1.10	0.85	3.05	1.10	-0.85	-3.05	1.10	-0.90	-4.50
		3	4.30	3.25	2.70	4.30	3.25	2.70	4.40	7.00	2.80
		4	1.00	0.95	2.00	1.00	0.95	2.00	1.30	1.10	2.20

SPEED = 37 MPH. CONSIST NO.1. GAUGE 5L

ORIENT.	DIR.	AXLE	ABSOLUTE AVERAGE (KIPS)			ALGEBRAIC AVERAGE (KIPS)			MAXIMUM VALUE (KIPS)		
			BARBER	LIST	SCHEFFEL	BARBER	LIST	SCHEFFEL	BARBER	LIST	SCHEFFEL
UNWYED	WEST	1	3.60	2.20	2.00	3.60	2.20	2.00	3.60	2.20	2.00
		2	2.60	2.00	1.00	-2.60	-2.00	1.00	-2.60	-2.00	1.00
		3	1.80	2.20	3.60	1.80	2.20	3.60	1.80	2.20	3.60
		4	2.40	2.20	4.00	-2.40	-2.20	-4.00	-2.40	-2.20	-4.00
UNWYED	EAST	4	3.70	3.20	1.40	3.70	3.20	1.40	3.80	3.40	1.80
		3	1.50	2.10	2.05	-1.50	-2.10	2.05	-1.80	-2.40	2.60
		2	2.70	1.95	1.60	2.70	1.95	1.60	3.00	2.00	2.20
		1	1.20	2.50	2.20	-1.20	-2.50	-2.20	-1.40	-2.60	-2.40
WYED	WEST	4	0.00	2.00	3.70	0.00	2.00	3.70	0.00	2.00	3.70
		3	1.70	0.90	3.70	-1.70	-0.90	-3.70	-1.70	-0.90	-3.70
		2	2.30	3.70	1.70	2.30	3.70	1.70	2.30	3.70	1.70
		1	3.20	3.20	1.20	-3.20	-3.20	-1.20	-3.20	-3.20	-1.20
WYED	EAST	1	1.60	1.40	2.10	1.60	1.40	2.10	1.80	1.40	2.10
		2	1.70	1.30	1.90	-1.70	-1.30	-1.90	-1.70	-1.30	-1.90
		3	4.10	0.00	1.70	4.10	0.00	1.70	4.10	0.00	1.70
		4	1.90	1.70	2.00	1.90	-1.70	2.00	1.90	-1.70	2.00

SPEED = 37 MPH. CONSIST NO.2. GAUGE 2L

ORIENT.	DIR.	AXLE	ABSOLUTE AVERAGE (KIPS)			ALGEBRAIC AVERAGE (KIPS)			MAXIMUM VALUE (KIPS)		
			BARBER	SCALE	SWING	BARBER	SCALE	SWING	BARBER	SCALE	SWING
UNWYED	WEST	1	4.70	4.40	4.70	4.70	4.40	4.70	5.00	4.70	4.70
		2	0.65	1.35	0.65	0.65	-1.35	-0.65	1.30	-1.00	-0.70
		3	1.90	1.55	2.30	1.90	1.55	2.30	2.30	1.90	2.40
		4	1.35	1.10	1.65	1.35	-0.50	-1.65	1.50	-1.00	-1.80
UNWYED	EAST	4	7.00	5.00	10.65	7.00	5.00	10.65	7.00	5.00	10.80
		3	4.25	3.05	1.20	4.25	3.05	1.20	4.40	3.20	1.20
		2	5.47	5.65	9.95	5.47	5.65	9.95	9.90	5.00	10.80
		1	1.05	1.05	3.50	1.05	1.05	-3.50	1.20	1.20	-4.10
WYED	WEST	4	3.20	4.20	4.40	3.20	4.20	4.40	3.20	4.20	4.40
		3	1.00	4.40	2.20	1.00	-4.40	-2.20	1.00	-4.40	-2.20
		2	1.00	2.10	2.00	1.00	2.10	2.00	1.00	2.10	2.00
		1	1.60	2.00	1.20	-1.60	2.00	-1.20	-1.60	2.00	-1.20
WYED	EAST	1	5.40	5.00	9.30	5.40	5.00	9.30	5.00	5.00	5.40
		2	1.40	1.60	1.00	1.40	1.60	-1.00	1.60	2.00	-1.40
		3	6.00	5.00	10.10	6.00	5.00	10.10	6.30	5.20	10.00
		4	1.90	1.00	3.90	1.90	1.00	-3.90	2.20	2.00	-4.00

SPEED = 37 MPH. CONSIST NO.2. GAUGE 3L

ORIENT.	DIR.	AXLE	ABSOLUTE AVERAGE (KIPS)			ALGEBRAIC AVERAGE (KIPS)			MAXIMUM VALUE (KIPS)		
			BARBER	SCALE	SWING	BARBER	SCALE	SWING	BARBER	SCALE	SWING
UNWYED	WEST	1	4.00	5.10	6.20	4.00	5.10	6.20	4.00	5.10	6.20
		2	2.00	0.00	1.40	2.00	0.00	1.40	2.00	0.00	1.40
		3	4.30	1.40	0.20	4.30	1.40	0.20	4.30	1.40	0.20
		4	1.70	2.10	2.60	1.70	-2.10	-2.60	1.70	-2.10	-2.60
UNWYED	EAST	4	3.70	2.30	4.30	3.70	2.30	4.30	3.70	2.30	4.30
		3	0.30	0.90	2.30	-0.30	0.90	-2.30	-0.30	0.90	-2.30
		2	4.00	3.10	5.70	4.00	3.10	5.70	4.00	3.10	5.70
		1	0.00	0.30	2.00	0.00	0.30	-2.00	0.00	0.30	-2.00
WYED	WEST	4	3.00	4.50	5.00	3.00	4.50	5.00	3.00	4.50	5.00
		3	2.40	2.00	0.20	2.40	-2.00	-0.20	2.40	-2.00	-0.20
		2	3.00	3.00	7.50	3.00	3.00	7.50	3.00	3.00	7.50
		1	4.00	1.00	2.00	-4.00	-1.00	-2.00	-4.00	-1.00	-2.00
WYED	EAST	1	2.45	2.90	4.05	2.45	2.90	4.05	2.50	3.40	4.90
		2	3.00	1.40	4.30	-3.00	-1.40	-4.30	-3.00	-1.00	-4.40
		3	2.20	2.20	5.70	2.20	2.20	5.70	2.00	2.40	6.00
		4	0.00	0.00	1.40	0.00	0.00	-1.40	0.00	1.00	-1.00

SPEED = 37 MPH. CONSIST NO.2. GAUGE 5L

ORIENT.	DIR.	AXLE	ABSOLUTE AVERAGE (KIPS)			ALGEBRAIC AVERAGE (KIPS)			MAXIMUM VALUE (KIPS)		
			BARBER	SCALE	SWING	BARBER	SCALE	SWING	BARBER	SCALE	SWING
UNWYED	WEST	1	1.15	3.60	1.35	1.15	3.60	1.35	1.40	3.70	1.40
		2	0.75	2.70	1.30	0.75	-2.70	-0.40	0.90	-2.80	-1.70
		3	3.50	2.75	6.15	3.50	2.75	6.15	3.90	3.20	6.30
		4	0.95	3.45	3.55	-0.85	-3.45	-3.55	-1.70	-3.70	-3.70
UNWYED	EAST	4	2.00	1.70	1.25	2.00	1.70	1.25	2.30	2.00	1.60
		3	1.05	0.85	1.70	1.05	0.85	-1.70	1.20	1.70	-1.70
		2	3.65	0.30	4.60	3.65	0.30	4.60	3.70	0.80	6.60
		1	1.00	2.00	2.05	-1.00	-2.00	-2.05	-2.20	-2.30	-2.90
WYED	WEST	4	1.40	4.00	2.00	1.40	4.00	2.00	1.40	4.00	3.60
		3	1.20	3.90	2.40	-1.20	-3.90	-2.40	-1.00	-4.40	-3.00
		2	3.00	1.50	4.00	0.40	1.50	4.00	1.00	1.00	5.20
		1	1.70	0.20	3.40	-1.70	-0.20	-3.40	-1.00	-0.40	-3.00
WYED	EAST	1	2.00	2.60	1.30	2.00	2.00	1.00	2.00	2.00	1.00
		2	1.80	2.20	2.40	-1.80	-2.20	-2.40	-1.80	-2.20	-2.40
		3	1.00	1.00	3.40	1.60	1.00	3.40	1.00	1.00	3.40
		4	3.60	1.60	3.00	0.00	-1.60	-3.00	3.00	-1.00	-3.00

TABLE 4 - Continued

TABLE 4 - Continued

SPEED = 37 MPH, CONSIST NO.3, GAUGE 2L

ORIENT.	DIR.	AXLE	ABSOLUTE AVERAGE (KIPS) BARBER	C-PEP	STUCKI	ALGEBRAIC AVERAGE (KIPS) BARBER	C-PEP	STUCKI	MAXIMUM VALUE (KIPS) BARBER	C-PEP	STUCKI
UNMVED	WEST	1	1.80	2.80	2.90	1.80	2.80	2.90	4.60	3.40	3.00
		2	2.30	1.10	2.10	2.00	3.50	2.10	2.40	1.60	2.46
		3	2.00	2.60	3.00	2.00	2.60	3.00	2.80	3.40	3.46
		4	2.20	1.10	1.30	-2.20	1.10	1.30	-2.80	2.20	1.80
UNMVED	EAST	4	4.50	8.30	9.30	8.50	8.30	9.30	9.00	9.00	5.40
		3	3.40	5.30	4.80	3.80	5.30	4.80	6.00	6.00	5.00
		2	19.00	8.40	9.00	16.00	8.40	9.00	10.20	8.40	9.00
		1	1.50	3.20	1.75	1.50	3.20	1.75	2.00	3.60	1.80
MVED	WEST	4	5.25	4.50	4.25	5.25	4.50	4.25	7.00	5.00	5.20
		3	1.05	1.20	2.90	1.05	1.20	2.90	1.50	1.20	3.20
		2	3.40	4.20	3.35	3.40	4.20	3.35	5.30	9.80	4.16
		1	0.15	0.60	1.75	-6.15	-0.30	1.75	-0.30	-0.90	2.00
MVED	EAST	1	8.40	6.55	10.05	8.40	6.55	10.05	9.30	7.60	10.26
		2	2.60	7.00	5.80	2.60	7.20	5.80	2.40	7.00	6.18
		3	9.60	9.20	10.65	6.60	9.20	10.65	9.40	9.40	11.10
		4	2.10	4.25	2.75	2.40	4.25	2.75	3.53	4.70	3.20

SPEED = 37 MPH, CONSIST NO.3, GAUGE 3L

ORIENT.	DIR.	AXLE	ABSOLUTE AVERAGE (KIPS) BARBER	C-PEP	STUCKI	ALGEBRAIC AVERAGE (KIPS) BARBER	C-PEP	STUCKI	MAXIMUM VALUE (KIPS) BARBER	C-PEP	STUCKI
UNMVED	WEST	1	5.30	4.80	5.70	5.30	4.80	5.70	5.00	4.80	6.00
		2	3.55	3.25	3.70	3.55	3.25	3.70	4.30	3.90	3.20
		3	5.50	3.90	4.20	5.50	3.90	4.20	6.20	4.00	4.40
		4	1.70	3.15	3.60	1.70	3.15	3.60	1.00	3.80	4.66
UNMVED	EAST	4	4.60	3.40	3.70	4.00	3.40	3.70	4.00	3.60	3.66
		3	1.30	1.70	1.50	0.10	-3.10	0.00	1.40	-1.80	2.20
		2	4.80	4.10	5.50	4.80	4.10	5.50	4.80	4.40	5.60
		1	1.40	1.10	1.10	1.40	1.10	1.10	1.60	2.00	1.40
MVED	WEST	4	7.40	5.80	5.95	7.40	5.80	5.95	9.10	7.10	6.20
		3	1.95	2.85	3.55	1.85	2.85	3.55	2.80	3.40	3.70
		2	7.10	5.55	3.95	7.10	5.55	3.95	10.20	7.10	5.10
		1	6.55	1.45	2.30	-6.55	1.45	2.30	-1.40	2.60	2.30
MVED	EAST	1	4.85	2.70	4.10	4.85	2.70	4.10	6.00	2.80	5.46
		2	1.40	1.00	1.85	-1.40	1.00	1.85	-1.70	1.10	2.30
		3	4.10	4.85	6.95	4.10	4.85	6.95	4.40	5.40	7.70
		4	1.05	1.85	1.30	1.05	1.85	1.30	2.00	2.30	2.00

SPEED = 37 MPH, CONSIST NO.3, GAUGE 5L

ORIENT.	DIR.	AXLE	ABSOLUTE AVERAGE (KIPS) BARBER	C-PEP	STUCKI	ALGEBRAIC AVERAGE (KIPS) BARBER	C-PEP	STUCKI	MAXIMUM VALUE (KIPS) BARBER	C-PEP	STUCKI
UNMVED	WEST	1	1.20	4.80	5.20	1.20	4.80	5.20	1.80	5.00	6.00
		2	2.20	1.75	1.95	2.20	1.05	1.95	2.00	2.00	3.40
		3	4.00	5.10	4.70	4.00	5.10	4.70	4.00	5.00	5.40
		4	3.20	1.10	2.05	-3.20	-1.10	-2.05	-3.20	-2.20	-2.90
UNMVED	EAST	4	1.90	2.90	1.40	1.90	2.90	1.40	2.00	1.40	1.60
		3	0.80	1.50	1.40	0.80	-0.30	0.80	1.60	-1.80	1.40
		2	4.30	4.50	3.20	4.30	4.50	3.20	4.00	5.00	3.40
		1	6.90	1.10	2.50	-6.90	-1.10	-2.50	-1.00	-2.20	-2.80
MVED	WEST	4	5.35	5.30	5.20	5.35	5.30	5.20	8.10	0.90	6.50
		3	2.60	1.30	1.30	-2.60	1.30	1.30	-2.90	1.60	2.00
		2	4.60	5.90	5.60	4.60	5.90	5.60	6.90	6.90	8.30
		1	1.30	2.30	2.35	-1.30	-2.30	-2.35	-1.70	-2.60	-2.40
MVED	EAST	1	3.90	2.25	2.30	3.90	2.25	2.30	4.30	2.00	2.30
		2	1.10	1.75	1.15	-1.10	0.85	-0.25	-1.30	2.60	-1.40
		3	3.80	3.60	2.00	3.80	3.60	2.00	3.70	4.00	2.60
		4	1.30	1.15	2.30	1.30	-1.15	-2.30	2.30	-2.30	-2.20

SPEED = 37 MPH, CONSIST NO.4, GAUGE 2L

ORIENT.	DIR.	AXLE	ABSOLUTE AVERAGE (KIPS) BARBER	RIDE	NEW AAR	ALGEBRAIC AVERAGE (KIPS) BARBER	RIDE	NEW AAR	MAXIMUM VALUE (KIPS) BARBER	RIDE	NEW AAR
UNMVED	WEST	1	4.10	3.90	7.90	4.10	3.90	7.90	4.10	3.90	7.60
		2	1.40	2.50	2.60	1.80	2.50	2.60	1.80	2.50	2.60
		3	1.80	3.60	7.80	1.80	3.60	7.00	1.80	3.60	7.80
		4	3.40	3.20	3.20	-0.60	3.20	3.20	-0.60	3.20	3.20
UNMVED	EAST	4	6.70	6.60	10.20	6.70	6.60	10.20	6.70	6.60	10.20
		3	1.50	4.40	5.50	1.20	4.40	5.50	1.50	4.40	5.50
		2	5.90	5.70	11.40	5.60	5.70	11.40	5.90	5.70	11.40
		1	0.60	3.10	6.40	0.60	3.10	6.40	0.60	3.10	6.40
MVED	WEST	4	3.50	2.20	4.40	3.50	2.20	4.40	4.10	2.90	4.76
		3	1.20	1.80	1.75	1.20	1.80	1.75	1.50	1.80	2.20
		2	1.80	2.10	3.50	1.80	2.10	3.50	2.00	2.30	4.40
		1	1.90	1.30	1.90	-1.90	1.30	1.90	-2.00	2.30	2.56
MVED	EAST	1	6.70	5.50	7.90	6.70	5.50	7.90	7.00	5.50	9.10
		2	3.20	4.85	3.65	3.20	4.65	3.65	3.50	5.00	5.00
		3	9.45	5.85	7.60	8.45	5.55	7.60	9.30	5.00	7.60
		4	1.65	3.05	1.60	1.65	3.05	1.00	1.80	3.20	2.60

SPEED = 37 MPH, CONSIST NO.4, GAUGE 3L

ORIENT.	DIR.	AXLE	ABSOLUTE AVERAGE (KIPS) BARBER	RIDE	NEW AAR	ALGEBRAIC AVERAGE (KIPS) BARBER	RIDE	NEW AAR	MAXIMUM VALUE (KIPS) BARBER	RIDE	NEW AAR
UNMVED	WEST	1	4.55	5.05	7.10	4.55	5.05	7.10	5.40	6.50	8.00
		2	2.55	3.00	2.10	2.55	3.00	2.10	3.10	4.00	2.80
		3	5.00	3.55	6.25	5.00	3.55	6.25	5.70	4.00	8.20
		4	1.00	2.10	3.00	-1.00	2.10	3.00	-1.70	3.10	4.30
UNMVED	EAST	4	4.00	1.70	5.10	4.30	1.70	5.10	4.00	1.70	5.10
		3	2.00	1.70	1.10	-2.00	1.76	1.10	-2.00	1.70	1.10
		2	4.00	2.90	7.10	4.00	2.90	7.10	4.00	2.90	7.10
		1	0.00	2.30	3.40	0.00	2.30	3.40	0.00	2.30	3.40
MVED	WEST	4	4.00	3.25	4.05	4.00	3.25	4.05	4.30	3.40	4.80
		3	2.30	3.70	3.25	2.30	3.76	3.25	2.30	4.30	4.20
		2	4.10	3.85	4.25	4.10	3.85	4.25	4.50	4.80	4.00
		1	0.65	1.85	2.40	-0.65	1.85	2.40	-1.00	2.30	3.70
MVED	EAST	1	4.30	2.60	2.80	4.30	2.00	2.00	4.30	2.60	2.80
		2	1.10	1.40	2.80	1.10	1.40	-2.00	1.10	1.40	-2.00
		3	3.40	2.70	4.50	3.40	2.76	4.50	3.40	2.70	4.50
		4	2.00	2.30	0.80	2.00	2.30	0.00	2.00	2.30	0.66

SPEED = 37 MPH, CONSIST NO.4, GAUGE 5L

ORIENT.	DIR.	AXLE	ABSOLUTE AVERAGE (KIPS) BARBER	RIDE	NEW AAR	ALGEBRAIC AVERAGE (KIPS) BARBER	RIDE	NEW AAR	MAXIMUM VALUE (KIPS) BARBER	RIDE	NEW AAR
UNMVED	WEST	1	0.90	3.70	8.40	0.90	3.73	8.40	0.90	3.70	8.40
		2	0.30	2.90	3.50	0.30	2.90	3.50	0.30	2.90	3.50
		3	3.20	4.00	7.80	3.20	4.00	7.00	3.20	4.00	7.80
		4	1.40	0.60	1.40	-1.40	0.60	1.40	-1.40	0.60	1.40
UNMVED	EAST	4	2.50	1.50	7.60	2.50	1.53	7.60	2.50	1.50	7.60
		3	1.40	3.40	1.60	-1.40	3.43	1.60	-1.40	3.40	1.60
		2	2.00	2.50	8.30	2.00	2.50	8.30	2.00	2.50	8.30
		1	0.00	1.80	2.50	0.00	1.80	2.50	0.00	1.80	2.50
MVED	WEST	4	0.75	1.45	4.60	0.15	1.45	4.60	0.90	2.30	5.20
		3	0.60	2.15	3.60	0.60	2.15	3.60	0.46	2.60	4.60
		2	2.45	2.45	6.05	2.45	2.45	6.05	3.50	3.50	6.60
		1	2.15	0.75	2.00	-2.15	-0.75	2.00	-2.60	-0.90	2.00
MVED	EAST	1	2.10	1.70	5.05	2.10	1.76	5.05	2.40	2.00	5.80
		2	1.40	2.45	1.55	1.40	2.45	0.15	1.80	2.90	1.70
		3	4.30	2.30	6.65	4.30	2.30	6.65	4.60	2.60	8.30
		4	1.45	1.55	2.30	0.25	1.55	-2.30	1.70	1.70	-2.60

SPEED = 45 MPH, CONSIST NO.1, GAUGE 2L

ORIENT.	DIR.	AXLE	ABSOLUTE AVERAGE (KIPS) BARBER	LIST	SCHEFFEL	ALGEBRAIC AVERAGE (KIPS) BARBER	LIST	SCHEFFEL	MAXIMUM VALUE (KIPS) BARBER	LIST	SCHEFFEL
UNMVED	WEST	1	7.44	3.31	3.31	7.44	3.31	3.31	7.80	3.58	4.09
		2	1.65	0.77	2.73	1.05	-3.77	2.73	2.64	-1.48	3.21
		3	3.11	0.80	0.60	3.11	0.49	0.98	3.56	1.17	1.17
		4	2.36	0.83	2.44	2.36	-0.84	-2.44	2.03	0.50	-2.03
UNMVED	EAST	4	4.83	7.40	7.45	5.83	7.40	7.49	10.22	7.59	7.25
		3	3.90	2.44	5.45	-6.90	2.44	5.45	-0.40	2.63	5.55
		2	11.29	6.47	9.37	11.29	6.47	8.37	11.08	6.57	8.47
		1	1.56	3.31	1.94	1.56	3.31	1.94	2.04	3.50	2.04
MVED	WEST	4	2.92	1.36	3.00	2.42	1.36	3.00	3.21	1.46	4.05
		3	1.40	0.78	0.20	2.40	0.19	-0.20	3.50	0.80	-0.30
		2	2.38	1.07	0.70	2.38	1.07	0.70	2.38	1.17	3.08
		1	1.56	0.93	2.73	1.56	-0.93	2.73	1.75	-1.20	2.92
MVED	EAST	1	7.40	6.42	5.63	7.40	6.42	5.63	7.59	6.72	5.78
		2	2.43	3.00	2.24	2.43	3.00	2.24	2.63	4.09	8.34
		3	11.58	5.35	7.11	11.58	5.35	7.11	11.97	5.55	7.30
		4	1.36	0.77	6.13	1.36	0.77	6.13	1.75	0.88	6.72

SPEED = 45 MPH, CONSIST NO.1, GAUGE 3L

ORIENT.	DIR.	AXLE	ABSOLUTE AVERAGE (KIPS) BARBER	LIST	SCHEFFEL	ALGEBRAIC AVERAGE (KIPS) BARBER	LIST	SCHEFFEL	MAXIMUM VALUE (KIPS) BARBER	LIST	SCHEFFEL
UNMVED	WEST	1	10.04	6.72	0.33	16.04	6.72	8.33	10.51	7.67	9.09
		2	1.98	1.23	4.07	1.00	3.67	4.07	1.99	1.70	5.11
		3	9.30	4.26	4.07	6.90	4.26	4.07	9.37	5.11	5.11
		4	1.52	0.76	3.31	1.52	3.76	-3.31	1.99	0.65	-3.41
UNMVED	EAST	4	4.73	3.00	1.99	4.73	3.00	1.99	5.11	3.98	2.27
		3	0.17	1.51	2.10	-0.17	1.51	2.10	-0.50	1.70	2.27
		2	3.79	3.22	4.45	3.79	3.22	4.45	3.98	3.41	4.84
		1	0.57	1.42	0.70	0.57	1.42	-0.70	0.57	1.42	-0.70
MVED	WEST	4	6.02	3.31	7.01	6.02	3.31	7.01	7.10	3.41	7.16
		3	1.70	0.76	1.42	1.70	0.76	1.42	1.99	0.08	1.70
		2	6.41	7.62	3.31	6.91	3.62	3.31	7.10	3.98	3.41
		1	1.51	1.23	1.70	1.51	-1.23	1.70	1.70	-1.42	1.70
MVED	EAST	1	3.50	2.93	2.10	3.50	2.93	2.10	3.69	3.18	2.87
		2	1.04	2.27	1.14	1.04	2.27	1.14	1.14	2.50	1.14
		3	3.76	2.08	2.46	3.79	2.08	2.46	3.98	2.27	2.98
		4	1.27	0.83	2.27	1.27	0.80	2.27	1.54	0.85	2.98

SPEED = 45 MPH, CONSIST NO.1, GAUGE 5L

ORIENT.	DIR.	AXLE	ABSOLUTE AVERAGE (KIPS) BARBER	LIST	SCHEFFEL	ALGEBRAIC AVERAGE (KIPS) BARBER	LIST	SCHEFFEL	MAXIMUM VALUE (KIPS) BARBER	LIST	SCHEFFEL
UNMVED	WEST	1	5.10	3.27	2.02	5.10	3.27	2.02	6.34	3.46	2.30
		2	0.67	1.33	2.08	-0.67	1.33	2.08	-1.15	1.44	3.17
		3	5.30	4.42	4.51	5.30	4.42	4.51	6.02	4.91	4.61
		4	1.11	1.97	0.40	-1.11	1.97	-0.40	-1.73	2.74	-1.15
UNMVED	EAST	4	2.98	1.46	1.63	2.58	1.46	1.63	3.46	1.73	1.73
		3	3.27	0.13	4.70	2.27	0.13	4.70	3.46	0.48	4.09
		2	2.98	0.20	4.03	2.98	-0.20	-4.03	3.46	-0.30	-4.03
		1	1.73	1.25	1.63	1.73	1.25	-1.63	2.30	1.44	-1.73
MVED	WEST	4	4.03	1.65	0.58	4.03	1.65	0.58	4.61	1.70	1.15
		3	0.57	2.65	2.88	-0.57	2.65	-2.88	-0.90	2.88	-2.88
		2	4.01	4.13	4.22	4.01	4.13	4.22	4.90	4.32	4.32
		1	3.30	1.29	2.93	-0.30	1.29	2.93	-0.96	2.02	3.40
MVED	EAST	1	3.07	0.07	1.44	3.07	0.07	1.44	3.46	0.20	1.44
		2	2.02	0.77	1.63	2.02	0.77	1.63	2.30	0.06	2.08
		3	2.30	2.49	3.07	2.30	-2.49	-3.07	2.30	-2.59	-3.17
		4	1.92	0.20	2.64	1.92	-0.20	2.64	2.02	-0.30	3.02

SPEED = 45 MPH, CONSIST NO.2, GAUGE 2L

ORIENT.	DIR.	AXLE	ABSOLUTE AVERAGE (KIPS) BARBER	SCALE	SWING	ALGEBRAIC AVERAGE (KIPS) BARBER	SCALE	SWING	MAXIMUM VALUE (KIPS) BARBER	SCALE	SWING
UNMVED	WEST	1	9.13	4.99	6.57	5.13	4.99	6.57	10.60	5.84	7.30
		2	6.95	1.10	1.58	6.95	1.10	1.58	8.03	1.10	8.19
		3	4.00	0.62	3.41	4.00	0.62	3.41	4.70	1.10	3.08
		4	4.01	3.09	0.05	4.01	3.09	0.05	4.82	4.02	1.46
UNMVED	EAST	4	9.84	0.65	12.98	5.84	0.65	12.98	10.60	9.98	14.23
		3	5.23	3.65	3.93	5.23	3.65	3.93	5.50	4.02	4.08
		2	13.62	7.80	13.79	13.62	7.80	13.79	14.48	8.90	14.60
		1	2.50	1.45	2.09	2.50	1.45	-2.09	2.60	1.00	-3.20
MVED	WEST	4	3.13	5.27	5.21	3.13	5.27	5.21	3.40	5.55	5.48
		3	1.91	0.39	2.10	1.91	0.39	-2.10	2.40	0.44	-2.35
		2	1.12	0.63	2.29	1.12	0.63	2.29	1.46	1.02	2.30
		1	1.26	4.57	1.66	1.26	4.57	1.66	1.75	4.67	2.19
MVED	EAST	1	6.87	5.46	8.08	6.87	5.46	8.08	7.20	6.30	8.32
		2	1.12	1.07	1.85	-1.12	1.07	-1.85	-1.75	1.46	-2.84
		3	8.83	5.59	10.46	8.83	5.59	10.46	9.20	5.84	10.95
		4	1.36	1.61	3.45	1.36	1.61	-3.45	1.60	1.98	-3.98

SPEED = 45 MPH, CONSIST NO.2, GAUGE 3L

ORIENT.	DIR.	AXLE	ABSOLUTE AVERAGE (KIPS) BARBER	SCALE	SWING	ALGEBRAIC AVERAGE (KIPS) BARBER	SCALE	SWING	MAXIMUM VALUE (KIPS) BARBER	SCALE	SWING
UNMVED	WEST	1	5.86	7.27	9.40	5.86	7.27	9.40	10.70	7.70	10.48
		2	3.37	0.83	1.57	3.37	0.83	1.57	4.18	1.98	2.48
		3	8.30	4.87	11.92	8.30	4.87	11.92	8.98	5.38	12.68
		4	3.47	0.03	1.51	3.47	-0.07	-1.51	3.08	-1.30	-1.08
UNMVED	EAST	4	3.83	4.20	7.24	3.83	4.20	7.24	4.40	4.50	7.81
		3	1.56	2.04	0.85	1.56	2.04	-0.85	2.13	2.98	-0.99
		2	6.06	3.46	6.63	6.06	3.46	6.63	6.82	3.55	7.53
		1	0.57	2.13	1.18	0.57	2.13	1.18	0.99	2.13	2.13
MVED	WEST	4	5.17	5.30	7.53	5.17	5.30	7.53	5.40	5.40	7.98
		3	0.72	2.10	1.75	0.72	-2.10	-1.75	0.99	-2.27	-1.81
		2	6.26	3.30	6.02	6.26	3.30	6.02	6.82	3.80	6.22
		1	0.93	0.54	2.12	-0.04	-3.06	-2.12	-1.30	-0.90	-2.40
MVED	EAST	1	3.00	2.33	5.35	3.00	2.33	5.35	3.70	2.00	5.40
		2	1.19	0.85	2.38	-0.32	0.85	-2.38	1.30	0.05	-2.98
		3	1.27	2.41	4.78	1.27	2.41	4.78	1.98	2.70	4.03
		4	0.00	2.17	0.57	0.00	2.17	0.57	0.05	2.27	6.71

SPEED = 45 MPH, CONSIST NO.2, GAUGE 5L

ORIENT.	DIR.	AXLE	ABSOLUTE AVERAGE (KIPS) BARBER	SCALE	SWING	ALGEBRAIC AVERAGE (KIPS) BARBER	SCALE	SWING	MAXIMUM VALUE (KIPS) BARBER	SCALE	SWING
UNMVED	WEST	1	5.02	5.21	6.33	5.02	5.21	4.33	5.70	5.58	5.80
		2	2.74	0.07	2.08	2.74	-0.07	-2.08	1.28	-2.38	-2.58
		3	6.03	3.38	6.62	6.03	3.38	6.62	6.60	3.98	7.28
		4	2.02	0.02	1.79	2.02	0.73	-1.79	2.98	1.00	-2.48
UNMVED	EAST	4	5.66	2.11	1.49	5.66	2.11	1.49	6.30	2.60	1.73
		3	2.06	3.49	1.10	2.06	3.09	1.10	2.45	4.03	1.15
		2	3.07	0.34	7.26	3.07	0.34	7.26	3.46	0.43	8.04
		1	0.71	0.19	1.90	0.71	0.19	-1.90	1.29	0.29	-2.16
MVED	WEST	4	4.14	5.28	6.42	4.14	5.28	6.42	4.40	5.47	6.70
		3	1.02	0.07	1.92	1.02	-0.07	-1.92	1.06	-0.92	-2.02
		2	3.55	1.98	5.16	3.65	1.98	5.16	4.05	2.43	5.36
		1	3.41	2.20	0.30	0.33	2.20	-0.24	1.38	2.61	-0.62
MVED	EAST	1	4.31	3.90	6.73	4.93	3.98	6.73	5.30	4.45	6.80
		2	1.15	1.00	2.13	-6.72	1.00	-2.13	-1.44	1.20	-2.30
		3	5.07	4.02	7.02	5.07	4.02	7.02	5.37	4.38	7.98
		4	1.10	1.98	1.65	1.10	1.90	-1.65	1.21	2.14	-1.99

TABLE 4 - Continued

SPEED = 45 MPH, CONSIST NO.3, GAUGE 2L

ORIENT.	DIR.	AXLE	ABSOLUTE AVERAGE (KIPS) BARBER	C-PEP	STUCKI	ALGEBRAIC AVERAGE (KIPS) BARBER	C-PEP	STUCKI	MAXIMUM VALUE (KIPS) BARBER	C-PEP	STUCKI
UNWYED	WEST	1	7.50	5.75	5.17	7.50	5.75	5.17	9.00	7.00	5.50
		2	4.83	2.33	2.83	4.83	2.33	2.83	5.50	3.00	3.00
		3	1.83	3.67	2.00	1.83	3.67	2.00	3.50	4.50	3.50
		4	1.34	4.00	2.83	2.60	4.00	2.83	3.25	4.50	3.50
UNWYED	EAST	4	2.67	4.17	10.83	5.67	4.17	10.83	10.00	10.50	12.00
		3	4.17	4.17	5.00	4.17	4.17	5.00	4.00	4.50	5.00
		2	11.50	9.33	10.67	11.50	9.33	10.67	12.00	11.00	11.50
		1	2.30	3.17	1.67	2.00	3.17	0.10	2.50	4.00	2.50
WYED	WEST	4	5.83	6.67	7.00	5.83	6.67	7.00	6.70	7.70	8.20
		3	1.67	1.73	1.37	1.63	1.73	1.37	2.30	2.00	2.00
		2	2.77	4.40	3.37	2.77	4.40	3.37	2.30	3.00	3.00
		1	1.63	2.27	2.13	1.63	2.27	2.13	2.00	2.70	2.00
WYED	EAST	1	12.10	7.37	9.50	12.10	7.37	9.56	13.10	7.00	10.50
		2	2.20	4.87	5.30	2.20	5.03	5.30	2.80	4.40	5.00
		3	12.10	9.00	10.77	12.10	9.06	10.77	12.00	10.20	11.70
		4	3.07	3.17	3.20	3.03	3.17	3.20	3.00	3.70	3.50

SPEED = 45 MPH, CONSIST NO.3, GAUGE 3L

ORIENT.	DIR.	AXLE	ABSOLUTE AVERAGE (KIPS) BARBER	C-PEP	STUCKI	ALGEBRAIC AVERAGE (KIPS) BARBER	C-PEP	STUCKI	MAXIMUM VALUE (KIPS) BARBER	C-PEP	STUCKI
UNWYED	WEST	1	9.13	5.00	4.93	5.13	5.00	4.93	9.00	5.00	5.20
		2	1.70	1.40	2.67	1.70	1.40	2.67	2.00	1.80	2.00
		3	7.20	6.83	2.77	7.20	6.83	2.77	7.50	6.00	5.00
		4	2.10	2.60	2.07	2.10	2.60	2.07	2.30	3.00	3.00
UNWYED	EAST	4	4.00	4.57	5.37	4.00	4.57	5.37	5.00	5.00	5.70
		3	1.30	1.20	1.07	1.30	4.33	0.63	1.60	1.50	1.40
		2	5.20	4.67	6.07	5.20	4.67	6.07	5.50	5.00	7.00
		1	0.43	1.33	2.13	0.07	1.33	2.13	-1.30	2.00	2.00
WYED	WEST	4	4.83	6.73	6.57	5.03	6.73	6.57	11.00	8.00	7.50
		3	1.13	1.83	2.27	1.13	1.63	2.27	1.80	1.80	2.00
		2	10.13	7.47	6.00	10.13	7.47	6.00	11.00	8.20	6.30
		1	1.23	1.30	1.27	1.03	1.30	1.27	1.70	1.40	1.80
WYED	EAST	1	6.47	4.27	5.17	-6.47	4.27	5.17	5.00	4.50	5.30
		2	0.50	1.23	1.63	-0.40	1.23	1.63	-0.00	1.70	1.70
		3	4.70	5.20	5.07	4.70	5.20	5.07	5.00	5.00	5.00
		4	3.80	1.30	2.20	0.80	1.30	2.20	1.10	1.40	2.30

SPEED = 45 MPH, CONSIST NO.3, GAUGE 5L

ORIENT.	DIR.	AXLE	ABSOLUTE AVERAGE (KIPS) BARBER	C-PEP	STUCKI	ALGEBRAIC AVERAGE (KIPS) BARBER	C-PEP	STUCKI	MAXIMUM VALUE (KIPS) BARBER	C-PEP	STUCKI
UNWYED	WEST	1	5.70	5.73	5.83	5.70	5.73	5.83	6.10	6.00	6.00
		2	2.03	1.70	1.03	2.03	0.77	0.77	2.10	2.00	1.50
		3	5.73	6.13	6.13	5.73	6.13	6.13	5.80	6.00	6.00
		4	2.47	2.13	1.70	1.60	1.13	0.67	3.20	2.00	2.00
UNWYED	EAST	4	3.77	2.83	2.20	2.83	-1.77	-1.27	4.90	3.70	2.50
		3	1.27	0.70	0.20	1.27	-0.20	-0.20	2.10	-1.00	0.00
		2	2.27	0.83	2.57	2.27	-0.83	2.57	3.00	-1.00	3.00
		1	0.80	1.53	1.40	0.00	-0.20	-1.40	-1.20	-2.00	-1.50
WYED	WEST	4	6.20	6.07	7.23	6.20	6.07	7.23	7.20	6.00	8.20
		3	1.20	0.33	1.13	-1.20	0.33	1.13	-1.50	1.00	1.50
		2	5.47	3.67	0.60	5.47	3.67	0.60	6.00	4.00	1.00
		1	1.07	0.00	1.00	-1.07	-0.00	-0.00	-1.00	-1.00	-1.00
WYED	EAST	1	6.27	5.10	5.57	2.47	5.10	5.57	6.00	5.00	6.00
		2	2.67	1.23	1.67	2.67	1.23	1.67	3.00	1.00	2.00
		3	5.33	5.67	6.03	5.33	5.67	6.03	6.00	6.00	6.00
		4	1.00	1.50	1.13	1.00	0.83	-1.13	2.00	2.00	-1.00

SPEED = 45 MPH, CONSIST NO.4, GAUGE 2L

ORIENT.	DIR.	AXLE	ABSOLUTE AVERAGE (KIPS) BARBER	RIDE	NEW AAR	ALGEBRAIC AVERAGE (KIPS) BARBER	RIDE	NEW AAR	MAXIMUM VALUE (KIPS) BARBER	RIDE	NEW AAR
UNWYED	WEST	1	6.30	4.67	5.65	6.30	4.67	5.65	6.67	5.00	6.42
		2	3.01	1.85	1.70	3.01	1.85	-1.70	3.21	2.00	-2.00
		3	1.56	2.24	2.00	1.56	2.24	2.00	2.00	2.00	2.00
		4	2.06	4.30	2.65	2.06	4.30	2.65	2.05	4.63	3.50
UNWYED	EAST	4	6.87	6.91	8.66	6.87	6.91	8.66	8.20	7.20	9.53
		3	0.76	2.73	1.00	0.30	2.73	1.00	0.00	3.20	5.00
		2	10.80	6.50	8.00	10.80	6.50	8.00	11.00	6.00	6.00
		1	1.85	4.30	2.24	1.85	4.30	2.24	2.34	4.67	3.50
WYED	WEST	4	6.23	6.00	5.00	6.22	6.90	5.00	6.72	5.20	5.00
		3	2.50	3.00	0.00	2.50	3.00	0.00	3.00	3.00	3.17
		2	5.00	5.00	6.00	5.00	5.00	6.00	5.00	5.00	6.00
		1	1.36	3.60	1.50	1.36	3.60	0.07	1.75	4.00	2.00
WYED	EAST	1	9.36	8.08	7.45	5.36	8.08	7.45	9.60	8.67	7.00
		2	3.60	4.67	1.75	3.60	4.67	1.75	4.38	5.00	1.00
		3	11.36	7.00	8.37	11.36	7.00	8.37	11.97	8.67	9.00
		4	2.26	3.60	0.53	2.26	3.60	-0.53	2.34	4.00	-0.73

SPEED = 45 MPH, CONSIST NO.4, GAUGE 3L

ORIENT.	DIR.	AXLE	ABSOLUTE AVERAGE (KIPS) BARBER	RIDE	NEW AAR	ALGEBRAIC AVERAGE (KIPS) BARBER	RIDE	NEW AAR	MAXIMUM VALUE (KIPS) BARBER	RIDE	NEW AAR
UNWYED	WEST	1	5.77	4.87	4.92	5.77	4.87	-4.92	6.53	5.11	-5.11
		2	1.23	2.37	0.96	1.23	2.37	-0.96	1.42	2.56	-1.00
		3	5.02	4.07	5.38	-5.02	4.07	-5.38	7.38	4.26	-5.56
		4	1.14	1.90	0.38	-1.14	1.90	-0.38	-1.02	2.27	-0.95
UNWYED	EAST	4	2.05	2.90	6.69	2.05	2.90	6.69	2.50	3.12	5.66
		3	1.33	0.74	0.73	1.33	0.74	0.73	1.50	0.00	1.10
		2	3.70	3.22	4.26	3.00	3.22	4.26	4.00	3.60	4.11
		1	1.14	1.95	1.23	1.14	1.95	1.23	1.42	2.27	1.42
WYED	WEST	4	6.53	4.54	5.58	6.53	4.54	5.58	7.10	4.83	5.00
		3	1.61	3.91	1.14	1.61	3.91	-1.14	2.27	3.56	-1.42
		2	7.10	5.73	5.07	7.10	5.73	-5.07	7.38	5.96	-5.00
		1	1.42	2.50	1.01	0.95	2.56	-0.44	1.99	3.41	-1.20
WYED	EAST	1	7.00	3.03	4.07	7.50	3.03	4.07	8.02	4.20	4.26
		2	1.37	1.14	1.14	1.37	1.14	1.14	1.42	1.42	1.42
		3	4.35	3.31	3.41	4.35	3.31	3.41	4.56	3.00	3.69
		4	0.95	1.61	1.37	0.95	1.61	1.37	1.14	1.99	1.42

SPEED = 45 MPH, CONSIST NO.4, GAUGE 5L

ORIENT.	DIR.	AXLE	ABSOLUTE AVERAGE (KIPS) BARBER	RIDE	NEW AAR	ALGEBRAIC AVERAGE (KIPS) BARBER	RIDE	NEW AAR	MAXIMUM VALUE (KIPS) BARBER	RIDE	NEW AAR
UNWYED	WEST	1	3.72	4.13	5.10	-3.72	4.13	-5.10	-4.02	4.32	-5.47
		2	2.21	1.92	0.23	-2.21	-1.92	-0.23	-2.30	-2.30	-0.00
		3	4.32	3.66	6.33	-4.32	3.66	-6.33	-4.61	4.03	-6.51
		4	1.63	0.67	1.73	-1.63	0.67	-1.73	-2.02	1.00	-1.73
UNWYED	EAST	4	3.61	6.08	6.72	3.61	6.08	6.72	3.69	6.90	6.51
		3	2.50	0.32	2.66	2.50	0.32	2.66	3.00	0.60	3.00
		2	2.40	2.76	5.36	2.40	2.76	5.36	2.69	3.00	5.70
		1	1.50	1.60	0.52	1.50	1.60	0.52	1.07	2.02	0.62
WYED	WEST	4	3.74	4.60	1.09	3.74	4.60	-3.56	-4.02	4.75	-4.46
		3	1.09	1.63	1.25	0.20	-1.63	-1.25	-1.15	-2.20	-1.70
		2	4.32	3.76	6.70	4.32	3.76	-6.70	-4.00	3.60	-6.62
		1	2.70	1.34	0.77	-2.30	-1.34	-0.77	-2.00	-2.50	-1.73
WYED	EAST	1	3.65	3.01	7.30	3.65	3.02	7.30	3.74	4.32	7.70
		2	1.09	1.25	3.12	1.09	1.25	3.12	1.00	1.60	3.46
		3	3.12	3.03	7.00	3.12	3.03	7.00	3.31	3.00	8.00
		4	1.77	1.54	2.00	1.77	1.54	2.00	2.30	1.73	2.20

TABLE 4 - Continued

SPEED = 29 MPH, CONSIST NO.1, ALL GAUGES

DIRECTION	TRUCK	AXLE	ABSOLUTE AVERAGE (KIPS)			ALGEBRAIC AVERAGE (KIPS)			MAXIMUM VALUE (KIPS)		
			BARBER	LIST	SCHEFFEL	BARBER	LIST	SCHEFFEL	BARBER	LIST	SCHEFFEL
WEST	LEADING	1	[illegible]	[illegible]	[illegible]	[illegible]	[illegible]	[illegible]	[illegible]	[illegible]	[illegible]
		2	[illegible]	[illegible]	[illegible]	[illegible]	[illegible]	[illegible]	[illegible]	[illegible]	[illegible]
	TRAILING	1	[illegible]	[illegible]	[illegible]	[illegible]	[illegible]	[illegible]	[illegible]	[illegible]	[illegible]
		2	[illegible]	[illegible]	[illegible]	[illegible]	[illegible]	[illegible]	[illegible]	[illegible]	[illegible]
EAST	LEADING	1	[illegible]	[illegible]	[illegible]	[illegible]	[illegible]	[illegible]	[illegible]	[illegible]	[illegible]
		2	[illegible]	[illegible]	[illegible]	[illegible]	[illegible]	[illegible]	[illegible]	[illegible]	[illegible]
	TRAILING	1	[illegible]	[illegible]	[illegible]	[illegible]	[illegible]	[illegible]	[illegible]	[illegible]	[illegible]
		2	[illegible]	[illegible]	[illegible]	[illegible]	[illegible]	[illegible]	[illegible]	[illegible]	[illegible]

SPEED = 29 MPH, CONSIST NO.2, ALL GAUGES

DIRECTION	TRUCK	AXLE	ABSOLUTE AVERAGE (KIPS)			ALGEBRAIC AVERAGE (KIPS)			MAXIMUM VALUE (KIPS)		
			BARBER	SCALE	SWING	BARBER	SCALE	SWING	BARBER	SCALE	SWING
WEST	LEADING	1	[illegible]	[illegible]	[illegible]	[illegible]	[illegible]	[illegible]	[illegible]	[illegible]	[illegible]
		2	[illegible]	[illegible]	[illegible]	[illegible]	[illegible]	[illegible]	[illegible]	[illegible]	[illegible]
	TRAILING	1	[illegible]	[illegible]	[illegible]	[illegible]	[illegible]	[illegible]	[illegible]	[illegible]	[illegible]
		2	[illegible]	[illegible]	[illegible]	[illegible]	[illegible]	[illegible]	[illegible]	[illegible]	[illegible]
EAST	LEADING	1	[illegible]	[illegible]	[illegible]	[illegible]	[illegible]	[illegible]	[illegible]	[illegible]	[illegible]
		2	[illegible]	[illegible]	[illegible]	[illegible]	[illegible]	[illegible]	[illegible]	[illegible]	[illegible]
	TRAILING	1	[illegible]	[illegible]	[illegible]	[illegible]	[illegible]	[illegible]	[illegible]	[illegible]	[illegible]
		2	[illegible]	[illegible]	[illegible]	[illegible]	[illegible]	[illegible]	[illegible]	[illegible]	[illegible]

SPEED = 29 MPH, CONSIST NO.3, ALL GAUGES

DIRECTION	TRUCK	AXLE	ABSOLUTE AVERAGE (KIPS)			ALGEBRAIC AVERAGE (KIPS)			MAXIMUM VALUE (KIPS)		
			BARBER	C-PEP	STUCKI	BARBER	C-PEP	STUCKI	BARBER	C-PEP	STUCKI
WEST	LEADING	1	[illegible]	[illegible]	[illegible]	[illegible]	[illegible]	[illegible]	[illegible]	[illegible]	[illegible]
		2	[illegible]	[illegible]	[illegible]	[illegible]	[illegible]	[illegible]	[illegible]	[illegible]	[illegible]
	TRAILING	1	[illegible]	[illegible]	[illegible]	[illegible]	[illegible]	[illegible]	[illegible]	[illegible]	[illegible]
		2	[illegible]	[illegible]	[illegible]	[illegible]	[illegible]	[illegible]	[illegible]	[illegible]	[illegible]
EAST	LEADING	1	[illegible]	[illegible]	[illegible]	[illegible]	[illegible]	[illegible]	[illegible]	[illegible]	[illegible]
		2	[illegible]	[illegible]	[illegible]	[illegible]	[illegible]	[illegible]	[illegible]	[illegible]	[illegible]
	TRAILING	1	[illegible]	[illegible]	[illegible]	[illegible]	[illegible]	[illegible]	[illegible]	[illegible]	[illegible]
		2	[illegible]	[illegible]	[illegible]	[illegible]	[illegible]	[illegible]	[illegible]	[illegible]	[illegible]

SPEED = 29 MPH, CONSIST NO.4, ALL GAUGES

DIRECTION	TRUCK	AXLE	ABSOLUTE AVERAGE (KIPS)			ALGEBRAIC AVERAGE (KIPS)			MAXIMUM VALUE (KIPS)		
			BARBER	RIDE	NEW AAR	BARBER	RIDE	NEW AAR	BARBER	RIDE	NEW AAR
WEST	LEADING	1	[illegible]	[illegible]	[illegible]	[illegible]	[illegible]	[illegible]	[illegible]	[illegible]	[illegible]
		2	[illegible]	[illegible]	[illegible]	[illegible]	[illegible]	[illegible]	[illegible]	[illegible]	[illegible]
	TRAILING	1	[illegible]	[illegible]	[illegible]	[illegible]	[illegible]	[illegible]	[illegible]	[illegible]	[illegible]
		2	[illegible]	[illegible]	[illegible]	[illegible]	[illegible]	[illegible]	[illegible]	[illegible]	[illegible]
EAST	LEADING	1	[illegible]	[illegible]	[illegible]	[illegible]	[illegible]	[illegible]	[illegible]	[illegible]	[illegible]
		2	[illegible]	[illegible]	[illegible]	[illegible]	[illegible]	[illegible]	[illegible]	[illegible]	[illegible]
	TRAILING	1	[illegible]	[illegible]	[illegible]	[illegible]	[illegible]	[illegible]	[illegible]	[illegible]	[illegible]
		2	[illegible]	[illegible]	[illegible]	[illegible]	[illegible]	[illegible]	[illegible]	[illegible]	[illegible]

SPEED = 37 MPH, CONSIST NO.1, ALL GAUGES

DIRECTION	TRUCK	AXLE	ABSOLUTE AVERAGE (KIPS)			ALGEBRAIC AVERAGE (KIPS)			MAXIMUM VALUE (KIPS)		
			BARBER	LIST	SCHEFFEL	BARBER	LIST	SCHEFFEL	BARBER	LIST	SCHEFFEL
WEST	LEADING	1	[illegible]	[illegible]	[illegible]	[illegible]	[illegible]	[illegible]	[illegible]	[illegible]	[illegible]
		2	[illegible]	[illegible]	[illegible]	[illegible]	[illegible]	[illegible]	[illegible]	[illegible]	[illegible]
	TRAILING	1	[illegible]	[illegible]	[illegible]	[illegible]	[illegible]	[illegible]	[illegible]	[illegible]	[illegible]
		2	[illegible]	[illegible]	[illegible]	[illegible]	[illegible]	[illegible]	[illegible]	[illegible]	[illegible]
EAST	LEADING	1	[illegible]	[illegible]	[illegible]	[illegible]	[illegible]	[illegible]	[illegible]	[illegible]	[illegible]
		2	[illegible]	[illegible]	[illegible]	[illegible]	[illegible]	[illegible]	[illegible]	[illegible]	[illegible]
	TRAILING	1	[illegible]	[illegible]	[illegible]	[illegible]	[illegible]	[illegible]	[illegible]	[illegible]	[illegible]
		2	[illegible]	[illegible]	[illegible]	[illegible]	[illegible]	[illegible]	[illegible]	[illegible]	[illegible]

SPEED = 37 MPH, CONSIST NO.2, ALL GAUGES

DIRECTION	TRUCK	AXLE	ABSOLUTE AVERAGE (KIPS)			ALGEBRAIC AVERAGE (KIPS)			MAXIMUM VALUE (KIPS)		
			BARBER	SCALE	SWING	BARBER	SCALE	SWING	BARBER	SCALE	SWING
WEST	LEADING	1	[illegible]	[illegible]	[illegible]	[illegible]	[illegible]	[illegible]	[illegible]	[illegible]	[illegible]
		2	[illegible]	[illegible]	[illegible]	[illegible]	[illegible]	[illegible]	[illegible]	[illegible]	[illegible]
	TRAILING	1	[illegible]	[illegible]	[illegible]	[illegible]	[illegible]	[illegible]	[illegible]	[illegible]	[illegible]
		2	[illegible]	[illegible]	[illegible]	[illegible]	[illegible]	[illegible]	[illegible]	[illegible]	[illegible]
EAST	LEADING	1	[illegible]	[illegible]	[illegible]	[illegible]	[illegible]	[illegible]	[illegible]	[illegible]	[illegible]
		2	[illegible]	[illegible]	[illegible]	[illegible]	[illegible]	[illegible]	[illegible]	[illegible]	[illegible]
	TRAILING	1	[illegible]	[illegible]	[illegible]	[illegible]	[illegible]	[illegible]	[illegible]	[illegible]	[illegible]
		2	[illegible]	[illegible]	[illegible]	[illegible]	[illegible]	[illegible]	[illegible]	[illegible]	[illegible]

SPEED = 37 MPH, CONSIST NO.3, ALL GAUGES

DIRECTION	TRUCK	AXLE	ABSOLUTE AVERAGE (KIPS)			ALGEBRAIC AVERAGE (KIPS)			MAXIMUM VALUE (KIPS)		
			BARBER	C-PEP	STUCKI	BARBER	C-PEP	STUCKI	BARBER	C-PEP	STUCKI
WEST	LEADING	1	[illegible]	[illegible]	[illegible]	[illegible]	[illegible]	[illegible]	[illegible]	[illegible]	[illegible]
		2	[illegible]	[illegible]	[illegible]	[illegible]	[illegible]	[illegible]	[illegible]	[illegible]	[illegible]
	TRAILING	1	[illegible]	[illegible]	[illegible]	[illegible]	[illegible]	[illegible]	[illegible]	[illegible]	[illegible]
		2	[illegible]	[illegible]	[illegible]	[illegible]	[illegible]	[illegible]	[illegible]	[illegible]	[illegible]
EAST	LEADING	1	[illegible]	[illegible]	[illegible]	[illegible]	[illegible]	[illegible]	[illegible]	[illegible]	[illegible]
		2	[illegible]	[illegible]	[illegible]	[illegible]	[illegible]	[illegible]	[illegible]	[illegible]	[illegible]
	TRAILING	1	[illegible]	[illegible]	[illegible]	[illegible]	[illegible]	[illegible]	[illegible]	[illegible]	[illegible]
		2	[illegible]	[illegible]	[illegible]	[illegible]	[illegible]	[illegible]	[illegible]	[illegible]	[illegible]

SPEED = 37 MPH, CONSIST NO.4, ALL GAUGES

DIRECTION	TRUCK	AXLE	ABSOLUTE AVERAGE (KIPS)			ALGEBRAIC AVERAGE (KIPS)			MAXIMUM VALUE (KIPS)		
			BARBER	RIDE	NEW AAR	BARBER	RIDE	NEW AAR	BARBER	RIDE	NEW AAR
WEST	LEADING	1	[illegible]	[illegible]	[illegible]	[illegible]	[illegible]	[illegible]	[illegible]	[illegible]	[illegible]
		2	[illegible]	[illegible]	[illegible]	[illegible]	[illegible]	[illegible]	[illegible]	[illegible]	[illegible]
	TRAILING	1	[illegible]	[illegible]	[illegible]	[illegible]	[illegible]	[illegible]	[illegible]	[illegible]	[illegible]
		2	[illegible]	[illegible]	[illegible]	[illegible]	[illegible]	[illegible]	[illegible]	[illegible]	[illegible]
EAST	LEADING	1	[illegible]	[illegible]	[illegible]	[illegible]	[illegible]	[illegible]	[illegible]	[illegible]	[illegible]
		2	[illegible]	[illegible]	[illegible]	[illegible]	[illegible]	[illegible]	[illegible]	[illegible]	[illegible]
	TRAILING	1	[illegible]	[illegible]	[illegible]	[illegible]	[illegible]	[illegible]	[illegible]	[illegible]	[illegible]
		2	[illegible]	[illegible]	[illegible]	[illegible]	[illegible]	[illegible]	[illegible]	[illegible]	[illegible]

SPEED = 45 MPH, CONSIST NO.1, ALL GAUGES

DIRECTION	TRUCK	AXLE	ABSOLUTE AVERAGE (KIPS)			ALGEBRAIC AVERAGE (KIPS)			MAXIMUM VALUE (KIPS)		
			BARBER	LIST	SCHEFFEL	BARBER	LIST	SCHEFFEL	BARBER	LIST	SCHEFFEL
WEST	LEADING	1	[illegible]	[illegible]	[illegible]	[illegible]	[illegible]	[illegible]	[illegible]	[illegible]	[illegible]
		2	[illegible]	[illegible]	[illegible]	[illegible]	[illegible]	[illegible]	[illegible]	[illegible]	[illegible]
	TRAILING	1	[illegible]	[illegible]	[illegible]	[illegible]	[illegible]	[illegible]	[illegible]	[illegible]	[illegible]
		2	[illegible]	[illegible]	[illegible]	[illegible]	[illegible]	[illegible]	[illegible]	[illegible]	[illegible]
EAST	LEADING	1	[illegible]	[illegible]	[illegible]	[illegible]	[illegible]	[illegible]	[illegible]	[illegible]	[illegible]
		2	[illegible]	[illegible]	[illegible]	[illegible]	[illegible]	[illegible]	[illegible]	[illegible]	[illegible]
	TRAILING	1	[illegible]	[illegible]	[illegible]	[illegible]	[illegible]	[illegible]	[illegible]	[illegible]	[illegible]
		2	[illegible]	[illegible]	[illegible]	[illegible]	[illegible]	[illegible]	[illegible]	[illegible]	[illegible]

SPEED = 45 MPH, CONSIST NO.2, ALL GAUGES

DIRECTION	TRUCK	AXLE	ABSOLUTE AVERAGE (KIPS)			ALGEBRAIC AVERAGE (KIPS)			MAXIMUM VALUE (KIPS)		
			BARBER	SCALE	SWING	BARBER	SCALE	SWING	BARBER	SCALE	SWING
WEST	LEADING	1	[illegible]	[illegible]	[illegible]	[illegible]	[illegible]	[illegible]	[illegible]	[illegible]	[illegible]
		2	[illegible]	[illegible]	[illegible]	[illegible]	[illegible]	[illegible]	[illegible]	[illegible]	[illegible]
	TRAILING	1	[illegible]	[illegible]	[illegible]	[illegible]	[illegible]	[illegible]	[illegible]	[illegible]	[illegible]
		2	[illegible]	[illegible]	[illegible]	[illegible]	[illegible]	[illegible]	[illegible]	[illegible]	[illegible]
EAST	LEADING	1	[illegible]	[illegible]	[illegible]	[illegible]	[illegible]	[illegible]	[illegible]	[illegible]	[illegible]
		2	[illegible]	[illegible]	[illegible]	[illegible]	[illegible]	[illegible]	[illegible]	[illegible]	[illegible]
	TRAILING	1	[illegible]	[illegible]	[illegible]	[illegible]	[illegible]	[illegible]	[illegible]	[illegible]	[illegible]
		2	[illegible]	[illegible]	[illegible]	[illegible]	[illegible]	[illegible]	[illegible]	[illegible]	[illegible]

SPEED = 45 MPH, CONSIST NO.3, ALL GAUGES

DIRECTION	TRUCK	AXLE	ABSOLUTE AVERAGE (KIPS)			ALGEBRAIC AVERAGE (KIPS)			MAXIMUM VALUE (KIPS)		
			BARBER	C-PEP	STUCKI	BARBER	C-PEP	STUCKI	BARBER	C-PEP	STUCKI
WEST	LEADING	1	[illegible]	[illegible]	[illegible]	[illegible]	[illegible]	[illegible]	[illegible]	[illegible]	[illegible]
		2	[illegible]	[illegible]	[illegible]	[illegible]	[illegible]	[illegible]	[illegible]	[illegible]	[illegible]
	TRAILING	1	[illegible]	[illegible]	[illegible]	[illegible]	[illegible]	[illegible]	[illegible]	[illegible]	[illegible]
		2	[illegible]	[illegible]	[illegible]	[illegible]	[illegible]	[illegible]	[illegible]	[illegible]	[illegible]
EAST	LEADING	1	[illegible]	[illegible]	[illegible]	[illegible]	[illegible]	[illegible]	[illegible]	[illegible]	[illegible]
		2	[illegible]	[illegible]	[illegible]	[illegible]	[illegible]	[illegible]	[illegible]	[illegible]	[illegible]
	TRAILING	1	[illegible]	[illegible]	[illegible]	[illegible]	[illegible]	[illegible]	[illegible]	[illegible]	[illegible]
		2	[illegible]	[illegible]	[illegible]	[illegible]	[illegible]	[illegible]	[illegible]	[illegible]	[illegible]

SPEED = 45 MPH, CONSIST NO.4, ALL GAUGES

DIRECTION	TRUCK	AXLE	ABSOLUTE AVERAGE (KIPS)			ALGEBRAIC AVERAGE (KIPS)			MAXIMUM VALUE (KIPS)		
			BARBER	RIDE	NEW AAR	BARBER	RIDE	NEW AAR	BARBER	RIDE	NEW AAR
WEST	LEADING	1	[illegible]	[illegible]	[illegible]	[illegible]	[illegible]	[illegible]	[illegible]	[illegible]	[illegible]
		2	[illegible]	[illegible]	[illegible]	[illegible]	[illegible]	[illegible]	[illegible]	[illegible]	[illegible]
	TRAILING	1	[illegible]	[illegible]	[illegible]	[illegible]	[illegible]	[illegible]	[illegible]	[illegible]	[illegible]
		2	[illegible]	[illegible]	[illegible]	[illegible]	[illegible]	[illegible]	[illegible]	[illegible]	[illegible]
EAST	LEADING	1	[illegible]	[illegible]	[illegible]	[illegible]	[illegible]	[illegible]	[illegible]	[illegible]	[illegible]
		2	[illegible]	[illegible]	[illegible]	[illegible]	[illegible]	[illegible]	[illegible]	[illegible]	[illegible]
	TRAILING	1	[illegible]	[illegible]	[illegible]	[illegible]	[illegible]	[illegible]	[illegible]	[illegible]	[illegible]
		2	[illegible]	[illegible]	[illegible]	[illegible]	[illegible]	[illegible]	[illegible]	[illegible]	[illegible]

TABLE 5 - LATERAL FORCE RESULTS TABULATED BY LEADING AND TRAILING AXLES FOR EASTWARD AND WESTWARD DIRECTIONS

SPEED = 25 MPH. CONSIST NO.1. ALL GAUGES. ALL DIRECTIONS

		ABSOLUTE AVERAGE (KIPS)			ALGEBRAIC AVERAGE (KIPS)			MAXIMUM VALUE (KIPS)		
TRUCK	AXLE	BARBER	LIST	SCHEFFEL	BARBER	LIST	SCHEFFEL	BARBER	LIST	SCHEFFEL
LEADING	1	3.12	2.47	2.52	2.02	2.17	1.95	10.20	7.30	6.50
	2	2.01	2.45	2.59	-0.49	-2.30	-1.27	-4.00	-4.00	-4.50
TRAILING	1	3.10	2.33	2.38	2.13	1.75	1.66	10.50	5.10	6.10
	2	2.07	2.40	2.85	-1.60	-2.40	-2.20	-4.00	-5.20	-5.20

SPEED = 25 MPH. CONSIST NO.2. ALL GAUGES. ALL DIRECTIONS

		ABSOLUTE AVERAGE (KIPS)			ALGEBRAIC AVERAGE (KIPS)			MAXIMUM VALUE (KIPS)		
TRUCK	AXLE	BARBER	SCALE	SWING	BARBER	SCALE	SWING	BARBER	SCALE	SWING
LEADING	1	2.07	3.00	4.57	2.02	2.65	4.52	6.70	5.70	10.00
	2	2.69	2.77	2.59	0.44	-1.75	-2.31	5.20	-5.00	-5.20
TRAILING	1	3.77	2.45	5.17	2.77	1.20	5.17	9.90	4.40	11.10
	2	2.59	2.53	3.23	-1.66	-2.13	-3.23	-4.90	-5.00	-4.60

SPEED = 25 MPH. CONSIST NO.3. ALL GAUGES. ALL DIRECTIONS

		ABSOLUTE AVERAGE (KIPS)			ALGEBRAIC AVERAGE (KIPS)			MAXIMUM VALUE (KIPS)		
TRUCK	AXLE	BARBER	C-PEP	STUCKI	BARBER	C-PEP	STUCKI	BARBER	C-PEP	STUCKI
LEADING	1	4.69	4.57	4.69	4.62	4.57	4.69	9.30	9.30	11.70
	2	2.50	2.24	2.24	-0.18	-0.03	0.20	4.40	4.40	3.80
TRAILING	1	4.50	4.70	4.60	4.47	4.70	4.60	10.00	9.50	11.40
	2	2.16	2.16	2.02	-1.44	-0.72	-0.87	-4.90	-4.30	-3.70

SPEED = 25 MPH. CONSIST NO.4. ALL GAUGES. ALL DIRECTIONS

		ABSOLUTE AVERAGE (KIPS)			ALGEBRAIC AVERAGE (KIPS)			MAXIMUM VALUE (KIPS)		
TRUCK	AXLE	BARBER	RIDE	NEW AAR	BARBER	RIDE	NEW AAR	BARBER	RIDE	NEW AAR
LEADING	1	2.46	2.13	3.66	1.99	1.06	3.66	5.30	4.10	7.30
	2	2.09	1.55	1.55	-1.24	0.05	-1.38	-5.10	3.80	-3.50
TRAILING	1	2.20	1.72	3.49	1.35	1.30	3.49	6.40	5.20	5.80
	2	2.32	1.76	1.84	-2.32	-0.73	-1.57	-5.20	-3.50	-3.70

SPEED = 37 MPH. CONSIST NO.1. ALL GAUGES. ALL DIRECTIONS

		ABSOLUTE AVERAGE (KIPS)			ALGEBRAIC AVERAGE (KIPS)			MAXIMUM VALUE (KIPS)		
TRUCK	AXLE	BARBER	LIST	SCHEFFEL	BARBER	LIST	SCHEFFEL	BARBER	LIST	SCHEFFEL
LEADING	1	4.66	3.37	3.87	4.66	3.37	3.87	8.40	7.20	7.30
	2	2.17	1.77	2.47	0.20	-1.32	-0.45	4.40	-3.20	-4.50
TRAILING	1	4.20	2.94	3.09	4.20	2.94	3.09	8.80	5.90	7.00
	2	1.47	1.73	2.50	-0.01	-1.26	-0.91	-3.20	-3.20	-4.40

SPEED = 37 MPH. CONSIST NO.2. ALL GAUGES. ALL DIRECTIONS

		ABSOLUTE AVERAGE (KIPS)			ALGEBRAIC AVERAGE (KIPS)			MAXIMUM VALUE (KIPS)		
TRUCK	AXLE	BARBER	SCALE	SWING	BARBER	SCALE	SWING	BARBER	SCALE	SWING
LEADING	1	3.30	3.04	4.70	3.30	3.04	4.70	7.00	5.00	10.00
	2	1.72	2.10	1.75	0.67	-1.03	-1.25	4.40	-4.40	-4.40
TRAILING	1	3.57	2.51	5.93	3.57	2.51	5.93	9.90	5.00	10.00
	2	1.30	1.45	2.69	-0.20	-0.41	-2.69	-4.00	-3.70	-4.10

SPEED = 37 MPH. CONSIST NO.3. ALL GAUGES. ALL DIRECTIONS

		ABSOLUTE AVERAGE (KIPS)			ALGEBRAIC AVERAGE (KIPS)			MAXIMUM VALUE (KIPS)		
TRUCK	AXLE	BARBER	C-PEP	STUCKI	BARBER	C-PEP	STUCKI	BARBER	C-PEP	STUCKI
LEADING	1	5.00	4.51	5.00	5.00	4.51	5.00	9.30	9.00	10.20
	2	2.02	2.47	2.67	1.07	1.99	2.36	4.30	7.00	6.10
TRAILING	1	5.25	5.16	5.17	5.25	5.16	5.17	10.20	9.60	11.10
	2	1.60	1.86	2.09	0.20	0.45	0.55	3.50	4.70	4.00

SPEED = 37 MPH. CONSIST NO.4. ALL GAUGES. ALL DIRECTIONS

		ABSOLUTE AVERAGE (KIPS)			ALGEBRAIC AVERAGE (KIPS)			MAXIMUM VALUE (KIPS)		
TRUCK	AXLE	BARBER	RIDE	NEW AAR	BARBER	RIDE	NEW AAR	BARBER	RIDE	NEW AAR
LEADING	1	3.67	3.31	6.31	3.62	3.26	6.31	7.00	6.60	10.20
	2	1.61	2.05	2.08	1.05	2.05	2.23	3.50	5.00	9.50
TRAILING	1	3.93	3.43	6.70	3.93	3.43	6.70	9.30	5.80	11.40
	2	1.12	1.99	2.51	-0.27	1.07	2.07	-2.00	3.20	6.40

SPEED = 45 MPH. CONSIST NO.1. ALL GAUGES. ALL DIRECTIONS

		ABSOLUTE AVERAGE (KIPS)			ALGEBRAIC AVERAGE (KIPS)			MAXIMUM VALUE (KIPS)		
TRUCK	AXLE	BARBER	LIST	SCHEFFEL	BARBER	LIST	SCHEFFEL	BARBER	LIST	SCHEFFEL
LEADING	1	5.67	3.48	3.70	5.67	3.40	3.70	10.51	7.67	5.05
	2	1.64	1.54	2.63	1.25	1.30	2.11	3.50	4.09	5.05
TRAILING	1	5.50	3.10	3.55	5.50	2.73	2.76	11.97	6.57	8.47
	2	1.40	1.20	2.43	1.16	0.76	0.98	2.63	3.50	6.72

SPEED = 45 MPH. CONSIST NO.2. ALL GAUGES. ALL DIRECTIONS

		ABSOLUTE AVERAGE (KIPS)			ALGEBRAIC AVERAGE (KIPS)			MAXIMUM VALUE (KIPS)		
TRUCK	AXLE	BARBER	SCALE	SWING	BARBER	SCALE	SWING	BARBER	SCALE	SWING
LEADING	1	5.87	5.00	6.77	5.87	5.00	6.77	10.70	9.50	14.22
	2	2.42	1.62	1.90	1.50	0.98	-0.61	8.03	4.03	4.02
TRAILING	1	5.61	3.20	7.33	5.61	3.20	7.33	14.00	8.00	14.60
	2	1.61	1.67	1.63	1.46	1.60	-0.91	4.02	4.67	-3.50

SPEED = 45 MPH. CONSIST NO.3. ALL GAUGES. ALL DIRECTIONS

		ABSOLUTE AVERAGE (KIPS)			ALGEBRAIC AVERAGE (KIPS)			MAXIMUM VALUE (KIPS)		
TRUCK	AXLE	BARBER	C-PEP	STUCKI	BARBER	C-PEP	STUCKI	BARBER	C-PEP	STUCKI
LEADING	1	7.85	5.79	6.20	6.96	5.70	6.20	13.10	10.50	13.00
	2	2.04	1.89	2.30	1.70	1.00	2.04	6.50	5.40	5.60
TRAILING	1	6.29	5.99	5.94	6.29	5.99	5.94	12.80	11.00	11.70
	2	1.75	2.07	1.96	1.34	1.69	1.19	3.90	4.50	3.50

SPEED = 45 MPH. CONSIST NO.4. ALL GAUGES. ALL DIRECTIONS

		ABSOLUTE AVERAGE (KIPS)			ALGEBRAIC AVERAGE (KIPS)			MAXIMUM VALUE (KIPS)		
TRUCK	AXLE	BARBER	RIDE	NEW AAR	BARBER	RIDE	NEW AAR	BARBER	RIDE	NEW AAR
LEADING	1	5.26	4.78	5.02	5.26	4.78	5.02	9.64	8.47	9.93
	2	1.98	2.14	1.45	1.52	1.56	0.53	4.38	4.96	3.46
TRAILING	1	5.25	4.35	5.01	5.25	4.35	5.01	11.57	9.04	9.64
	2	1.62	2.41	1.40	0.73	2.16	0.67	-2.00	4.67	3.50

TABLE 6 - LATERAL FORCE RESULTS TABULATED BY LEADING AND TRAILING AXLES FOR ALL DIRECTIONS

SPEED = 25 MPH., CONSIST NO. 1

ORIENT.	DIR.	AXLE	ABSOLUTE AVERAGE ANGLE (MIN) BARBER	ABSOLUTE AVERAGE ANGLE (MIN) LIST	ABSOLUTE AVERAGE ANGLE (MIN) SCHEFFEL	ALGEBRAIC AVERAGE ANGLE (MIN) BARBER	ALGEBRAIC AVERAGE ANGLE (MIN) LIST	ALGEBRAIC AVERAGE ANGLE (MIN) SCHEFFEL	MAXIMUM ANGLE (MINS) BARBER	MAXIMUM ANGLE (MINS) LIST	MAXIMUM ANGLE (MINS) SCHEFFEL
REG.	WEST	1	30.716	7.345	16.514	30.716	7.345	16.514	32.728	9.197	19.861
		2	7.742	6.575	12.601	7.742	6.575	12.601	12.983	9.570	16.835
		3	30.112	10.164	6.945	30.112	10.164	6.945	30.904	12.399	8.443
		4	6.634	7.306	7.346	6.634	7.306	7.346	9.049	10.243	9.379
REG.	EAST	4	26.800	17.166	23.207	26.800	17.166	23.207	28.751	19.160	26.895
		3	7.605	8.837	15.523	7.605	8.837	15.523	14.346	9.205	17.186
		2	25.017	13.712	11.028	25.017	13.712	11.028	28.221	14.990	12.163
		1	6.769	10.490	10.511	6.769	10.490	10.511	8.392	11.687	12.651
WYED	WEST	4	25.138	6.557	3.659	25.138	6.557	3.659	27.426	7.836	4.322
		3	9.665	7.729	6.759	9.665	7.729	6.759	10.369	8.310	7.703
		2	22.571	7.656	10.639	22.571	7.656	10.639	24.237	8.406	11.796
		1	5.723	7.243	10.319	5.723	7.243	10.319	6.897	8.287	11.180
WYED	EAST	1	21.845	12.104	9.608	21.845	12.104	9.608	23.786	12.346	16.193
		2	6.714	9.295	11.381	6.714	9.295	11.381	8.021	9.719	12.198
		3	17.283	10.167	16.566	17.283	10.167	16.566	18.024	11.451	17.946
		4	3.876	7.840	11.205	3.876	7.840	11.205	5.524	8.691	12.488

SPEED = 25 MPH., CONSIST NO. 2

ORIENT.	DIR.	AXLE	ABSOLUTE AVERAGE ANGLE (MIN) BARBER	ABSOLUTE AVERAGE ANGLE (MIN) SCALE	ABSOLUTE AVERAGE ANGLE (MIN) SWING	ALGEBRAIC AVERAGE ANGLE (MIN) BARBER	ALGEBRAIC AVERAGE ANGLE (MIN) SCALE	ALGEBRAIC AVERAGE ANGLE (MIN) SWING	MAXIMUM ANGLE (MINS) BARBER	MAXIMUM ANGLE (MINS) SCALE	MAXIMUM ANGLE (MINS) SWING
REG.	WEST	1	35.865	13.142	31.720	35.865	13.142	31.720	37.586	15.358	32.615
		2	22.923	9.974	13.996	22.923	9.974	13.996	29.895	11.377	15.403
		3	25.670	8.626	20.063	25.670	8.626	20.063	27.885	9.961	22.106
		4	10.102	10.360	6.360	10.102	10.360	6.360	11.219	12.885	7.576
REG.	EAST	4	25.442	13.828	25.709	25.442	13.828	25.709	27.776	15.678	26.243
		3	11.011	10.138	10.914	11.011	10.138	10.914	13.317	19.068	12.529
		2	20.642	14.575	23.438	20.642	14.575	23.438	21.431	15.757	25.528
		1	7.367	10.067	3.782	7.367	10.067	3.782	8.102	11.244	4.461
WYED	WEST	4	33.228	9.749	28.990	33.228	9.749	28.990	34.477	10.317	29.882
		3	11.529	5.734	6.648	11.529	5.734	6.648	13.144	6.148	8.298
		2	30.466	11.871	25.091	30.466	11.871	25.091	31.122	12.986	25.516
		1	7.407	11.344	6.393	7.407	11.344	6.393	8.607	12.433	7.574
WYED	EAST	1	31.881	13.840	22.044	31.881	13.840	22.044	32.545	14.297	23.168
		2	7.095	13.372	6.171	7.095	13.372	6.171	7.359	14.749	7.520
		3	28.517	17.961	26.539	28.517	17.961	26.539	29.658	16.706	27.697
		4	6.425	9.298	3.512	6.425	9.298	3.512	7.458	10.428	4.726

SPEED = 25 MPH., CONSIST NO. 3

ORIENT.	DIR.	AXLE	ABSOLUTE AVERAGE ANGLE (MIN) BARBER	ABSOLUTE AVERAGE ANGLE (MIN) C-PEP	ABSOLUTE AVERAGE ANGLE (MIN) STUCKI	ALGEBRAIC AVERAGE ANGLE (MIN) BARBER	ALGEBRAIC AVERAGE ANGLE (MIN) C-PEP	ALGEBRAIC AVERAGE ANGLE (MIN) STUCKI	MAXIMUM ANGLE (MINS) BARBER	MAXIMUM ANGLE (MINS) C-PEP	MAXIMUM ANGLE (MINS) STUCKI
REG.	WEST	1	29.755	31.394	28.936	29.755	31.394	28.936	31.995	21.762	30.517
		2	14.566	9.902	9.062	14.566	9.902	9.062	16.883	11.901	10.932
		3	22.206	27.258	25.935	22.206	27.258	25.935	23.164	29.201	27.774
		4	5.761	9.286	7.546	5.761	9.286	7.546	6.339	10.697	10.355
REG.	EAST	4	21.785	23.254	25.237	21.785	23.254	25.237	23.139	24.288	26.570
		3	7.970	10.127	9.316	7.970	10.127	9.316	9.394	11.131	10.206
		2	19.052	26.638	23.056	19.052	26.638	23.056	19.860	28.138	23.479
		1	5.676	8.844	3.368	5.676	8.844	3.368	7.733	8.900	3.611
WYED	WEST	4	31.034	30.100	32.409	31.034	30.100	32.409	35.187	32.914	32.563
		3	9.865	12.546	14.585	9.865	12.546	14.585	14.527	19.333	22.051
		2	30.983	30.154	28.682	30.983	30.154	28.682	33.428	31.398	31.302
		1	7.722	11.859	10.257	7.722	11.859	10.257	10.916	16.760	12.992
WYED	EAST	1	29.141	26.602	27.008	29.141	26.602	27.008	34.861	34.866	37.341
		2	5.800	7.623	9.817	5.800	7.623	9.817	10.527	13.523	18.335
		3	24.739	22.568	20.964	24.739	22.568	20.964	28.680	26.268	24.523
		4	4.292	4.253	2.272	4.292	4.253	2.272	7.448	7.611	5.725

SPEED = 25 MPH., CONSIST NO. 4

ORIENT.	DIR.	AXLE	ABSOLUTE AVERAGE ANGLE (MIN) BARBER	ABSOLUTE AVERAGE ANGLE (MIN) RIDE	ABSOLUTE AVERAGE ANGLE (MIN) NEW-AAR	ALGEBRAIC AVERAGE ANGLE (MIN) BARBER	ALGEBRAIC AVERAGE ANGLE (MIN) RIDE	ALGEBRAIC AVERAGE ANGLE (MIN) NEW-AAR	MAXIMUM ANGLE (MINS) BARBER	MAXIMUM ANGLE (MINS) RIDE	MAXIMUM ANGLE (MINS) NEW-AAR
REG.	WEST	1	33.863	34.032	19.066	33.863	34.032	19.066	35.469	34.606	15.865
		2	12.572	19.173	4.818	12.572	19.173	4.818	13.580	20.243	5.339
		3	32.202	36.206	19.688	32.202	36.206	19.688	33.043	37.651	26.843
		4	9.428	18.293	5.697	9.428	18.293	5.697	10.097	19.379	6.515
REG.	EAST	4	28.346	30.946	11.961	28.346	30.946	11.961	29.743	33.335	14.955
		3	5.635	12.449	0.632	5.635	12.449	0.456	6.668	13.865	1.484
		2	23.009	23.794	13.862	23.009	23.794	13.862	23.855	26.017	10.063
		1	2.271	7.678	0.813	2.271	7.678	-0.813	3.867	9.890	-1.839
WYED	WEST	4	33.251	31.077	23.245	33.251	31.077	23.245	34.658	31.619	25.294
		3	18.444	15.705	5.621	18.444	15.705	5.621	20.643	16.357	7.631
		2	26.121	34.039	26.613	26.121	34.039	26.613	26.685	35.233	27.944
		1	9.492	17.345	5.859	9.492	17.345	5.859	10.170	10.638	7.576
WYED	EAST	1	19.087	23.309	17.360	19.087	23.309	17.360	21.961	25.711	19.081
		2	3.995	6.561	1.428	3.995	6.561	-0.132	7.795	8.056	3.241
		3	16.524	18.912	17.836	16.524	18.912	17.036	17.785	19.561	14.768
		4	3.010	5.111	1.619	3.010	5.111	1.047	6.358	6.141	4.635

TABLE 7 - ANGLE-OF-ATTACK RESULTS TABULATED BY LEADING AND TRAILING AXLES FOR EACH CONSIST AT THREE TEST SPEEDS

SPEED = 37 MPH., CONSIST NO. 1

ORIENT.	DIR.	AXLE	ABSOLUTE AVERAGE ANGLE (MIN)			ALGEBRAIC AVERAGE ANGLE (MIN)			MAXIMUM ANGLE (MINS)		
			BARBER	LIST	SCHEFFEL	BARBER	LIST	SCHEFFEL	BARBER	LIST	SCHEFFEL
REG.	WEST	1	31.776	4.506	17.201	31.776	4.506	17.201	35.523	9.836	16.333
		2	10.599	5.629	8.735	10.599	5.629	8.735	15.637	6.425	9.526
		3	28.640	9.487	4.566	28.640	9.487	4.566	29.864	10.652	6.410
		4	6.570	6.011	3.887	6.570	6.011	3.887	8.095	6.946	4.077
REG.	EAST	4	26.873	12.472	26.698	26.873	12.472	26.698	27.965	13.740	26.419
		3	6.439	9.259	15.080	6.439	9.259	15.080	8.015	10.016	17.634
		2	26.956	14.474	7.503	26.956	14.474	7.503	28.718	14.942	9.205
		1	9.111	10.703	9.339	9.111	10.703	9.339	10.324	11.885	10.385
WYED	WEST	4	21.900	3.347	1.248	21.900	3.347	1.248	25.517	3.645	2.136
		3	8.389	6.454	2.403	8.389	6.454	2.403	11.565	7.161	3.090
		2	19.321	5.176	10.317	19.321	5.176	10.317	20.795	5.607	12.832
		1	3.550	5.205	6.402	3.550	5.205	6.402	4.683	5.442	7.664
WYED	EAST	1	24.255	13.799	10.265	24.255	13.799	10.265	28.192	16.839	12.423
		2	10.107	10.755	11.164	10.107	10.755	11.164	12.807	11.386	12.552
		3	18.496	12.198	18.085	18.496	12.198	18.085	22.045	13.276	20.996
		4	7.010	8.553	11.860	7.010	8.553	11.860	9.215	9.849	12.545

SPEED = 37 MPH., CONSIST NO. 2

ORIENT.	DIR.	AXLE	ABSOLUTE AVERAGE ANGLE (MIN)			ALGEBRAIC AVERAGE ANGLE (MIN)			MAXIMUM ANGLE (MINS)		
			BARBER	SCALE	SWING	BARBER	SCALE	SWING	BARBER	SCALE	SWING
REG.	WEST	1	29.803	12.009	24.612	29.803	12.009	24.612	31.508	12.688	26.734
		2	25.016	8.792	14.976	25.016	8.792	14.976	26.199	9.867	26.469
		3	27.180	4.487	19.112	27.180	4.487	19.112	28.985	5.229	26.236
		4	11.751	8.996	3.822	11.751	8.996	3.822	12.869	9.624	4.103
REG.	EAST	4	29.430	14.242	25.580	29.430	14.242	25.580	30.885	16.028	26.084
		3	13.525	19.122	11.672	13.525	19.122	11.672	14.926	20.775	14.711
		2	22.360	16.861	24.151	22.360	16.861	24.151	24.735	18.303	24.955
		1	10.215	10.778	5.710	10.215	10.778	5.710	12.218	12.279	6.250
WYED	WEST	4	29.823	6.476	28.385	29.823	6.476	28.385	31.638	8.236	30.588
		3	9.777	4.660	5.088	9.777	4.660	5.088	9.955	6.656	8.049
		2	28.913	10.671	21.915	28.913	10.671	21.915	29.986	11.763	22.845
		1	7.284	11.729	2.955	7.284	11.729	2.955	8.217	12.938	4.272
WYED	EAST	1	32.097	17.132	26.270	32.057	17.132	26.270	33.288	18.719	27.306
		2	9.268	15.701	8.325	9.268	15.701	8.325	10.619	16.937	8.931
		3	31.059	19.621	27.423	31.059	19.621	27.423	31.836	21.135	27.813
		4	12.025	11.916	5.089	12.025	11.916	5.089	12.500	13.225	5.706

SPEED = 37 MPH., CONSIST NO. 3

ORIENT.	DIR.	AXLE	ABSOLUTE AVERAGE ANGLE (MIN)			ALGEBRAIC AVERAGE ANGLE (MIN)			MAXIMUM ANGLE (MINS)		
			BARBER	C-PEP	STUCKI	BARBER	C-PEP	STUCKI	BARBER	C-PEP	STUCKI
REG.	WEST	1	30.845	27.877	26.801	30.845	27.877	26.801	33.259	31.482	28.467
		2	17.681	7.975	8.937	17.681	7.975	8.937	20.423	12.719	16.838
		3	20.997	23.573	22.461	20.997	23.573	22.461	21.887	27.104	25.870
		4	5.176	6.128	4.778	5.176	6.128	4.778	6.682	8.638	8.697
REG.	EAST	4	21.398	22.538	24.626	21.990	22.538	24.626	25.528	26.764	30.142
		3	8.295	10.524	8.406	8.295	10.524	8.406	11.731	14.394	13.731
		2	17.968	24.650	23.653	17.988	24.650	23.653	21.140	28.288	20.014
		1	7.118	7.965	3.359	7.118	7.965	3.359	9.720	11.443	5.981
WYED	WEST	4	27.940	29.170	31.216	27.940	29.170	31.216	28.624	30.428	32.610
		3	7.833	11.727	11.761	7.833	11.727	11.761	9.373	12.880	12.215
		2	29.393	27.972	26.575	29.393	27.972	26.575	30.584	28.855	27.196
		1	7.589	10.264	9.277	7.589	10.264	9.277	8.191	10.710	9.998
WYED	EAST	1	28.465	25.049	26.355	28.465	25.049	26.355	31.755	28.495	30.363
		2	5.086	9.725	9.977	5.086	9.725	9.977	8.759	12.874	13.242
		3	24.709	23.910	22.014	24.709	23.910	22.014	27.813	25.393	23.518
		4	5.252	6.974	2.477	5.252	6.974	2.477	8.994	8.996	4.592

SPEED = 37 MPH., CONSIST NO. 4

ORIENT.	DIR.	AXLE	ABSOLUTE AVERAGE ANGLE (MIN)			ALGEBRAIC AVERAGE ANGLE (MIN)			MAXIMUM ANGLE (MINS)		
			BARBER	RIDE	NEW-AAR	BARBER	RIDE	NEW-AAR	BARBER	RIDE	NEW-AAR
REG.	WEST	1	34.874	35.186	21.542	34.874	35.186	21.542	36.842	37.873	23.812
		2	14.273	20.325	7.388	14.273	20.325	7.388	15.359	23.169	9.851
		3	30.151	38.318	21.507	30.151	38.318	21.507	31.317	43.069	24.262
		4	8.392	22.852	8.491	8.392	22.852	8.491	9.651	23.884	10.864
REG.	EAST	4	28.658	36.139	16.626	28.650	36.139	16.626	31.129	46.525	18.580
		3	6.899	21.364	5.923	6.899	21.364	5.923	10.381	30.905	7.928
		2	24.856	26.214	18.239	24.856	26.214	18.239	27.509	32.168	20.897
		1	6.383	12.856	6.314	6.383	12.856	6.314	8.158	16.129	8.512
WYED	WEST	4	34.189	32.791	28.885	34.189	32.791	28.885	37.908	36.508	31.675
		3	19.913	17.487	11.876	19.913	17.487	11.876	22.148	21.350	13.849
		2	25.324	35.046	29.091	25.324	35.046	29.091	26.928	39.414	32.187
		1	9.044	15.913	10.565	9.044	15.913	10.565	11.111	19.581	14.215
WYED	EAST	1	24.135	29.151	22.206	24.135	29.151	22.206	27.045	40.411	32.120
		2	9.015	12.551	5.088	9.015	12.551	5.088	12.195	21.133	10.357
		3	20.238	23.826	20.081	20.238	23.826	20.081	22.866	32.511	23.691
		4	7.082	9.839	3.247	7.082	9.839	3.247	10.545	19.457	7.848

TABLE 7- Continued

SPEED = 45 MPH., CONSIST NO. 1

ORIENT.	DIR.	AXLE	ABSOLUTE AVERAGE ANGLE (MIN) BARBER	LIST	SCHEFFEL	ALGEBRAIC AVERAGE ANGLE (MIN) BARBER	LIST	SCHEFFEL	MAXIMUM ANGLE (MINS) BARBER	LIST	SCHEFFEL
REG.	WEST	1	23.624	2.968	9.555	23.624	2.968	9.555	25.249	4.681	11.457
		2	3.046	3.180	4.954	3.046	3.180	4.954	3.463	3.896	6.779
		3	25.358	5.914	1.664	25.358	5.914	-0.596	26.462	7.156	-2.482
		4	4.724	6.615	2.123	4.724	6.615	1.457	5.360	8.487	3.581
REG.	EAST	4	23.992	0.0	20.459	23.992	0.0	20.459	24.638	0.0	20.660
		3	4.533	8.018	10.493	4.533	8.018	10.493	5.108	8.496	10.565
		2	22.498	12.505	7.792	22.498	12.505	7.792	23.365	13.111	8.489
		1	3.972	8.655	5.230	3.972	8.655	5.230	4.404	9.764	5.992
WYED	WEST	4	16.284	2.575	1.241	16.284	2.575	-1.241	17.175	3.808	-2.016
		3	5.776	4.915	0.392	5.776	4.915	0.392	6.358	5.595	0.639
		2	15.836	4.586	5.555	15.836	4.586	5.555	16.381	5.272	5.917
		1	3.356	5.073	4.181	3.356	5.073	4.181	3.650	5.443	4.418
WYED	EAST	1	15.756	8.548	7.695	15.756	8.548	7.695	16.442	9.021	8.170
		2	2.979	5.332	7.970	2.979	5.332	7.970	3.808	5.399	8.360
		3	13.099	8.396	11.572	13.099	8.396	11.572	14.014	8.681	12.250
		4	0.400	4.868	5.821	0.165	4.868	5.821	0.847	5.280	6.570

SPEED = 45 MPH., CONSIST NO. 2

ORIENT.	DIR.	AXLE	ABSOLUTE AVERAGE ANGLE (MIN) BARBER	SCALE	SWING	ALGEBRAIC AVERAGE ANGLE (MIN) BARBER	SCALE	SWING	MAXIMUM ANGLE (MINS) BARBER	SCALE	SWING
REG.	WEST	1	32.605	8.074	26.253	32.605	8.074	26.253	36.057	9.455	20.671
		2	21.093	8.442	7.968	21.093	8.442	7.968	26.286	10.101	10.330
		3	24.306	5.040	17.335	24.306	5.040	17.335	24.805	6.294	18.258
		4	12.175	9.190	3.406	12.175	9.190	3.406	13.623	10.888	4.518
REG.	EAST	4	23.240	12.083	20.752	23.240	12.083	20.752	24.060	13.294	22.012
		3	7.788	15.322	6.409	7.788	15.322	6.409	9.595	16.919	7.264
		2	19.069	13.158	20.864	19.069	13.158	20.864	19.857	14.110	22.322
		1	5.937	6.079	2.413	5.937	6.079	2.413	7.630	8.291	3.503
WYED	WEST	4	24.535	6.006	24.548	24.535	6.006	24.548	27.535	6.547	27.054
		3	4.379	5.526	2.414	4.379	5.526	2.414	4.379	6.300	2.892
		2	26.105	7.372	20.183	26.105	7.372	20.183	27.172	9.123	22.085
		1	5.274	9.148	2.948	5.274	9.148	2.948	5.621	10.620	3.312
WYED	EAST	1	28.672	11.866	22.720	28.672	11.866	22.720	29.651	12.875	21.315
		2	4.410	11.191	5.497	4.410	11.191	5.497	4.557	11.596	6.230
		3	25.893	15.299	24.831	25.893	15.299	24.831	28.174	15.809	25.207
		4	5.751	7.461	2.655	5.751	7.461	2.655	7.081	8.556	3.093

SPEED = 45 MPH., CONSIST NO. 3

ORIENT.	DIR.	AXLE	ABSOLUTE AVERAGE ANGLE (MIN) BARBER	C-PEP	STUCKI	ALGEBRAIC AVERAGE ANGLE (MIN) BARBER	C-PEP	STUCKI	MAXIMUM ANGLE (MINS) BARBER	C-PEP	STUCKI
REG.	WEST	1	30.259	29.512	30.078	30.259	29.512	30.078	30.976	20.286	32.208
		2	17.872	10.933	12.404	17.872	10.933	12.404	18.305	11.932	14.937
		3	21.870	24.383	23.419	21.870	24.383	23.419	23.197	25.369	24.824
		4	8.166	9.827	8.014	8.166	9.827	8.014	8.827	10.374	9.227
REG.	EAST	4	19.721	20.536	21.753	19.721	20.536	21.753	20.386	21.011	22.407
		3	7.239	9.526	5.659	7.239	9.526	5.659	9.388	10.965	7.305
		2	16.468	25.246	21.760	16.468	25.246	21.760	16.998	25.258	22.196
		1	4.939	7.406	1.737	4.939	7.406	1.737	6.907	9.267	2.660
WYED	WEST	4	26.472	26.951	26.963	26.472	26.951	26.963	26.587	27.276	27.654
		3	7.207	11.323	8.720	7.207	11.323	8.720	7.893	11.919	8.971
		2	28.288	26.851	24.377	28.288	26.851	24.377	29.173	27.039	24.462
		1	7.793	9.976	8.488	7.793	9.976	8.488	8.342	10.247	8.055
WYED	EAST	1	21.946	21.833	21.183	21.946	21.833	21.183	22.089	24.437	23.580
		2	0.622	4.996	5.199	0.130	4.996	5.199	-0.738	9.276	6.430
		3	21.005	20.424	18.770	21.005	20.424	18.770	21.625	21.488	19.656
		4	1.907	2.953	0.526	1.907	2.953	-0.304	2.061	3.164	-1.068

SPEED = 45 MPH., CONSIST NO. 4

ORIENT.	DIR.	AXLE	ABSOLUTE AVERAGE ANGLE (MIN) BARBER	RIDE	NEW-AAR	ALGEBRAIC AVERAGE ANGLE (MIN) BARBER	RIDE	NEW-AAR	MAXIMUM ANGLE (MINS) BARBER	RIDE	NEW-AAR
REG.	WEST	1	30.545	24.642	17.528	30.545	24.642	17.528	31.657	25.242	16.546
		2	12.453	12.567	6.260	12.453	12.567	6.260	13.901	12.925	8.162
		3	28.480	31.697	17.629	28.480	31.697	17.629	29.420	32.329	18.148
		4	8.128	16.013	6.352	8.128	16.013	6.352	10.154	16.598	7.668
REG.	EAST	4	20.077	19.442	13.034	20.077	19.442	13.034	20.512	20.826	14.522
		3	1.976	3.629	2.646	-1.976	3.629	-2.646	-3.535	4.512	-4.333
		2	20.082	17.290	11.667	20.082	17.290	11.667	21.017	18.802	12.665
		1	1.057	3.312	0.887	0.415	3.312	-0.715	1.401	3.533	-2.386
WYED	WEST	4	28.345	27.899	20.474	28.345	27.899	20.474	29.446	28.533	21.983
		3	16.130	14.185	6.618	16.130	14.185	6.618	17.913	15.420	6.449
		2	22.085	29.734	21.662	22.085	29.734	21.662	22.750	30.518	21.956
		1	8.963	13.817	5.176	8.963	13.817	5.176	9.563	14.839	7.192
WYED	EAST	1	12.745	18.051	13.234	12.745	18.051	13.234	14.866	19.527	13.652
		2	0.560	1.694	3.598	0.560	1.694	-3.598	0.855	2.043	-4.640
		3	11.450	13.496	11.019	11.450	13.496	11.019	11.766	13.767	11.711
		4	0.915	1.064	3.683	-0.915	1.064	-3.683	-2.168	1.511	-4.042

TABLE 7 - Continued

TABLE 8 - ANGLE-OF-ATTACK RESULTS TABULATED BY LEADING AND TRAILING AXLES FOR EASTWARD AND WESTWARD DIRECTIONS

SPEED = 25 MPH., CONSIST NO. 1

DIRECTION	TRUCK	AXLE	ABSOLUTE AVERAGE ANGLE (MIN) BARBER	LIST	SCHEFFEL	ALGEBRAIC AVERAGE ANGLE (MIN) BARBER	LIST	SCHEFFEL	MAXIMUM ANGLE (MINS) BARBER	LIST	SCHEFFEL
WEST	LEADING	1	27.027	6.091	10.200	27.027	6.051	10.200	37.720	4.147	19.061
		2	9.729	7.152	9.400	9.703	7.152	9.600	17.941	5.570	15.035
	TRAILING	1	26.301	8.910	9.707	26.341	8.913	8.702	10.500	12.366	11.700
		2	6.179	7.276	9.032	6.170	7.276	8.032	6.609	10.207	11.190
EAST	LEADING	1	26.922	14.634	10.407	26.122	14.635	10.407	28.781	14.166	25.865
		2	7.159	9.066	13.452	7.159	9.066	13.452	10.366	5.716	17.198
	TRAILING	1	21.150	11.939	13.707	21.150	11.939	13.707	29.221	14.940	17.500
		2	5.327	9.145	10.858	5.327	9.145	10.858	8.957	11.047	12.651

SPEED = 25 MPH., CONSIST NO. 2

DIRECTION	TRUCK	AXLE	ABSOLUTE AVERAGE ANGLE (MIN) BARBER	SCALE	SWING	ALGEBRAIC AVERAGE ANGLE (MIN) BARBER	SCALE	SWING	MAXIMUM ANGLE (MINS) BARBER	SCALE	SWING
WEST	LEADING	1	30.566	11.465	30.395	30.566	11.465	30.395	37.482	14.354	34.615
		2	17.226	7.856	10.322	17.226	7.856	10.322	25.895	11.377	15.403
	TRAILING	1	28.060	10.240	22.577	28.060	10.240	22.577	31.172	12.566	27.516
		2	8.756	10.092	6.376	8.756	10.052	6.376	11.214	12.005	7.578
EAST	LEADING	1	28.601	13.036	23.876	28.601	13.034	23.876	32.569	17.878	27.267
		2	9.053	15.755	8.562	9.053	15.755	8.562	17.917	14.028	12.524
	TRAILING	1	24.574	10.268	24.988	24.574	10.268	24.988	29.650	18.706	27.057
		2	6.996	9.602	3.667	6.996	9.602	3.667	8.102	11.266	8.726

SPEED = 25 MPH., CONSIST NO. 3

DIRECTION	TRUCK	AXLE	ABSOLUTE AVERAGE ANGLE (MIN) BARBER	C-PEP	STUCKI	ALGEBRAIC AVERAGE ANGLE (MIN) BARBER	C-PEP	STUCKI	MAXIMUM ANGLE (MINS) BARBER	C-PEP	STUCKI
WEST	LEADING	1	30.305	30.767	30.673	30.305	30.767	30.673	35.147	32.416	34.503
		2	12.215	11.224	11.023	12.215	11.224	11.023	14.801	19.377	22.671
	TRAILING	1	26.594	28.702	27.304	26.594	28.702	27.304	33.078	31.900	31.726
		2	6.701	10.172	8.931	6.701	10.172	8.931	10.416	17.700	12.599
EAST	LEADING	1	25.461	24.928	26.122	25.461	24.928	26.122	36.261	34.026	37.141
		2	8.405	8.875	9.566	8.889	8.875	9.566	10.427	13.923	10.335
	TRAILING	1	21.995	24.601	22.010	21.995	24.601	22.010	28.660	28.178	24.523
		2	6.386	6.168	2.878	6.986	6.168	2.878	7.731	9.468	5.725

SPEED = 25 MPH., CONSIST NO. 4

DIRECTION	TRUCK	AXLE	ABSOLUTE AVERAGE ANGLE (MIN) BARBER	RIDE	NEO-AAR	ALGEBRAIC AVERAGE ANGLE (MIN) BARBER	RIDE	NEO-AAR	MAXIMUM ANGLE (MINS) BARBER	RIDE	NEO-AAR
WEST	LEADING	1	33.557	32.556	21.195	33.557	32.556	21.155	35.664	36.688	25.248
		2	15.908	17.639	5.210	15.508	17.639	5.214	20.763	20.261	7.631
	TRAILING	1	29.161	35.122	23.150	29.161	35.122	23.150	37.069	37.651	27.546
		2	9.460	17.819	5.778	9.460	17.813	5.778	10.170	15.375	7.576
EAST	LEADING	1	23.716	27.128	14.000	23.716	27.128	14.000	25.761	37.395	17.081
		2	4.915	9.509	1.030	4.915	9.505	0.162	7.705	11.089	3.261
	TRAILING	1	19.706	21.951	15.649	19.706	21.951	15.649	23.855	27.017	19.780
		2	2.661	8.396	1.218	2.661	8.396	0.117	7.358	9.050	4.436

SPEED = 37 MPH., CONSIST NO. 1

DIRECTION	TRUCK	AXLE	ABSOLUTE AVERAGE ANGLE (MIN) BARBER	LIST	SCHEFFEL	ALGEBRAIC AVERAGE ANGLE (MIN) BARBER	LIST	SCHEFFEL	MAXIMUM ANGLE (MINS) BARBER	LIST	SCHEFFEL
WEST	LEADING	1	26.938	3.926	9.224	26.038	3.926	9.224	35.523	7.734	10.333
		2	9.696	6.042	5.960	9.696	6.042	5.563	15.037	7.181	9.520
	TRAILING	1	23.900	7.332	7.461	23.900	7.332	7.461	25.864	10.652	12.032
		2	5.000	5.608	5.144	5.000	5.608	5.144	8.005	6.566	7.604
EAST	LEADING	1	25.564	13.135	10.401	25.564	13.135	10.401	27.102	16.875	15.615
		2	8.273	10.007	13.122	8.273	10.007	13.122	12.007	11.706	17.614
	TRAILING	1	22.726	13.336	12.796	22.726	13.336	12.796	27.718	16.562	[illegible]
		2	8.060	9.028	10.599	8.060	9.028	10.599	10.326	11.865	12.565

SPEED = 37 MPH., CONSIST NO. 2

DIRECTION	TRUCK	AXLE	ABSOLUTE AVERAGE ANGLE (MIN) BARBER	SCALE	SWING	ALGEBRAIC AVERAGE ANGLE (MIN) BARBER	SCALE	SWING	MAXIMUM ANGLE (MINS) BARBER	SCALE	SWING
WEST	LEADING	1	29.013	9.262	26.490	29.013	9.262	26.449	31.980	12.688	30.506
		2	17.306	6.726	10.032	17.306	6.726	10.032	26.199	9.067	19.045
	TRAILING	1	28.046	7.576	20.513	28.046	7.576	20.513	29.906	11.763	22.005
		2	9.517	10.362	3.308	9.517	10.362	3.308	12.069	12.030	4.276
EAST	LEADING	1	30.763	15.687	25.525	30.763	15.687	25.525	37.286	18.715	28.084
		2	11.396	17.611	9.998	11.396	17.611	9.998	14.026	20.775	14.711
	TRAILING	1	28.710	17.841	25.707	28.710	17.841	25.707	31.836	21.135	27.013
		2	11.128	11.367	5.398	11.128	11.367	5.304	12.400	17.334	6.250

SPEED = 37 MPH., CONSIST NO. 3

DIRECTION	TRUCK	AXLE	ABSOLUTE AVERAGE ANGLE (MIN) BARBER	C-PEP	STUCKI	ALGEBRAIC AVERAGE ANGLE (MIN) BARBER	C-PEP	STUCKI	MAXIMUM ANGLE (MINS) BARBER	C-PEP	STUCKI
WEST	LEADING	1	29.303	28.523	29.088	29.303	28.523	29.088	33.250	31.002	32.816
		2	12.757	9.051	10.349	12.757	9.051	10.349	20.421	12.888	15.038
	TRAILING	1	25.195	25.772	24.510	25.195	25.772	24.510	30.504	28.899	27.196
		2	6.382	8.196	7.028	6.382	8.196	7.028	9.191	10.710	9.540
EAST	LEADING	1	28.327	23.703	25.498	28.327	23.703	25.498	31.755	28.059	30.363
		2	8.691	10.124	9.191	8.691	10.124	9.191	11.731	16.396	13.731
	TRAILING	1	21.339	24.200	22.033	21.339	24.200	22.033	27.013	28.270	26.614
		2	6.105	7.460	2.910	6.105	7.460	2.910	5.728	11.461	5.501

SPEED = 37 MPH., CONSIST NO. 4

DIRECTION	TRUCK	AXLE	ABSOLUTE AVERAGE ANGLE (MIN) BARBER	RIDE	NEO-AAR	ALGEBRAIC AVERAGE ANGLE (MIN) BARBER	RIDE	NEO-AAR	MAXIMUM ANGLE (MINS) BARBER	RIDE	NEO-AAR
WEST	LEADING	1	34.531	33.988	25.173	34.531	33.988	25.173	37.988	37.073	31.675
		2	17.901	18.866	9.232	17.093	18.866	9.232	22.148	23.165	13.046
	TRAILING	1	27.710	36.682	25.299	27.738	36.682	25.299	31.317	43.065	32.107
		2	8.710	19.382	9.928	8.718	19.382	9.928	11.111	23.886	14.215
EAST	LEADING	1	26.392	32.065	19.410	26.392	32.065	19.410	31.129	40.924	34.146
		2	7.957	16.957	5.909	7.957	16.957	5.909	12.195	30.908	14.357
	TRAILING	1	22.547	25.020	15.108	22.547	25.020	15.108	27.989	32.611	23.041
		2	6.733	11.367	4.708	6.733	11.367	4.700	10.945	15.457	9.712

SPEED = 65 MPH., CONSIST NO. 1

DIRECTION	TRUCK	AXLE	ABSOLUTE AVERAGE ANGLE (MIN) BARBER	LIST	SCHEFFEL	ALGEBRAIC AVERAGE ANGLE (MIN) BARBER	LIST	SCHEFFEL	MAXIMUM ANGLE (MINS) BARBER	LIST	SCHEFFEL
WEST	LEADING	1	19.956	2.767	5.908	19.054	2.767	6.157	29.269	4.871	11.657
		2	6.411	6.067	2.673	6.411	4.067	2.673	6.350	7.559	6.774
	TRAILING	1	20.597	5.250	3.009	20.597	5.250	2.679	26.402	7.158	5.617
		2	6.940	5.044	3.152	6.040	5.044	2.014	8.960	8.487	6.416
EAST	LEADING	1	19.876	8.548	14.077	19.876	8.548	14.077	24.678	5.821	19.606
		2	3.756	6.675	9.231	3.756	6.675	9.231	7.100	8.096	10.585
	TRAILING	1	17.798	10.450	9.002	17.798	10.450	4.892	27.565	13.131	14.696
		2	2.186	6.751	5.529	2.068	6.751	5.525	4.404	6.784	6.576

SPEED = 65 MPH., CONSIST NO. 2

DIRECTION	TRUCK	AXLE	ABSOLUTE AVERAGE ANGLE (MIN) BARBER	SCALE	SWING	ALGEBRAIC AVERAGE ANGLE (MIN) BARBER	SCALE	SWING	MAXIMUM ANGLE (MINS) BARBER	SCALE	SWING
WEST	LEADING	1	28.570	7.040	25.400	20.570	7.040	25.400	35.057	5.897	28.671
		2	12.736	8.986	5.191	12.736	6.986	5.191	26.296	10.101	10.336
	TRAILING	1	25.209	9.206	18.759	25.205	6.206	18.759	27.172	9.127	[illegible]
		2	4.726	9.160	3.177	8.726	9.160	3.177	13.623	10.860	4.716
EAST	LEADING	1	25.956	11.076	21.736	25.556	11.076	21.736	29.091	17.256	13.315
		2	6.095	13.256	5.953	6.095	13.256	5.953	5.595	16.515	7.606
	TRAILING	1	22.401	14.228	22.067	22.401	14.228	22.067	20.174	19.805	5.287
		2	5.064	6.770	2.434	5.064	6.770	2.430	7.830	8.990	3.563

SPEED = 65 MPH., CONSIST NO. 3

DIRECTION	TRUCK	AXLE	ABSOLUTE AVERAGE ANGLE (MIN) BARBER	C-PEP	STUCKI	ALGEBRAIC AVERAGE ANGLE (MIN) BARBER	C-PEP	STUCKI	MAXIMUM ANGLE (MINS) BARBER	C-PEP	STUCKI
WEST	LEADING	1	28.365	24.231	20.520	28.365	24.231	20.520	30.876	[illegible]	34.290
		2	12.530	11.170	10.562	12.530	11.120	10.502	19.109	11.032	16.477
	TRAILING	1	25.079	25.617	23.000	25.074	25.617	23.000	29.173	27.036	20.826
		2	7.379	9.901	4.251	7.676	9.901	4.251	8.077	10.376	4.277
EAST	LEADING	1	20.837	21.186	21.460	20.833	21.180	21.460	22.086	24.617	13.586
		2	3.731	7.241	5.629	3.806	7.261	5.624	5.586	10.969	7.105
	TRAILING	1	18.736	22.038	20.265	18.736	22.039	20.265	21.027	29.290	12.140
		2	3.623	5.179	1.132	3.623	5.179	0.716	4.507	4.267	4.466

SPEED = 65 MPH., CONSIST NO. 4

DIRECTION	TRUCK	AXLE	ABSOLUTE AVERAGE ANGLE (MIN) BARBER	RIDE	NEO-AAR	ALGEBRAIC AVERAGE ANGLE (MIN) BARBER	RIDE	NEO-AAR	MAXIMUM ANGLE (MINS) BARBER	RIDE	NEO-AAR
WEST	LEADING	1	29.465	26.270	19.001	29.445	26.270	19.001	31.697	28.833	13.597
		2	16.291	13.376	6.439	16.291	13.376	6.439	17.013	19.026	8.844
	TRAILING	1	25.281	30.715	19.065	25.281	30.715	19.065	29.020	32.325	11.656
		2	8.565	16.015	5.706	8.565	16.015	5.706	17.156	16.590	7.602
EAST	LEADING	1	15.411	18.766	13.136	16.411	18.769	13.136	26.612	20.948	16.526
		2	1.708	2.661	3.122	-0.708	2.661	-3.122	-1.594	6.912	-6.333
	TRAILING	1	15.766	15.303	11.363	15.766	15.301	11.363	21.017	17.602	12.665
		2	6.400	2.198	2.249	-0.250	2.190	-2.156	-2.100	5.633	-6.094

SPEED = 20 MPH., CONSIST NO. 1 ALL DIRECTIONS

TRUCK	AXLE	ABSOLUTE AVERAGE ANGLE (MIN)			ALGEBRAIC AVERAGE ANGLE (MIN)			MAXIMUM ANGLE (MIN)		
		BARBER	LIST	SCHEFFEL	BARBER	LIST	SCHEFFEL	BARBER	LIST	SCHEFFEL
LEADING	1	20.125	10.797	13.307	20.125	10.797	13.307	37.720	[illegible]	[illegible]
	2	7.011	9.109	11.986	7.011	9.134	11.986	16.906	[illegible]	[illegible]
TRAILING	1	21.766	10.029	11.294	21.766	10.029	11.294	30.506	[illegible]	[illegible]
	2	5.799	9.220	9.965	5.710	9.223	9.965	5.064	11.297	[illegible]

SPEED = 20 MPH., CONSIST NO. 2 ALL DIRECTIONS

TRUCK	AXLE	ABSOLUTE AVERAGE ANGLE (MIN)			ALGEBRAIC AVERAGE ANGLE (MIN)			MAXIMUM ANGLE (MIN)		
		BARBER	SCALE	SWING	BARBER	SCALE	SWING	BARBER	SCALE	SWING
LEADING	1	31.004	12.640	27.110	31.004	12.640	27.110	[illegible]	[illegible]	[illegible]
	2	13.139	11.804	9.632	13.139	11.804	9.632	[illegible]	[illegible]	[illegible]
TRAILING	1	26.324	13.259	23.703	26.324	13.259	23.703	31.172	[illegible]	[illegible]
	2	7.825	10.267	5.012	7.825	10.267	5.012	11.219	[illegible]	[illegible]

SPEED = 20 MPH., CONSIST NO. 3 ALL DIRECTIONS

TRUCK	AXLE	ABSOLUTE AVERAGE ANGLE (MIN)			ALGEBRAIC AVERAGE ANGLE (MIN)			MAXIMUM ANGLE (MIN)		
		BARBER	C-PEP	STUCKI	BARBER	C-PEP	STUCKI	BARBER	C-PEP	STUCKI
LEADING	1	27.929	27.037	20.397	27.929	27.037	20.397	35.107	9.066	[illegible]
	2	9.950	10.049	10.095	9.950	10.049	10.095	17.803	14.311	[illegible]
TRAILING	1	24.249	20.652	24.659	24.249	20.652	24.659	39.029	21.950	[illegible]
	2	5.061	8.170	5.061	5.061	8.170	5.061	19.919	16.730	[illegible]

SPEED = 20 MPH., CONSIST NO. 4 ALL DIRECTIONS

TRUCK	AXLE	ABSOLUTE AVERAGE ANGLE (MIN)			ALGEBRAIC AVERAGE ANGLE (MIN)			MAXIMUM ANGLE (MIN)		
		BARBER	RIDE	NEO-ARM	BARBER	RIDE	NEO-ARM	BARBER	RIDE	NEO-ARM
LEADING	1	20.037	29.001	17.900	20.037	29.001	17.930	35.006	36.089	[illegible]
	2	10.101	13.672	3.125	10.101	13.672	2.601	20.003	20.269	7.031
TRAILING	1	26.606	20.230	15.306	26.606	20.230	15.306	33.043	37.651	27.466
	2	8.398	12.107	3.067	8.050	12.107	2.067	16.170	16.379	7.576

SPEED = 37 MPH., CONSIST NO. 1 ALL DIRECTIONS

TRUCK	AXLE	ABSOLUTE AVERAGE ANGLE (MIN)			ALGEBRAIC AVERAGE ANGLE (MIN)			MAXIMUM ANGLE (MIN)		
		BARBER	LIST	SCHEFFEL	BARBER	LIST	SCHEFFEL	BARBER	LIST	SCHEFFEL
LEADING	1	20.201	8.531	13.053	20.201	8.531	13.053	39.523	17.876	20.815
	2	8.003	8.024	8.305	8.003	8.024	5.305	15.637	11.900	17.030
TRAILING	1	23.353	10.336	10.110	23.353	10.336	10.110	25.006	14.402	26.560
	2	6.560	7.618	7.072	6.560	7.618	7.072	16.726	11.893	12.545

SPEED = 37 MPH., CONSIST NO. 2 ALL DIRECTIONS

TRUCK	AXLE	ABSOLUTE AVERAGE ANGLE (MIN)			ALGEBRAIC AVERAGE ANGLE (MIN)			MAXIMUM ANGLE (MIN)		
		BARBER	SCALE	SWING	BARBER	SCALE	SWING	BARBER	SCALE	SWING
LEADING	1	30.200	12.405	26.212	30.200	12.405	26.212	37.200	18.715	36.300
	2	14.390	12.069	10.015	14.390	12.360	10.015	20.105	20.776	19.405
TRAILING	1	27.370	12.710	23.150	27.370	12.710	23.150	31.030	21.139	27.913
	2	10.314	10.955	6.390	10.314	10.955	6.390	12.900	12.776	6.250

SPEED = 37 MPH., CONSIST NO. 3 ALL DIRECTIONS

TRUCK	AXLE	ABSOLUTE AVERAGE ANGLE (MIN)			ALGEBRAIC AVERAGE ANGLE (MIN)			MAXIMUM ANGLE (MIN)		
		BARBER	C-PEP	STUCKI	BARBER	C-PEP	STUCKI	BARBER	C-PEP	STUCKI
LEADING	1	27.310	20.150	27.209	27.310	20.150	27.209	33.259	31.692	32.510
	2	9.724	9.988	9.770	9.724	9.988	9.770	20.423	10.330	10.030
TRAILING	1	23.267	25.020	23.070	23.267	25.020	23.070	38.500	29.000	27.100
	2	6.204	7.033	6.973	6.204	7.033	6.973	5.728	11.667	9.650

SPEED = 37 MPH., CONSIST NO. 4 ALL DIRECTIONS

TRUCK	AXLE	ABSOLUTE AVERAGE ANGLE (MIN)			ALGEBRAIC AVERAGE ANGLE (MIN)			MAXIMUM ANGLE (MIN)		
		BARBER	RIDE	NEO-ARM	BARBER	RIDE	NEO-ARM	BARBER	RIDE	NEO-ARM
LEADING	1	30.462	33.317	22.295	30.462	33.317	22.295	37.500	66.929	32.120
	2	12.929	17.012	7.309	12.929	17.012	7.309	22.140	26.589	13.049
TRAILING	1	29.142	30.051	22.229	29.142	30.051	22.229	31.317	61.026	32.107
	2	7.725	15.309	7.154	7.725	15.309	7.154	11.111	[illegible]	10.219

SPEED = 65 MPH., CONSIST NO. 1 ALL DIRECTIONS

TRUCK	AXLE	ABSOLUTE AVERAGE ANGLE (MIN)			ALGEBRAIC AVERAGE ANGLE (MIN)			MAXIMUM ANGLE (MIN)		
		BARBER	LIST	SCHEFFEL	BARBER	LIST	SCHEFFEL	BARBER	LIST	SCHEFFEL
LEADING	1	19.916	6.696	9.737	19.916	6.696	6.117	29.205	5.621	[illegible]
	2	6.003	5.301	5.992	6.003	5.301	5.992	6.350	8.050	[illegible]
TRAILING	1	19.100	7.058	6.606	19.100	7.058	6.091	29.462	13.111	[illegible]
	2	5.113	6.301	4.339	5.094	6.301	6.172	5.300	5.796	[illegible]

SPEED = 65 MPH., CONSIST NO. 2 ALL DIRECTIONS

TRUCK	AXLE	ABSOLUTE AVERAGE ANGLE (MIN)			ALGEBRAIC AVERAGE ANGLE (MIN)			MAXIMUM ANGLE (MIN)		
		BARBER	SCALE	SWING	BARBER	SCALE	SWING	BARBER	SCALE	SWING
LEADING	1	27.203	9.507	23.500	27.203	9.507	23.500	30.657	17.254	[illegible]
	2	9.615	10.120	5.572	9.615	10.120	5.572	29.206	15.915	[illegible]
TRAILING	1	23.063	10.217	20.003	23.063	10.217	26.003	20.176	19.006	[illegible]
	2	7.206	7.064	2.099	7.206	7.064	2.099	17.027	10.676	[illegible]

SPEED = 65 MPH., CONSIST NO. 3 ALL DIRECTIONS

TRUCK	AXLE	ABSOLUTE AVERAGE ANGLE (MIN)			ALGEBRAIC AVERAGE ANGLE (MIN)			MAXIMUM ANGLE (MIN)		
		BARBER	C-PEP	STUCKI	BARBER	C-PEP	STUCKI	BARBER	C-PEP	STUCKI
LEADING	1	26.509	24.700	26.000	26.505	24.700	[illegible]	36.476	30.299	[illegible]
	2	8.235	9.196	7.990	8.112	9.196	[illegible]	19.709	11.595	[illegible]
TRAILING	1	21.300	24.220	22.001	21.300	24.220	22.191	[illegible]	[illegible]	[illegible]
	2	5.701	7.540	6.601	5.701	7.543	[illegible]	[illegible]	10.376	[illegible]

SPEED = 65 MPH., CONSIST NO. 4 ALL DIRECTIONS

TRUCK	AXLE	ABSOLUTE AVERAGE ANGLE (MIN)			ALGEBRAIC AVERAGE ANGLE (MIN)			MAXIMUM ANGLE (MIN)		
		BARBER	RIDE	NEO-ARM	BARBER	RIDE	NEO-ARM	BARBER	RIDE	NEO-ARM
LEADING	1	22.928	22.508	10.067	22.920	22.104	[illegible]	[illegible]	[illegible]	[illegible]
	2	7.700	8.819	6.770	6.702	8.214	1.956	[illegible]	17.660	[illegible]
TRAILING	1	20.526	23.056	15.600	20.526	23.056	[illegible]	[illegible]	[illegible]	[illegible]
	2	6.766	8.551	6.000	6.100	8.551	1.852	19.216	16.566	[illegible]

TABLE 9 - ANGLE-OF-ATTACK RESULTS TABULATED BY LEADING AND TRAILING AXLES FOR ALL DIRECTIONS

SPEED = 25 MPH, ALL GAUGES, ALL DIRECTIONS
NORMALIZED ALGEBRAIC AVERAGE (KIPS)

TRUCK	AXLE	BARBER	LIST	SCHEFFEL	SCALE	SWING	C-PEP	STUCKI	RIDE	NEW AAR
LEADING	1	3.11	2.23	2.08	3.15	4.99	3.08	3.16	2.91	5.74
TRAILING	1	2.93	1.64	1.55	1.26	5.47	3.08	3.01	2.82	7.66

SPEED = 37 MPH, ALL GAUGES, ALL DIRECTIONS
NORMALIZED ALGEBRAIC AVERAGE (KIPS)

TRUCK	AXLE	BARBER	LIST	SCHEFFEL	SCALE	SWING	C-PEP	STUCKI	RIDE	NEW AAR
LEADING	1	4.15	3.02	3.48	4.75	5.82	3.72	4.13	3.77	7.25
TRAILING	1	4.26	2.92	3.07	3.60	7.08	4.18	4.20	3.72	7.25

SPEED = 45 MPH, ALL GAUGES, ALL DIRECTIONS
NORMALIZED ALGEBRAIC AVERAGE (KIPS)

TRUCK	AXLE	BARBER	LIST	SCHEFFEL	SCALE	SWING	C-PEP	STUCKI	RIDE	NEW AAR
LEADING	1	5.93	3.65	3.96	5.66 0.83	6.85	4.87	5.30	5.35	6.56
TRAILING	1	5.66	2.79	2.81	3.24	7.42	5.41	5.37	4.76	6.29

TABLE 10- NORMALIZED LATERAL FORCES FOR THE OUTER
LEADING WHEELS OF ALL TEST TRUCKS

SPEED = 25 MPH., ALL DIRECTIONS
NORMALIZED ABSOLUTE AVERAGE ANGLES (MINS)

TRUCK	AXLE	BARBER	LIST	SCHEFFEL	SCALE	SWING	C-PEP	STUCKI	WIDE	ALB-AAN
LEADING	1	28.574	11.805	14.558	11.428	24.516	28.480	29.053	25.778	17.868
	2	10.196	10.424	14.868	9.160	7.319	10.729	11.418	13.517	3.135
TRAILING	1	24.695	10.841	11.746	12.438	22.311	27.147	25.117	28.504	16.802
	2	6.172	9.108	10.910	8.361	4.081	8.870	6.370	12.781	3.683

SPEED = 25 MPH., ALL DIRECTIONS
NORMALIZED ALGEBRAIC AVERAGE ANGLES (MINS)

TRUCK	AXLE	BARBER	LIST	SCHEFFEL	SCALE	SWING	C-PEP	STUCKI	WIDE	ALB-AAN
LEADING	1	28.574	11.805	14.558	11.428	24.516	28.480	29.053	25.778	17.068
	2	10.196	10.424	14.968	9.160	7.319	10.729	11.418	13.517	2.726
TRAILING	1	24.695	10.841	11.746	12.438	22.311	27.147	25.117	28.504	14.896
	2	6.172	9.108	10.910	8.361	4.081	8.870	6.370	12.781	1.136

SPEED = 37 MPH., ALL DIRECTIONS
NORMALIZED ABSOLUTE AVERAGE ANGLES (MINS)

TRUCK	AXLE	BARBER	LIST	SCHEFFEL	SCALE	SWING	C-PEP	STUCKI	WIDE	ALB-AAN
LEADING	1	28.565	9.381	15.103	11.756	24.721	27.381	28.502	21.242	20.637
	2	11.382	10.281	11.974	9.542	7.918	11.691	11.437	16.277	6.696
TRAILING	1	24.785	10.967	10.738	11.506	20.958	26.655	25.221	30.413	21.914
	2	7.722	8.967	9.268	8.123	3.288	9.626	6.111	15.359	7.151

SPEED = 37 MPH., ALL DIRECTIONS
NORMALIZED ALGEBRAIC AVERAGE ANGLES (MINS)

TRUCK	AXLE	BARBER	LIST	SCHEFFEL	SCALE	SWING	C-PEP	STUCKI	WIDE	ALB-AAN
LEADING	1	28.565	9.381	15.103	11.756	24.721	27.381	28.502	21.242	20.637
	2	11.382	10.281	11.974	9.542	7.918	11.691	11.437	16.277	6.696
TRAILING	1	24.785	10.967	10.738	11.806	20.958	26.655	25.221	30.413	21.914
	2	7.722	8.967	9.268	8.123	3.288	9.626	6.111	15.356	7.151

SPEED = 65 MPH., ALL DIRECTIONS
NORMALIZED ABSOLUTE AVERAGE ANGLES (MINS)

TRUCK	AXLE	BARBER	LIST	SCHEFFEL	SCALE	SWING	C-PEP	STUCKI	WIDE	ALB-AAN
LEADING	1	23.676	9.581	11.577	8.256	20.467	23.781	24.056	23.243	16.594
	2	7.378	9.687	10.785	7.931	4.386	8.238	7.164	7.665	4.936
TRAILING	1	21.368	8.738	7.397	9.157	18.044	23.629	21.578	24.062	17.131
	2	5.816	10.561	7.278	5.707	2.845	6.898	4.292	5.360	4.382

SPEED = 65 MPH., ALL DIRECTIONS
NORMALIZED ALGEBRAIC AVERAGE ANGLES (MINS)

TRUCK	AXLE	BARBER	LIST	SCHEFFEL	SCALE	SWING	C-PEP	STUCKI	WIDE	ALB-AAN
LEADING	1	23.676	9.581	10.839	8.256	20.467	23.781	24.056	23.243	16.556
	2	7.181	9.323	10.358	7.632	4.282	8.848	6.999	8.389	1.732
TRAILING	1	21.368	8.738	6.788	9.157	18.044	23.629	21.538	24.002	16.131
	2	5.047	10.418	6.894	5.522	1.978	6.675	3.969	10.489	2.163

TABLE 11 - NORMALIZED ANGLE-OF-ATTACK FOR ALL TEST TRUCKS

Consist No.	Truck	Misalignment Angle (Min.)
1	Barber S-2 with 'A' Wheel Profile	11.4
	DR-1	5.5
	Barber Scheffel	4.1
2	Barber S-2 with 'A' Wheel Profile	13.5
	Devine-Scales	4.7
	Swing Motion	9.8
3	Barber S-2 with 'A' Wheel Profile	14.6
	Barber S-2 with C-PEP	13.5
	Barber S-2 with Stucki C.C.S.B.	14.2
4	Barber S-2 with 'A' Wheel Profile	18.7
	Ride Control	18.8
	Barber S-2 with AAR Profile Wheels	16.3

TABLE 12 - MISALIGNMENT ANGLES

Truck	Sum of the Lateral Forces (Leading + Trailing Axles) of Test Truck / Sum of the Lateral Forces (Leading + Trailing Axles) of the Reference* Truck		
	25 mph	37 mph	45 mph
DR-1	0.26	0.41	0.60
Barber-Scheffel	0.31	0.60	0.70
Devine-Scale	0.59	0.66	0.73
Swing Motion	1.2	0.92	0.85
Ride Control	1.6	1.38	1.01
Barber S-2 with C-PEP	1.17	1.08	0.92
Barber S-2 with Stucki C.C.S.B.	1.17	1.12	0.94
Barber S-2 with AAR Profile Wheels	2.5	2.11	1.01

* The reference truck is the Barber S-2 with 'A' profile wheels.

TABLE 13: RATIO OF SUM OF THE LATERAL FORCES OF TEST TRUCKS TO THAT OF THE REFERENCE TRUCK

CONSIST	TRUCK	25 MPH		37 MPH		45 MPH	
		α DEGREE	$\frac{\alpha\ \text{(TEST TRUCK)}}{\alpha\ \text{(REFERENCE TRUCK)}}$	α DEGREE	$\frac{\alpha\ \text{(TEST TRUCK)}}{\alpha\ \text{(REFERENCE TRUCK)}}$	α DEGREE	$\frac{\alpha\ \text{(TEST TRUCK)}}{\alpha\ \text{(REFERENCE TRUCK)}}$
I	Barber S-2 (Reference Truck)	0.417	1.00	0.413	1.00	0.326	1.00
	DR-1	0.176	0.42	0.157	0.38	0.105	0.32
	Barber-Scheffel	0.205	0.49	0.200	0.48	0.126	0.39
II	Barber S-2 (Reference Truck)	0.483	1.00	0.481	1.00	0.426	1.00
	Devine-Scales	0.216	0.45	0.210	0.44	0.164	0.39
	Swing Motion	0.424	0.88	0.411	0.86	0.370	0.87
III	Barber S-2 (Reference Truck)	0.435	1.00	0.421	1.00	0.388	1.00
	Barber S-2 with C-PEP	0.454	1.04	0.427	1.01	0.408	1.05
	Barber S-2 with Stucki C.C.S.B.	0.442	1.02	0.424	1.01	0.392	1.01
IV	Barber S-2 (Reference Truck)	0.443	1.00	0.463	1.00	0.362	1.00
	Ride Control	0.484	1.09	0.535	1.15	0.380	1.05
	Barber S-2 with AAR Profile Wheels	0.310	0.70	0.371	0.80	0.263	0.73

TABLE 14: ANGLE-OF-ATTACK VALUES OF ALL TEST TRUCKS

CONSIST	TRUCK	25 MPH		37 MPH		45 MPH	
		$Y\alpha^*$ LB. DEGREE	$\frac{Y\alpha\ (\text{TEST TRUCK})}{Y\alpha\ (\text{REFERENCE TRUCK})}$	$Y\alpha$ LB. DEGREE	$\frac{Y\alpha\ (\text{TEST TRUCK})}{Y\alpha\ (\text{REFERENCE TRUCK})}$	$Y\alpha$ LB. DEGREE	$\frac{Y\alpha\ (\text{TEST TRUCK})}{Y\alpha\ (\text{REFERENCE TRUCK})}$
I	Barber S-2 (Reference Truck)	1458	1.00	2090	1.00	2055	1.00
	DR-1	575	0.40	543	0.26	318	0.15
	Barber-Scheffel	591	0.40	698	0.33	490	0.24
II	Barber S-2 (Reference Truck)	1464	1.00	1688	1.00	2348	1.00
	Devine-Scale	641	0.44	634	0.38	638	0.26
	Swing Motion	2712	1.85	2427	1.40	2763	1.17
III	Barber S-2 (Reference Truck)	2090	1.00	2338	1.00	2813	1.00
	Barber S-2 with C-PEP	2131	1.02	1904	0.81	2280	0.81
	Barber S-2 with Stucki C.S.B.	1960	0.94	2134	0.91	2198	0.78
IV	Barber S-2 (Reference Truck)	770	1.00	1955	1.00	1973	1.00
	Ride Control	815	1.06	1732	0.91	1560	0.79
	Barber S-2 with AAR Profile Wheels	881	1.15	1909	0.97	1326	0.66

Y is the lateral force of the outer leading wheel.

α is the angle-of-attack of the outer leading wheel

TABLE 15: THE WEAR INDEX OF THE TEST TRUCKS

MILEAGE	SPEED mph	SURFACE DEFECTS				CROSS-LEVEL (in 11 ft.)				OVER GAUGE (ft./occ.)		
		¼ to ½	½ to ¾	¾ to 1	1 -	¼ to ½	½ to ¾	¾ to 1	1 -	½ to ¾	¾ to 1	1 -
158.00 - 158.25	45	8	0	0	0	4	0	0	0	0/0	0/0	0/0
158.25 - 158.50	46	16	0	0	0	1	0	0	0	0/0	0/0	0/0
158.50 - 158.75	47	3	0	0	0	1	0	0	0	0/0	0/0	0/0
158.75 - 159.00	46	7	1	0	0	4	1	0	0	0/0	0/0	0/0
159.00 - 159.25	45	1	0	0	0	1	0	0	0	0/0	0/0	0/0
159.25 - 159.50	44	3	0	0	0	3	0	0	0	0/0	0/0	0/0
159.50 - 159.75	43	7	0	0	0	3	0	0	0	0/0	0/0	0/0
159.75 - 160.00	43	1	0	0	0	1	0	0	0	0/0	0/0	0/0

TABLE 16: TRACK RECORDER CAR SUMMARY REPORT IN TEST ZONE BETWEEN MILEAGE 160-152 ON THE BROOKS SUBDIVISION - TAKEN ON JUNE 23rd, 1978

TEST CAR NOS.	CP 351668	CP 349157	CP 349537
Test Car Description & Type	100-Ton Bathtub Coal Car	100-Ton Bathtub Coal Car	100-Ton Bathtub Coal Car
Year Built	1-76	5-76	5-76
Load Limits	208,900 lbs.	209,100 lbs.	209,100 lbs.
Light Weight	54,100 lbs.	53,900 lbs.	53,900 lbs.
Scaled Light Weight	56,600 lbs.	55,800 lbs.	57,700 lbs.
Length over End Sills	55'11½"	55'11½"	55'11½"
Internal Length	48'	48'	48'
Truck Centres	45'	45'	45'
Height of Centre of Gravity Above Rails (Light)	49"	49"	49"

TABLE 17: TEST CAR DATA FOR THE HIGH SPEED STABILITY TESTS

TRUCK	BARBER S-2 (REFERENCE TRUCK)	DR-I RADIAL RETROFITTED TO BARBER S-2 TRUCK	BARBER-SCHEFFEL TRUCK	DEVINE-SCALE TRUCK	SWING MOTION TRUCK	RIDE CONTROL TRUCK
Capacity	100-ton	100-ton	100-ton	100-ton	100-ton	100-ton
Wheels 36" Diameter	'A' Profile	'A' Profile	'A' Profile	'A' Profile	'A' Profile	'A' Profile
Axle Type	Standard AAR	Standard AAR	Standard AAR	Standard AAR	Standard AAR	Standard AAR
Roller Bearings	6½" x 12"	6½" x 12"	6½" x 12"	6½" x 12"	6½" x 12"	6½" x 12"
Wheel Base	70"	70"	75"	70"	72"	70"
Weight - lbs./Carset	20,400	21,600	22,200	24,800	N.A.	20,500
Bolster Centre Plate Diameter	14"	14"	16"*	14"	16"*	14"
Springs, Type and No./Nest	Special two rate spring, 7 Main springs, 7 Top springs held in cups in series with main springs 2 Outer Side Springs 3 Inner Side Springs	Tested with 1. Conventional D-5 springs. 2. Special two rate springs as on Barber S-2 Reference Truck	6, D-5 outer 7, D-5 inner 2, B-355 2, B-356	Each Primary suspension consists of 4, D-5 outer 4, D-6 inner 2, B-331	6, D-7 Outer 6, D-6 Inner	D-7 spring 9 Outer 5 Inner

* Special adaptor rings were welded to the car body centre plate to fit the 16" diameter centre plates on the truck.

TABLE 18: TRUCK DATA FOR HIGH SPEED STABILITY TESTS

TEST NO. AND DATE	TRUCK TYPE	45 mph	50 mph	55 mph	60 mph	65 mph	70 mph	75 mph
1 June 22	Barber S-2 (Reference Car)	-	-	-	Intermittent Hunting(27%)	Intermittent Hunting(62%)	Intermittent Hunting(70%)	Intermittent Hunting(85%)
	DR-1 Radial (Retrofit to Barber S-2 with Conventional Springs)	-	-	-	Intermittent Hunting(12%)	Intermittent Hunting(20%)	Intermittent Hunting(20%)	Intermittent Hunting(30%)
	Barber-Scheffel	-	-	-	-	-	-	-
1 (Repeated) June 23	Barber S-2 (Reference Car)	-	-	-	Intermittent Hunting(28%)	Intermittent Hunting(66%)	Hunting (100%)	Hunting (100%)
	DR-1 Radial (Retrofit to Barber S-2 with two rate springs)	-	-	-	-	-	Intermittent Hunting 11%	Intermittent Hunting 20%
	Barber-Scheffel	-	-	-	-	-	-	-
2 June 24	Barber S-2 (Reference Car)	-	-	-	Intermittent Hunting(35%)	Intermittent Hunting(32%)	Intermittent Hunting(62%)	Intermittent Hunting(59%)
	Devine-Scale	-	-	-	-	-	Intermittent Hunting(39%)	Intermittent Hunting(40%)
	Swing Motion	-	-	-	-	-	-	-
3 June 27	Barber S-2 (Reference Car)	-	-	-	Intermittent Hunting (7%)	Intermittent Hunting(29%)	Intermittent Hunting(45%)	Intermittent Hunting(50%)
	Barber S-2 with C-PEP	-	-	-	-	-	-	-
	Barber S-2 with Stucki C.C.S.B.	-	-	-	-	-	-	-
4 June 28	Barber S-2 (Reference Car)	-	-	-	-	Intermittent Hunting 14%	Intermittent Hunting 39%	Intermittent Hunting 82%
	Barber S-S with AAR Wheels						Intermittent Hunting(18%)	Intermittent Hunting(32%)
	Ride Control					Intermittent Hunting(12%)	Intermittent Hunting(32%)	Intermittent Hunting(74%)

- Denotes trucks were stable.

Figures in parenthesis denotes % time test trucks were hunting in the two mile test zone as observed from the longitudinal accelerometer output.
All trucks were tested with 'A' profile wheels except Test 4 where the Barber S-2 Truck was tested with AAR wheels.

TABLE 19: TEST TRUCK PERFORMANCE DURING HIGH SPEED STABILITY TESTS

TEST NO.	DATE	TRUCK TYPE	45 mph	50 mph	55 mph	60 mph	65 mph	70 mph	75 mph	REMARKS
1	June 22	Barber S-2 (Reference)	.0252	.03	.0423	.0578	.1548	.1691	.1746	DR-1 radial retrofitted to Barber S-2 truck with conventional D-5 springs.
		DR-1 Radial	.0260	.0401	.0520	.0676	.0884	.1052	-	
		Barber-Scheffel	.0266	.0309	.0368	.0452	.0543	.0657	.0823	
1 (Repeated)	June 23	Barber S-2 (Reference)	.0235	.0352	.0475	.0915	.1667	.1986	.2104	DR-1 radial retrofitted to Barber S-2 truck with two rate springs
		DR-1 Radial	.0202	.0361	.0366	.0495	.0664	.0934	.1083	
		Barber-Scheffel	.0247	.0304	.0368	.0450	.0524	.0610	.0698	
2	June 24	Barber S-2 (Reference)	.0230	.0377	.0504	.1395	.1055	.1525	.1513	
		Devine-Scales	.0225	.032	.043	.0586	.0799	.1134	.1189	
		Swing Motion	.0269	.0245	.0307	.0391	.0495	.0625	.0738	
3	June 27	Barber S-2 (Reference)	.0239	.0304	.0421	.0641	.0908	.1272	.1451	
		Barber S-2 with Stucki C.C.S.B.	.0145	.0198	.0201	.0233	.0294	.0317	.0301	
		Barber S-2 with C-PEP	.025	.030	.0346	.0407	.0479	.0568	.0532	
4	June 28	Barber S-2 (Reference)	.0236	.0307	.0387	.0554	.0980	.1463	.1808	
		Barber S-2 with AAR Wheels	.0235	.0301	.0481	.0508	.0809	.0903	.1236	
		Ride Control	.0309	.0365	.0465	.0596	.0758	.1058	.1649	

FIGURE 20: R.M.S. 'g' VALUES (FREQUENCY RANGE 1-5 Hz) FOR LATERAL ACCELEROMETER ON THE AXLE BEARING END CAP

TEST NO.	DATE	TRUCK TYPE	45 mph	50 mph	55 mph	60 mph	65 mph	70 mph	75 mph	REMARKS
1	June 22	Barber S-2 (Reference)	.0267	.0320	.0414	.0607	.1702	.1827	.1881	DR-1 radial retrofitted to Barber S-2 truck with conventional D-5 springs.
		DR-1 Radial	.0427	.0598	.0801	.0982	.1212	.1295	.1436	
		Barber-Scheffel	.0327	.0337	.0388	.0461	.0511	.0586	.0718	
1 (Repeated)	June 23	Barber S-2 (Reference)	.0235	.0332	.0492	.0841	.1919	.1989	.2040	DR-1 radial retrofitted to Barber S-2 truck with two rate springs
		DR-1 Radial	.0317	.0363	.0440	.0619	.0850	.1050	.1118	
		Barber-Scheffel	.0303	.0370	.0411	.0495	.0558	.0575	.0683	
2	June 24	Barber S-2 (Reference)	.0262	.0397	.0503	.1398	.1242	.1555	.1530	
		Devine-Scales	.0278	.0378	.0445	.0621	.0825	.1308	.1375	
		Swing Motion	.0286	.0321	.0355	.0424	.0536	.0697	.0794	
3	June 27	Barber S-2 (Reference)	.0237	.0301	.0396	.0608	.0962	.1292	.1568	
		Barber S-2 with Stucki C.C.S.B.	.0287	.0355	.0418	.0459	.0489	.0535	.0558	
		Barber S-2 with C-PEP	.0279	.0338	.0413	.0491	.0640	.0675	.0675	
4	June 28	Barber S-2 (Reference)	.027	.0286	.0362	.0576	.0965	.1327	.1922	
		Barber S-2 with AAR Wheels	.0253	.0294	.0365	.0504	.0778	.100	.1306	
		Ride Control	.0356	.0408	.0530	.0779	.0865	.1365	.2093	

FIGURE 21: R.M.S. 'g' (FREQUENCY RANGE 1-5 Hz) FOR LATERAL ACCELEROMETER ON THE CAR BODY NEAR THE CENTRE PLATE

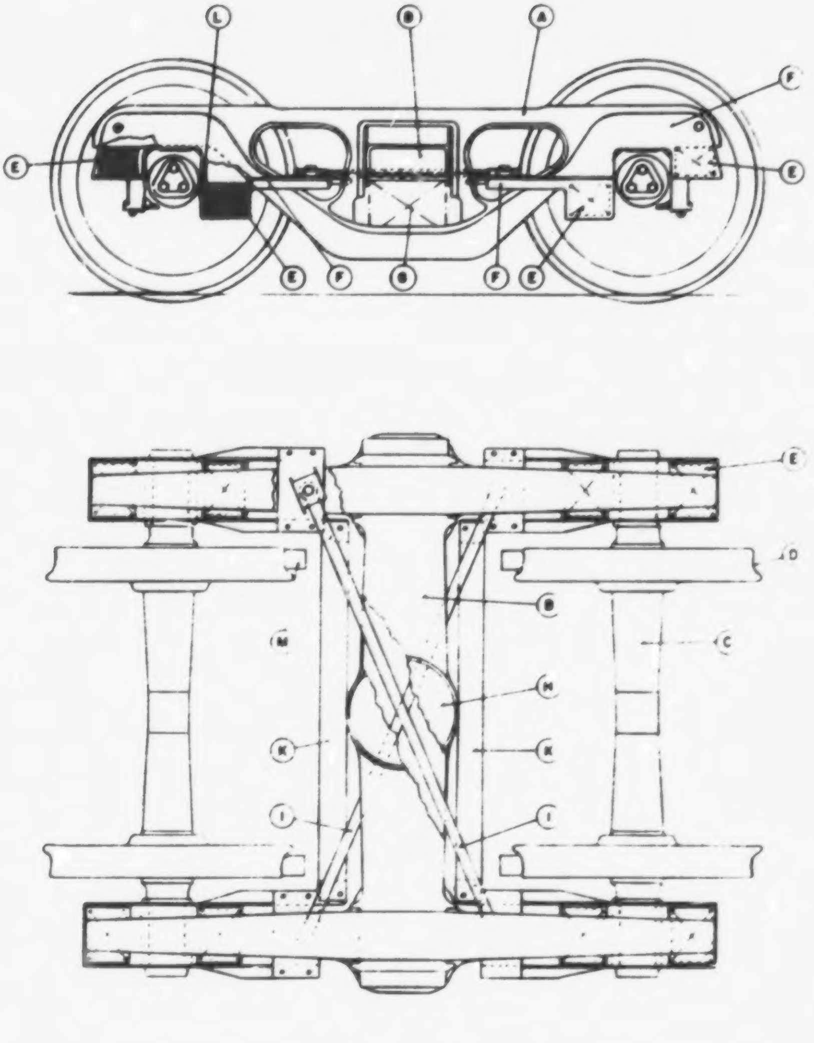

A : load carrying side frames;
B : bolster,
C : wheelset,
D : profiled wheel tread;
E : rubber sandwiches,
F : axle box adaptor;
G : bolster springs,
H : centre pivot,
I : cross-anchor,
K : stay,
L : longitudinal clearance between adaptor and side frame,
M : single brakes.

Figure 1 - BARBER-SCHEFFEL TRUCK

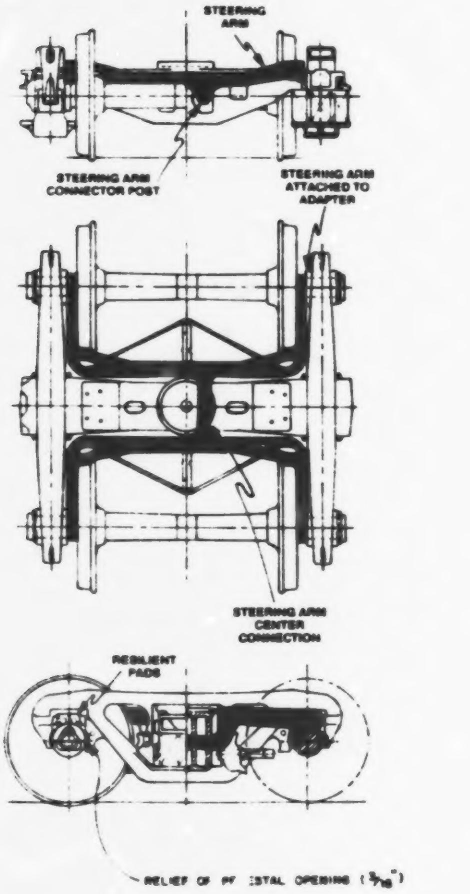
STEERING ARM
STEERING ARM CONNECTOR POST
STEERING ARM ATTACHED TO ADAPTER
STEERING ARM CENTER CONNECTION
RESILIENT PADS
RELIEF OF PEDESTAL OPENING ($\frac{3}{16}$")

Figure 2 - GENERAL ARRANGEMENT OF A TRUCK EQUIPPED WITH DR-1 STEERING ASSEMBLY

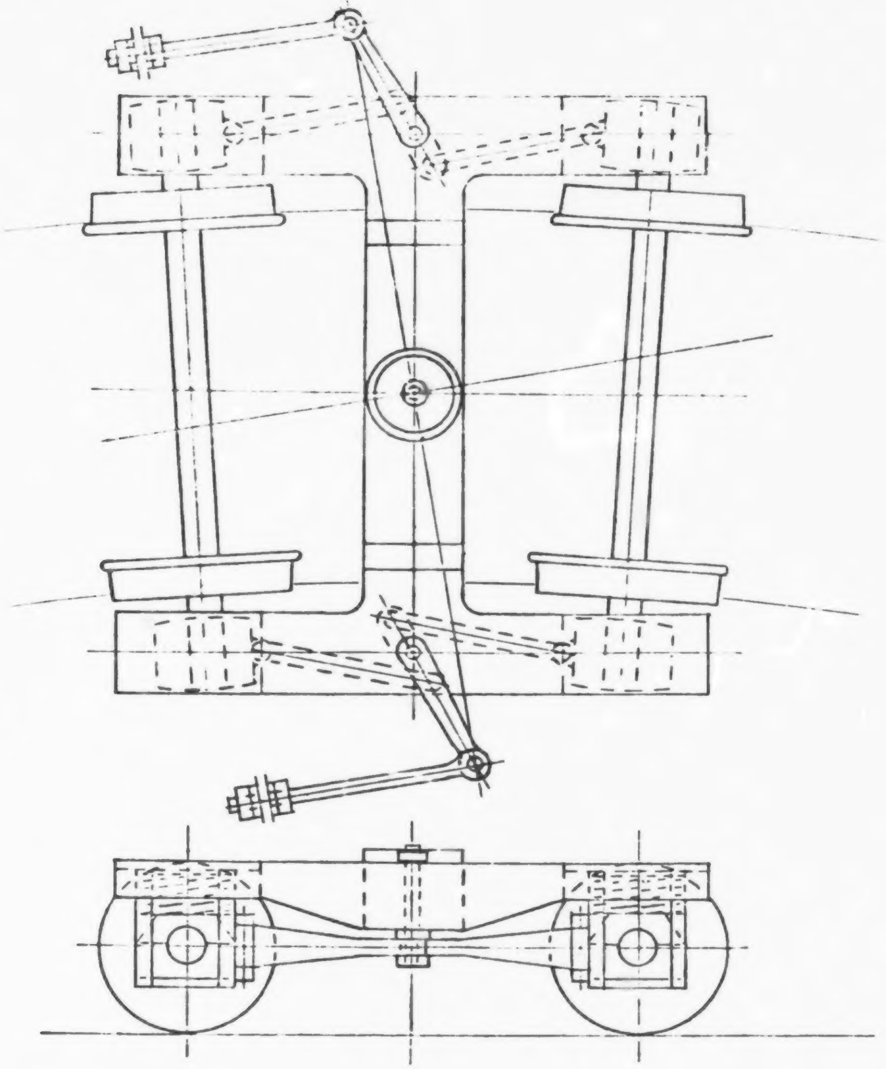

Figure 3 - DEVINE-SCALE RADIAL TRUCK

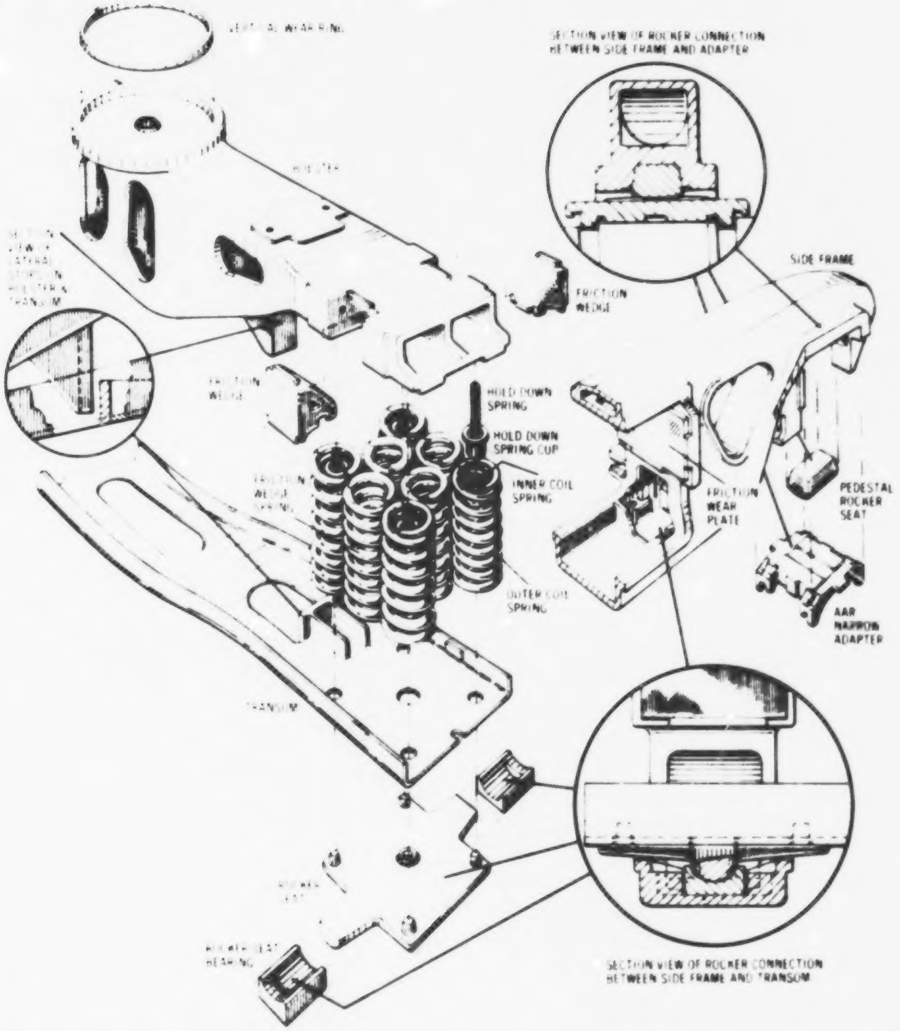
VERTICAL WEAR RING
BOLSTER
SECTION VIEW OF LATERAL STOPS IN BOLSTER & TRANSOM
FRICTION WEDGE
FRICTION WEDGE
HOLD DOWN SPRING
HOLD DOWN SPRING CUP
FRICTION WEDGE SPRING
INNER COIL SPRING
OUTER COIL SPRING
TRANSOM
ROCKER SEAT
ROCKER SEAT BEARING
SECTION VIEW OF ROCKER CONNECTION BETWEEN SIDE FRAME AND ADAPTER
SIDE FRAME
FRICTION WEAR PLATE
PEDESTAL ROCKER SEAT
AAR NARROW ADAPTER
SECTION VIEW OF ROCKER CONNECTION BETWEEN SIDE FRAME AND TRANSOM

Figure 4 - SWING MOTION TRUCK

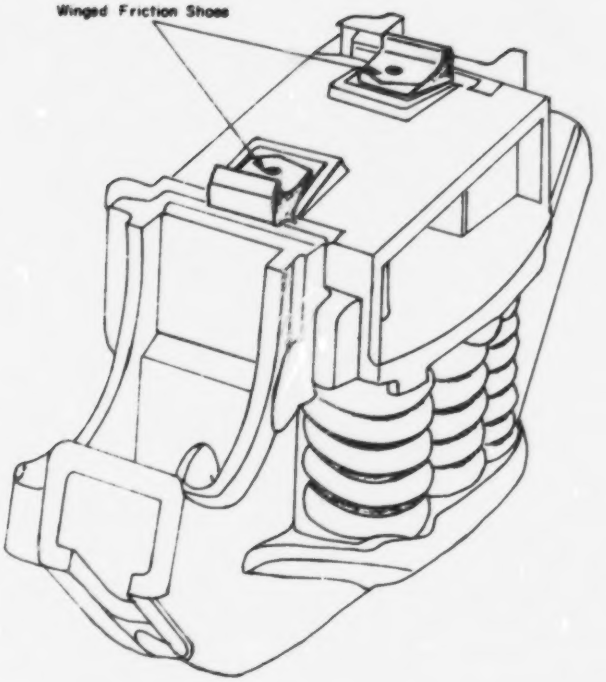
Winged Friction Shoes

Figure 4(b) - WINGED FRICTION SHOES OF RIDE CONTROL TRUCK

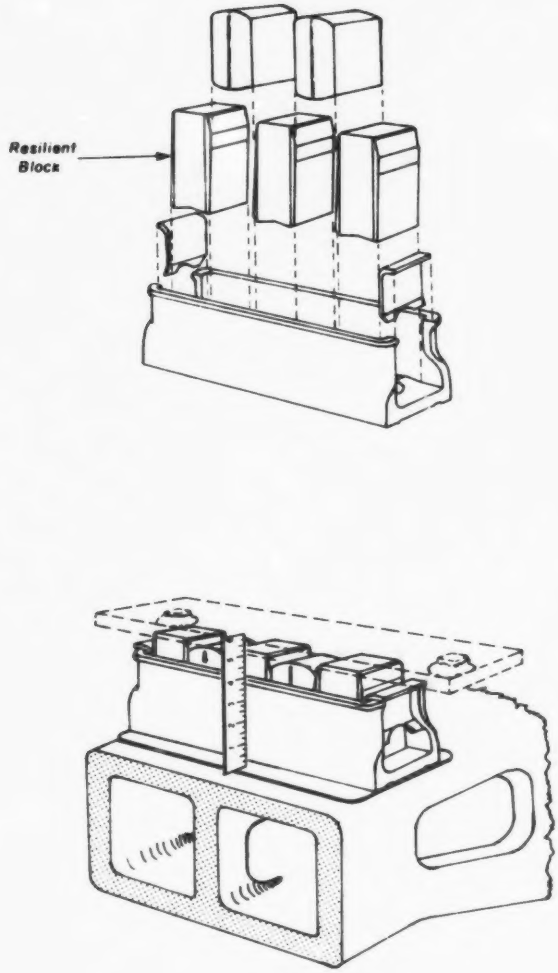
Resilient Block

Figure 5 - STUCKI CONSTANT CONTACT SIDE BEARING

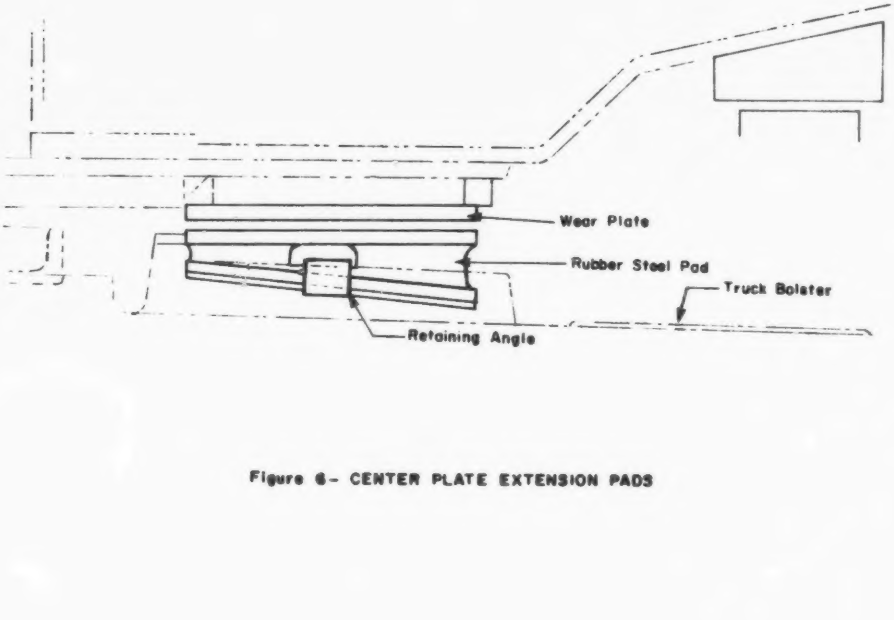
Wear Plate
Rubber Steel Pad
Truck Bolster
Retaining Angle

Figure 6- CENTER PLATE EXTENSION PADS

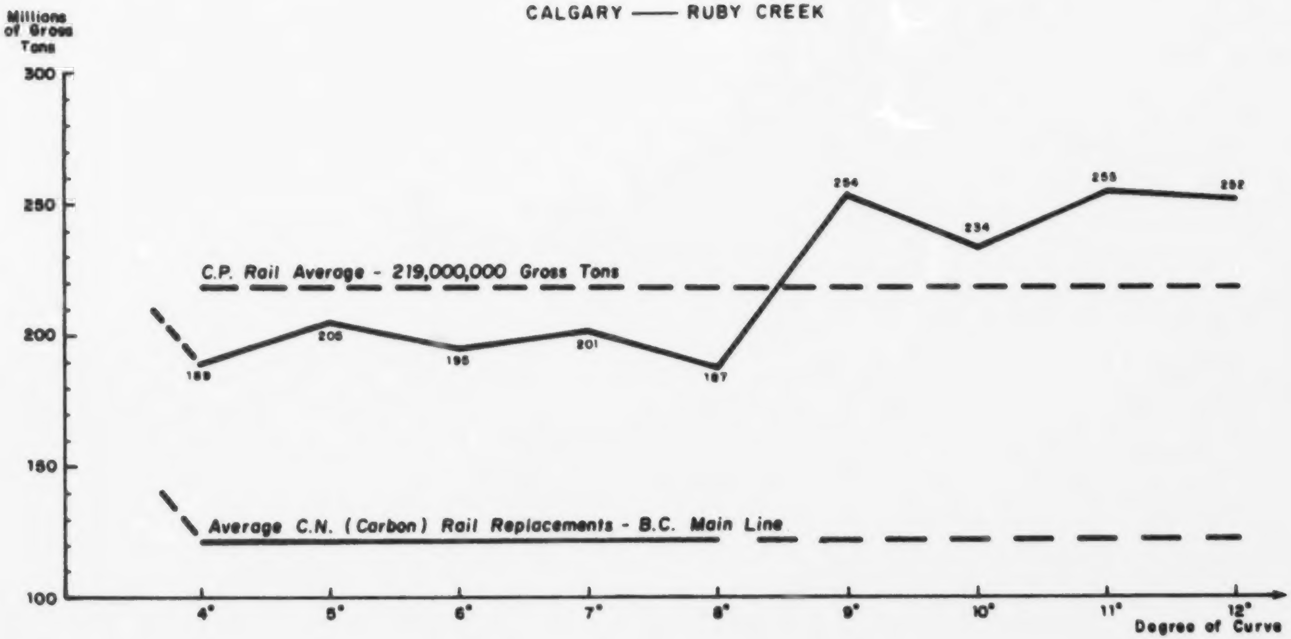

Figure 7 - AVERAGE MILLIONS OF GROSS TONS MOVED BETWEEN RAIL REPLACEMENTS

132# CHROME ALLOY

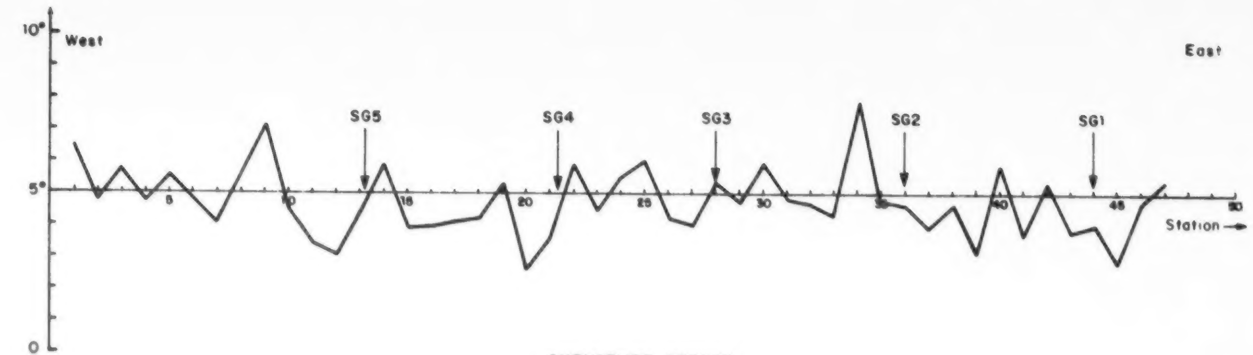

CURVATURE RECORD

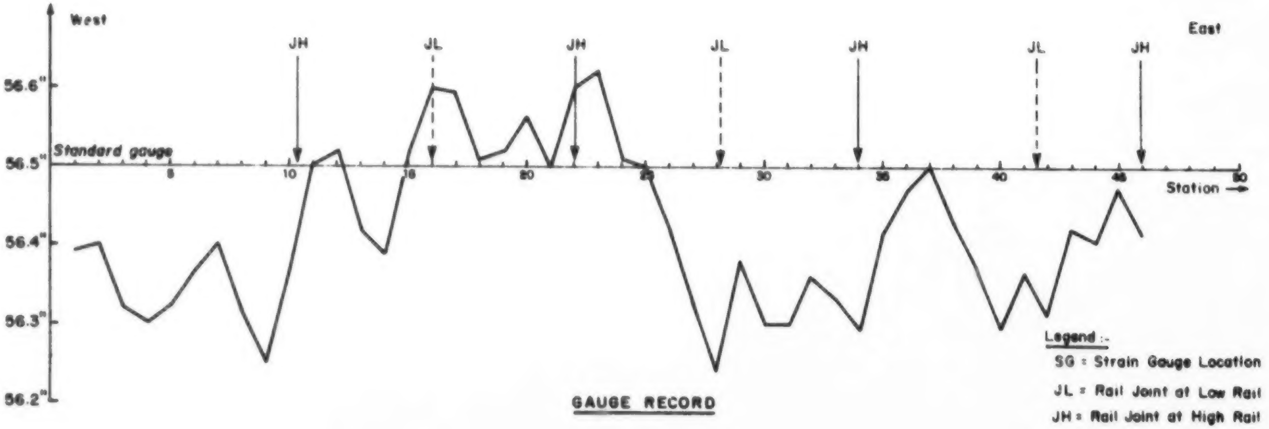

GAUGE RECORD

Figure 8 - CURVATURE AND STATIC GAUGE MEASUREMENT OF THE TEST CURVE

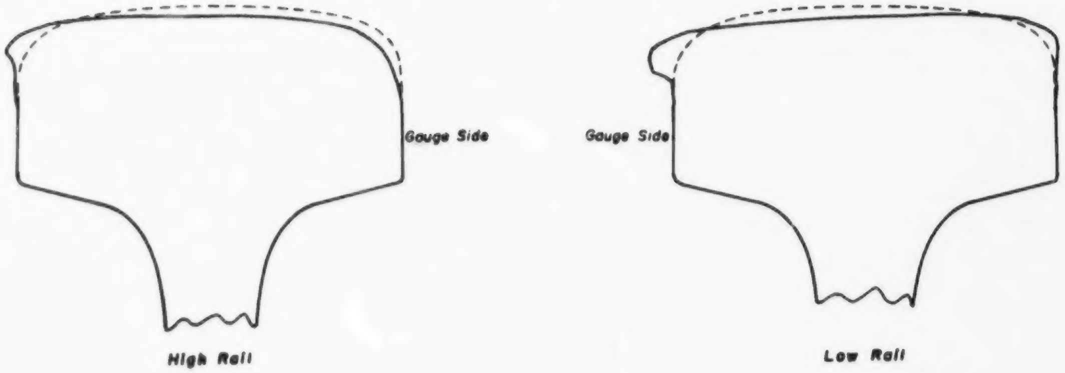
Gauge Side
Gauge Side
High Rail
Low Rail

Figure 9 - TYPICAL RAIL HEAD PROFILE ON THE TEST CURVE

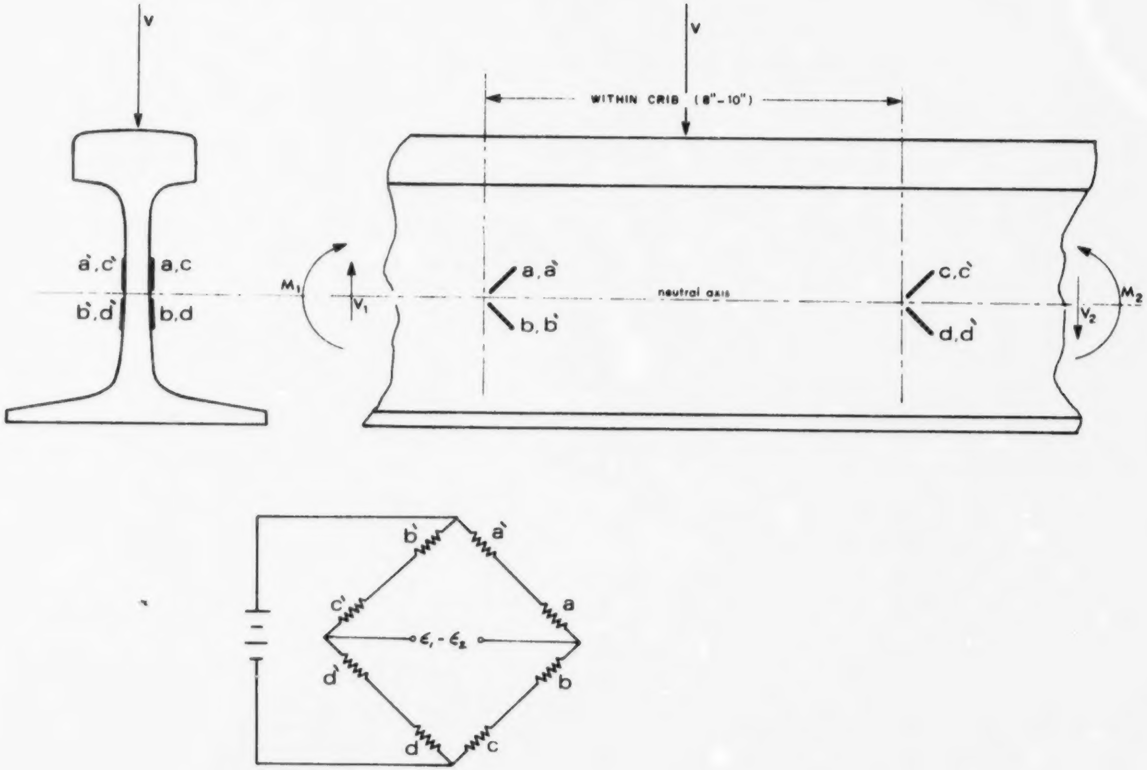
V
a',c'
a,c
b',d'
b,d
V
WITHIN CRIB (8"-10")
M₁
V₁
a,a'
b,b'
neutral axis
c,c'
d,d'
V₂
M₂
b'
a'
c'
a
ε₁ - ε₂
d'
b
d
c

Figure 10 - STRAIN GAUGE CIRCUIT FOR MEASURING VERTICAL WHEEL/RAIL LOADS

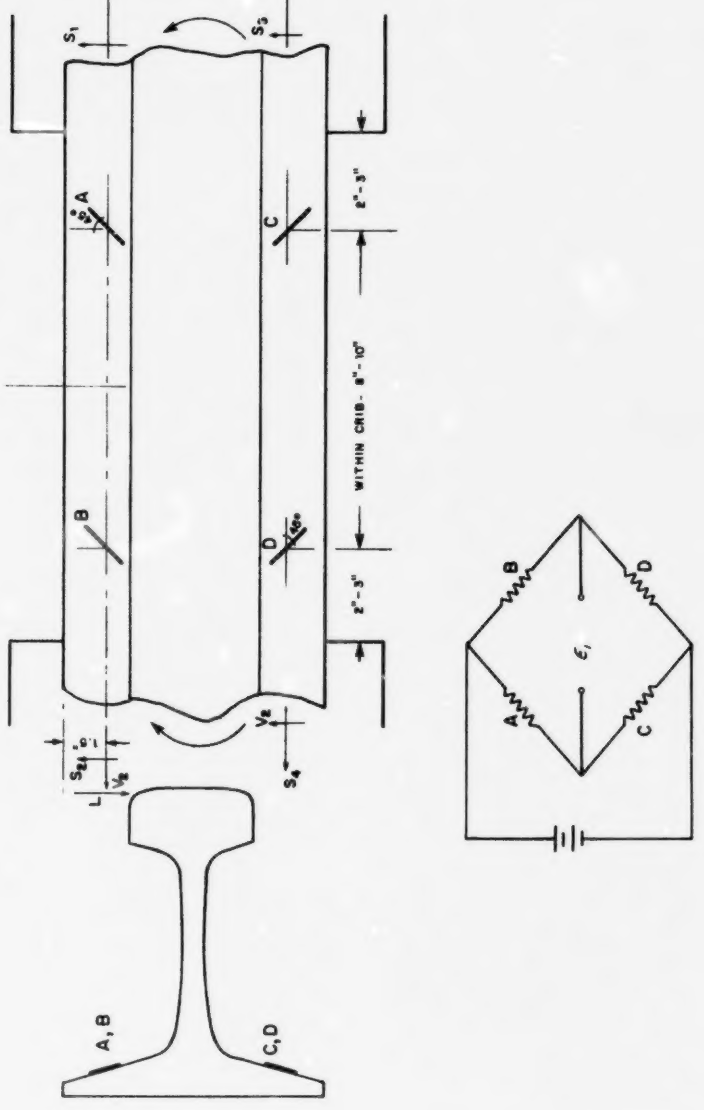
S1
V1
S3
V3
A
45°
C
B
D
45°
2"-3"
WITHIN CRIB - 8"-10"
2"-3"
S2
1.0"
L
V2
V2
S4
A, B
C, D
B
D
A
C
ε1

Figure 11- STRAIN GAUGE CIRCUIT FOR MEASURING LATERAL WHEEL/RAIL LOADS

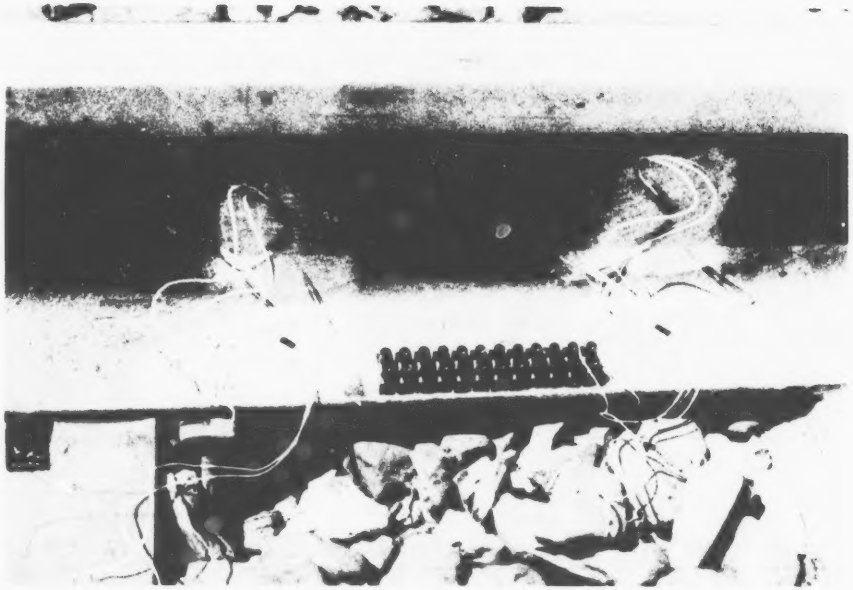

FIGURE 12: VERTICAL AND LATERAL STRAIN GAUGE CIRCUITS ON RAIL

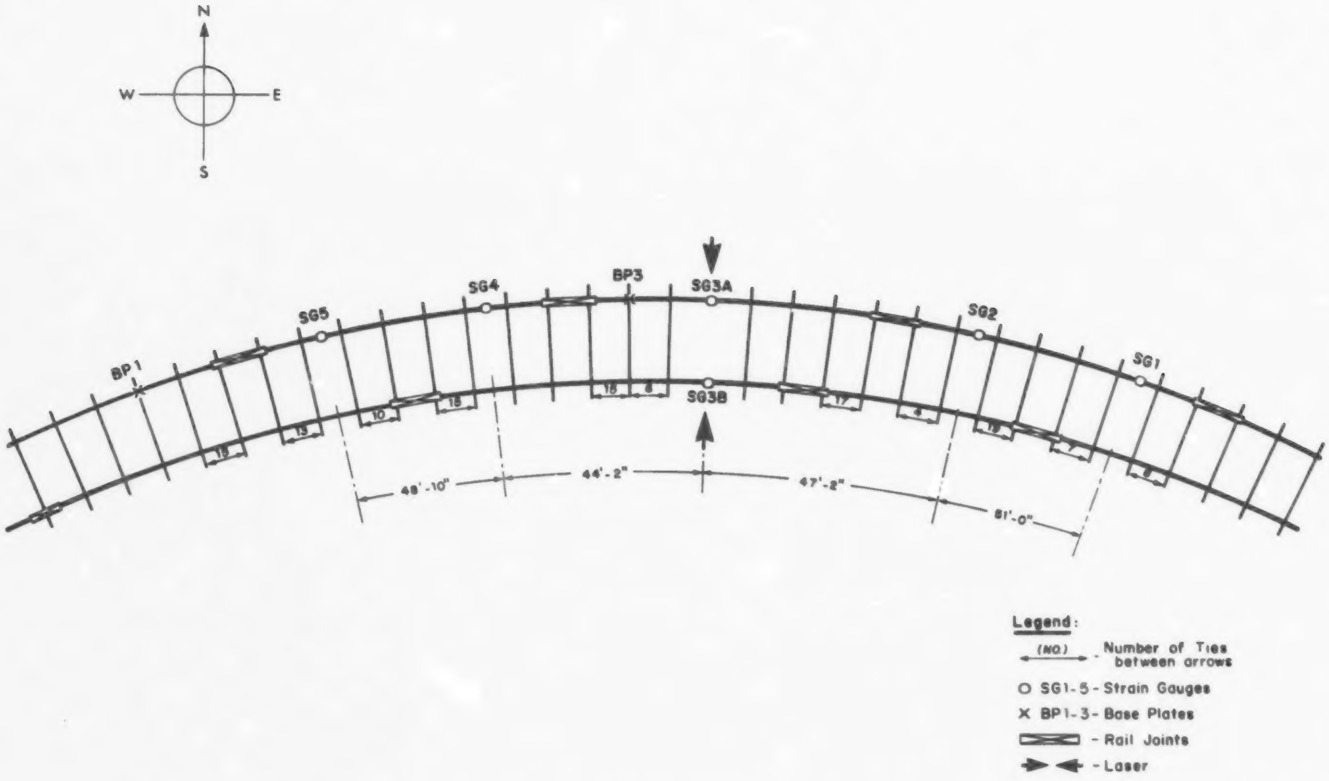
N
W
E
S
BP1
SG5
SG4
BP3
SG3A
SG3B
SG2
SG1
15
13
10
15
15
8
17
4
19
7
8
48'-10"
44'-2"
47'-2"
81'-0"
Legend:
(NO.) - Number of Ties between arrows
O SG1-5 - Strain Gauges
X BP1-3 - Base Plates
- Rail Joints
- Laser

Figure 13 - LOCATIONS OF INSTRUMENTATION IN THE CURVE TESTING

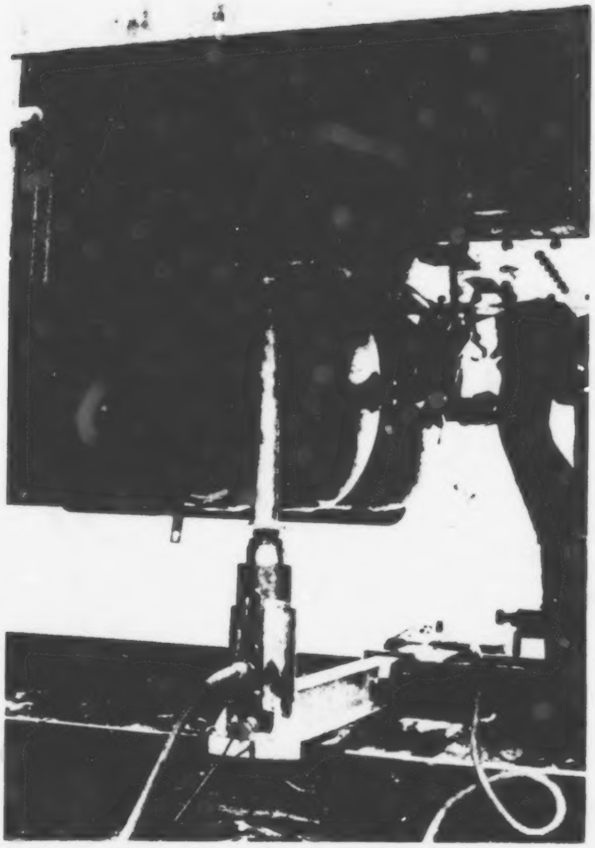

FIGURE 14: FRAME FIXTURE USED IN CALIBRATING THE STRAIN GAUGE CIRCUITS

Figure 15 VERTICAL CALIBRATION OF STRAIN GAUGE No. 2

(recording sensitivity - 10 uv/division)

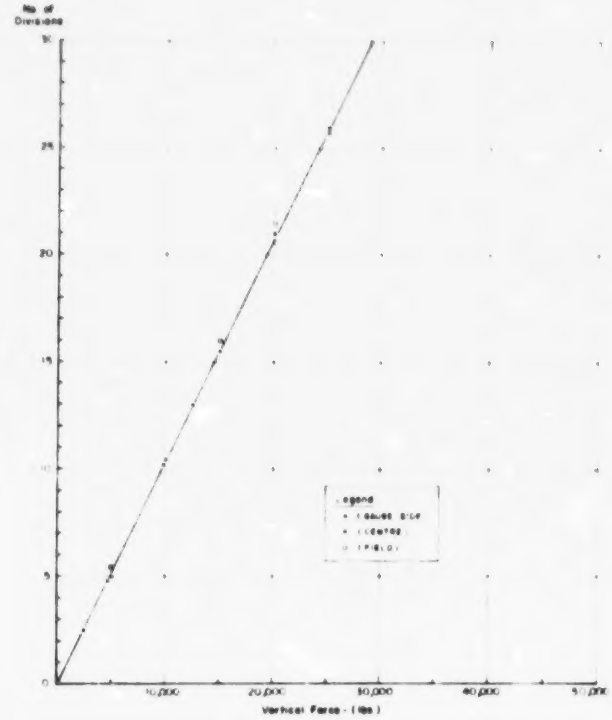

Figure 16 - VERTICAL CALIBRATION OF STRAIN GAUGE No. 3A

- ALL POSITIONS -

(recording sensitivity - 20 uv/division)

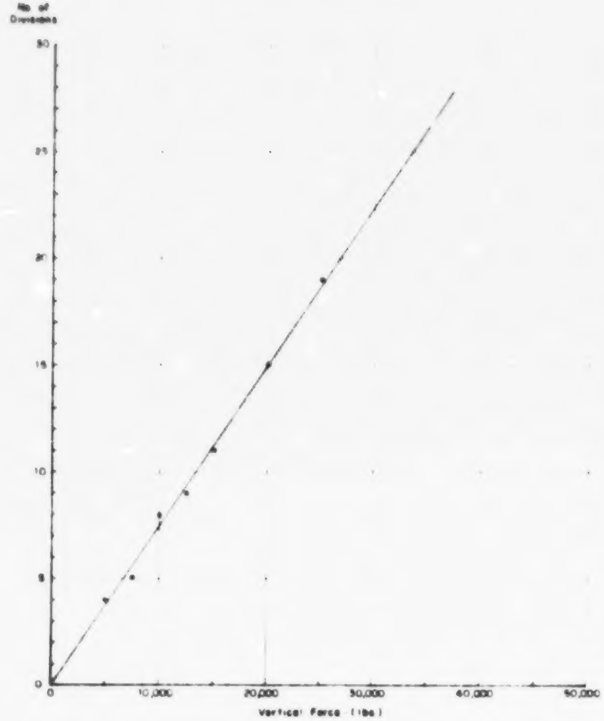

Figure 17: VERTICAL CALIBRATION OF STRAIN GAUGE No 38

- ALL POSITIONS -

(recording sensitivity = 20 mv/division)

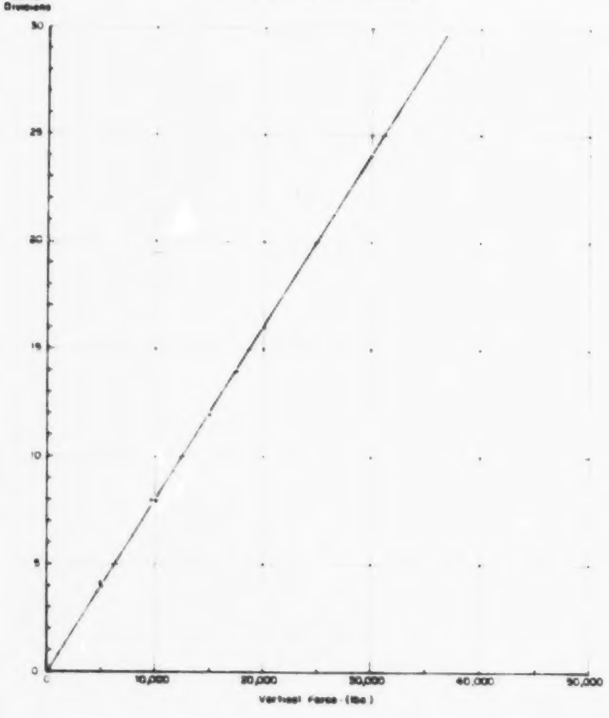

Figure 18 - VERTICAL CALIBRATION OF STRAIN GAUGE No 5

(recording sensitivity 10 mv/division)

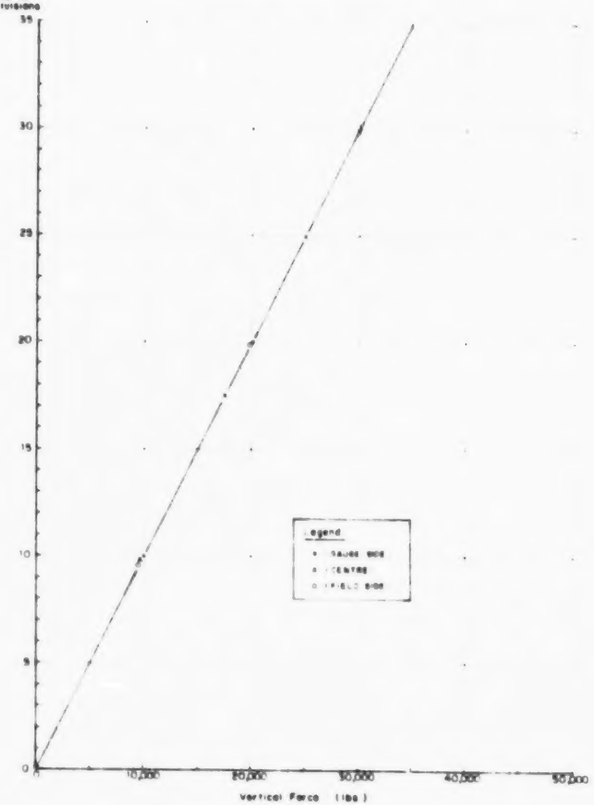

Figure 19: LATERAL CALIBRATION OF STRAIN GAUGE No 2

(recording sensitivity 5 mv/division)

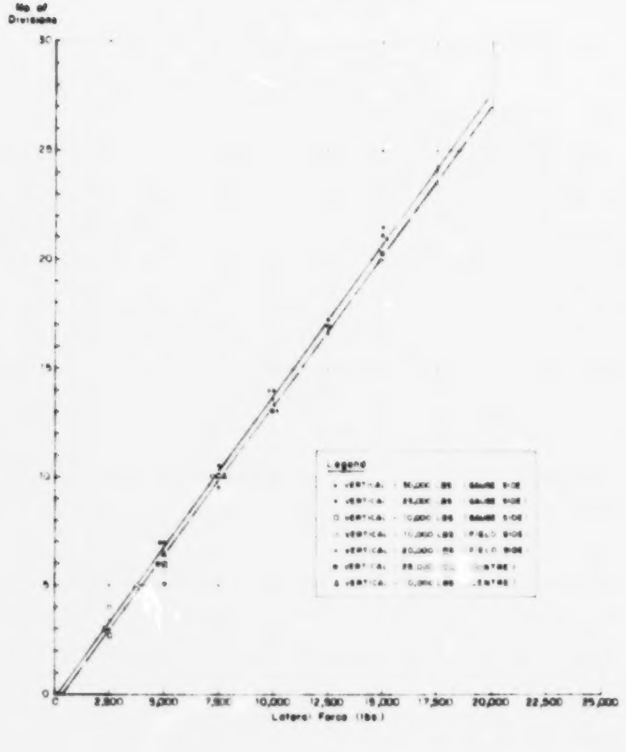

Figure 20 LATERAL CALIBRATION OF STRAIN GAUGE No 3A

(recording sensitivity 50 mv/division)

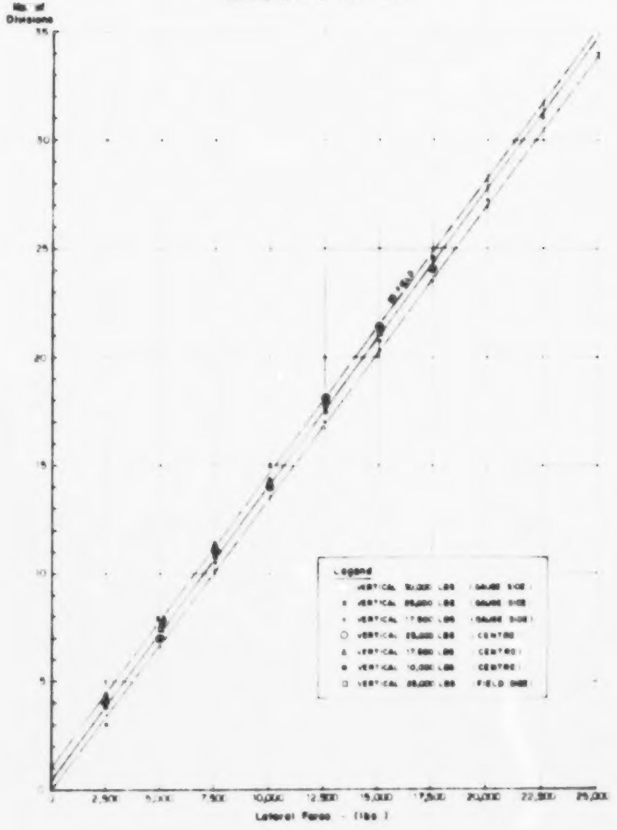

Figure 21 - LATERAL CALIBRATION OF STRAIN GAUGE No 38

recording sensitivity 50 mv/division

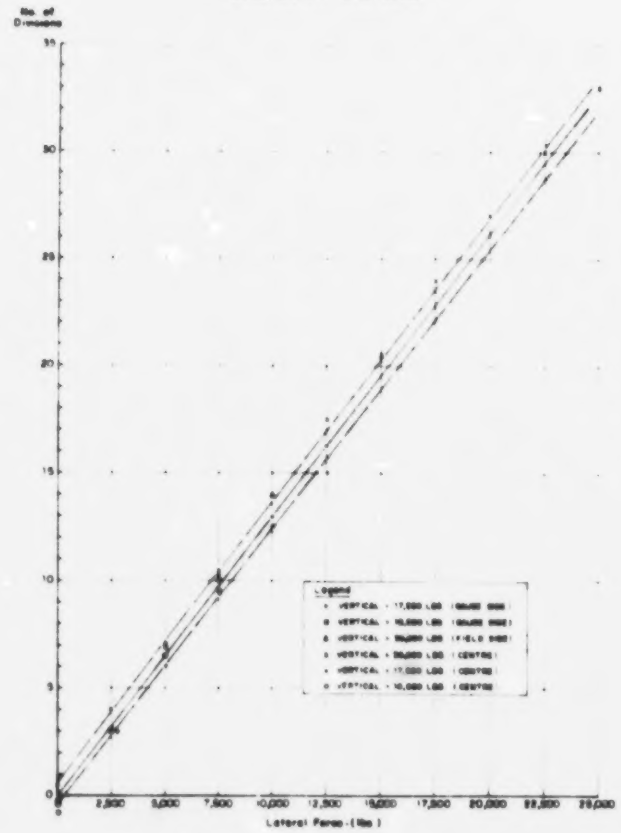

Figure 22 - LATERAL CALIBRATION OF STRAIN GAUGE No 5

recording sensitivity 50 mv/division

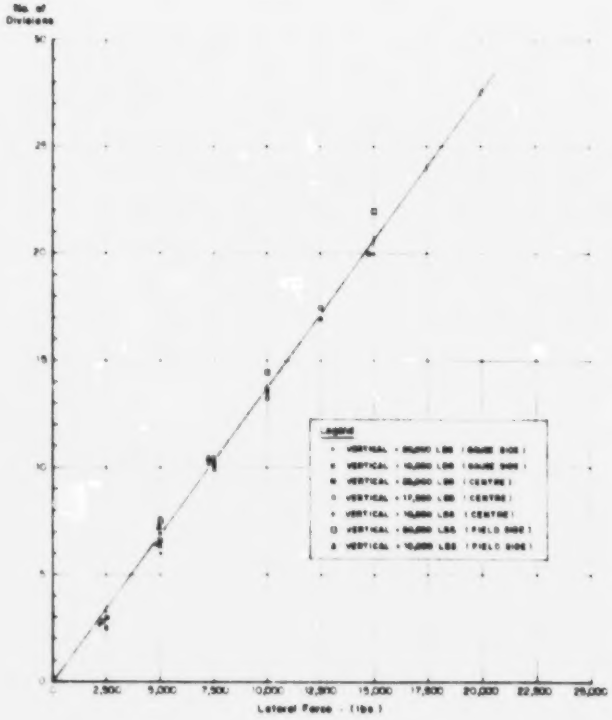

FIGURE 23: ANGLE-OF-ATTACK MEASUREMENT SYSTEM

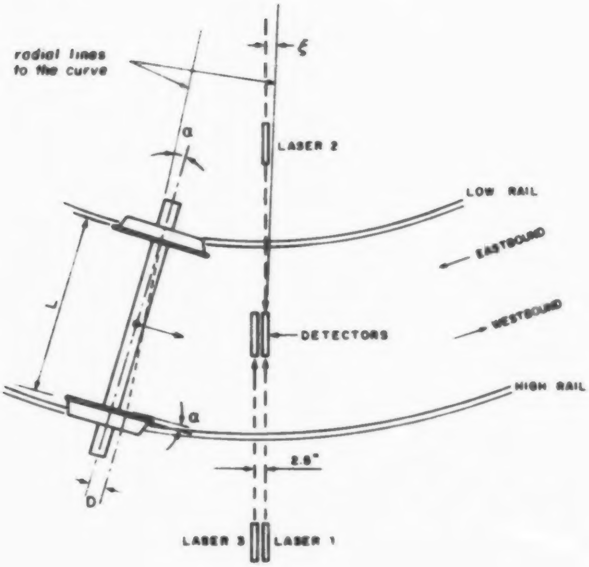
radial lines
to the curve
ξ
α
LASER 2
LOW RAIL
EASTBOUND
L
DETECTORS
WESTBOUND
HIGH RAIL
α
2.5"
D
LASER 3
LASER 1

Figure 24- ALIGNMENT OF LASERS AND DETECTORS USED IN ANGLE OF ATTACK MEASUREMENTS

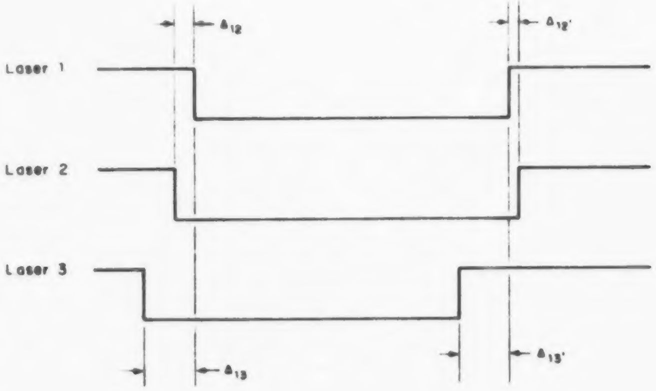
Δ_{12}
$\Delta_{12'}$
Laser 1
Laser 2
Laser 3
Δ_{13}
$\Delta_{13'}$

d = time interval corresponding to angle-of-attack

$= \frac{\Delta_{12} + \Delta_{12'}}{2}$ [m sec]

T = time for 1" of travel

$= \frac{(\Delta_{13} + \Delta_{13'})/2}{2.5}$ $[\frac{m\,sec}{in}]$

$D = \frac{d}{T}$ [inch], $\tan \alpha = \frac{D}{L}$ [rad]

α = angle-of-attack

$= \tan^{-1}(\frac{d}{LT}) \times 60$ [min]

Note: $\Delta_{12'}$ is negative with respect to Laser 2 in this example

Figure 25- LASER SIGNAL TRACES OF A WESTBOUND WHEELSET AND CALCULATION OF ANGLE-OF-ATTACK

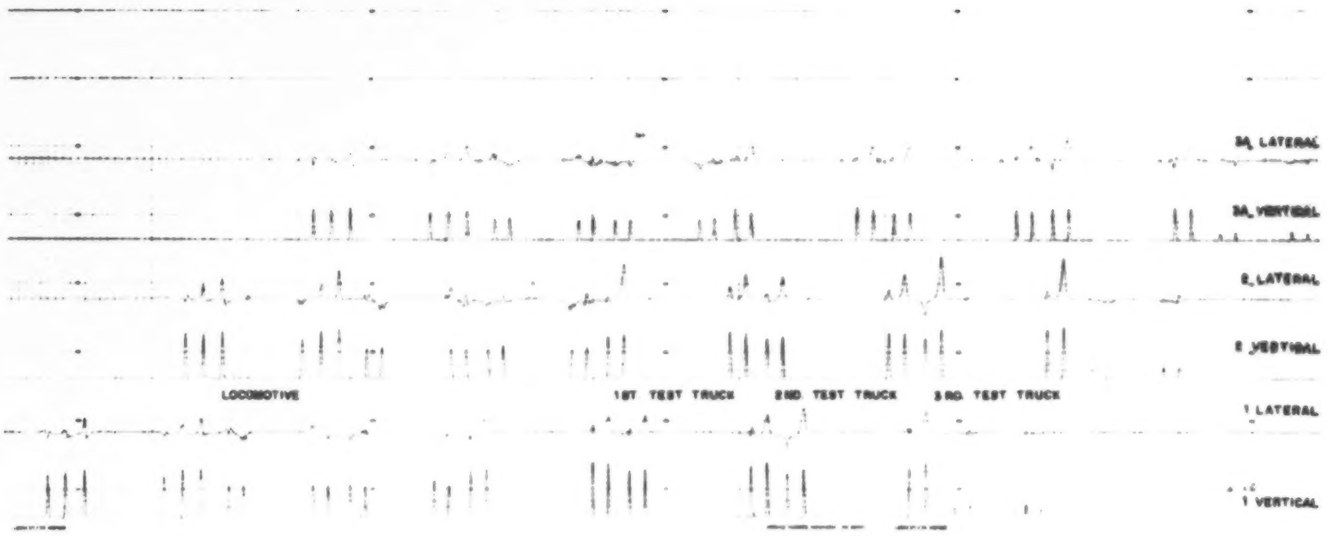

Figure 26- TYPICAL OUTPUT OF THE LATERAL AND VERTICAL STRAIN GAUGE CIRCUITS

(Speed = 37 mph, run no. 65 East, Consist II)

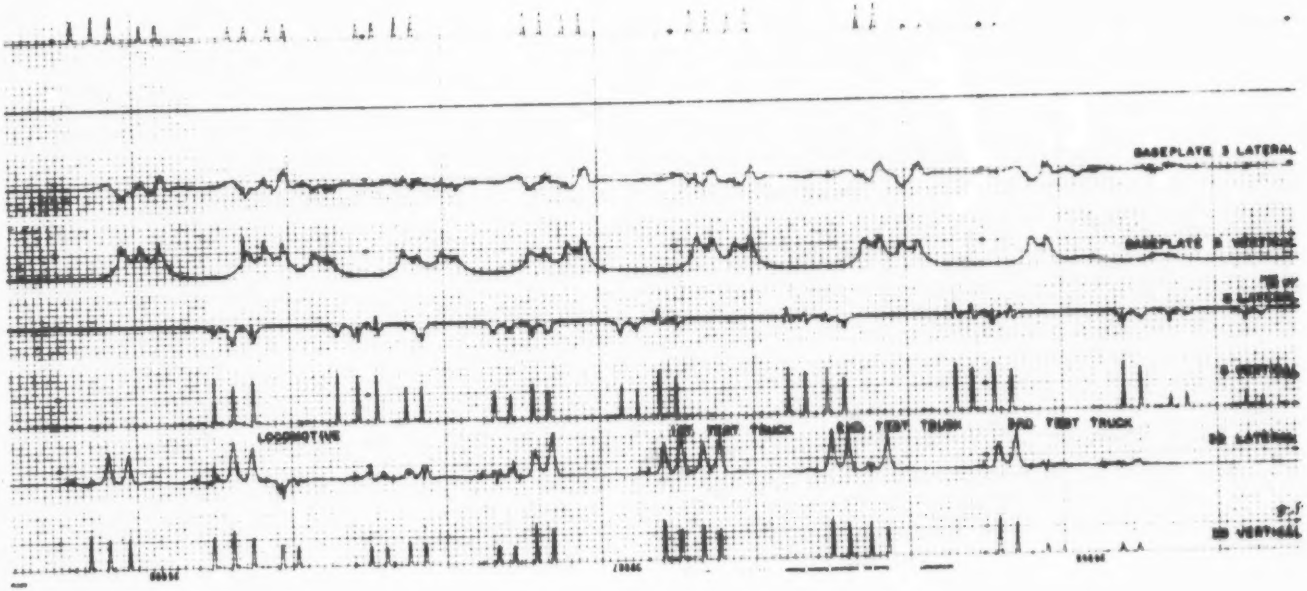

Figure 26 - Continued

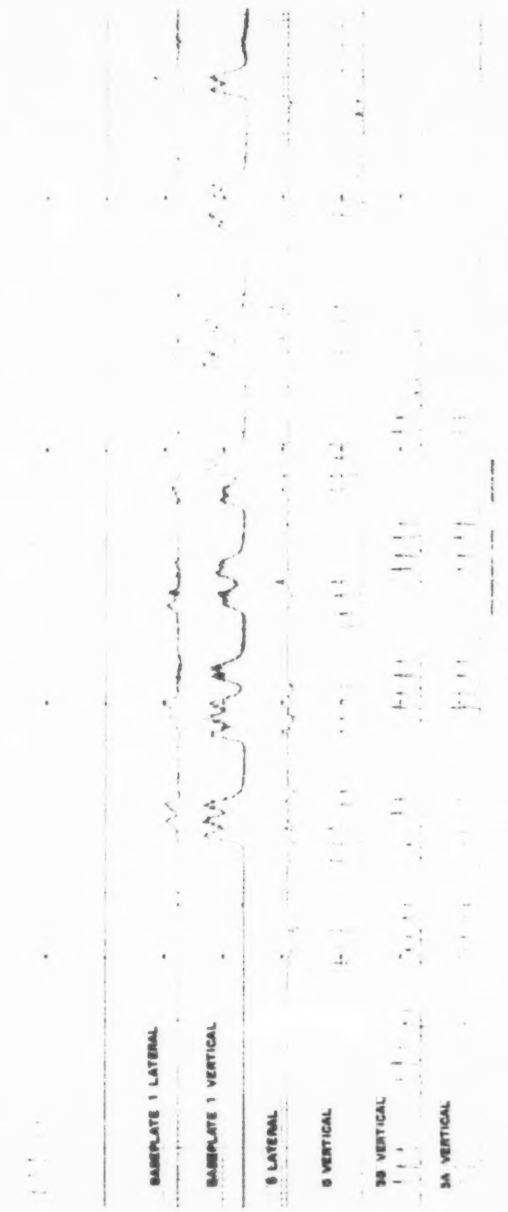

Figure 26- Continued

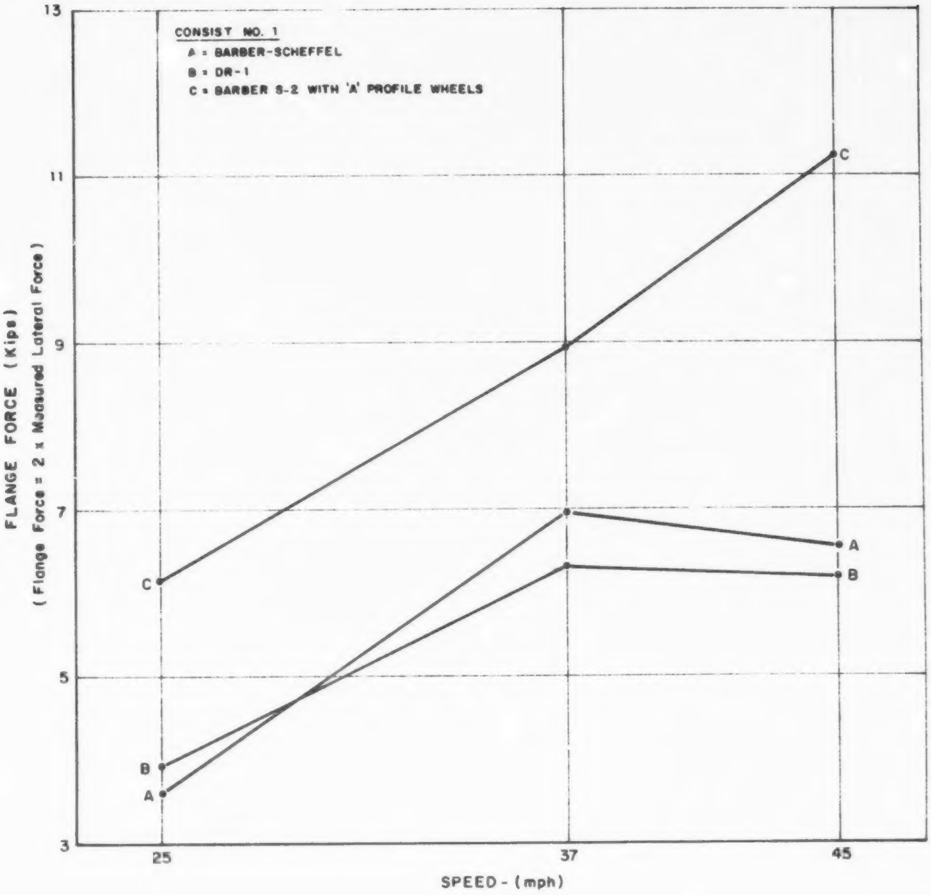

Figure 27 (a) 1- AVERAGE FLANGE FORCE VS SPEED - CONSIST I

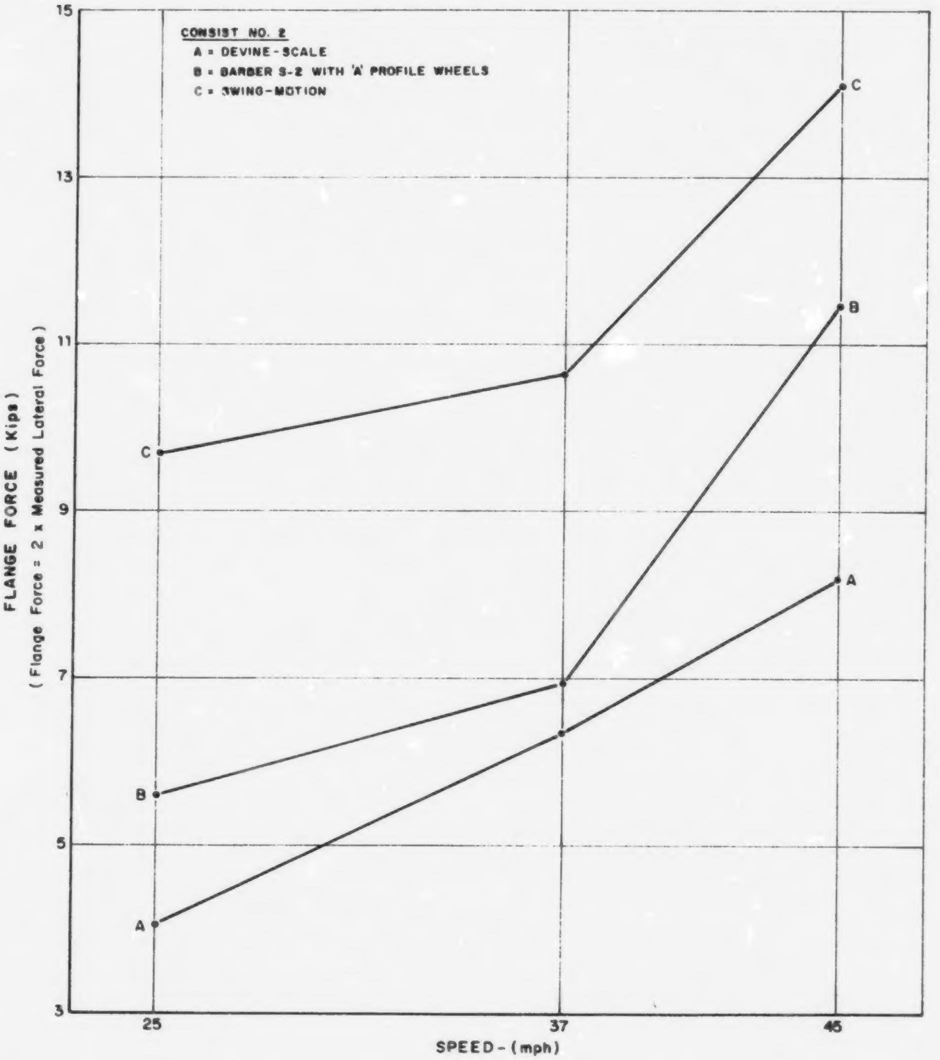

Figure 27(a) 2- AVERAGE FLANGE FORCE VS SPEED - CONSIST II

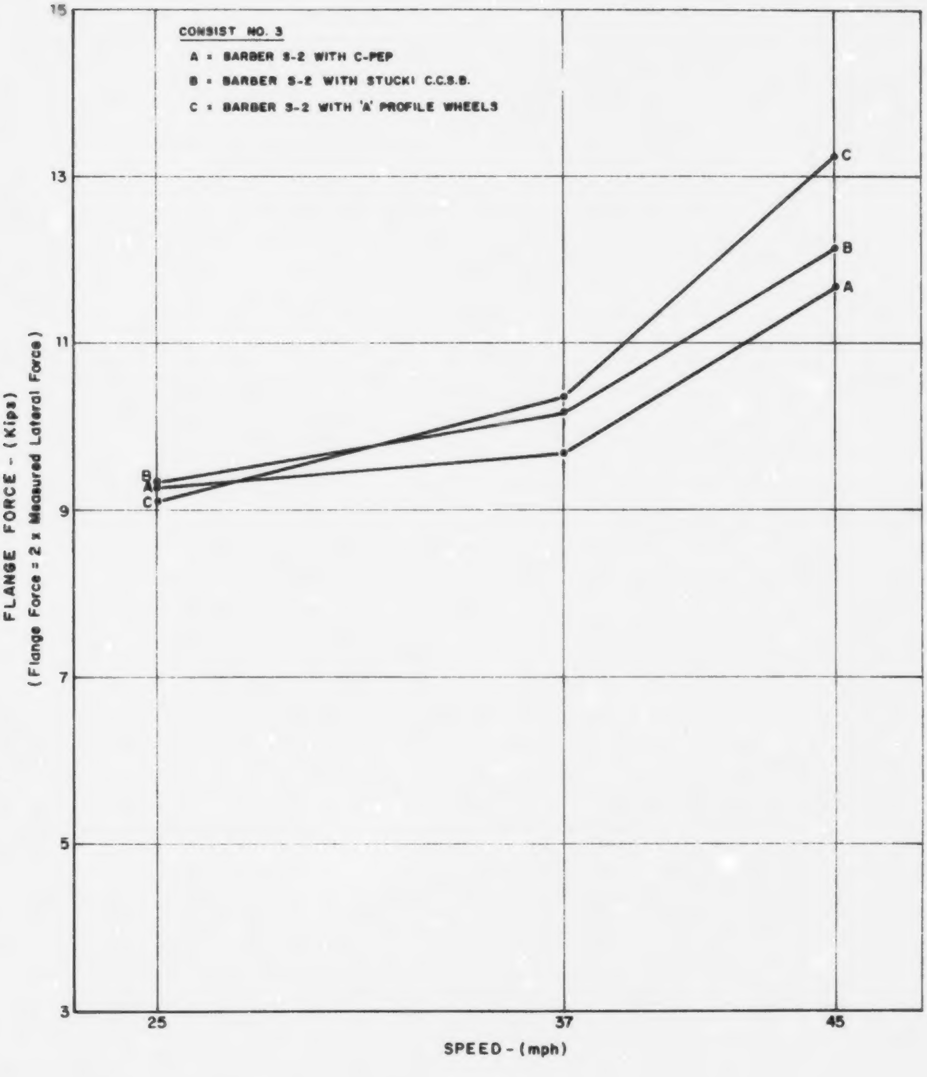

Figure 27(a) 3- AVERAGE FLANGE FORCE VS SPEED- CONSIST III

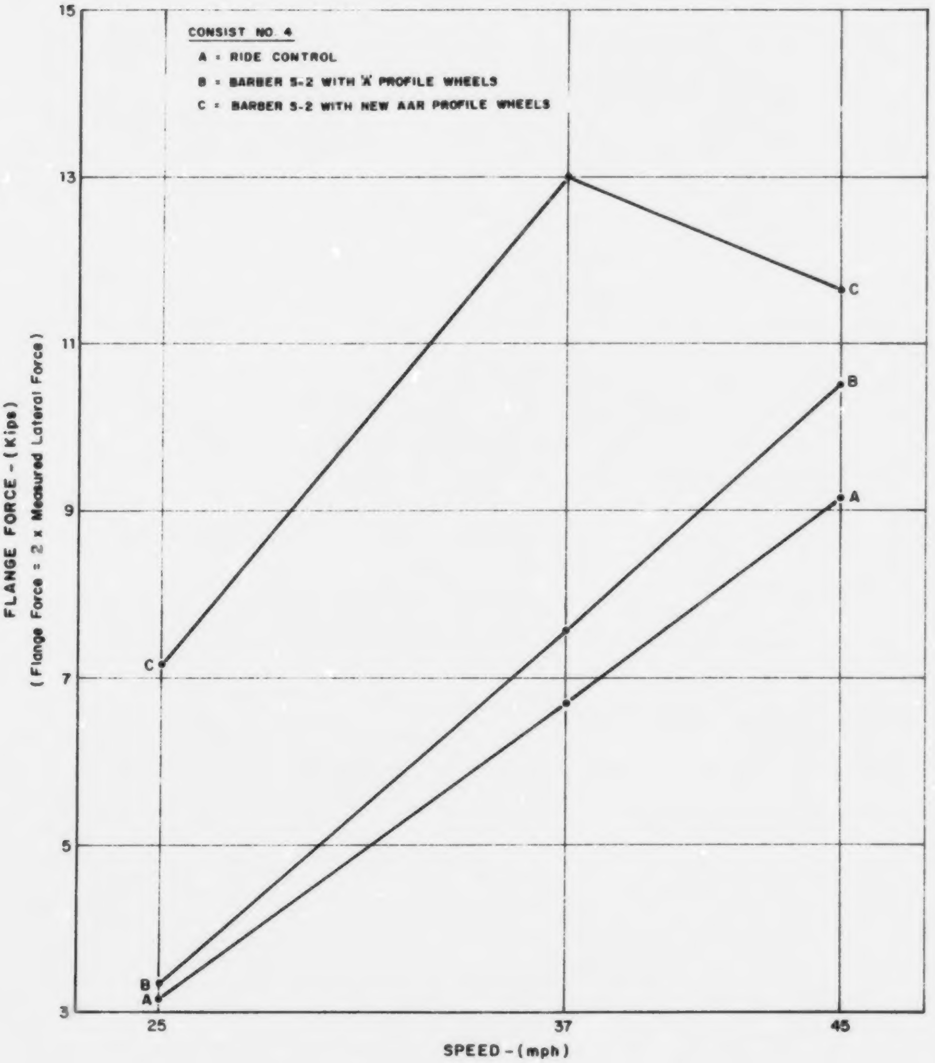

Figure 27(a) 4 - AVERAGE FLANGE FORCE VS SPEED - CONSIST IV

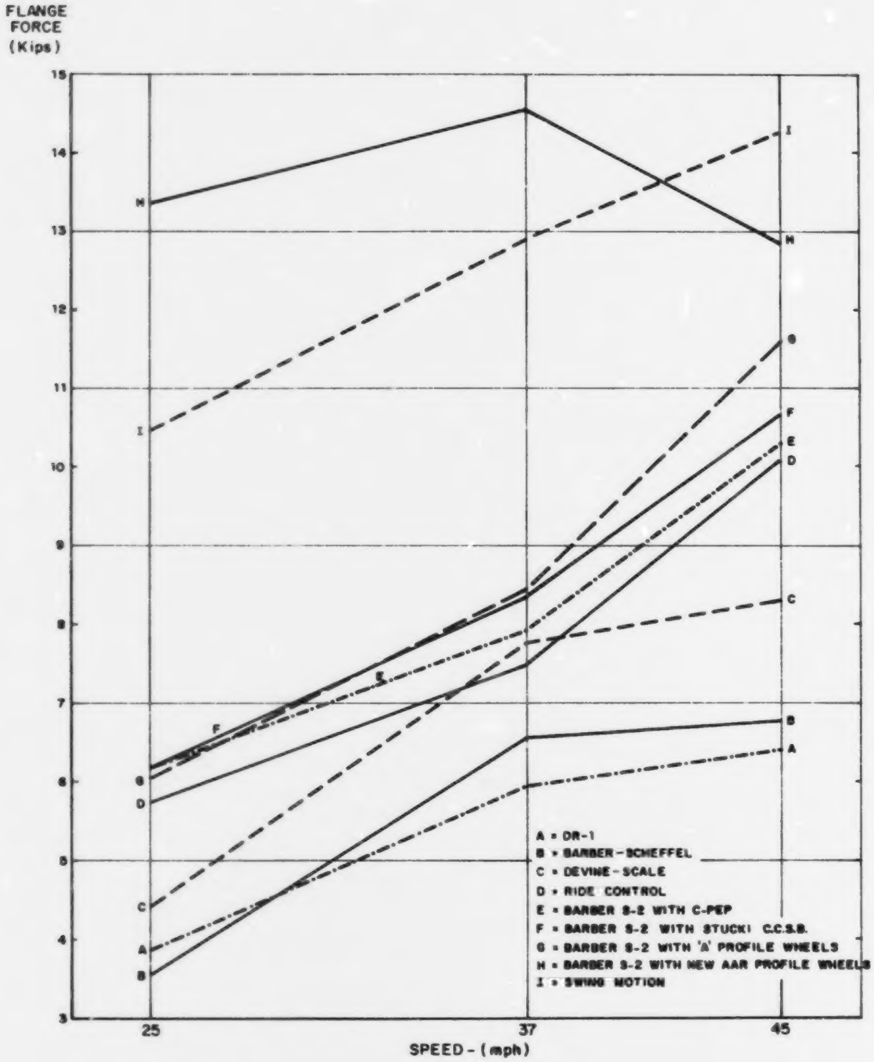

Figure 27 (b) - AVERAGE NORMALIZED FLANGE FORCES OF ALL TEST TRUCKS

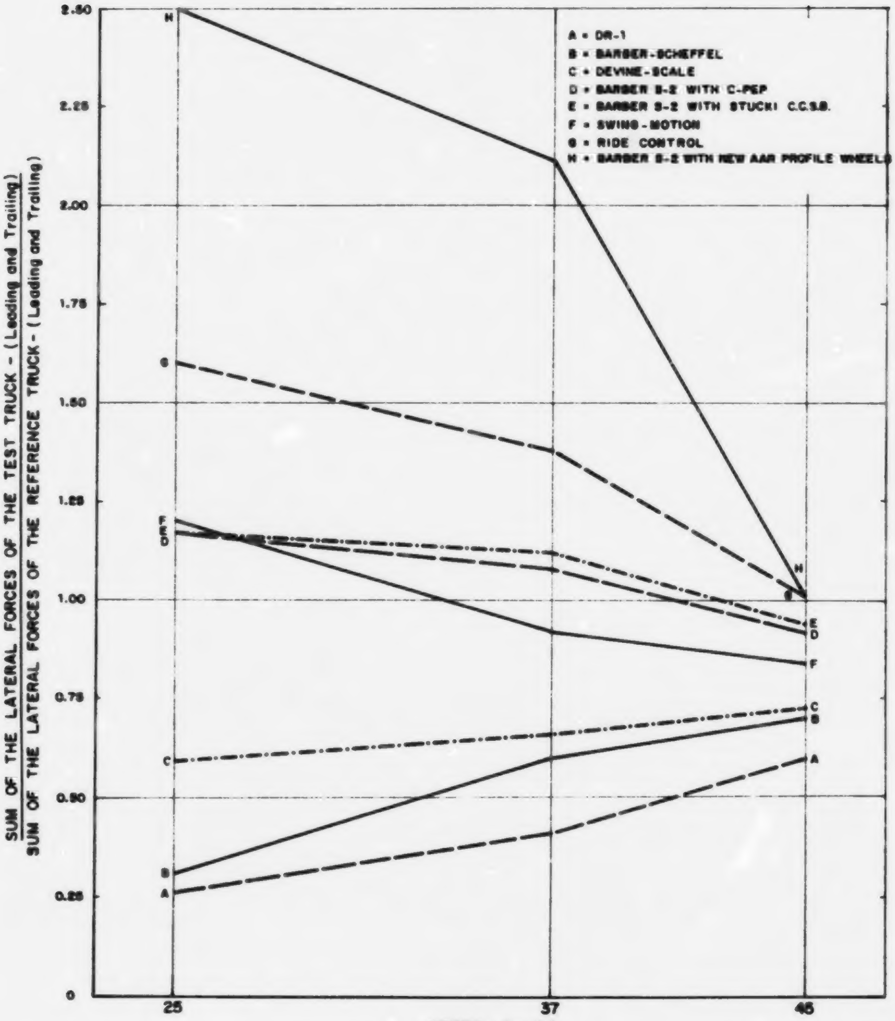

Figure 28- SUM OF THE LATERAL FORCES OF EACH TEST TRUCK
IN RELATION TO THE REFERENCE TRUCK

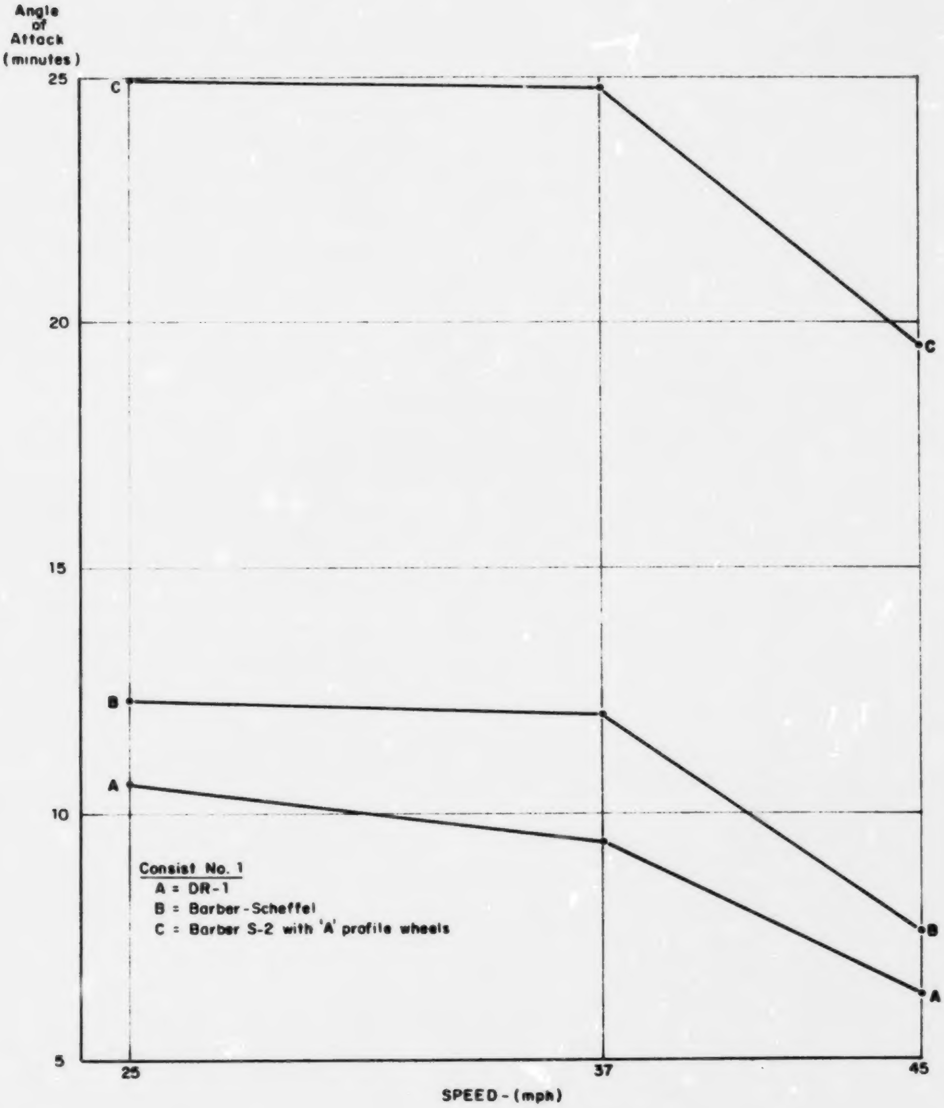

Figure 29(a)- AVERAGE ANGLE-OF-ATTACK VS SPEED

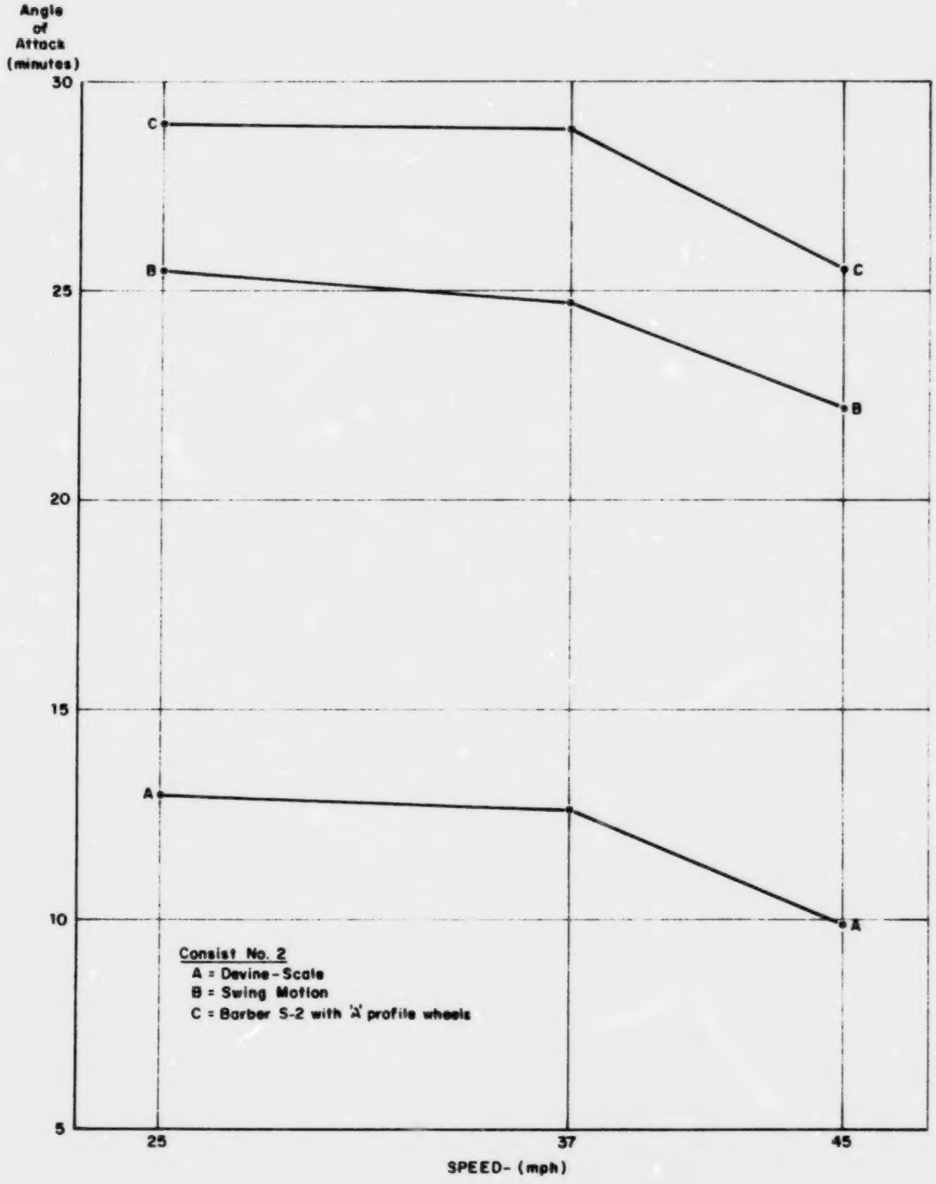

Figure 29 (a) - Continued

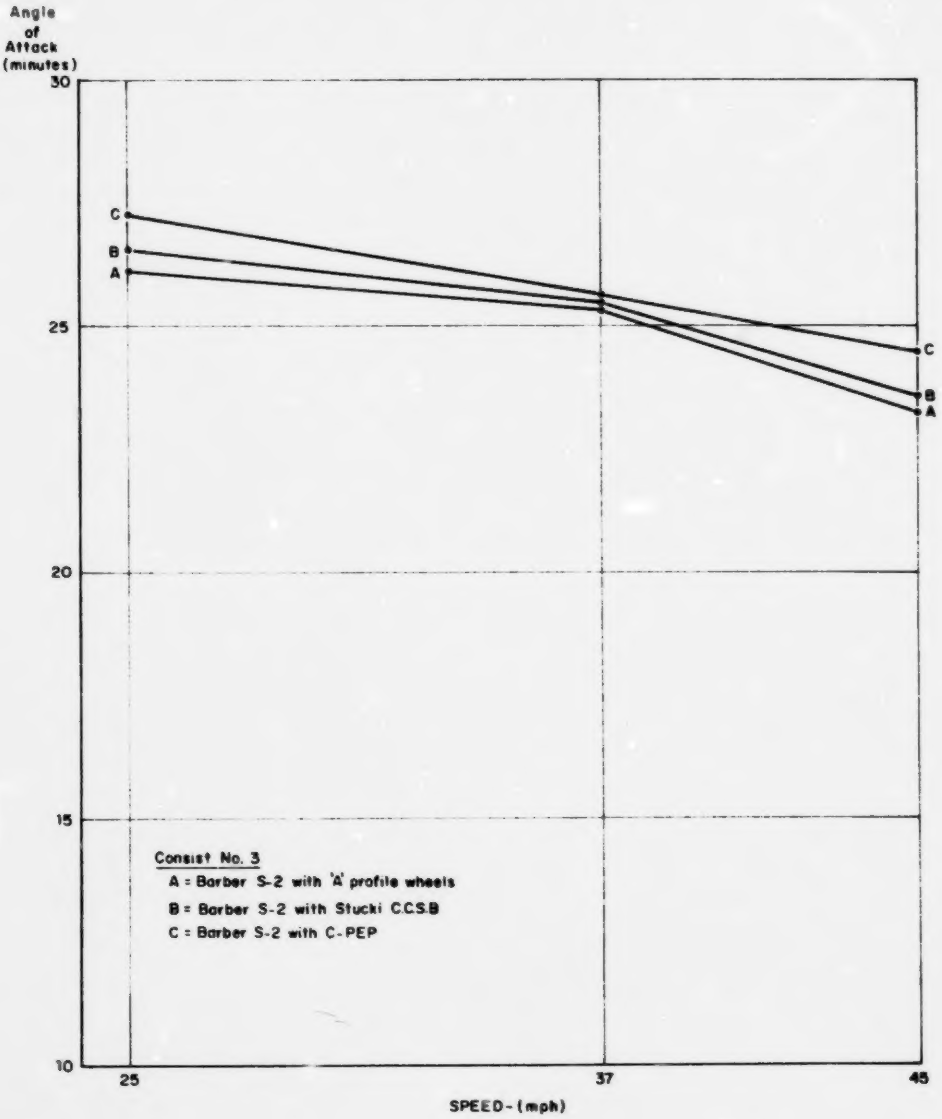

Figure 29(a) – Continued

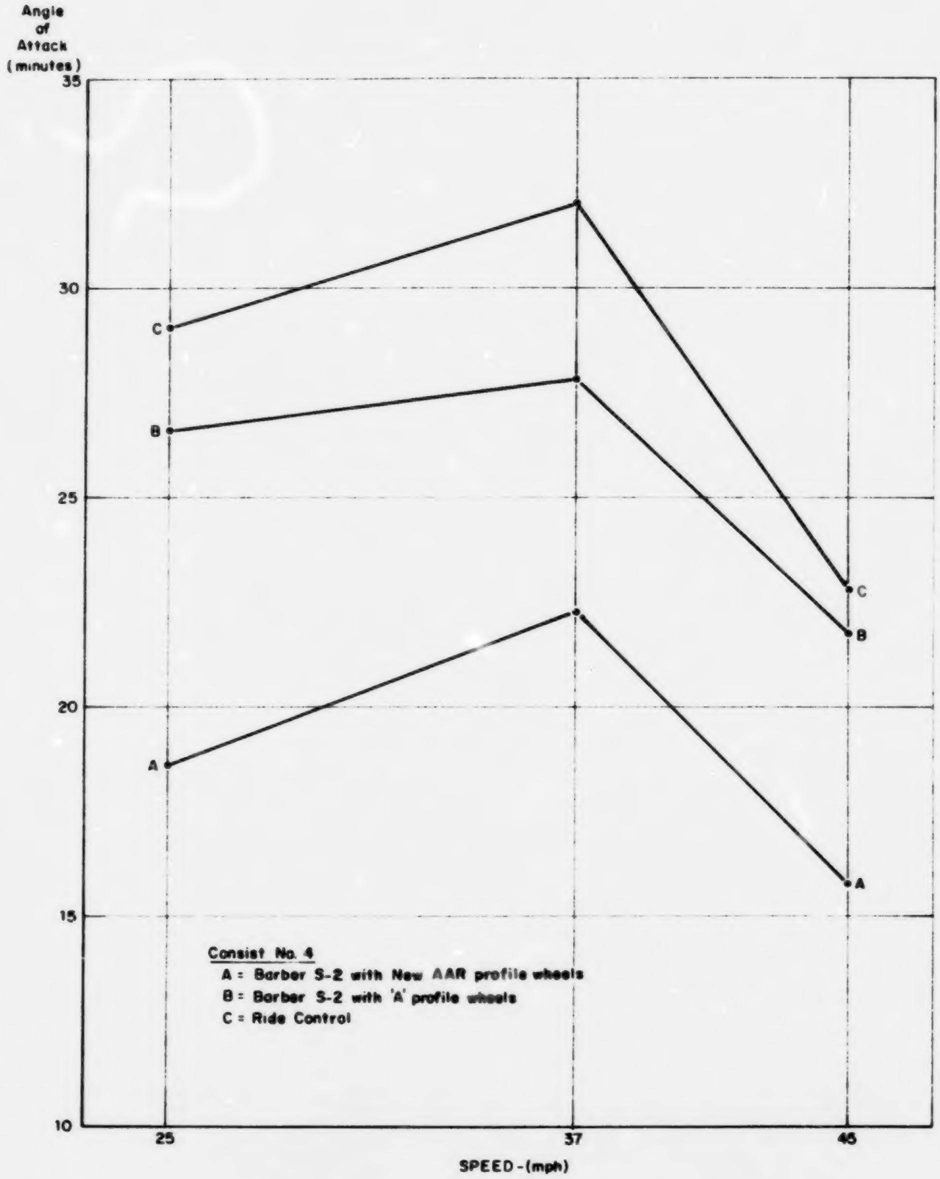

Figure 29(a) - Continued

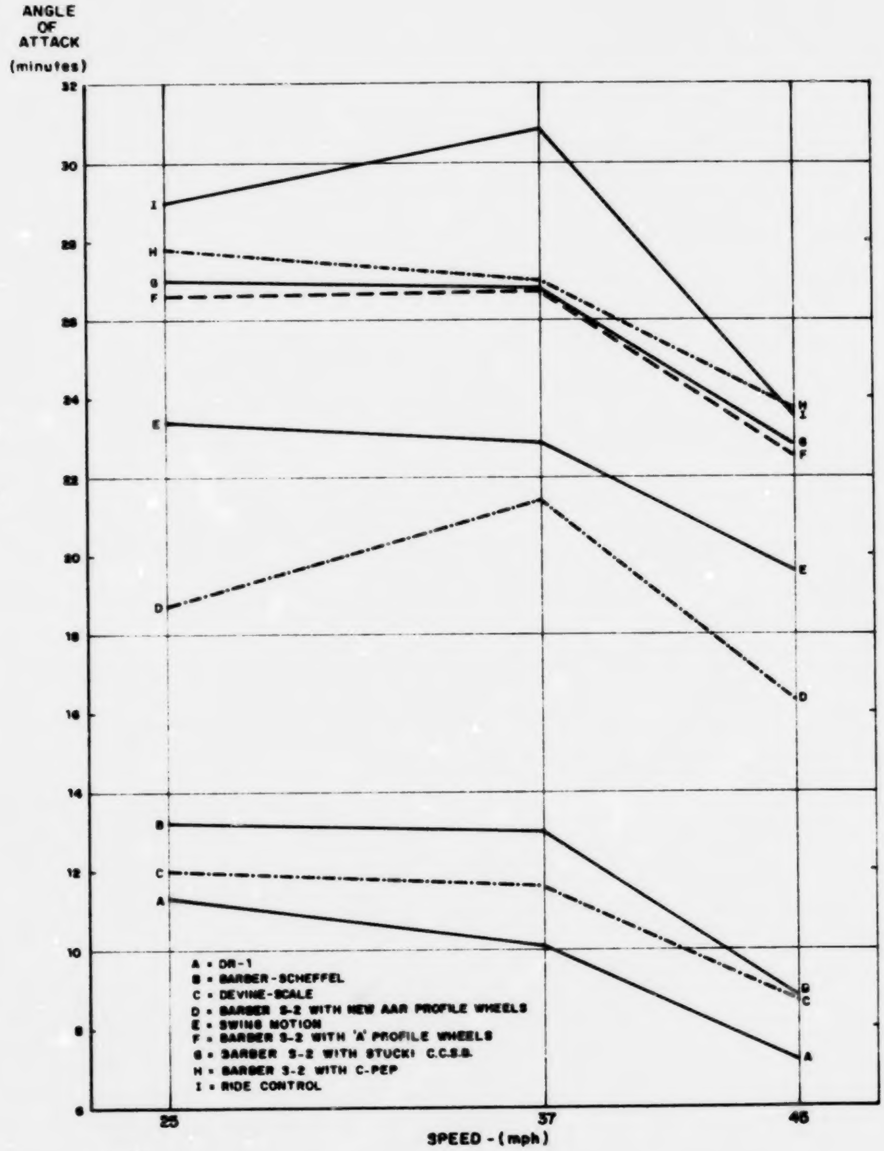

Figure 29(b)- AVERAGE NORMALIZED VALUE OF ANGLE-OF-ATTACK OF EACH TEST TRUCK

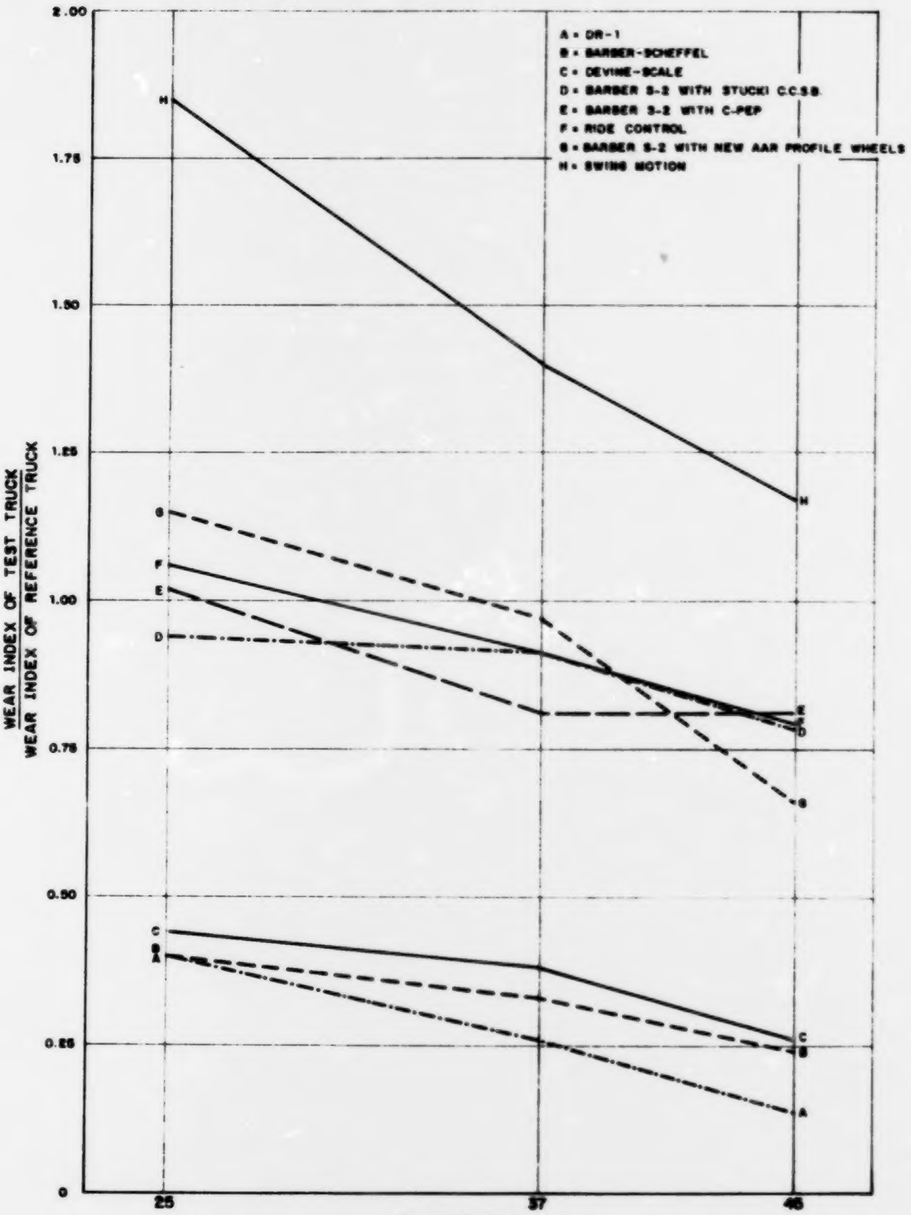

Figure 30- WEAR INDEX OF TEST TRUCKS IN RELATION TO THE REFERENCE TRUCK

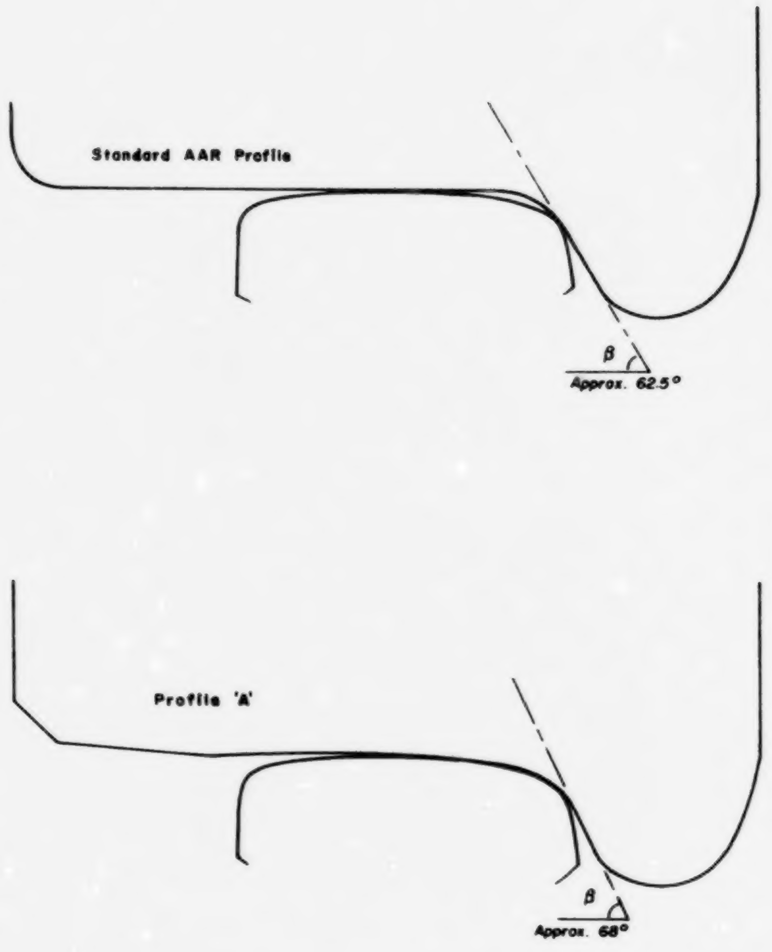
Standard AAR Profile
β
Approx. 62.5°
Profile 'A'
β
Approx. 68°

β = angle of flange contact (under condition of no angle of attack of wheelset/rail)

Figure 30(b)- FLANGE CONTACT GEOMETRY OF THE TWO NEW PROFILES ON THE TEST CURVE OUTER RAIL

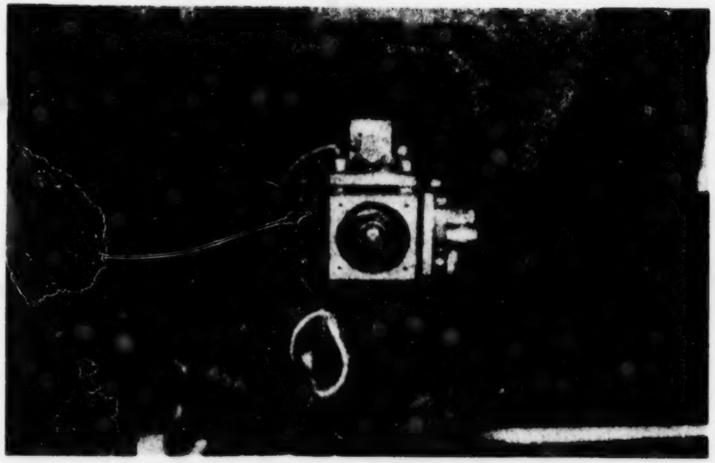

FIGURE 31(a): LOCATION OF ACCELEROMETER ON AXLE BEARING END CAP

Note: All Test Trucks equipped with 'A' profile wheels.
X = Instrumented bearing end caps.
[→] = TV Camera locations.

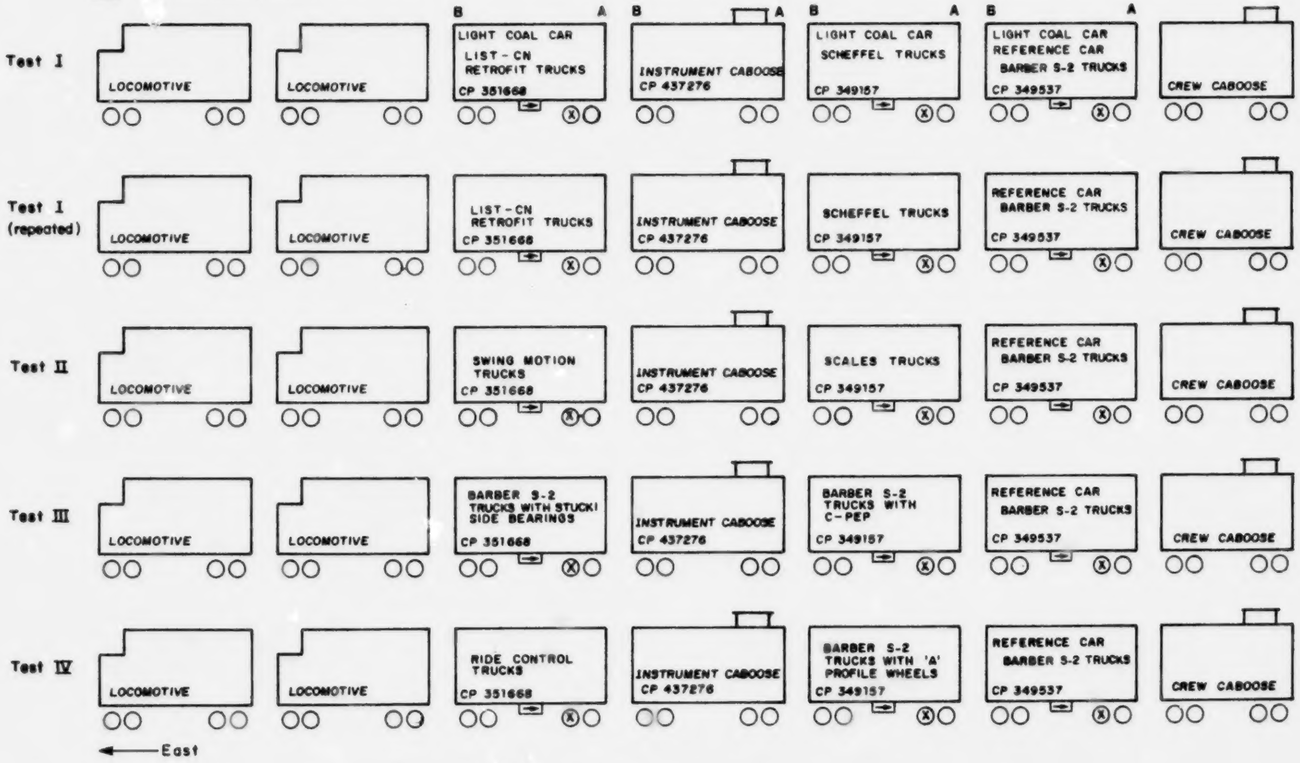
Test I
LOCOMOTIVE
LOCOMOTIVE
B A
LIGHT COAL CAR LIST-CN RETROFIT TRUCKS CP 351668
INSTRUMENT CABOOSE CP 437276
LIGHT COAL CAR SCHEFFEL TRUCKS CP 349157
LIGHT COAL CAR REFERENCE CAR BARBER S-2 TRUCKS CP 349537
CREW CABOOSE
Test I (repeated)
LIST-CN RETROFIT TRUCKS CP 351668
SCHEFFEL TRUCKS CP 349157
REFERENCE CAR BARBER S-2 TRUCKS CP 349537
Test II
SWING MOTION TRUCKS CP 351668
SCALES TRUCKS CP 349157
Test III
BARBER S-2 TRUCKS WITH STUCKI SIDE BEARINGS CP 351668
BARBER S-2 TRUCKS WITH C-PEP CP 349157
Test IV
RIDE CONTROL TRUCKS CP 351668
BARBER S-2 TRUCKS WITH 'A' PROFILE WHEELS CP 349157
X
East

Figure 31(b) - TRAIN CONSISTS FOR HIGH SPEED STABILITY TESTS

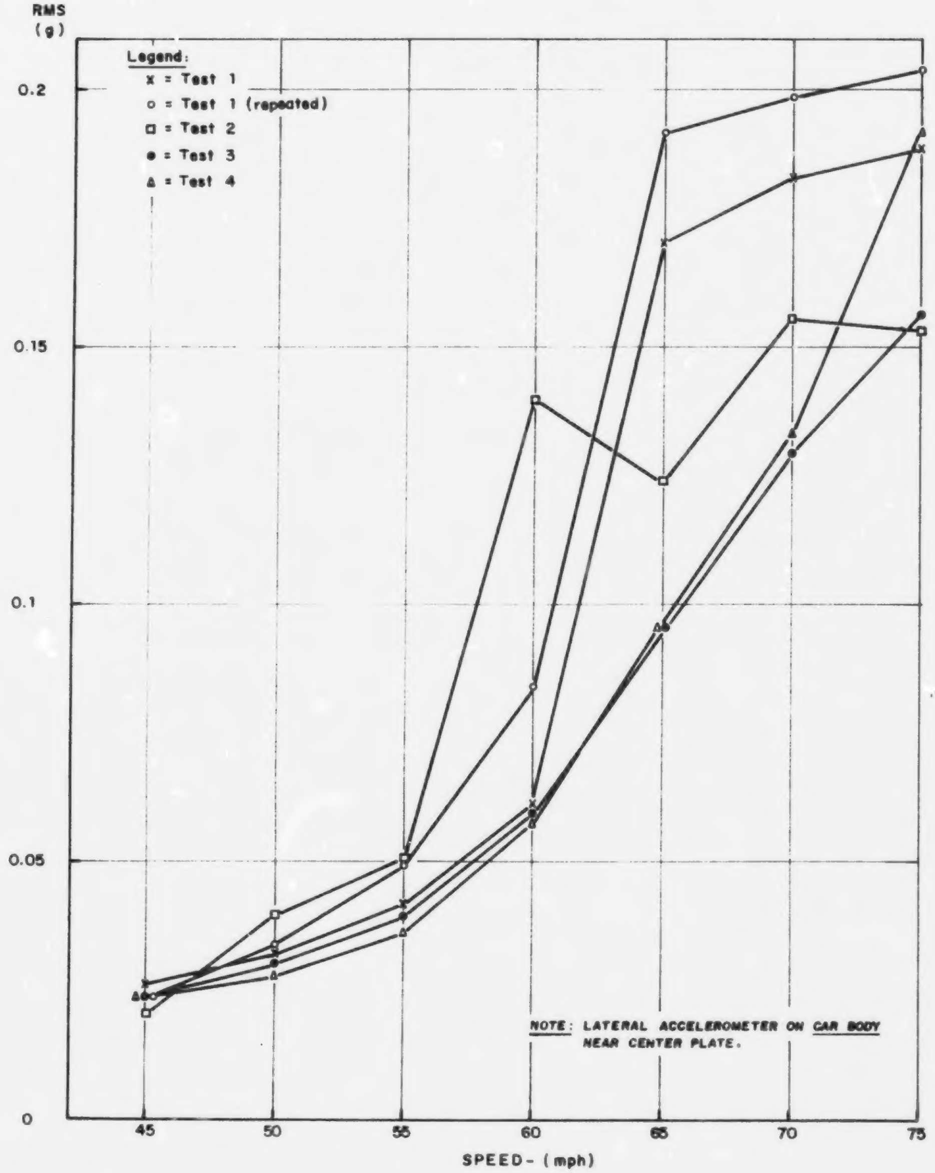

Figure 32 - LATERAL ACCELERATION OF CAR BODY (RMS (g)) VS SPEED FOR BARBER S-2 REFERENCE TRUCK

(5 Tests)

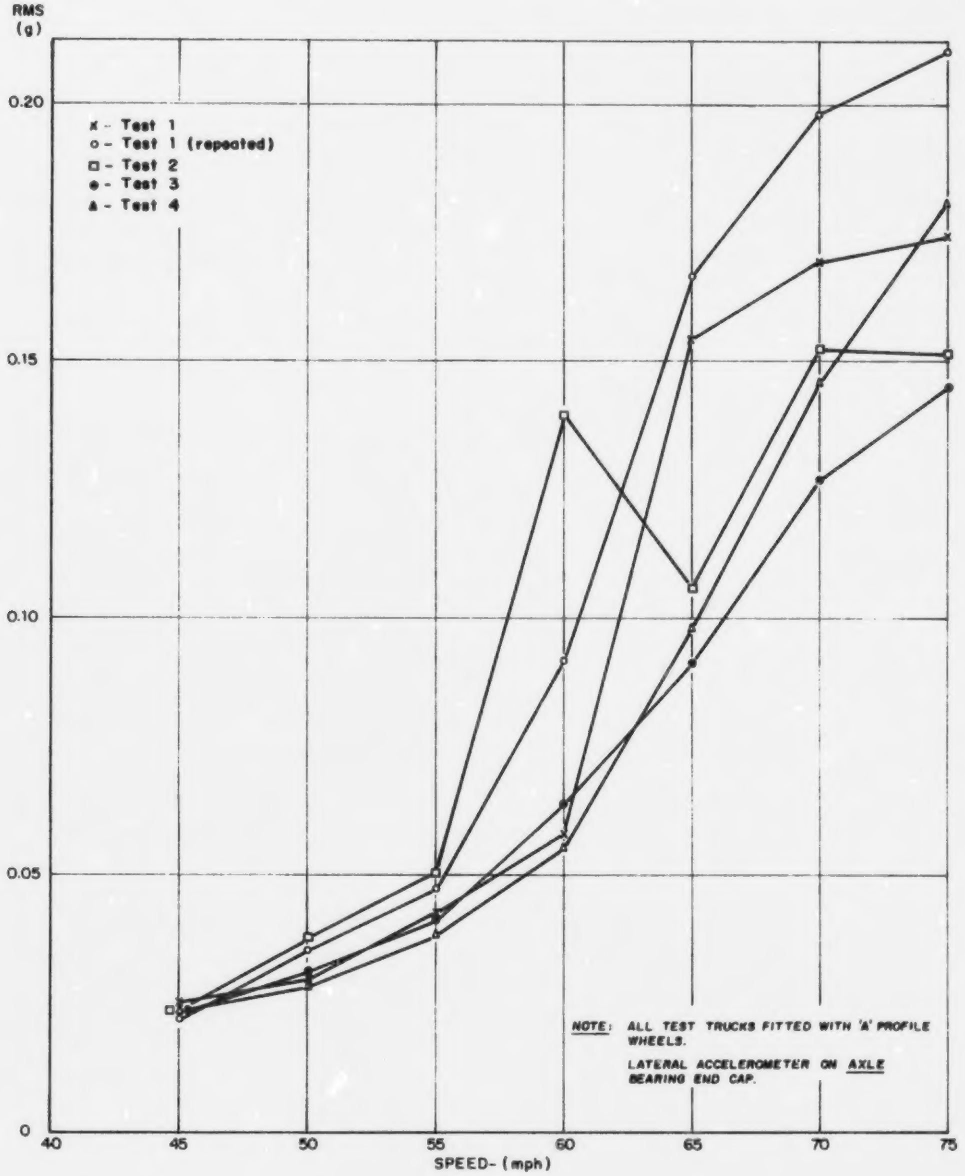

NOTE: ALL TEST TRUCKS FITTED WITH 'A' PROFILE WHEELS.

LATERAL ACCELEROMETER ON AXLE BEARING END CAP.

Figure 33 - LATERAL ACCELERATION ON AXLE BEARING END CAP (RMS (g)) VS SPEED FOR BARBER S-2 REFERENCE TRUCK (5 Tests)

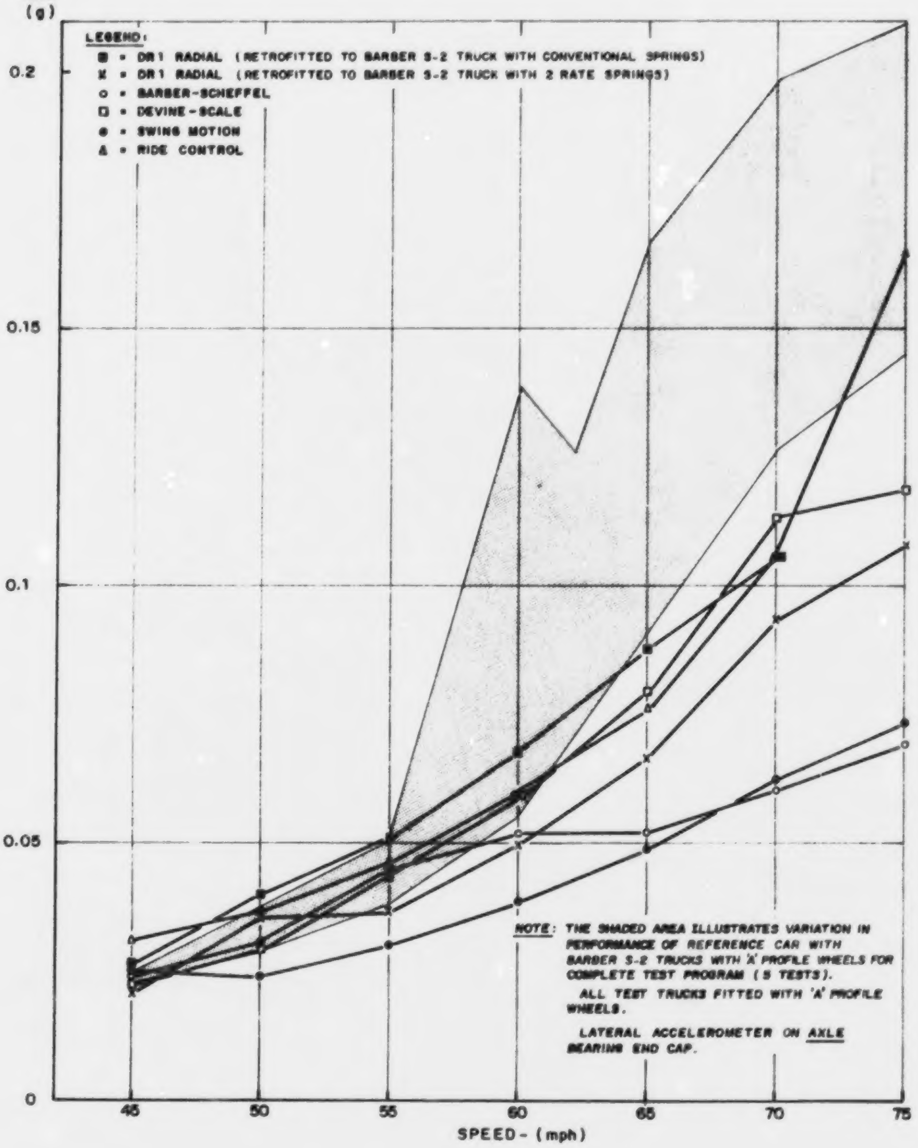

NOTE: THE SHADED AREA ILLUSTRATES VARIATION IN PERFORMANCE OF REFERENCE CAR WITH BARBER S-2 TRUCKS WITH 'A' PROFILE WHEELS FOR COMPLETE TEST PROGRAM (5 TESTS).

ALL TEST TRUCKS FITTED WITH 'A' PROFILE WHEELS.

LATERAL ACCELEROMETER ON AXLE BEARING END CAP.

Figure 34- LATERAL ACCELERATION ON AXLE BEARING END CAP (RMS (g)) VS SPEED FOR VARIOUS TEST TRUCKS

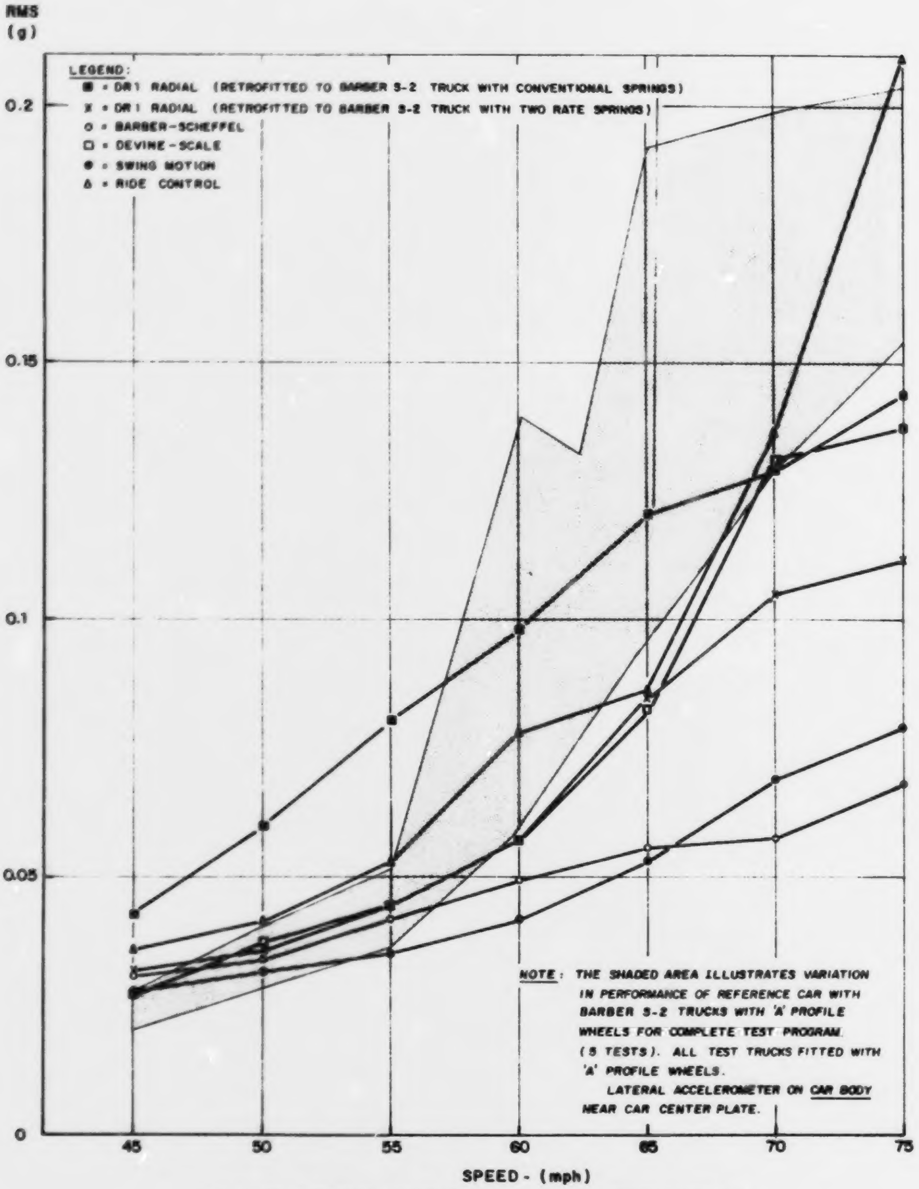

NOTE: THE SHADED AREA ILLUSTRATES VARIATION IN PERFORMANCE OF REFERENCE CAR WITH BARBER S-2 TRUCKS WITH 'A' PROFILE WHEELS FOR COMPLETE TEST PROGRAM. (5 TESTS). ALL TEST TRUCKS FITTED WITH 'A' PROFILE WHEELS.

LATERAL ACCELEROMETER ON CAR BODY NEAR CAR CENTER PLATE.

Figure 35 - LATERAL ACCELERATION OF CAR BODY (RMS (g)) VS SPEED FOR VARIOUS TEST TRUCKS

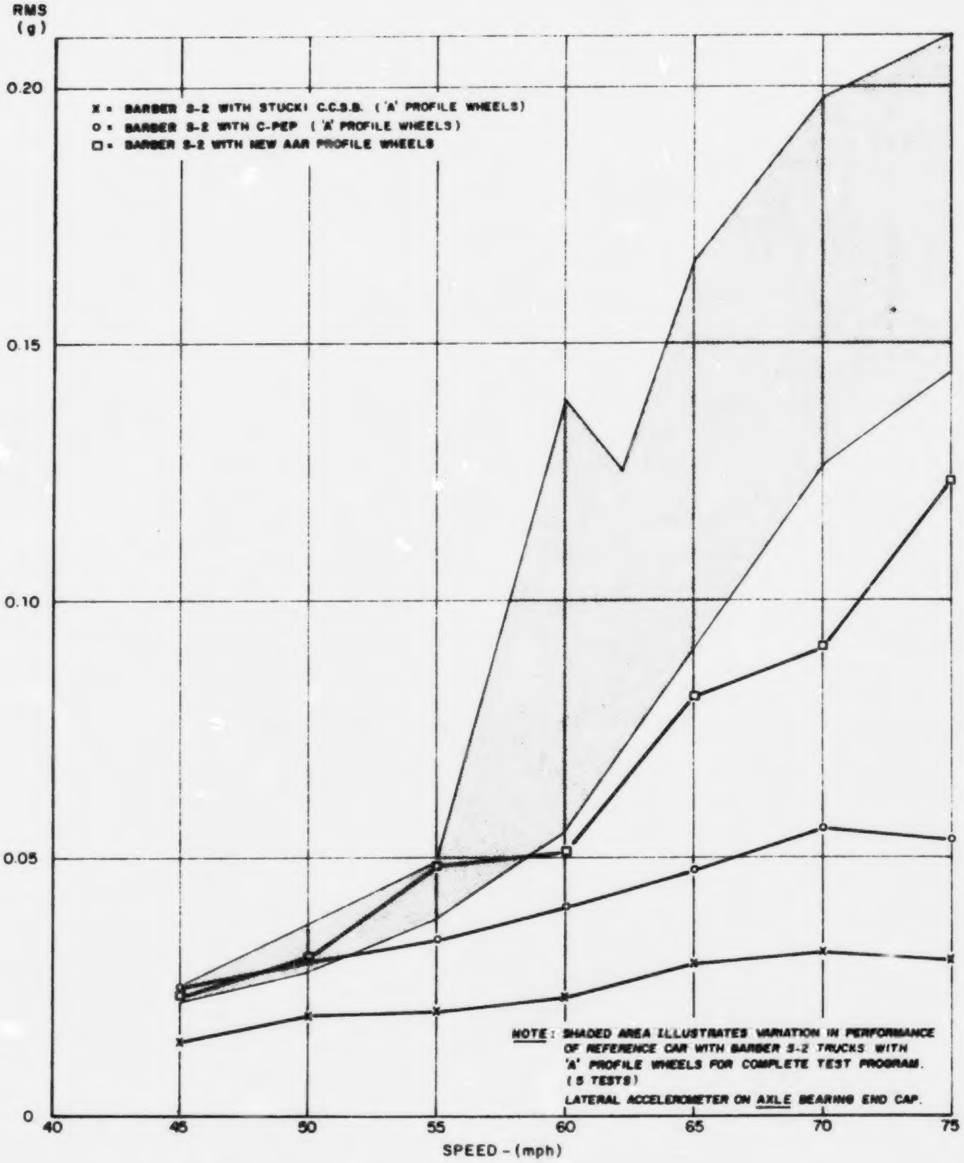

Figure 36 - EFFECT OF C.C.S.B., C-PEP AND NEW PROFILE AAR WHEELS ON BARBER S-2 TRUCKS
(5 Tests)

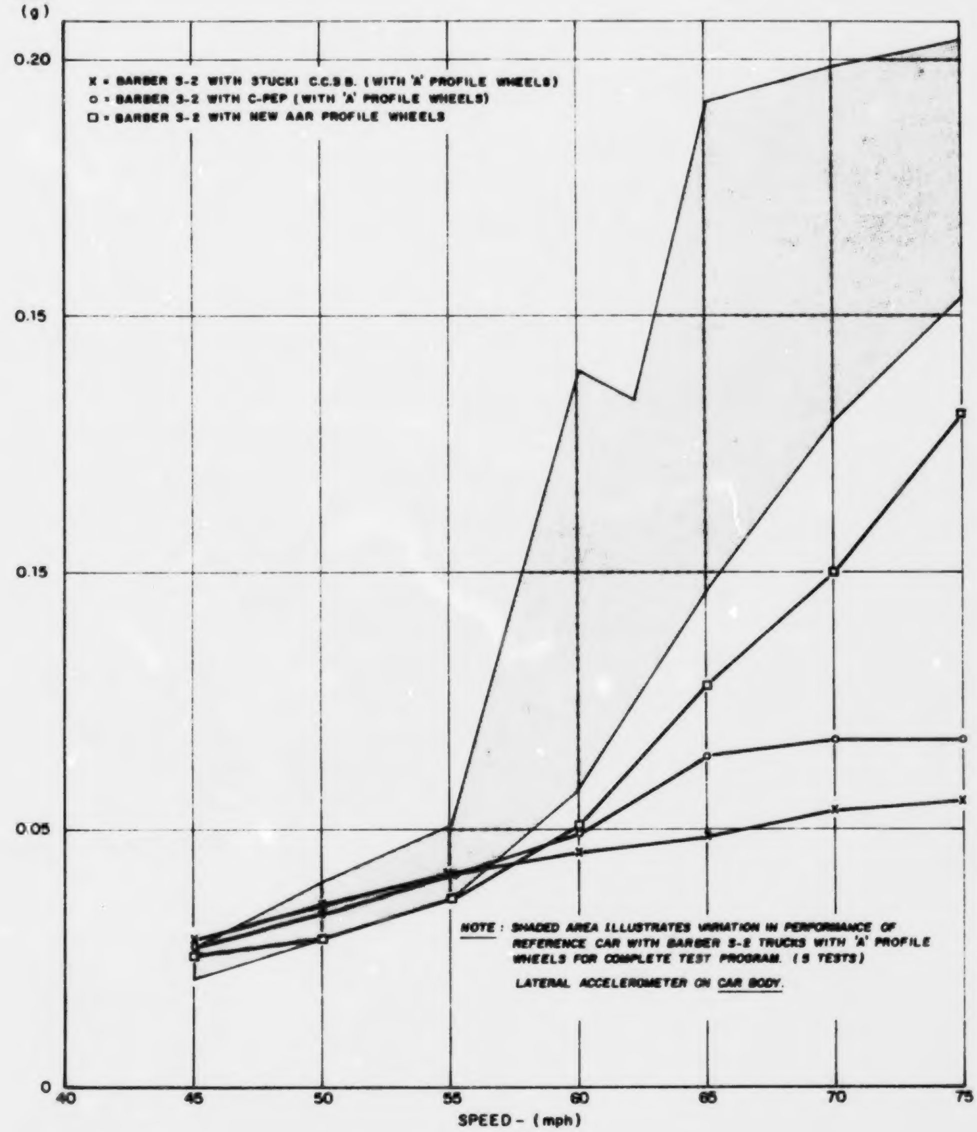

NOTE : SHADED AREA ILLUSTRATES VARIATION IN PERFORMANCE OF REFERENCE CAR WITH BARBER S-2 TRUCKS WITH 'A' PROFILE WHEELS FOR COMPLETE TEST PROGRAM. (5 TESTS)

LATERAL ACCELEROMETER ON CAR BODY.

Figure 37 – EFFECT OF C.C.S.B., C-PEP AND NEW PROFILE AAR WHEELS ON BARBER S-2 TRUCKS

(5 Tests)

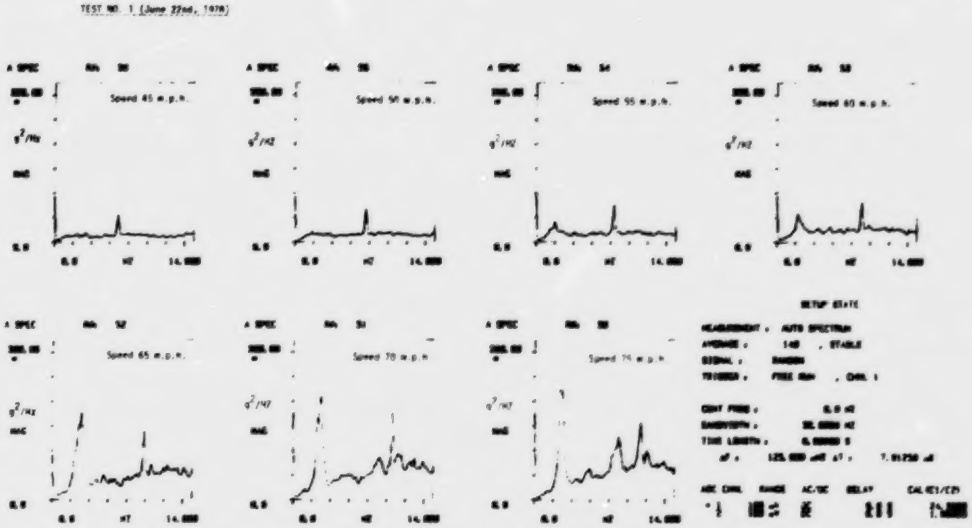

FIGURE 38: P.S.D. OF LATERAL ACCELEROMETER OUTPUT ON THE AXLE OF THE BARBER S-2 TRUCK (REFERENCE TRUCK)

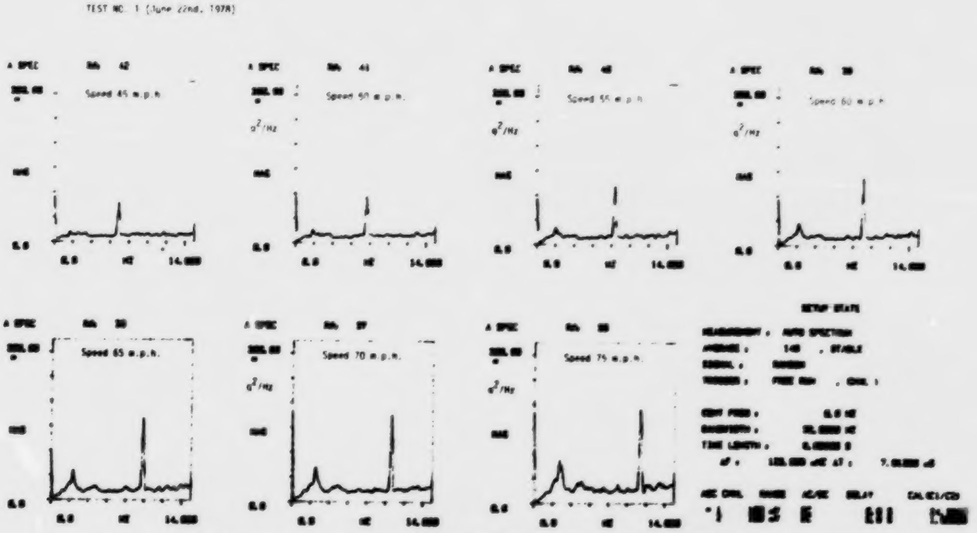

FIGURE 39: P.S.D. OF THE LATERAL ACCELEROMETER OUTPUT ON THE AXLE OF THE BARBER-SCHEFFEL TRUCK

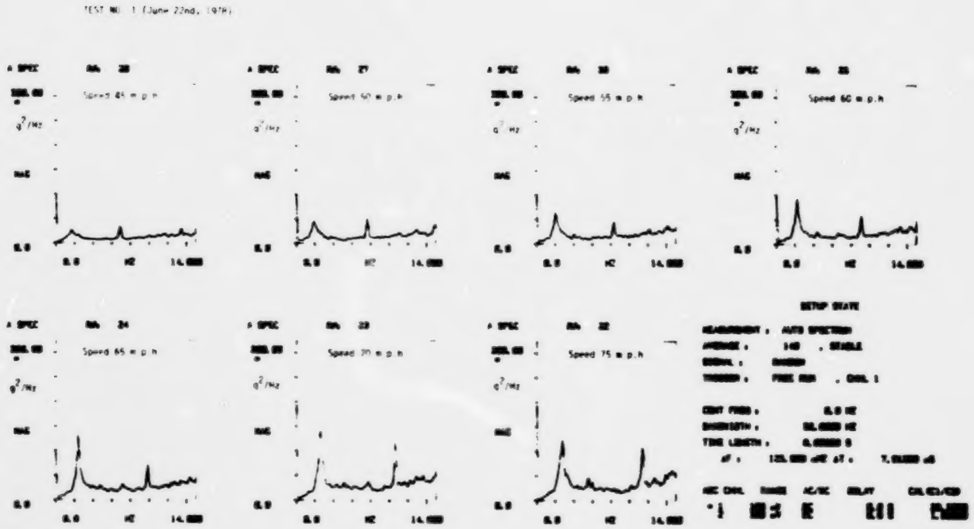

FIGURE 40: P.S.D. OF THE LATERAL ACCELEROMETER OUTPUT ON THE AXLE OF DR-1 (RETROFIT TO BARBER S-2 TRUCK WITH CONVENTIONAL SPRINGS)

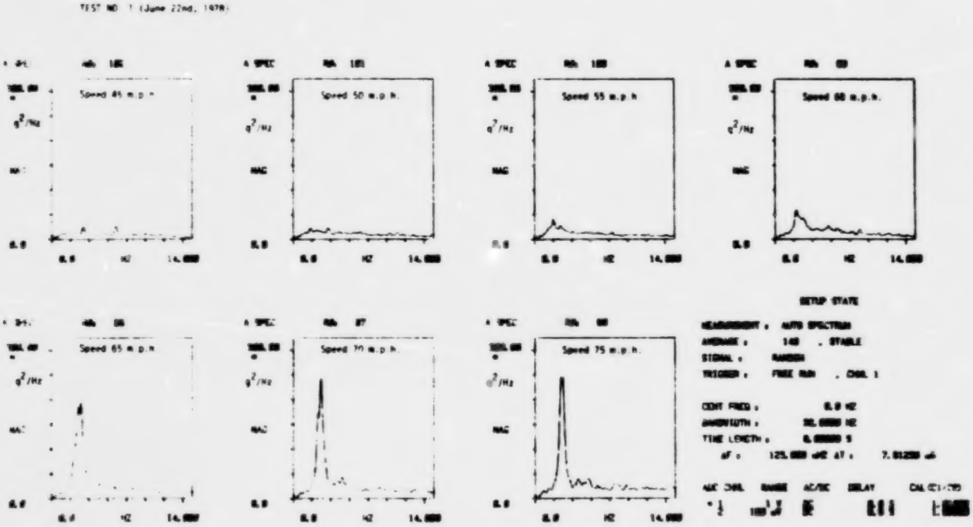

FIGURE 41: P.S.D. OF THE LATERAL ACCELEROMETER OUTPUT ON THE CAR BODY OF THE REFERENCE CAR WITH BARBER S-2 TRUCKS

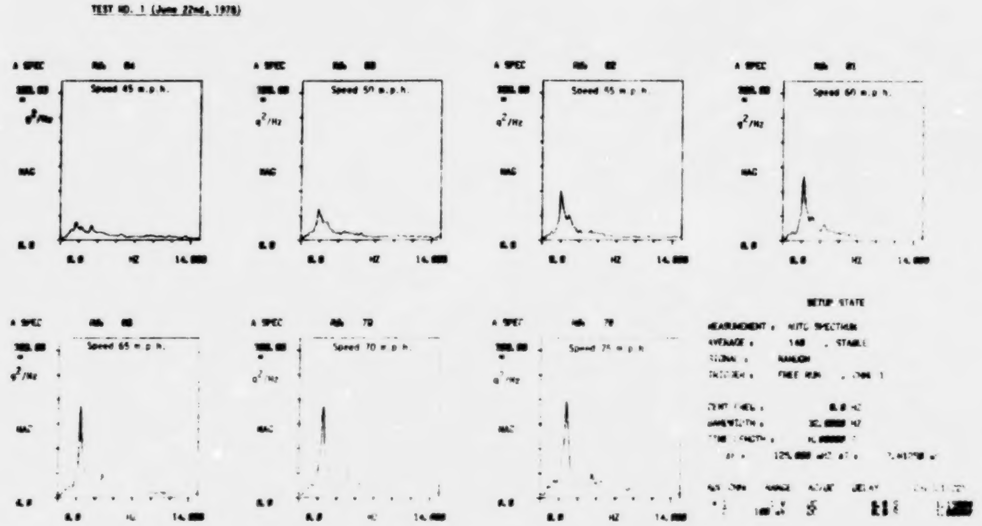

FIGURE 42: P.S.D. OF THE LATERAL ACCELEROMETER OUTPUT ON THE CAR BODY OF THE CAR WITH DR-1 TRUCKS (RETROFIT TO BARBER S-2 TRUCK WITH CONVENTIONAL SPRINGS)

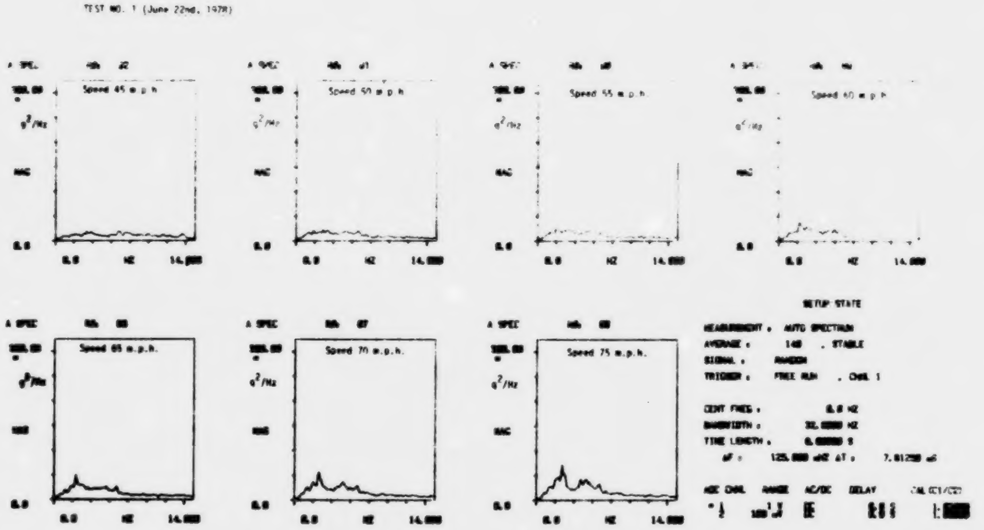

FIGURE 43: P.S.D. OF THE LATERAL ACCELEROMETER OUTPUT ON THE CAR BODY OF THE CAR WITH BARBER-SCHEFFEL TRUCKS

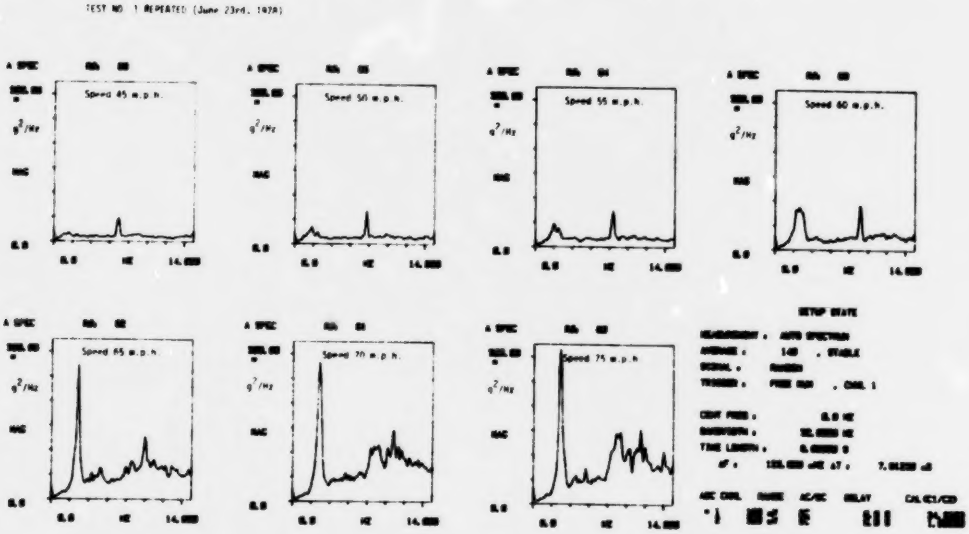

FIGURE 44: P.S.D. OF THE LATERAL ACCELEROMETER OUTPUT ON THE AXLE OF THE BARBER S-2 TRUCK (REFERENCE TRUCK)

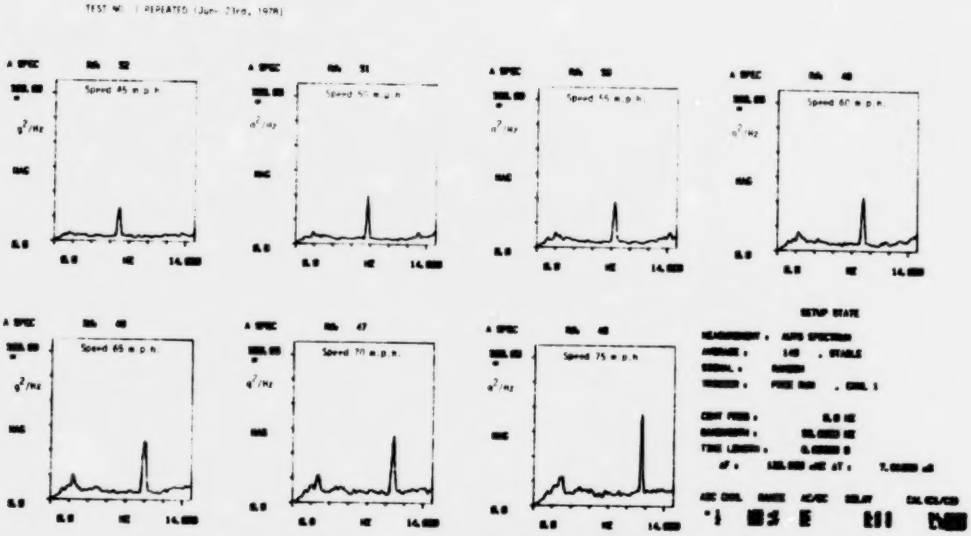

FIGURE 45: P.S.D. OF THE LATERAL ACCELEROMETER OUTPUT ON THE AXLE OF THE BARBER-SCHEFFEL TRUCK

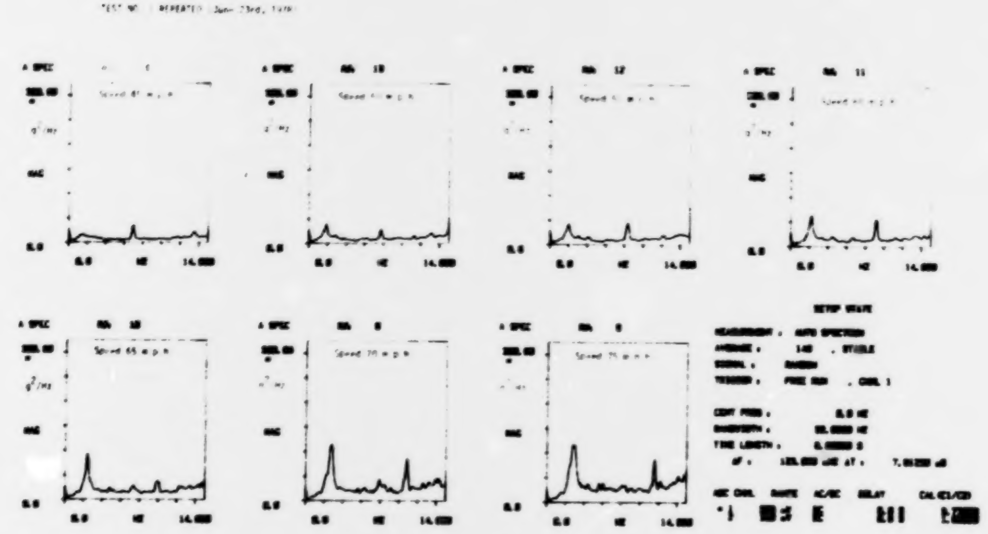

FIGURE 46: P.S.D. OF THE LATERAL ACCELEROMETER OUTPUT ON THE AXLE OF THE DR-1 TRUCK (RETROFIT TO BARBER S-2 TRUCK WITH TWO RATE SPRINGS)

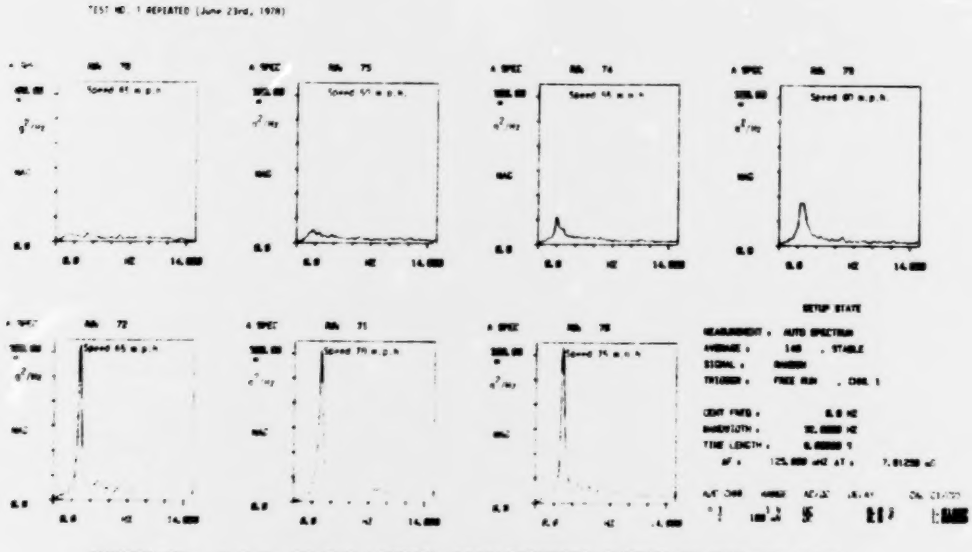

FIGURE 47: P.S.D. OF THE LATERAL ACCELEROMETER OUTPUT ON THE CAR BODY OF THE REFERENCE CAR WITH BARBER S-2 TRUCKS

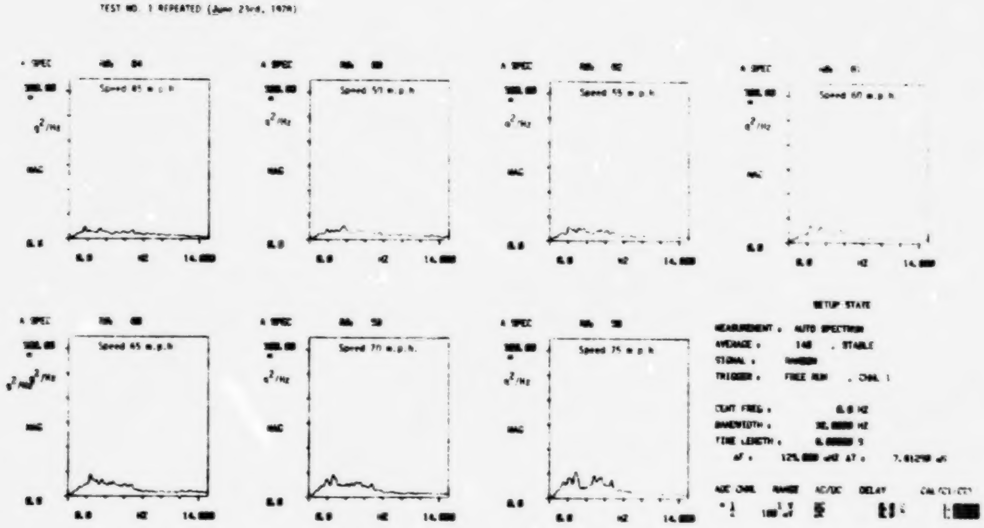

FIGURE 48: P.S.D. OF THE LATERAL ACCELEROMETER OUTPUT ON THE CAR BODY OF THE CAR WITH BARBER-SCHEFFEL TRUCKS

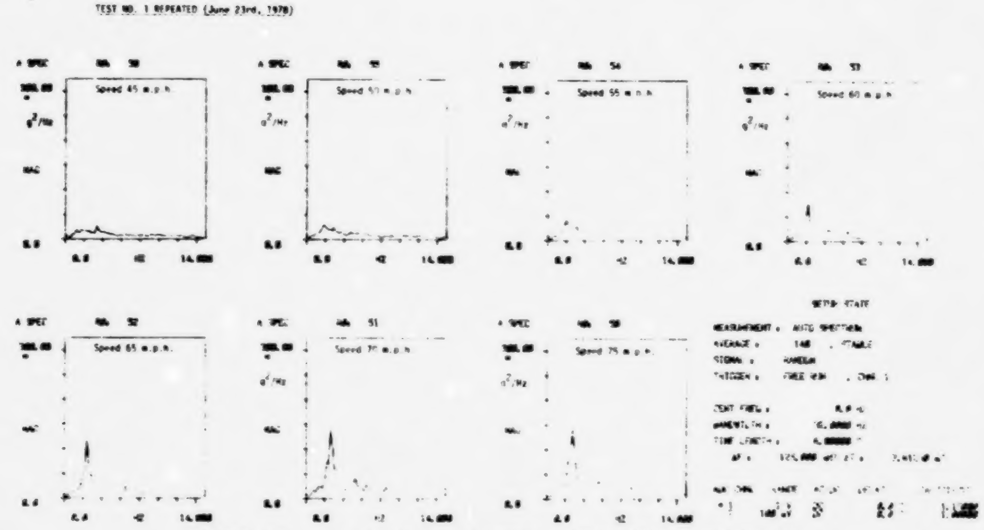

FIGURE 49: P.S.D. OF THE LATERAL ACCELEROMETER OUTPUT ON THE CAR BODY OF THE CAR WITH DR-1 TRUCKS (RETROFITTED TO BARBER S-2 TRUCKS WITH TWO RATE SPRINGS)

TEST NO. 2 (June 24th, 1978)

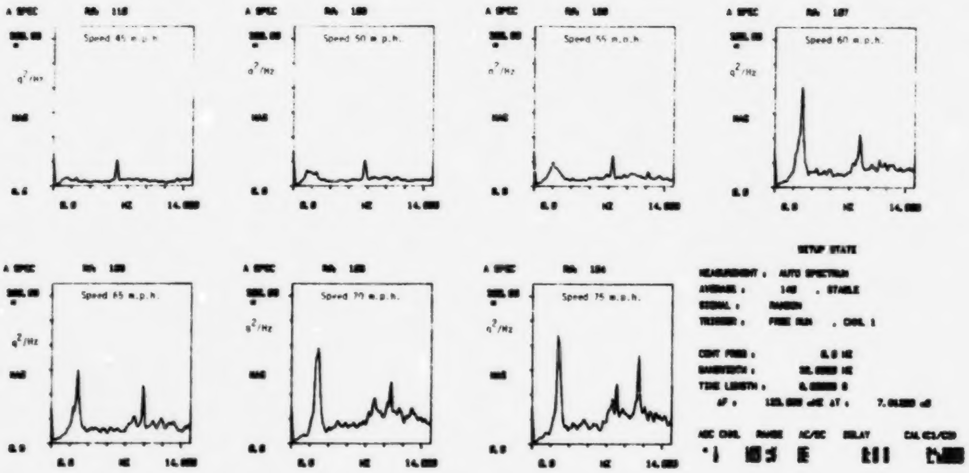

FIGURE 50: P.S.D. OF THE LATERAL ACCELEROMETER OUTPUT ON THE AXLE OF THE BARBER S-2 TRUCK (REFERENCE TRUCK)

TEST NO. 2 (June 24th, 1978)

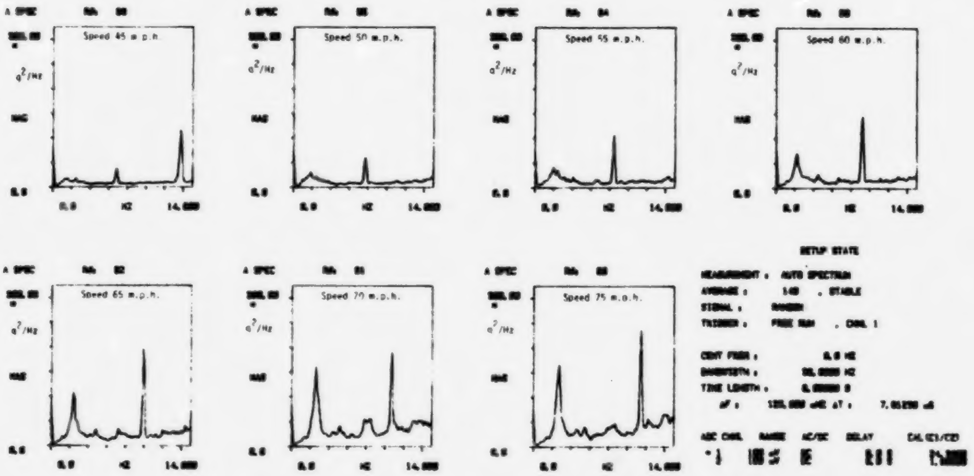

FIGURE 51: P.S.D. OF THE LATERAL ACCELEROMETER OUTPUT ON THE AXLE OF THE DEVINE-SCALES TRUCK

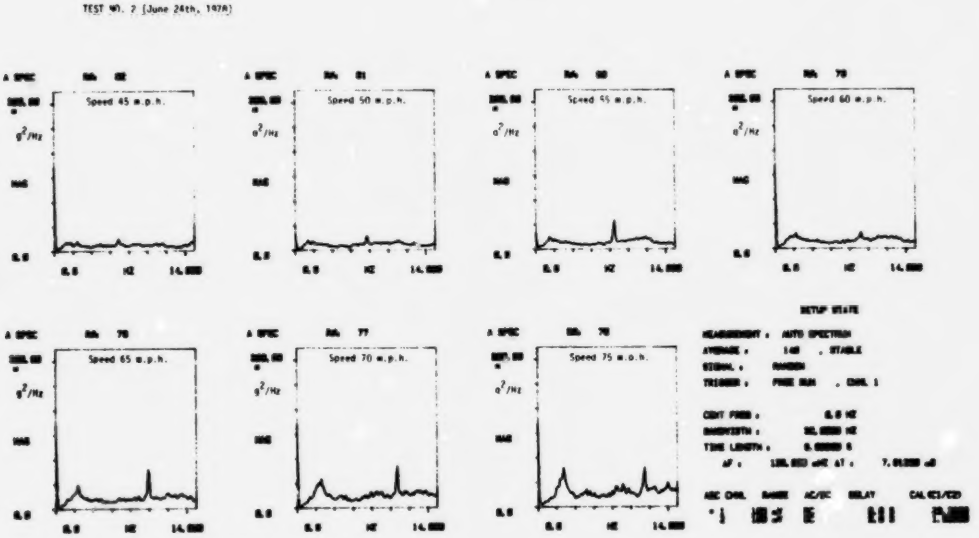

FIGURE 52: P.S.D. OF THE LATERAL ACCELEROMETER OUTPUT ON THE AXLE OF THE SWING MOTION TRUCK

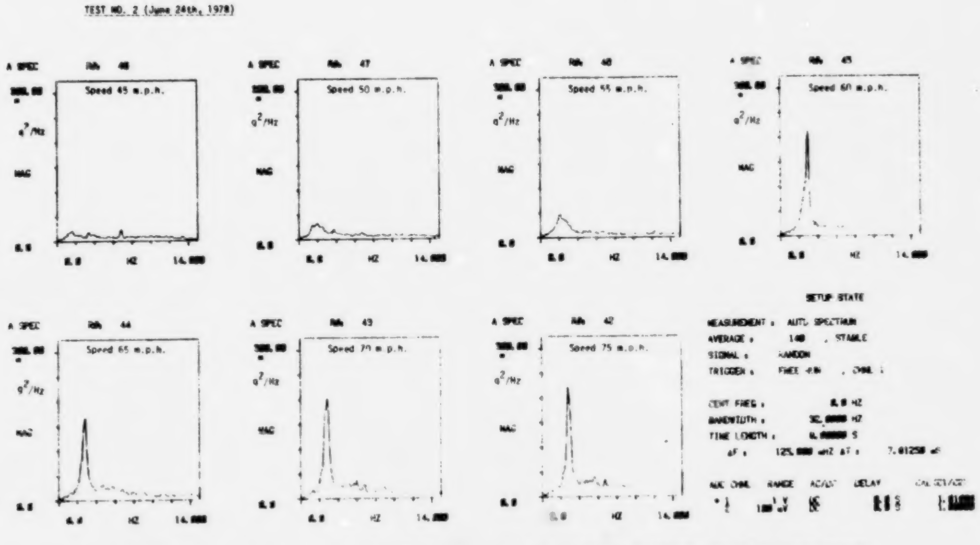

FIGURE 53: P.S.D. OF THE LATERAL ACCELEROMETER OUTPUT ON THE CAR BODY OF THE CAR WITH BARBER S-2 TRUCKS (REFERENCE TRUCK)

TEST NO. 2 (June 24th, 1978)

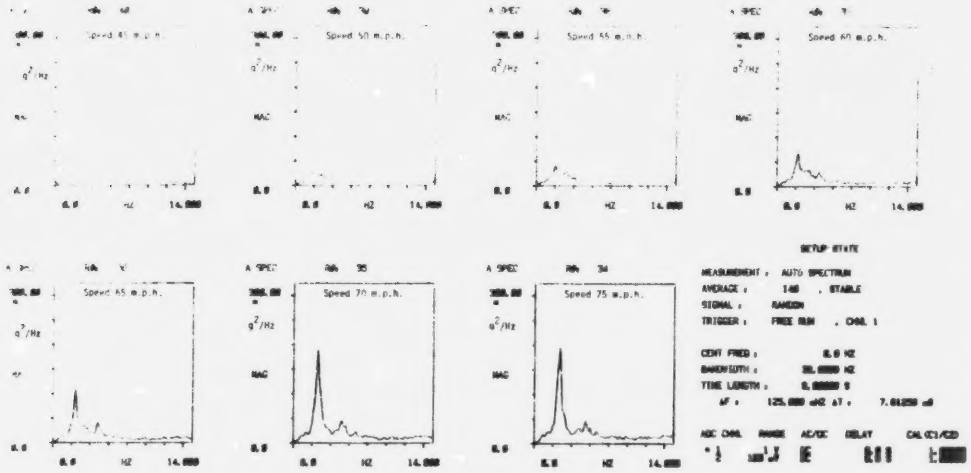

FIGURE 54: P.S.D. OF THE LATERAL ACCELEROMETER OUTPUT ON THE CAR BODY OF THE CAR WITH DEVINE-SCALES TRUCKS

TEST NO. 2 (June 24th, 1978)

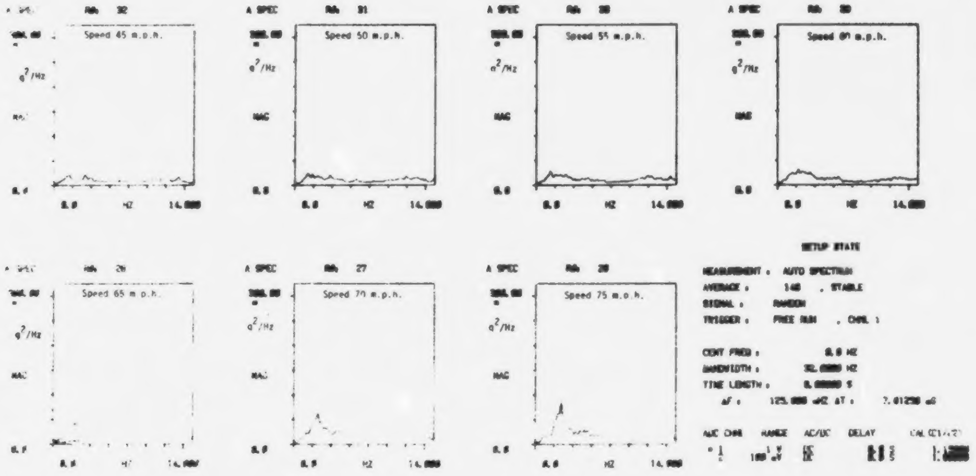

FIGURE 55: P.S.D. OF THE LATERAL ACCELEROMETER OUTPUT ON THE CAR BODY OF THE CAR WITH SWING MOTION TRUCKS

TEST NO. 3 (June 27th, 1978)

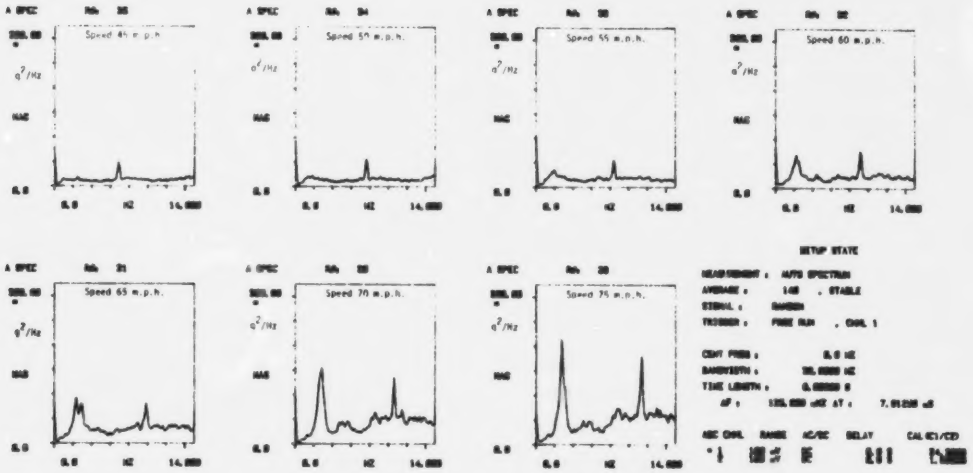

FIGURE 56: P.S.D. OF THE LATERAL ACCELEROMETER OUTPUT ON THE AXLE OF THE BARBER S-2 TRUCK (REFERENCE TRUCK)

TEST NO. 3 (June 27th, 1978)

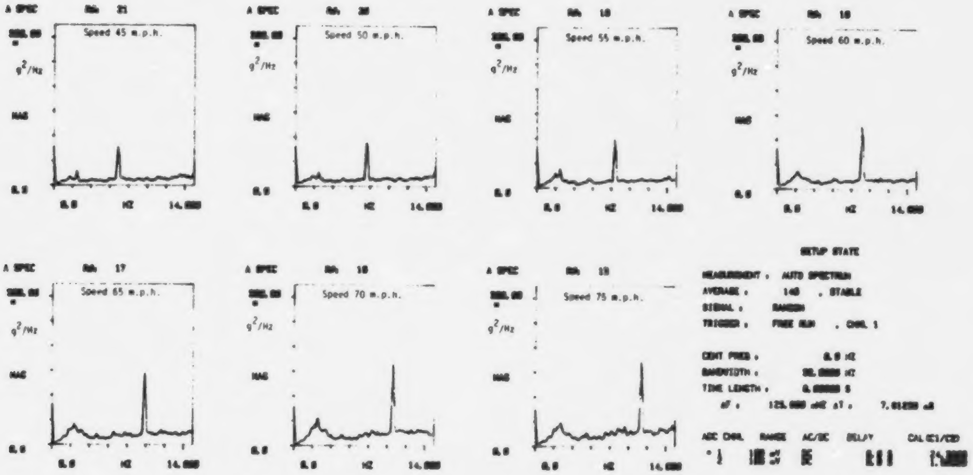

FIGURE 57: P.S.D. OF THE LATERAL ACCELEROMETER OUTPUT ON THE AXLE OF THE BARBER S-2 TRUCK WITH C-PEP

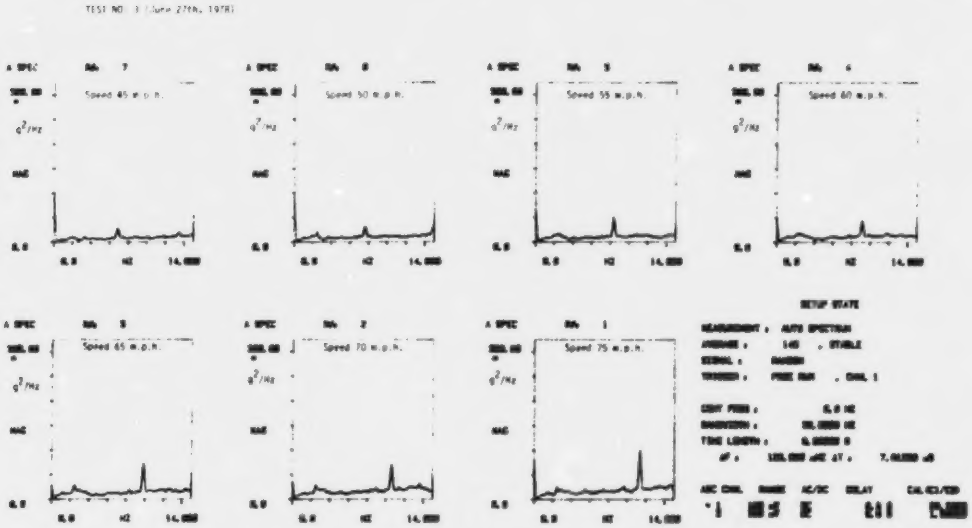

FIGURE 58: P.S.D. OF THE LATERAL ACCELEROMETER OUTPUT ON THE AXLE OF THE BARBER S-2 TRUCK WITH STUCKI C.C.S.B.

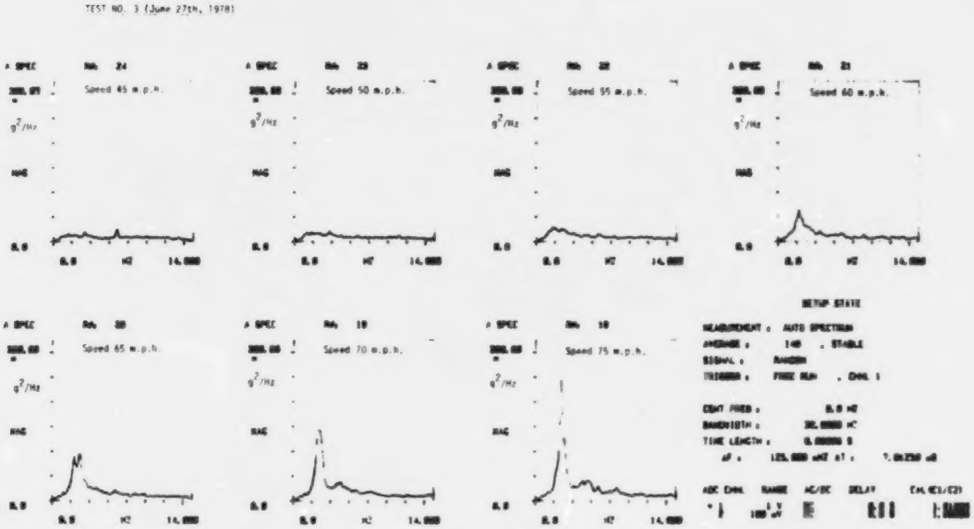

FIGURE 59: P.S.D. OF THE LATERAL ACCELEROMETER OUTPUT ON THE CAR BODY OF THE CAR WITH BARBER S-2 TRUCKS (REFERENCE TRUCK)

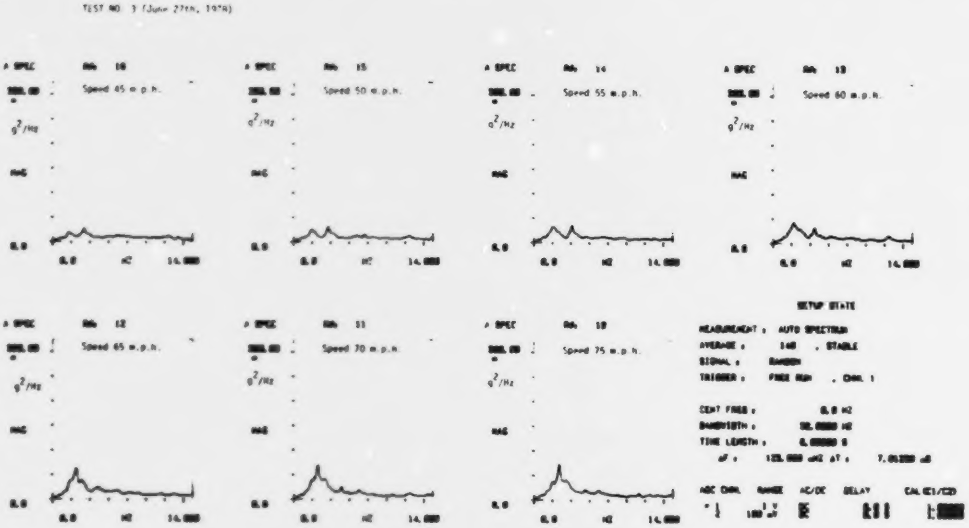

FIGURE 60: P.S.D. OF THE LATERAL ACCELEROMETER OUTPUT ON THE CAR BODY OF THE CAR WITH BARBER S-2 TRUCKS WITH C-PEP

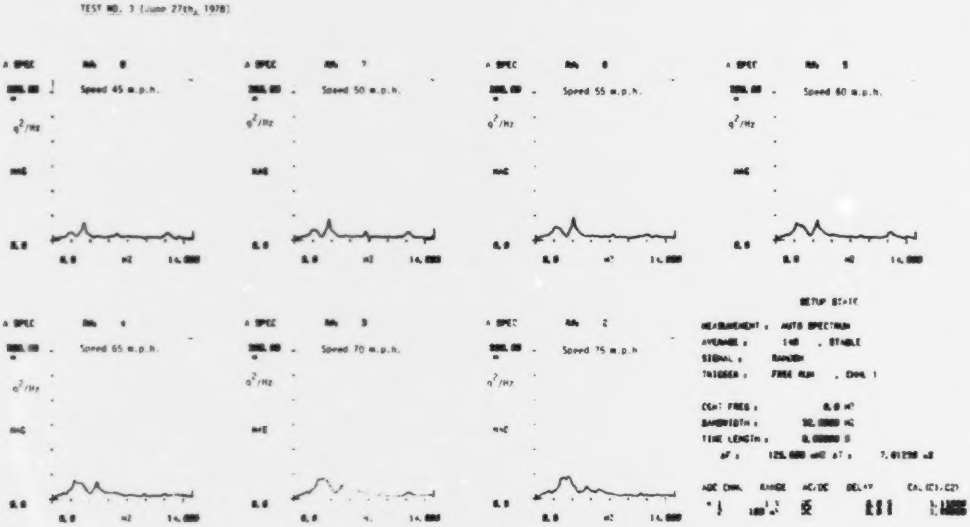

FIGURE 61: P.S.D. OF THE LATERAL ACCELEROMETER OUTPUT ON THE CAR BODY OF THE CAR WITH BARBER S-2 TRUCKS WITH STUCKI C.C.S.B.

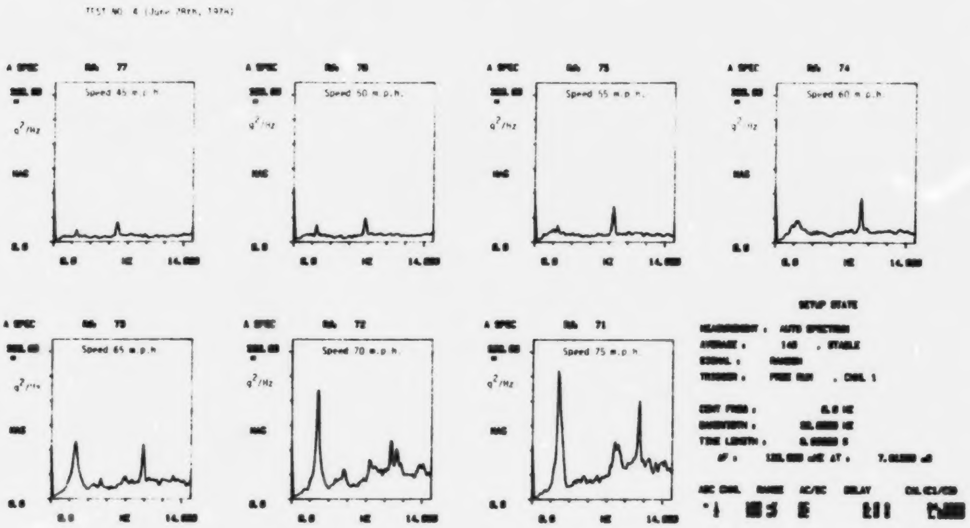

FIGURE 62: P.S.D. OF THE LATERAL ACCELEROMETER OUTPUT ON THE AXLE OF THE BARBER S-2 TRUCK (REFERENCE TRUCK)

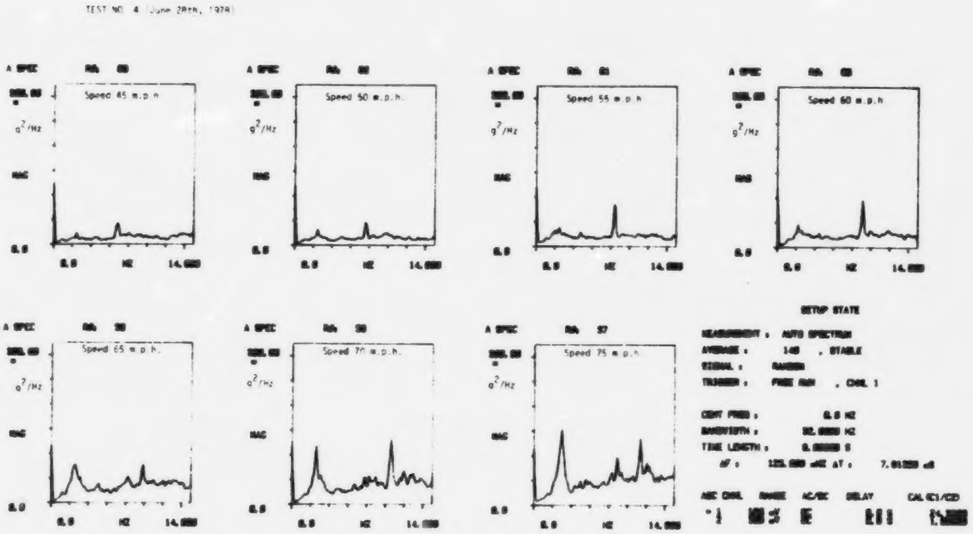

FIGURE 63: P.S.D. OF THE LATERAL ACCELEROMETER OUTPUT ON THE BARBER S-2 TRUCK WITH NEW AAR WHEELS

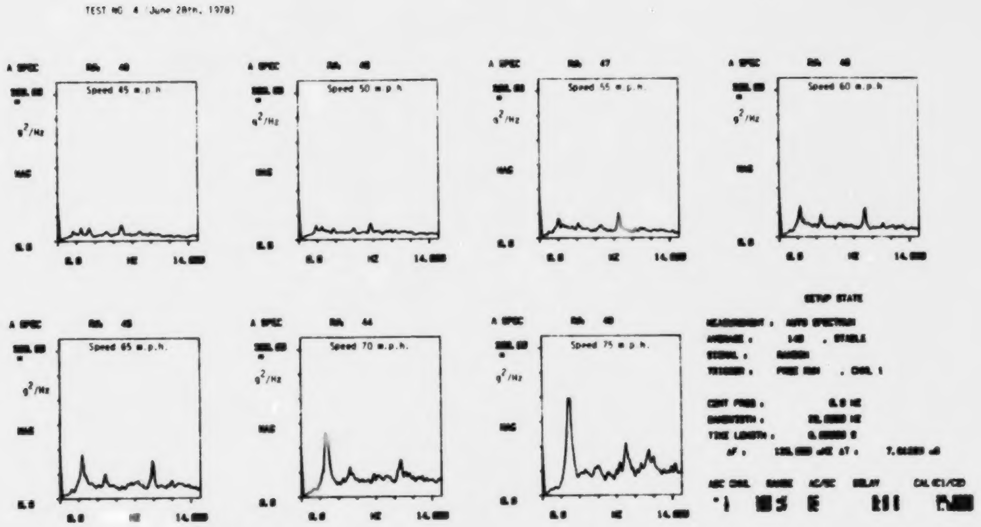

FIGURE 64: P.S.D. OF THE LATERAL ACCELEROMETER OUTPUT ON THE AXLE OF THE RIDE CONTROL TRUCK

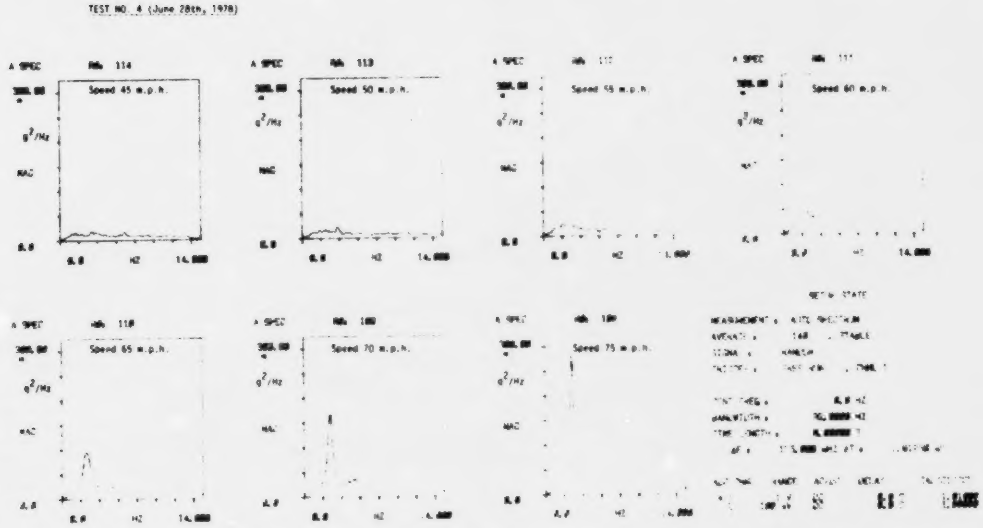

FIGURE 65: P.S.D. OF THE LATERAL ACCELEROMETER OUTPUT ON THE CAR BODY OF THE CAR WITH BARBER S-2 TRUCKS (REFERENCE TRUCK)

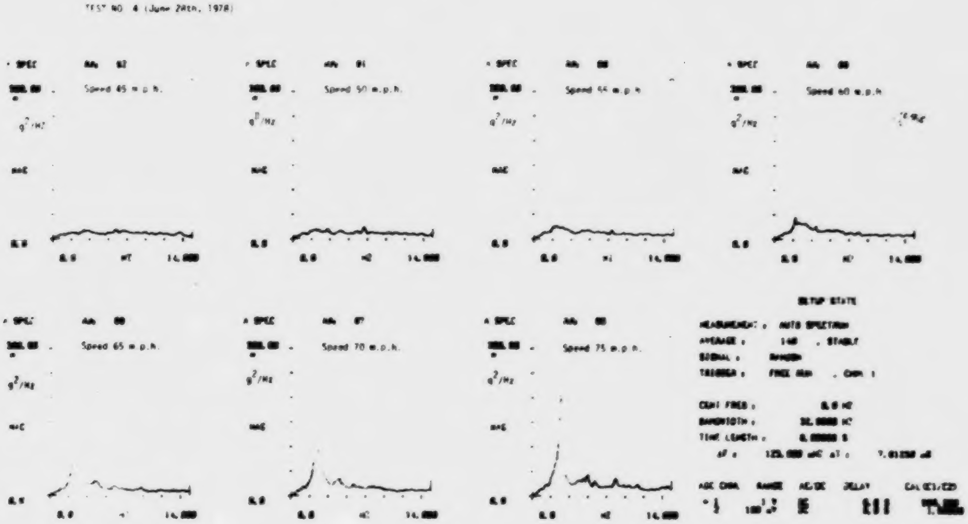

FIGURE 66: P.S.D. OF THE LATERAL ACCELEROMETER OUTPUT ON THE CAR BODY OF THE CAR WITH BARBER S-2 TRUCKS WITH NEW AAR WHEELS

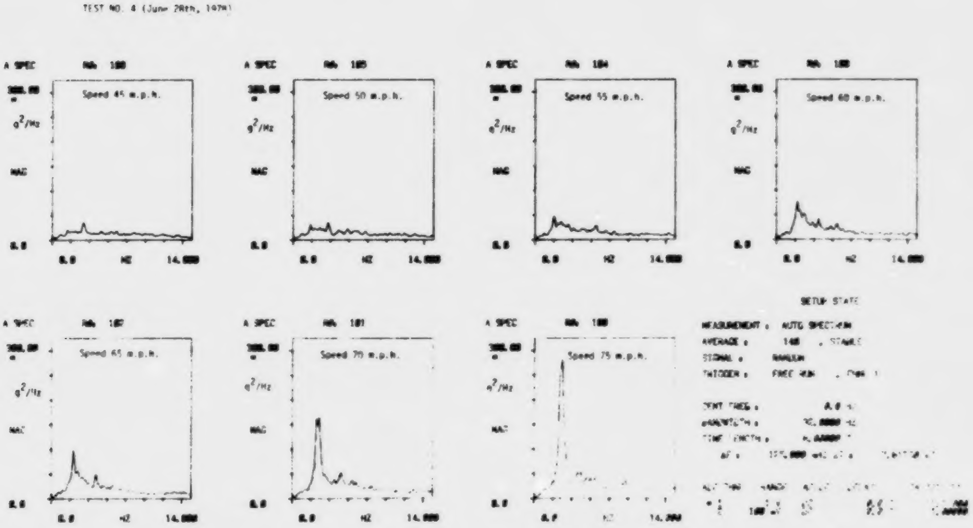

FIGURE 67: P.S.D. OF THE LATERAL ACCELEROMETER OUTPUT ON THE CAR BODY OF THE CAR WITH RIDE CONTROL TRUCKS

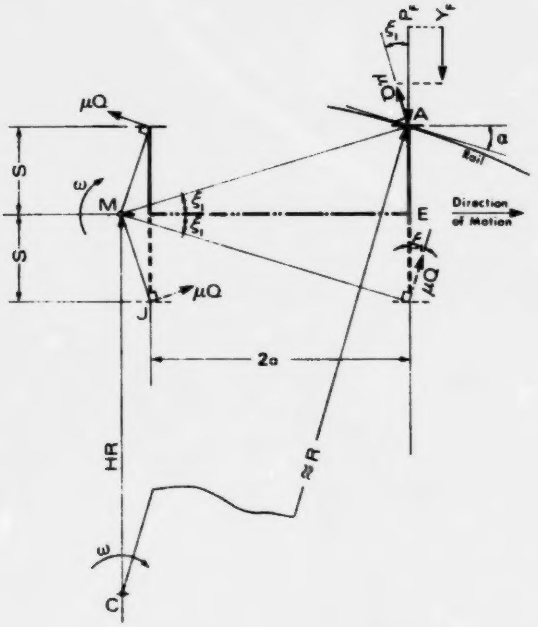
Y_f
P_f
ξ_1
μQ
A
α
Rail
μQ
S
S
ω
M
ξ_1
ξ_1
E
Direction of Motion
ξ_1
μQ
J
μQ
D
2a
HR
$\approx R$
ω
C

M = *Friction Force Centre*
P_f = *Flange Force*
Y_f = *Guiding Force*
μ = *Coefficient of Sliding Friction*
Q = *Vertical Load*
α = *Angle-of-Attack*
C = *Curve Center*
HR = *Radius of the Curve negotiated by the vehicle*
R = *Radius of the Curve through which the vehicle moves under steady state conditions*

Figure 68 - FORCES ACTING ON WHEELSETS OF A TRUCK IN A CURVE

J. Robert

Effect of Unsprung Weight on Vertical Track Dynamics

ABSTRACT: With recent studies concerning the development of a high speed passenger service in the major population corridor between Quebec City and Windsor, there is increasing interest in the effects of high speed trains on track structure. In this context the Chief Engineer, CP Rail requested the Technical Research group to undertake a study to define the effect of unsprung weight upon vertical track forces. The Transport Canada Research and Development Centre (TDC) was approached about including this area under the terms of an existing Track/Train Dynamics contract and subsequently agreed. An interim review of the work completed is summarized in the following pages.

A methodology has been developed which will enable us to investigate the influence of various equipment and track parameters upon dynamic force levels. Before more detailed work can be initiated it will be necessary to obtain a comprehensive plot of the spectral distribution of track irregularities for typical Canadian jointed and continuous rail.

Introduction

With increasing train speed vertical dynamic forces on the track are becoming of increasing concern. Locomotive dynamic forces are superimposed on the already heavy static axle loading. In particular, unsprung weight, which is not insulated from the shocks of the ride by any suspension element, is thought to give rise to large forces at high speed.

Review of Literature Search

The approaches taken by railroads from various countries regarding vertical dynamics were reviewed: Japan, France, England, Russia. Attention was paid especially to the British and Russian programs since they were well described in the available literature.

British Railways has studied the effect of unsprung weight on dynamic loading (Nield and Goodwin, 1969) and designed a computer program to simulate a wheelset passing a rail joint. Field tests were performed which validated the model. Canadian National Railways used the British program with some input specifications of their own vehicles and track to determine a maximum speed limit for locomotives with a given unsprung weight and static axle load (Radford, 1977). They found that axle hung traction motors were suitable for operation at speeds not much higher than 90 mph. The criterion used was that maximum combined static and dynamic load should not exceed the vertical loading imposed by a GPA-17 passenger diesel locomotive.

Russian scientists (Kogan, 1973) developed a program to fully simulate a locomotive operating on jointed or continuous welded rails. The Soviet computer program was developed to determine how much of the dynamic loading is attributable not only to the unsprung weight, but to the sprung truck and body as well.

Model Description

The USSR model is very comprehensive: it can simulate a complete vehicle on any segment of track. This is why we have decided to employ the Russian computer program with appropriate modifications to assess the effects of unsprung weight and other parameters. The program has been run with two models: complete and simplified.

The first model is pictorially shown in Figure 1a. The track mass is per unit length and includes the rail, the distributed mass of the ties, ballast and part of the sub-grade. The unsprung weight includes the wheels, axles, bearings and part of the traction motor. The following motions are allowed in that model:

- body and truck pitch and bounce,
- wheel bounce,
- deformation of the track considered as a beam on an elastic foundation.

A complete model such as this shows quite a large number of resonance peaks and in order to identify the prevailing resonant frequencies, i.e., to isolate the main bounce frequencies from the pitch frequencies, a simplified model has also been used in this preliminary work. The second model consists of a quarter body mounted on half a truck and a single wheelset as shown in Figure 1b.

Discussion of Computer Model Input

The inputs to the program (both the complete and the simplified model) are the track and vehicle characteristics and a power spectral density plot (PSD) of track irregularities. Vehicle data have been prepared for a number of locomotives including the LRC, the GPA-17, the SD40-2 and for a 100 ton coal car. A data sample for the LRC locomotive is shown in Figure 2a. The track characteristics shown in Figure 2b and used in this preliminary work are those of Russian track, since these were available. Characteristics for Canadian track will be measured or estimated for further work.

Figure 3 shows a power spectral density plot of track irregularities from various countries. The plot is expressed in units of amplitude of irregularities squared per unit band width of wavelength. The PSD plot is actually a spectral analysis of the amplitude of track irregularities for different wavelengths. For example, the PSD plot of track with a dominant sine wavelength of 39 feet would show a relatively high peak at such a wavelength. The depth and dip angle of joints, as adopted by Nield, Goodwin and Radford, can also be represented by a combination of other wavelengths. A PSD plot of typical Canadian track is shown but is incomplete as it does not include the amplitude of irregularities at longer wavelengths. This curve was obtained by processing a signal from an accelerometer mounted on the axle of a car in recent tests carried out near Kamloops, British Columbia. It is planned to establish a complete PSD plot with a track recording car which is equipped to pick up longer wavelengths.

Results

Typical output of the program for simulating a complete model of the LRC locomotive on Russian track is shown in Figure 4. The average value of the dynamic forces, as shown, represents the forces which would be encountered when riding on an ideal track without irregularities. The mean square value is the mean deviation (on a statistical basis) from the average value. Figure 5 illustrates the situation for axle No. 4, which is the leading axle.

The program has been modified to plot the power spectral density of the wheel-rail force using the simplified model, as shown in Figure 6. Four important resonances can be identified from this curve and are sketched in Figure 7. The first peak is body bounce which occurs at about 1 Hz in this example. The second peak is truck bounce at about 4 Hz whilst the body is responding with relatively small amplitude. A third resonance peak occurs at about 18 Hz and is excited mainly by track irregularities of 10 foot wavelength when travelling at 120 mph. This peak is caused by the unsprung mass and the track mass oscillating in phase. These two masses also resonate out of phase at 120 Hz, that is they move toward each other and then away from each other, the contact zone providing a stiff spring between the two masses. Vehicle suspension stiffness and track modulus do not influence this fourth resonance peak since they are negligible when compared to the contact stiffness.

The mean deviation of the dynamic loads from the average load is the area under the curve of Figure 6. The relative magnitudes of dynamic loads from the four resonance peaks are shown as a bar graph on Figure 8. The root mean square (RMS) level of forces corresponds to the mean deviation and is the force level that would be exceeded during 16% of the ride, whilst the peak level represented on the second graph would be exceeded during 0.6% of the ride. Although body bounce produced the largest peak, in the diagram shown in Figure 6, its resonance frequency has such a narrow bandwidth that it is actually responsible for only a small portion of the total dynamic loading.

Future Work

A more extensive analysis will begin once the characteristics and the PSD plot of typical Canadian track are obtained. It will then be possible to simulate the effect of some changes to the vehicle or to the track and to establish a comparison between various vehicles, including locomotives and cars. Some simple field tests may be required to assess the validity of the theory. Finally, it will be necessary to estimate the effect of the vertical forces on track maintenance.

References

Kogan A.Y. 1973 "Track Design Allowing for Vertical Dynamic Load" (Translated from Russian) Proceedings of the All Union Scientific Research Institute of Railway Transportation, No. 502, 1973.

Nield B.J. and Goodwin W.H. (British Railways) 1969 "Dynamic Loading at Rail Joints" Railway Gazette, August 15, 1969.

Radford R.W. (Canadian National Railways) "Wheel/Rail Vertical Forces in High-speed Railway Operation" ASME paper No. 77-RT-1.

Sources for the Power Spectral Density (PSD) Curves of Figure 3

Canada	(Preliminary results obtained by the National Research Council, Railway Lab from accelerometers mounted on an empty car. CP mainline near Kamloops. New 132 lbs. rail on wood ties.)
England	Newland, D.E., Cassidy, R.J.; "Suspension and Structures: Some Fundamental Design Considerations for Railway Vehicles". REJ, March 1975. (Simplified approximate track displacement spectrum. Typical. Does not actually represent a specific piece of track.)
France	Prudhomme, A., Weber, O.; "L'aspect technique des grandes vitesses. La voie et les installations électriques des lignes à grande vitesse". Travaux, Août-Septembre 1973, Editions Science et Industrie, Paris. (Mauzin recording car. 200 km/hr line Les Aubrais-Vierzon. 50 kg welded rails on wood ties.)
Japan	Ikemori, M., Itagaki, Y.; "Some Statistical Characteristics of Track Irregularities" Quarterly Reports, Vol. 17, No. 1, 1976. (Average power spectral density of cross-level. Three different classes of track lie within the shaded area on Figure 3.)
Russia	Kogan, A.Y.; "Track Design allowing for Vertical Dynamic Load" (Translated from Russian) Proceedings of the All Union Scientific Research Institute of Railway Transportation, No. 502, 1973. (Average from a geometric survey. Good track. 50 kg/m rail on wood ties.)

U.S.A. Ahlbeck, D.R., Prause, R.H., Meacham, H.C.; "On Application of Computer Modelling Techniques to Predict the Effects of Railroad Track Geometry". Battelle Research Report, Columbus, Ohio. (Range of measured data from high-speed demonstration. Northeast Corridor, U.S.A.)

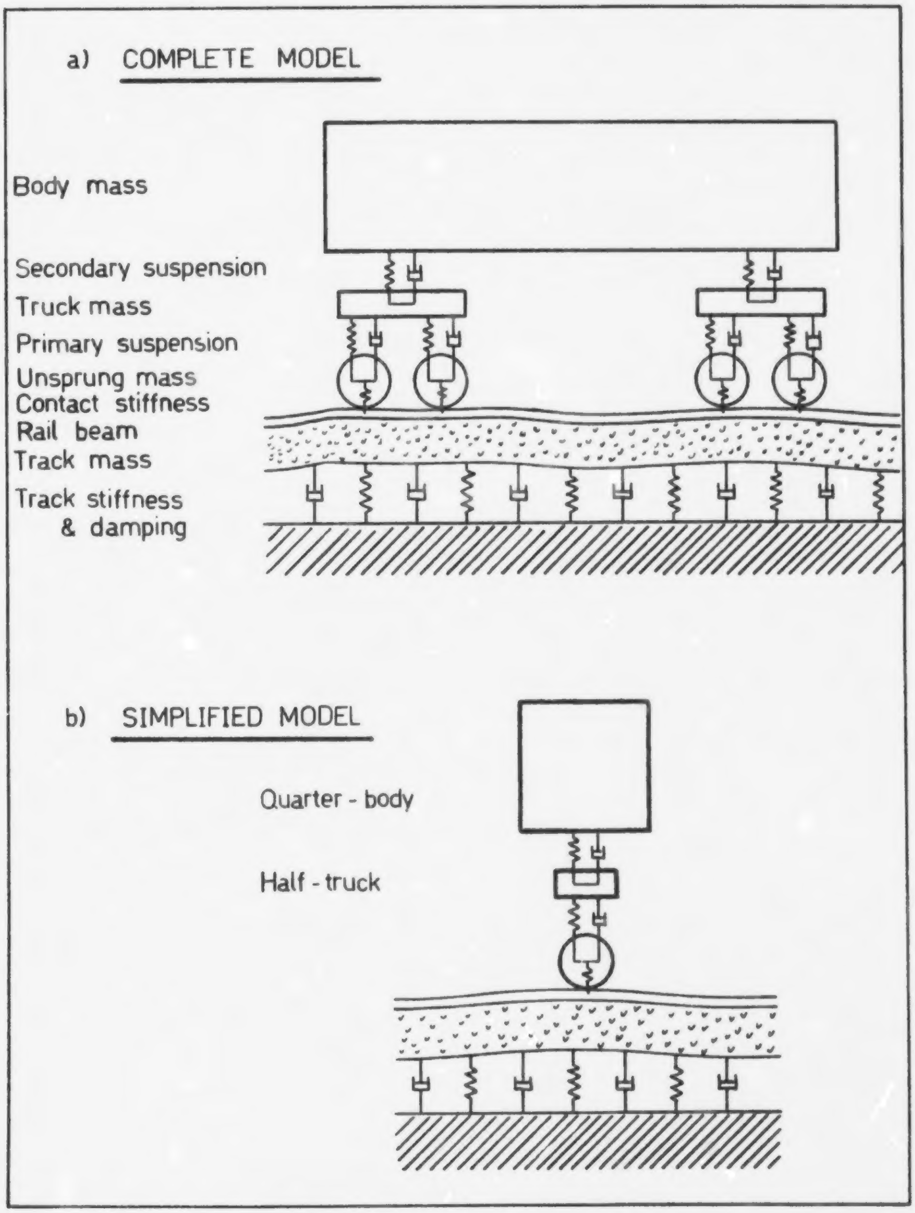
a) COMPLETE MODEL
Body mass
Secondary suspension
Truck mass
Primary suspension
Unsprung mass
Contact stiffness
Rail beam
Track mass
Track stiffness
& damping
b) SIMPLIFIED MODEL
Quarter - body
Half - truck

FIGURE 1: MODELS FOR STUDYING VERTICAL DYNAMICS

a) Vehicle Characteristics

"785" LRC locomotive with PD1 motor, hollow axle

For one rail only		Mass kg s^2/cm	Stiffness kg/cm	Damping kg-s/cm	Position cm	Wheel load or Inertia kg//kg cm s^2
Wheel	1	1.763	1607	4.465	0	13,360
	2	1.763	1607	4.465	290	13,360
	3	1.763	1607	4.465	1250	13,360
	4	1.763	1607	4.465	1540	13,360
	5	-	-	-	-	-
	6	-	-	-	-	-
Truck	1	2.297	1285	75.90	145	0.1728 E5
	2	2.297	1285	75.90	1395	0.1728 E5
Body	1	37.70	-	-	770	48.39 E5

b) Track characteristics

Russian track
R50 Rail 50 kg/m (115 lb/yard)
1840 wood ties/km (2960 ties/mile)
45 cm of crushed rock (18 inches)

All data for one rail only.

Mass	9.381 E-3	kg s^2/cm^2
Damping	0.60	kg s^2/cm
Foundation stiffness	260	kg/cm^2
Contact stiffness	.5E6	kg/cm
Rail moment of inertia	2018	cm^4
Rail moment of resistance	286	cm^3
Mass of a half crosstie	35.68 E-3	kg s^2/cm
Tie spacing	55	cm

FIGURE 2: VEHICLE AND TRACK CHARACTERISTICS

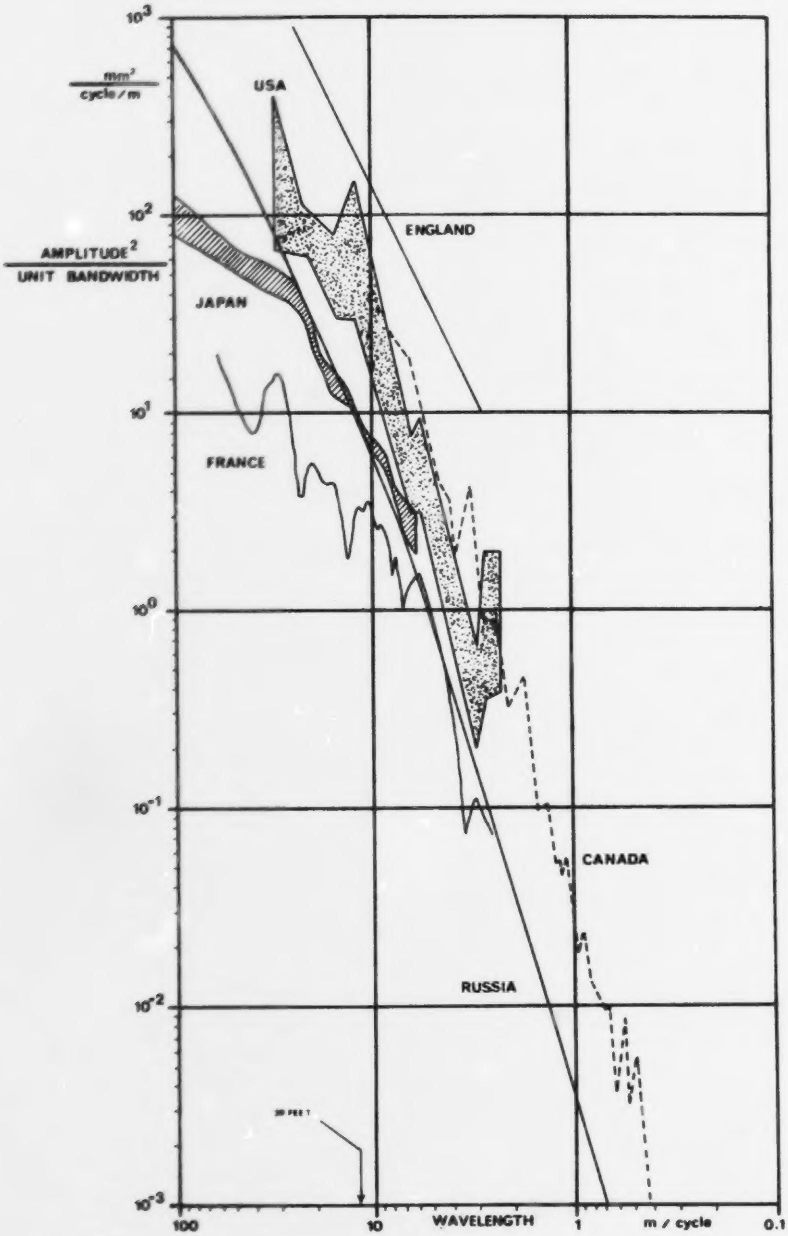

FIGURE 3: POWER SPECTRAL DENSITY OF TRACK IRREGULARITIES

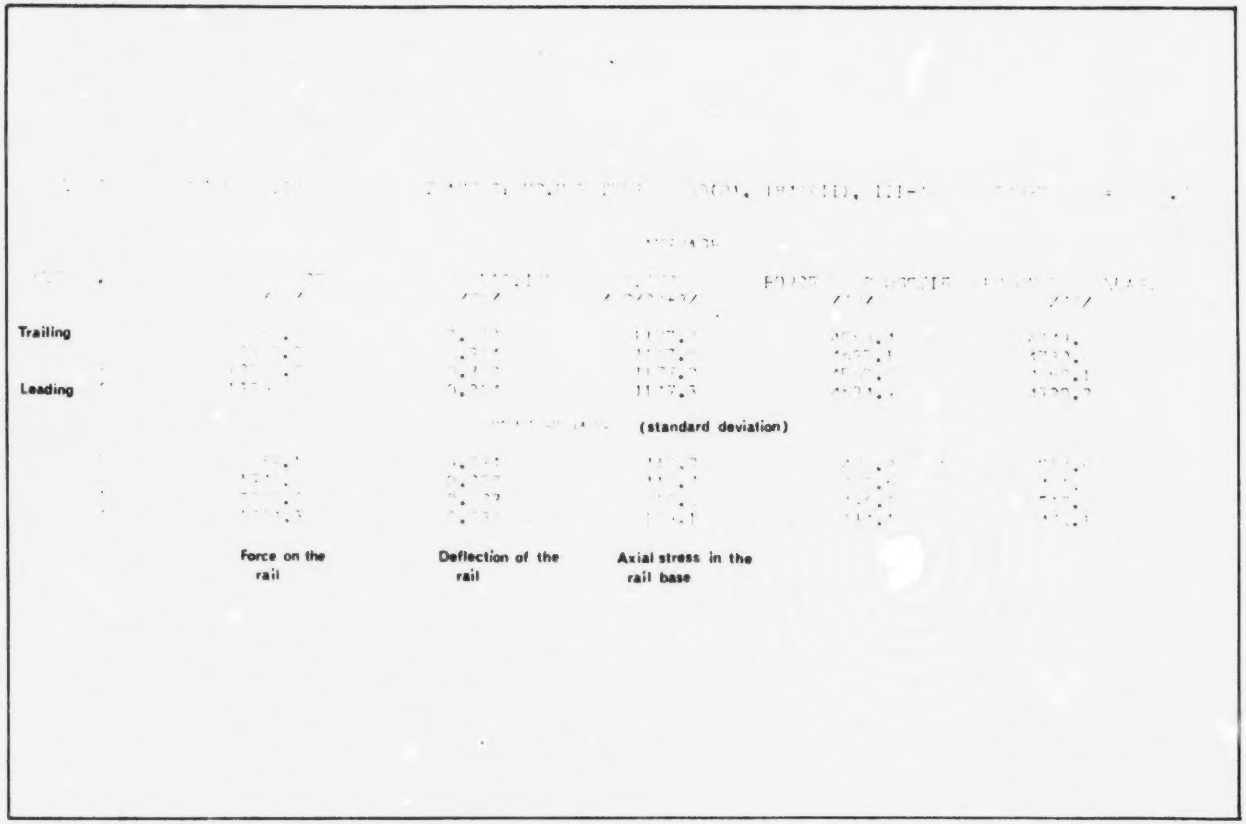

Trailing

Leading

(standard deviation)

Force on the rail

Deflection of the rail

Axial stress in the rail base

FIGURE 4:
DYNAMIC FORCES FOR THE LRC ON A TYPICAL RUSSIAN TRACK

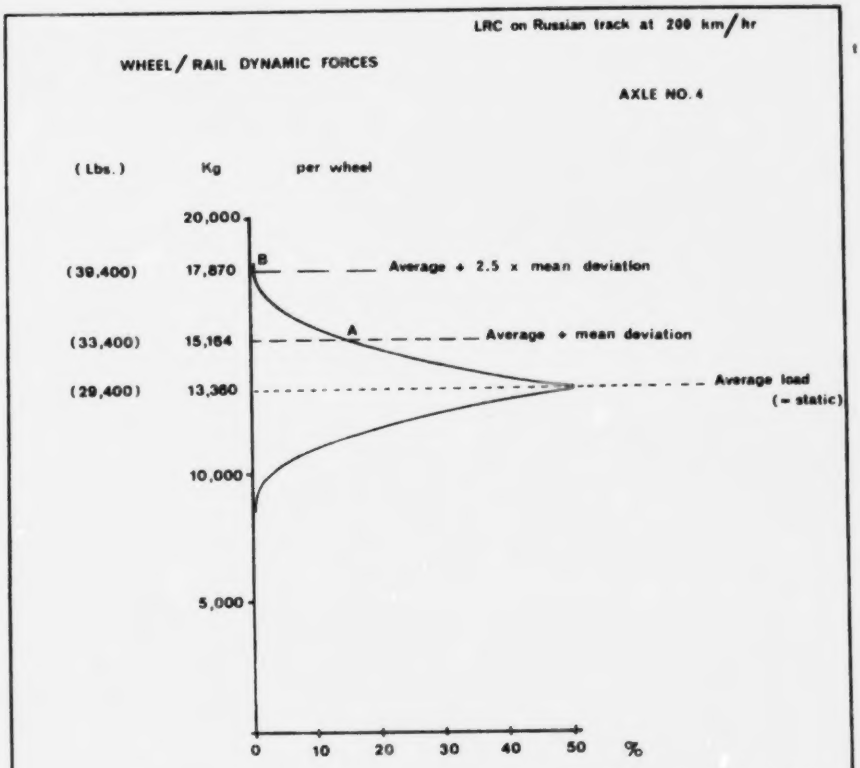

Probability of deviation of dynamic forces from the average.

Point A: The force exceeds 15,164 kg during 16% of the time.

Point B: The force exceeds 17,870 kg during 0.6% of the time.

FIGURE 5:
NORMAL PROBABILITY OF DEVIATION OF DYNAMIC FORCES FROM THE AVERAGE

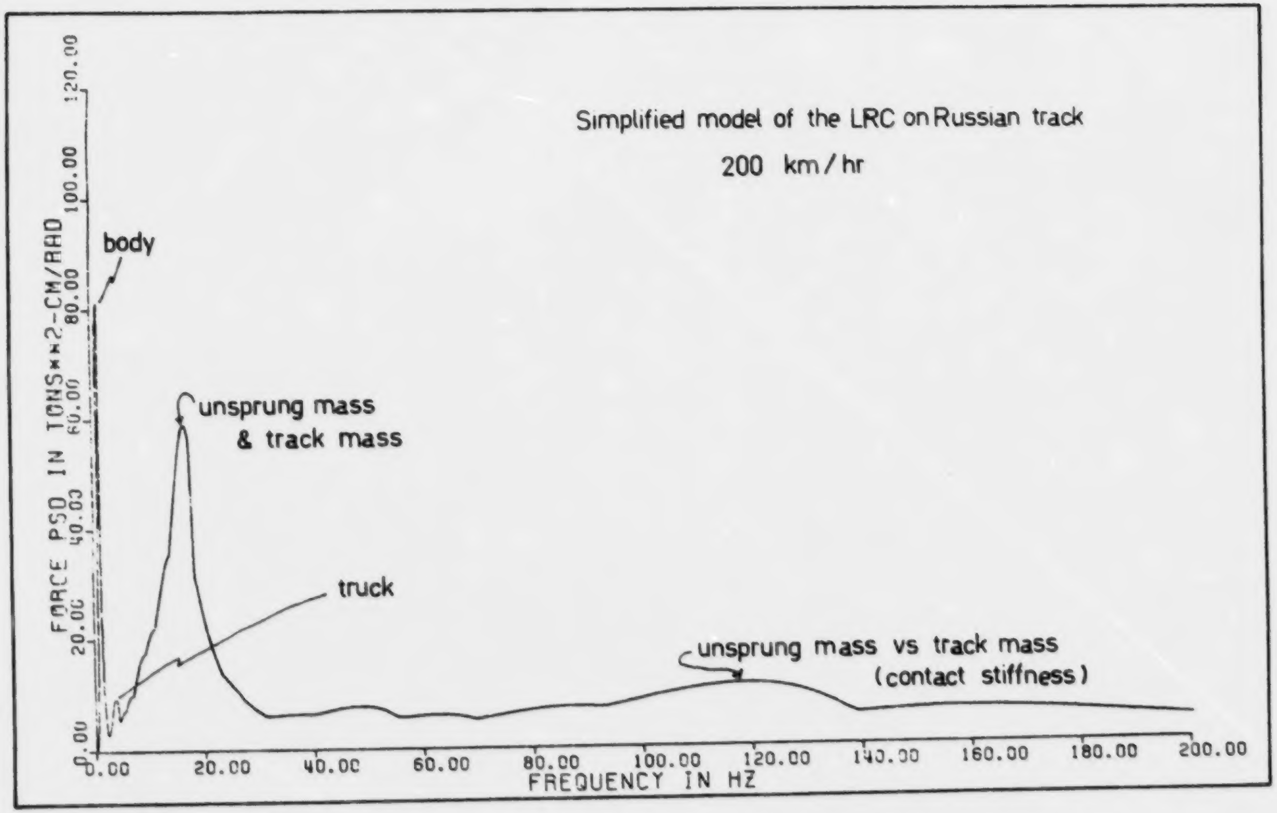

FIGURE 6: POWER SPECTRAL DENSITY PLOT OF THE WHEEL/RAIL FORCE

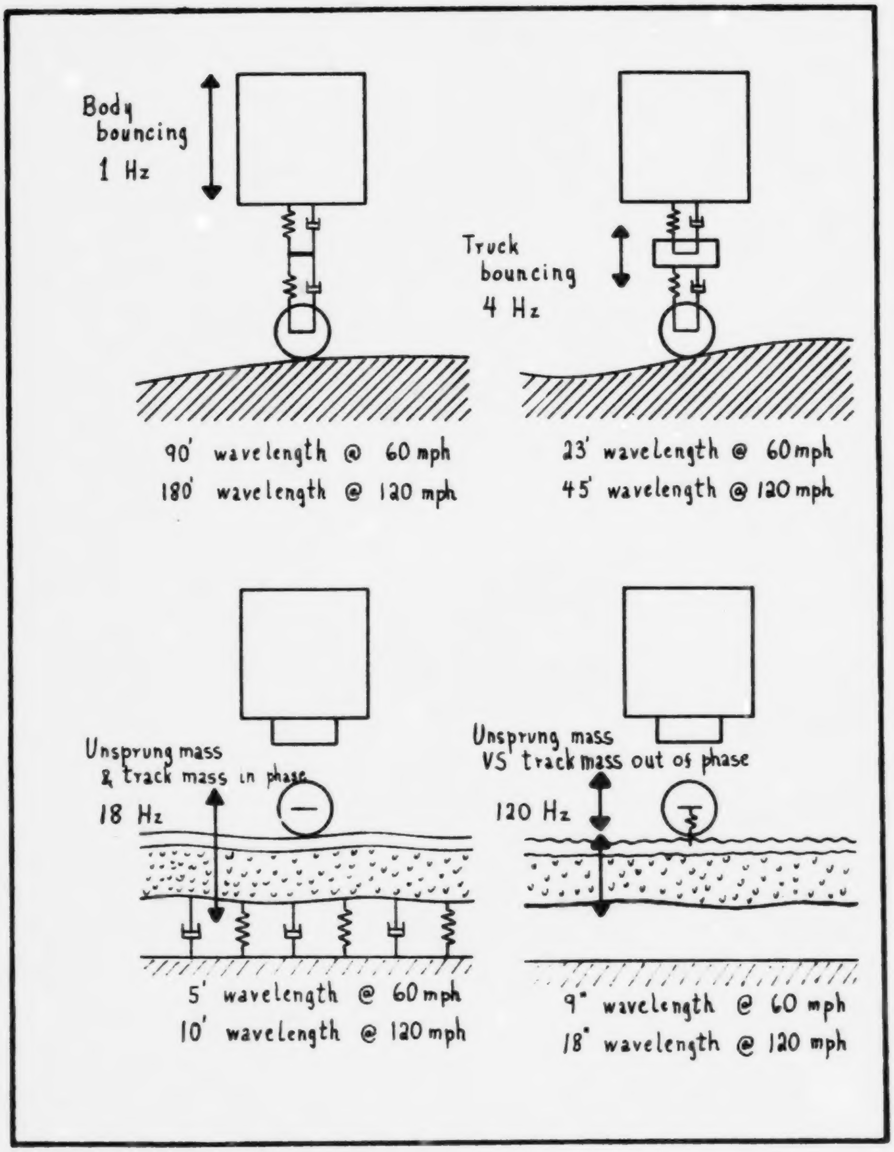
Body bouncing
1 Hz
90' wavelength @ 60 mph
180' wavelength @ 120 mph
Truck bouncing
4 Hz
23' wavelength @ 60 mph
45' wavelength @ 120 mph
Unsprung mass & track mass in phase
18 Hz
5' wavelength @ 60 mph
10' wavelength @ 120 mph
Unsprung mass VS track mass out of phase
120 Hz
9" wavelength @ 60 mph
18" wavelength @ 120 mph

FIGURE 7: FOUR MAIN RESONANCES OF THE SIMPLIFIED MODEL

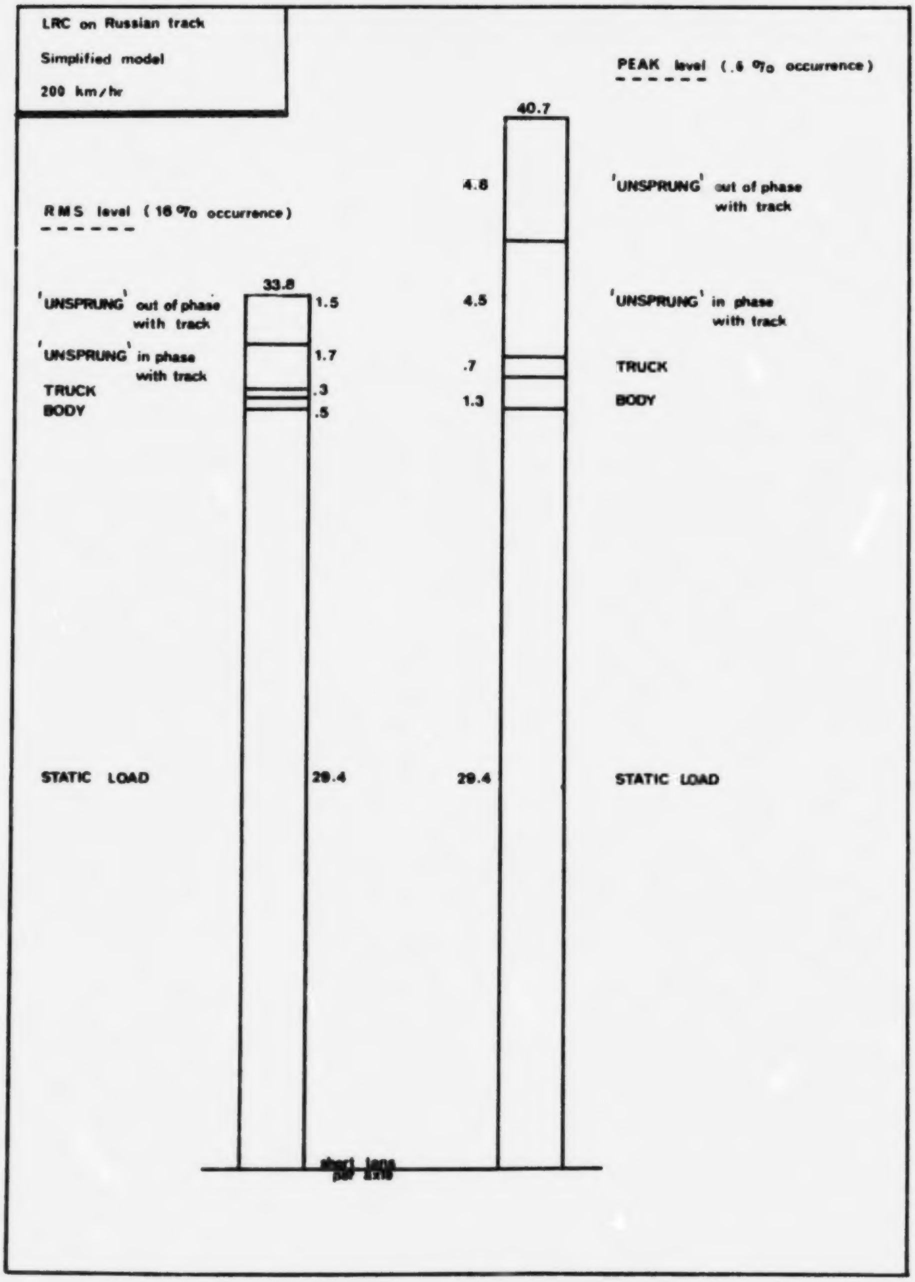

FIGURE 8: RELATIVE MAGNITUDE OF DYNAMIC FORCES

H Ghonem and W Pak

Design of Lockable Draw Gear

ABSTRACT: The present report, which is the first in a series covering this investigation, will present a literature review of various discussions on the subject of longitudinal shock problems encountered in freight train service and discuss general characteristics of different types of draft gears. This report concludes by presenting some suggestions as guidelines for the future design of a lockable draw gear.

1. INTRODUCTION

During normal train operations, longitudinal shocks are constantly being generated by run-in and run-out of the cars. These occur when the train is starting, stopping or running up or down grades in undulating regions. The following are two factors causing this phenomenon:

a) Free slack existing in the couplers due to the nature of the design and/or the wear process.

b) The non-rigid, elastic nature of the cushioning device, i.e. draft gears, end of car cushioning, etc.

Longitudinal shock in freight train operation is undesirable for the following reasons(1)*:

1. Fragile merchandise in transit may be damaged.
2. Lading shift longitudinally.
3. The car itself is subjected to severe acceleration.
4. A risk of a broken coupler during violent run-out.
5. Train crew may be injured.
6. Derailment may result on curves due to exceptionally violent longitudinal shock.

---

* The number in parenthesis refers to the references at the end of this report.

In view of the above, an investigation for the design of a new lockable draw gear was initiated as a project in the "Railway Research Program for Canada"(2). This design should aim at reducing the above-mentioned longitudinal shocks during train running, as well as retaining the cushioning abilities of the present coupling system during yard impact. In addition, this design should take into account safety considerations such as the ability of restoring end float in some emergency situations, such as an impending crossing collision.

Before the actual design of such a draw gear is initiated, it is desirable at this stage to gain a better knowledge concerning the subject of running shock, and the role of couplers and draft gears in minimizing this shock.

2. COUPLER SLACK AND ITS RELATIONSHIP TO THE LONGITUDINAL SHOCK PROBLEM

Slack in a coupler may be considered to consist of two types: contour slack and attachment slack. Contour slack arises from rough casting interface between knuckles and bodies of two mating couplers. This slack varies from 25/32" to 3/8" from the old E type to the new F type couplers for freight cars (see Figures 1 and 2). The H type safety tightlock coupler used in passenger trains have machined mating interfaces and design had called for zero contour slack.

For rigid shank E type couplers, attachment slack occurs due to the wear between key and shank, key and yoke, and between yoke and gear (see Figures 3 and 4). F couplers do not use yoke and key arrangement, thus attachment slack is less and occurs mainly in the shank pin and bearing block. For an E type coupler, the slack could be summarized as follows(4):

	New Car	Average Condition	Condemning Limit
Contour Slack	25/32"	1-9/32"	2-1/32"
Attachment Slack	0	7/8"	2"
Total Slack	25/32"	2-5/32"	4-1/32"

It is to be noted here that the old E type coupler is the worst in terms of the amount of slack inherent in the coupling system.

It was suggested in the draft of "A Railway Research Program for Canada" that coupler slack might be important to assist in starting a train. However, the necessity of bunching coupler slack before moving a train forward might be a concept related to the use of journal bearings. With the new roller bearings, starting resistance of a train could be reduced by 80%(3). One should also not forget the low resistance of the draft gears at initial travel, which is equivalent to a small amount of slack already inherent in the train.

In order to understand the effect of slack and other variables on longitudinal shock generation, the subject of longitudinal train action was studied by various investigators. In the fifties, classical mathematics were applied to different mathematical train models to calculate the intensity of the longitudinal waves. These models were ranging from simple elastic bars(5,6) to models of uniform cars connected by springs and viscous damping(7). These calculations were limited to the capabilities of classical mathematics and required drastic simplifying assumptions in order to keep the mathematics within manipulation.

With advances in analogue and digital computers, the capabilities and sophistication of train action simulation is broadened, and numerous researchers were involved in this type of computer analysis(8,9,10). Among these, one of the more comprehensive studies was made by R.C. Roggeveen. As part of his paper(11), the effect of slack reduction on the force peak generated in standard friction draft gears were discussed. The theoretical model he used was based on a train consist of 29 empty cars followed by 4 heavy cars going through a 2% downgrade. The output of this simulation program is in the form of a sequential force peak plot depicting each successive force peak that would occur in a series of couplers linking the train model. The plotting starts from the first coupler recording its force versus time until a greater force occurs in the following coupler. The plotter will then follow the second coupler until a higher force occurs in the third. In this fashion, the maximum shock force at any time is recorded.

Figure 6 illustrates the result obtained from a series of computer runs made each time with a different value of coupler slack. From this figure, it is clear that complete removal of slack in a train does not give zero coupler force. This phenomenon is understandable if we consider the low resistance of the draft gears at initial travel as an additional slack. Other important information obtained from this figure is that initial slack reduction will cause a minimal reduction in the running shock force peak. The reduction of shock level would be maximum only when the coupler slack removal is nearly complete.

From the above, it can be concluded that slack reduction is fundamental in eliminating violent running shocks. However, the elimination of slack should be complete in a new draw gear in order to achieve maximum reduction in shock level.

3. CURRENT STATE-OF-THE-ART OF DRAFT GEARS

3.1 Introduction

The second most important aspect affecting the intensity of running shock is the characteristics of shock absorbing devices such as draft gears, end of car cushionings, or cushion underframes. Accordingly, a study of the characteristics of the various shock absorber devices is indispensable since it may lead to the choice or modification of a particular device to be used as a lockable draw gear.

Presently, there are three basic types of draft gears in use. These are respectively:

1. the friction draft gear,
2. the rubber draft gear, and
3. the hydraulic draft gear.

The purpose of employing any of these devices is twofold. Firstly, its presence is necessary to absorb and dissipate impact energy for yard impact situations. Secondly, it is required to cushion relative shock between cars during train running. Up to the present, yard impact absorption capabilities of the gears are considered as the major determining factor in the design of a draft gear. Thus, the maximum buff and draft travel, reaction forces, capacity, etc., which determine the design of a draft gear are specified by specially designed impact conditions. Not until problems occurred during train running were the gears modified to alleviate the shock.

3.2 General Draft Gear Characteristics

Before entering the discussion of various types of draft gears, it is advantageous to know the various features of a draft gear as a cushioning device.

Basically, a draft gear can be described as a cushion device which develops a cycle of work during closure and release under various intensities of draft or buff impact. The general shape of a draft gear force-displacement characteristics is shown in Figure 7. The total work done by a draft gear during compression is usually called draft gear capacity and it is shown as Area OAC in Figure 7. In general, the higher the capacity of the draft gear, the greater the impact severity that can be accommodated with full cushioning. The old AAR standard specified gears fitting a 24-5/8" pocket to have a minimum travel of 2" in buff and combined maximum buff and pull travel of not more than 5-1/2". Recent specifications had aimed more to relate draft gear capacity to reaction force rather than travel.

When the car is coupled at a switching speed which results in impact force beyond the capacity of the draft gear, the overload is absorbed by the coupler shank, draft gear column, rear stop lug construction, and finally the centre sill of the car. This overload saturation is represented as the "beam solid" portion of the draft gear shown in Figure 8. During overload, the coupler shank, being the weakest and cheapest to replace, among the different shock absorbing components, is used as a safety valve to reduce pressure and damaging effects upon structure and lading.

3.2.1 Train Running Conditions

To understand the role of a draft gear during train action, a simple model shown in Figure 9 is used to simulate the behaviour of a car during train running. This model consists of a single car attached to a rigid wall by a draft gear, and it is assumed that, initially, the whole system is undisturbed and the draft gear force is zero. Shock generated by run-in or run-out can be represented by a constant tensile or compressive force, F, suddenly applied to the car body at point A as shown in Figure 9. When this force, F, is applied, the car moves towards the wall, and spring force is generated to oppose this action. As this continues, the draft gear follows the load path AB and the car body accelerates towards the wall. When point B is reached, i.e. when draft gear force equals the applied constant force, the car is at its maximum velocity. Further compression decelerates the car until point C is reached and the car velocity is zero. At this point the spring force is the highest. Beyond this point, the draft gear re-extends and the car accelerates away from the wall.

Now, energy balance of the system, shown in Figure 9, can be considered from the gear characteristics as follows: At any point Y, during the initial compression stage AB, the distance travelled by the car body is represented by AZ in Figure 9. Therefore, the work done by the externally applied force F is given by the area AFXZ, while the energy stored in the gear is represented by the area AYZ. Hence at point Y, the kinetic energy of the car body correspond to the area AFXY. Similarly, the maximum kinetic energy which occurs at point B, can be described by the area AFB.

At point C, where the kinetic energy of the car is zero, the work done by the external force F, which is represented by Area AFDE, must equal the energy stored in the gear, i.e. Area ACE. From this, it is concluded that Area AFB equals Area BCD.

The above discussions can be summarized as follows: When a constant force is applied to the car-spring system during run-in or run-out, the gear force reaches its maximum value when the maximum kinetic energy of the car is absorbed by the gear action.

In Figure 9, a comparison between two linear gears having different stiffness is shown. From this figure it is clear that they will attain the same force level CC' by subjecting them to the same external force F. Figure 10 shows that non-linear draft gears, with little initial energy absorption capability, will soar to high forces under the same external applied load.

The A.A.R. specification for friction draft gears sets a minimum for the amount of initial work at half travel at not less than 20% of capacity

and preferably more than 25%(12). One example of the long travel, low reaction force level characteristics generating high forces during train running is the hydraulic end of car cushioning.
Shock wave theory had shown a similar result. The theory had shown that a draft gear efficiency of 50% or better is necessary to prevent a shock build-up. A draft gear efficiency is defined as the energy absorbed divided by peak force multiplied by travel. Hence 50% efficiency means a straight line of 45° angle. Any gear stiffer than this will attenuate or damp the shock in trains and any gear softer than this will tend to magnify the amplitude of the shock. It should be noted here that in this theory, slack is considered absent.

3.2.2 Yard Impact Conditions

The behaviour of a draft gear during yard impact can be deduced from the physics of impact of two masses. It is known that when two masses collide, there is a certain amount of work done during the process of momentum transfer until their relative velocity is zero. At this instant, the kinetic energy of the whole system is minimum and the force of interaction maximum. After this, the two masses involved will either spring apart or travel together at the same terminal velocity depending on whether the collision is elastic or in-elastic.

The work done which is absorbed by colliding masses can be calculated as:

$$IQ = \frac{1}{2} \; Mm/(M-m) \; V^2 \qquad \text{(Ref. 13)}$$

where IQ is termed Impact Quantum for the case of a mass M moving with velocity V impact into a stationary mass m.

This quantity, IQ, is a constant for the same two masses impacting at a certain velocity, and must be taken up completely by the force displacement curve of the draft gears, assuming that the draft gears alone control the energy transfer.

Hence, though the shape of force displacement curves of different draft gears may be different, under identical impact conditions they will all be loaded to the point having the same area under their curves. Figures 11 and 12 show the behaviour of two different draft gears under the same impact conditions. It can be seen that in order to accommodate the "Impact Quantum", the reaction force for Case 1 (Figure 11) has to rise to high values. This is an undesirable feature that should be avoided in the choice of a draft gear.

From the above, it is obvious that the requirement of maximum energy absorption while developing minimum reaction force could be met by a draft gear which has a rectangular force travel diagram as shown in Figure 13.

In practice, however, a rectangular force travel curve is impractical for the reason that high forces must be developed before any deflection of draft gear will occur(14) and thus it will not be efficient in cushioning low speed, light weight impacts. Therefore an ideal force-travel diagram for cushioning should be as shown as the dotted line figure in Figure 13.

3.3 Friction Draft Gear

Friction draft gear is used extensively in freight cars. The basic structure consists of a spring and friction clutch arrangement to store and dissipate the impact energy (see Figures 14 and 15).

In the friction draft gear, the total reaction force consists of a spring force and a friction force. The latter is proportional to the spring force in magnitude and lags behind it. The general force displacement characteristics of friction draft gear in a complete cycle can be described, with reference to Figure 16, as follows.

During compression, the linear region AB corresponds to the combination of the spring and the friction force while BC is the characteristic of the "beam solid" condition when the spring is fully compressed. During recoil, car beam returns to its original extension point B and due to the reversal of direction of the friction force, the resultant force decreases following the path BA'.

During train running, however, the gear force is constantly reversing direction and follows hysterisis cycles as shown in Figure 18.

A graphical representation of the force-time characteristics of friction draft gear is shown in Figure 17. This illustrates the time-lag phenomenon of the friction force and explains the reason for low reaction forces (BA' in Figure 16) during gear re-extension.

From previous discussions, it was shown that in order to reduce running shocks, it is desirable to have high reaction force in the draft gear at initial travel. This can be achieved by preloading the draft gear to obtain a high initial compression, see Figure 19. However, preloading the draft gear means a loss of impact capabilities.

In Figure 19, Area ABCD is the shock energy being eliminated due to preloading while Area ADE is the loss of impact capacity of this specific gear. Since Area ABCD is much greater than Area ADE, it is obvious that an initial preload on friction draft gear is indeed beneficial, especially in gears with low stiffness.

The second way to reduce running shock is by increasing the stiffness of the gear as discussed previously. Computer simulation were carried out to verify these conjectures(11). From these simulations it was shown that the amount of existing slack allows large relative motion between cars regardless of friction draft gear stiffness. These relative motions will be stopped by draft gears having lower stiffness. Preloading the gear will have the same effect of giving the appearance of a stiffer draft gear and hence offer limited improvement. Some computer simulation results are presented in Figure 20, illustrating the above discussions.

Figure 20A shows the run-out of a standard consist (as in discussion of coupler slack) with friction draft gears stiffness of 1,000,000 lb./ft. A tractive force of 30,000 lb. pulls on the front of the cars, which is, at the same time, being run off the level onto a 2% downgrade. Figure 20B shows the result when the stiffness is halved and the travel doubled. The heavy cars at the end did not pick up until 5.85 second mark and the average force had been reduced from 159,000 lbs. to 129,000 lbs.

Other runs have been discussed(11), nonetheless, in all tests the softer longer travel draft gears have a better performance than the regular gear by virtue of their higher energy absorbing capacity.

Figure 20D shows the effect of preloading in the identical situation as in Figure 20A or 20C. From the top down, the three cases correspond to preloading of 30,000, 50,000 or 70,000 lbs., respectively. As expected, the run-outs complete themselves more rapidly as preloading is increased. However, the force had risen from 159,000 lbs. in the datum run (Figure 20A, 20C) to 165,000 lbs. by the time preload is increased to 70,000 lbs. The salutary effect obtained from controlling the slack is apparently overweighed by the deleterious effect of the higher apparent stiffness.

It is the belief of the authors that one way to understand the above phenomenon is as follows:

> preloading or stiffening a draft gear is similar in effect to an initial reduction in slack. This gives very little improvement to shock reduction and can be easily overweighed by any other change in the system. However, the improvements by preloading or stiffening should manifest themselves once the free slack has been completely eliminated.

3.4 Rubber Draft Gear

Rubber friction draft gears are commonly used. The characteristics of rubber draft gears are low capacity of energy absorption and high recoil force, see Figure 21. Due to the low absorption characteristics, they require supplementary friction for absorption or damping. The high recoil, i.e. low-damping, is undesirable in train running, because of low energy dissipation. As can be observed in Figure 21, rubber draft gear normally produce a force travel diagram which approaches even less the ideal rectangular shape than friction draft gears, and hence less efficient in yard impact.

In reference (2), R.C. Roggeveen discussed the comparison between a standard friction draft gear and an advertized rubber draft gear preloaded by 1/2". Figure 22 shows that the preload rubber draft gear is superior in that it offers a higher energy absorption and a more gradual force increase. However, no simulation results were available for this comparison.

3.5 Hydraulic Draft Gears

It was mentioned before that an ideal force-displacement characteristic of a draft gear pertaining to yard impact would be the rectangular type. Hydraulic draft gear is the one that was designed based on this concept. The basic structure of a hydraulic draft gear consists of a fluid damping device and a spring (steel or air spring) contained in one casing as shown in Figures 23 and 24.

The gear shown in these figures consists of an inner and outer cylinder separated by hydraulic seals. The outer cylinder contains hydraulic fluid and a metering pin, while the inner cylinder contains an orifice plate, floating piston and a charge of inert gas such as nitrogen. When dynamic force is applied, the cylinders close on one another causing the metering pin and fluid to pass through the orifice. By controlling the area of the orifice during the whole travel, a rectangular force displacement characteristic can be achieved. The details of mathematical expressions and derivations concerning hydraulic gear characteristics can be obtained in references (11, 17, 19). It should be mentioned here that the force generated at any time in a hydraulic draft gear is directly proportional to the square of the piston velocity and inversely proportional to the square of the orifice area.

Since force generated in the hydraulic plunger arrangement is due to piston velocity, a steady tractive pull will exhaust the whole traverse of the gear, rendering it "solid". Free slack would thus develop when the dynamic force reverses its direction. Hence return spring is always included to resist a steady pull. An example of a hydraulic draft gear using ordinary spring arrangement is shown in Figure 25.

The rectangular force travel response is geared only for the impact of a design mass at a design velocity. The response due to the design mass impact at different speed is shown in Figure 26. The response to different mass impact at the design velocity is shown in Figure 27. It was shown in reference (18) that, for impact situation, both rectangular and falling force characteristics are superior in that they will have minimum impact force level. Hence, hydraulic draft gear will efficiently cushion any condition of impact except when the impact mass exceeds the design mass.

The train running characteristics of a hydraulic draft gear are complex due to velocity and positions dependence of hydraulic draft gears force. It was shown in reference (1) that for the case of run-ins, using analogy to rake impacts*, the impact condition is equivalent to impact between 2 cars of twice the design weight originally considered. The corresponding force displacement curve can be easily derived and is shown in Figure 28. Again, this illustrates rising force characteristics when impact mass exceeds the design mass. Experimental work by V.T. Hawthorne for rake impact also showed similar results(19).

Hydraulic draft gears offers good possibilities of modification to suit various needs in yard impact and train running from orifice design or release valve designs.

---

*Rake impact is impact between rakes of cars, i.e. number of cars coupled together.

4. CONCLUSIONS

An attempt has been made in this report to review the running shock problem and the important features of different types of couplers and draft gears. From this study, it was shown that draft gear characteristics and coupler slack constitute the two main variables affecting the running shock intensity. The exact relationship of these variables to the running shock generation were analyzed in this report and the conclusions can be summarized as follows:

1. The E type coupler which is characterized by large inherent slack, and the hydraulic end of car cushioning which has long travel at low reaction force, are the worst type of devices with respect to running shock generation and intensity.

2. Running shock intensity can be reduced by preloading or stiffening of draft gears. However, this beneficial effect will manifest itself only after total reduction of the system slack.

3. An initial reduction of slack will result in an ineffective reduction in the intensity of running shock. Based on this fact, a design of new lockable draw gear should be preceded by an investigation aiming at a complete removal of slack in the present couplers.

5. REFERENCES

1. B.T. Scales. "Longitudinal Shock Problems in Freight-Train Operations", ASME Paper 64-WA/RR-4.

2. P.J. Detmold. "A Railway Research Program for Canada", first draft December 20th, 1977.

3. Hay. "Railroad Engineering", Vol. I, Chapter 6, pg. 80.

4. R.C. Roggeveen. "The Outlook for Simulations of Longitudinal Train Actions", NRC INS-27.

5. L.H. Donnell. "Longitudinal Wave Transmission and Impact", Trans. ASME, 1930, Paper APM-52-14-153.

6. O.R. Wikander. "Draft Gear Action in Long Trains", Trans. ASME, Vol. 57, 1935, pg. 317.

7. L.A. Pipes. "Analysis of Longitudinal Motions of Trains by Electric Analog", Journal of Applied Physics, December 1942, pg. 780.

8. R.C. Roggeveen. "Analog-Computer Simulations of End Impact of Railway Cars", ASME Paper 65-RR-3.

9. V.T. Hawthorne. "Modeling and Simulating Longitudinal Train Action Forces", ASME Paper 74-RT-1.

10. Masayoshi Kobayashi. "A Simulation of Freight Car Motion Due to End-to-End Impact", JNR Report Vol. 15, No. 2, 1974.

11. R.C. Roggeveen. "Computer Prediction of Freight Train Shock Actions", ASME Paper 72-WA/RT-9.

12. W.D. Wallace. "Evaluation of Railway Draft Gears", ASME Paper 57-RR-8.

13. Wallace E. Baillie. "Impact as Related to Freight-Car and Lading Damage", ASME Paper 59-A-249.

14. R.E. Abbott. "Increased Cushioning Capacity - A Requirement of Tomorrow's Freight Car", ASME Paper 59-A-224.

15. R.C. Roggeveen. "Review of Digital Computer Impact of Train Simulation", NRC INS-26.

16. R.C. Roggeveen. "The Details and Functioning of a Simulation of Longitudinal Train Action", NRC INS-29.

17. Robert L. Hassenauer, George E. Novak. "The Design of Cushioning Gears for Railway Applications", Anthology of Rail Vehicle Dynamics, Vol. I by S.G. Guins & C.E. Tack, 1971.

18. C.A.M. Smith. "Freight Car Draft Gear Impact Performance Characteristics and Their Evaluation Criteria", June 1968. Mechanical Engineering Report MI-834.

19. V.T. Hawthorne. "Hydraulic Draft Gear for Locomotives", ASME Paper 71-WA/RT-1.

20. Car and Locomotive Cyclopedia, 1974.

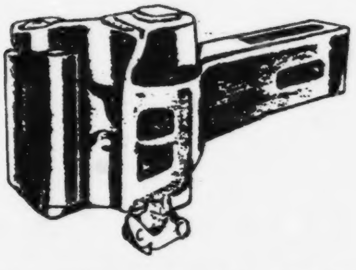

Figure 1- A.A.R. STANDARD E COUPLER, RIGID SHANK

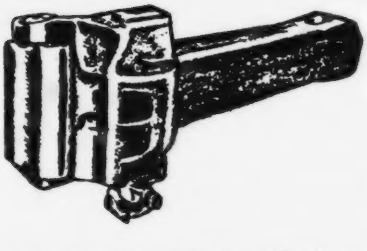

Figure 2- A.A.R. STANDARD E/F COUPLER, VERTICAL PIN CONNECTION

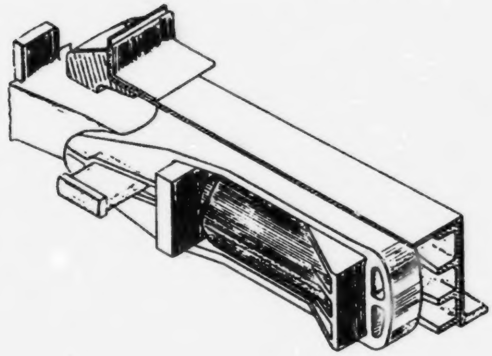

Figure 3- MINER A-22-XL DRAFT GEAR

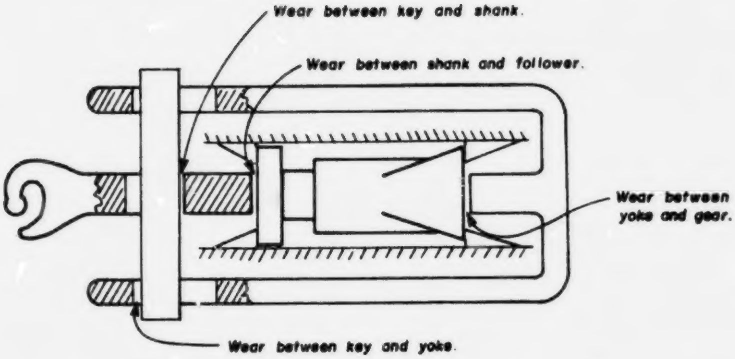
Wear between key and shank.
Wear between shank and follower.
Wear between yoke and gear.
Wear between key and yoke.

Figure 4 - SCHEMATIC VIEW OF STANDARD ATTACHMENT

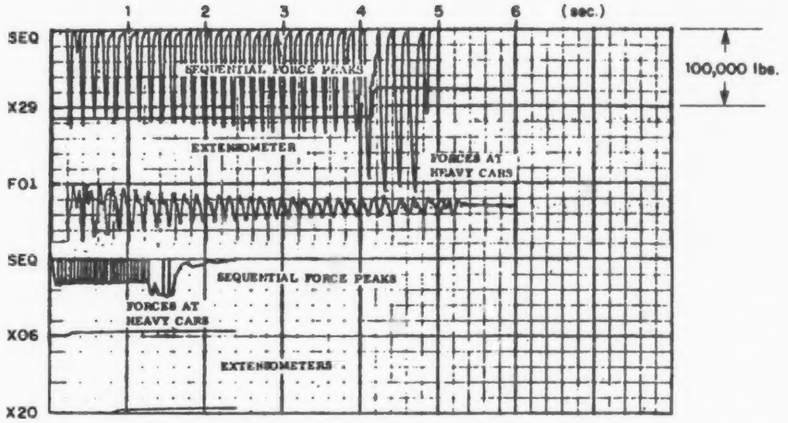

Figure 5 - EFFECT OF COUPLER SLACK ON RUNOUT

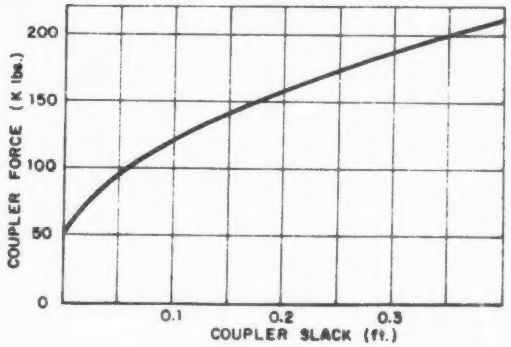

Figure 6 - COUPLER FORCE PLOTTED AGAINST VARYING COUPLER SLACK

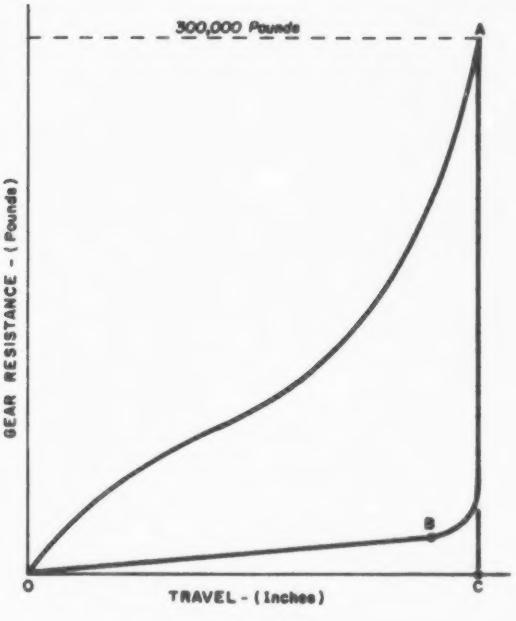

O-C = 2.60 INCHES

Figure 7- STANDARD FRICTION DRAFT GEAR CHARACTERISTICS

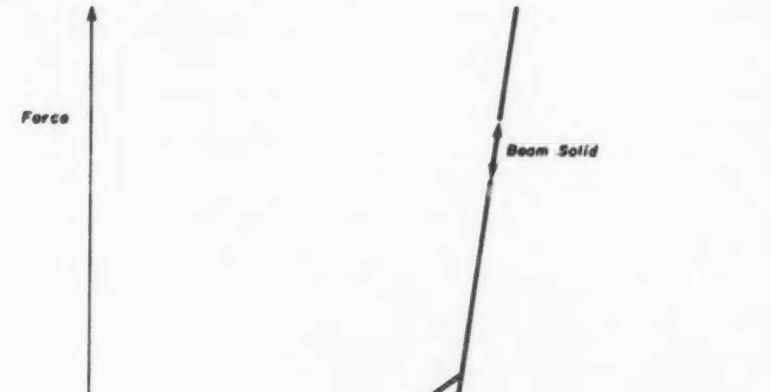

Figure 8- FORCE DISPLACEMENT CHARACTERISTICS

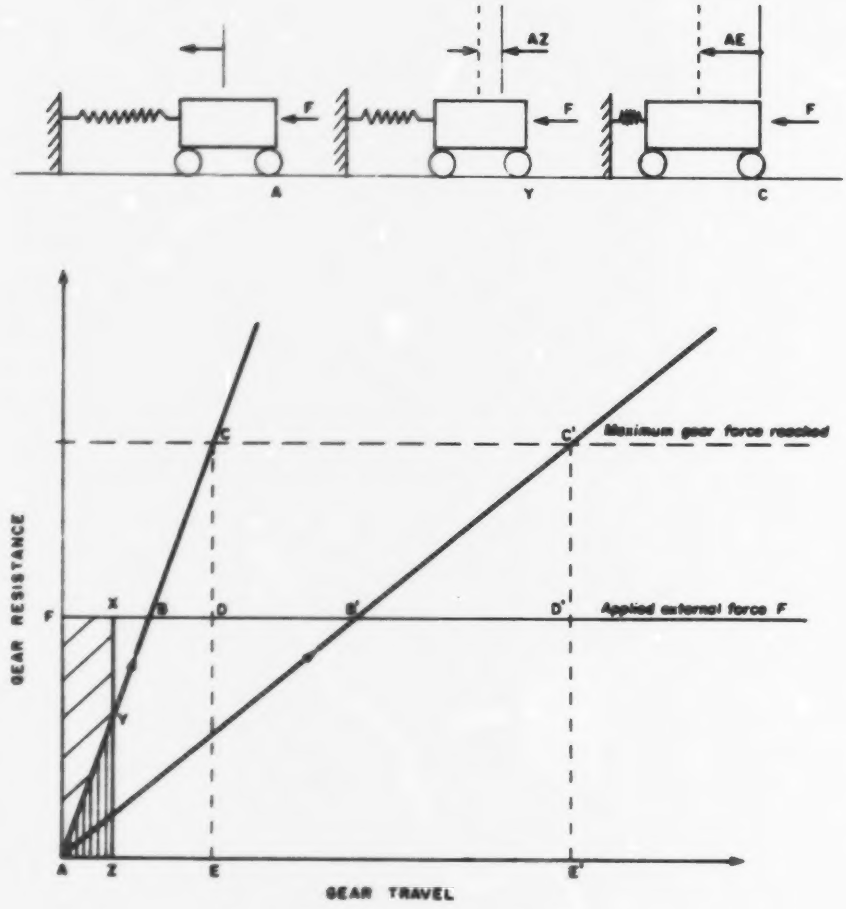
AZ
AE
F
F
F
A
Y
C
GEAR RESISTANCE
C
C'
Maximum gear force reached
F
X
B
D
B'
D'
Applied external force F
Y
A
Z
E
E'
GEAR TRAVEL

Figure 9- TRAIN RUNNING GEAR ACTION

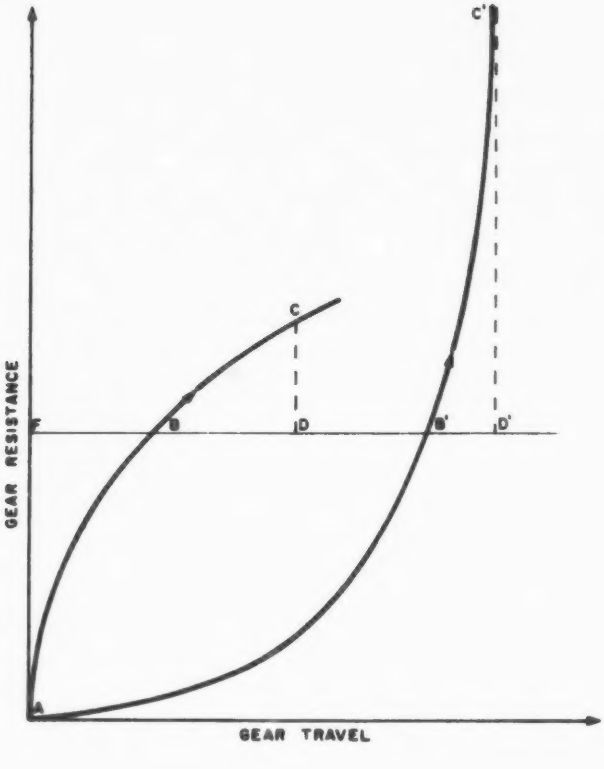

Figure 10- COMPARISON OF FORCE LEVELS GENERATED BY NON-LINEAR SPRINGS UNDER SAME EXTERNAL LOAD.

Figure 11

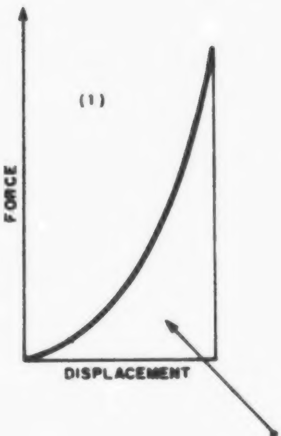
(1)
FORCE
DISPLACEMENT

Same area (work)

Figure 12

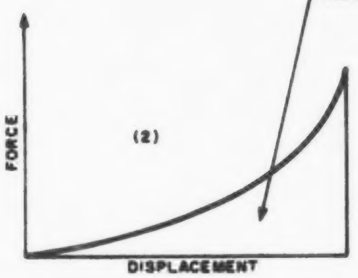
(2)
FORCE
DISPLACEMENT

TWO FORCE-DISPLACEMENT CURVES WHICH SATISFY ENERGY REQUIREMENTS OF TWO MASSES, IMPACTING AT A CERTAIN VELOCITY.

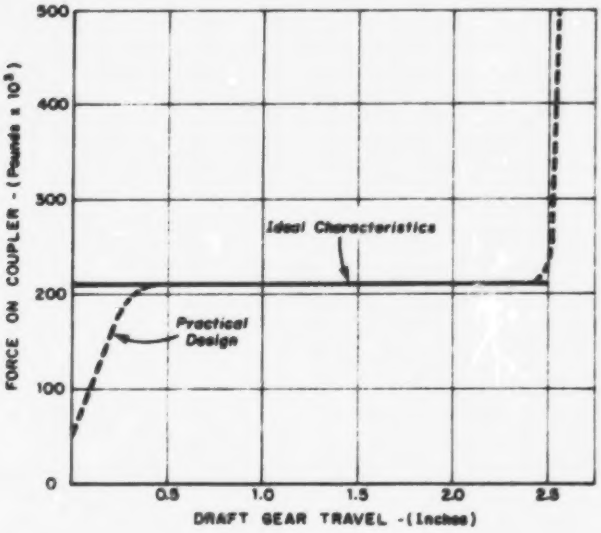

Figure 13 - IDEAL RECTANGULAR FORCE-TRAVEL DIAGRAM

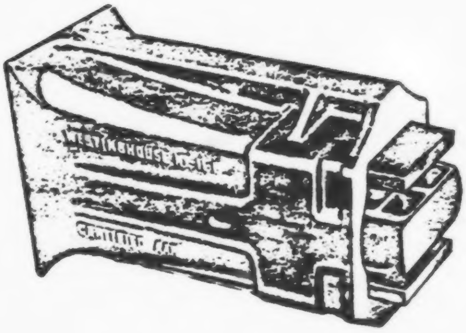

Figure 14- WESTINGHOUSE, TYPE NY-11-F DRAFT GEAR. CERTIFIED A.A.R.

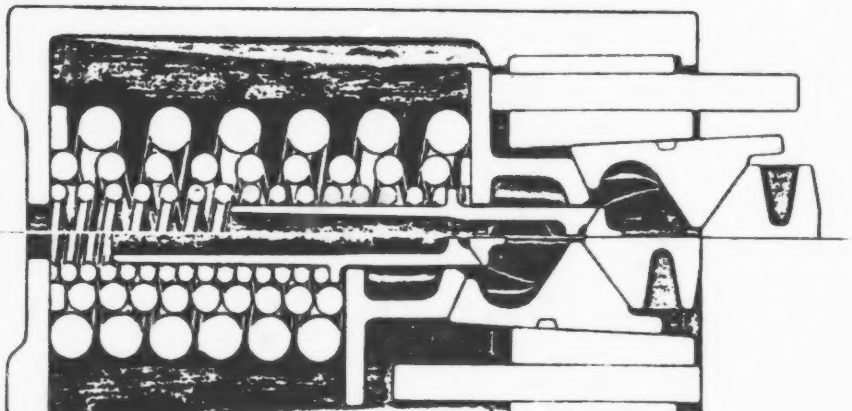

Figure 15 - CROSS SECTION OF WESTINGHOUSE TYPE MARK 40 FRICTION DRAFT GEAR.

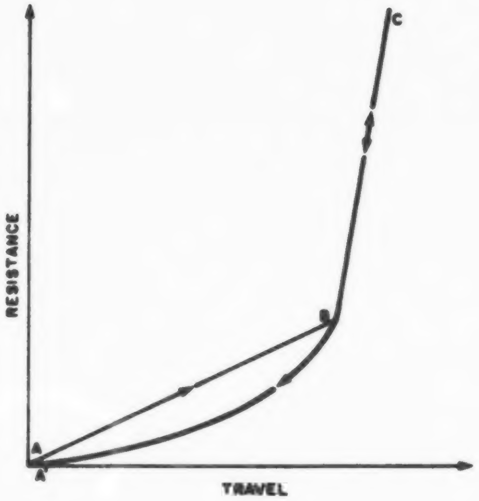

Figure 16- FRICTION DRAFT GEAR FORCE-TRAVEL DIAGRAM

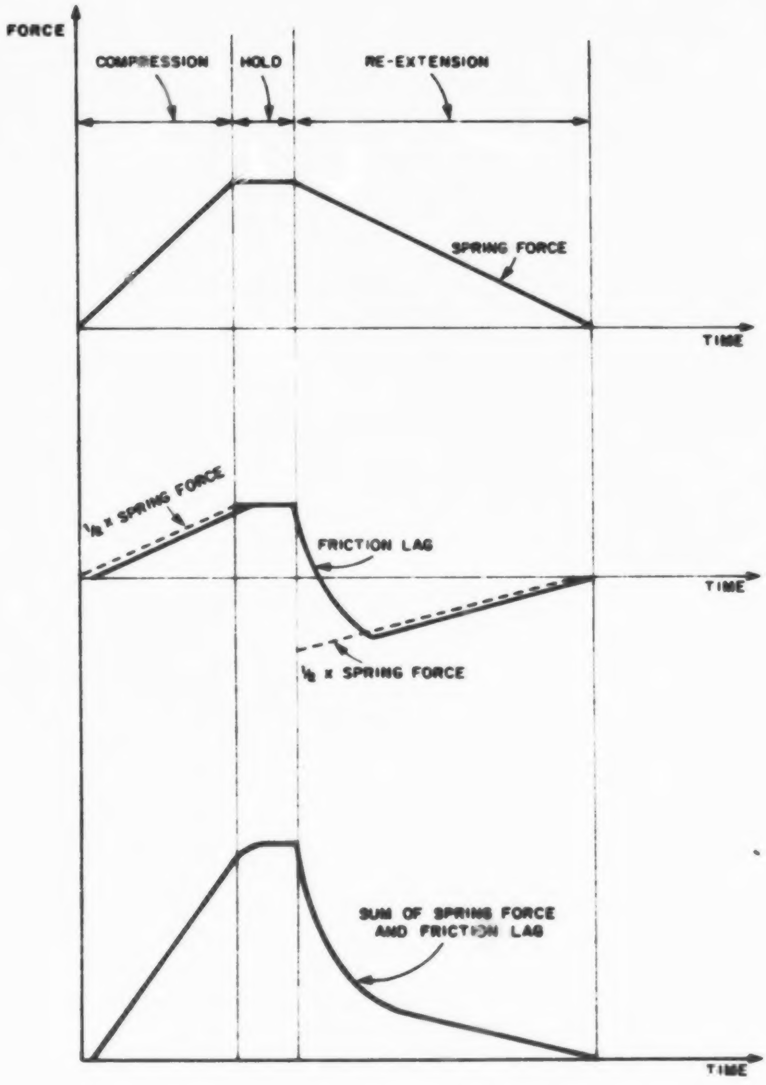
FORCE
COMPRESSION
HOLD
RE-EXTENSION
SPRING FORCE
TIME
½ x SPRING FORCE
FRICTION LAG
TIME
½ x SPRING FORCE
SUM OF SPRING FORCE AND FRICTION LAG
TIME

Figure 17- FORCE-TIME CHARACTERISTICS OF FRICTION DRAFT GEAR

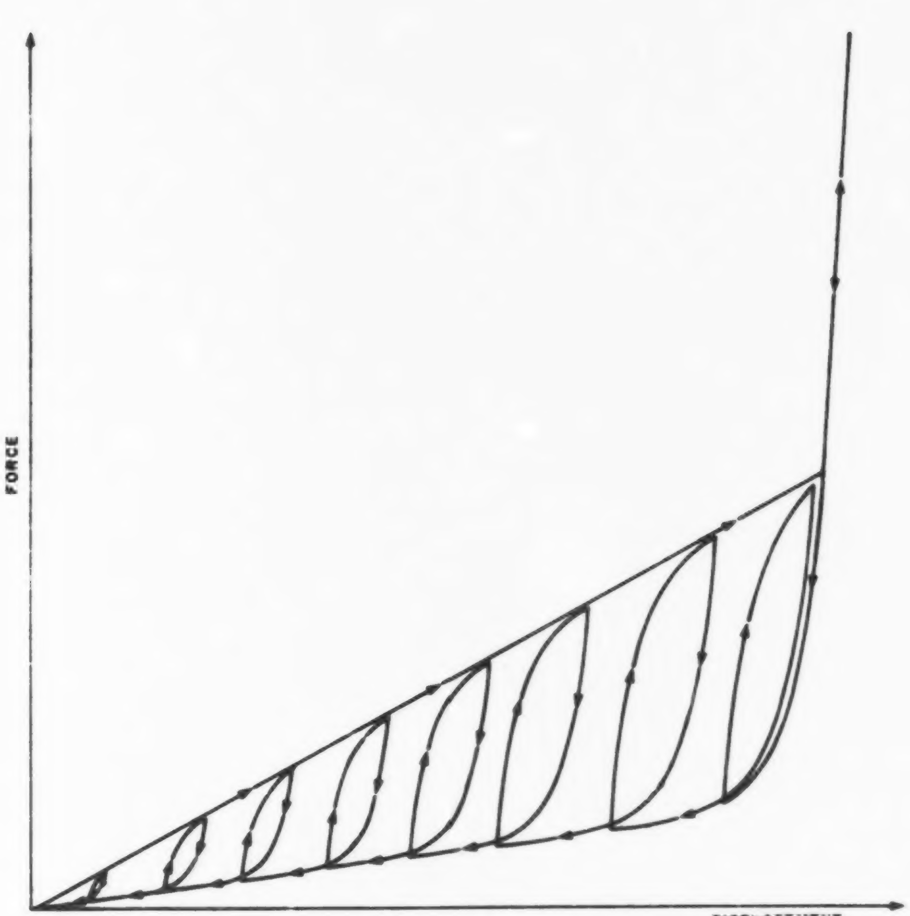

Figure 16- FORCE-DISPLACEMENT CHARACTERISTICS WITH TIME INDEPENDENT DRAFT GEAR

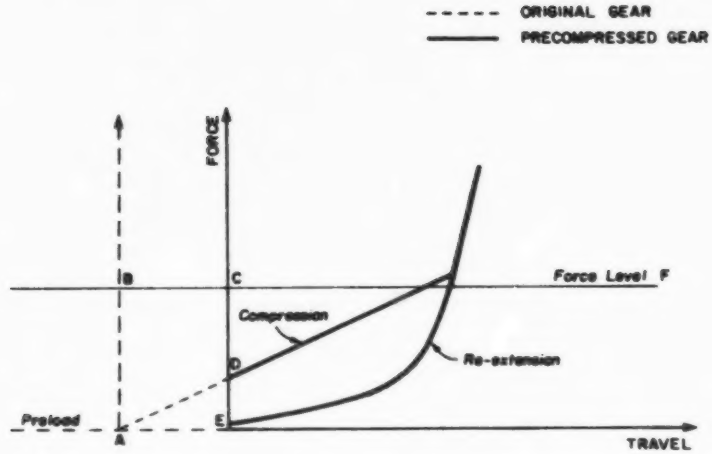

Figure 19- EFFECT OF PRELOAD

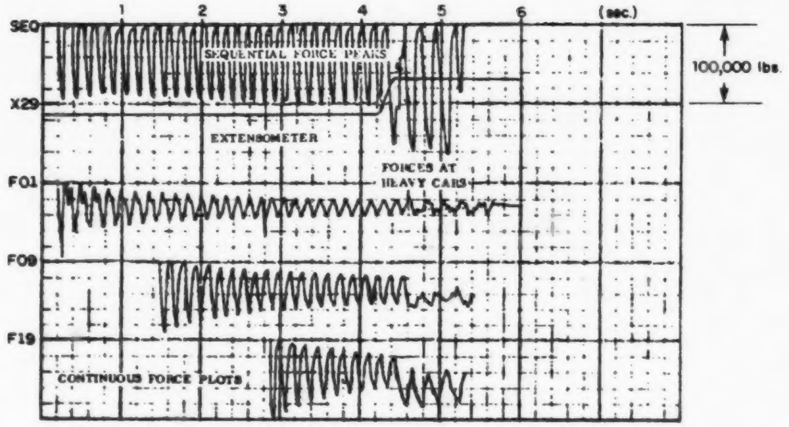

Figure 20A - DATUM RUN-OUT OVER 2 PERCENT GRADE CHANGE

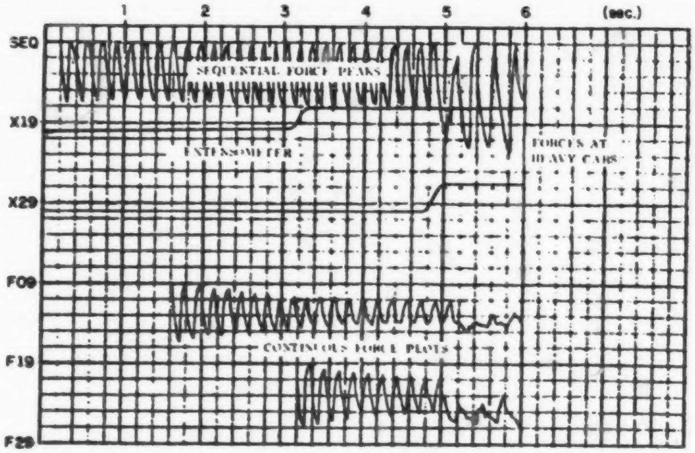

Figure 20B - RUN-OUT WITH SOFTER DRAFT GEAR AND 2 PERCENT GRADE CHANGE

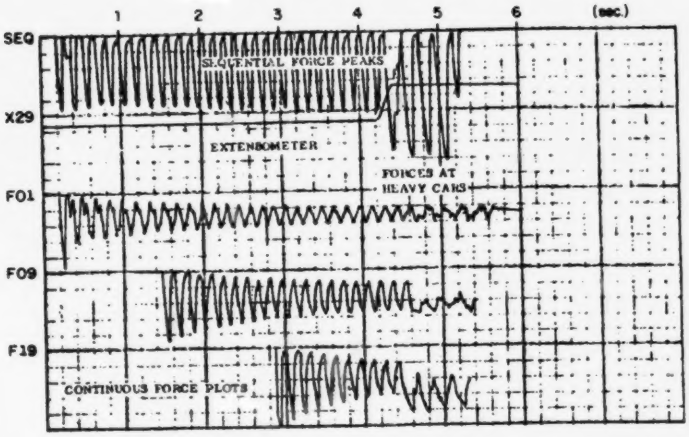

Figure 20C - DATUM RUN-OUT OVER 2 PERCENT GRADE CHANGE

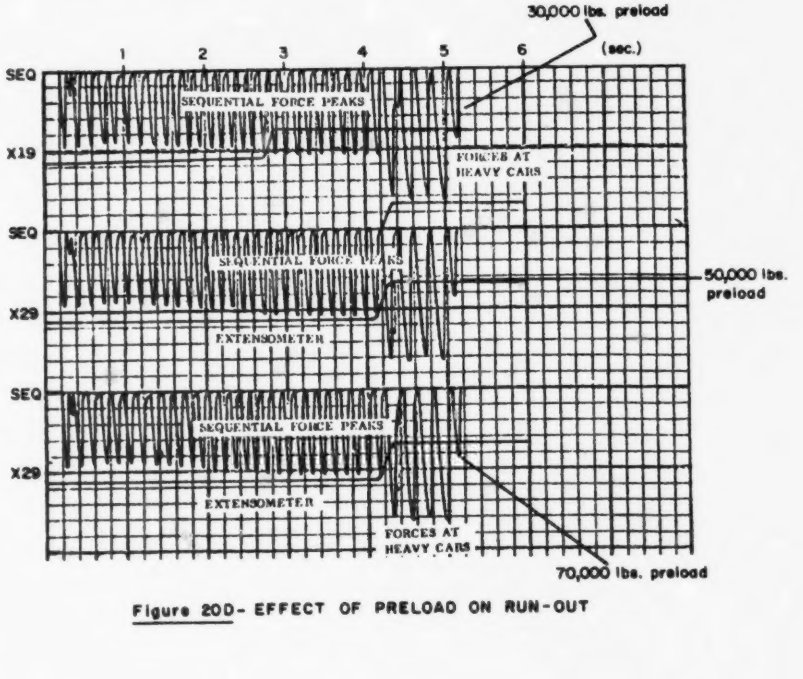

Figure 20D - EFFECT OF PRELOAD ON RUN-OUT

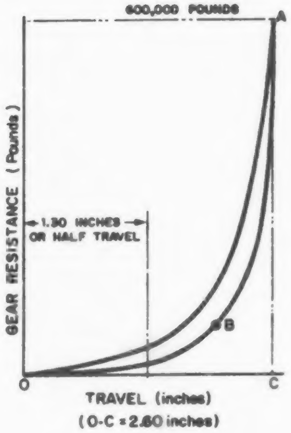

Figure 21- RUBBER DRAFT GEAR CHARACTERISTICS

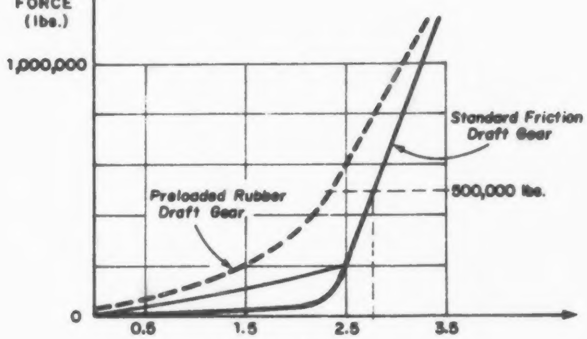

Figure 22- STANDARD FRICTION DRAFT GEAR VS PRELOADED RUBBER DRAFT GEAR

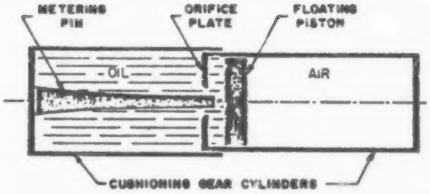
METERING PIN
ORIFICE PLATE
FLOATING PISTON
OIL
AIR
CUSHIONING GEAR CYLINDERS

Figure 23 - SCHEMATIC OF A HYDRAULIC DRAFT GEAR

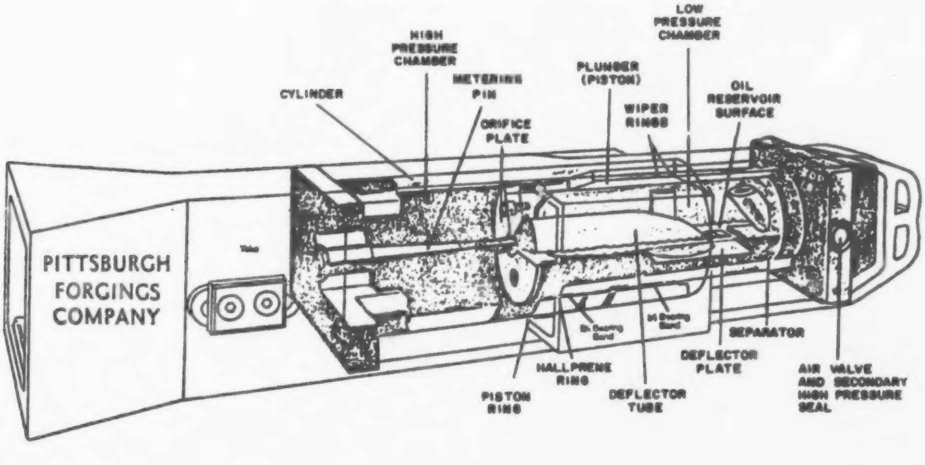
LOW PRESSURE CHAMBER
HIGH PRESSURE CHAMBER
PLUNGER (PISTON)
METERING PIN
CYLINDER
OIL RESERVOIR SURFACE
WIPER RINGS
ORIFICE PLATE
PITTSBURGH FORGINGS COMPANY
SEPARATOR
DEFLECTOR PLATE
HALLPRENE RING
AIR VALVE AND SECONDARY HIGH PRESSURE SEAL
PISTON RING
DEFLECTOR TUBE

Figure 24 - HYDRAULIC DRAFT GEAR

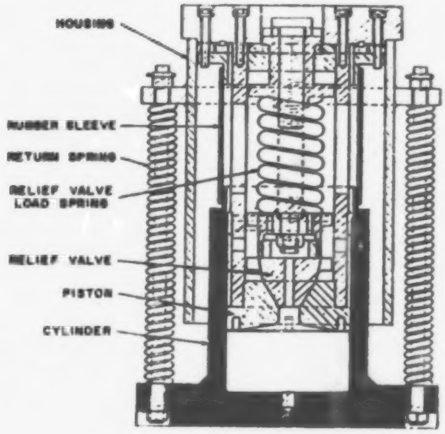
HOUSING
RUBBER SLEEVE
RETURN SPRING
RELIEF VALVE LOAD SPRING
RELIEF VALVE
PISTON
CYLINDER

Figure 25- HYDRAULIC DRAFT GEAR WITH RETURN SPRING

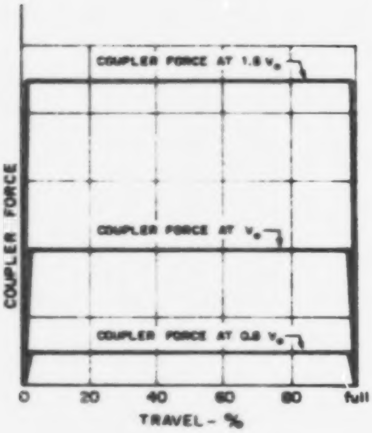

Figure 26 - COUPLER FORCE AT DESIGN MASS AND VARYING SPEED

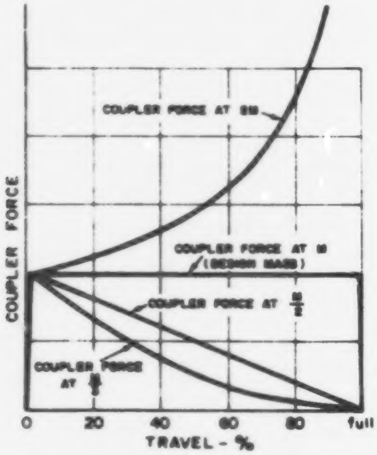

Figure 27 - COUPLER FORCE AT FIXED SPEED AND VARYING MASS

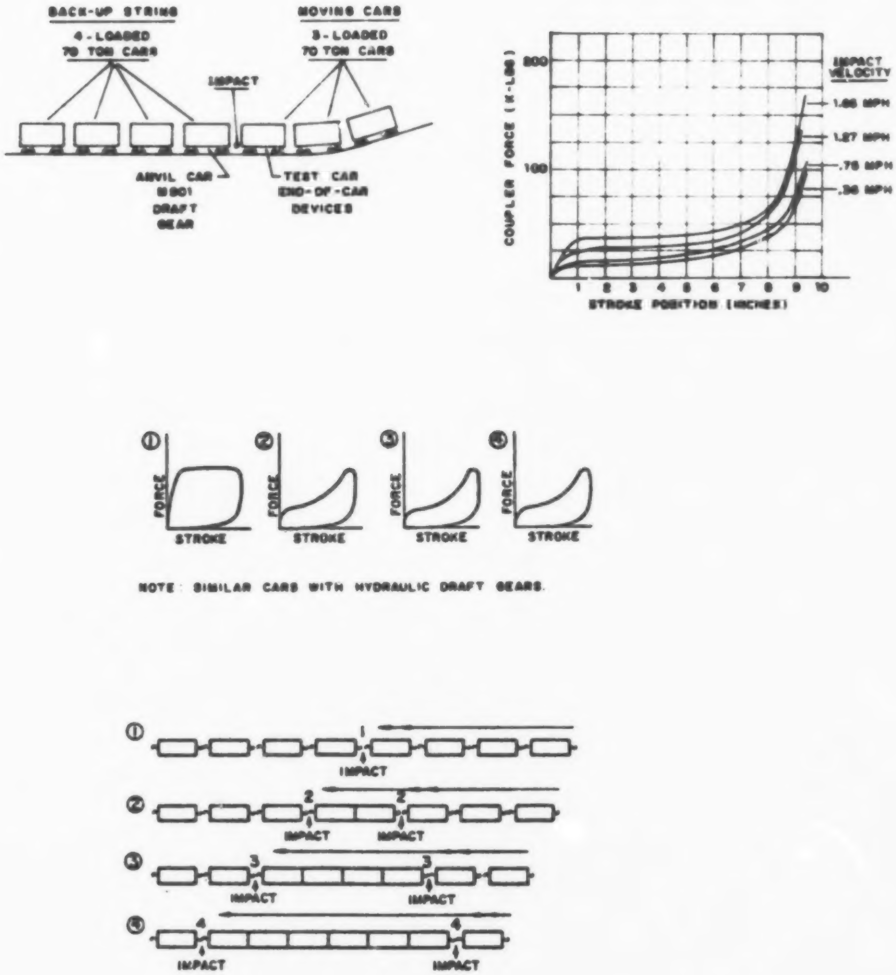
BACK-UP STRING
4-LOADED
70 TON CARS
MOVING CARS
3-LOADED
70 TON CARS
IMPACT
ANVIL CAR
M901
DRAFT
GEAR
TEST CAR
END-OF-CAR
DEVICES
COUPLER FORCE (K-LBS)
200
100
IMPACT VELOCITY
1.66 MPH
1.27 MPH
.75 MPH
.36 MPH
1
2
3
4
5
6
7
8
9
10
STROKE POSITION (INCHES)
①
②
③
④
FORCE
STROKE
NOTE: SIMILAR CARS WITH HYDRAULIC DRAFT GEARS.
①
1
IMPACT
②
2
2
IMPACT
IMPACT
③
3
3
IMPACT
IMPACT
④
4
4
IMPACT
IMPACT

Figure [illegible] - RAKE IMPACT FOR RUN-IN SIMULATION

J Kalousek and A E Bethune

Stringer Stress Measurements on Bridge, Mile. 51.5, Windermere Subdivision

ABSTRACT: 1. In late 1975, a number of cracks, up to 4 inches in length, were found in stringer webs on several bridges of the same design on the Windermere and Cranbrook Subdivisions (Figure 1). Corrective measures were immediately undertaken by the Bridge Department of CP Rail. In order to improve our understanding of crack initiation and propagation in stringer webs, a test program was proposed to measure stress levels at various locations on the stringers, particularly in the areas of crack initiation. Bridge 51.5 Windermere Subdivision was selected as the most suitable site for testing. Several stringers on the bridge were strain gauged in early May 1976 and stress levels recorded during passage of fully laden and light cars.

This report describes the test site, instrumentation and procedures in Chapter 2, and presents experimental data in Chapter 3. Discussion of design and material considerations concerning the stringers is presented in Chapter 4.

2. TEST DESCRIPTION

2.1 Test Site

Bridge 51.5 Windermere Subdivision was selected as a test site for stringer stress measurements for two reasons. A number of stringers on the bridge had experienced cracks in the web section. Secondly, since the bridge is comprised of two spans, each of slightly different design and with different stringer lengths, information on both types of stringers could be collected simultaneously. Additionally, the bridge was easily accessible by road to transport personnel and delicate recording instrumentation.

The general philosophy of this test, as conceived by the authors called for the installation of large numbers of strain gauges at pre-selected locations on various stringers in such a way that any excessive or unusual stresses contributing to the formation of cracks would be recorded. A total of 19 different locations on 10 stringers were selected for application of strain gauges. Three different strain gauge types were employed depending on the information sought. The gauge locations are indicated in Figure 2. More specific details concerning the location of several gauges are independently shown in Figure 3. A comprehensive list of gauges including pertinent technical data is presented in Table 1.

No difficulties were encountered in placing the tension-compression and shear gauges, however rosettes B, D, I and L could not be placed as close to the edge of the stringer copes as desired because of limitations arising from the large diameter of the grinding disc. The same difficulty was experienced in placing torque measuring rosettes O and R. The upper corner of the stringer web (formed by the angle clips and the stringer upper flange), where cracks have been observed, was inaccessible for grinding and strain gauge application. Following a few test runs, the desirability of placing a rosette as near as possible to the copes was recognized and an additional rosette S was installed as close as possible to the stringer cope (see Figure 4a). This however necessitated a modification to the grinding equipment. It should also be mentioned that rosettes B and L were applied to discoloured webs, as depicted in Figure 4b, while rosettes D and I were applied to non-discoloured webs.

2.2 Instrumentation

The instrumentation used in this test was provided by the National Research Council of Canada - Division of Mechanical Engineering and is described in detail in NRC report No. INS-46(1). The instruments were shipped in an NRC instrument van via CP Rail to Golden. The van contained three 18-channel CEC paper recorders and the necessary electronic hardware to connect installed gauges to appropriate Wheatstone bridge circuits. The gauges were calibrated by placing a resistor of known resistance on the gauge and measuring the resulting gauge output, from which the amount of stress or strain per 1" of trace deflection on CEC recorder could be calculated. This calibrating procedure is described in Reference 1 as the "proper" calibration, as opposed to the so called "convenient" calibration. The proper calibrated values for each gauge are presented in Table 1. The sample traces of recorders 1, 2 and 3 are shown in Graphs 1, 2 and 3 respectively.

2.3 Test Procedure

Stress levels were recorded during the passage of 11 trains with various car types both laden and empty (see Table 2). In addition, the effect of speed on stress levels in stringers was investigated throughout a range of 10 mph to 27 mph.

3. RESULTS

3.1 Tension-Compression and Shear Stresses

The general level of stresses on stringers as measured by tension-compression and shear gauges was simply determined by measuring the maximum deflection of the appropriate trace (see Graphs 1, 2 and 3) and multiplying it by the calibrated stress equivalent taken from Table 1. The peak values of this stress with empty and loaded coal cars at various speeds are listed in Table 3. It can be seen from this table that the stresses are low for empty trains and fall beneath the allowable limit calculated according to AREA Manual for Railway Engineering (Chapter 15, Part 2) with loaded 100-ton coal cars. No discernible speed effect on stress levels was observed within the speed range of 10-26 mph. Very interesting results were obtained from the rosette readings.

3.2 Plane Stress Near Coped Areas

Each rectangular rosette measured strain in three directions (45° apart), giving three traces on the CEC recorders. The trace readings were multiplied by the proper calibration values to determine strain. The strain values were then fed to a computer to evaluate the principle stresses and strains and directions in which σ_{max}'s were acting, based on the formulas described in References 2 or 3. As the readings from each gauge repeated themselves in a distinct manner, each such repetition may be considered as a "cycle". It is evident from the records that each loading cycle was caused by the passage of two trucks from neighbouring cars and/or locomotives.

Typical stress cycles evaluated from each rosette are shown in Graphs 4 to 9. Three variations in stress cycles are apparent. The first stress cycle pattern is that measured by rosettes B and L applied to discoloured areas. The second stress cycle pattern is that measured by rosettes D and I which were applied to non-discoloured areas. All rosettes B, D, as well as I and L measured strain at a distance 1-7/8" away from the cope (see Figure 2). The rosettes were intentionally installed on both discoloured and non-discoloured webs to find if the discolouration had any effect on stresses. Our results indicate that the stresses on the discoloured webs are substantially lower than those on the non-discoloured webs (compare Graphs 4 and 5 with Graphs 6 and 7), but we are not able to provide a satisfactory explanation. Two possible explanations are offered for consideration. Stress relieving due to the application of heat may be a factor. Second, development and "bleeding" of two or more hairline non-propagating cracks may have discoloured the web and redistributed the pattern of stress concentrations.

The third stress cycle pattern is that measured by rosette S, which measured stress 3/8" away from the cope on a non-discoloured web. The peak stress measured by this rosette is appreciably higher than that measured by rosettes D and I and indicates that copes act as stress raisers. Considering the non-linear nature of stress risers such as notches, copes, holes, etc., it is quite probable that the macro-stress in the immediate vicinity of the cope reaches 31 ± 3 ksi (see Figure 5) on non-discoloured webs. The effects of micro-stresses arising from the quality of the surface finish and the corrosive effect of atmospheric moisture will be discussed later in this report.

3.3 Torsional Rosettes

Graph 10 shows the stresses and orientation measured by torque rosettes Q and R applied on opposite sides of a web as shown in Figure 2. The original purpose of installing this pair of rosettes was to determine whether ties, when deflected by loading, impose a torsional moment on the stringers in addition to pure bending. In other words, we were interested in establishing whether the loading from ties is symmetrical or asymmetrical with respect to the centerline of the stringer's upper flange.

Examination of Graph 10 confirms the asymmetrical nature of tie loading on the stringer flanges and hence the presence of a torsional moment on the stringer. Surprisingly, the torque acts on this stringer in a direction opposite to that expected. With the tie loadings asymmetrical toward the gauge side of the stringer and with the stringer web fixed at each end to the floorbeam, compression on rosette R (applied to the gauge side of the web), and tension on rosette Q (applied to the field side of the web) should result. Since the opposite combination of stresses was measured by rosettes Q and R, it may be concluded that the tie loadings were displaced toward the field sides of the stringer upper flange.

The torsional moment direction being toward the field side of the bridge can be most plausibly explained by the fact that the beam flanges have not been rolled exactly perpendicular to the web. This type of rolling defect had been actually observed on several stringers in the bridge floor. The top flange of instrumented stringer was slightly higher on the field side than at the gauge side.

In any event, the stresses resulting from bending and torsional loads on a stringer are low and their existence alone does not account for the formation of cracks observed at the top of the stringer web. Additional factors, such as stress concentration at the boltholes and/or the possibility of fretting fatigue must also be taken into account.

4. DISCUSSION

During the course of the investigation, the authors of this report have been somewhat overwhelmed by the large amount of literature available dealing with fatigue related subjects (about 7,000 papers and several dozen books). Most of this information is highly specialized and narrow in scope. A few sources, which were found to contain a reasonable blend of practical and theoretical information are listed in references 4 to 8.

The general feeling obtained from examination of the literature reviewed is that high strength structural steels are more advantageous when utilized in statically rather than dynamically loaded structures.

For statically loaded structures, high strength structural steels have a strength ratio of 1.5 to 3 with respect to plain carbon structural steel when comparing yield point. In our case, tests performed on a sample taken from the bridge stringers under investigation showed that the yield point of the stringer steel was 62,000 psi and ultimate tensile strength was approximately 79,000 psi. The strength ratio of high strength steel as compared to typical plain carbon construction steel (with approximately 33,000 psi yield) is approximately 1.9.

With dynamically loaded structures, the fatigue strength (namely the fatigue limit or endurance limit) must be carefully taken into consideration in the design. While fatigue data on high strength steels, based on the rotating beam test with polished specimens, indicates higher fatigue strength, in actual fact, higher fatigue endurance is rarely realized in the finished structure. Stress raisers such a notches, bolt holes, welds, riveted joints, and other defects from welding, or present in the "as rolled" steel, have a greater net effect on high strength steel than on plain carbon structural steel. In some instances, the structures made from these two types of steel have the same overall fatigue endurance.

The findings contained in previous sections of this report, namely the existance of a higher filament stress in the vicinity of the cope, indicate that the cracks are indeed of fatigue origin. In this chapter, we will be concerned with a few specific aspects of fatigue cracking of stringers. These are:

1. Number of cycles
2. Stress concentration
3. Surface finish
4. Corrosion environment

Other aspects of less importance which have an influence on fatigue cracking of stringers, are described in the generalized texts 4 to 8.

4.1 Number of Cycles

Modern methods to determine stress cycles are well described in reference 8. With bridge stringers, it is possible to quite accurately determine the number of cycles from a knowledge of loading patterns on the stringers and the amount of traffic which passed during the time the stringers were in service. The loading cycle stress pattern on the stringers, as measured by rosettes J and S, is one cycle per car or locomotive. We have estimated that stringers in Bridge 51.5 were subject to approximately 500,000 to 600,000 loading cycles by laden 100-ton capacity cars and locomotives, and approximately the same number of empty car cycles, with perhaps an additional 100,000 loading cycles caused by mixed traffic in the period between 1969 and 1975.

The empty car loading cycles did not contribute to stringer cracking since their peak loads fall well beneath the fatigue limit as will be shown later. Therefore, fatigue cracking of the stringers must be due to approximately 600,000 cycles caused by 100-ton capacity cars, locomotives and heavier cars from mixed traffic. The double peak observed on the rosette D stress pattern has an additional damaging effect on the fatigue endurance of stringers.

4.2 Stress Concentration Near Copes

A measure of the severity of a stress concentration is given by the stress concentration factor K_t which is defined as the ratio of the maximum local stresses in the region of the notch to the nominal local stress evaluated by simple theory. According to Figure 3, the stress concentration factor for stringer copes would be:

$$K_t = \frac{\sigma'_{max}}{\sigma_{nom}} = 2.5 \text{ to } 3.1$$

The value of $\sigma'_{max} = 31 \pm 3$ ksi has been derived from the stress concentration curve, the slope of which and two points through which it has to pass being known.

Fatigue strength is considerably reduced by geometric stress concentrations, but the effect of stress concentration varies with different materials. To account for this variation in material behaviour, a fatigue strength reduction factor K_f has been introduced which is defined as the ratio of fatigue strength of a specimen with no stress concentration to the fatigue strength of a specimen with a notch. The relationship between K_f and K_t is given by the notch sensitivity factor q which is defined as:

$$q = \frac{K_f - 1}{K_t - 1}$$

When $K_f = K_t$, $q = 1$, and the material is said to be fully notch sensitive. If the presence of a notch does not affect the fatigue strength, $K_f = 1$, $q = 0$ and the material is notch insensitive.

The q value of high strength construction steel CSA/G40.11 Grade B was not discovered by the authors in any available literature. The notch sensitivity of mild steel (.17% carbon) is .3. It is mentioned by several investigators that notch sensitivity of high strength structural steel is approximately twice that of mild steel, giving a notch sensitivity value of approximately .6 for high strength structural steel.

4.3 Effect of Surface Finish and Corrosion Environment on Fatigue Limit

A fatigue test, in which fatigue limit is usually reached after 2 or more million stress cycles, may be carried out on a large variety of specimens. These may be polished round bars, bars with grooves or notches, and "as rolled" flats in the case of construction steel. If data from these tests are available for a given material, one may make allowance for factors such as stress concentration, notch sensitivity, surface finished and environmental effects to estimate the fatigue life of a structure. For example, if fatigue test data was available for flat rolled bars with ground edges, we would have to consider the effect of stress concentration due to a cope and environmental effects, to finalize the design. Since no fatigue data of any kind could be found for CSA/G40.11 Grade B or its equivalent ASTM/A588 Grade B steel, we are left with general considerations which are summarized in graphical form in Figure 6. From this diagram, it may be seen that the fatigue ratio (fatigue limit divided by ultimate tensile strength) is approximately .50 as determined by polished, un-notched specimen, subject to completely reversed cycles of flexural stress. For various varieties of steel with the same tensile strength, this fatigue ratio may vary from .40 to .60. The degree of polish also influences the fatigue limit.

The surface finish, which may be ground, peened, turned or "as rolled", etc., contains irregularities which act as microscopic stress raisers which reduce fatigue endurance. Rough ground surfaces usually have significant stress raising effects, due to the presence of V-shape grooves on the surface profile. Grinding marks perpendicular to the web inside the coped area approximately .004" (1 mm) deep containing many 60°V groove notches observed on the copes, bring the fatigue limit of the stringer steel into the range of 22 to 30 ksi. If we consider notch sensitivity of steel, which is the same for large or small V-shape notches, the fatigue limit of ground steel may be derived from a knowledge of the fatigue limit of a polished specimen and the notch sensitivity factor. Thus, taking the fatigue limit of polished specimens (approximately 40 ksi) and multiplying it by the notch sensitivity factor (.6), gives the fatigue endurance limit of the roughly ground specimen at 24 ksi, which falls into range of 22 to 30 ksi just mentioned.

The bottom area of Figure 6 relates to steel subject to a corrosive atmosphere or liquid water while being dynamically stressed. This figure also indicates that steels which have improved corrosion resistance due to the addition of alloying elements, do not possess improved fatigue corrosion resistance. Hence, for our material with an ultimate tensile strength of approximately 80 ksi, the fatigue endurance in a corrosive atmosphere would fall between 10 and 20 ksi.

This type of fatigue behaviour on high strength steel is acnowledge in AREA Manual for Railway Engineering, Chapter 15-2-1, paragraph 3, which reads "The fatigue strength of high-strength steels is not materially greater than that of ASTM A36 steel."

Fatigue cracks on stringer copes which appeared after 600,000 cycles actually give us the fatigue life (or 1 point on the S-N curve) of our material, for our given combination of nominal stress, stress raisers, notch effect, and corrosive effects of the environment. It may be concluded that other stringers of the same design will also eventually fail if all three factors, i.e. cope, grinding marks and corrosive environment are present. However, the severity of these factors may vary from location to location (i.e. corrosive environment) or from manufacturer to manufacturer (coarseness of grinding wheels used to grind the copes) so that the time to failure may vary considerably. However, in view of Figure 6, all floor stringers, coped in this manner, and loaded by locomotives and 100-ton capacity cars may be expected to eventually fail in fatigue.

4.4 Fretting Fatigue

The cracks observed in the upper portion of the web were most likely caused by fretting fatigue since no other rational explanation of their occurrence could be found. Fretting occurs when two pieces of material pressed together by an external static load, such as from a tightened bolt, are subjected to a transverse cyclic loading so that one contacting face is relatively displaced cyclically parallel to the other face. The magnitude of the tangential displacement is usually small and does not exceed more than about .0004" (.1 mm). During fretting, small fragments of metal are broken and oxidize, forming oxide particles, which are, for most engineering metals, harder than the metal itself. This leads to surface pitting, wear, scoring and the transfer of metal from one surface to another. If the material is simultaneously subjected to fretting and alternating stress, fatigue cracks may originate at a fretted surface and propagate in the direction of maximum shear stresses.

With riveted or bolted joints, fretting can occur in the rivet or bolt hole or between the plates themselves causing fatigue failure at low alternating stresses. As might be expected, the fatigue strength of a riveted or bolted joint is not related to the plain fatigue limit of the plate material or to the static strength of the joint itself. Detailed descriptions of various types of bolted joints and their behaviour under fatigue loading may be found in references 10, 11 and 12.

Methods of increasing the fatigue strength of either riveted or bolted joints in a structure such as bridges include the insertion of anti-fretting compounds between the bolt or rivet shank and the hole wall or by increasing the tensile stress in the rivets or bolts, which permits more of the load to be transmitted by friction at the contacting surfaces rather than by shear in the bolt. In fact, the basic principle underlying the use of high tensile steel bolts is that they are sufficiently strong to enable them to be tightened to such an extent that the working loads are transmitted by frictional forces between the plates. As might be expected, many researchers (reference 13) have found that the fatigue strength of a bolted joint having properly tightened high tensile strength steel bolts is superior to that of a joint of similar geometry fastened with partially tightened bolts or rivets.

In our case, fretting could have occured either between the bolt and the bolt hole if the bolt was not tightened properly, or between the angle clips and stringer web due to the presence of a lateral moment as indicated by rosettes Q and R. The fretting most likely occured in the top area of the angle clips where the absence of the bolt permitted fretting in the vertical direction. The cracks may have initiated at low stress levels and then propagated in the direction of maximum shear stress, that is horizontally, as may be interpreted from Graph 10. It is believed that a type III joint (Figure 7) would eliminate fretting caused by the presence of a lateral moment acting on a stringer.

It is not possible to accurately predict the fretting fatigue strength of a joint, especially with numerous bolts, from a knowledge of fatigue strength of the material and the joint geometry. However, a corrosive environment has the same effect on the fretting fatigue endurance of joints as it does on the fatigue life of materials in general. The crack in the stringer web observed in the top portion of the angle clip joint is actually an accurate assessment of fatigue life of the joint under the specific environmental, metallurgical and loading conditions experienced. The very rare occurrence of these types of failures defies any kind of generalization or specific recommendations to be made.

5. CONCLUSIONS AND RECOMMENDATION

Stress measurements carried out by Canadian Pacific Department of Research and the National Research Council have clearly revealed the stress distribution in stringers under dynamic conditions, particularly in the vicinity of the origin of cracks. These measurements have shown that the cracks are of fatigue or fretting fatigue origin. Train speed was found to have no effect upon stringer stress level. Based on the discussion presented in the previous chapter the following recommendations are made.

1. All stringers with the copes of the design investigated in this report should be repaired according to CPR Bridge Department recommendations.

2. The use of unpainted steel for bridges should be reviewed. Some form of corrosion prevention should be used on joints, copes, fillets, or any portion of the bridge where stress concentration may occur.

3. Copes in the floor members should be avoided in future design.

4. In view of increasing traffic densities and usage of heavier freight cars, a recommendation to the AREA Bridge Committee should be made to incorporate a sentence in Chapter 15, Section 1.8 of AREA Manual as follows:

   "Floor members shall not be coped or notched."

REFERENCES

1)	W.J. Watson L.A. Weatherston	Measurement Systems & Reduction Techniques Used in Railway Engineering. NRC Report No. INS-46.
2)	Parry & Lissner	The Strain Gage Primer, McGraw Hill (1962)
3)	J.W. Dally W.F. Riley	Experimental Stress Analysis, McGraw Hill (1965)
4)	O.J. Horger (Ed.)	Metals Engineering Design, ASME Handbook McGraw Hill, 1953.
5)	P.G. Forrest	Fatigue of Metals, Pergamon Press (1962)
6)	E.H. Spaulding	Metal Fatigue, McGraw Hill (1969)
7)	L. Sors	Fatigue Design of Machine Components, Pergamon Press (1971)
8)	N.E. Frost K.J. March L.P. Pook	Metal Fatigue, Clarendon Press, Oxford (1974)
9)	P. Watson R.G. Rebbeck	Modern Methods of Fatigue Assessment REJ, November 1975, p.10.
10)	W.H. Munse D.T. Wright N.M. Newark	"Laboratory Test of Bolted Joints" Proc. Am. Soc. Civil Engrs. 120 p.1299 (1955)
11)	R.S. Fountain W.H. Munse R.D. Sunbury	Specifications and Design Relations Proc. Am. Soc. Civil Engrs. - Struct. Division, 94, No. ST12 1968.
12)	J.W. Fisher L.S. Beedle	Criteria for Designing Bearing-Type Bolted Joints Proc. Am. Soc. Civil Engrs. Struct. Division 91, 129 (1965)
13)	C.W. Lewitt E. Chesson W.H. Munse	"New Concepts in Structural Joint Design" Proc. Am. Soc. Civ. Engrs. - Struct. Division 89, p.49 (1963)
14)	C.T. Webster	Bridges 22.6, 35.7 and 51.5 Windemere Subdivision, CPR Internal Correspondence
15)	Battelle Memorial Institute	"Prevention of the Failure of Metals Under Repeated Stress" Wiley & Sons (1946)

TABLE 1

"PROPER" CALIBRATED VALUES FOR VARIOUS GAUGE TYPES

Gauge	Gauge Type	Gauge Factor	Recorder No.	Trace No.	Proper Stress psi/x1" T.D.*	Proper Strain µin./in./1"T.D.*
A	Shear (12")	2.065	3	1	23,200	770
B	Rosette (1-5/8") (Discoloured)	2.075 2.075 2.075	3	3 4 5	21,900 21,900 23,100	730 730 770
C	Shear (Center)	2.065	3	2	21,000	700
D	Rosette (1-1/4")	2.075 2.105 2.075	3	10 11 12	23,100 26,700 23,700	770 890 790
E	Tens-Comp (Top-Center)	2.100	3	8	24,500	810
F	Tens-Comp (Top-Center)	2.100	3	9	22,500	720
G	Shear (Center)	2.065	3	6	23,500	780
H	Shear (3")	2.075	3	7	23,800	790
I	Rosette (1-5/8")	2.075 2.105 2.075	2	1 2 3	20,600 21,600 21,400	690 720 710
J	Tens-Comp (Bottom 6")	2.100	2	4	20,900	700
K	Tens-Comp (Bottom Center)	2.100	2	5	20,600	690
L	Rosette (1-5/8") (Discoloured)	2.075 2.105 2.075	2	6 7 8	21,100 20,300 20,400	700 690 680
M	Shear (Center)	2.065	2	9	21,000	700
N	Shear (6")	2.065	2	10	22,600	750
O	Tens-Comp (Bottom 3")	2.100	1	1	45,000	510
P	Tens-Comp (Bottom Center)	2.100	1	2	22,200	1500
Q	Rosette	2.075 2.105 2.075	1	3 4 5	20,900 21,300 21,100	700 710 700
R	Rosette	2.075 2.105 2.075	1	6 7 8	20,900 20,800 20,900	700 700 700
S	Rosette (3/8")	2.075 2.105 2.075	1	9 10 11	19,200 18,000 18,400	640 600 610

* T.D. -- Trace Deflection

TABLE 2

List of Test Runs by Train Type and Speed

Test Number	Date 1976	Train Number	Train Type	Speed Range MPH
1	May 6	5802N	100 Ton Bathtub Coal Cars - Loaded	20 Constant
2		5655N	70 Ton Coal Cars - Loaded	10-20
3	May 7	5800N	100 Ton Bathtub Coal Cars - Loaded	20-25
4		82-5670	Mixed Train - 6 Loads, 2 Empty	20-25
5		80-5809	Empty Bathtub Coal Cars	5-25
6		863IN	Mixed Train - 4 Loads, 36 Empty	24-27
7		84-5777	Empty Bathtub Coal Cars	25 Constant
8		5806	100 Ton Bathtub Coal Cars - Loaded	24-26
9	May 8	5809	70 Ton Coal Cars - Loaded	10-15
10		5810	70 Ton Coal Cars - Loaded	20-25
11		5681	100 Ton Bathtub Coal Cars - Loaded	15-20

TABLE 3

MAXIMUM TENSION-COMPRESSION AND SHEAR STRESSES AT VARIOUS LOCATIONS ON THE STRINGERS FROM EMPTY AND LOADED COAL CARS AT VARIOUS SPEEDS

Gauge	Gauge Type	STRESS σ_{max} OR τ_{max} (psi)										
	COAL CAR	EMPTY		LOADED								
	Speed MPH	10	25	10	12	14	16	18	20	22	24	26
O	Tens-Comp (Bottom 3")	0	0	0	0	0	0	0	0	0	0	0
J	Tens-Comp (Bottom 6")	0	0	0	0	630	420	840	1,050	840	630	1,050
K	Tens-Comp (Bottom Center)	2,060	2,270	9,270	9,480	9,480	9,480	9,890	10,100	10,300	9,890	9,890
P	Tens-Comp (Bottom Center)	1,350	1,800	9,000	8,100	8,550	8,100	9,000	9,450	9,000	8,100	8,550
E	Tens-Comp (Top Center)	-1,470	-2,205	-7,840	-8,090	-8,330	-8,820	-8,820	-9,070	-8,330	-9,310	-9,800
F	Tens-Comp (Top Center)	-2,030	-2,250	-7,200	-6,080	-7,880	-7,880	-7,880	-7,880	-8,100	-9,000	-9,000
H	Shear (3")	2,380	2,870	11,900	11,660	14,040	12,850	12,850	12,850	13,090	12,610	11,660
N	Shear (6")	2,710	2,490	11,300	10,850	10,620	10,850	11,300	11,300	12,430	11,980	11,300
A	Shear (12")	2,090	2,320	11,600	11,600	11,370	11,140	13,000	10,900	12,300	11,370	11,370
C	Shear (Center)	630	630	2,100	2,310	2,100	2,310	2,100	2,520	2,730	2,940	2,310
G	Shear (Center)	940	1,180	2,600	2,820	2,820	3,060	3,060	2,350	3,060	2,820	3,060
M	Shear (Center)	840	630	2,940	3,150	3,150	2,940	3,360	3,360	3,570	3,150	2,940

FIGURE 1: Crack observed in the web near the coped area.

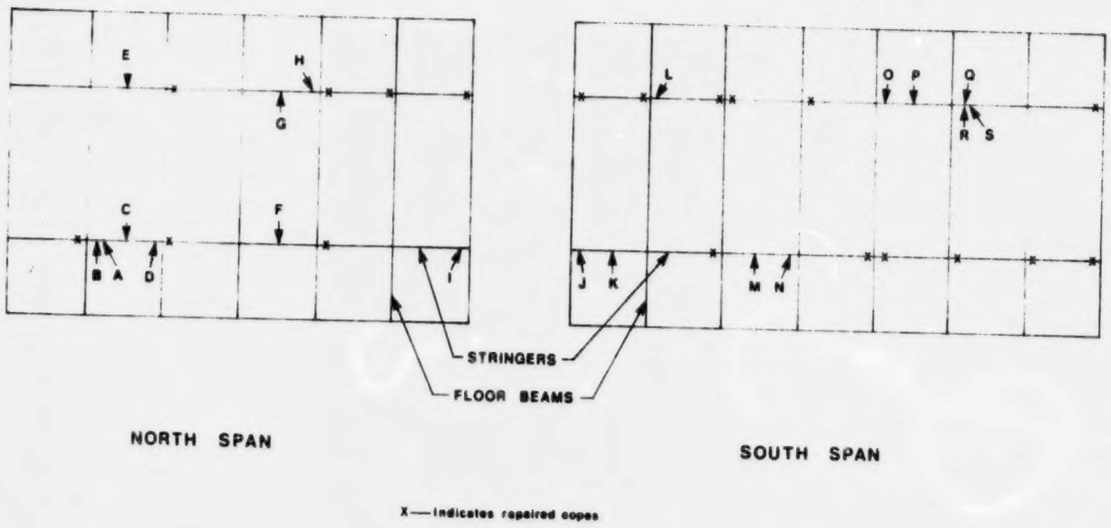
E
H
G
C
F
B
A
D
I
L
O
P
Q
R
S
J
K
M
N
STRINGERS
FLOOR BEAMS
NORTH SPAN
SOUTH SPAN
X — Indicates repaired copes

Figure 2: GAUGE LOCATIONS ON BRIDGE 51.5 WINDERMERE SUB.

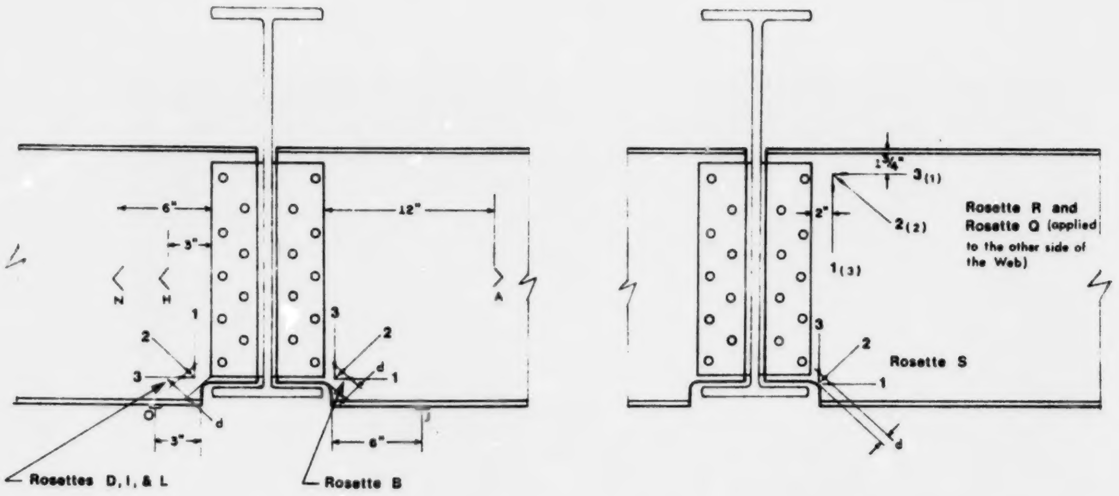
6"
3"
12"
N
H
A
1
2
3
d
3"
3
2
d
1
6"
Rosettes D, I, & L
Rosette B
1 3/4"
3(1)
2"
2(2)
1(3)
Rosette R and
Rosette Q (applied
to the other side of
the Web)
3
2
Rosette S
1
d

A) Location of Gauges on various Stringers
(viewed towards the center of the track)

B) Actual positions of Torsion measuring Rosettes 'Q' and 'R'
and Rosette 'S' (viewed towards the field side of track)

d = DISTANCE BETWEEN FILAMENT CENTERS OF ROSETTES AND THE ROOT OF COPES.
FOR ROSETTES B, D, I AND L: d = 1 5/8". FOR ROSETTE S: d = 3/8".

Figure 3 - SPECIFIC POSITION OF SEVERAL GAUGES WITH RESPECT TO STRINGERS

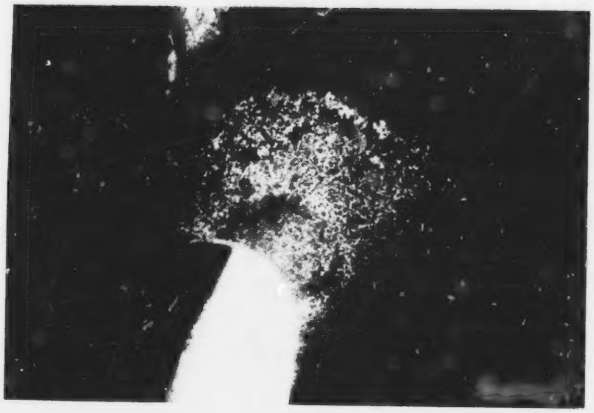

(a) Discoloured Area Near the Cope.

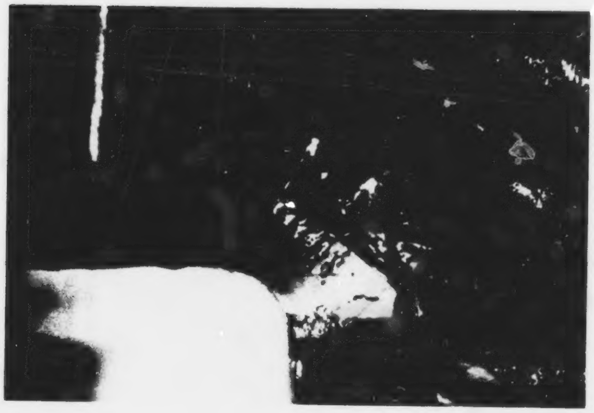

(b) Rosette 'S'

FIGURE 4

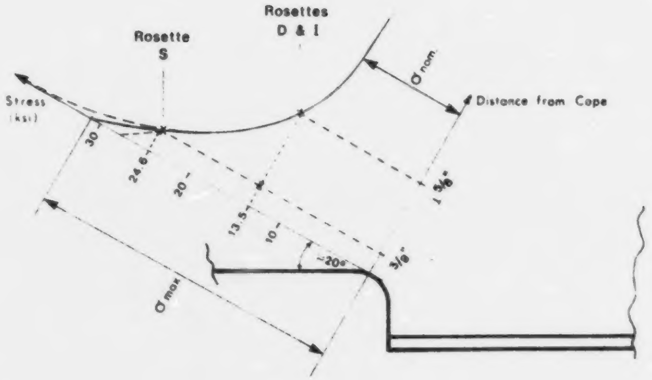
Rosette
S
Rosettes
D & I
Stress
(ksi)
σ_{nom}
Distance from Cope
30
24.6
20
13.5
10
~20°
1 5/8"
3/8"
σ_{max}

Figure 5 - STRESS CONCENTRATION CAUSED BY COPE

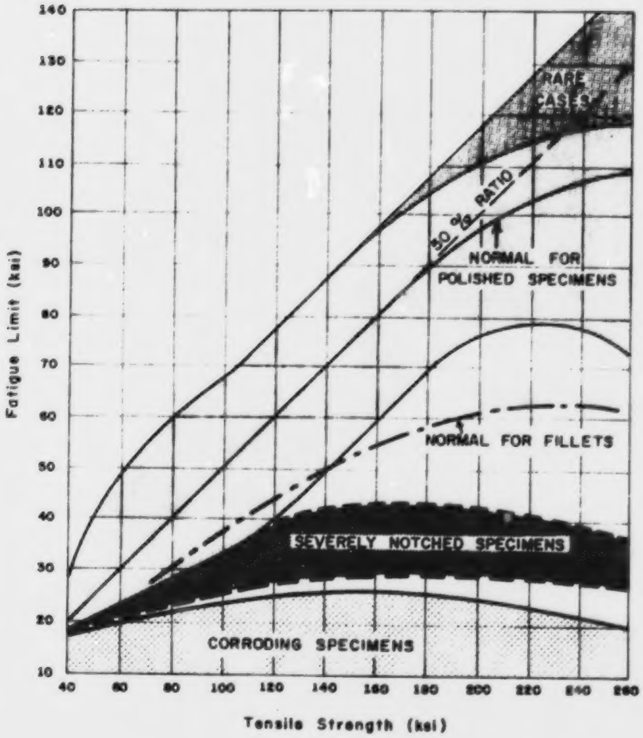

Figure 6- GENERAL BEHAVIOUR OF FATIGUE IN STEEL OF POLISHED, NOTCHED OR CORRODING SPECIMENS AS RELATED TO TENSILE STRENGTH. (After Batelle Memorial Institute (15))

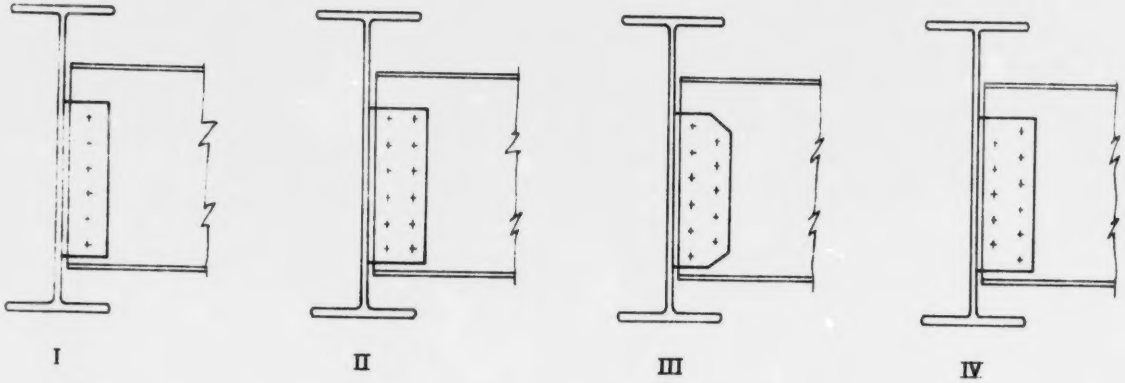

FIGURE 7- VARIOUS PATTERNS OF TYPICAL RAILWAY BRIDGE CONNECTIONS

(After Webster (14))

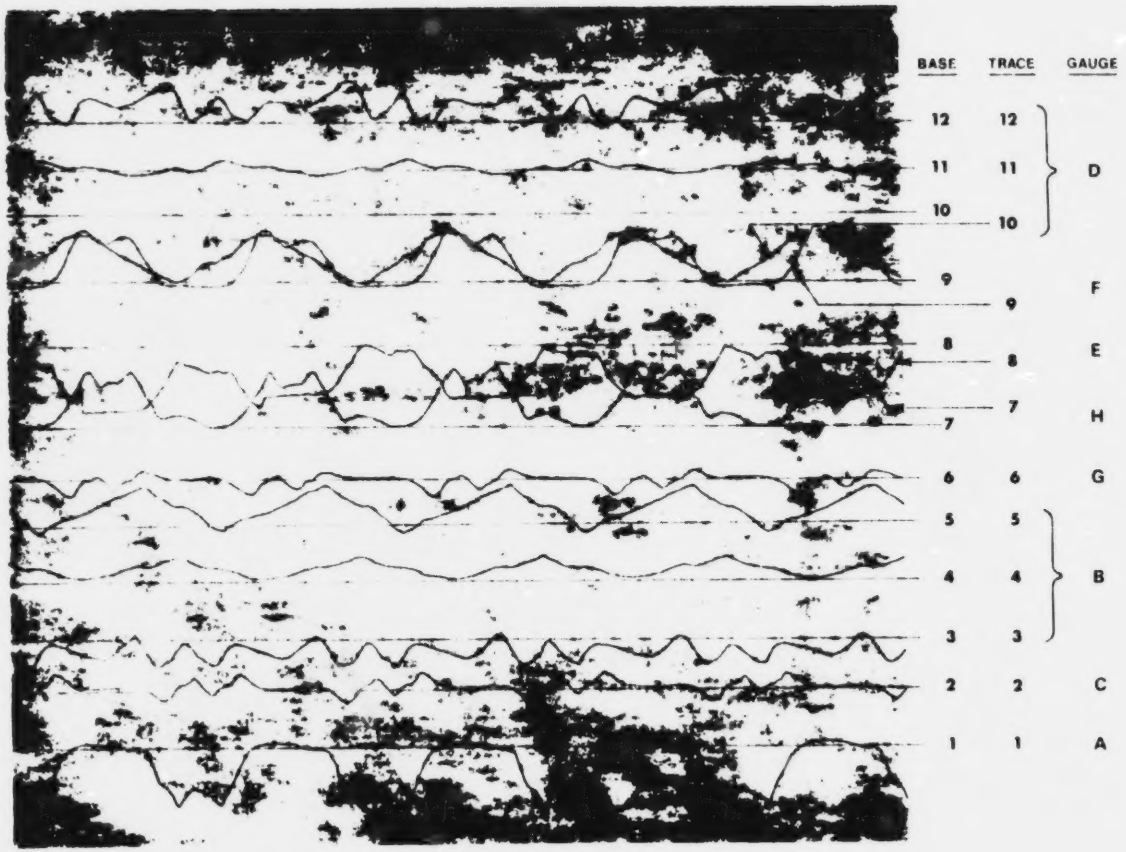

GRAPH NO 1 - TRACE SAMPLE OF RECORDER NO 1, TEST NO 8

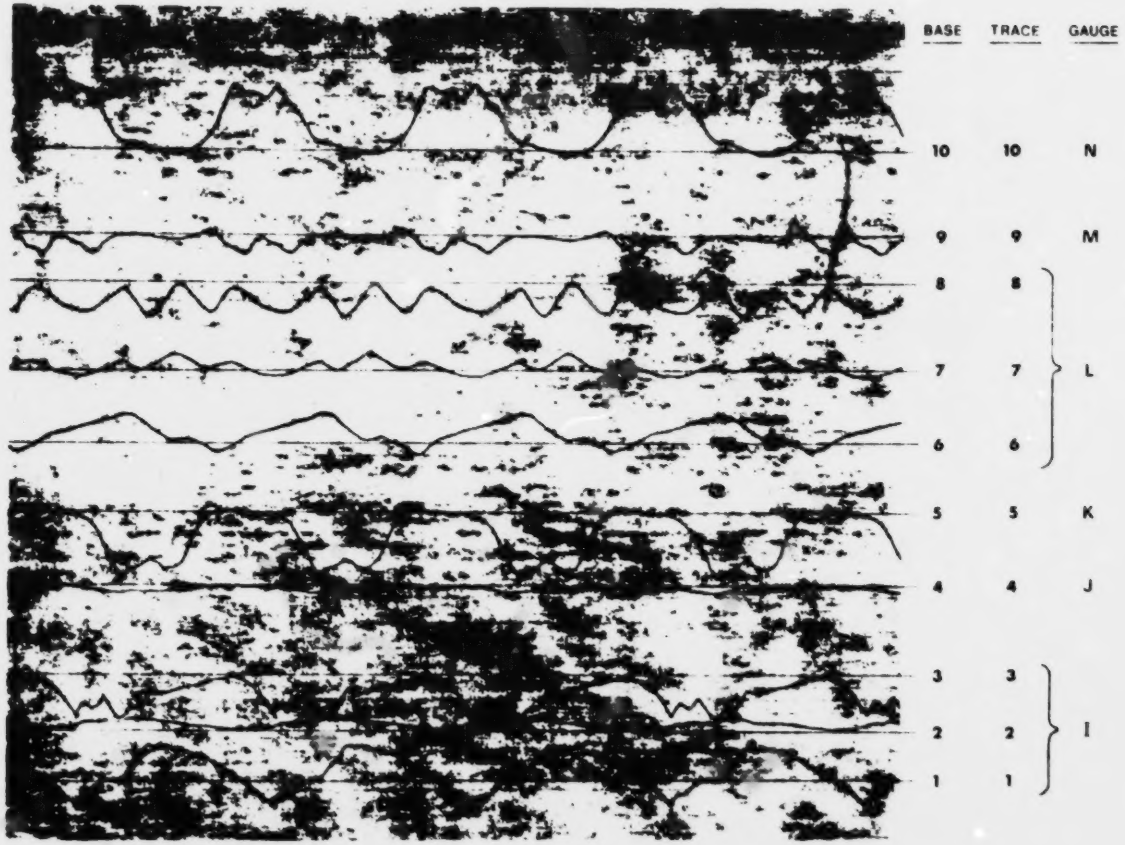

GRAPH NO. 2- TRACE SAMPLE OF RECORDER NO. 2. TEST NO. 8

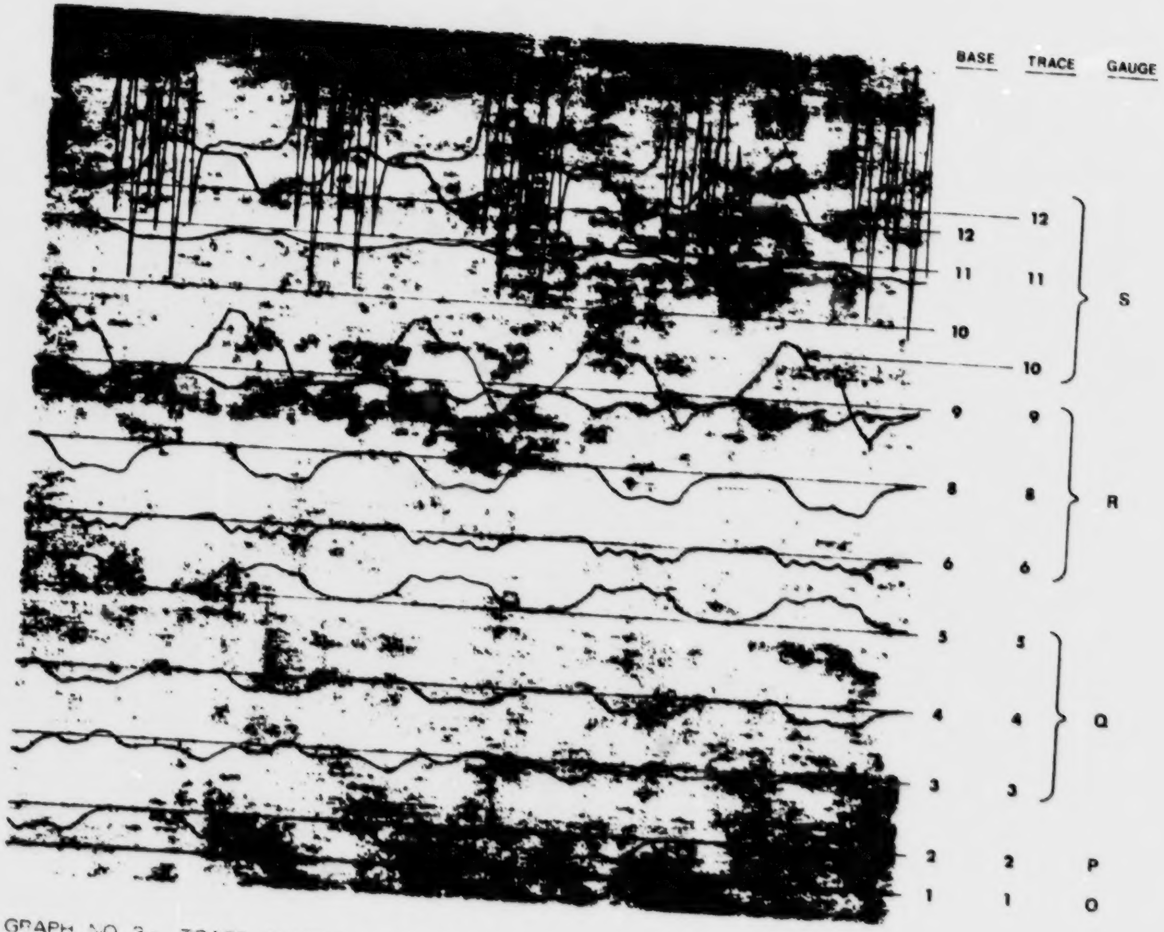

GRAPH NO 3 · TRACE SAMPLE OF RECORDER NO 3. TEST NO 8

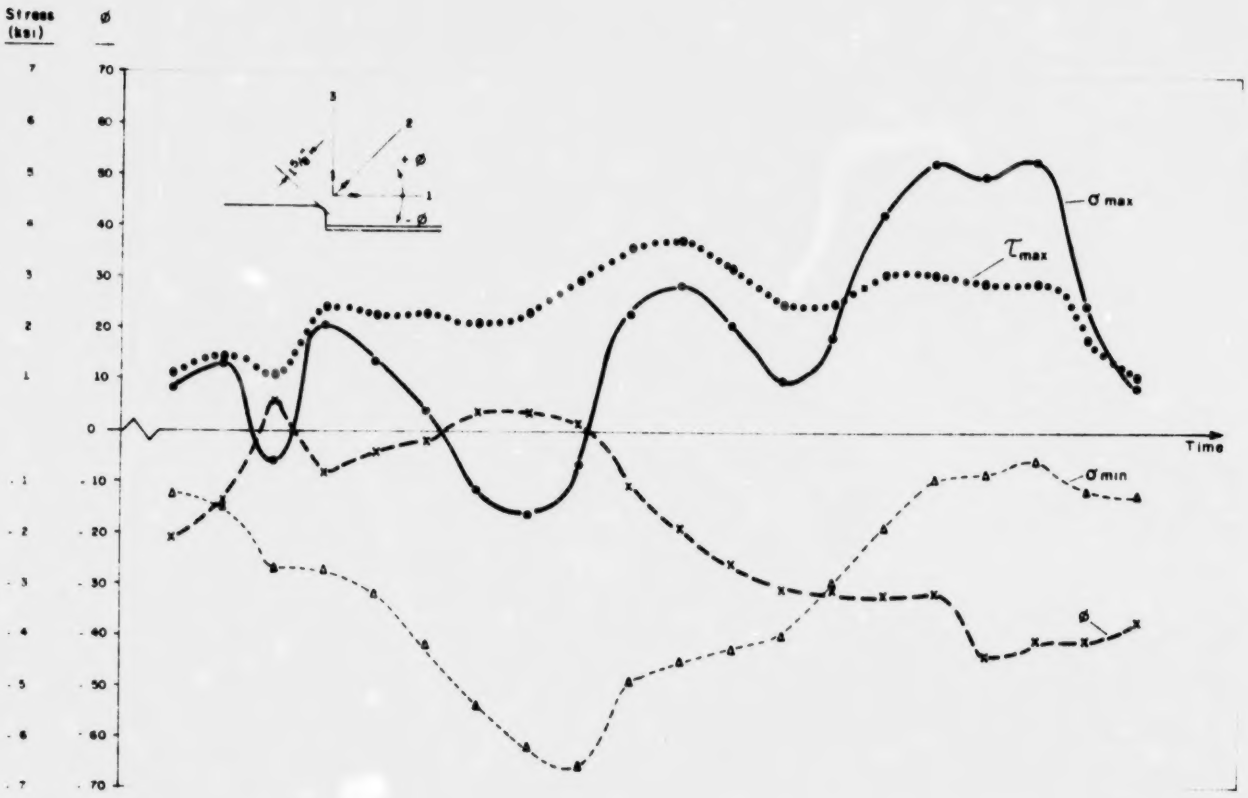

GRAPH NO. 4 - STRESS CYCLE MEASURED BY ROSETTE 'B' - (DISCOLOURED), TEST NO. 8, 26 MPH.

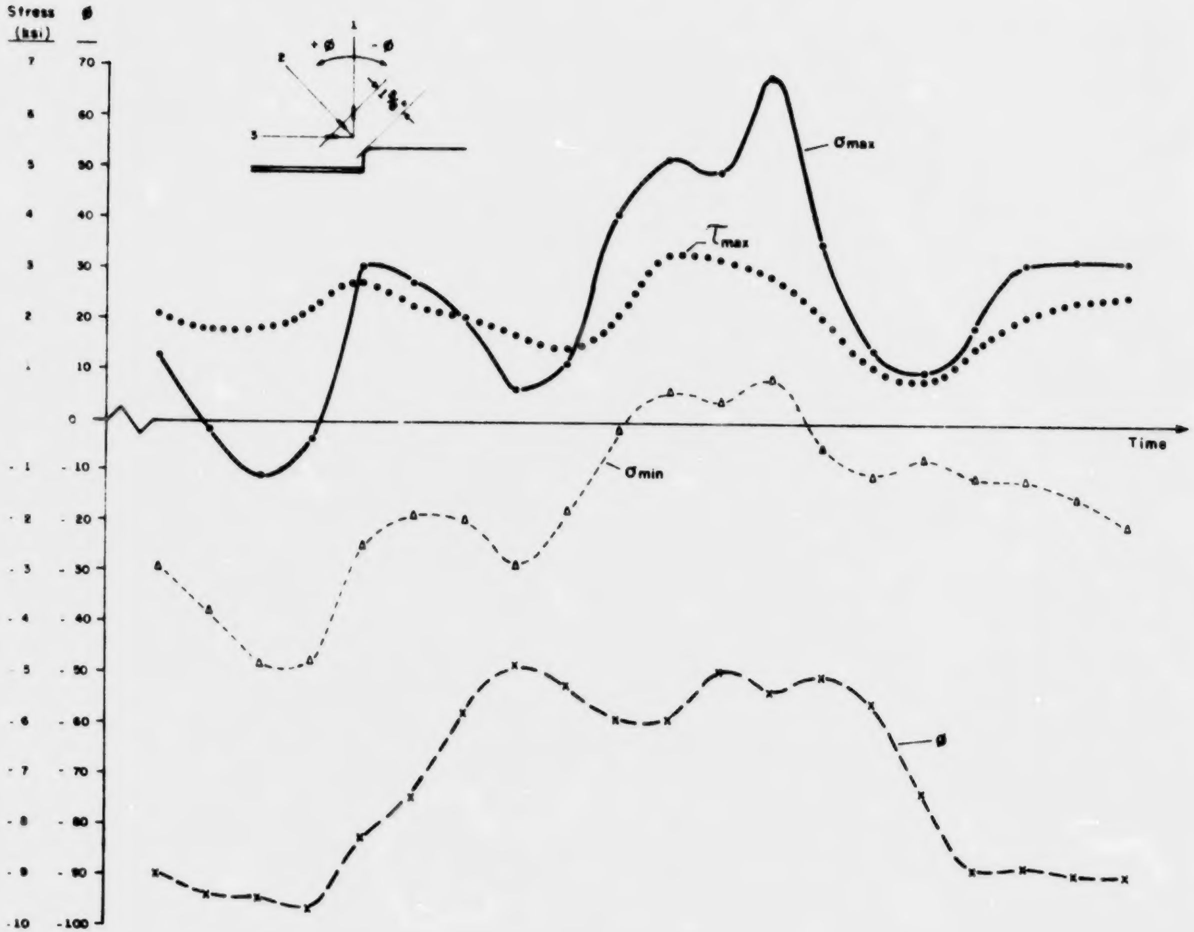

GRAPH NO. 5 - STRESS CYCLE MEASURED BY ROSETTE 'L' - (Discoloured), TEST NO. 8, 26 MPH

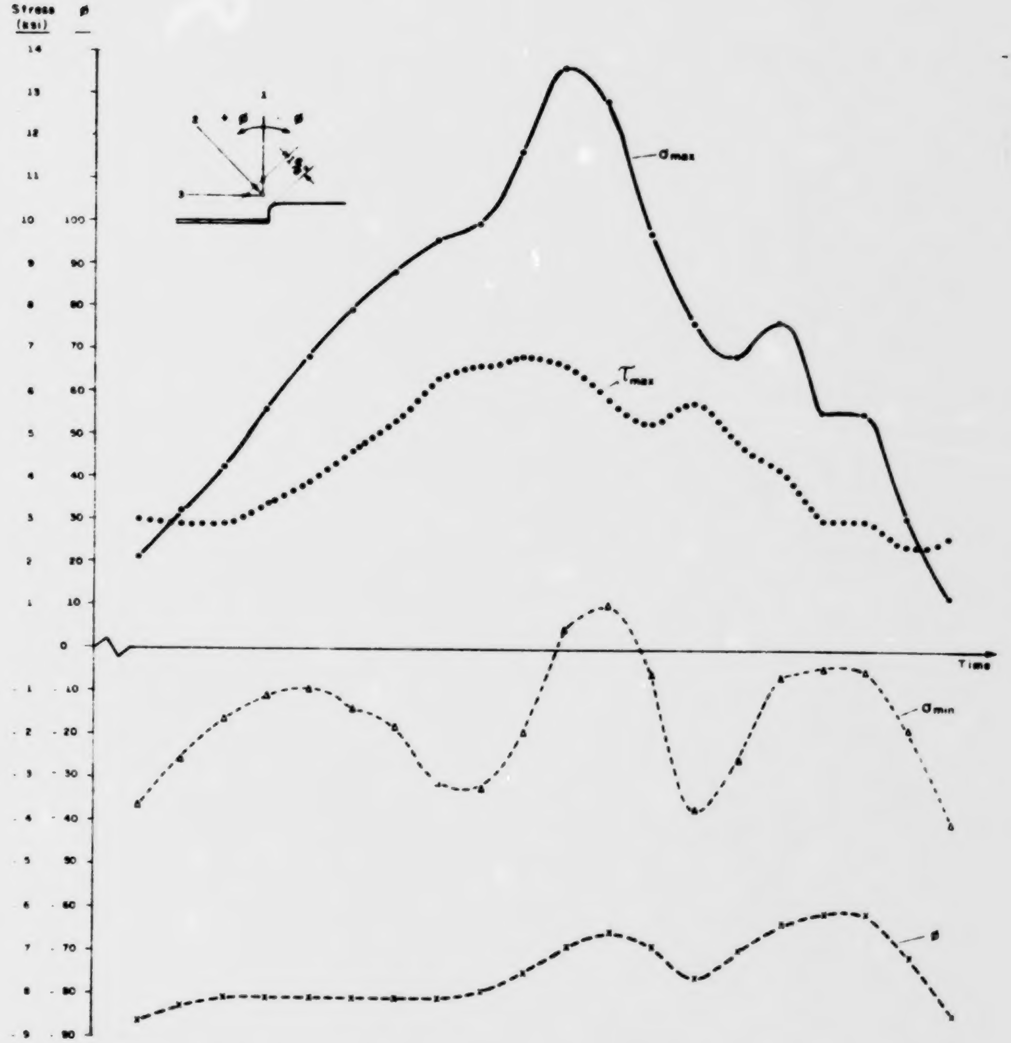

GRAPH NO 6 - STRESS CYCLE MEASURED BY ROSETTE 'D' - TEST NO. 8, 28 MPH

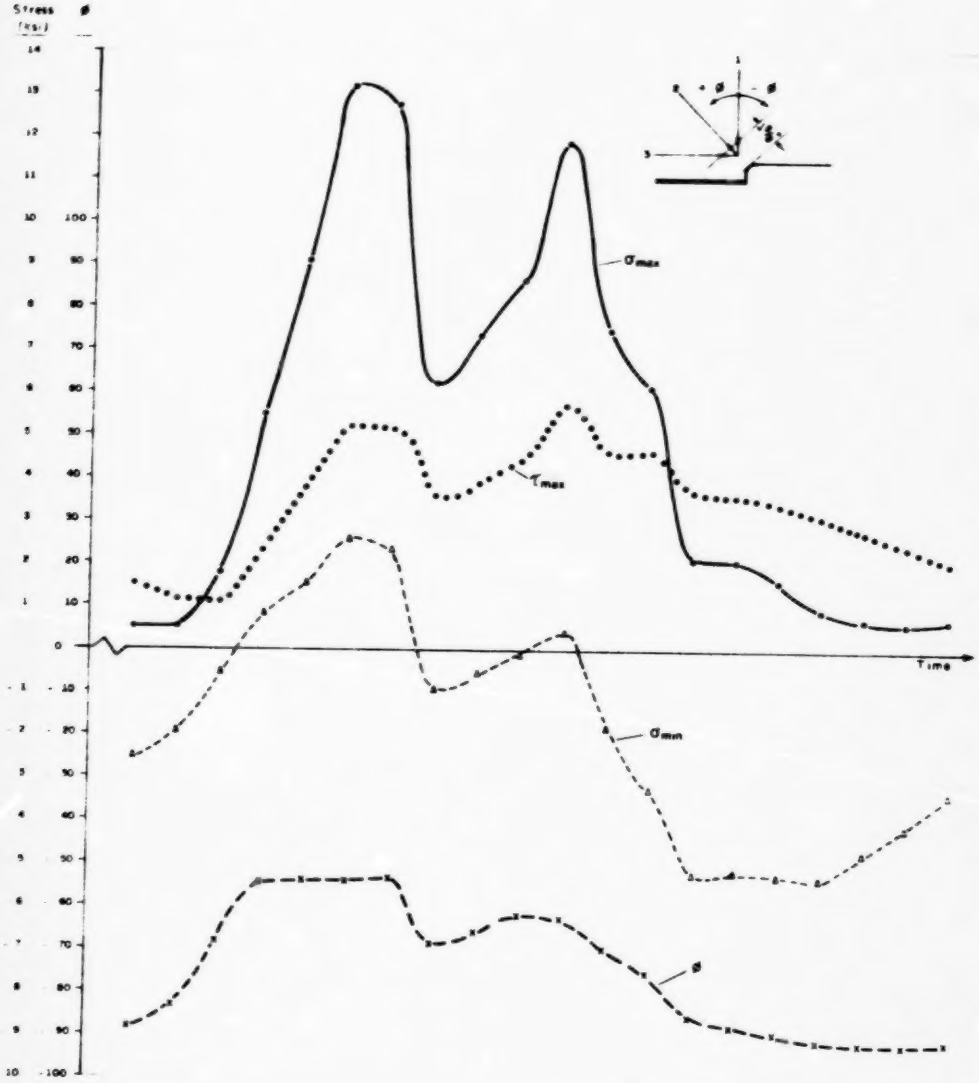

GRAPH NO. 7 - STRESS CYCLE MEASURED BY ROSETTE 'I', -TEST NO. 8, 20 MPH.

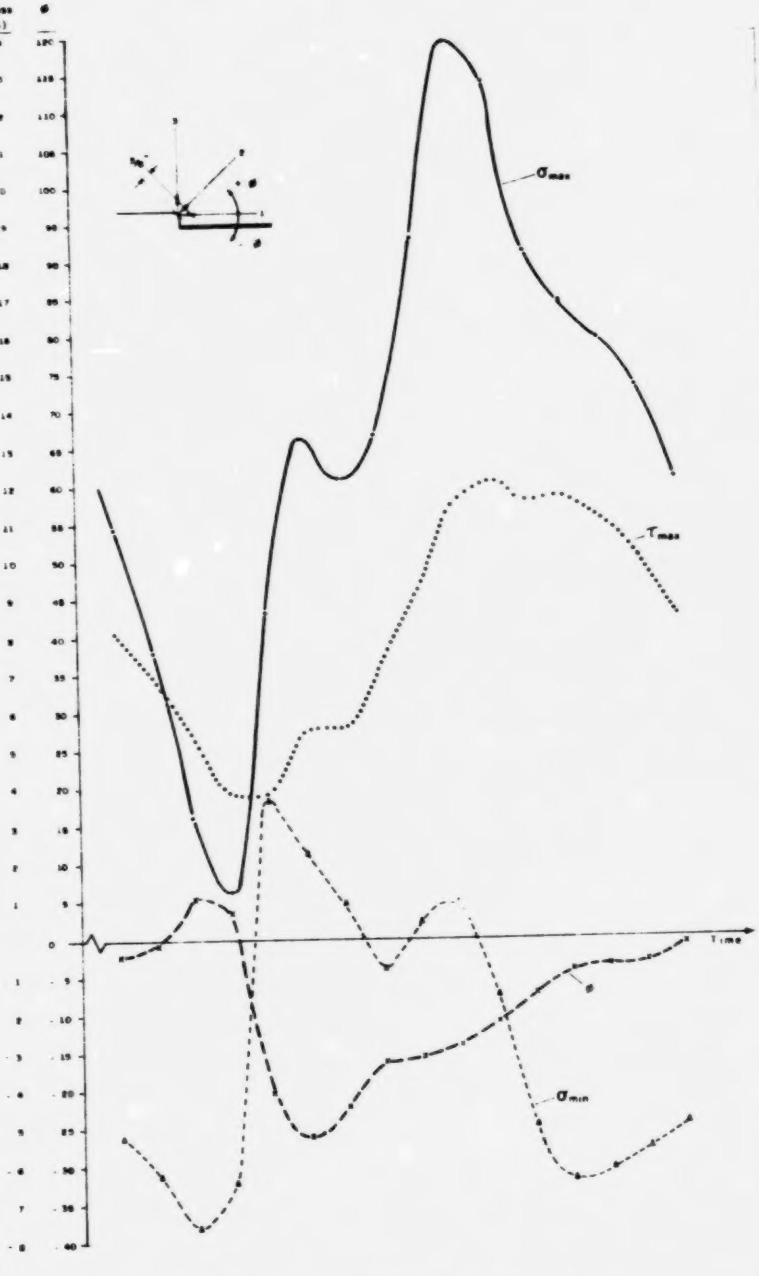

GRAPH NO 8 - STRESS CYCLE MEASURED BY ROSETTE 'S'. - TEST NO 8. 28 MPH

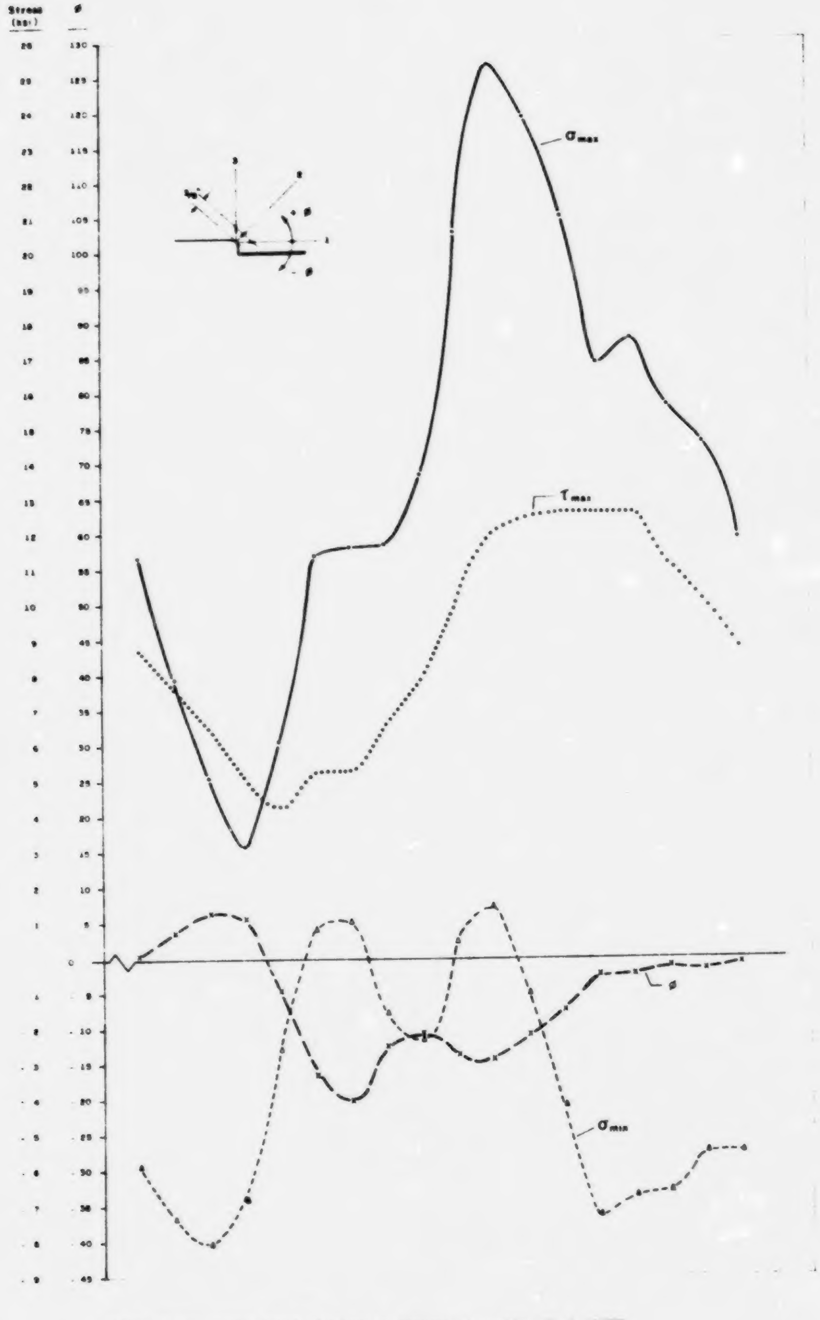

GRAPH NO 9 - STRESS CYCLE MEASURED BY ROSETTE 'S', - TEST NO. 11, 16 MPH

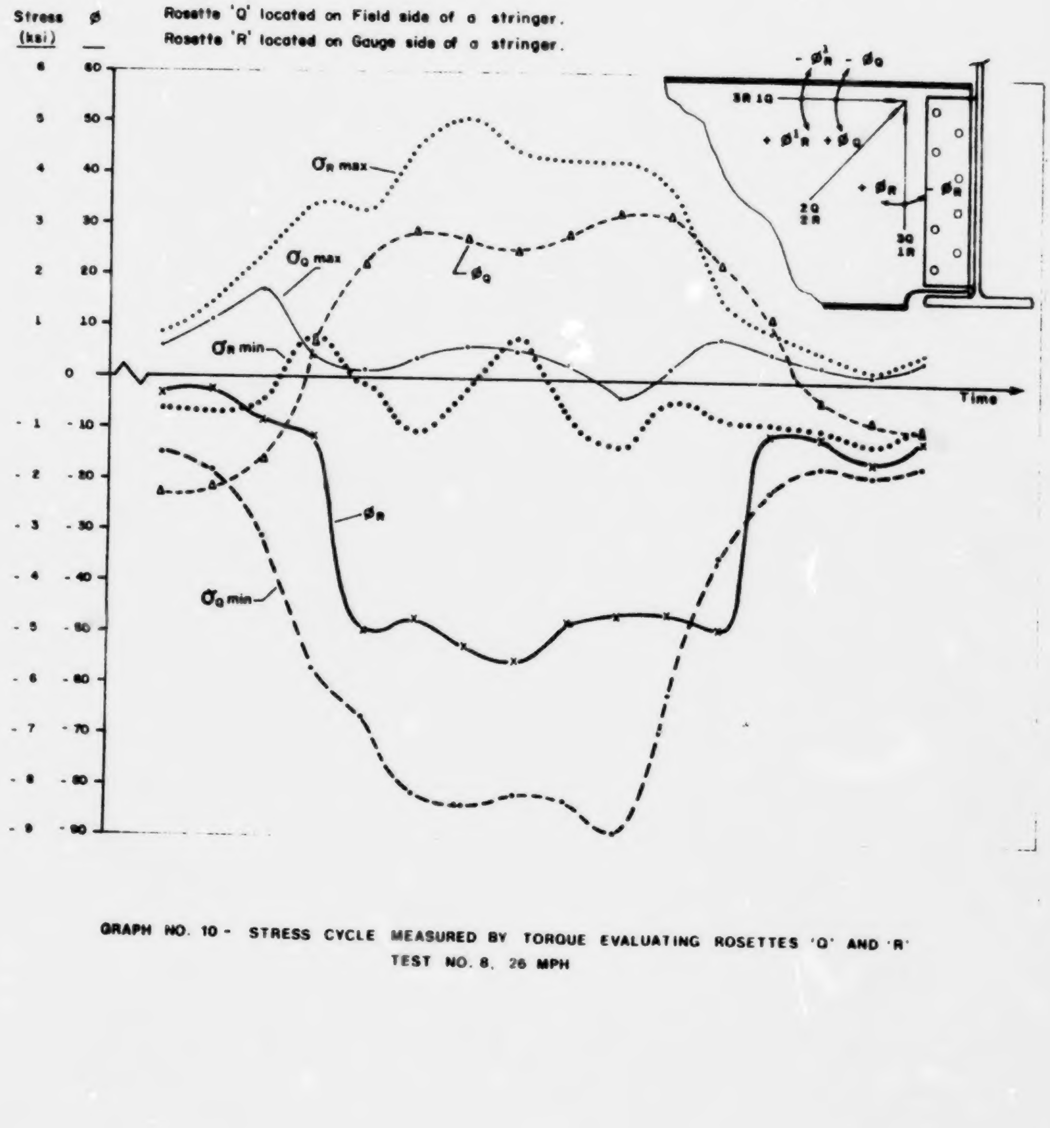

GRAPH NO. 10 - STRESS CYCLE MEASURED BY TORQUE EVALUATING ROSETTES 'Q' AND 'R'
TEST NO. 8, 26 MPH

Number/
Numéro

2

TP 4183 E

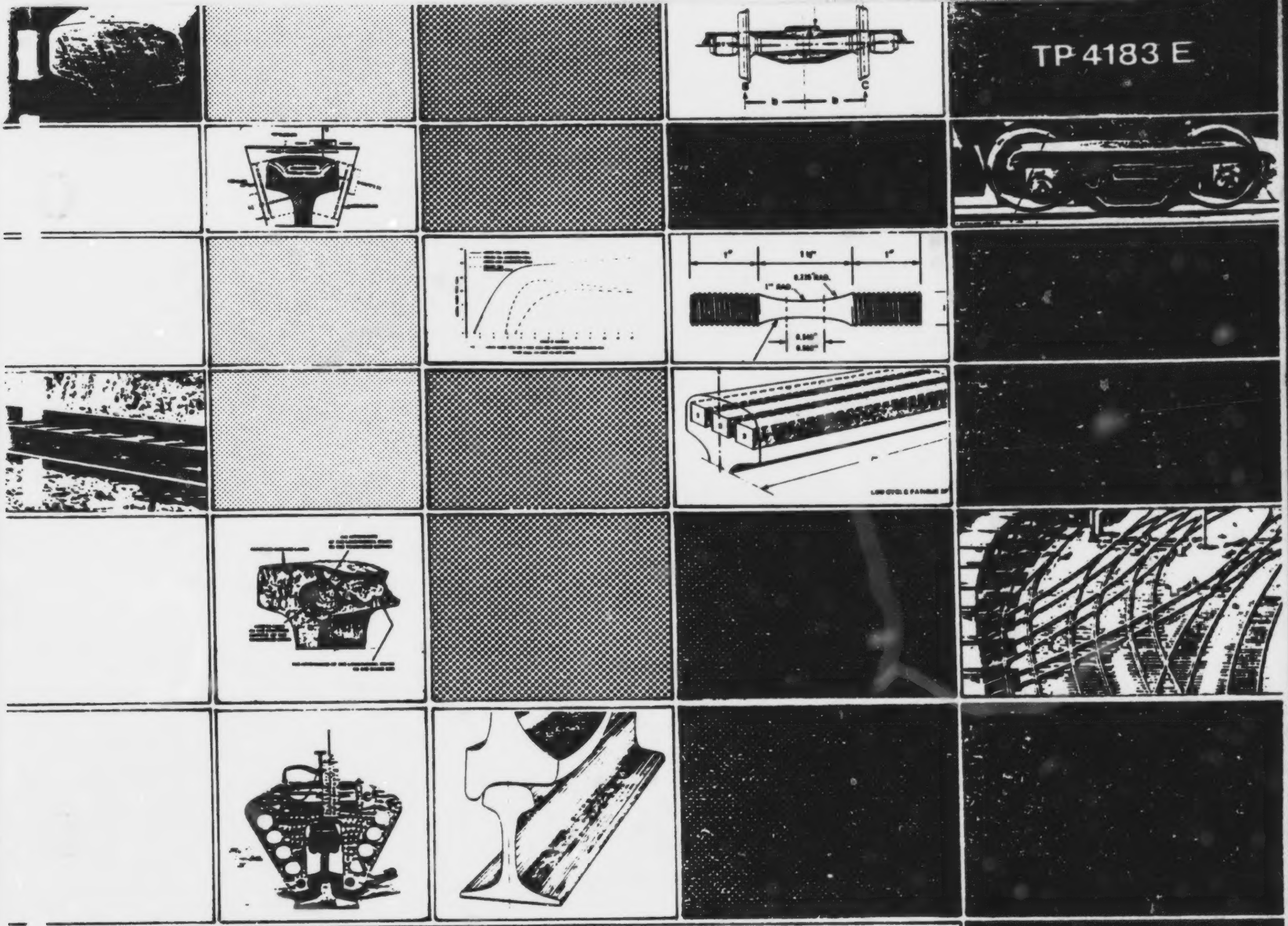

TRACK/TRAIN DYNAMICS

TECHNICAL AND OPERATIONS RESEARCH

Canadian Pacific

MONTREAL CANADA 1982

CP Rail
4242

CA1
DTC 801
83
T673

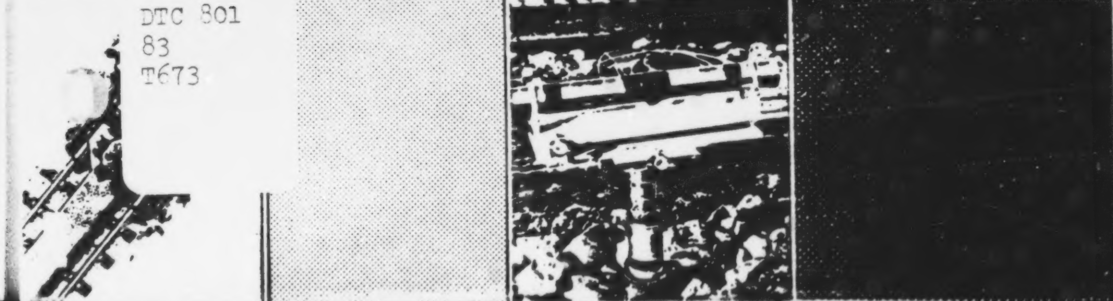

VOLUME 3
1982

TP 4183 E

Library and Information Centre /
Centre de Documentation (GSLA)
RECEIVED – REÇU LE
[illegible] 27 1983
Transport Canada / Transports Canada

TRACK/TRAIN DYNAMICS

VOLUME 3

Prepared for:

Transportation Development Centre
TRANSPORT CANADA

By:

TECHNICAL AND OPERATIONS RESEARCH
Canadian Pacific
MONTREAL, CANADA

1982

THE CONTENTS OF THE REPORT REFLECT THE VIEWS OF THE CONTRACTOR AND NOT NECESSARILY THE OFFICIAL VIEWS OR POLICIES OF THE TRANSPORTATION DEVELOPMENT CENTRE OF TRANSPORT CANADA

REPORT DOCUMENTATION FORM

1 Transport Canada Report No. TP 4183E	2. TDC Project No 4289	3 Recipient's Catalogue No

4 Title and Subtitle

TRACK/TRAIN DYNAMICS
Volume 3, 1982

5 Report Date
FEBRUARY 1983

6 Performing Organization Report No

7 Author(s)

8 Transport Canada File No
D1465-198-7-5

9 Performing Organization Name and Address
Canadian Pacific Limited
Department of Research
Windsor Station
Montreal, Quebec H3C 3E4

10 DSS File No
09SD.T8200-0-0532

11 DSS or Transport Canada Contract No
0SD81-00006

12 Sponsoring Agency Name and Address
Transportation Development Centre (TDC)
1000 Sherbrooke Street West
Suite 2421
Montreal, Quebec H3A 2R3

13 Type of Report and Period Covered
Final
April 1981 - December 1982

14 Sponsoring Agency Code
TDC 4289

15 Supplementary Notes
Canadian Pacific Ltd. and TDC equally shared the cost of this program.

16 TDC Project Officer
D.W. Dibble

17 Abstract

This final report is a collection of individual reports on research activities carried out under the shared cost Canadian Pacific/Transportation Development Centre research agreement during the period April 1981 to December 1982.

This collection includes results of both theoretical and field work in the areas of development of wheel and rail profilometers for assessment of wheel/rail wear, curving and hunting performance of modified freight car and locomotive trucks, wheelset angle-of-attack distribution of freight trains, study of wheel/rail quasi-static and dynamic systems and assessment of the performance of experimental Bainitic Chromium-Molybdenum rail and Russian P-65 rail.

18 Key Words
Track/Train Dynamics, curving and hunting, rail metallurgy, angle-of-attack, wheel/rail wear assessment

19 Distribution Statement
Copies available from TDC

20 Security Classification (of this report) Unclassified	21. Security Classification (of this page) Unclassified	22 No of Pages 192	23 Price No charge

TDC CDT 79-005

FORMULE DE DOCUMENTATION POUR RAPPORT

1 N° du rapport Transports Canada
TP 4183E

2 N° de l'étude — CDT
4289

3 N° de catalogue du destinataire

4 Titre et sous-titre
TRACK/TRAIN DYNAMICS
Volume 3, 1982

5 Date du rapport
février 1983

6 N° du rapport de l'organisme executant

7 Auteur(s)

8 N° de dossier Transports Canada
D1465-108-7-5

9 Nom et adresse de l'organisme executant
Canadien Pacifique Limitée
Département de recherche
Gare Windsor
Montréal, Québec H3C 3E4

10 N° de dossier — ASC
09SD.T8200-0-0532

11 N° de contrat — ASC ou Transports Canada
0SD81-00006

12 Nom et adresse de l'organisme parrain
Centre de développement des transports (CDT)
1000 o., rue Sherbrooke
Suite 2421
Montréal, Québec H3A 2R3

13 Genre de rapport et periode visee
Final
avril 1981 - décembre 1982

14 Code de l'organisme parrain
CDT 4289

15 Remarques additionnelles
Le CP et le CDT se sont paragés également les coûts de ce projet.

16 Agent de projet — CDT
D.W. Dibble

17 Resume

Ce rapport final rassemble les divers rapports touchant la recherche faite dans le cadre de la convention sur le partage des frais conclue entre le Canadien Pacifique et le Centre de développement des transports, pour la période allant d'avril 1981 à décembre 1982.

Ce corpus rend compte des résultats des études théoriques et des expérimentations in situ visant la mise au point de profilomètres de roues et de rails pour la détermination des phénomène suivants: usure roue-rail; tenue dans les courbes et les alignements (effet de lacet) de bogies modifiés équipant les wagons et les locomotives d'un convoi de marchandises; répartition des angles d'inscription des essieux d'un convoi de marchandises; étude de l'interaction roue-rail en régimes quasi statique et dynamique; évaluation du rail en bainite au chrome et molybdène et du rail P-65 fabriqué en Russie.

18 Mots-cles
Interaction roue-rail, comportement dans les voies en alignement et en courbe, Métallurgie du rail, angle d'inscription, évaluation de l'usure roue-rail

19 Diffusion
Le CDT dispose d'un nombre limité d'exemplaires

20 Classification de sécurité (de ce rapport)
non-classifié

21 Classification de sécurité (de cette page)
non-classifiée

22 Nombre de pages
192

23 Prix
Gratuit

CDT TDC 79-005

Preface

This report is a continuation of a series of publications intended to present the results of investigations conducted by the Research Department (Technical and Operations Research section) of Canadian Pacific Limited related to track/train dynamics.

The introduction of the jointly sponsored AAR Track/Train Dynamics Program several years ago initiated a broadly based industry effort in Canada and the United States to obtain a better understanding of the fundamental principles governing the interaction of rail vehicles and the supporting track structure. Canadian Pacific has actively supported and participated in these industry activities while conducting cooperative research in areas of special interest to CP Rail.

The following chapters of this report describe the methodology, results and recommendations of several track/train dynamics investigations undertaken by the Department between April 1981 and December 1982.

It is very satisfying to be able to acknowledge the suggestions and assistance provided by many railway personnel and industry colleagues who participated in these investigations. Cost shared financial support provided by the Transportation Development Centre (Transport Canada) permitted our activities to be more extensive and vigorous than would have otherwise been possible.

R. Klein
General Manager, Research
Montreal, Quebec

TABLE OF CONTENTS

	PAGE NO.
PREFACE R. Klein	i
ELASTO-CUSHION TRUCK PERFORMANCE STUDY R. Gonsalves, W. Pak and G. Izbinsky	1
THEORETICAL CURVING PERFORMANCE OF FOUR FREIGHT CAR TRUCKS W. Pak and G. Rosval	24
CURVING PERFORMANCE TEST OF GM SD40, SD40-2 AND MLW M636 LOCOMOTIVE TRUCKS W. Pak, R. Gonsalves and G. Izbinsky	52
EFFECT OF AXLE LATERAL CLEARANCE AND WHEEL PROFILE VARIATION ON THE CURVING PERFORMANCE OF SD40-2 LOCOMOTIVE TRUCKS W. Pak and R. Gonsalves	70
WHEELSET ANGLE-OF-ATTACK MEASUREMENT OF REGULAR TRAIN CONSISTS W. Pak, G. Izbinsky and H. Soares	113
ON THE PERFORMANCE OF THE EXPERIMENTAL BAINITIC CHROMIUM-MOLYBDENUM RAIL STEEL H. Ghonem	124
CONCEPT OF A PROFILOMETER FOR RAIL WEAR DETERMINATION G. Izbinsky and G. Warshaw	154
ANALYTICAL STUDIES OF THE RAIL-WHEEL SYSTEM: AN OVERVIEW OF APPLICATIONS OF ROLLING CONTACT THEORY	187

ELASTO-CUSHION TRUCK PERFORMANCE STUDY

EXECUTIVE SUMMARY

A series of hunting and curving performance tests was conducted in the Fall of 1981 to study the behaviour of conventional 3-piece trucks modified by the insertion of elastomeric shear pads between the bearing adaptor and the side frame pedestal roof. The test cars with modified trucks and the reference car trucks were all equipped with new CN 'A' profile wheels.

Field test results indicate that the curving performance of elasto-cushion trucks is similar to radial trucks at or above the balance speed on a 5 degree curve. Below balance speed, however, the leading truck tended to parallelogram, and hence the full benefit from natural wheelset steering was not obtained.

The hunting tests indicate that the lateral stability of elasto-cushion trucks with shear pads of 21,000 lbs/in shear stiffness did not differ from conventional 3-piece trucks as tested with the experimental CN 'A' profile wheels. However, when pads with lower shear stiffness (15,000 lbs/in) were introduced, intermittent hunting occurred at 65 mph.

SOMMAIRE

Des essais sur le phénomène de lacet et sur les inscriptions en courbe on été faits à l'automne de 1981 pour étudier le comportement des bogies standard à 3 essieux, modifiés par l'adjonction de tampons en caoutchouc synthétique entre l'adapteur élastique et le sommet de la plaque de garde du châssis latéral du bogie. Les wagons d'essai équipés de ces bogies de même que les wagons témoins avaient des roues à profil CN 'A' neuves.

Les essais ont montré qu'à l'inscription, dans une courbe de 5^o, la tenue des bogies standard ainsi modifiés était comparable à celle des bogies articulés lorsque la vitesse était égale ou supérieure à celle d'équilibre. Cependant, en-dessous de cette vitesse, le bogie directeur se déformait ce qui empêchait les essieux de tirer le plein parti de ce type de roues.

Les essais sur le phénomène de lacet ont montré que la stabilité latérale des bogies équipés de tampons caoutchouc d'une raideur en cisaillement de 21 000 lb par pouce ne différait pas de celle des bogies standard équipés de roues neuves à profil CN 'A'. Toutefois, quand ces tampons étaient remplacés par d'autres ayant une raideur en cisaillement de 15 000 lb par pouce, un phénomène de lacet intermittent se manifestait à la vitesse de 65 mi/h.

Acknowledgements

The Research Department acknowledges the contribution of personnel from the following organizations.

- Office of the Chief Mechanical Officer for assistance during the course of this test program.

- The National Research Council of Canada, Railway Laboratory, Division of Mechanical Engineering for their contribution to the field work.

- Officers and personnel of the Calgary Division, Alberta South Division and Ogden Shops for assistance during the tests.

- Transportation Development Centre, Transport Canada for financial support under contract # OSD81-00006.

1. INTRODUCTION

Previous research has been conducted on a conventional three-piece freight car truck which had been modified by the insertion of a rubber shear pad (Elastomeric LC-Pad manufactured by Lord Kinematics) at the pedestal roof bearing adaptor interface. Field tests using instrumented wheelsets with these modified trucks indicated that there was a reduction in lateral wheel/rail forces on curves (Ref. 1). As a result, certain railways have since adopted this modification as standard on their freight car trucks. Subsequent service experience further indicated that there is a noticeable flange wear reduction compared with conventional unmodified trucks. However, no angle-of-attack measurements were ever made on these trucks, and hence the steering characteristics of these trucks were not fully investigated.

From previous testing (Ref. 2) conducted by CP Research, it was recognized that the horizontal suspension of a conventional 3-piece freight car truck is characterized by very high interaxle yaw stiffness and low interaxle shear stiffness. Hence in steady state curving, while the axles are kept parallel they tend to parallelogram relative to each other. This results in an increase in the angle-of-attack of the leading flanging wheel, thus causing heavy flange wear during curving.

Introducing LC-pads in the truck side frame pedestal roof area would allow the axles to yaw relative to each other and, therefore, utilize the benefit of longitudinal steering moments naturally generated at the wheel/rail interface, to reduce the angle-of-attack. However, introducing LC-pads also reduces the parallelogramming stiffness of a 3-piece truck, and thus compromises to a certain degree the benefits derived from wheelset steering. A clear understanding of the aforementioned trade off in curving behaviour is desirable before truck modifications are undertaken to improve curving performance.

Reducing the interaxle shear stiffness as well as the interaxle yaw stiffness by using LC-pads also affects the lateral stability of 3-piece trucks. According to linear hunting analysis, the stability threshold is lowered as interaxle shear stiffness is reduced from its nominal value in a 3-piece truck. Therefore, it is important to determine the hunting sensitivity of the truck to a reduction in its interaxle shear stiffness.

In view of the evidence of flange wear reduction experienced by other railways utilizing elasto-cushion trucks, curving and hunting tests as well as theoretical studies on this modified 3-piece truck were conducted in 1981 by CP Research to provide a better understanding of truck behaviour.

2. CURVING PERFORMANCE TESTS AND ANALYSIS OF ELASTO-CUSHION TRUCKS

2.1 Instrumentation and Test Site

Strain-gauges were installed on a 5 degree curve to measure lateral and vertical forces at both rails, as well as wheelset angle-of-attack as the test consist passed the instrumented site at various speeds. Data recorded were processed to generate a lateral/vertical wheel load distribution pattern for each truck and the lateral slippage (angle-of-attack) experienced by each wheelset. Instrumentation for this test was the same as used previously, details of which can be found in Reference 2.

The instrumented test section was located near Calgary at Mileage 12.4 on the Laggan Subdivision. The rail used in this curve consisted of Algoma 1971 RE 132 Lb., 78 ft. staggered jointed rail. The curve had an 0.5% ascending grade in the Westward direction, a superelevation of 4.5" and a corresponding equilibrium speed of 37 mph. The rail flange lubricator was shut off during the tests.

2.2 Test Consist and Procedure

Two series of curving tests were conducted on two different days. The consist in both days was comprised of three 6-axle locomotives, four laden 100-ton bathtub coal cars with Barber S-2 heavy duty trucks in the following sequence; Car 1: Barber S-2 trucks without modification, Car 2: Barber S-2 trucks with C-PEP, Car 3: Barber S-2 trucks with

LC-pads, and Car 4: Barber S-2 trucks with both C-PEP and LC-pads. Both curving tests were conducted with new CN experimental "A" profile wheels. Centre plate of each test truck was well lubricated.

The first tests (Oct. 15) were run with modified trucks equipped with LC-pads of 21,000 lb/in shear stiffness and the second tests (Oct. 17) were conducted with the trucks equipped with LC-pads of 15,000 lb/in shear stiffness. During each series of tests, three runs were made through the test curve in each direction at approximately 25, 37, 45 mph respectively. The test consist was wyed and this procedure repeated for a total of 36 runs. The consist was allowed to coast through the instrumented section of the curve during each test.

2.3 Discussion of Test Results

In order to present the complete curving characteristic of each truck, and to permit correlation between wheel rail forces and angle-of-attack for each wheel, the measured parameters for each test run are presented in one illustration (Fig. 1 to Fig. 5). In these illustrations, the same axle number always indicates the same axle on each truck, whether the consist is wyed or unwyed, moving Eastbound or Westbound. The sign conventions adopted in this report are that positive angle-of-attack signifies axles rolling towards outside of the curve (away from centre), and positive low rail and high rail forces are directed away from the centre of the curve.

From the plotted results, one can observe the general phenomena of reduction of angle-of-attack with increased curving speeds and an increase in angle-of-attack with higher lateral force on low rail. The centrifugal force and the weight transfer effect on vertical wheel loads within each truck due to the moment generated by interaxle shear forces and the net wheel/rail lateral force on each axle are evident. A similar coupling effect between leading and trailing trucks can also be observed. These effects have been discussed in detail in previous reports (Ref. 2).

Comparing the angle-of-attack of the elasto-cushion truck with those of conventional trucks, one can see that there is a marked reduction of angle-of-attack at the leading axle, as a result of wheelset steering. However, at less than balance speed, the leading truck of the cars with LC-pads have a tendency to parallelogram, thus increasing the angle-of-attack at both the leading and trailing axle of the leading truck and hence compromise the benefits of wheelset steering. Maximum lateral and vertical forces do not differ significantly between modified and unmodified trucks, although the lateral creep forces at the low rail are slightly lower at the leading axles of the modified trucks, due to angle-of-attack reduction when steering.

The modified trucks with softer LC-pads of lower shear stiffness (15,000 lbs/in) steers slightly better than those with stiffer LC-pads (21,000 lbs/in). However, the parallelogramming action is also more severe with LC-pads of lower shear stiffness for the leading truck below the balance speed.

From these Figures, it was also observed that the parallelogramming action on the leading truck at less than balance speed does not occur exclusively on modified trucks. Conventional trucks also possess this tendency, but to a lesser extent, as compared to the modified trucks.

2.4 Theoretical Analysis

In order to provide a theoretical explanation of the lead truck parallelogramming observed at less than balance speed on elasto-cushion trucks, computer simulations were conducted utilizing a non-linear steady-state curving model recently developed by CP Research (Ref. 3). Various computer runs were made to simulate elasto-cushion truck behaviour in response to cant deficiency and centre-plate torque. The interaxle yaw stiffness of the truck was kept constant and was computed from the 15,000 lbs/in shear stiffness of the LC pads, and the interaxle shear stiffness was allowed to vary, in order to study truck response as this parameter was lowered from nominal values of 4,000 lb_f/in.

The results indicate that as the parallelogramming stiffness is allowed to decrease keeping the interaxle yaw stiffness constant, the truck curving behaviour becomes more sensitive to centre-plate torque generated from truck bolster rotation experienced during curve entrance. Since bolsters rotate in opposite directions with respect to the car body on curves, the orientation of the centre-plate torque is also opposite in direction for leading and trailing trucks. From these computer simulations, it was concluded that the positive torque experienced on the leading truck tends to parallelogram the truck, while the negative torque experienced on the trailing truck tends to suppress this action.

2.5 Conclusions

1. Elasto- cushion trucks' curving performance is very similar to a radial truck at or above balance speed on a 5 degree curve. At less than balance speed, the lead truck tends to parallelogram, thus compromising the benefits from wheelset steering.

2. Since most radial trucks designed are essentially elasto-cushioned trucks with added cross-members or steering arms, in the event of failure of these interaxle linkage due to fatigue or damage, the curving performance of these trucks would be similar to that documented in the present report for elasto-cushion trucks.

3. HUNTING TESTS AND ANALYSIS OF ELASTO-CUSHION TRUCKS

3.1 Test Site

High speed stability tests were carried out on the Brooks Subdivision east of Calgary between Mileage 160-158. The two mile test zone consisted of tangent track with continuous welded 115 lb/yard rail in 1440 foot lengths laid in 1977.

3.2 Instrumentation

The four test cars were instrumented with accelerometers on the truck and car body to determine wheelset and car body lateral acceleration. The accelerometers on the lead axles of the trailing trucks of the test cars were mounted at the end of the axles on specially designed bearing end caps. The accelerometers on the car body were mounted on the stub sill near the centre plate of the trailing trucks.

Three video cameras were used on the two test cars with LC-pads. One video camera was mounted under the tub of each car body to observe wheelset lateral oscillation, while the other camera was mounted on one car and "angled in" to observe the pedestal/bearing adaptor interface.

The speed of the test cars during each test run were continuously monitored on the instrumentation car. Acceleration signal data was recorded on a 14 channel Phillips FM tape recorder on the instrumentation car.

3.3 Test Consist

The test consist was made up of one 3300 HP MLW locomotive, four empty 100-ton bathtub coal test cars, Dynamometer Car CP 62 (the instrumentation car to record the data) and a crew caboose. Two of the four test cars were fitted with LC pads between the bearing adapter and pedestal roof. One of the two cars with LC-pads had C-PEP. One of the other two cars with conventional trucks, was equipped with C-PEP. All four test cars were tested with new CN 'A' profile wheels, in order to generate similar wheel rail contact condition.

Two series of tests were carried out. The first test was carried out with LC-pads of 15,000 lb/in shear stiffness and the second test with LC-pads of 21,000 lb/in shear stiffness. A gradual in-step increase in the test car consist speed in 5 mph increments from 40 to 70 mph was carried out for each of the tests. In each case, the required test speed was attained prior to reaching the test zone (Mileage 160-158) and held constant throughout the two mile section for data collection. All tests were run in the same direction over the 2 mile test zone.

3.4 Data Analysis

The high speed lateral accelerometer data recorded during the tests was processed by the National Research Council Railway Laboratory using a Hewlett-Packard, Model 5420A Digital Signal Analyzer.

A power spectral density (psd) analysis of the data was carried out to determine if hunting did occur. The data was analyzed over a bandwidth up to 30 Hz with a resolution of .125 Hz. For both series of tests the signal was analyzed over the same section of track for each test run to avoid any difference of track input to the various test cars.

The outputs of the psd analysis are in the form of plots of signal power normalized to a 1 Hz bandwidth against frequency in units of g^2/Hz ($g = 32.2$ ft/sec^2). From the psd analysis the average lateral accelerations (rms 'g') within the bandwidth 1 to 5 Hz were calculated for all the test runs. The rms 'g' values were calculated for the frequency range 1-5 Hz to include the hunting frequency and avoid frequencies unrelated to wheelset oscillation. Similar sample outputs can be seen in the previous report (Ref. 2).

Truck hunting occurs when a sharp increase in the rms lateral acceleration values is observed between one test speed and the next. However, since the rms 'g' value is an average value, and if hunting was intermittent, the increase in rms 'g' from one test speed to the next will not be so pronounced.

3.5 Discussion of Test Results

Figures 6 to 9 illustrate the rms lateral acceleration on the wheelsets and carbody for the test cars during two days of testing utilizing LC-pads of different shear stiffnesses.

The test results indicate that the conventional Barber S-2 truck with C-PEP and the one without C-PEP, both used as the reference cars, showed a slight difference in rms 'g' values during the two days of testing for speeds above 55 mph. This may have been due to environmental test conditions not being exactly similar on both days of testing. On both days of testing, trucks of both reference cars were stable throughout the test speed range of 40 to 70 mph. The car equipped with C-PEP had a lower average lateral acceleration (rms 'g') as compared to the car without C-PEP.

From the graphs plotted, it can be seen that for the modified trucks with LC-pads of 21,000 lb/in shear stiffness the average lateral acceleration (rms 'g') was the same as for the conventional trucks. However, with LC-pads of a lower shear stiffness of 15,000 lb/in intermittent truck hunting commenced at 65 mph. The intermittent truck hunting which could have been caused by local track irregularities showed no signs of being sustained in the two mile test zone. With LC-pads of a lower shear stiffness (15,000 lb/in) the car body lateral acceleration values (rms 'g') were slightly higher than those from the axle. This would be due to the introduction of a softer primary suspension (LC-pads) which allows the wheelset freedom to move independently of the car body. Even though the lateral acceleration values (rms 'g') were slightly higher on the car body with the LC-pads of lower shear stiffness there were no signs of violent car body hunting to a maximum test speed of 70 mph.

Figure 10 illustrates how the predominant wheelset frequency varies with speed on the lead axles of the leading and trailing truck for the conventional Barber S-2 truck with LC pads of 15,000 lb/in shear stiffness. It was found that the frequency of oscillation of the two trucks and car body were the same up to 60 mph.

3.6 Conclusions

1. Test cars with conventional Barber S-2 trucks equipped with LC-pads of 21,000 lb/in shear stiffness and CN 'A' profile wheels exhibited the same lateral ride of the carbody and trucks up to a maximum speed of 70 mph when compared to the reference cars with conventional Barber S-2 trucks and new CN 'A' profile wheels. The test results were similar whether cars were equipped with C-PEP or not.

2. With LC pads of 15,000 lb/in shear stiffness on the conventional Barber S-2 trucks with CN 'A' profile wheels intermittent truck hunting commenced at 65 mph on the cars with C-PEP as well as without C-PEP.

4. REFERENCES

1.	L.W. Peterson W.H. Freeman J.M. Wandrisco	Measurement and Analysis of Wheel-Rail Forces. ASME paper 71-WA/RT-4
2.	R. Gonsalves W. Pak G. Izbinsky	Railroad Dynamics Incorporated (RDI) Truck Evaluation Test CP report No. S670-81, March 1981, Transport Canada report No. TP 2970.
3.	W. Pak G. Rosval	Theoretical Curving Performance of Four Freight Car Trucks CP report No. S712-82, December 1981, Transport Canada report No. TP 3449.

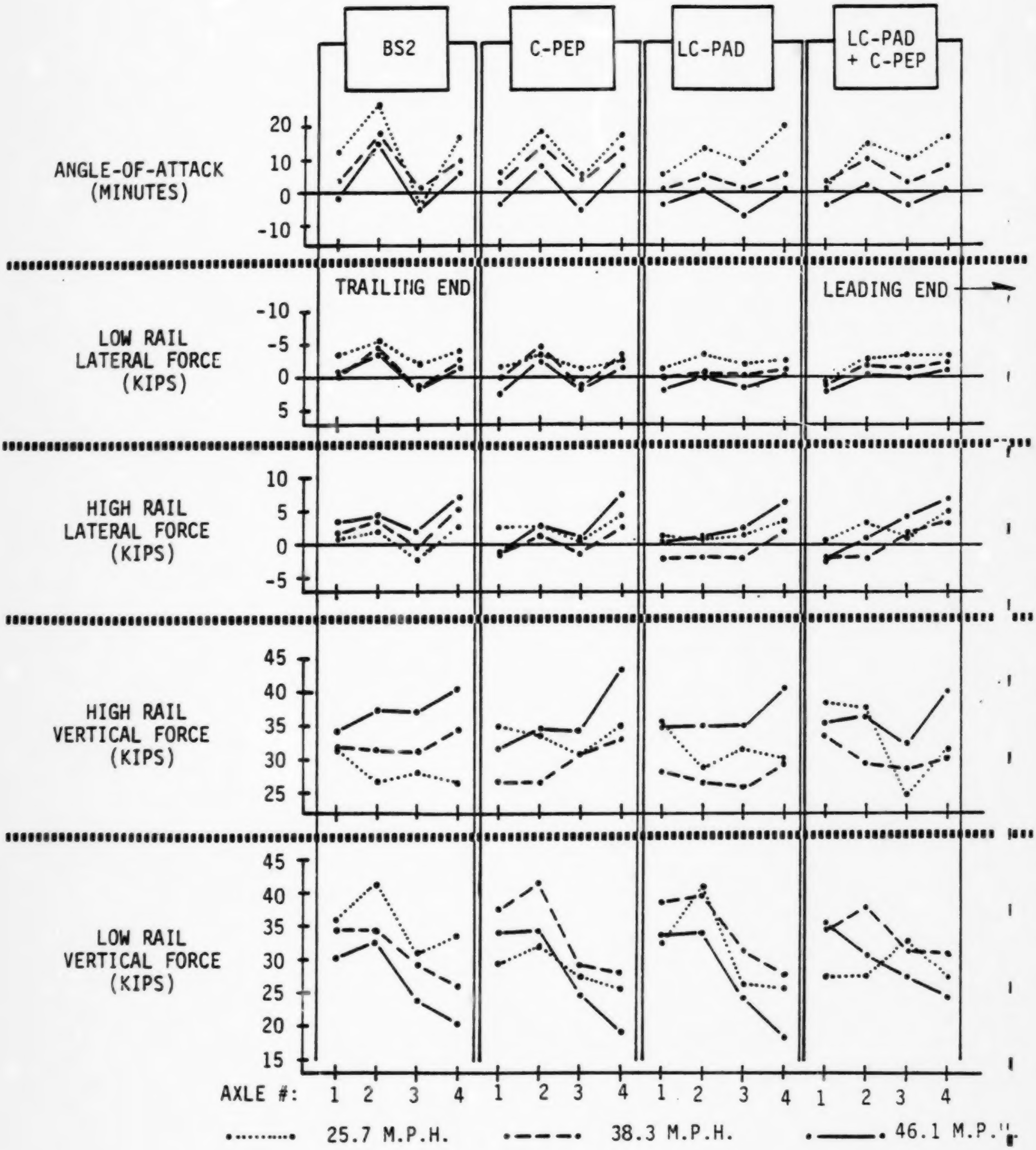

FIG: 1 ANGLE-OF-ATTACK AND RAIL FORCES AT DIFFERENT CURVING SPEEDS WITH 21,000 lbs/in SHEAR PAD (eastbound, unwyed)

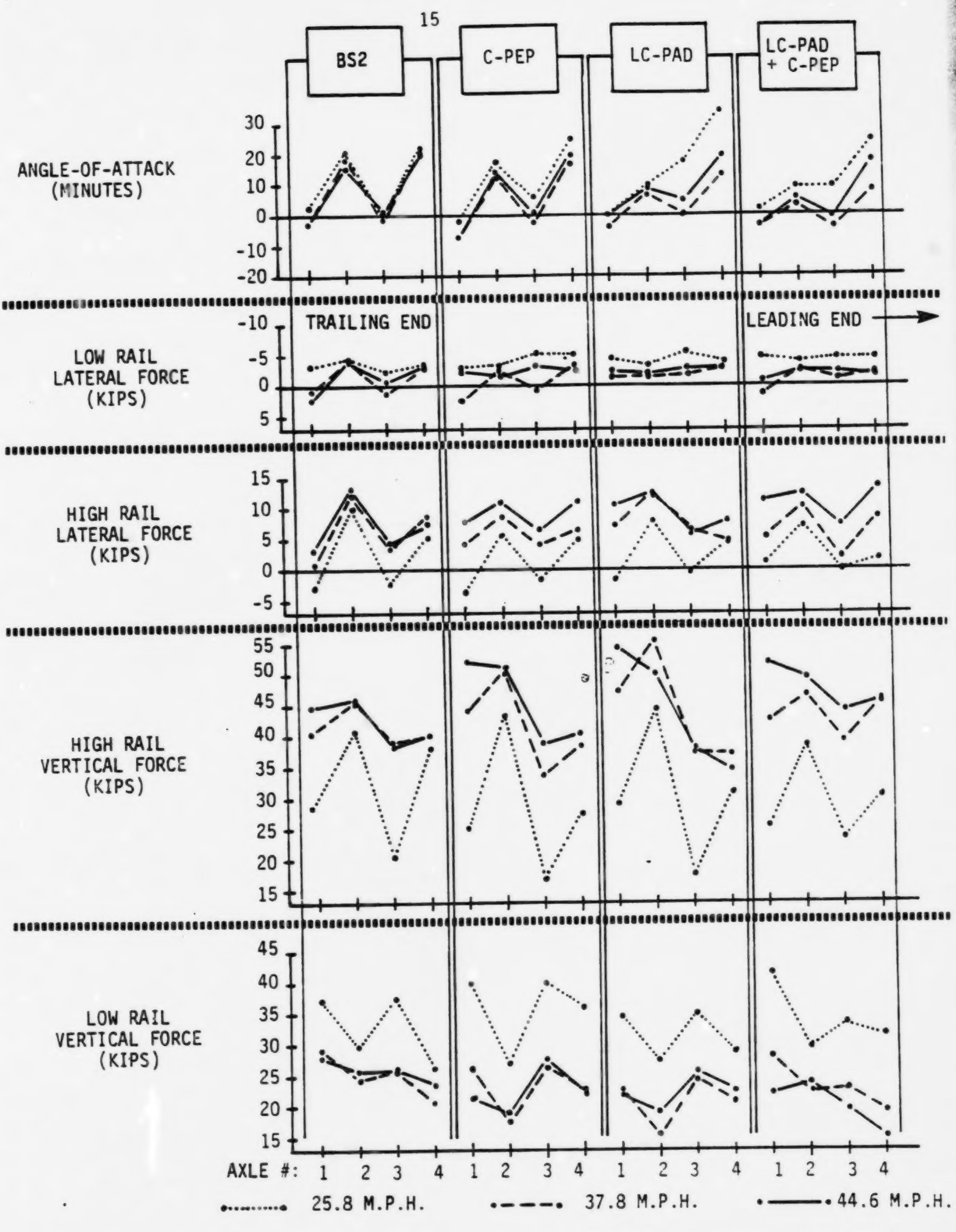

FIG: 2 ANGLE-OF-ATTACK AND RAIL FORCES AT DIFFERENT SPEEDS WITH 21,000 lbs/in SHEAR PAD (westbound, wyed)

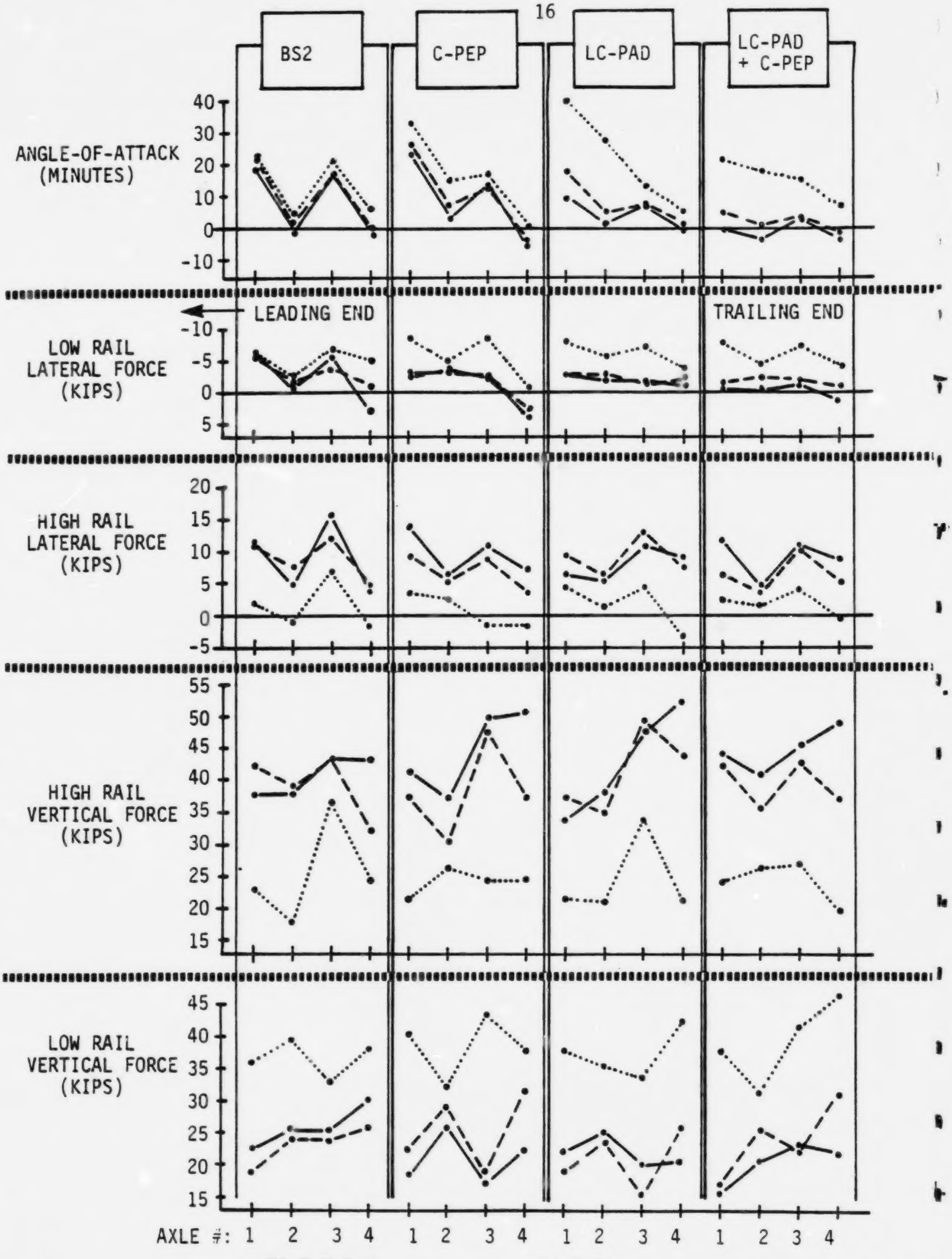

FIG: 3 ANGLE-OF-ATTACK AND RAIL FORCES AT DIFFERENT CURVING SPEEDS WITH 15,000 lbs/in SHEAR PAD
(westbound, unwyed)

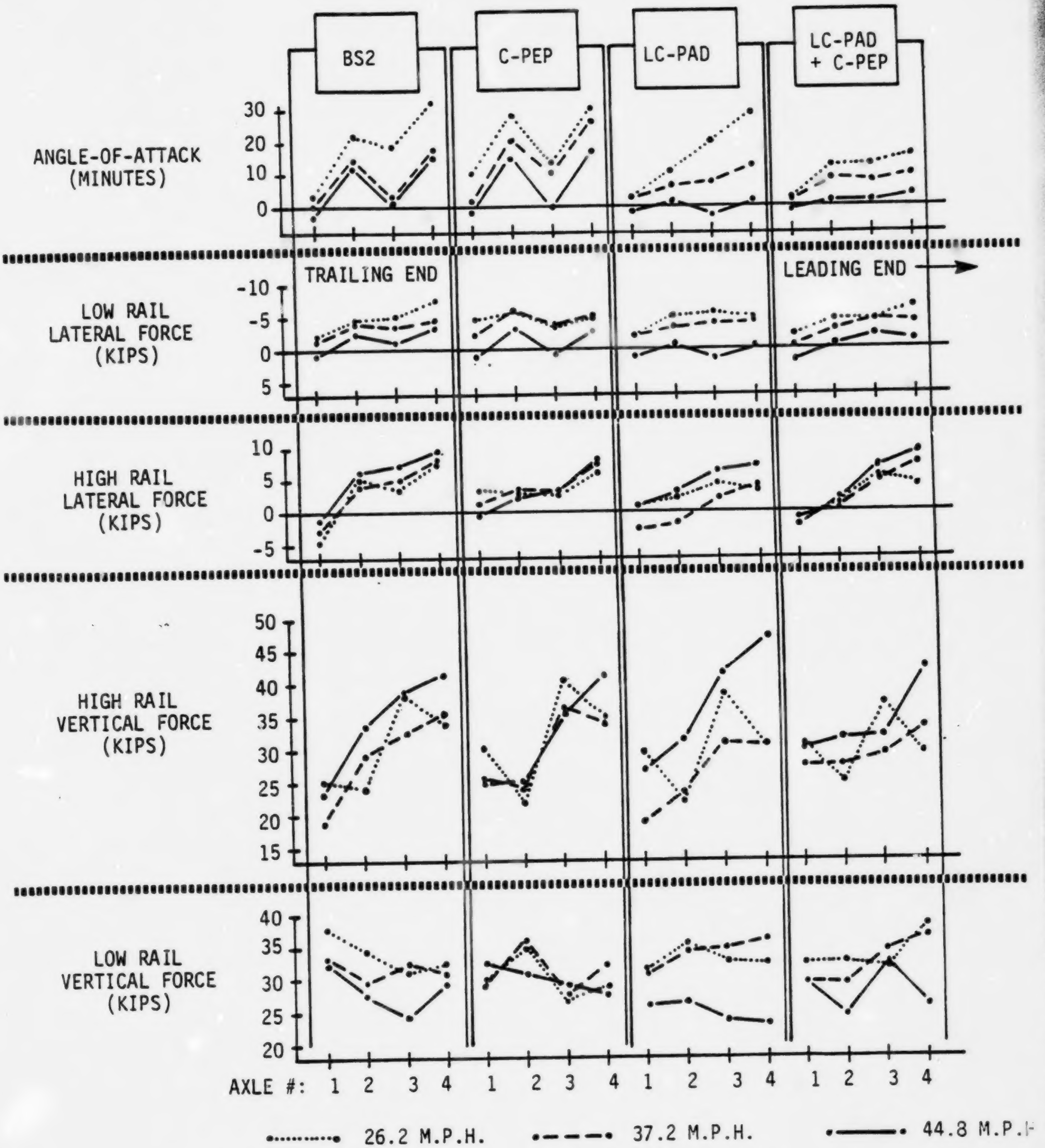

FIG: 4 ANGLE-OF-ATTACK AND RAIL FORCES AT DIFFERENT CURVING SPEEDS WITH 15,000 lbs/in SHEAR PAD
(eastbound, unwyed)

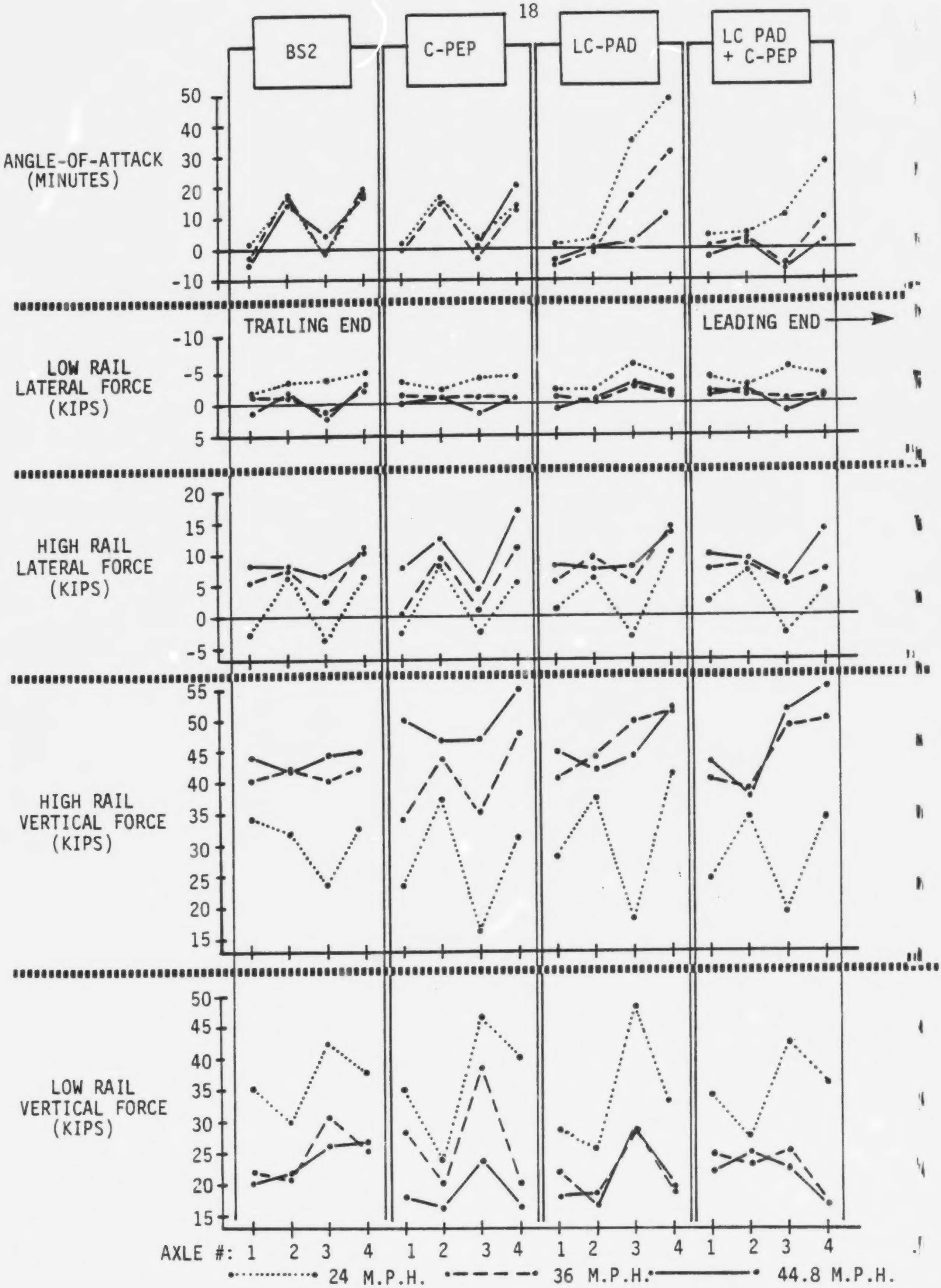

FIG: 5 ANGLE-OF-ATTACK AND RAIL FORCES AT DIFFERENT CURVING SPEEDS WITH 15,000 lbs/in SHEAR PAD (westbound, wyed)

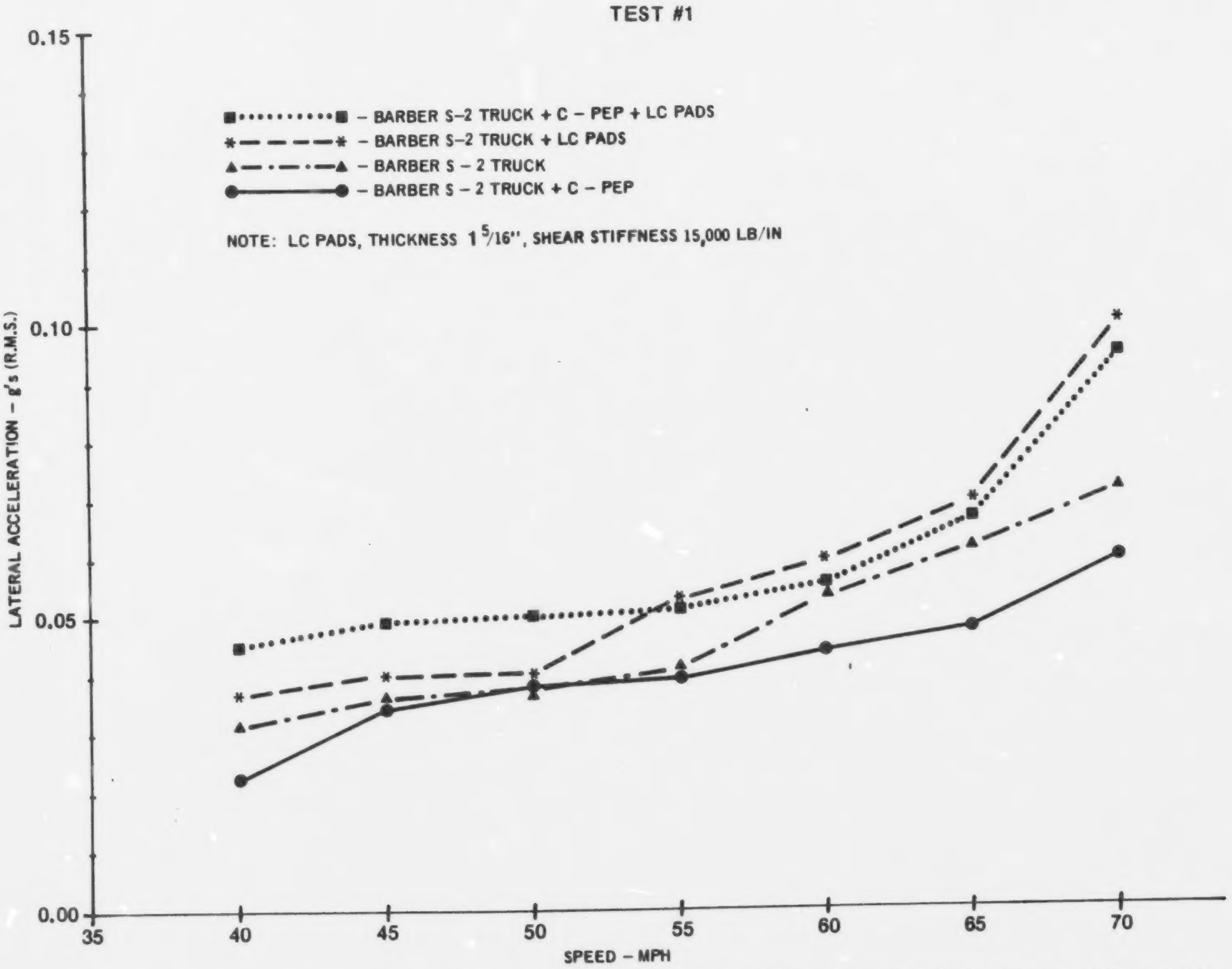

FIG. 6 : LATERAL ACCELERATION ON TRAILING TRUCK LEAD AXLE BEARING END CAP VS SPEED FOR TRUCKS WITH CN "A" PROFILE WHEELS

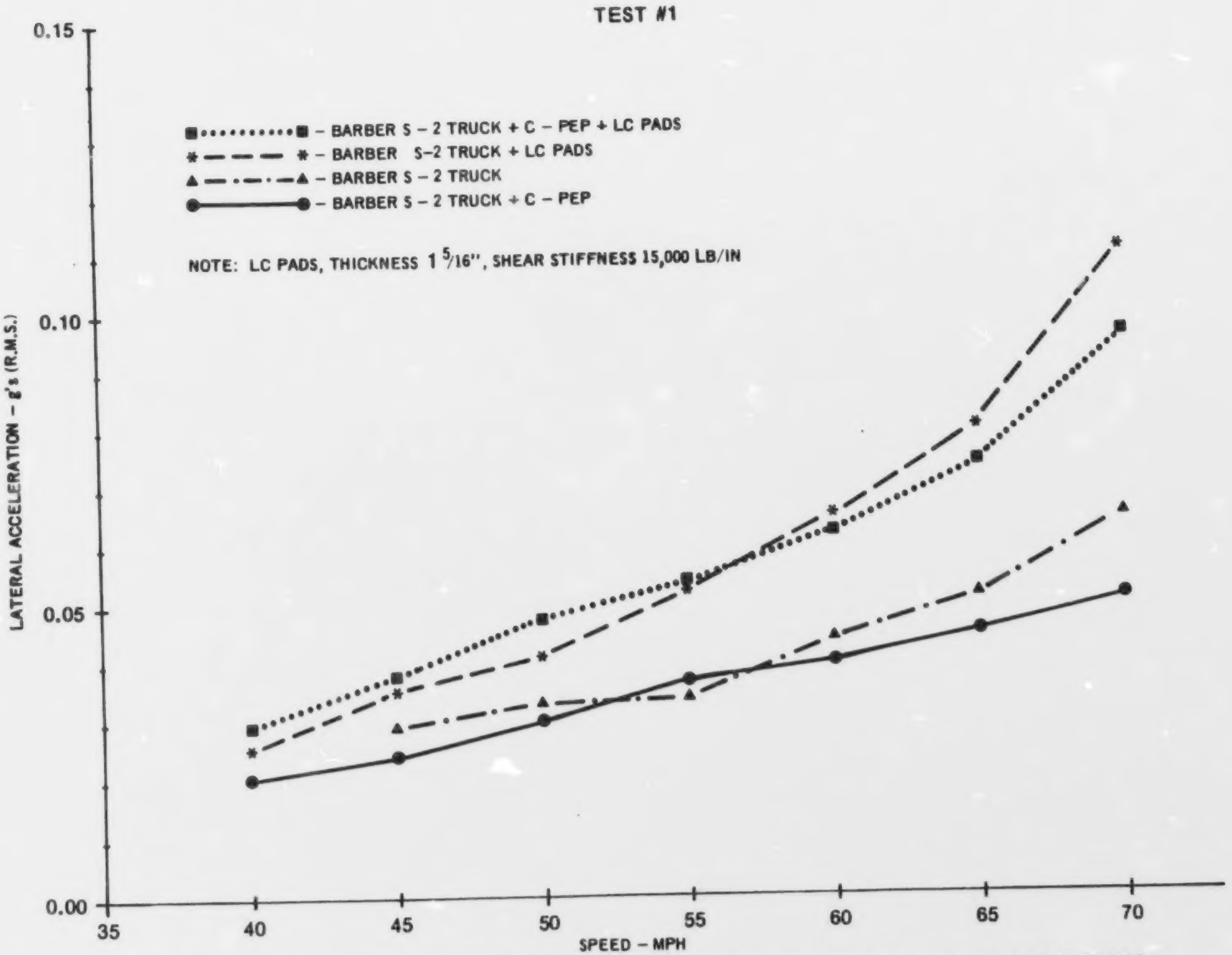

FIG.7 : LATERAL ACCELERATION OF CAR BODY AT THE TRAILING TRUCK VS SPEED FOR TRUCKS WITH CN "A" PROFILE WHEELS

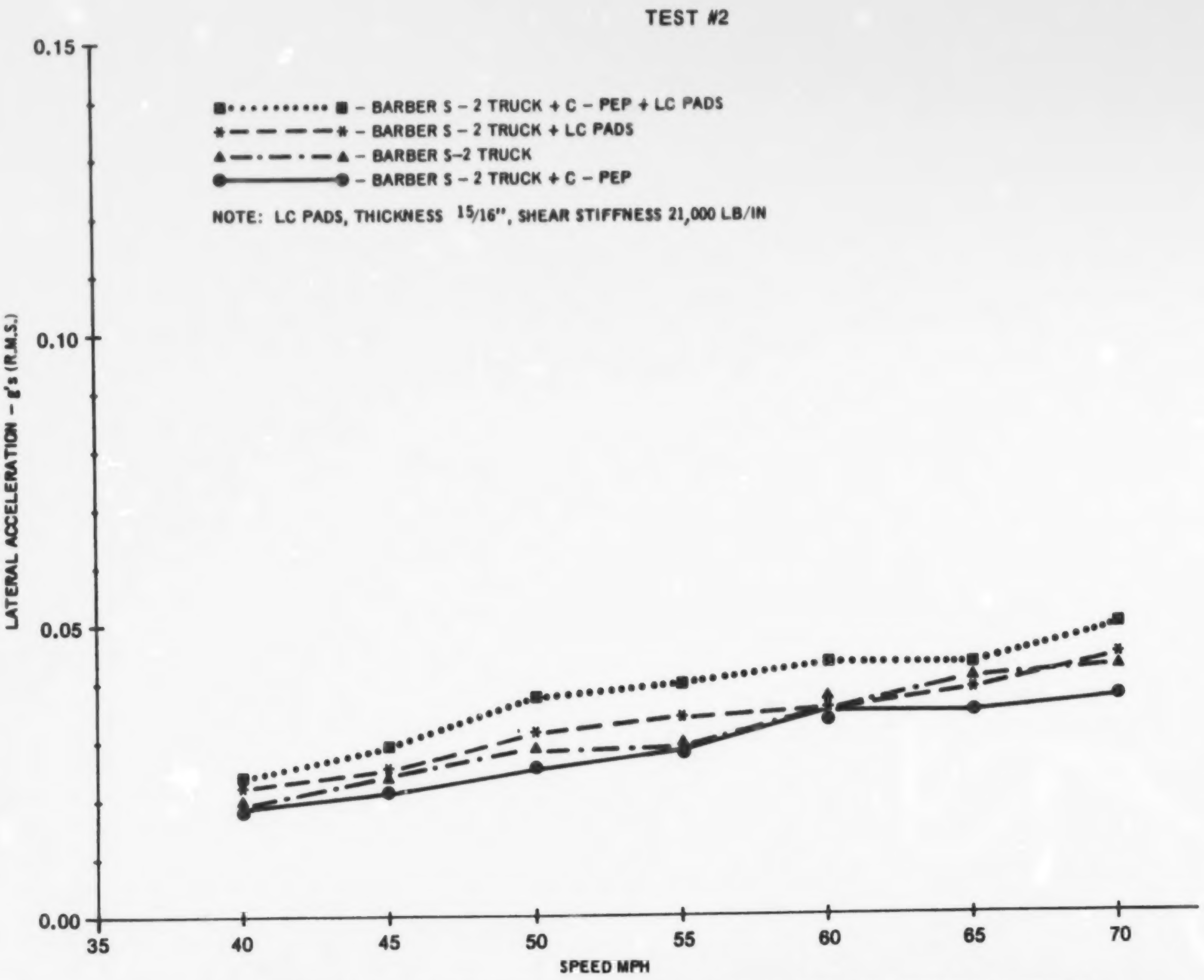

FIG. 8 : LATERAL ACCELERATION OF CAR BODY AT THE TRAILING TRUCK VS SPEED FOR TRUCKS WITH CN "A" PROFILE WHEELS

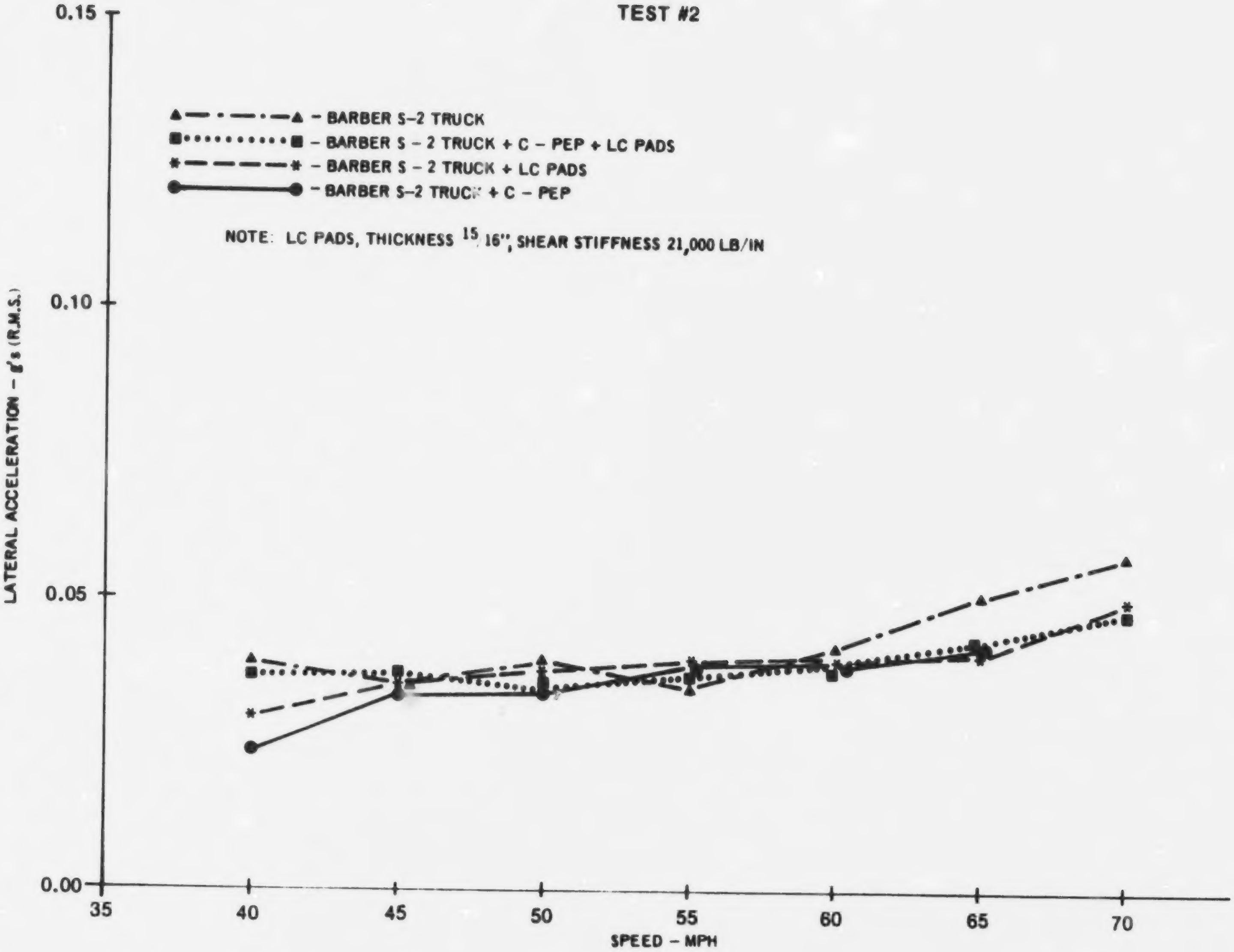

FIG. 9: LATERAL ACCELERATION ON TRAILING TRUCK LEAD AXLE BEARING END CAP VS SPEED FOR TRUCKS WITH CN "A" PROFILE WHEELS

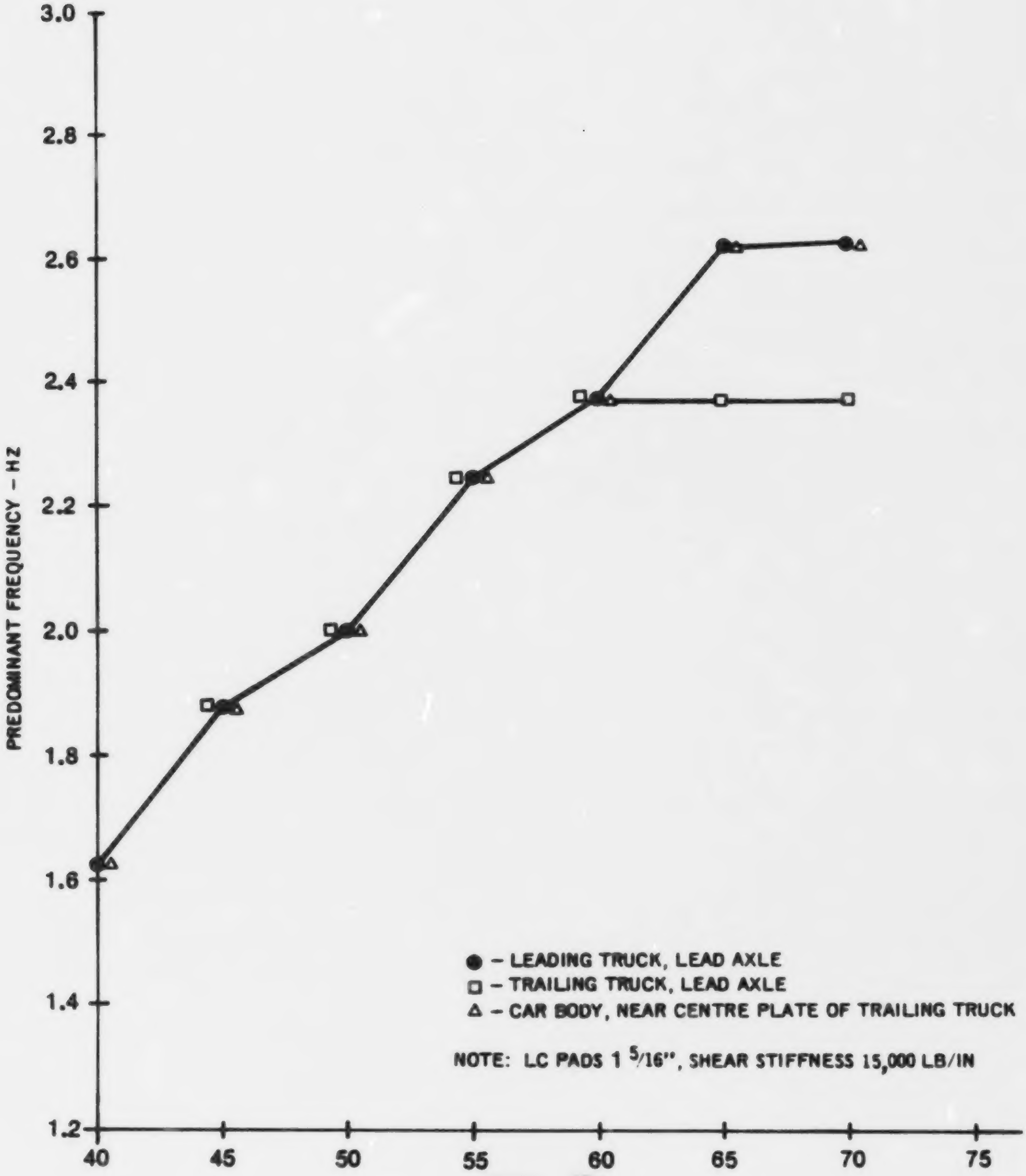

PREDOMINANT LATERAL WHEELSET AND CARBODY FREQUENCY VERSUS SPEED
FOR THE CONVENTIONAL BARBER S–2 TRUCK
WITH LC PADS AND CN "A" PROFILE WHEELS

FIG. 10

THEORETICAL CURVING PERFORMANCE OF FOUR FREIGHT CAR TRUCKS

EXECUTIVE SUMMARY

This report compares the relative theoretical curving performance of Barber-Scheffel, Barber S-2, DR1 and rigid frame trucks using a non-linear steady-state curving model developed by the CP Research Department.

The results indicate that considerable improvement in flange wear, derailment tendency and rolling resistance on curves could be achieved by using radial trucks instead of conventional Barber S-2 trucks. They also indicate that a rigid frame truck (e.g. RDI truck) does not offer significant improvement in wear, derailment tendency or rolling resistance.

Radial trucks utilize the self-steering action naturally existing from the wheel-rail interaction, and offer a means to suppress the parallelogramming tendency of trucks such as the Barber S-2 truck, in order to reduce the angle-of-attack of the leading wheelset and hence flange wear. By postponing the wheel flanging action to a higher degree of curvature, the radial trucks also generate less wheel drag associated with flanging and therefore reduce fuel consumption on curves. These benefits can be realized over the range of curvature (0-12 degrees) which exists on CP mainline track in the Pacific Region.

SOMMAIRE

Ce rapport compare les données théoriques du comportement en courbe de quatre bogies de wagons marchandises étudiés au moyen d'un modèle non linéaire de simulation en régime permanent mis au point par le service de la Recherche du CP. Les quatre bogies étudiés sont: le Barber Scheffel, le Barber S-2, le DR-1 et un bogie à châssis rigide.

L'étude a permis de dégager pour les bogies orientables une nette réduction de l'usure des boudins de roue, de la tendance au déraillement et de la résistance au roulement par rapport au bogie Barber S-2 d'usage courant. Elle indique également qu'un bogie à châssis rigide - le RDI par exemple - n'apporte aucune amélioration notable sous les aspects précités.

Les bogies orientables se conforment aux forces de guidage normalement présentes dans l'interaction roue-voie et offrent des moyens d'éliminer la tendance parallélogramme des bogies tel le bogie Barber S-2, afin de réduire l'angle d'inscription des paires de roues avant et l'usure des boudins de roue. En retardant l'apparition du frottement du boudin sur le rail aux courbes plus prononcées, les bogies orientables créent aussi moins de résistance au roulement dû au frottement des boudins sur les rails et conséquemment réduisent la consommation de carburant dans les courbes. Ces bénéfices peuvent être réalisés sur toute la gamme de courbure (0-12 degrés) sur la ligne principale du CP dans la région du Pacifique.

I. INTRODUCTION

The objective of this report is to compare the theoretical curving performance of four different types of freight car trucks currently in use or scheduled for service testing by CP Rail. The specific truck types considered are Barber-Scheffel (BSH), DR1, Barber S-2 (BS2) and rigid frame (RF) trucks.

Various comparative curving indices are derived using a non-linear steady state curving model recently developed by the Canadian Pacific Research Department. Specifically, the model is capable of predicting lateral flange force, angle-of-attack, flange wear index, derailment index (L/V ratio), rolling resistance and suspension forces for balanced and unbalanced speed curving at different degree curves and wheel-rail conditions. This report uses this information to evaluate the balanced speed curving of four types of trucks, and to investigate the self-steering mechanism of radial trucks.

II. STEADY-STATE CURVING MODEL

The steady-state curving model assumes a 2 point contact configuration on the flanging wheel. The tread forces are calculated using the Johnson-Vermeulen creep force/creepage relationship. The flange creepage is saturated, so the direction and magnitude of the flange sliding forces are calculated from relative velocity considerations of the wheel and rail, and from the track lateral elastic deflection after the flange clearance is exceeded. Prior to flanging, linear conicity is assumed.

A single truck is modelled with six degrees of freedom. These are the axle lateral displacement, yaw, and angular velocity for each wheelset. The suspension forces are calculated using Wickens' interaxle shear and bending formulation ($K_s;K_b$), with shear and bending stiffnesses derived from primary suspension characteristics.

The method of solution uses a numerical iterative technique to minimize the wheelset force, moment and torque unbalances on each wheelset. With a judicious choice of initial coordinates, usually less than 4 iterations are required for the solution to converge.

III. TRUCK SUSPENSION CHARACTERISTICS

The suspension values of Barber S-2, Barber-Scheffel and DR1 trucks were obtained from manufacturers, published data and from test results. The Barber S-2 truck has a very low interaxle shear stiffness and a very high interaxle bending stiffness. The Barber-Scheffel truck is much stiffer in shear than the BS2 truck, but is also very much softer in bending. The DR1 truck has approximately half the interaxle shear and double the interaxle bending stiffness of the Barber-Scheffel truck. This is due to the cross-anchor arrangement and the use of softer primary rubber shear springs in the pedestals of the Barber-Scheffel truck.

The calculations for the rigid frame truck assume an interaxle shear stiffness comparable to the DR1 truck and a high interaxle bending stiffness comparable to the BS2 truck. The model for this truck is equivalent to that of a DR1 truck with the rubber shear pads removed. The curving performance of the RDI bolster truck presently being considered by CP Rail will fall between the performances of this "rigid frame" truck and the BS2 truck.

IV. WHEEL-RAIL CONDITION

Computer results were obtained under both relatively new and worn wheel-rail conditions. This was done to obtain a quantitative measure of the improvement of curving performance of each truck under the worn wheel-rail conditions of high effective wheel conicity and large flange clearance. The relatively new conditions are simulated with a 0.375 inch flange clearance and a wheel conicity of 0.05. The worn conditions are simulated by using a 0.5 inch flange clearance and a wheel conicity of 0.15. In each case, a flange angle of 75 degrees is used, and a coefficient of friction of 0.3 assumed. Wheel load of 32875 lbs. is used to simulate 100-ton car fully laden conditions for all computer runs.

V. DISCUSSION OF RESULTS

Equilibrium free-body diagrams obtained from the computer simulation results are presented in figures 1 and 2 for the Barber-Scheffel and Barber S-2 trucks. The figures show all the creep, flange and suspension forces and the moments generated during steady-state curving. It is important to note that the slowdown of the flanging wheelsets from the nominal angular velocity (V/R) generates net longitudinal drag forces at the wheel-rail interface, and results in a higher rolling resistance in curves. The slowing down of the wheelsets also changes the longitudinal tread creep forces and hence affects the steering characteristics of the truck.

Figures 3 to 20 depict the variations of various curving parameters at different track curvatures. These are discussed in detail below.

1. Angles-of-Attack of Leading Axles: (Figures 3, 4)

For both new and worn conditions, the radial trucks generate a much lower angle-of-attack at the leading outer wheel. The RF and BS2 trucks have very similar angles-of-attack for worn conditions, and the RF truck generates a slightly lower angle-of-attack than the BS2 truck for new conditions. The BSH truck generates a lower angle-of-attack than the DR1 truck in both cases.

2. Angles-of-Attack of Trailing Axles: (Figure 5)

The trailing axles of all trucks assume a more or less radial position up to a 4 degree curve. After 4 degrees the BS2 truck generates a much higher angle-of-attack than the rest in the new wheel-rail condition. This large positive angle-of-attack of the trailing axle indicates that this truck is in a parallelogramming mode much more pronounced than those of the other trucks at these curvatures. The trailing axles are much more radial on all trucks for worn conditions. These are not illustrated here.

3. Lateral Flange Forces of Leading Axles: (Figures 6, 7)

All leading axles start flanging at below a 2 degree curve for the new condition, and the magnitudes of the flange forces do not differ considerably from one truck type to another. For the worn condition, the radial trucks postpone flanging until a 7 degree curve, thus eliminating flange wear up to that curvature.

4. Lateral Flange Forces of Trailing Axles: (Figure 8)

Under new wheel and rail conditions, the radial trucks' trailing wheelsets flange only for a certain curvature range. BS2 trucks however, flange consistently above a 3 1/2 degree curve. The trailing axles of RF trucks do not flange. Under worn wheel and rail conditions, no flanging action was observed on trailing wheelsets at all curvatures considered.

5. Flange Wear Index: (Figures 9, 10)

The flange wear index is calculated as the product of the angle-of-attack and the lateral flange force of the flanging wheel. It is an indicator of flange wear which still requires further correlation with service test results.

The vast difference observed in the wear index of radial and non-radial trucks for the new condition can be attributed to the angle-of-attack reduction of radial trucks, since the lateral flange force for this condition does not differ much among trucks.

For the worn wheel-rail condition, the radial truck flange wear index is lower because the radial truck axles simply do not flange at low curvature, and the angle-of-attack is considerably reduced compared with the BS2 and RF trucks after wheelset flanging takes place.

6. L/V Ratio of Leading Outer Wheel: (Figures 11, 12)

The L/V ratio is an index related to the wheel lifting tendancy and is computed by taking the net lateral force on the outer wheel divided by the wheel vertical load. The figures indicate that the derailment tendancy is improved marginally by radial trucks for the new wheel-rail condition. For the worn wheel and rail condition, the L/V ratios of the radial trucks are generally much smaller, due to the fact that flanging action is postponed to a higher degree curve.

The negative L/V ratios arise because the net lateral force on the wheel consists of the sum of the lateral flange force and the lateral creep force on the tread, which are opposite in direction for positive angles-of-attack.

7. Rolling Resistance: (Figures 13, 14)

Flanging action increases wheel drag around curves. Radial trucks, by postponing flanging to a higher curvature, are therefore beneficial from a fuel consumption viewpoint. The rolling resistances of the trucks are compared to a conventional formula used to calculate this resistance.

VI. SELF-STEERING MECHANISM OF RADIAL TRUCKS (Figures 15-20)

The suspension forces and moments arising from the shearing and yawing action of the trucks are presented to illustrate the self-steering principle of the radial trucks. For both the new and worn wheel and rail conditions, Figures 15 and 16 show that the parallelogramming direction is opposite for low and high curvatures. This reversal occurs at a much higher degree of curvature for the worn condition as compared to the new condition. The worn condition postpones to a higher curvature the parallelogramming action associated with the large positive angle-of-attack. Although the magnitude of the interaxle shear force of the BS2 truck is generally lower than that of the others, its very low interaxleshear stiffness results in a greater parallelogramming action.

The reduction of the angles-of-attack of the radial trucks results from the yawing of the axles relative to the truck frame such that they open up on the high rail. This yawing action can be seen by observing the relative magnitude and direction of the suspension yaw moments on both leading and trailing axles.

Figures 17 to 20 show that the yaw moments acting on the two axles can be either in-phase (same direction) or out-of-phase (opposite direction). With the exception of the trailing axle yaw moment of the BS2 truck, the direction of these moments as a function of curvature is consistent for all trucks and for both new and worn wheel and rail conditions.

At low curvatures the leading axle yaw moment is positive and the trailing moment is negative; they are out-of-phase. At a higher curvature both moments are positive, resulting in an in-phase condition which exists over a range of curvatures. At an even higher curvature, the leading axle moment is negative, with the trailing moment remaining positive. The worn wheel and rail condition shifts these phase-change points to higher degrees of curvature. The high range out-of-phase moments for the worn condition occur at curvatures higher than those of interest here.

The behaviour of the BS2 truck is quite different. The trailing axle suspension yaw moment is positive at all curvatures, resulting in two ranges of phases only; in-phase at low curvatures and out-of-phase at higher curvatures.

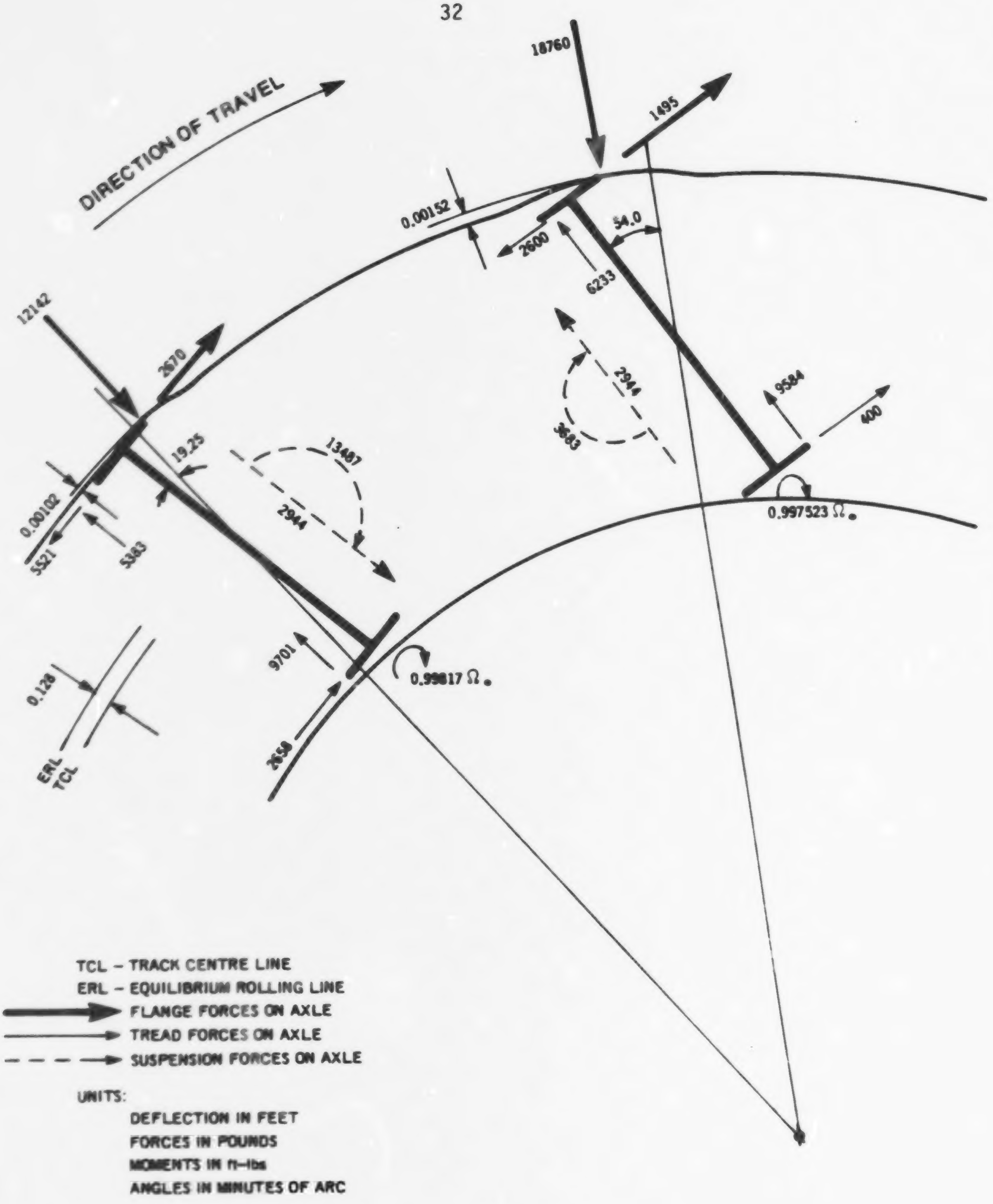
DIRECTION OF TRAVEL
18760
1495
0.00152
2600
6233
54.0
12142
2670
2944
3683
9584
400
19.25
13487
2944
0.00102
5521
5383
0.997523 Ω₀
9701
0.99817 Ω₀
0.128
2658
ERL
TCL
TCL – TRACK CENTRE LINE
ERL – EQUILIBRIUM ROLLING LINE
FLANGE FORCES ON AXLE
TREAD FORCES ON AXLE
SUSPENSION FORCES ON AXLE
UNITS:
DEFLECTION IN FEET
FORCES IN POUNDS
MOMENTS IN ft–lbs
ANGLES IN MINUTES OF ARC

FIG. 1 : STEADY STATE CURVING ATTITUDE OF BS2 TRUCK ON 10 DEGREE CURVE
(NEW WHEEL AND RAIL CONDITION)

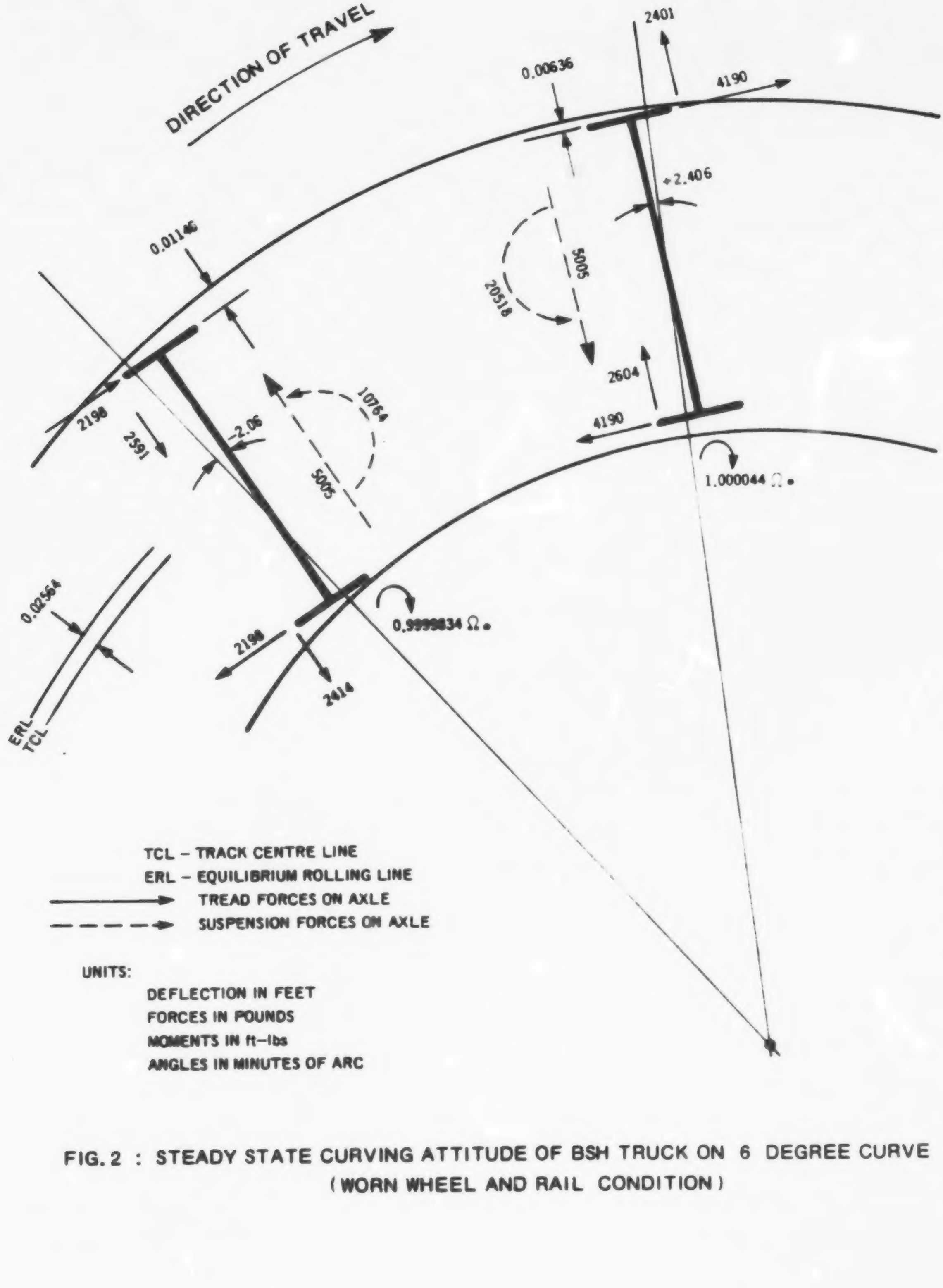
DIRECTION OF TRAVEL
2401
0.00636
4190
+2.406
5005
20518
0.01146
2604
4190
1.000044 Ω•
2198
2591
-2.06
10764
5005
0.02564
ERL
TCL
2198
2414
0.9999834 Ω•
TCL – TRACK CENTRE LINE
ERL – EQUILIBRIUM ROLLING LINE
TREAD FORCES ON AXLE
SUSPENSION FORCES ON AXLE
UNITS:
DEFLECTION IN FEET
FORCES IN POUNDS
MOMENTS IN ft–lbs
ANGLES IN MINUTES OF ARC

FIG. 2 : STEADY STATE CURVING ATTITUDE OF BSH TRUCK ON 6 DEGREE CURVE
(WORN WHEEL AND RAIL CONDITION)

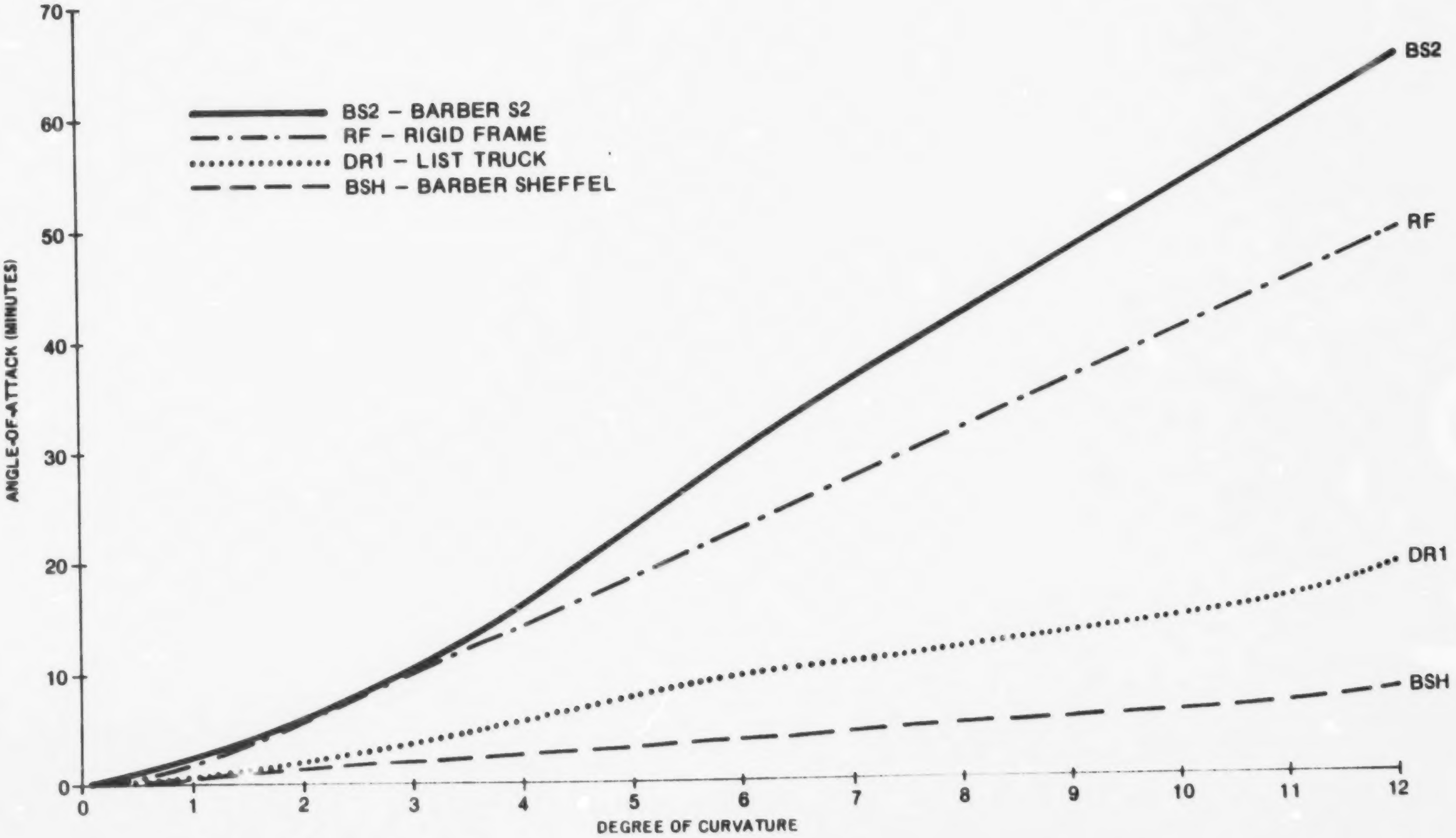

FIG.3 : ANGLE-OF-ATTACK OF LEADING OUTER WHEEL (WITH NEW WHEEL AND RAIL CONDITION)

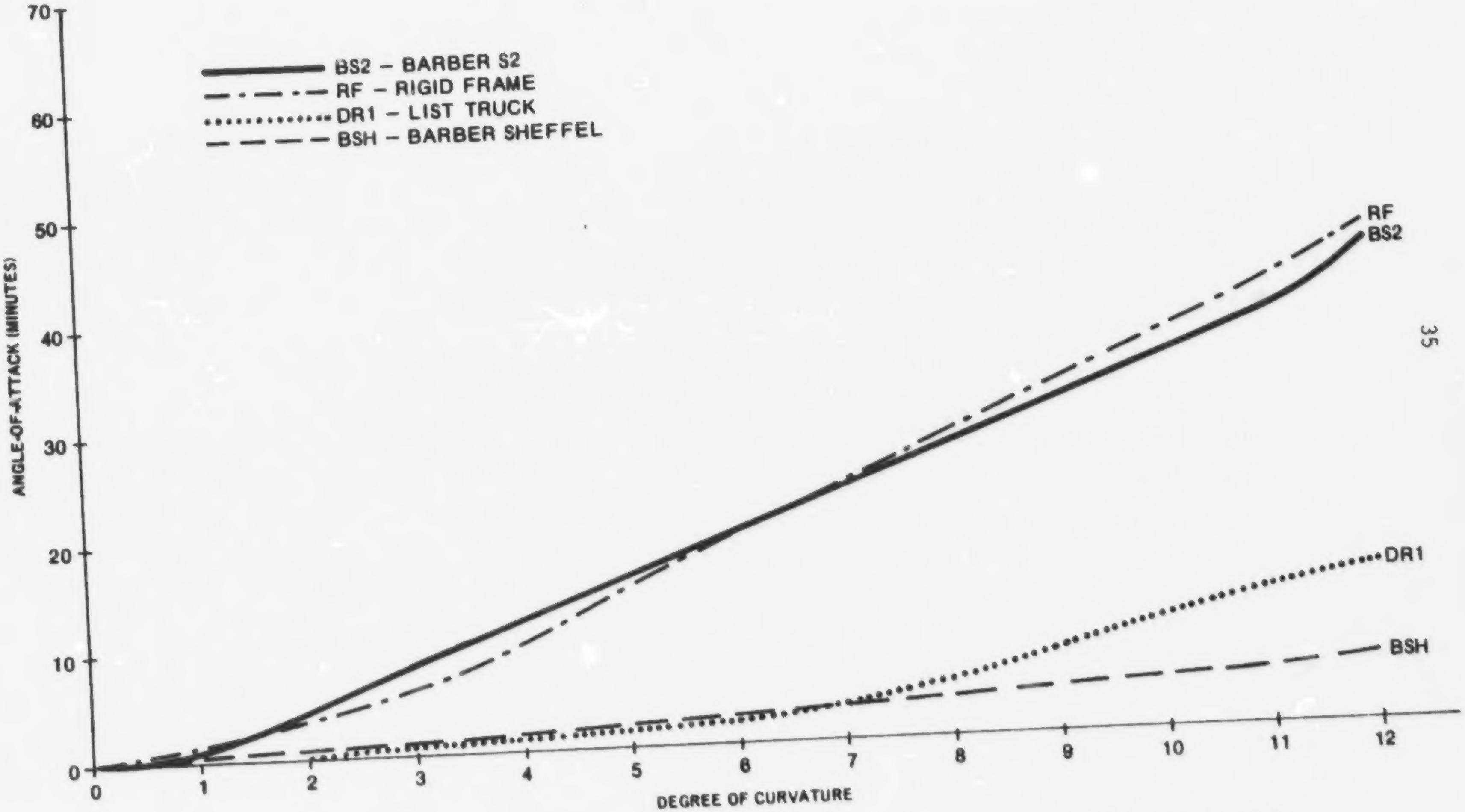

FIG. 4 : ANGLE-OF-ATTACK OF LEADING OUTER WHEEL (WITH WORN WHEEL AND RAIL CONDITION)

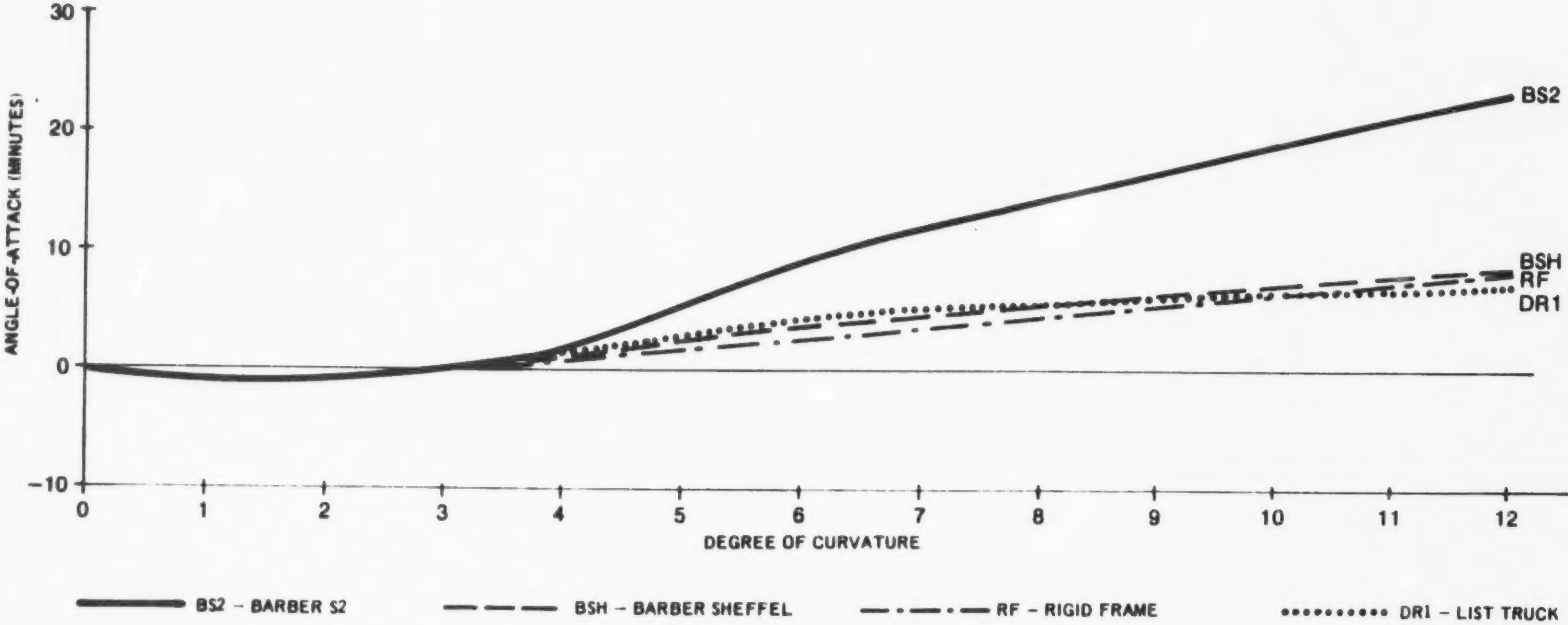

FIG. 5 : ANGLE-OF-ATTACK OF TRAILING AXLES (WITH NEW WHEEL AND RAIL CONDITION)

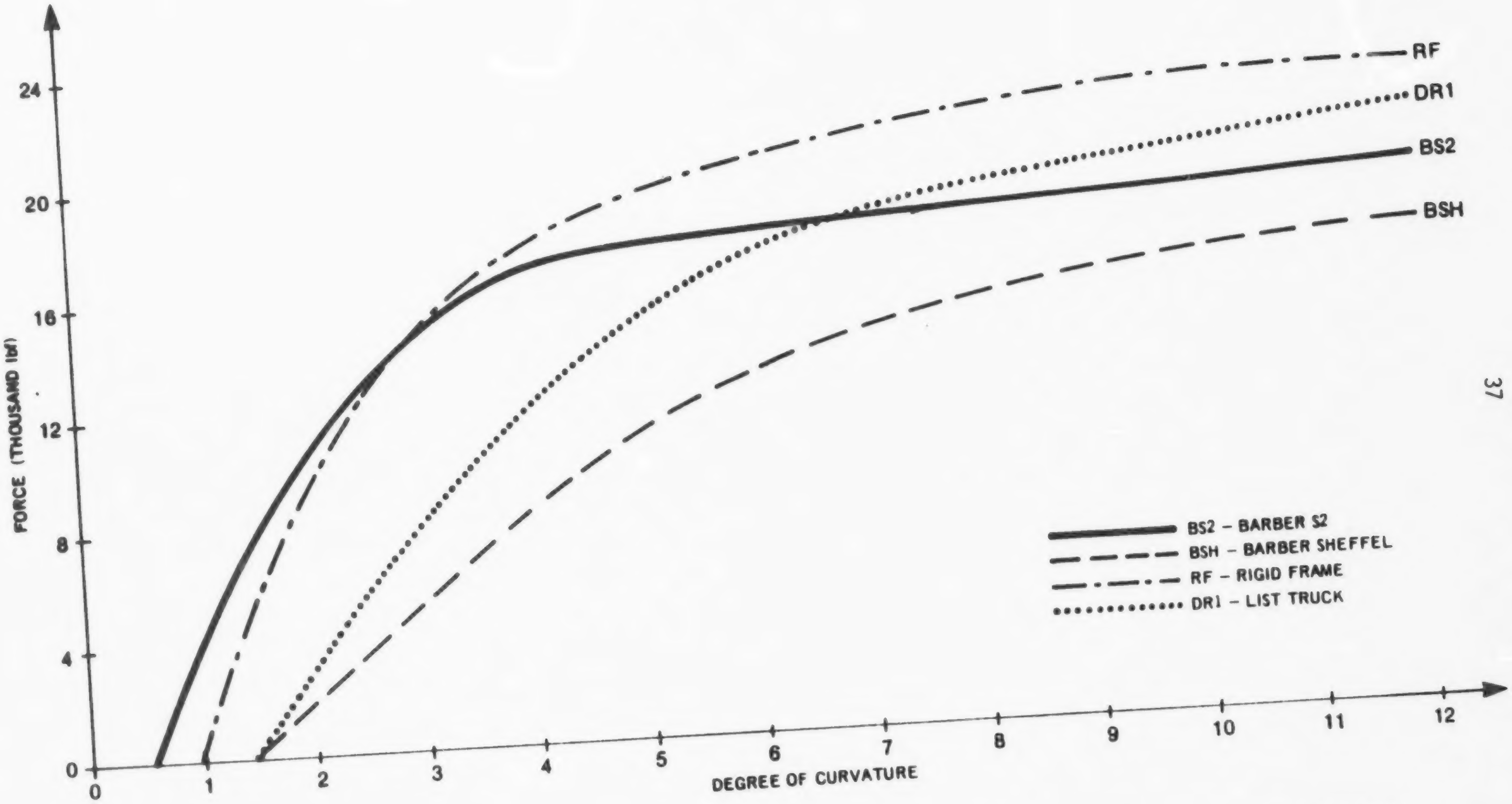

FIG.6 : LATERAL FLANGE FORCE OF LEADING OUTER WHEEL (WITH NEW WHEEL AND RAIL CONDITION)

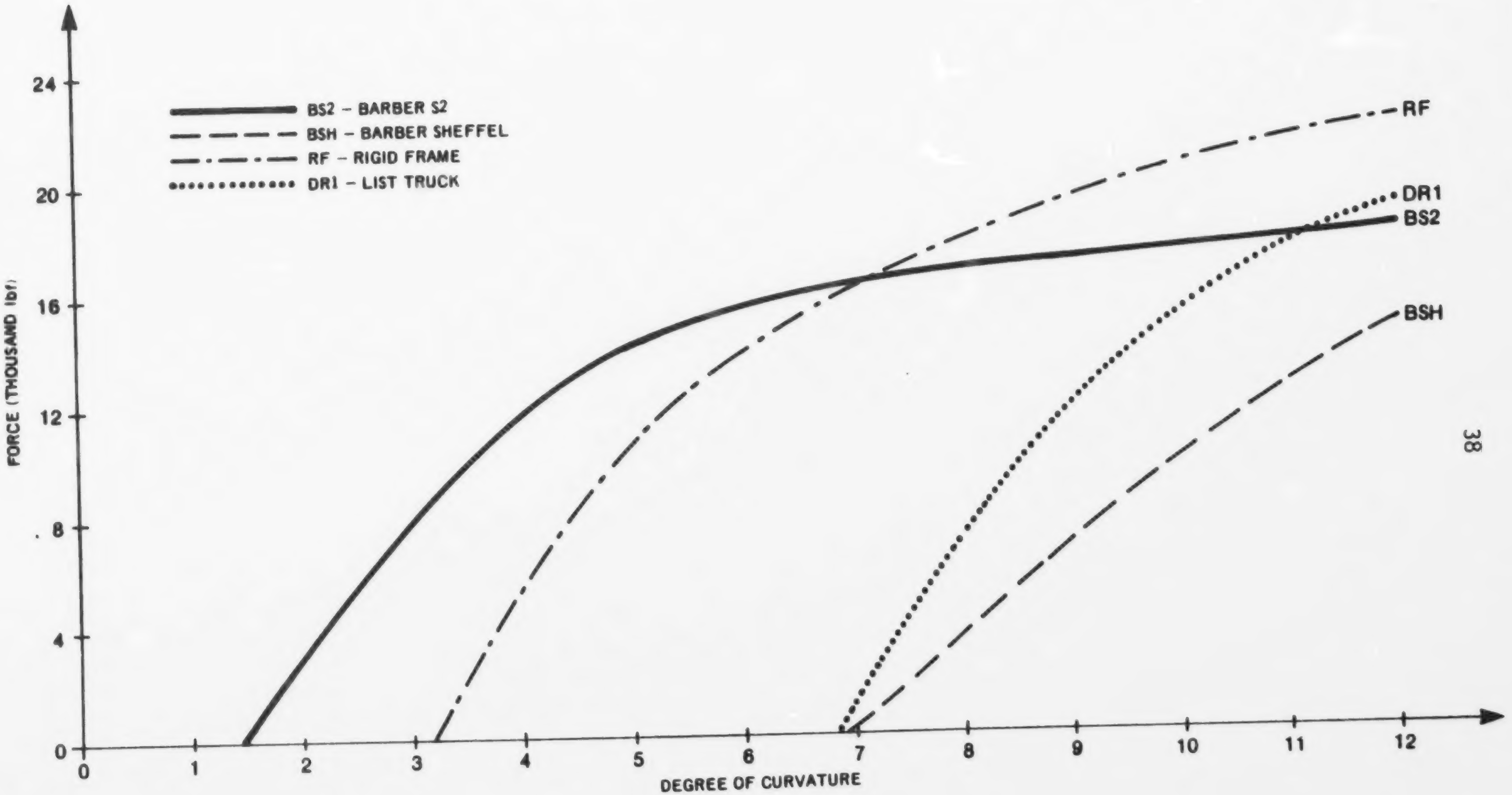

FIG.7 : LATERAL FLANGE FORCE OF LEADING OUTER WHEEL (WITH WORN WHEEL AND RAIL CONDITION)

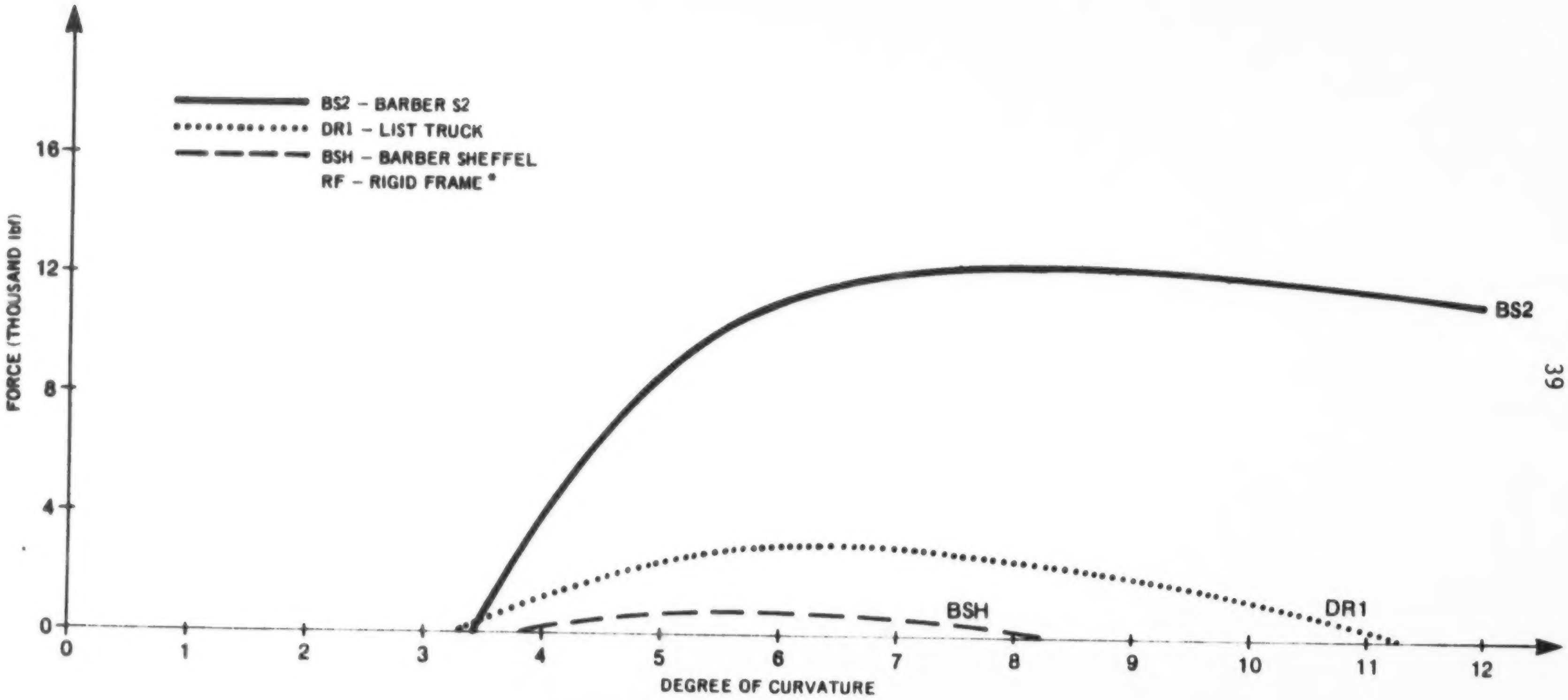

FIG. 8 : LATERAL FLANGE FORCE OF TRAILING OUTER WHEEL (WITH NEW WHEEL AND RAIL CONDITION)

*RF TRUCK NOT FLANGING

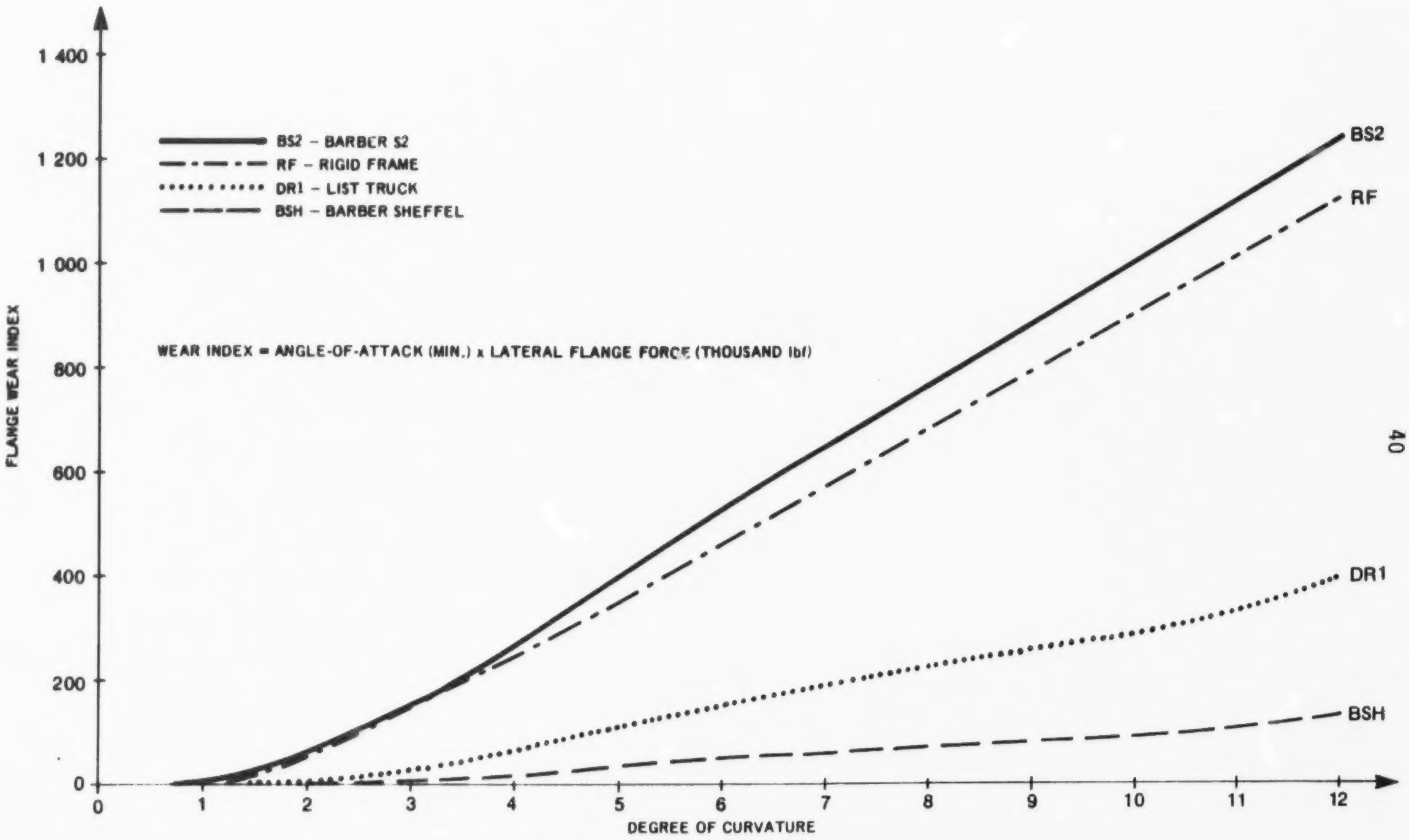

FIG. 9 : FLANGE WEAR INDEX OF LEADING OUTER WHEEL (WITH NEW WHEEL AND RAIL CONDITION)

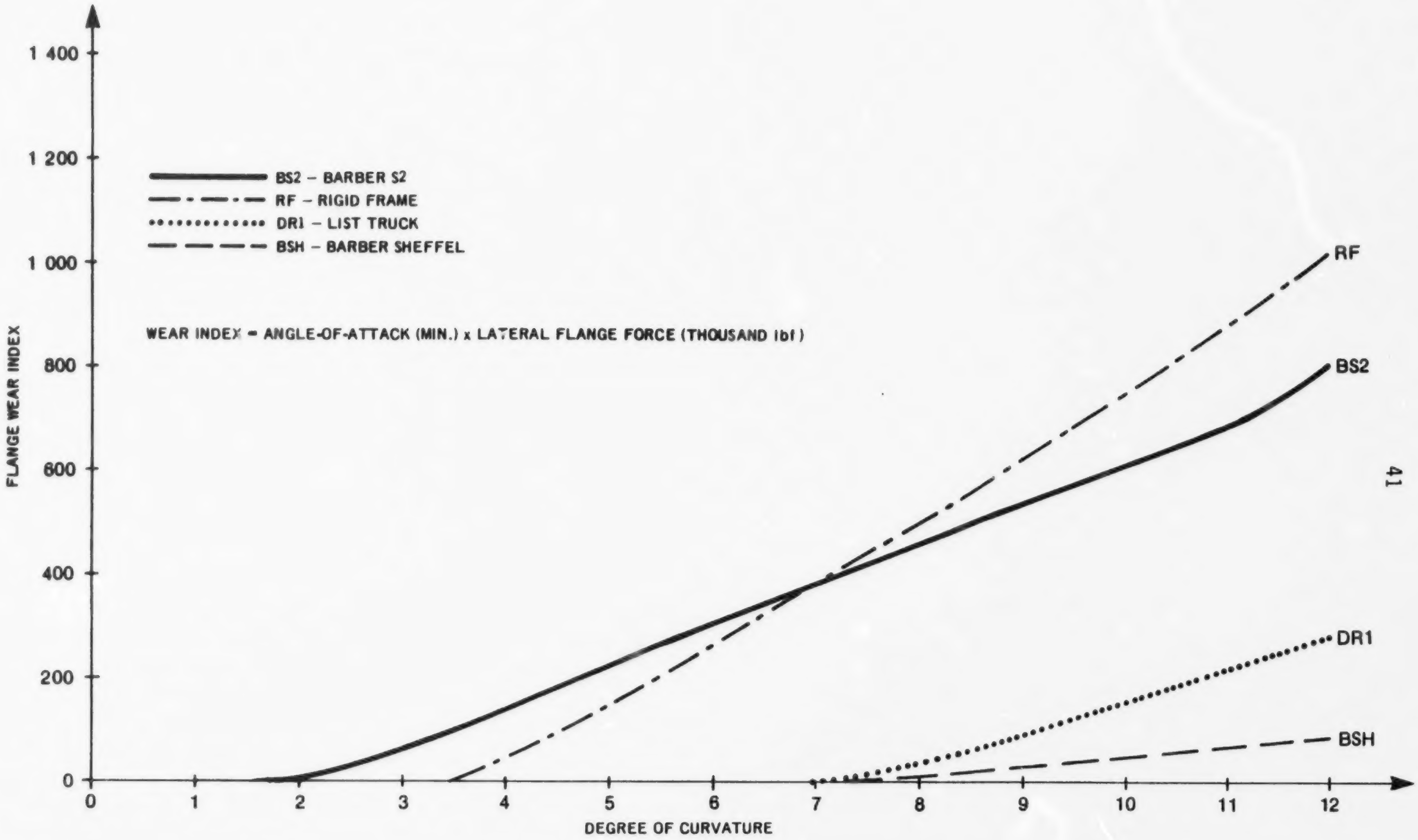

FIG.10 : FLANGE WEAR INDEX OF LEADING OUTER WHEEL (WITH WORN WHEEL AND RAIL CONDITION)

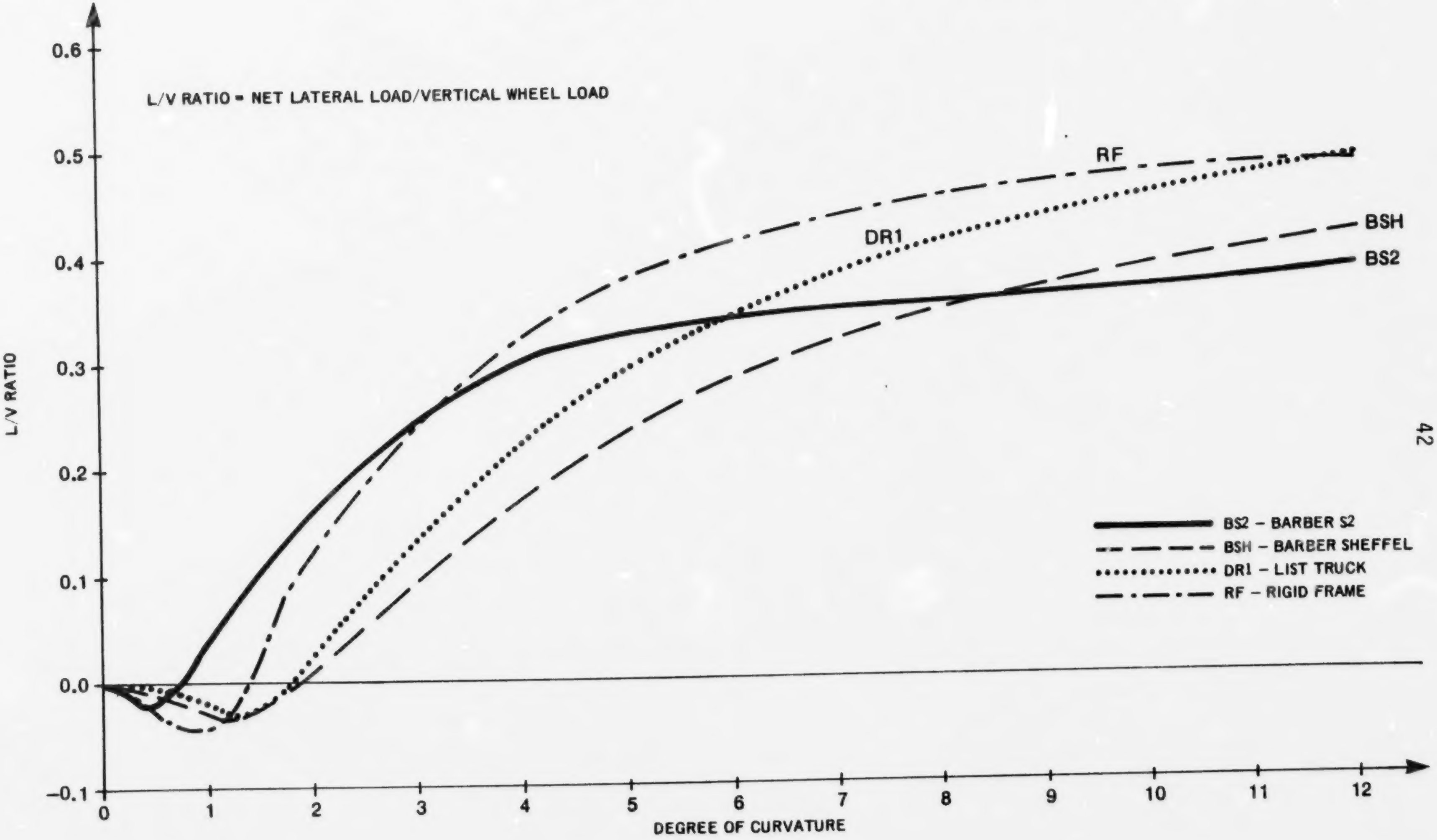

FIG.11 : RAIL L/V RATIO FOR LEADING OUTER WHEEL (NEW WHEEL AND RAIL CONDITION)

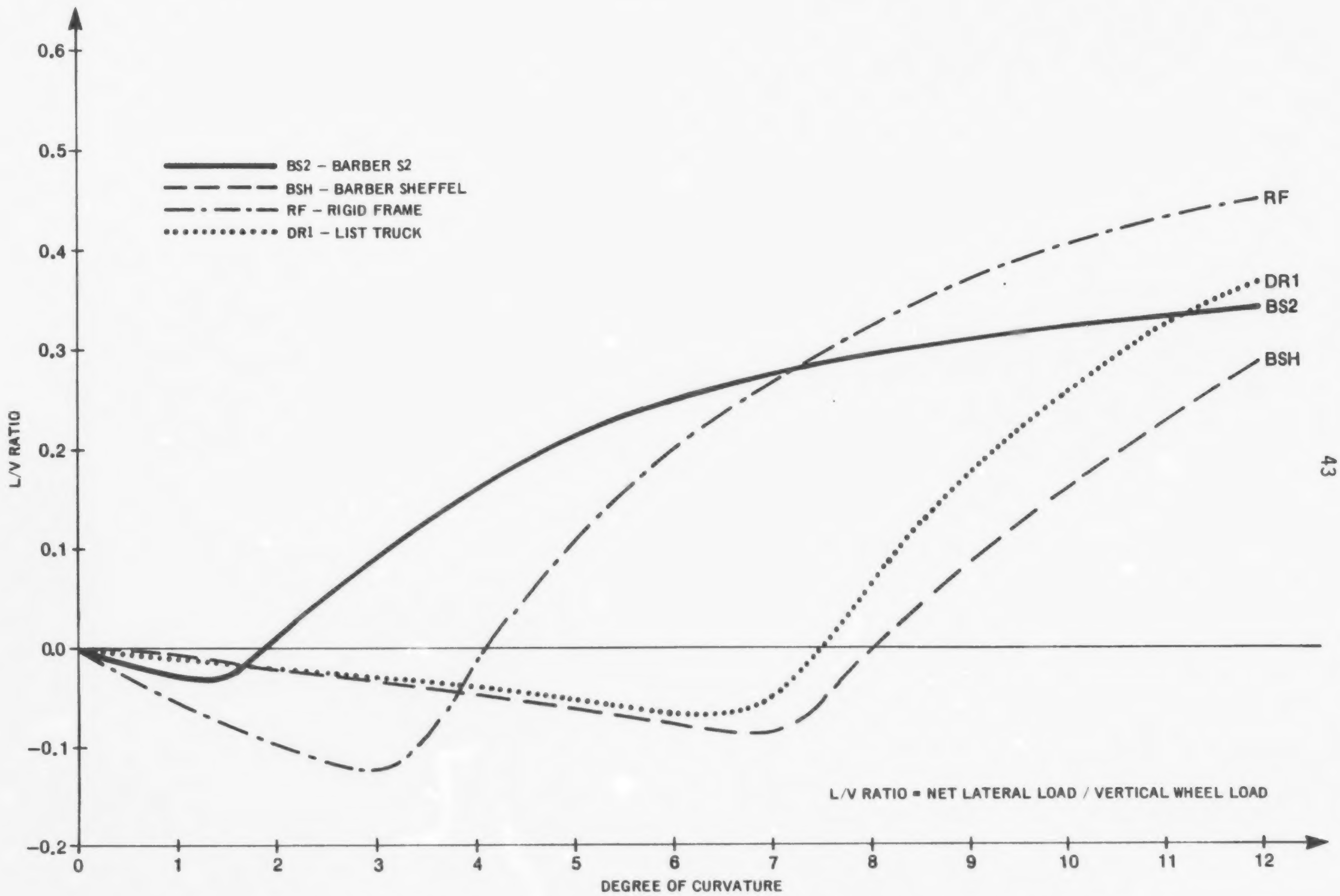

FIG.12: RAIL L/V RATIO FOR LEADING OUTER WHEEL (WORN WHEEL AND RAIL CONDITION)

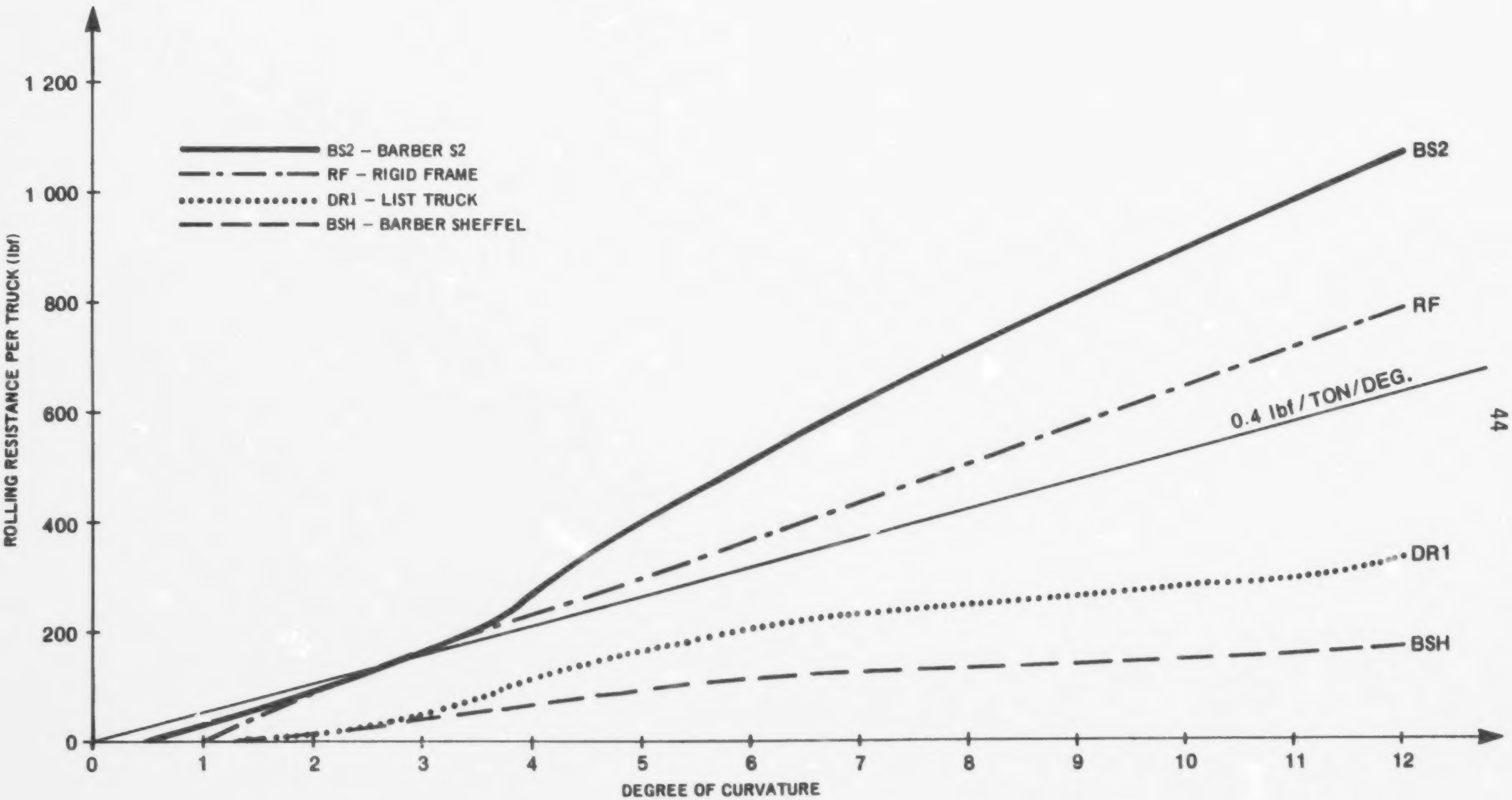

FIG.13 : ROLLING RESISTANCE PER TRUCK (FOR NEW WHEEL AND RAIL CONDITION)

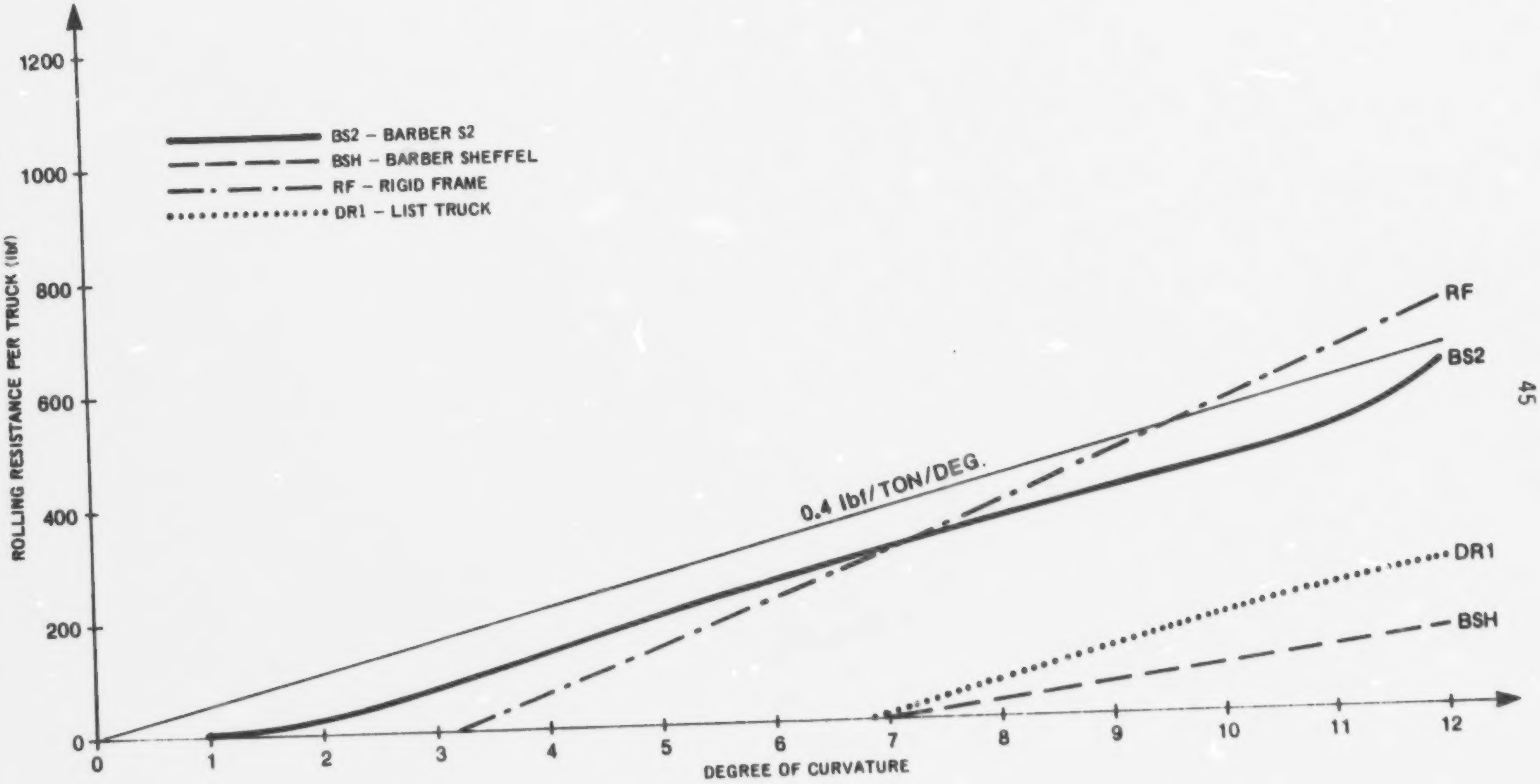

FIG. 14 : ROLLING RESISTANCE PER TRUCK (WORN WHEEL AND RAIL CONDITION)

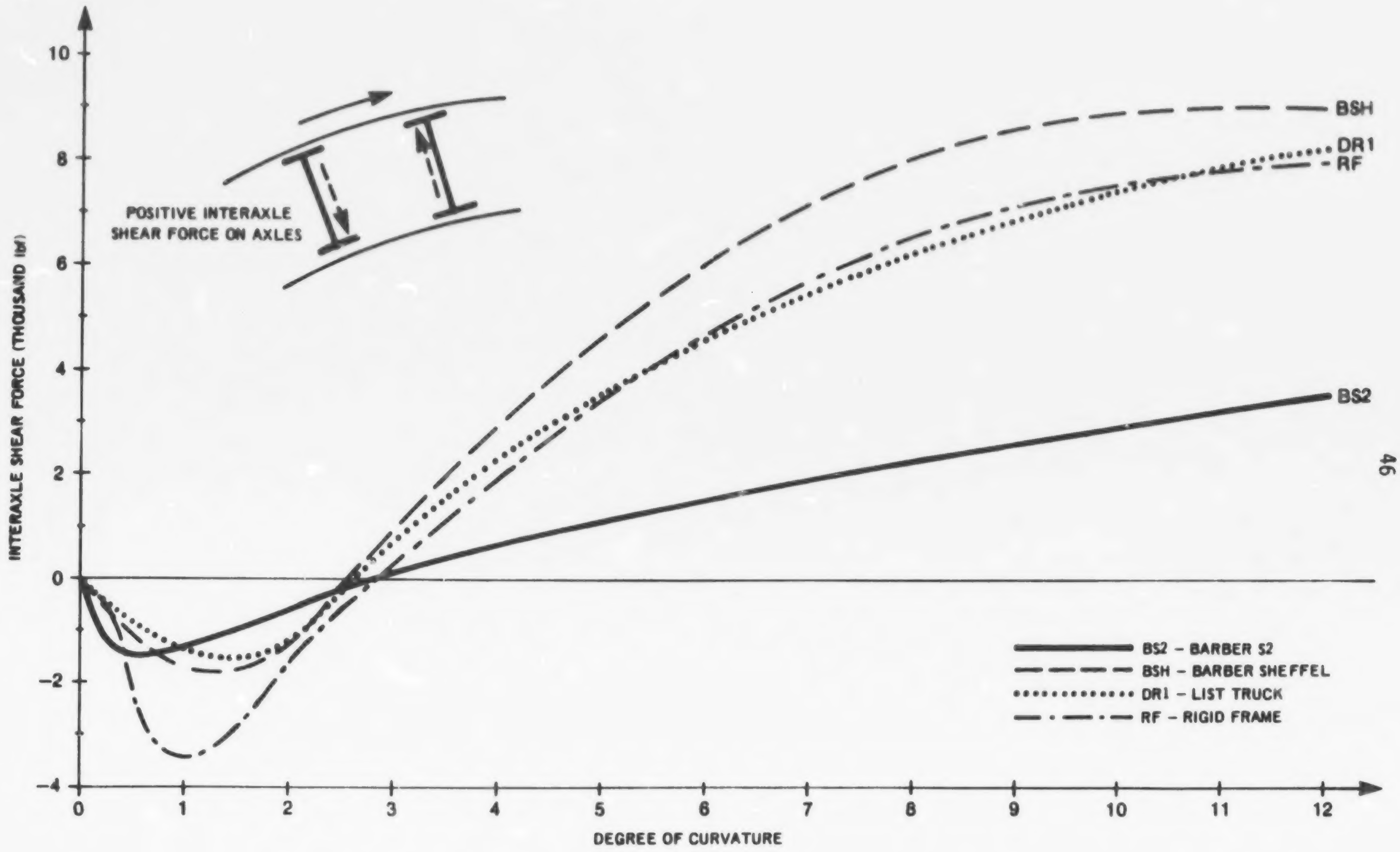

FIG.15: INTERAXLE SHEAR FORCE (NEW WHEEL AND RAIL CONDITION)

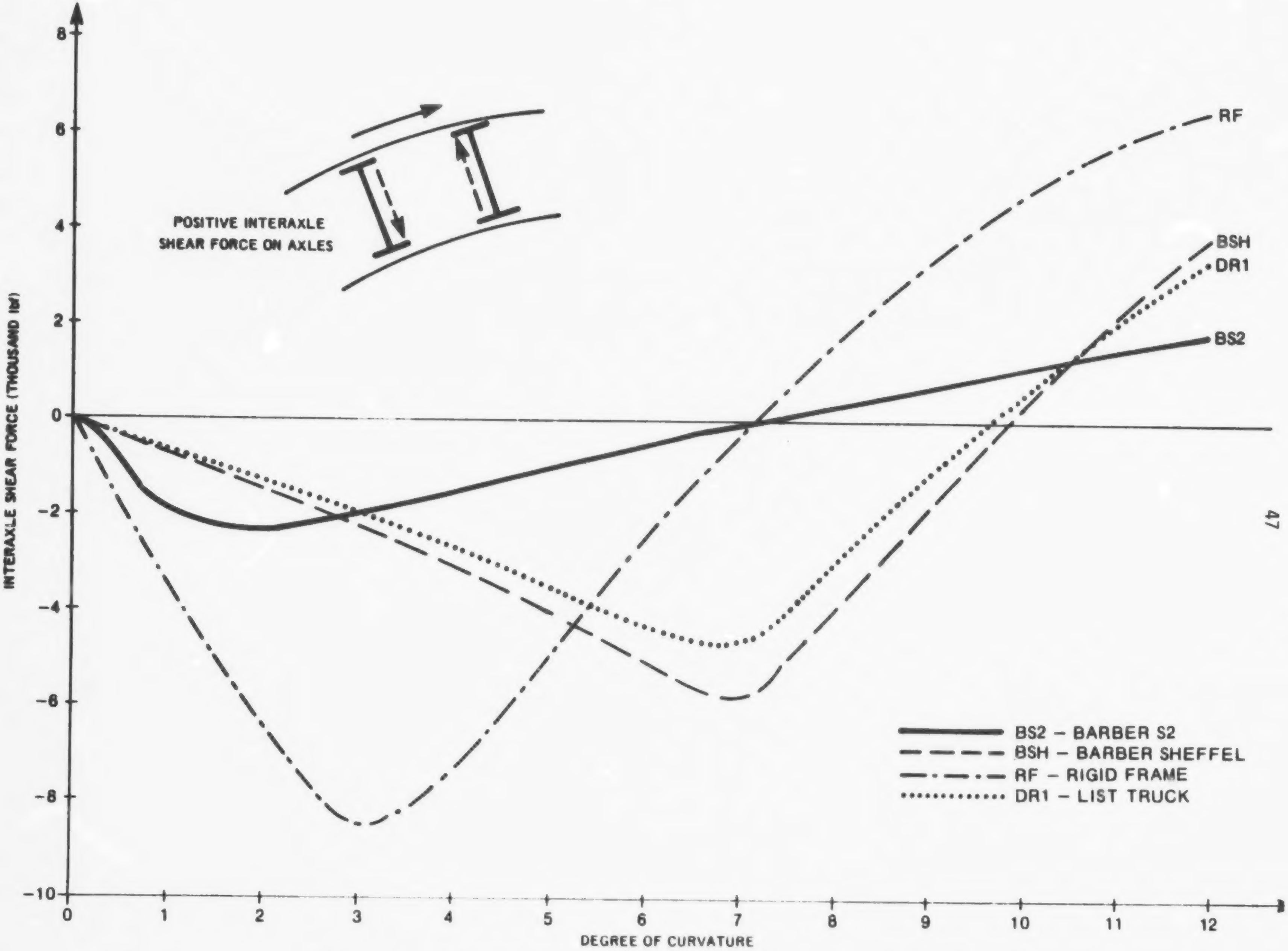

FIG.16 : INTERAXLE SHEAR FORCE (WORN WHEEL AND RAIL CONDITION)

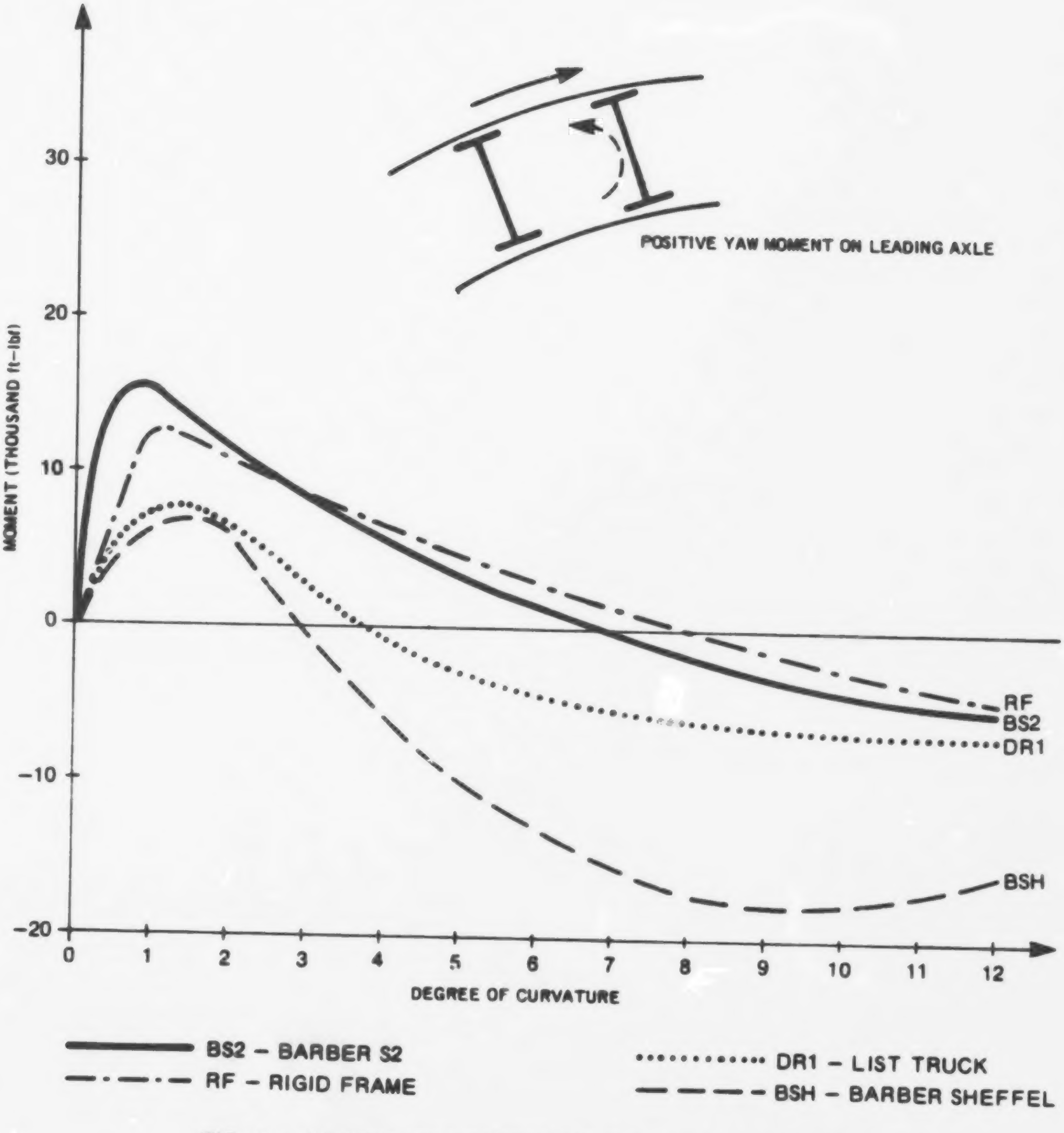

FIG.17 : MOMENT ON LEADING AXLE DUE TO SUSPENSION YAW (NEW WHEEL AND RAIL CONDITION)

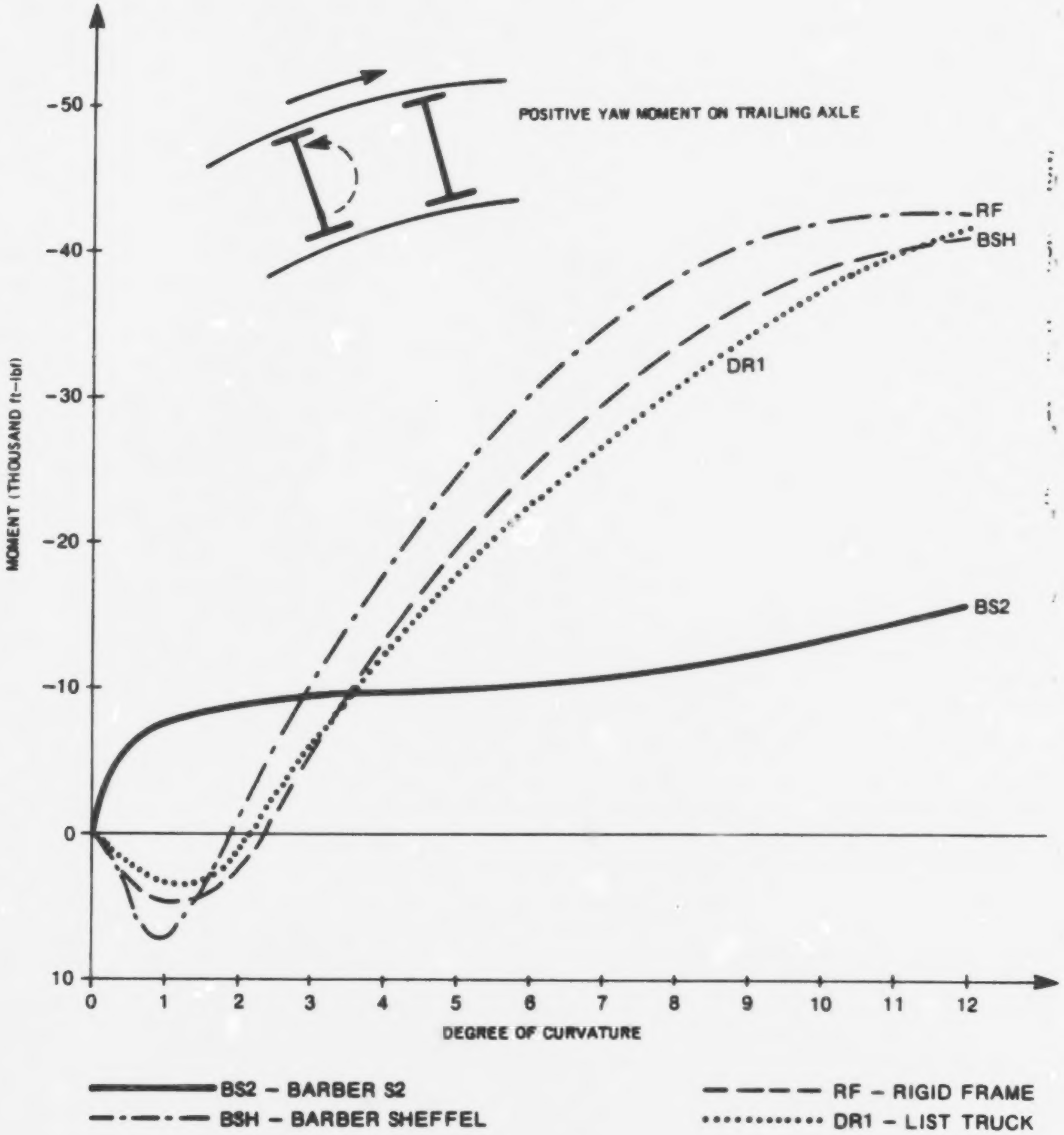

FIG.18 : MOMENT ON TRAILING AXLE DUE TO SUSPENSION YAW (NEW WHEEL AND RAIL CONDITION)

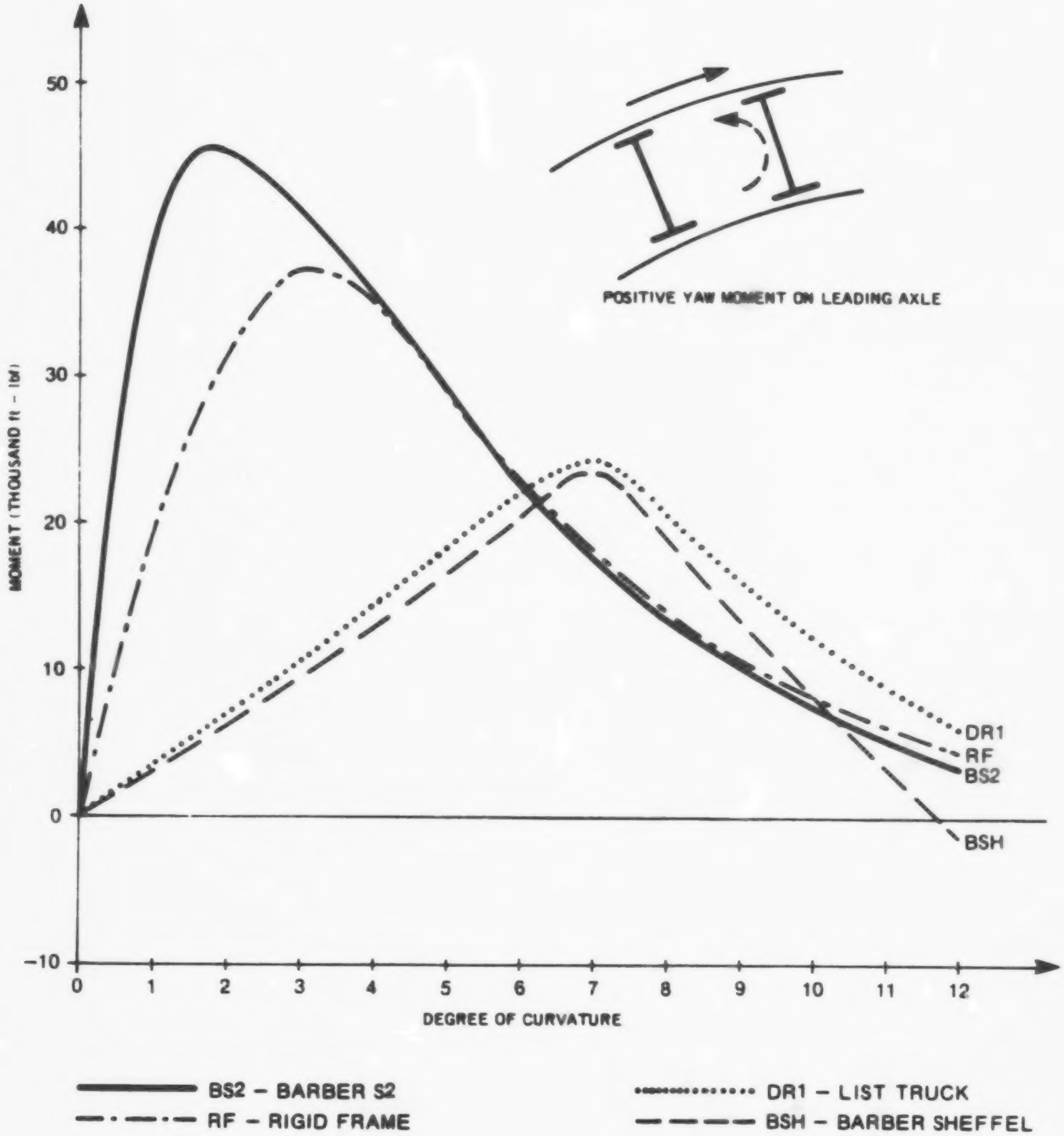

FIG.19 : MOMENT ON LEADING AXLE DUE TO SUSPENSION YAW
(WORN WHEEL AND RAIL CONDITION)

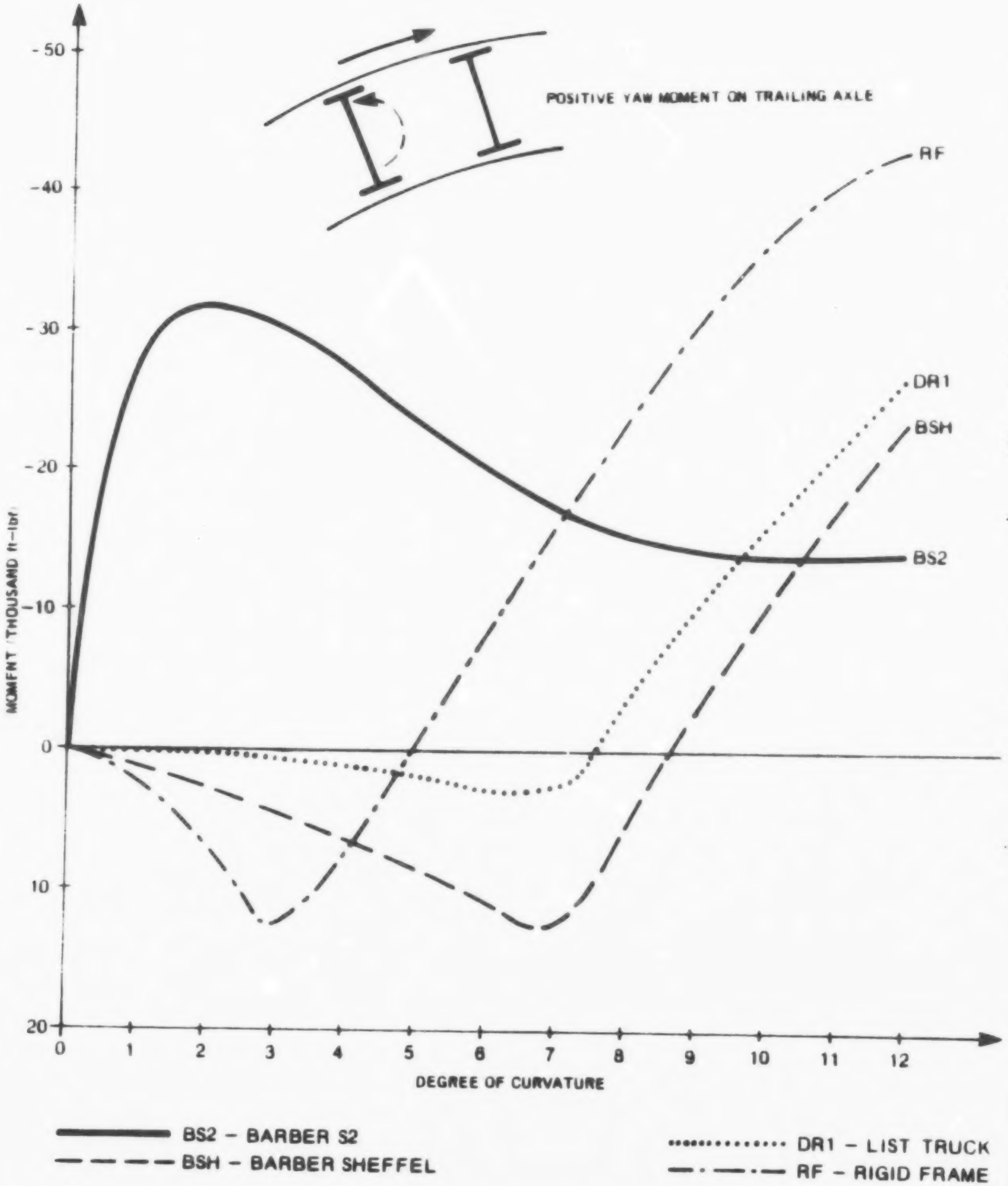

FIG. 20 : MOMENT ON TRAILING AXLE DUE TO SUSPENSION YAW (WORN WHEEL AND RAIL CONDITION)

CURVING PERFORMANCE TEST OF GM SD40, SD40-2 AND MLW M636 LOCOMOTIVE TRUCKS

Summary

A field test was conducted in October, 1981 in the Calgary area to evaluate the comparative curving performance of three types of locomotive trucks on a 5 degree curve. The locomotive test consist was comprised of a General Motors SD-40-2 3000 HP unit, a General Motors SD-40 3000 HP unit, and a Montreal Locomotive Works M636 3300 HP unit. Angle-of-attack, lateral and vertical forces data were collected for these 3 axle trucks.

The results indicate that the curving behaviour of these trucks is asymmetric in the Eastbound and Westbound runs with the trucks steering substantially better Eastbound. In addition, each truck retained its own curving characteristics when the tests were repeated within 2 days, indicating that the wheel/rail adhesion was not altered substantially between the two tests. As concluded from results of previous tests conducted in 1980, a correlation exists between high and low rail forces during steady-state curving and the importance of the mid-axle flanging action is discernible again in the results.

Among the locomotive trucks tested, SD-40 locomotive trucks generate slightly higher angle-of-attack at the lead axle, and have a slightly larger weight transfer effect among the axles in the same truck. This weight transfer effect is observable on all trucks tested and is a direct result of the moment generated from the difference in height of the lateral load path of the net wheel/rail forces and the net lateral bearing reaction load on a wheelset, and has a much more dominant effect in wheel load distribution in the case of a flanging wheelset than the effect of wheel size differential.

SOMMAIRE

Un essai fait en octobre 1981 sur une voie ayant 5° de courbure dans la région de Calgary a permis d'évaluer et de comparer les caractéristiques d'inscription en courbe de trois types de bogies de locomotives. Les locomotives essayées ont été les suivantes: une General Motors SD-40-2 d'une puissance de 3 000 HP, une autre General Motors SD-40 également de 3 000 HP et une Montreal Locomotive Works M636 de 3 300 HP. Les valeurs mesurées ont été l'angle d'inscription et les forces transversales et verticales exercées par les bogies à 3 essieux chacun.

Il ressort des résultats de l'essai que le comportement en courbe de ces bogies diffère selon que le train se dirige vers l'Est ou vers l'Ouest, la stabilité des bogies étant de loin meilleure lorsque le train se dirige vers l'Est. En outre, il a été constaté que le comportement en courbe des bogies n'a pas varié lorsque l'essai a été refait moins de deux jours plus tard, ce qui montre que l'adhérence rail/roue n'a guère changé entre-temps. Ces essais ont confirmé la corrélation entre les forces s'exerçant sur les deux files de rail en régime d'inscription en courbe permanent, ressortie lors d'essais faits en 1980. En outre, l'ampleur du frottement des boudins des rous de l'essieu intermédiaire a, de nouveau, pu être constatée.

Des trois bogies essayés, le SD-40 a été celui dont l'essieu directeur a accusé, par une légère marge, le plus grand angle d'inscription et celui où le transfert de poids entre les essieux d'un même bogie a été le plus prononcé, également par une faible marge. Ce transfert est observé dans tous les bogies essayés. C'est le résultat direct du moment engendré par la différence de hauteur entre les forces transversales nettes en jeu sur les deux files de rail et de l'effort de réaction transversal net des coussinets sur l'essieu monté. Son influence sur la distribution des charges de roue dans le cas d'un essieu monté qui frotte est de loin supérieure à celle due à une différence dans la dimension des roues.

Acknowledgements

The authors wish to express their sincere thanks to:

- Personnel of the National Research Council Railway Laboratory Division of Mechanical Engineering for assistance in measuring curving forces during the field tests.

- Office of the Chief Mechanical Officer for assistance during the course of the test program.

- Transportation Development Centre, Transport Canada for financial support under Contract # OSD81-00006.

1. Introduction

As a continuation of the locomotive curving and ride studies (Ref. 1) under the Track Train Dynamics Program with the Transportation Research and Development Centre, (TDC), Transport Canada, a series of locomotive curving performance tests with service worn wheels was conducted in the Calgary area in October, 1981. The objective of this test was to provide curving performance data, under the same test environment, for three types of 3 axle locomotive trucks: General Motors Flexicoil truck (SD-40), General Motors HTC Truck (SD-40-2), and Montreal Locomotive Works High Adhesion (HI-AD) truck.

Trackside instrumentation was installed at a specific location on a 5 degree curve to measure lateral, vertical rail forces, and angle-of-attack of each wheelset as it passed the instrumented site at different curving speeds. A more detailed description of instrumentation is given in previous reports (Ref. 1 & 2).

2. Test Curve and Test Sequence

The location chosen for trackside instrumentation was a 5 degree curve near Calgary at mileage 12.4 on the Laggan Subdivision. The track consists of Algoma 1971 RE132 lb, 78 ft. staggered jointed rail. The curve had a 0.5% ascending grade in the Westward direction, a super-elevation of 4.5" and a corresponding equilibrium speed of 37 mph. The flange lubricator was shut off during each test.

The test consist was comprised of one SD-40-2, one SD-40 and one M636 locomotive coupled in this sequence throughout the tests. During each series of tests, three runs were made by coasting the locomotives through the test curve in each direction at 25, 37 and 45 mph respectively. The test consist was then wyed and this procedure repeated for a total of 36 runs on October 15. Identical test runs were repeated on October 17 at the same location. Curving data for a total of 72 runs were collected and analyzed. At the end of the second day of testing some special condition runs were made to study locomotive truck behaviour under dynamic braking, automatic braking, and acceleration. These results are included at the end of the illustrations.

3. Sign Conventions

In order to demonstrate the correlation between angle-of-attack, lateral and vertical forces generated for all three axles of each truck, the curving results are illustrated by axle numbers in Figures 1 to 10. The same axle number indicates the same axle on each truck, whether the consist is wyed or unwyed, travelling Eastbound or Westbound.

For sign conventions, (Fig. 1A) a positive angle-of-attack signifies axles rolling toward the outside of the curve (away from centre), positive lateral low rail and high rail forces are directed away from the centre of curve.

4. Discussion of Test Results

1) The test results for both days of testing are presented in consecutive figures for each test run with the same test configuration. In each case, there is a remarkable resemblance in the test results, indicating that the locomotive trucks generally retain their angle-of-attack and rail force patterns at the same track location, and that the adhesion level variation is small. The slight variation in the force pattern is attributable to slight curving speed variations.

2) Due to the single point contact between low rail and wheel tread (when the trailing axle is not flanging on low rail), the angle-of-attack of each wheel strictly governs the amount of lateral slip force at the low rail. Since the angle-of-attack of a wheelset decreases with increasing speed, the low rail forces also manifest this characteristic.

3) Under an ideal steady state curving condition, no lateral acceleration is experienced on truck components, and therefore the net lateral force experienced on each truck component is zero. When a free body diagram of the whole truck is examined, one can see that the sum of the lateral wheel/rail loads on both high and low rails should balance the lateral centrifugal forces applied at the centre plate. Therefore, a large negative lateral slip force at low rail induces a high positive reaction flange force at the high rail. This is most evident for the two SD-40 trucks in the figures.

4) The weight transfer effect is also evident from observing the vertical wheel load distribution of each wheel in the truck. This effect is a result of the fact that the net lateral wheel rail force for each wheelset is balanced only at the bearing level. The difference in height of the load path creates a moment, which is balanced only by an uneven distribution of wheel load, provided the vertical bearing loads are fairly equalized. Thus a flanging wheelset tends to increase the high rail force and at the same time reduce the low rail vertical force. A non-flanging wheelset with positive angle-of-attack would distribute the vertical wheel loads in the exactly opposite manner.

5) Curve steering behaviour of locomotive trucks are asymmetric in the Eastbound and Westbound direction. Westbound runs have larger positive angle-of-attack, higher creep and flange forces and manifest larger weight transfer characteristics among axles of the same truck.

6) In the Westbound runs, the leading SD-40 truck generate higher angle-of-attack at the lead axle compared with the lead axles of leading trucks of the other two locomotives.

7) For both East and Westbound runs, the second SD-40 truck consistently generated higher low rail and high rail forces than the first truck.

8) The SD-40 trucks, in both East and Westbound runs, have higher vertical wheel load transfer characteristics than the other trucks.

9) No drastic difference was observed on locomotive truck behaviour under various effects of dynamic braking, automatic braking, or acceleration, (Figs: 9, 10) except for the MLW truck in the Westbound direction where the angle-of-attack of the mid-axle was substantially reduced under automatic braking.

10) The derailment ratio (L/V) for the flanging wheels on high rail can be readily deduced from these data. It was generally found to be less than 0.4.

References

1.	W. Pak	Curving Performance of SD-40-2 Locomotive Trucks CP Report S677-81, June 1981, Transport Canada Report No. TP 3050
2.	R. Gonsalves W. Pak G. Izbinsky	Railroad Dynamics Incorporated (RDI) Truck Evaluation Test CP Report S670-81, March 1981, Transport Canada Report No. TP 2970

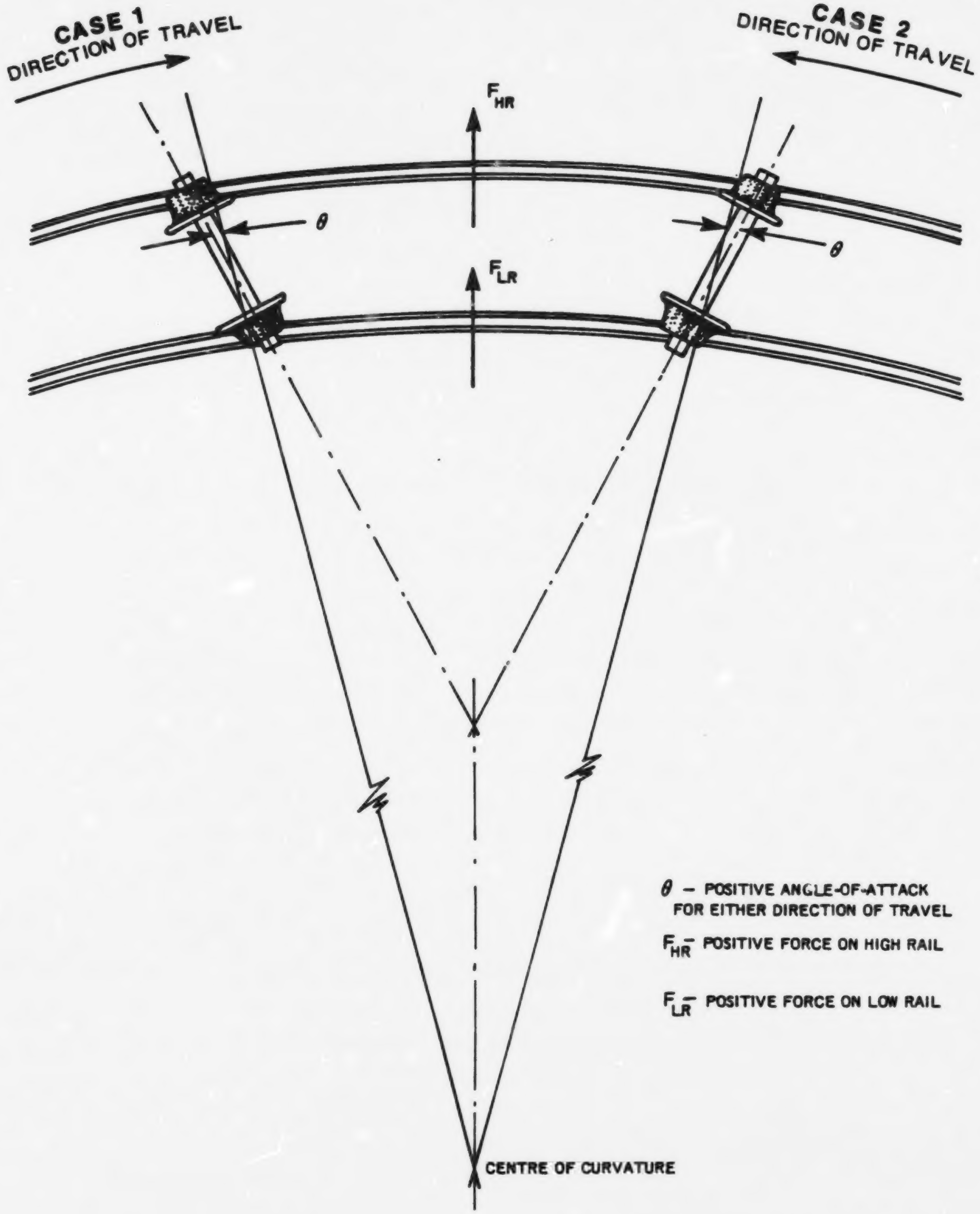
CASE 1
DIRECTION OF TRAVEL
CASE 2
DIRECTION OF TRAVEL
F_{HR}
F_{LR}
θ
θ
θ – POSITIVE ANGLE-OF-ATTACK FOR EITHER DIRECTION OF TRAVEL
F_{HR} – POSITIVE FORCE ON HIGH RAIL
F_{LR} – POSITIVE FORCE ON LOW RAIL
CENTRE OF CURVATURE

SIGN CONVENTION OF ANGLE-OF-ATTACK FOR A SINGLE WHEELSET TRAVELLING IN EITHER DIRECTION AND RAIL FORCES

FIG. 1a

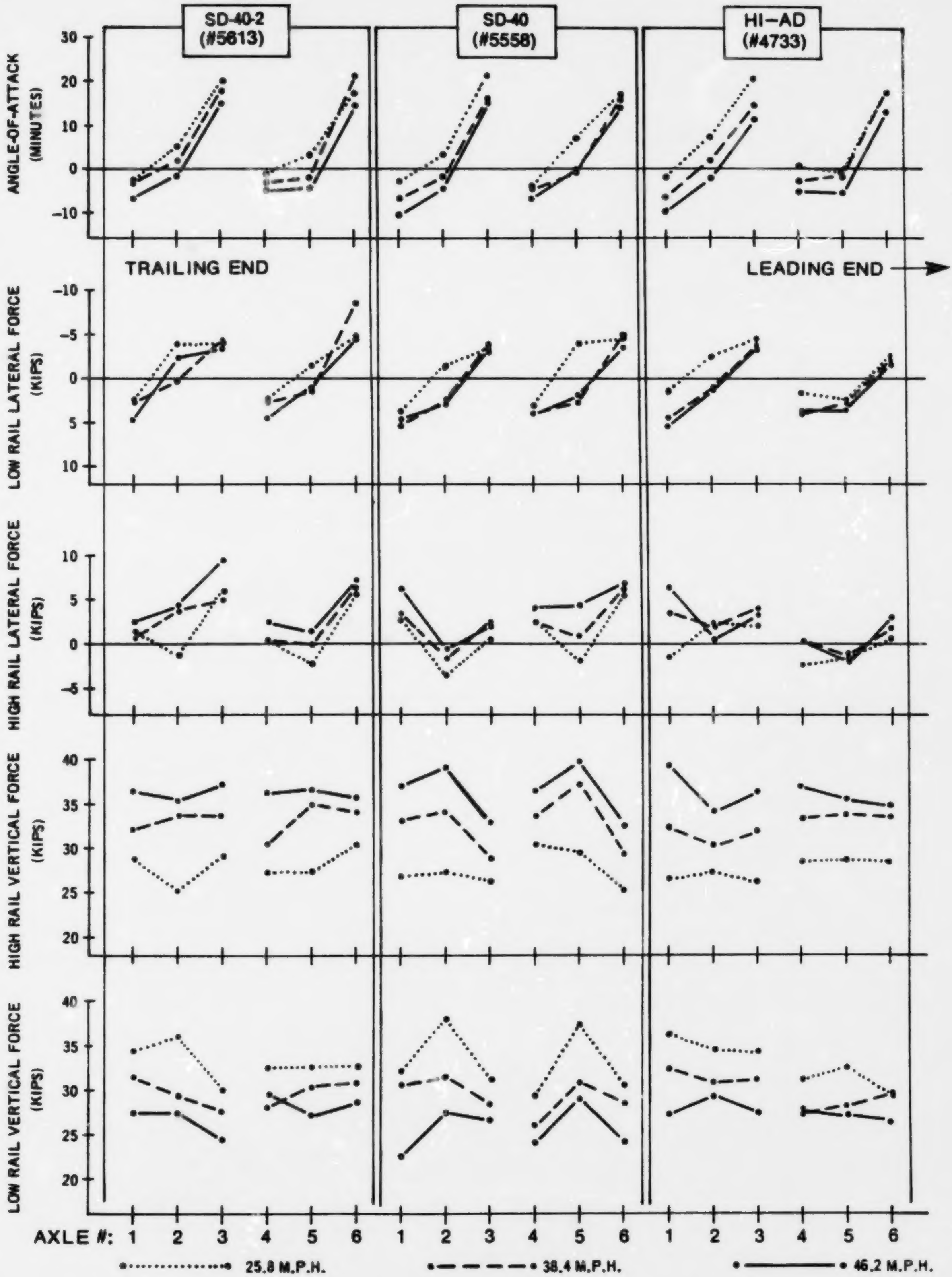

FIG. 1 : ANGLE-OF-ATTACK AND RAIL FORCES AT DIFFERENT CURVING SPEEDS
(EASTBOUND, UNWYED, DAY 1)

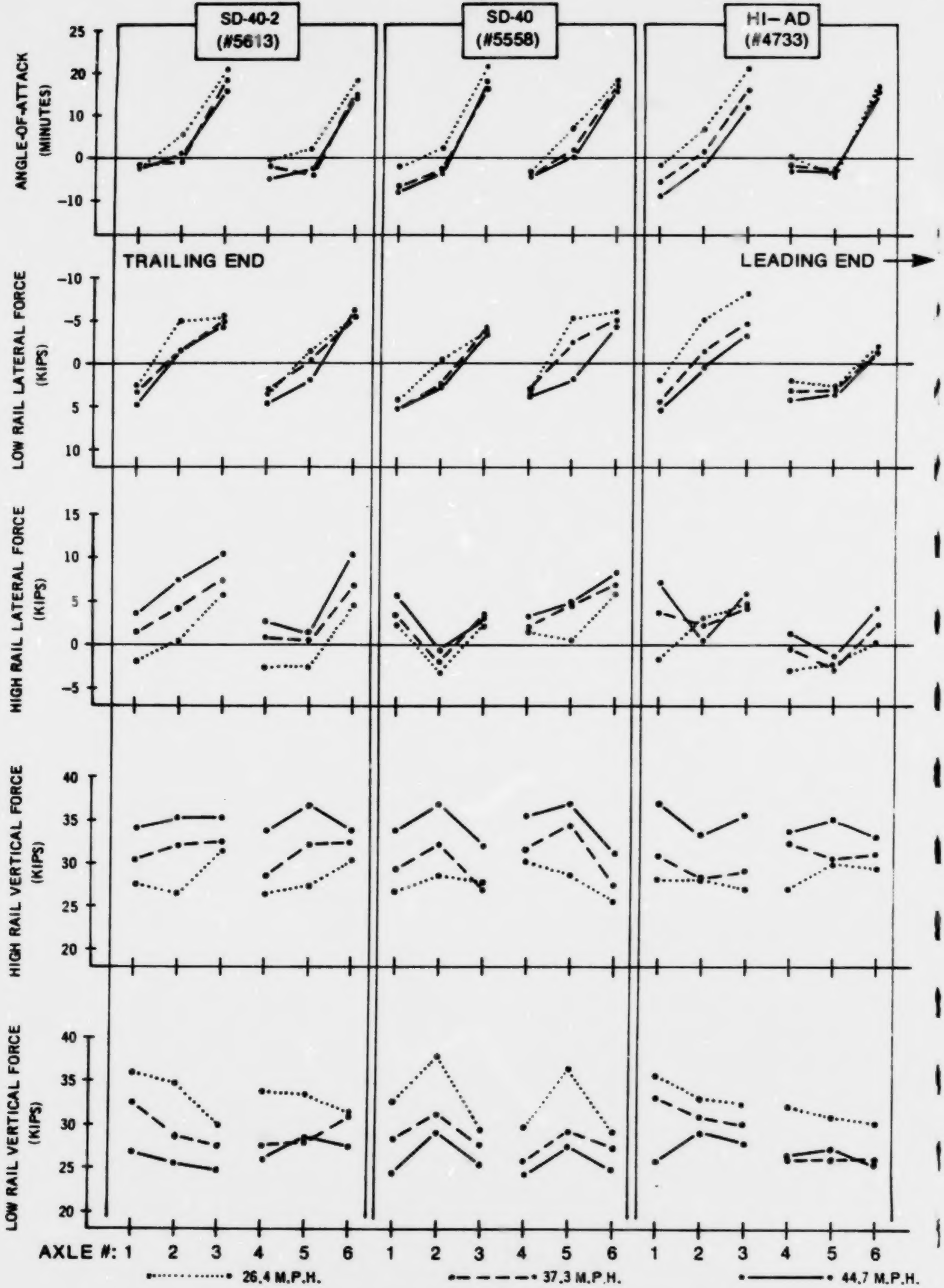

FIG. 2 : ANGLE-OF-ATTACK AND RAIL FORCES AT DIFFERENT CURVING SPEEDS

(EASTBOUND, UNWYED, DAY 2)

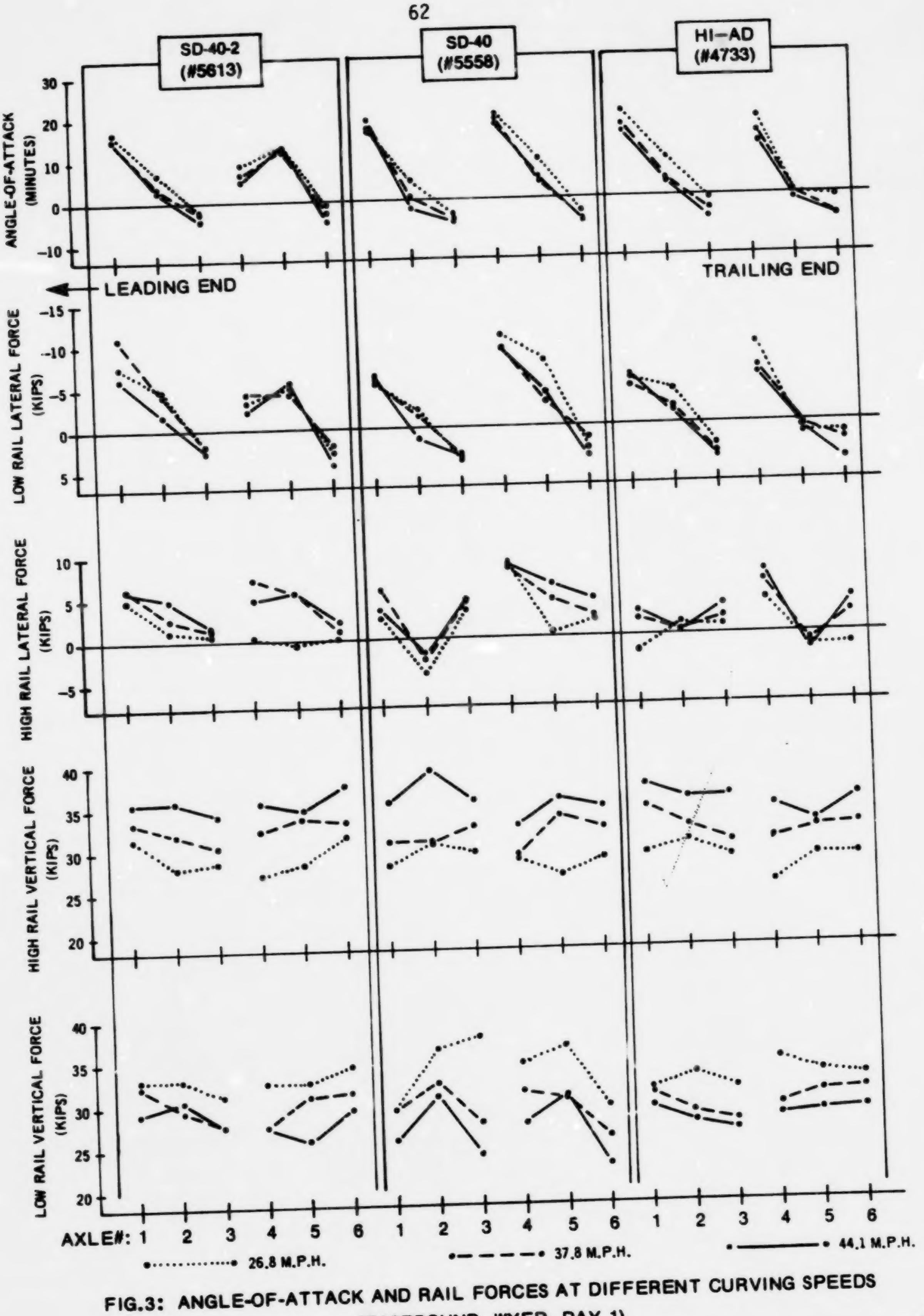

FIG.3: ANGLE-OF-ATTACK AND RAIL FORCES AT DIFFERENT CURVING SPEEDS
(EASTBOUND, WYED, DAY 1)

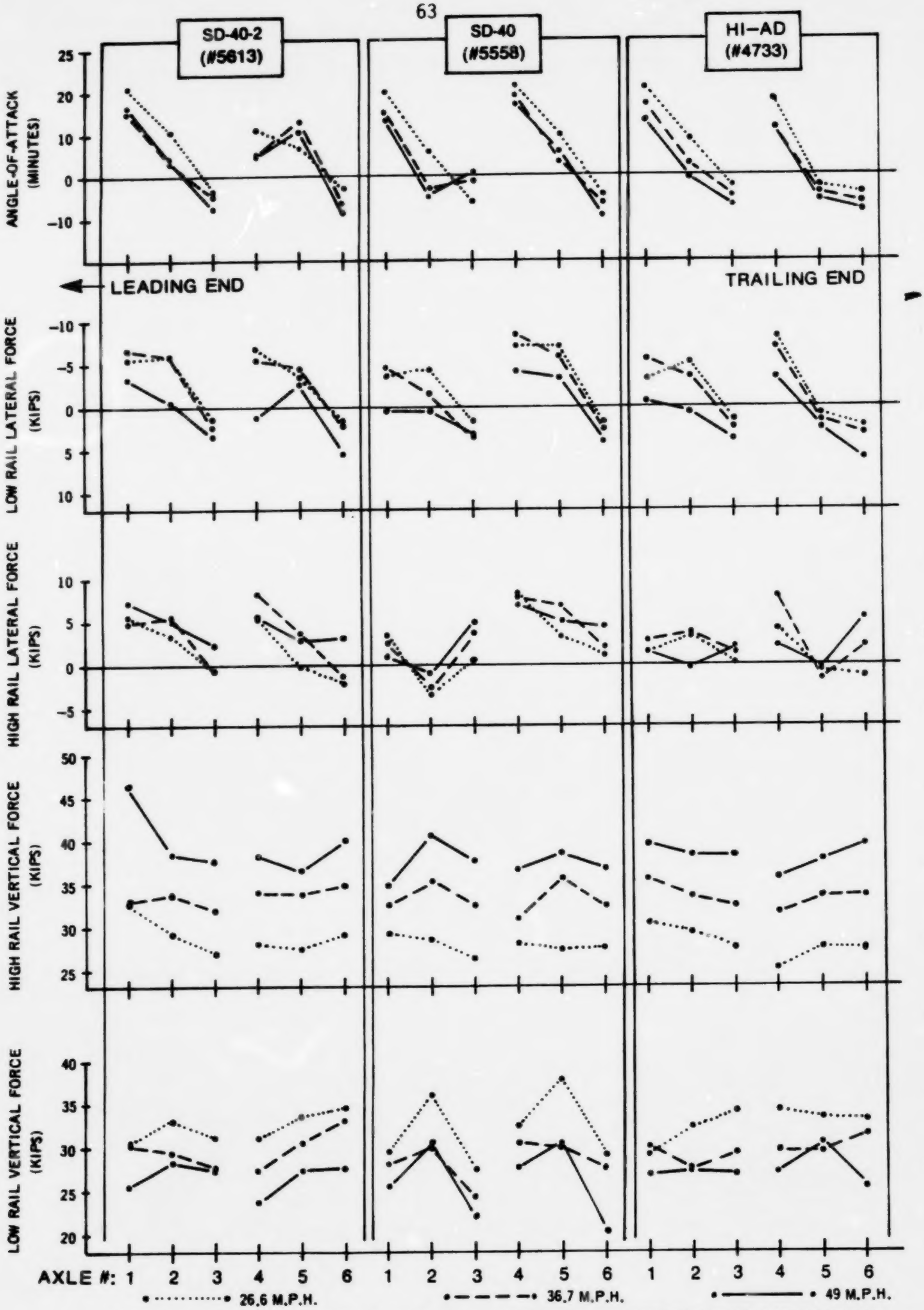

FIG.4: ANGLE-OF-ATTACK AND RAIL FORCES AT DIFFERENT CURVING SPEEDS

(EASTBOUND, WYED, DAY 2)

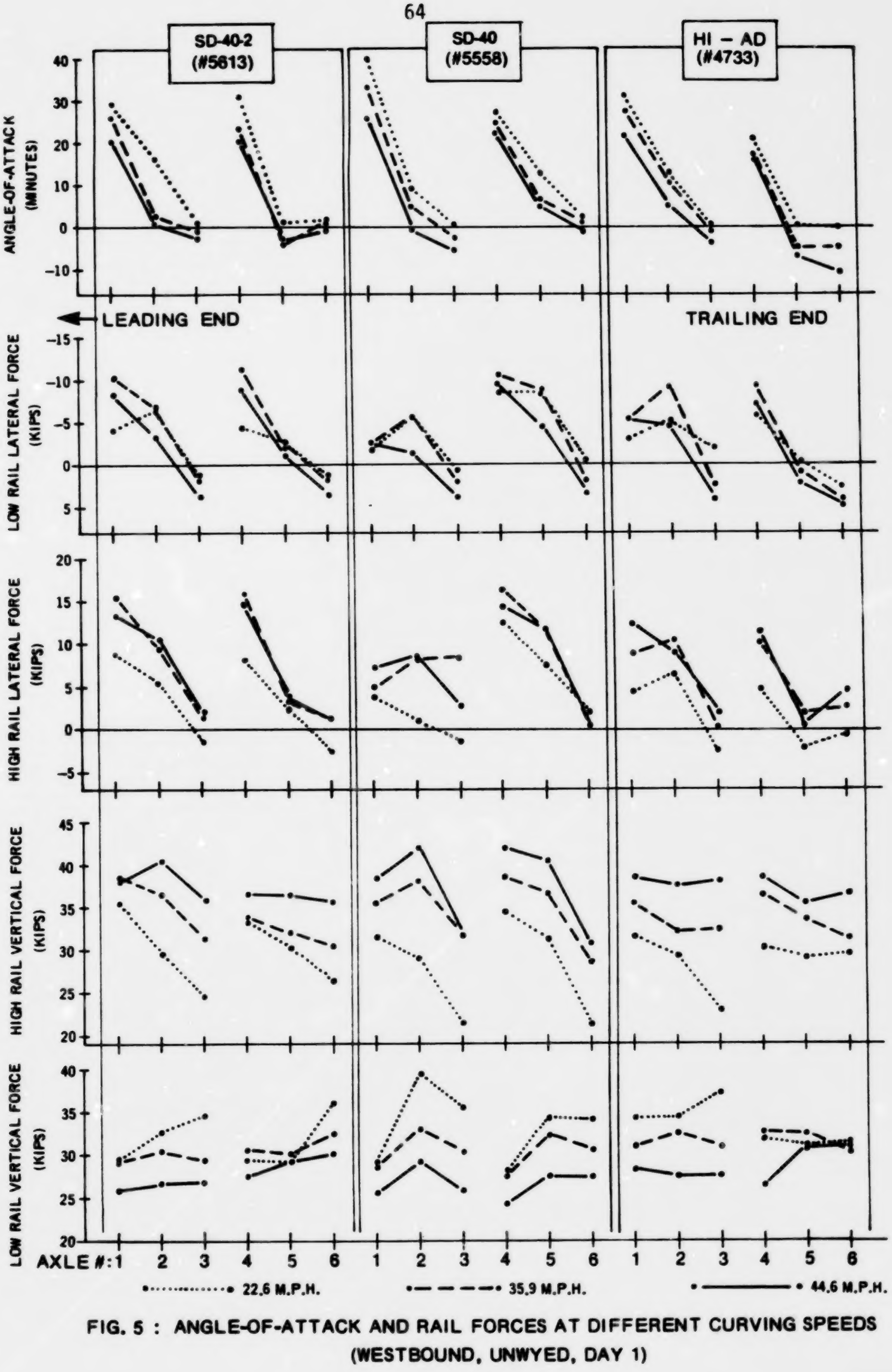

FIG. 5 : ANGLE-OF-ATTACK AND RAIL FORCES AT DIFFERENT CURVING SPEEDS (WESTBOUND, UNWYED, DAY 1)

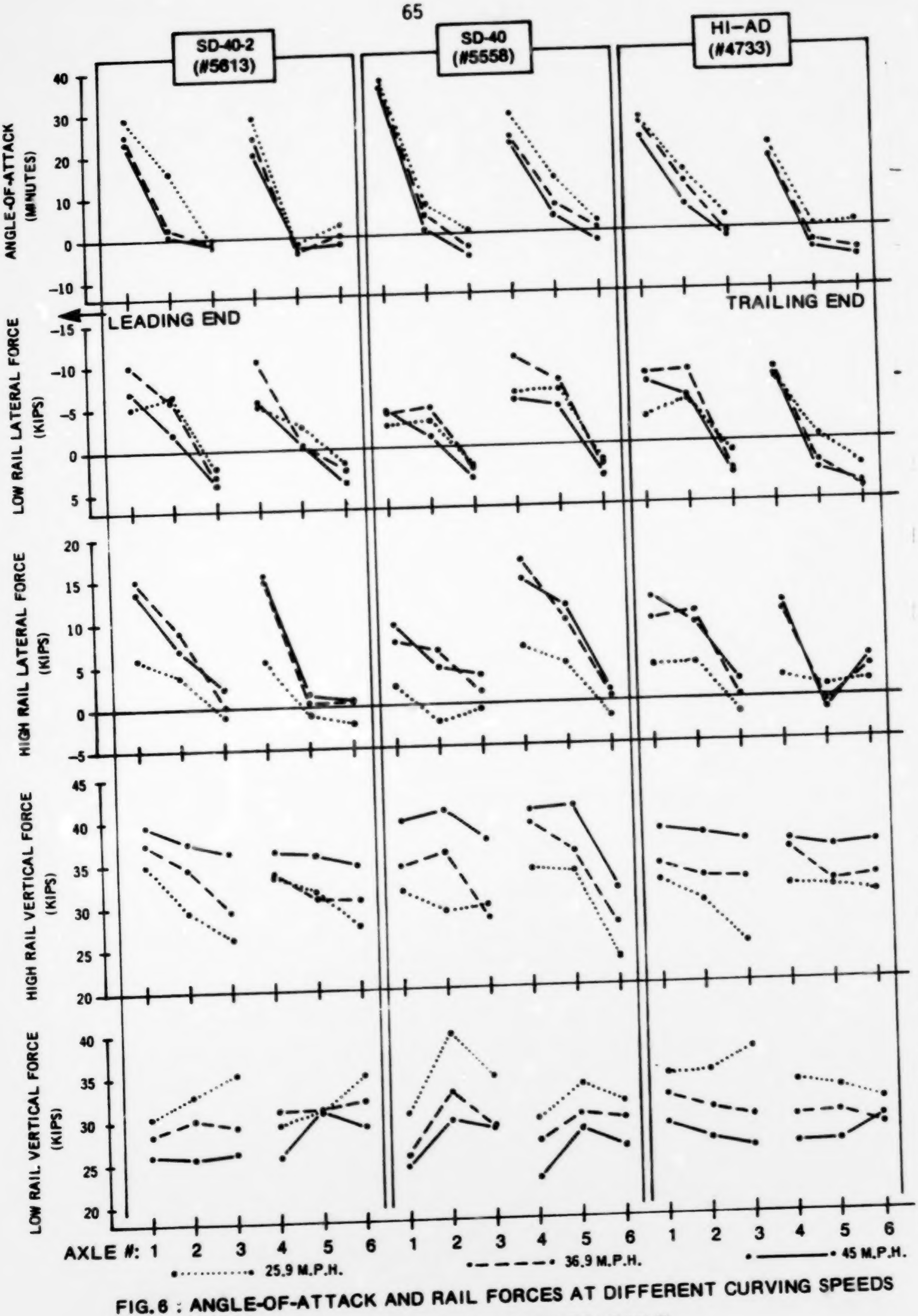

FIG. 6 : ANGLE-OF-ATTACK AND RAIL FORCES AT DIFFERENT CURVING SPEEDS

(WESTBOUND, UNWYED, DAY 2)

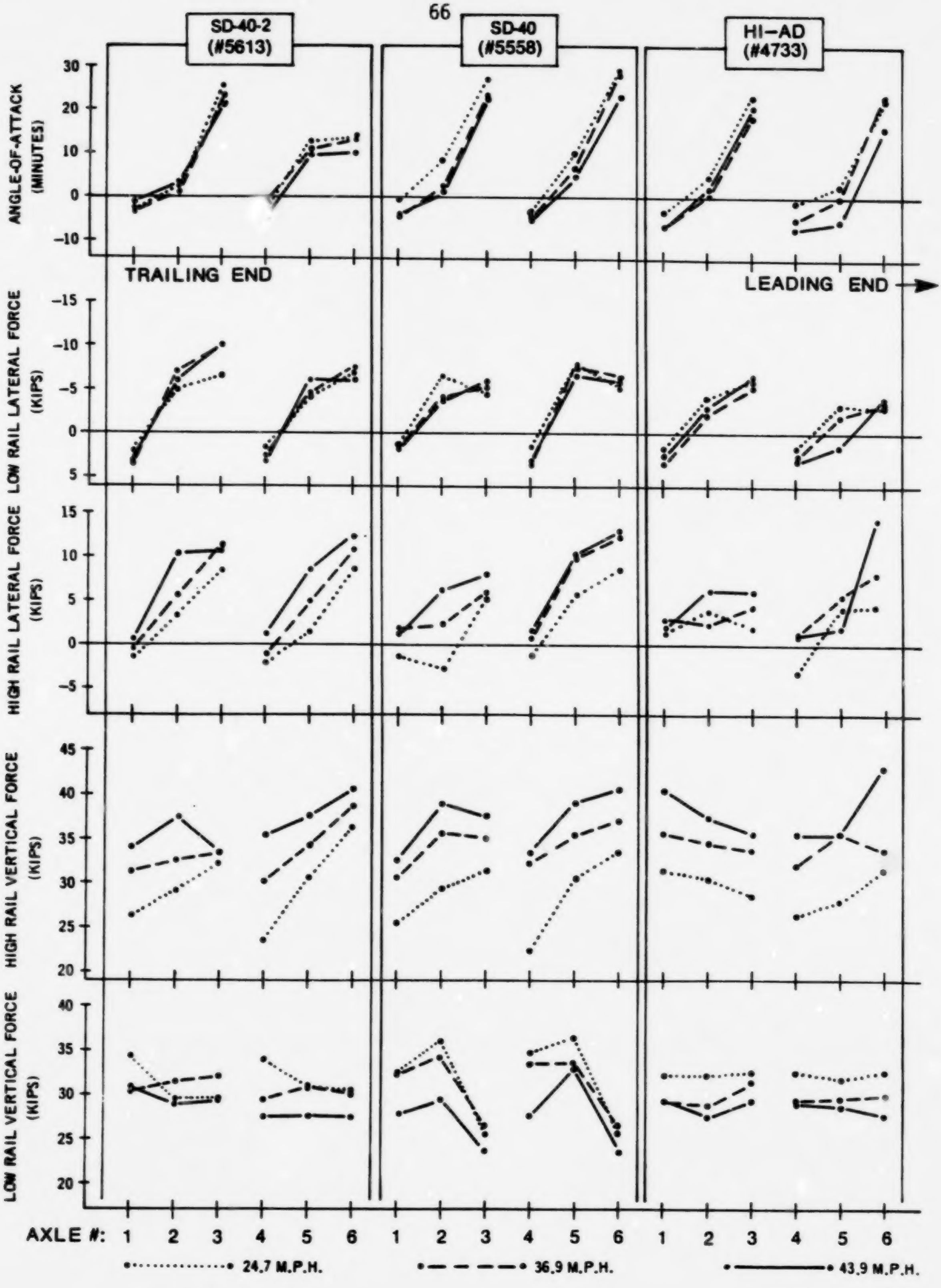

FIG.7: ANGLE-OF-ATTACK AND RAIL FORCES AT DIFFERENT CURVING SPEEDS (WESTBOUND, WYED, DAY 1)

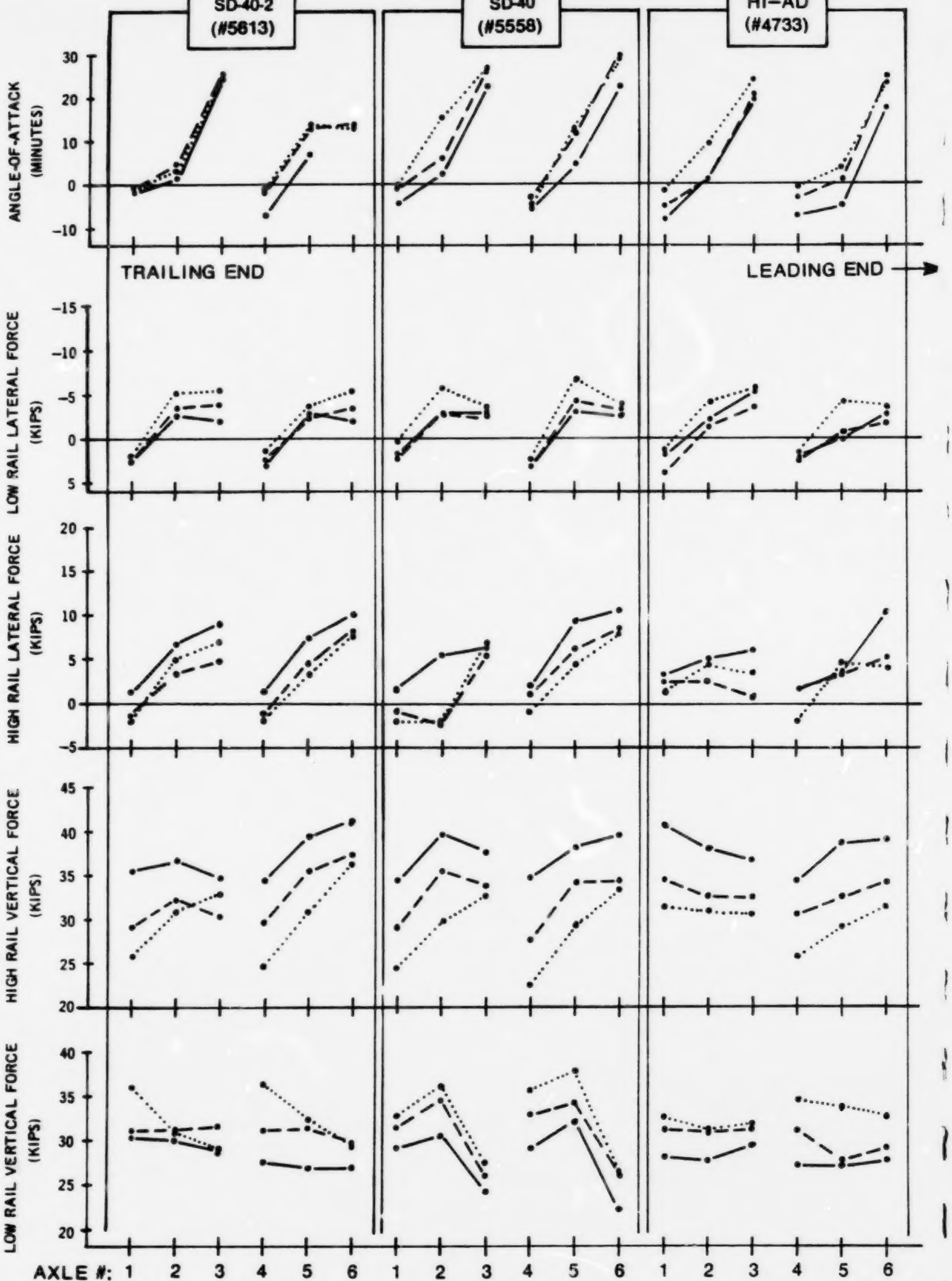

FIG. 8 : ANGLE-OF-ATTACK AND RAIL FORCES AT DIFFERENT CURVING SPEEDS

(WESTBOUND, WYED, DAY 2)

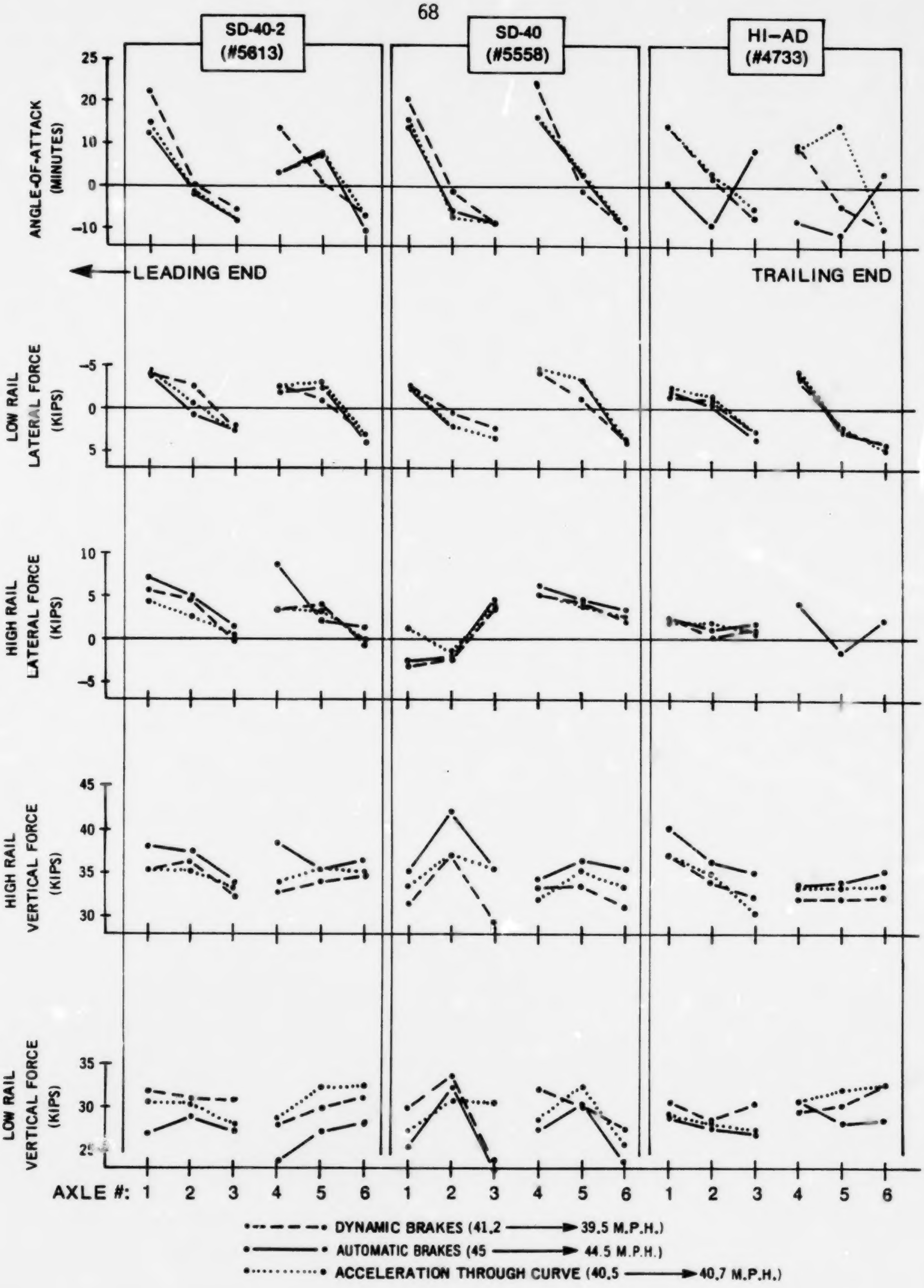

FIG. 9 :SPECIAL CONDITION TEST RUNS (EASTBOUND, WYED, DAY 2)

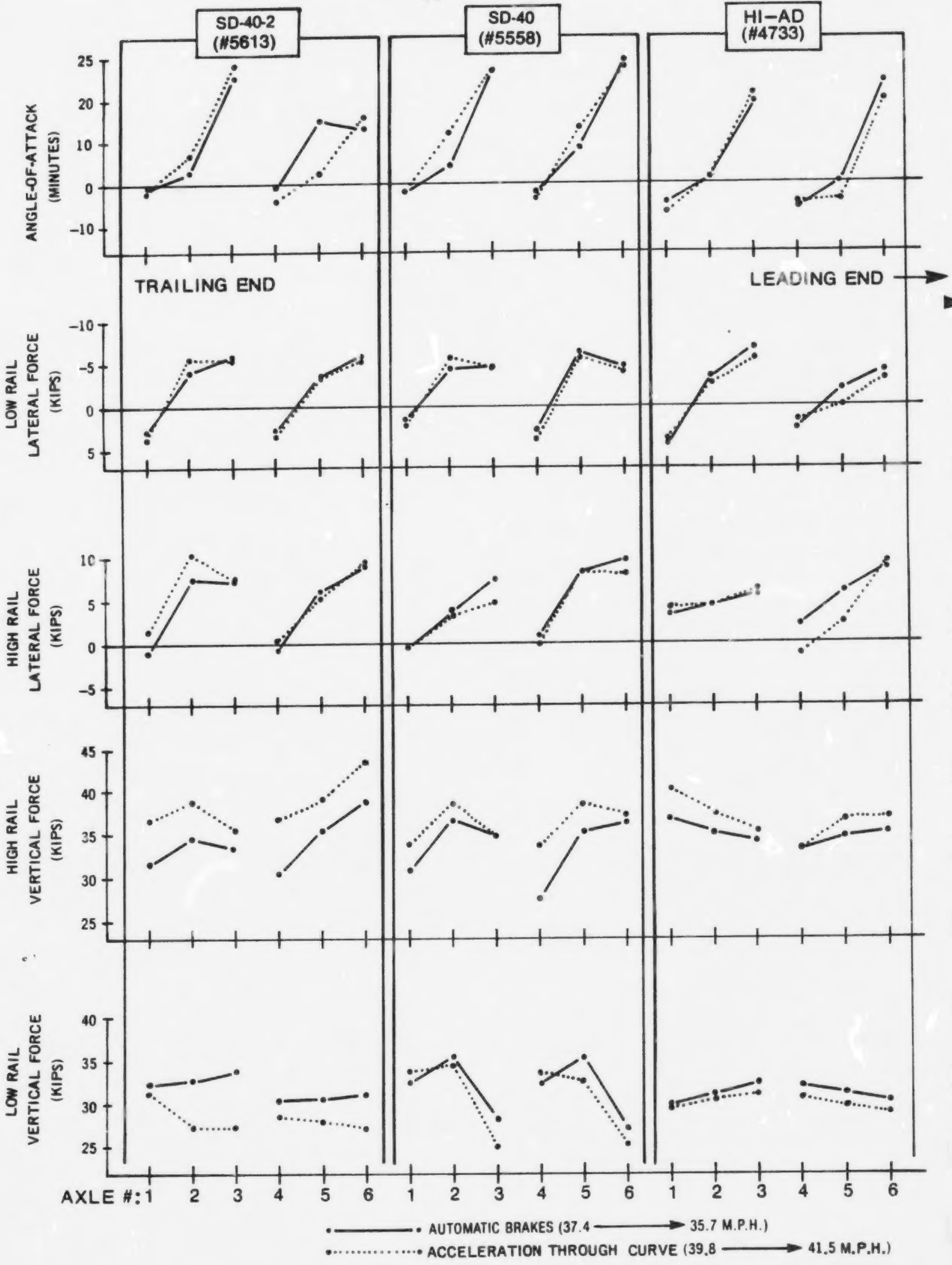

FIG.10: SPECIAL CONDITION TEST RUNS (WESTBOUND, WYED, DAY 2)

EFFECT OF AXLE LATERAL CLEARANCE AND WHEEL PROFILE VARIATION ON THE CURVING PERFORMANCE OF SD40-2 LOCOMOTIVE TRUCKS

Summary

A series of GM SD40-2 locomotive curving performance tests was conducted in May 1982 over 2°, 4° and 8° curves on the Thompson Subdivision, Pacific Region, CP Rail. The primary objectives of these tests were to investigate the effect of wheel profile variation and the effect of increasing locomotive truck mid-axle lateral clearance on the distribution of lateral loads among truck axles. A secondary objective was to investigate the effect of rail flange lubrication on curving performance of locomotive trucks.

From the test results, it was concluded that a new AAR wheel profile generates considerably larger lateral forces in the initial wear-in period of wheel life compared with service worn wheels. A wheel profile with better conformity to the worn rail gauge corner, should be considered for improved curving performance during the initial wear-in period.

Additional clearance obtained on the mid-axle by removing the inner strip liner did not significantly reduce lateral forces on locomotives with service worn wheels and existing lateral clearances.

Finally, it was found that high rail flange lubrication adversely affects the steering behavior of both freight car and locomotive trucks. Angles-of-attack and lateral flange forces both increased during the lubricated curving test runs. The significance of increased lateral flange forces and creepage on high rail shelling, low rail corrugation, and gauge widening of lubricated track should be further investigated.

SOMMAIRE

Des essais ont été faits en mai 1982 sur la ligne Thompson appartenant à CP Rail, région du Pacifique, avec un locomotive GM SD40-2 pour connaître son comportement dans des courbes de 2, 4 et 8 degrés. Le premier objectif de ces essais a été, d'abord, de connaître l'effet que pourraient avoir des variations dans les profils de roue et accroissement du mouvement latéral permis au niveau de l'essieu médian sur la répartition des charges latérales entre les essieux du bogie. Le deuxième objectif a été de vérifier l'effet d'un lubrifiant entre le champignon du rail et le boudin de roue sur l'inscription en courbe des bogies.

Ces essais ont montré que le nouveau profil de roue AAR produit des forces transversales beaucoup plus grandes lorsque les roues sont neuves et en rodage que lorsqu'elles ont été usées en service. On en conclut qu'il faudrait donner aux roues un profil mieux adapté au profil usé, du côté intérieur du champignon, de manière à améliorer l'inscription en courbe durant la période de rodage.

L'accroissement du jeu latéral de l'essieu médian, obtenu en ôtant la garniture intérieure de palier, n'a pas réduit perceptiblement les forces transversales par rapport à celles s'exerçant sur un bogie de locomotive dont les roues ont été usées en service et dont le jeu latéral n'a pas été augmenté.

Enfin, il a été constaté que le lubrifiant interposé entre le champignon du rail extérieur et le boudin de roue produit un effet négatif sur la conduite des wagons de marchandise et aussi sur celle des locomotives. L'angle d'inscription et les forces transversales d'inscription en courbe augmentent lorsque la voie a été lubrifiée. Il y a lieu de poursuivre la recherche sur l'influence que peuvent avoir des forces transversales et un fluage de boudin accrus sur l'écaillage du rail extérieur, l'usure ondulatorie du rail intérieur et l'écartement de la voie, dans le cas d'une voie lubrifiée.

Acknowledgements

The Research Department acknowledges the contribution of personnel from the following organizations:

- The National Research Council, Railway Laboratory, Division of Mechanical Engineering for their significant contribution in instrumentation and data acquisition during the field work.

- Personnel of the Engineering, Mechanical and Transportation Departments of CP Rail for their assistance during the course of the test program.

- Transportation Development Centre, Transport Canada for financial support under contract #OSD81-00006.

1. Introduction

A series of locomotive curving performance tests was conducted on SD40-2 General Motors 3-axle locomotive trucks in May 1982 on the Thompson Subdivision, Pacific Region, by CP Research Department personnel. The objective of this test was to investigate the effect of locomotive truck mid-axle lateral clearance on the distribution of lateral loads among truck axles. In addition, the effect of wheel profile variation on locomotive curving forces was investigated. The test was carried out in conjunction with the experimental rail profile grinding tests conducted for CP Rail's Engineering Department (Ref. 5).

2. Theoretical Background

In a recent computer simulation study conducted by Dynamic Sciences Ltd. (DSL) on behalf of CP Research, (Ref. 1), two areas for improvement in high curvature curving performance of GM SD40-2 trucks were identified. It was found that by increasing the existing conicity of AAR new wheel profiles, or by increasing the mid-axle lateral clearance on the 3-axle trucks, leading axle lateral forces on the high rail could be reduced. Subsequently, both conclusions were confirmed, using a non-linear steady state locomotive curving program developed by CP Research.

To illustrate the effect of increasing mid-axle lateral clearance, two sample CP computer simulation results are presented in Figure 1 and 2 respectively. Figure 1 illustrates an SD40-2 truck coasting on a 10 degree curve with no lateral axle clearance, and Figure 2 illustrates an identical case with lateral clearance in the centre axle bearing area. It can be observed that since the middle axle has a positive angle-of-attack, it generates a lateral creep force pushing the mid-axle toward the high rail. By allowing this mid-axle to flange independently on the high rail, the total lateral load of the 3-axle truck can be shared more evenly between the leading and the middle axle rather than being borne by the leading axle alone. It is important to note that although these simulation runs were carried out for the case of zero longitudinal bearing clearance, a similar lateral force reduction was also observed for the case of nominal longitudinal free clearance in the pedestals. However, it must also be noted that the two simulation runs only serve to illustrate the principle involved. In reality, each locomotive truck has different lateral and longitudinal clearances at each axle bearing, small wheel tape size differences and initial position errors relative to the truck frame which can be input into the computer program to study the effect of each individual parameter on the distribution of curving forces.

The improvement in curving behaviour using high conicity wheelsets has been observed in both freight car (Ref. 2) and locomotive simulation studies conducted by CP Research. High effective conicity, or a large rolling radii differential during curving, generates more favourable longitudinal creep forces and steering moments on the axles, and reduces lateral forces on curves.

It is also a known fact that as wheels wear, higher effective conicity is naturally achieved, and curving forces reduced. In order to investigate this phenomenon, actual matching of wheel/rail profiles was carried out in this study, in conjunction with force and angle-of-attack analyses.

3. Test Sites and Test Consist

Three test sites chosen included a 2°, 4° and 8° left hand curve between mileage 109 and 113 on the Thompson Subdivision. Each curve was instrumented to measure lateral/vertical forces on both high and low rails and wheelset angle-of-attack at the same location. A detailed description of instrumentation can be found in Reference 3. The curvature, superelevation and gauge of the three curves measured on site are illustrated in Figures 3 to 5.

A series of tests was conducted at the three test sites in May 1982, (Test 1) and the same tests repeated in June 1982, (Test 2), approximately 4 weeks later, after the rail had been newly ground to an experimental profile. In each test, three test locomotives coupled in the same order and orientation relative to the curves were run in both eastbound and westbound directions at different curving speeds and under different rail flange lubrication conditions. Between Test 1 and Test 2, the test locomotives were returned to revenue service.

Mid-axle lateral clearance on the test locomotives was increased by removing the inner strip liner on the mid-axle journal box in the pedestal area of each locomotive truck. The resulting total lateral clearances on each axle measured before Test 1 and 2 according to GM service instruction MI 1552 are tabulated in Table 1. The amount of existing shims in the journal box of each axle, noted at the end of Test 2, are tabulated in Table 2.

4. Wheel and Rail Profiles

The wheel profiles of the locomotives were recorded with a Seiki wheel profilometer. Wheel profiles were taken during Test 1 and repeated after Test 2 as the locomotives were returned to revenue service between the two tests. A complete record of the wheel profiles is shown in Figures 6 to 11.

From the wheel profiles taken during Test 1 it can be seen that all the wheelsets were well worn in the flange throat area except for the wheelsets of locomotives 5689 and some wheelsets on locomotive 5590. As the locomotives were in revenue service between the two tests, incremental flange wear was detected on all wheels. However, the wear pattern in the flange throat area was considerably different for the new wheelsets on locomotive 5689 and some wheelsets on locomotive 5590. In addition, it was observed that the 6R wheel of locomotive 5760 had a distinct false flange which traversed the low rail of the test curves.

Rail profiles on the high and low rail at the instrumented sites in the test curves were recorded before and after rail grinding using a recently designed CP Research rail profilometer (Ref. 4). The rail profilometer is of unique design with three potentiometer slides to independently measure the rail head profile down to the rail web. After proper matching of the recorded digital data, complete rail head profiles were plotted. Rail profiles on the high rail before and after grinding, together with a typical new wheel profile from locomotive 5689 in a flanging configuration, are illustrated in Fig. 13 and 14. In Figure 14, the new wheel profile of locomotive 5689 is shown after an initial "wear-in" in the flange throat area (approximately 10,000 miles of additional revenue service). From the rail profiles recorded prior to Test 1 (Fig. 15, 17, 19) before the rail was ground it can be seen that the high rail guage corner on all three test curves were well worn-in and possessed identical shape.

The experimental rail grinding pattern did not substantially alter the contour of the high rail gauge corner in the 2 and 8 degree curve in Test 2 (Fig. 16, 20) but did remove a substantial amount of material at the high rail gauge corner of the 4 degree curve (Fig. 18). Experimental grinding also removed material on the field side, resulting in a downward slope on the rail head profiles in that area.

5. Discussion of Results

Tables 3 to 6 depict some sample data of angle-of-attack of each axle of the 3-axle trucks in both eastbound and westbound runs over the 2, 4, and 8 degree curves in Test #1 and #2. Tables 7 and 8 show the lateral forces generated at the leading outer wheel of each truck for Test #2. From these results, the following can be concluded:

a. Each truck retains the same relative magnitude of angle-of-attack and lateral force compared with other trucks, regardless of the degree of curvature traversed. Steady state curving behaviour is dominant on all curves.

b. On the 4 degree and 8 degree curves, the leading axles of the trucks are flanging, producing large positive lateral forces which push the high rail outward. On the 2 degree curve, more negative lateral forces were measured indicating that the wheel tread steering action was more dominant. Some negative angles-of-attack were also recorded for the leading axles on the 2 degree curve.

c. Flange lubrication increases both the angles-of-attack and lateral flange force of the leading outer wheel. This phenomenon has also been observed on freight car trucks as was predicted by the CP Research curving simulation computer program. The increase in lateral force is due to the loss of the longitudinal high rail flange force which produces a favourable steering moment on the trucks, as well as the increase of lateral creep force from the vertical wheel load distributed on the tread rather than on the flange of the flanging wheel on the high rail (Ref. 5).

d. Locomotive 5689 fitted with new wheel profiles generates substantially higher forces than reference locomotive 5590 with service worn wheels. The same trend was observed for both Test #1 and 2, regardless of increased mid-axle lateral clearance suspension modifications.

e. The angle-of-attack and force pattern of the second truck of locomotive 5760 with the false flange wheelset is substantially different from the other trucks, especially with respect to the angle-of-attack pattern on the 2 degree curve. The influence of the false flange is evident on the curving behaviour of that truck.

Tables 9 to 12 show the difference in average lateral forces at similar curving speeds between Test #1 and Test #2. Among the three locomotives, #5689 has the maximum reduction in lateral load on the 8 degree curve, but a maximum increase in the 4 degree curve, compared with the other locomotives. Since the rail head gauge corner on the high rail of the 8 degree curve was not altered substantially, this lateral load reduction can be attributed to wheel profile variation due to initial wear-in at the flange throat area between Test #1 and Test #2. From the wheel/rail contact configuration shown in Figure 13 and 14, one can see that a much better conformity is achieved at the gauge corner on the 8 degree curve in Test #2, effectively shifting the vertical wheel load to a higher rolling radius on the high rail. This is equivalent to increasing the effective conicity of the wheelset, and hence decreasing curving forces.

Similarly, the increase in curving forces for locomotive 5689 on the 4 degree curve can also be explained from the wheel/rail contact geometry. Since the rail was heavily ground at the high rail gauge corner on the 4 degree curve prior test #2 (Fig. 17 & 18), even though the wheelsets were more worn-in during test #2, a large gap is still maintained at the gauge corner (Fig. 14). This type of wheel/rail contact shifts the vertical wheel load back to the wheel tread, effectively reducing the rolling radius on the high rail, and increasing the curving forces. Increase in angle-of-attack and lateral forces were also observed on the 4 degree curve from test #1 to test #2 for all freight car trucks in the test consist for the same reason.

From Tables 11 and 12 it can be observed that reference locomotive 5590 showed a lateral force reduction on the 8 degree curve only on the westbound runs. From examining the wheel profiles taken before test #1 and after test #2, it is suspected that locomotive 5590 was running predominantly unidirectional in revenue service between test #1 and test #2. This resulted in the lead axle wheelsets in the westbound direction developing more hollowness in the flange throat area and hence higher effective conicity. However, with the Seiki wheel profilometer, it is difficult to extract the exact flange wear accumulated on these wheels.

6. Mid-Axle Lateral Clearance

Because of the large reduction of lateral curving forces due to the new wheel profile change on locomotive 5689 between the two tests, it was difficult to distinctly isolate the effect of increased lateral clearance on this locomotive in test #2. However, the lateral force pattern on high and low rails suggested that increased conicity is the major contributor to the load reduction experienced. On locomotive 5760 with service worn wheels, the sensitivity of lateral load due to increased lateral clearance is also very low.

However, the principle of sharing high rail lateral load between the lead and mid-axle is well demonstrated in each individual test run. Figure 12 illustrates the lateral/vertical load pulses recorded during a test run. It can be observed from the high rail lateral force channel that if the mid-axle wheelsets of the locomotive trucks are allowed to flange harder, the lead axle lateral force of the same truck is somewhat relieved.

7. Conclusions and Recommendations

1. The sensitivity of lateral force, due to additional mid-axle lateral clearance by removing the inner strip liner, is low compared with that due to wheel profile variation. No strong correlation could be observed between the lateral forces and total lateral axle clearance. However, the principle of load distribution between lead and mid-axle is well demonstrated in the force pattern.

2. The new AAR wheel profile, being highly non-conformal to worn rail gauge corner, generates substantially higher lateral forces in the initial stage of wheel life due to a smaller rolling radius on the high rail. Adopting a new wheel profile, with better conformity with the worn rail gauge corner, would substantially reduce lateral flange forces compared with using the new AAR wheel profile. A more conformal wheel profile also has the added advantage of requiring less metal removal during wheel remachining.

3. Rail flange lubrication tends to increase angle-of-attack and lateral flange force on 3-axle locomotive trucks. Thus, although flange wear is reduced from lubrication, increased lateral load and lateral wheel slippage is imposed on the track structure. The significance of this trade-off should be further investigated with respect to rail shelling, corrugation and gauge widening on lubricated track.

4. To further reduce lateral forces and angle-of-attack on 3-axle trucks, a radial steering linkage must be applied to the truck suspensions.

References

1. Technical Report concerning four modifications to the SD40-2 Locomotive Trucks to reduce track loadings in curves and improve ride, by DSL Dynamic Science Ltd., September 1981.

2. Theoretical Curving Performance of Four Freight Car Trucks. CP report S712-82 (TP 3449), December 1981.

3. Railroad Dynamics Incorporated (RDI) Truck Evaluation Test. CP report S670-81 (TP 2970), March 1981.

4. Concept of a Profilometer for Rail Wear Determination. CP report S655-80, September 1980.

5. Effect of Experimental Rail Profile Grinding, Flange Lubrication and Wheel Profile on the Steering Behaviour of 100-Ton Freight Car Trucks.
CP report S742-82, November 1982.

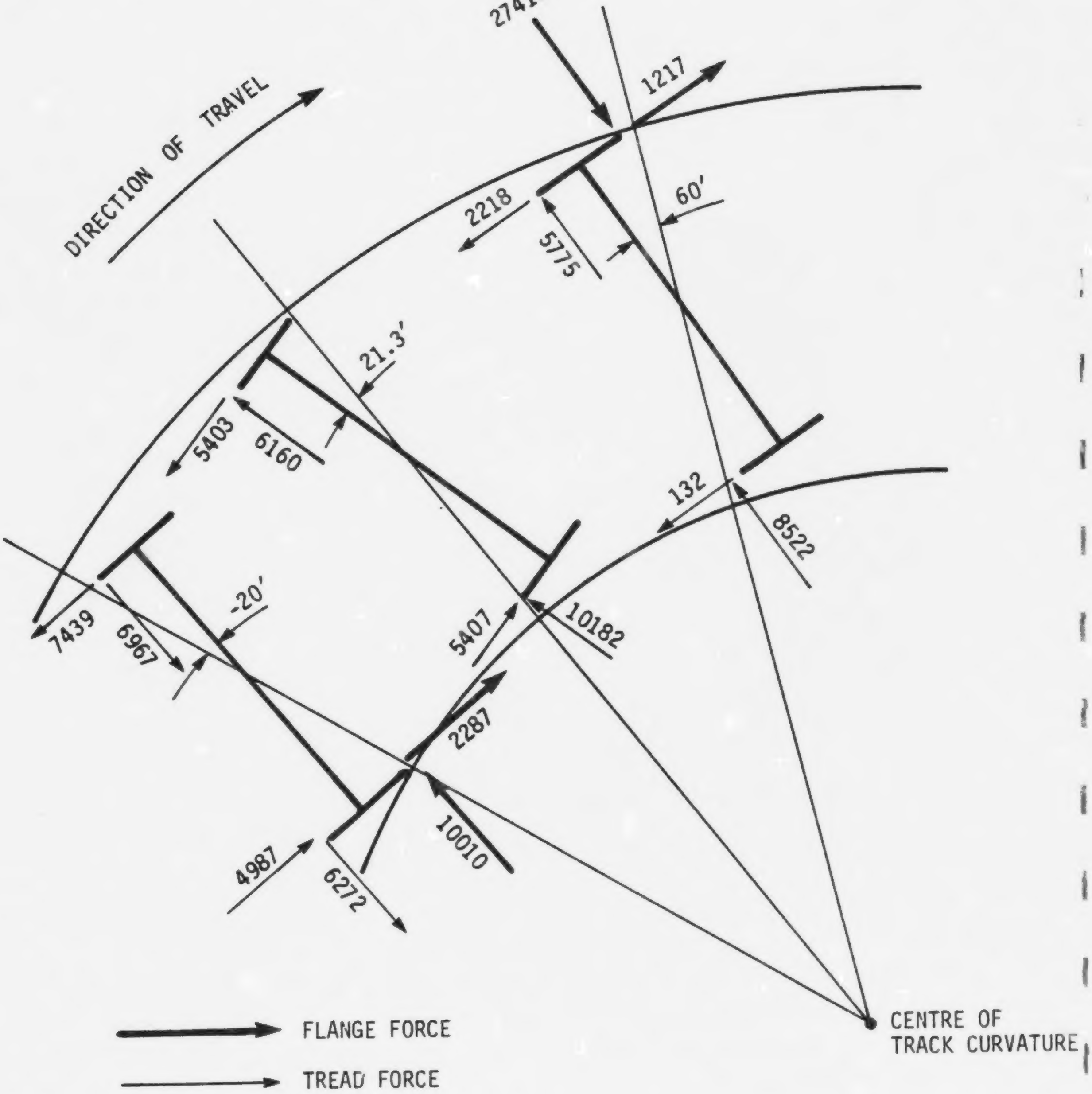
DIRECTION OF TRAVEL
27412
1217
60'
2218
5775
21.3'
5403
6160
132
8522
-20'
7439
6967
5407
10182
2287
10010
4987
6272
CENTRE OF TRACK CURVATURE
FLANGE FORCE
TREAD FORCE

Fig. 1: Non-linear steady state curving forces (lb_f) of an SD40-2 locomotive truck traversing a 10 degree curve with new wheel profile and nominal rail gauge clearance.(0.375")

Notes: 1 - Total lateral free clearance is assumed as zero for all bearings.
2 - Total longitudinal free clearance is assumed as zero for all bearings.

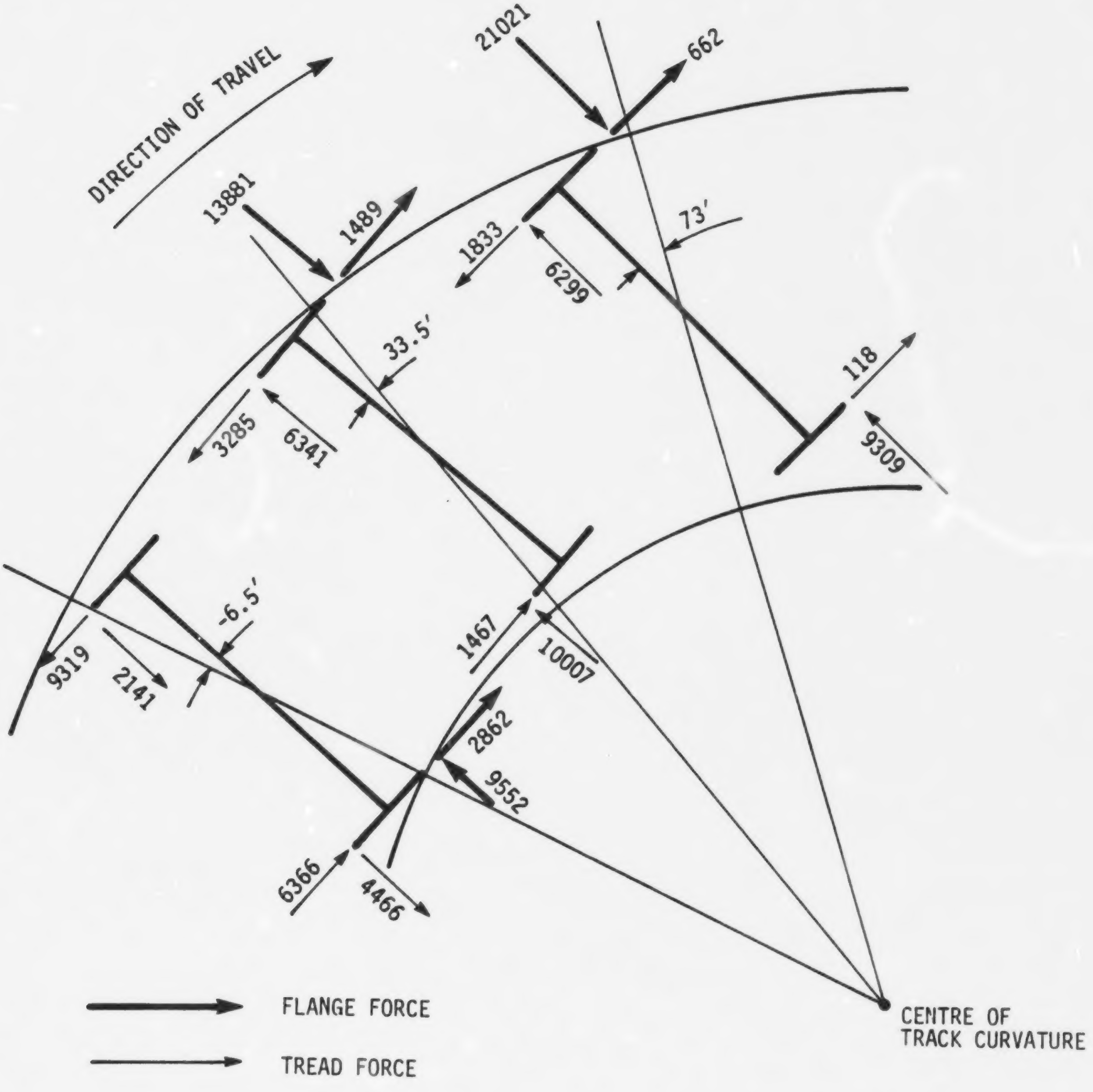
DIRECTION OF TRAVEL
21021
662
13881
1489
1833
6299
73'
33.5'
3285
6341
118
9309
-6.5'
1467
10007
9319
2141
2862
9552
6366
4466
FLANGE FORCE
TREAD FORCE
CENTRE OF
TRACK CURVATURE

Fig. 2: Non-linear steady state wheel/rail curving forces (lb_f) of an SD40-2 locomotive truck traversing a 10 degree curve with new wheel profile and nominal gauge clearance (0.375") with lateral clearance.

Notes: 1 - Total lateral clearance:

mid-axle - 1.4"
leading & trailing axles - 0.4"

2 - Total longitudinal clearance is assumed as zero for all bearings.

FIG. 3 : TRACK PROFILE OF 2 DEGREE TEST CURVE (MILEAGE 112.5 EQUILIBRIUM SPEED 38 MPH)

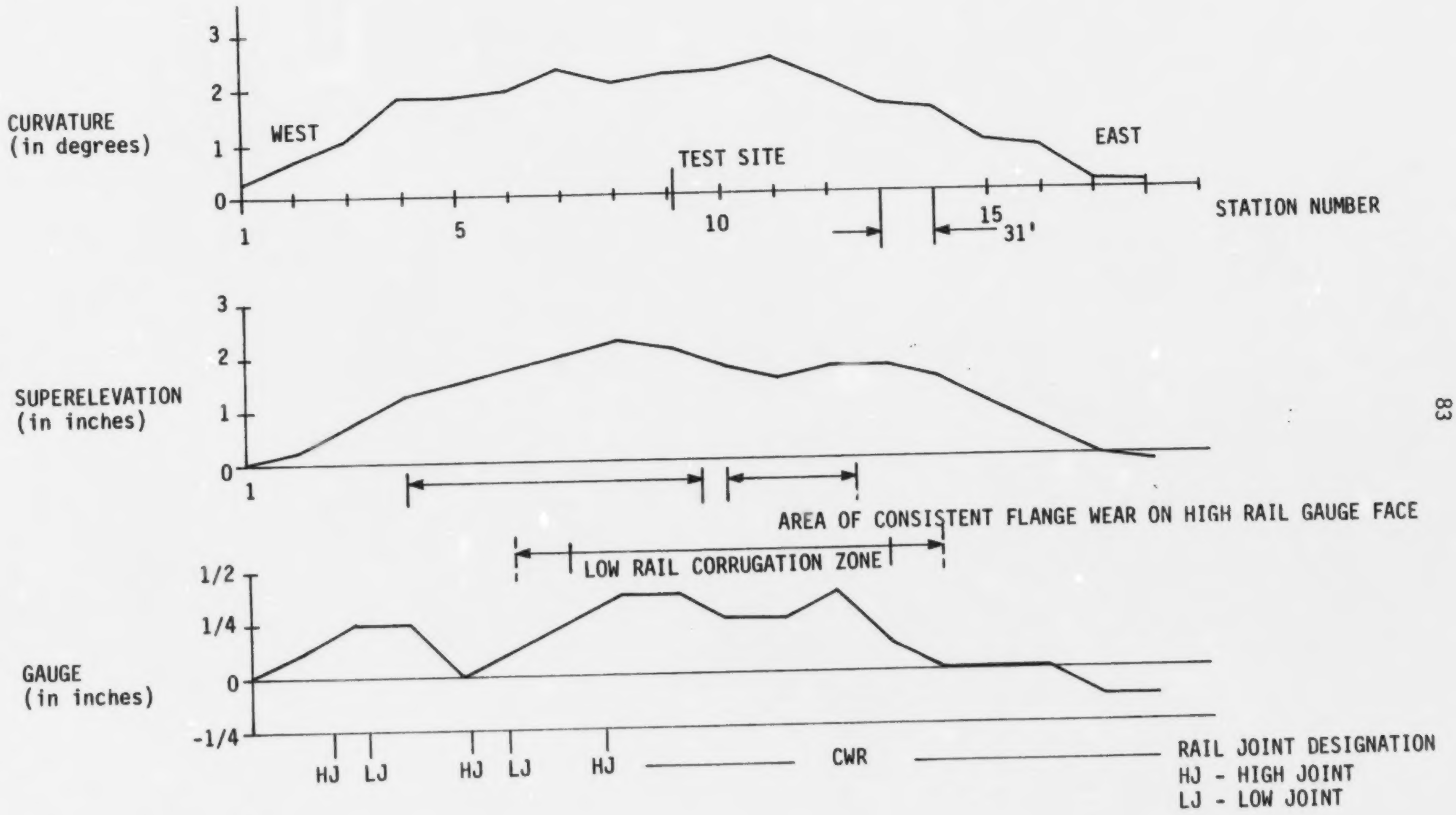

FIG. 4 : TRACK PROFILE OF 4 DEGREE TEST CURVE (CWR LOW RAIL, MILEAGE 109.9, EQUILIBRIUM SPEED 28.2 MPH)

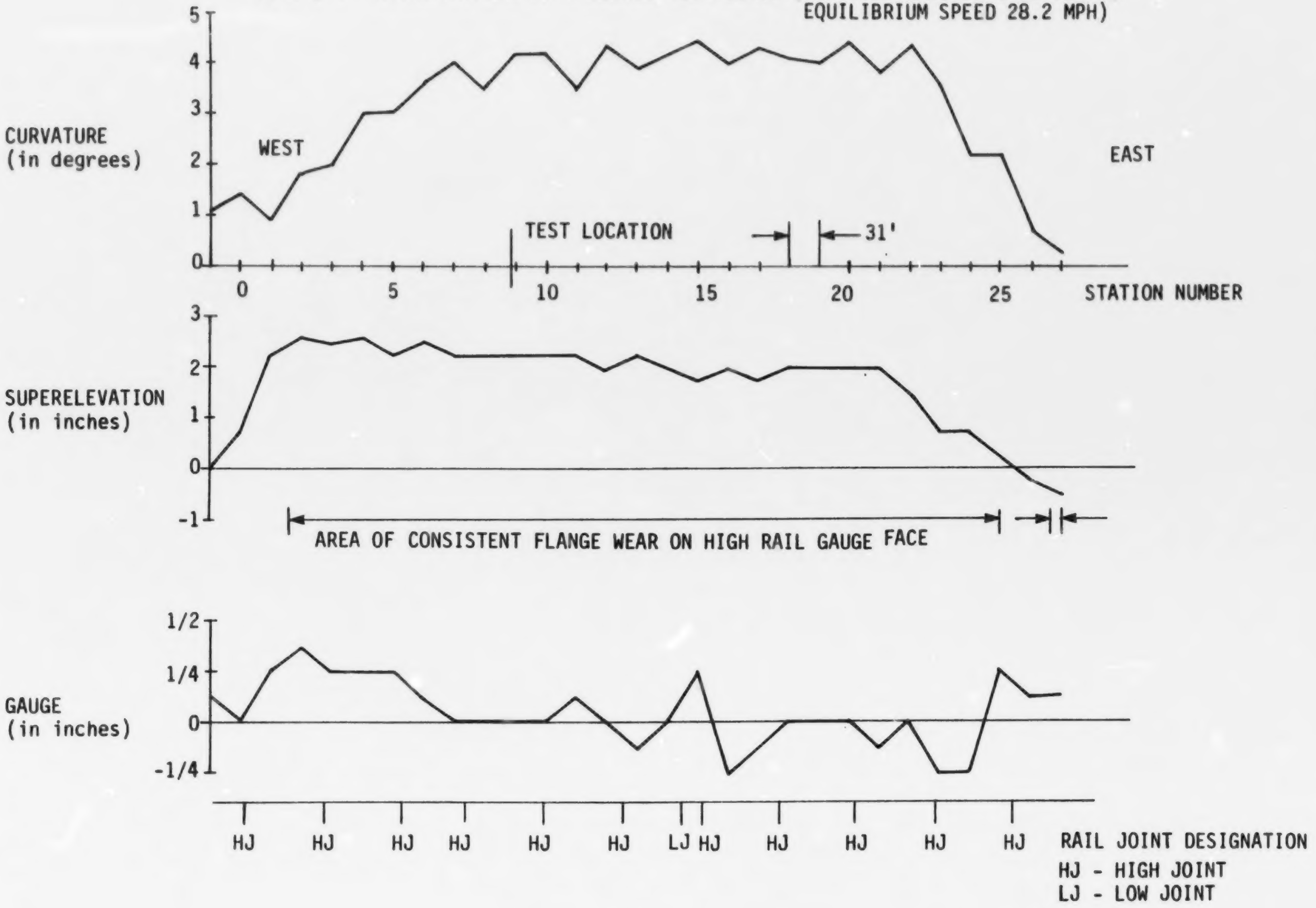

FIG. 5 : TRACK PROFILE OF THE 8 DEGREE TEST CURVE (MILEAGE 111, EQUILIBRIUM SPEED 25 MPH)

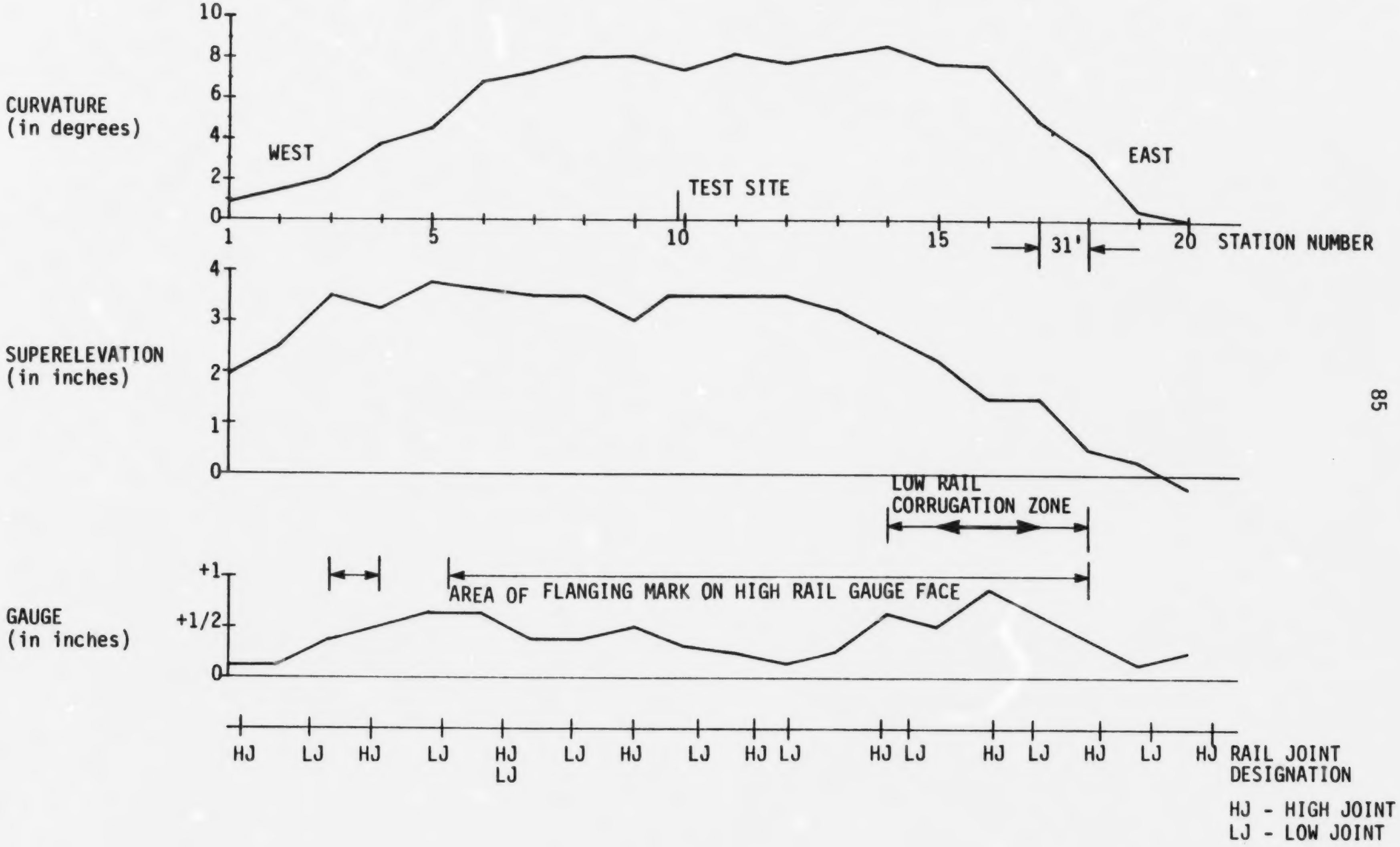

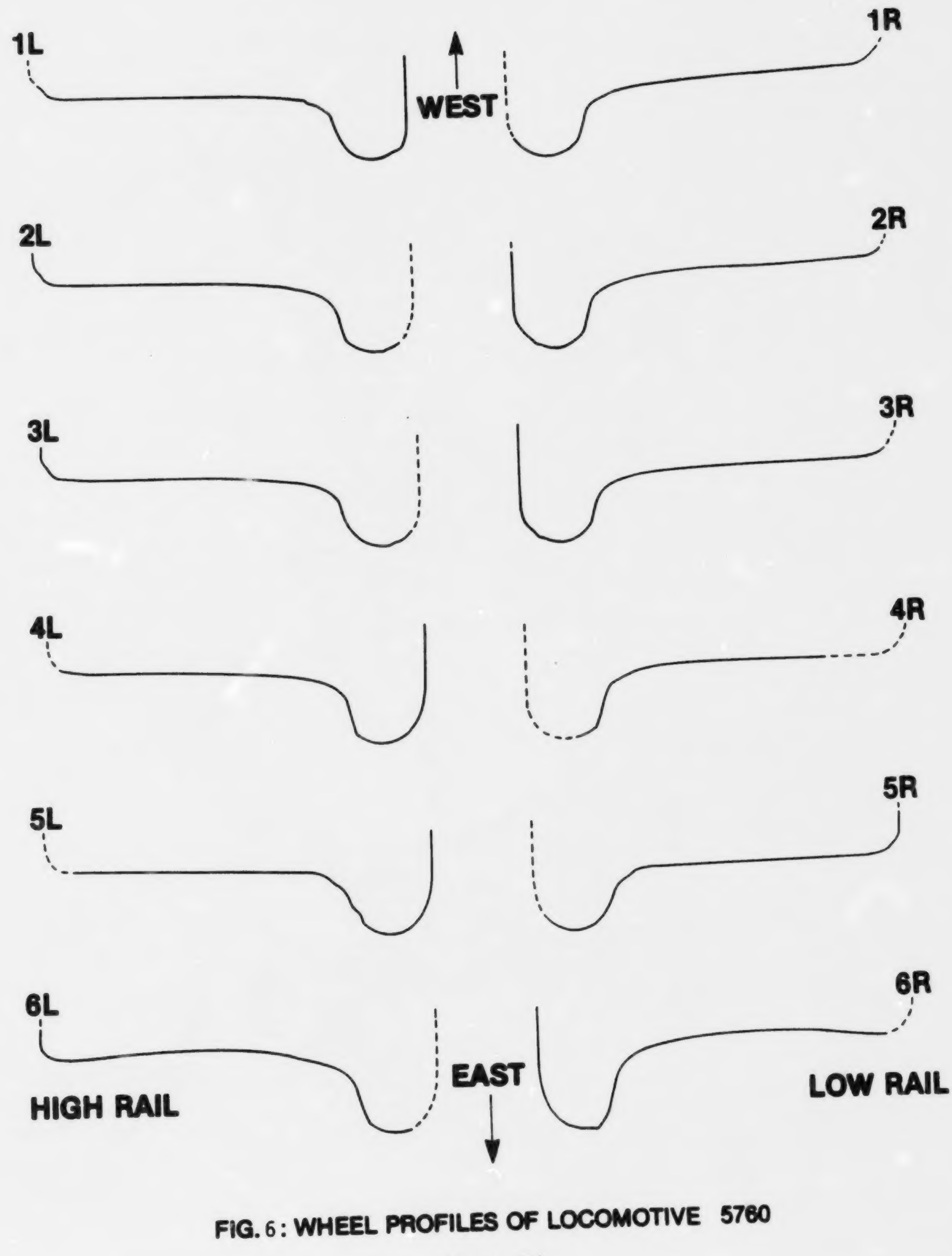
1L
1R
WEST
2L
2R
3L
3R
4L
4R
5L
5R
6L
6R
EAST
HIGH RAIL
LOW RAIL

FIG. 6: WHEEL PROFILES OF LOCOMOTIVE 5760

(Test #1)

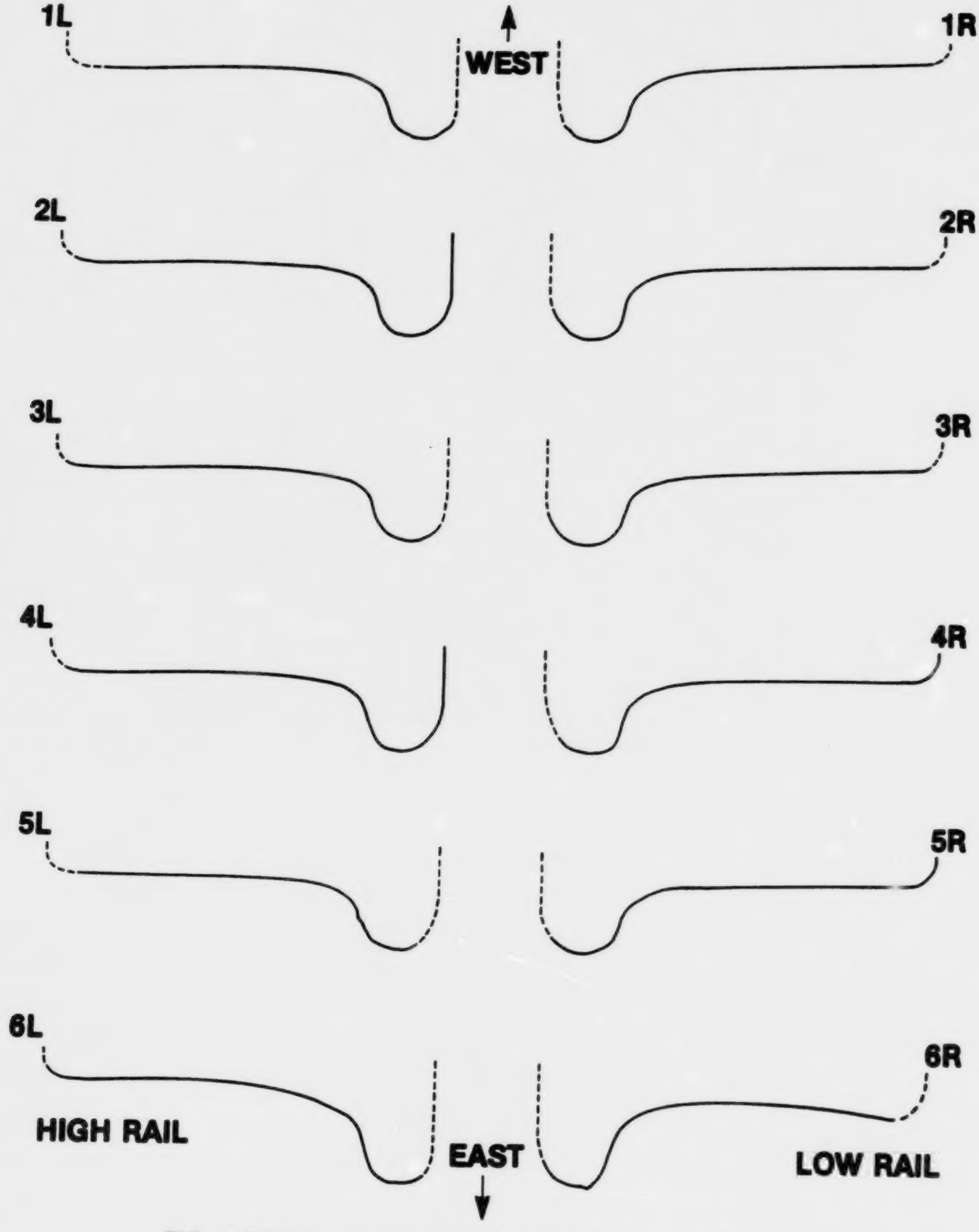
1L
WEST
1R
2L
2R
3L
3R
4L
4R
5L
5R
6L
6R
HIGH RAIL
EAST
LOW RAIL

FIG.7 : WHEEL PROFILES OF LOCOMOTIVE 5760

(Test #2)

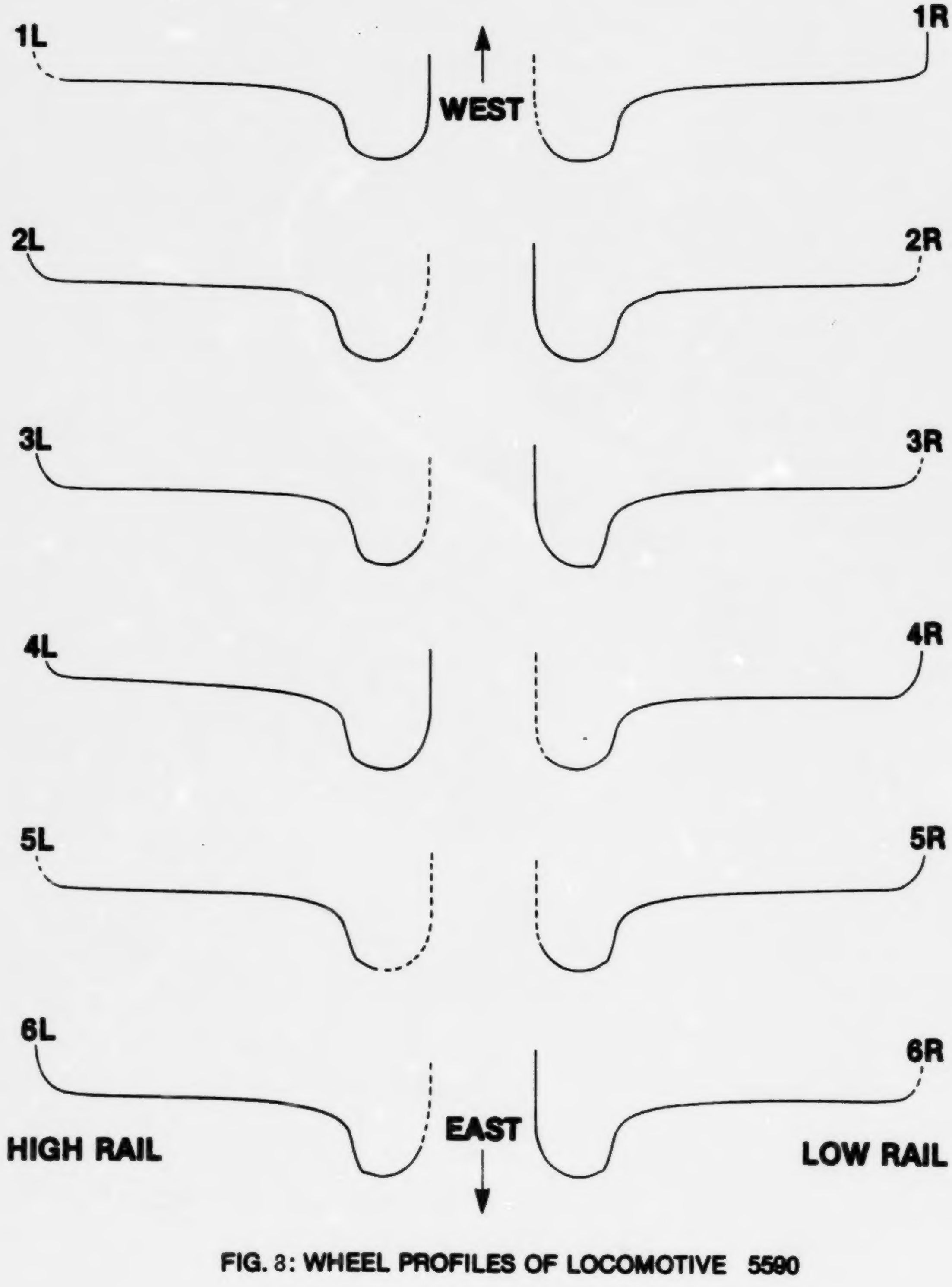
1L
1R
WEST
2L
2R
3L
3R
4L
4R
5L
5R
6L
6R
EAST
HIGH RAIL
LOW RAIL

FIG. 8: WHEEL PROFILES OF LOCOMOTIVE 5590

(Test #1)

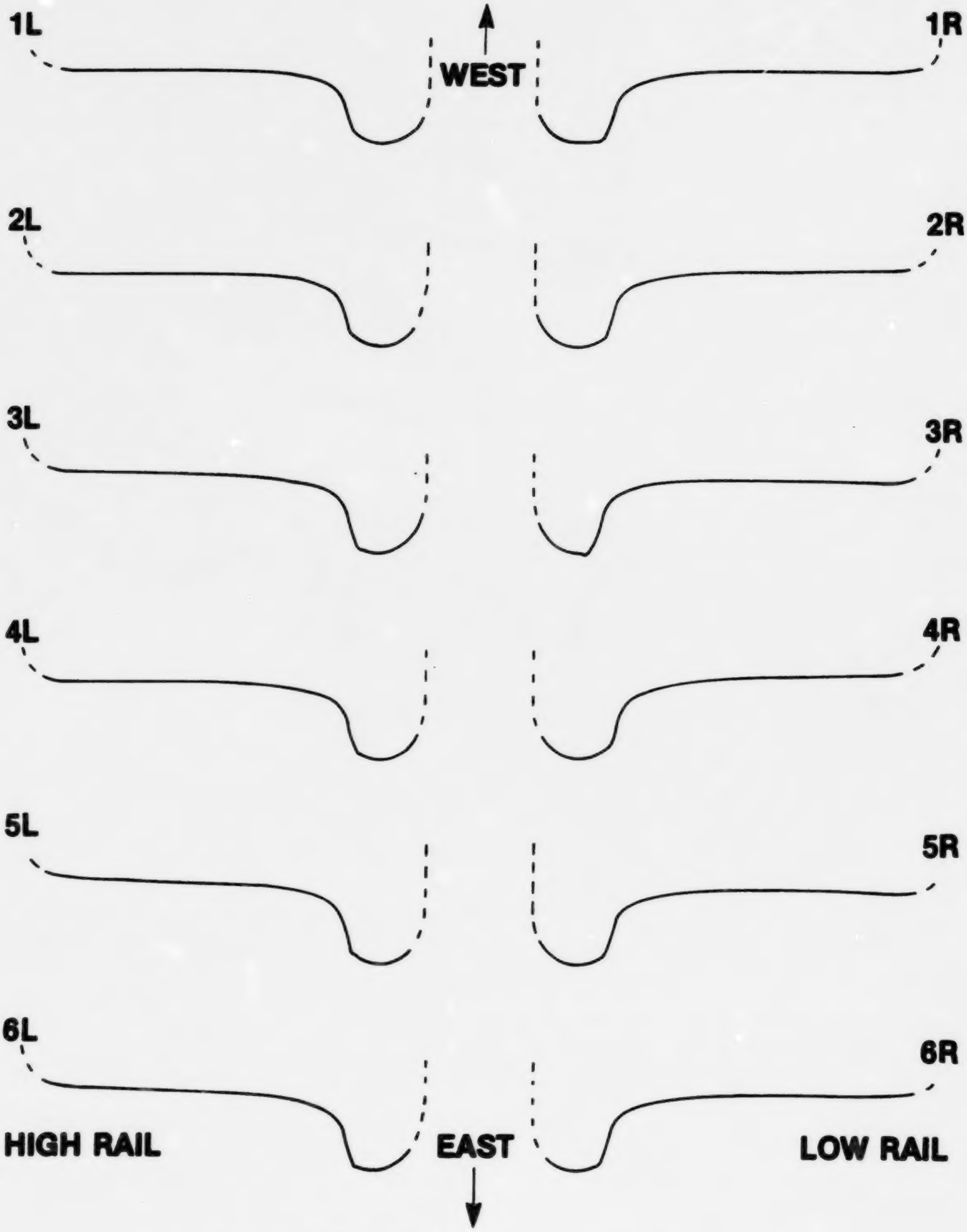
1L
1R
WEST
2L
2R
3L
3R
4L
4R
5L
5R
6L
6R
HIGH RAIL
EAST
LOW RAIL

FIG. 9: WHEEL PROFILES OF LOCOMOTIVE 5590

(Test #2)

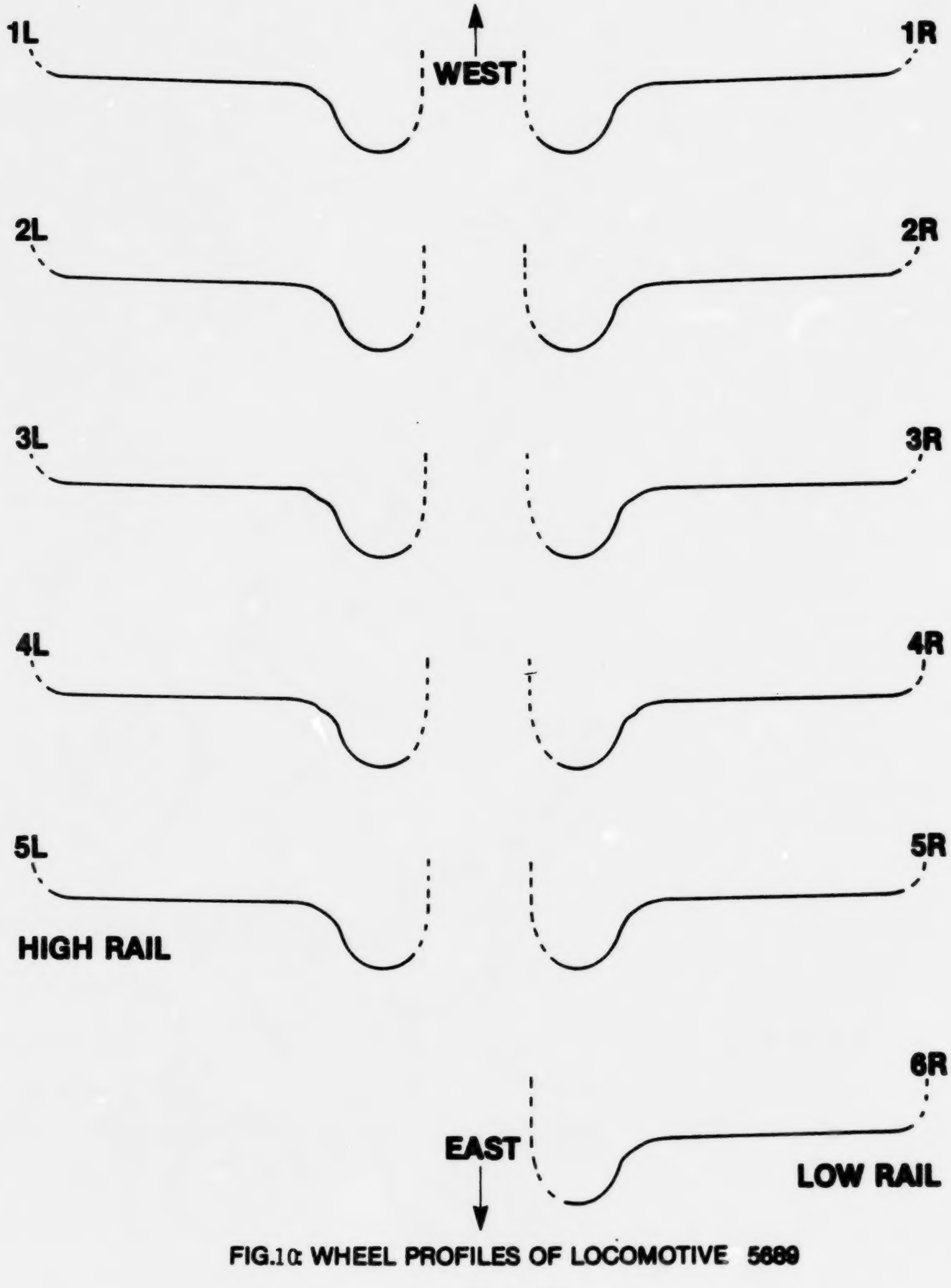
WEST
1L
1R
2L
2R
3L
3R
4L
4R
5L
5R
HIGH RAIL
6R
EAST
LOW RAIL

FIG.10: WHEEL PROFILES OF LOCOMOTIVE 5669

(Test #1)

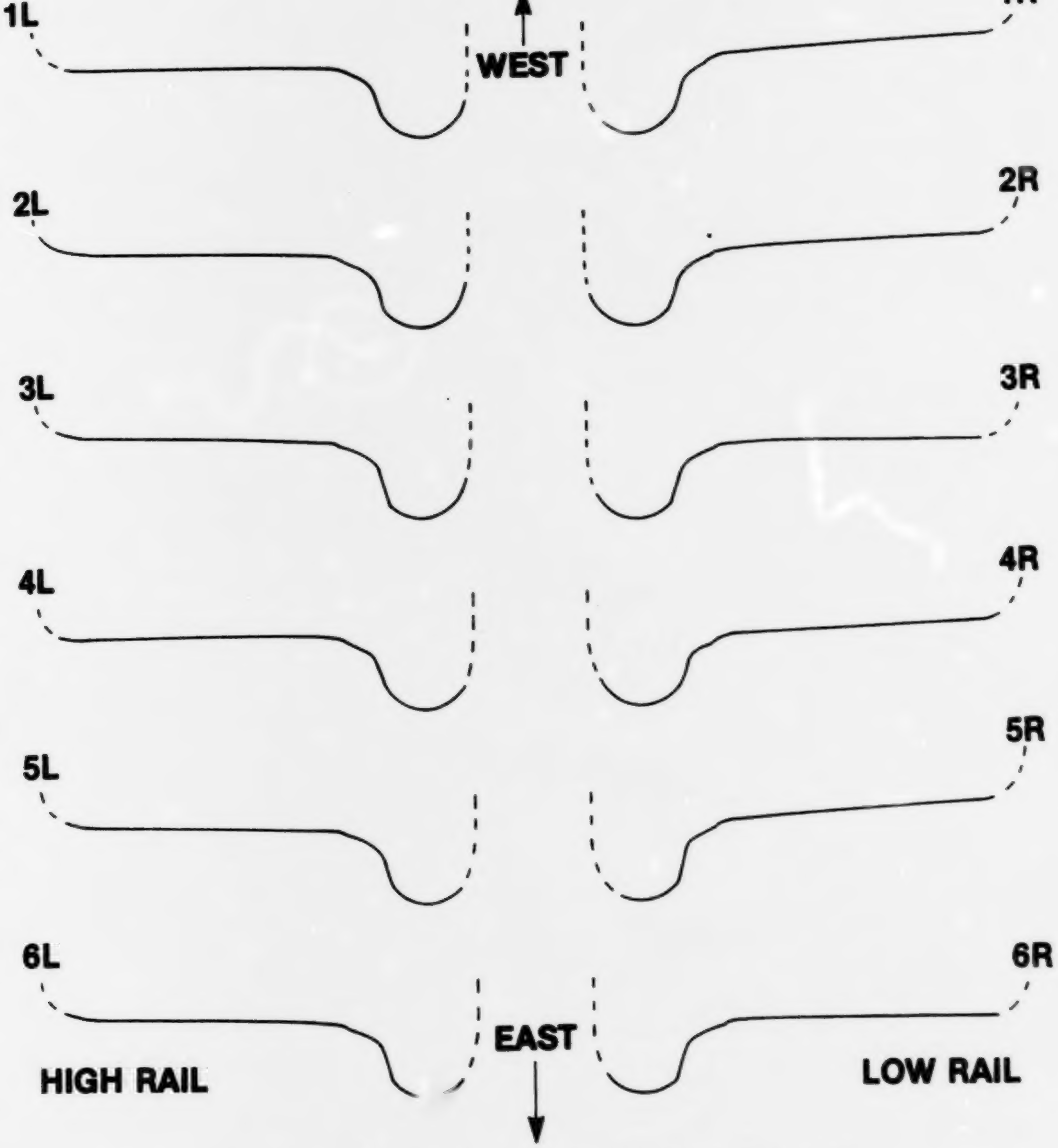
1L
WEST
1R
2L
2R
3L
3R
4L
4R
5L
5R
6L
EAST
6R
HIGH RAIL
LOW RAIL

FIG.11: WHEEL PROFILES OF LOCOMOTIVE 5689

(Test #2)

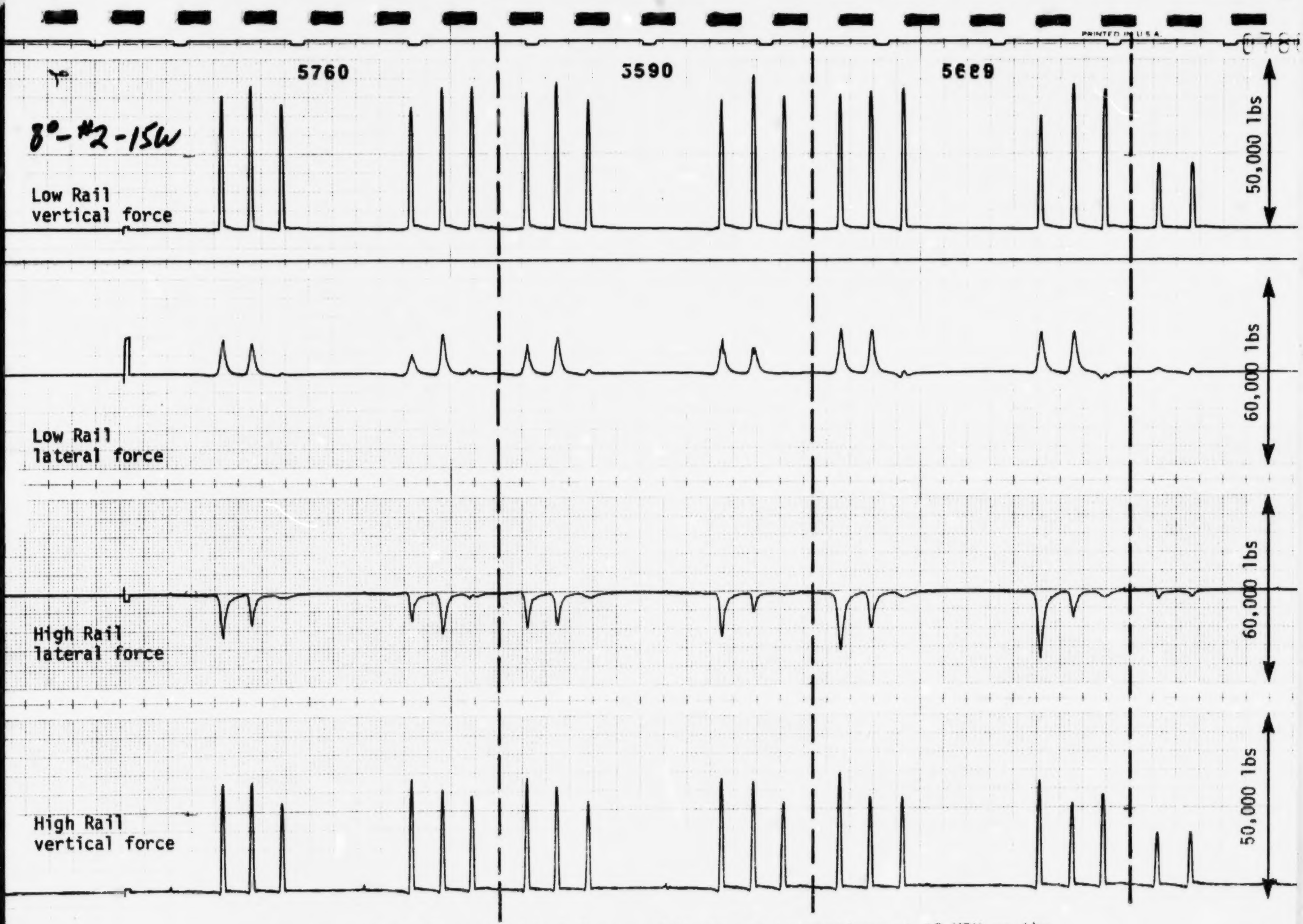

Fig. 12: Lateral and Vertical Forces of Westbound Locomotives at 15 MPH on the 8 degree curve unground rail with no flange lubrication.

TEST #1

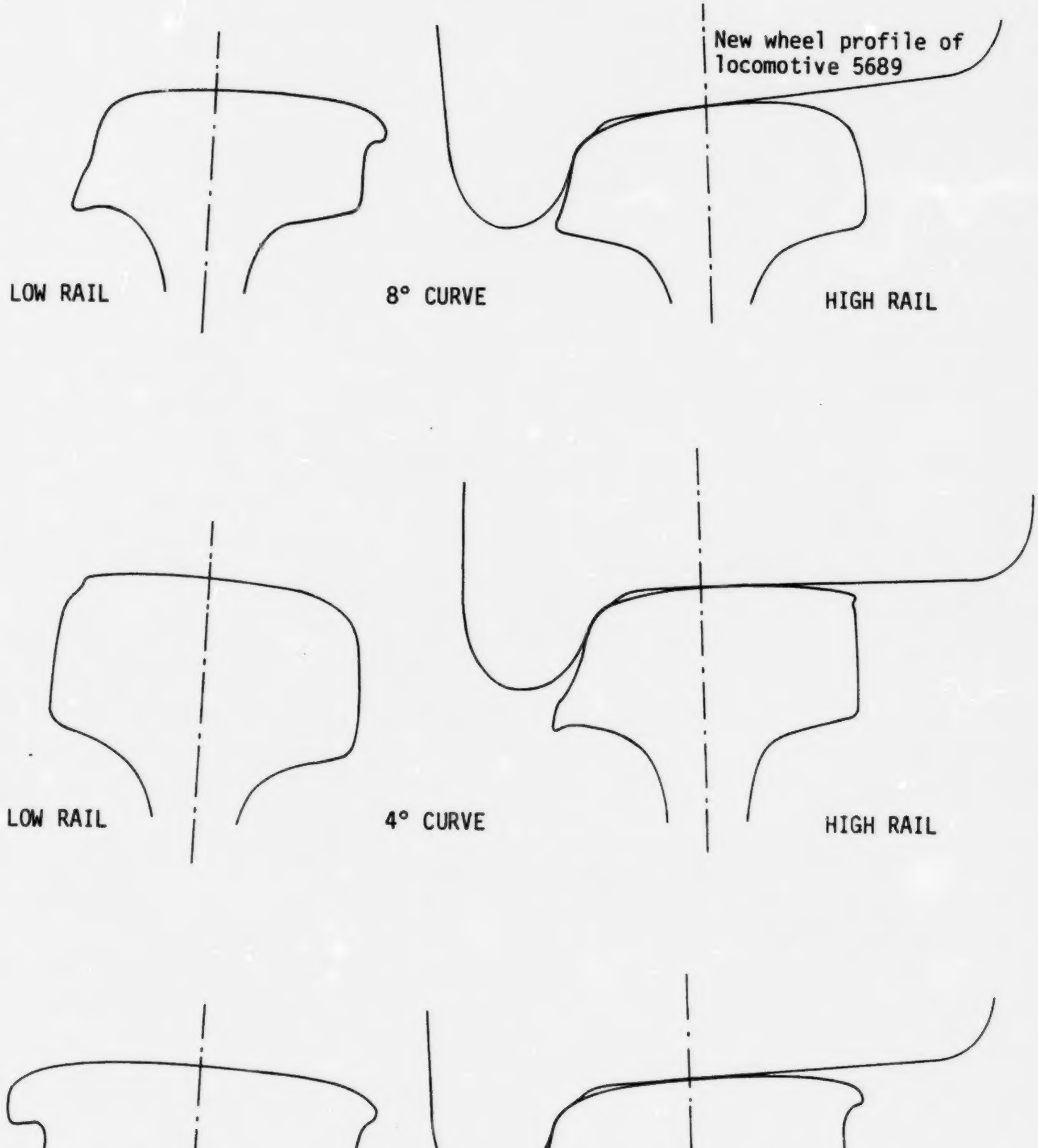
New wheel profile of locomotive 5689
LOW RAIL
8° CURVE
HIGH RAIL
LOW RAIL
4° CURVE
HIGH RAIL
LOW RAIL
2° CURVE
HIGH RAIL

FIG. 13: LOCOMOTIVE WHEEL CONTACT CONFIGURATION OVER UNGROUND RAIL

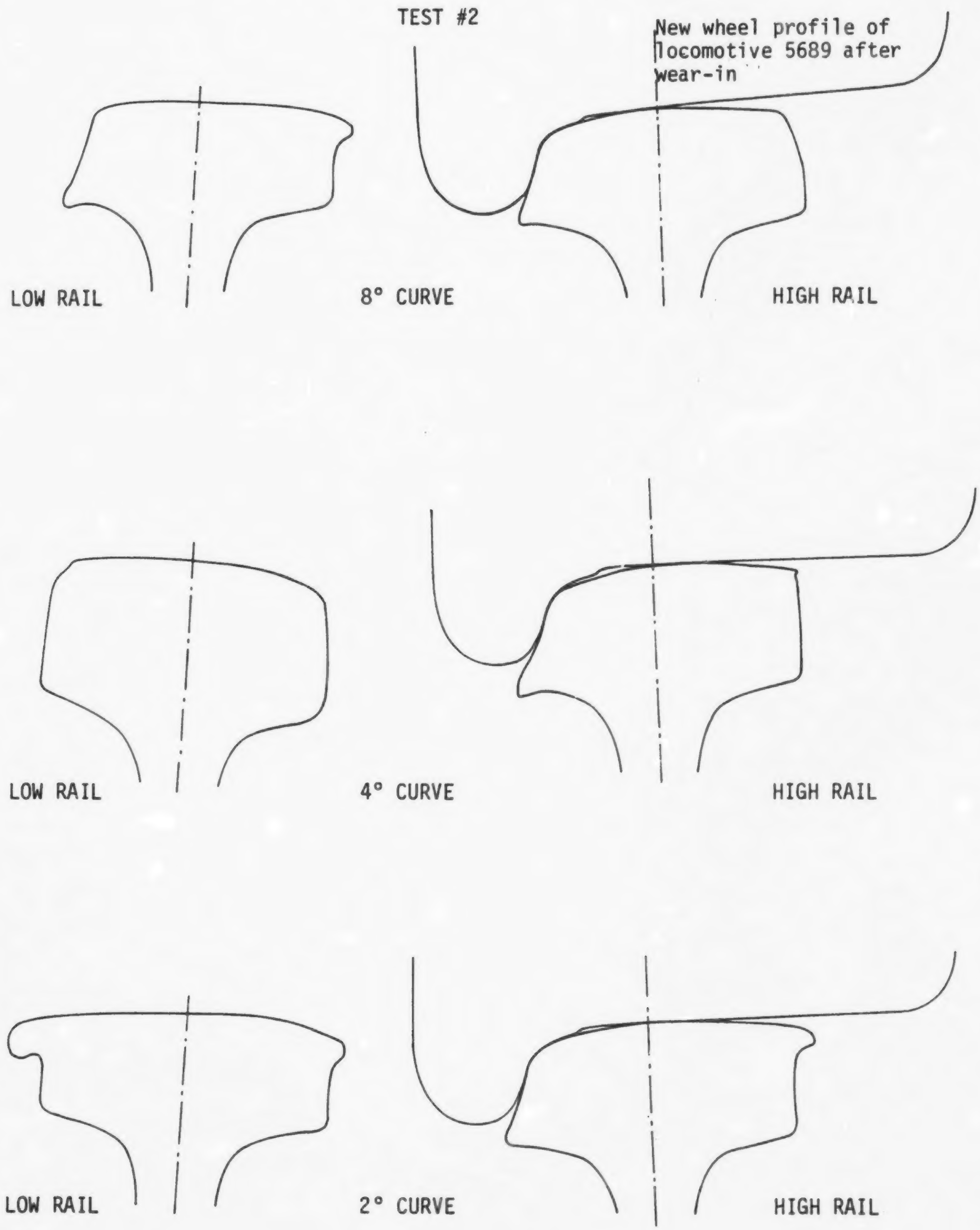
TEST #2
New wheel profile of locomotive 5689 after wear-in
LOW RAIL
8° CURVE
HIGH RAIL
LOW RAIL
4° CURVE
HIGH RAIL
LOW RAIL
2° CURVE
HIGH RAIL

FIG. 14: LOCOMOTIVE WHEEL CONTACT CONFIGURATION OVER GROUND RAIL

FIG. 15

2 DEGREE CURVE BEFORE GRINDING

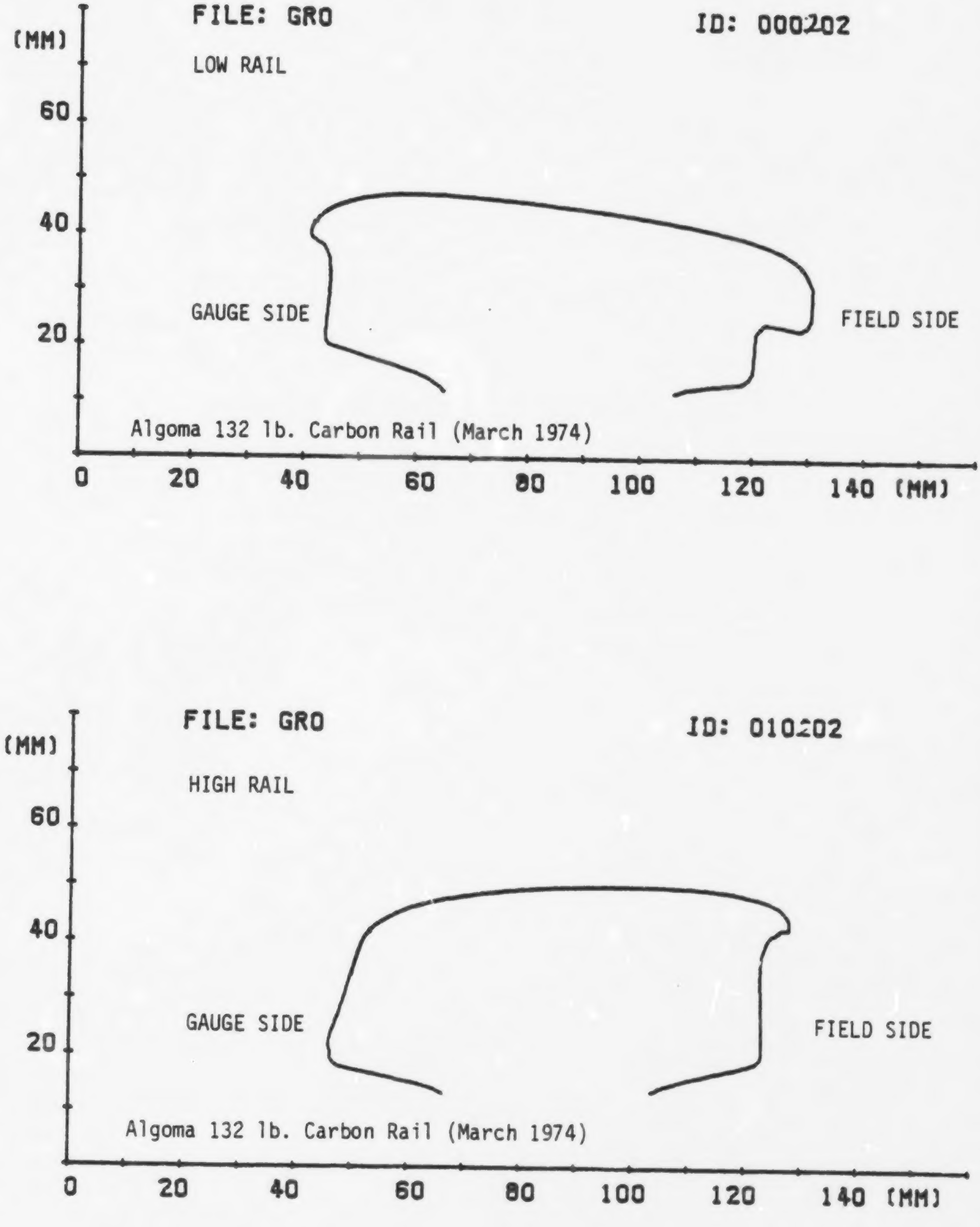

FIG. 16

2 DEGREE CURVE IMMEDIATELY AFTER GRINDING

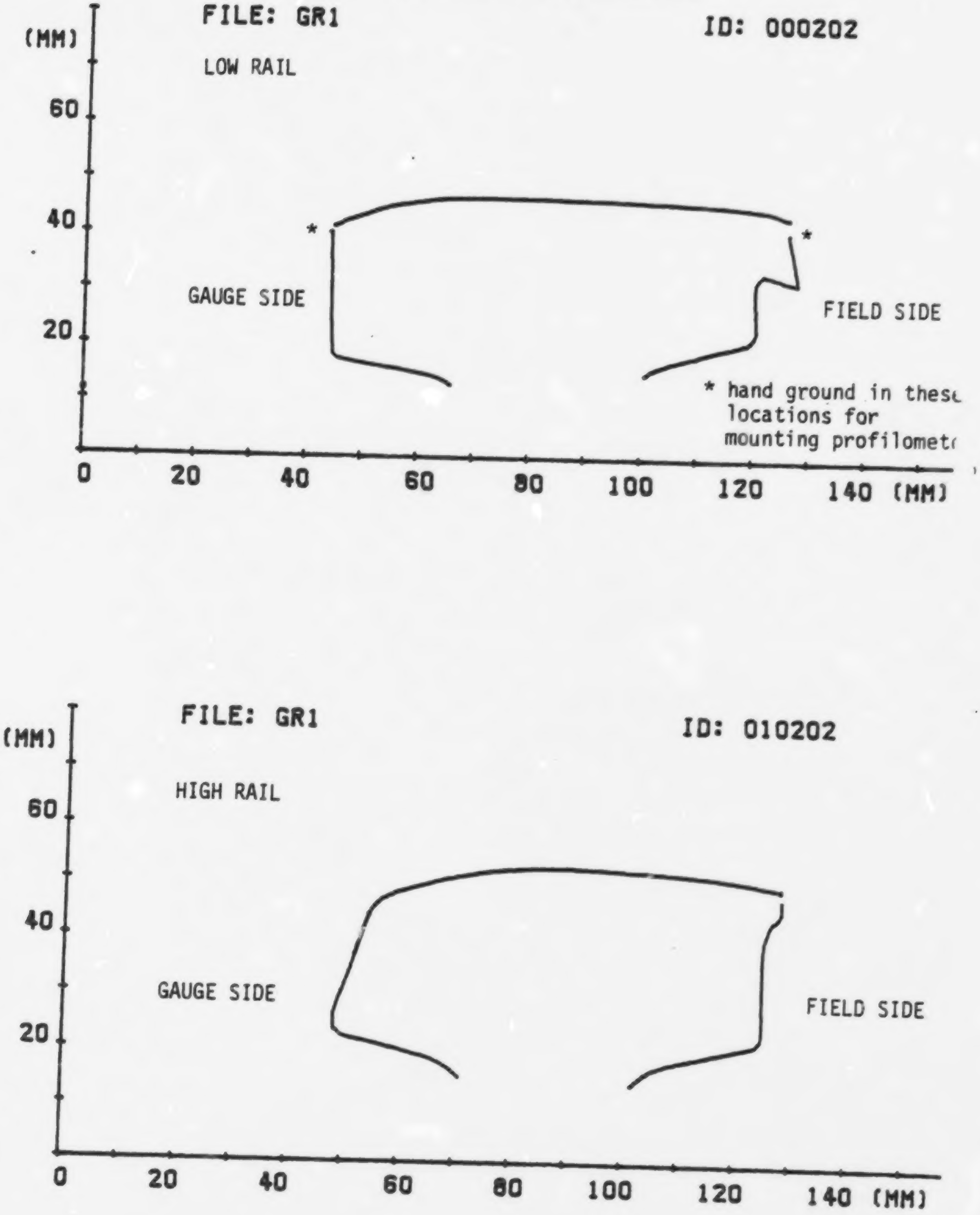

* hand ground in thes
locations for
mounting profilomet

FIG. 17

4 DEGREE CURVE BEFORE GRINDING

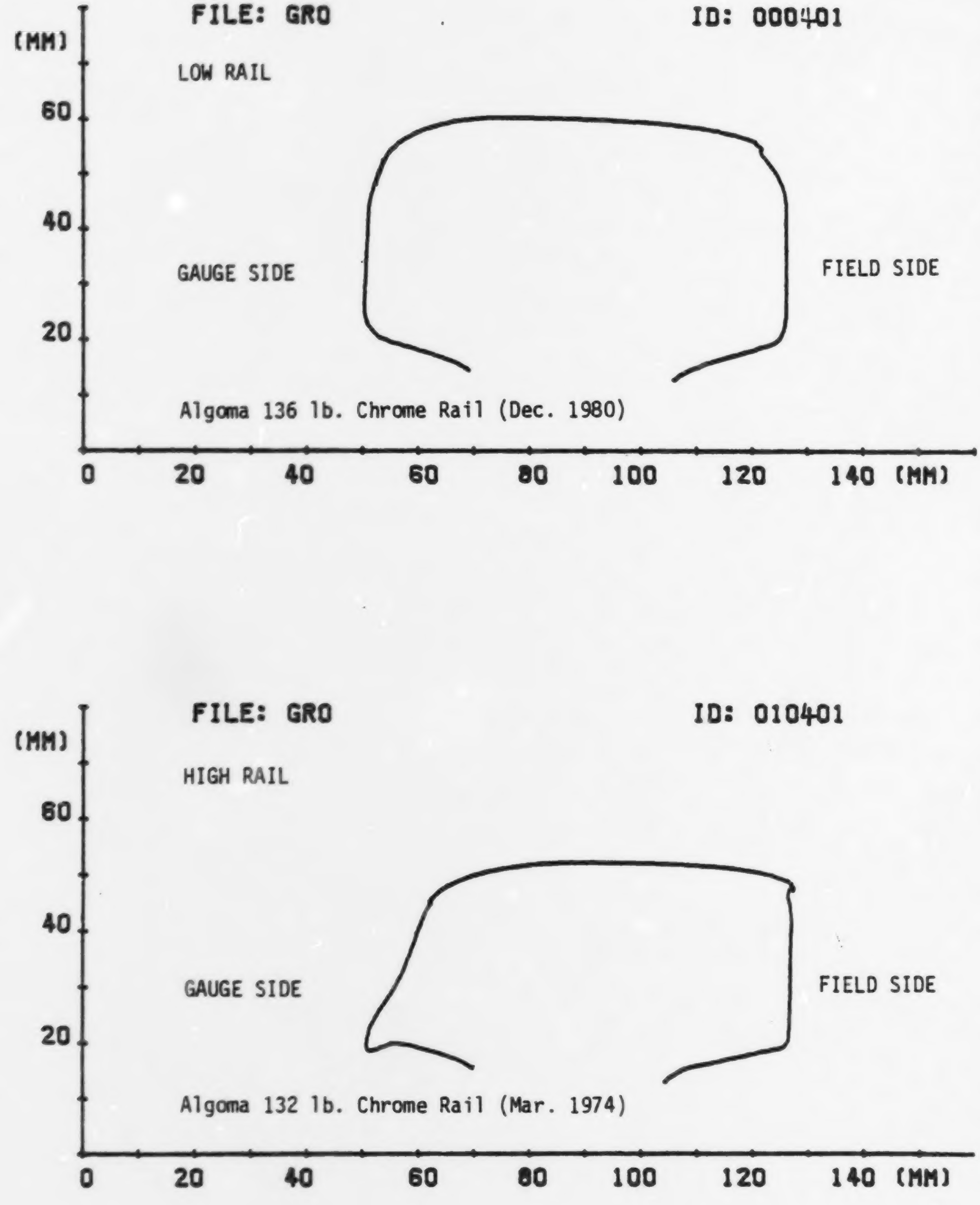

FIG. 18

4 DEGREE CURVE IMMEDIATELY AFTER GRINDING

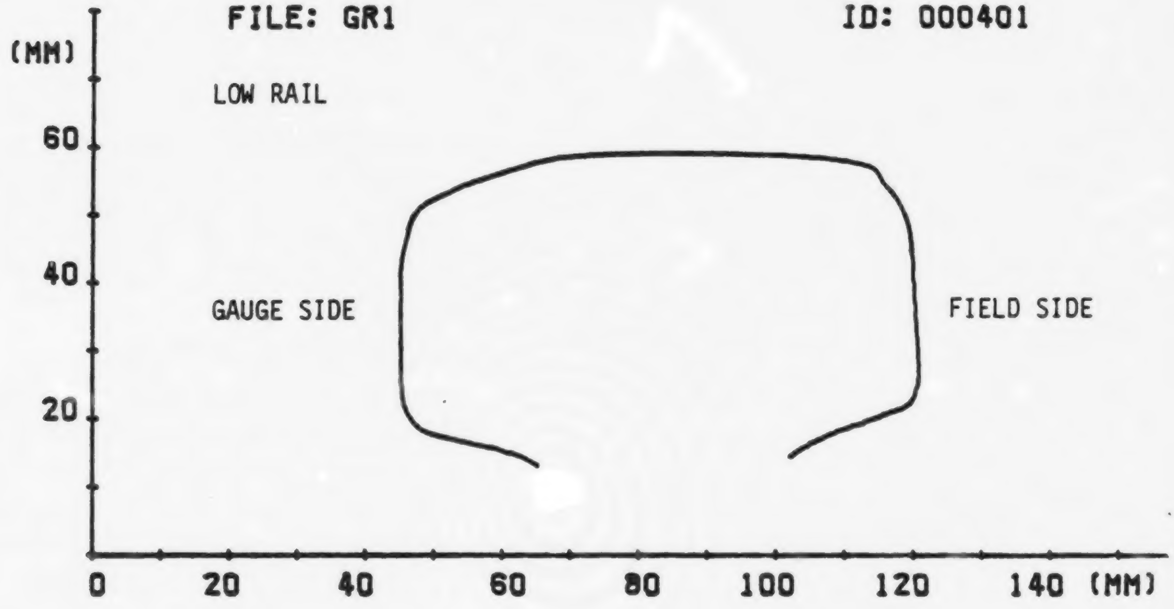

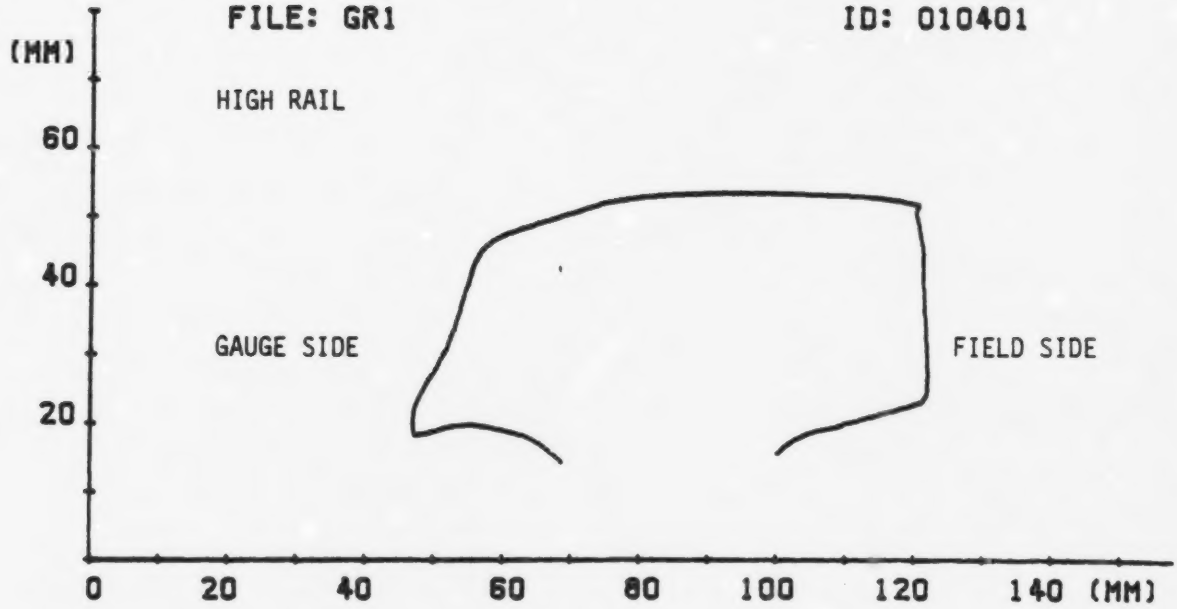

FIG. 19

8 DEGREE CURVE BEFORE GRINDING

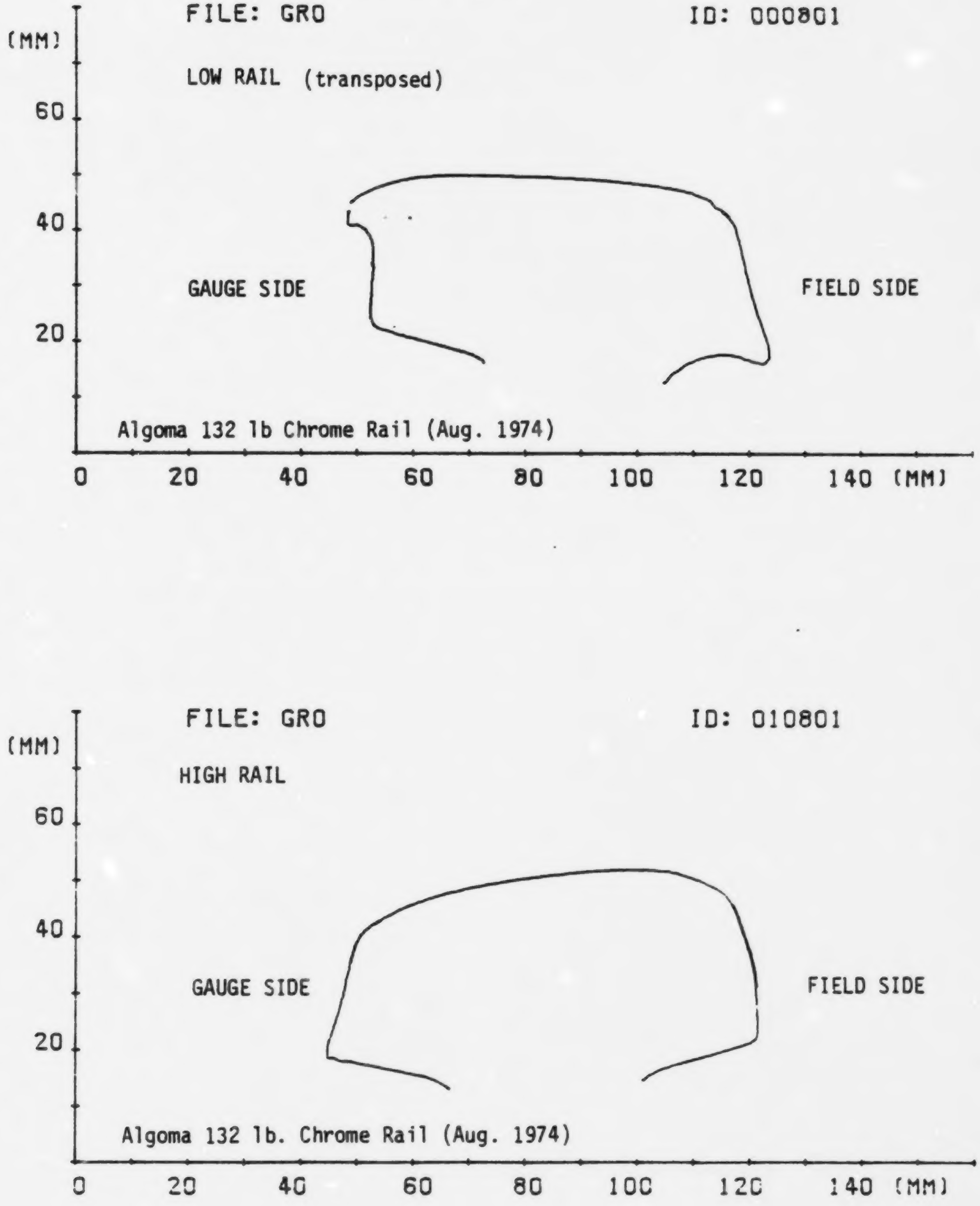

FIG. 20

8 DEGREE CURVE IMMEDIATELY AFTER GRINDING

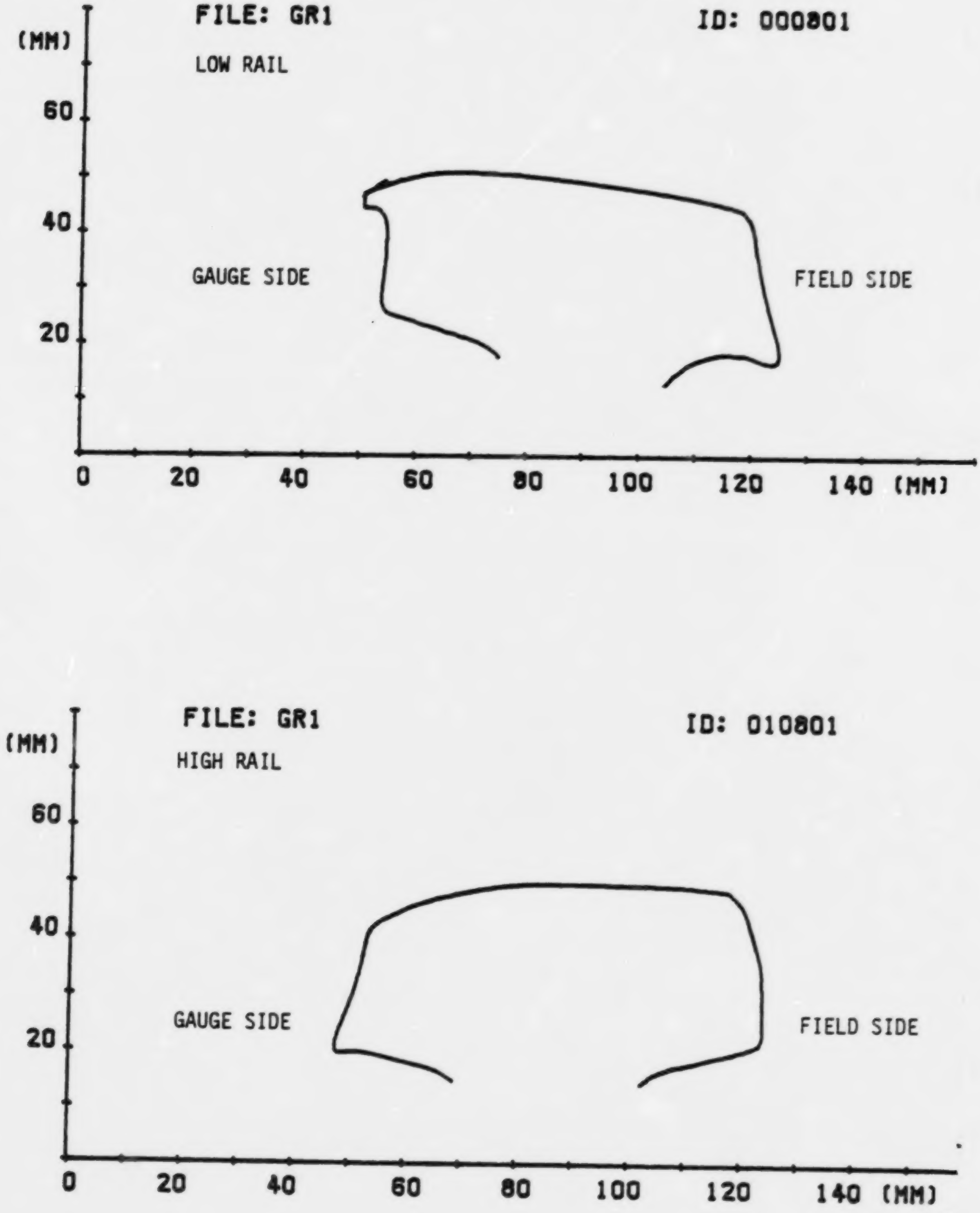

Test #1

Locomotive Number	Axle Number (#1 West, #6 East in the Test Configuration)					
	1	2	3	4	5	6
5760	16/32	46/32*	18/32	19/32	44/32*	23/32
5590	22/32	40/32***	18/32	18/32	30/32***	18/32
5689	22/32	24/32	21/32	18/32	24/32	18/32

Test #2

Locomotive Number	Axle Number (#1 East, #6 West in the Test Configuration)					
	1	2	3	4	5	6
5760	16/32	19/32	18/32	19/32	24/32	23/32
5590	22/32	40/32***	18/32	18/32	30/32***	18/32
5689	22/32	44/32**	21/32	18/32	33/32**	18/32

TABLE 1: Lateral clearance (inches) measured for each axle of the test locomotives.

*, ** modified axles

***

Test #2

Locomotive Number	Axle Number (#1 West, #6 East in the Test Configuration)					
	IR/IL	2R/2L	3R/3L	4R/4L	5R/5L	6R/6L
	No. of 1/16" Shims	No. of 1/16" Shims	No. of 1/16" Shims	No. of 1/16" Shims	No. of 1/16" Shims	No. of 1/16" Shims
5760	3/8	4/7	4/4	4/3	2*/3	8/4
5590	7/4	9/9	5/8	8/8	9/9	4/8
5689	4/4	8/6	4/4	8/8	6/8	8/8

TABLE 2 : Shims used on the journal boxes of test locomotives.

Note - * - 1/8" shims

- Rear strip liners on edge of inner stop lugs on the journal box removed on middle axle of trucks on locomotives 5590 and 5689.

Table 3 : Angle-of-Attack of Each Axle For Westbound Runs of Test Locomotives in Test #1

Degree of Curve	M.P.H.	Rail Flange Condition	Locomotive 5760 (Modified, Worn Wheels) Axle No.						Locomotive 5590 (Modified, Worn Wheels) Axle No.						Locomotive 5689 (Unmodified, New Wheels) Axle No.					
			1	2	3	4	5	6	1	2	3	4	5	6	1	2	3	4	5	6
2	41	Dry	-1.8	-4.3	-4.6	-1.0	-1.8	6.0	1.2	-3.9	-5.1	-2.7	-2.5	-2.4	0.7	-1.2	-3.6	4.3	0.1	-3.6
2	30	Dry	1.1	-3.3	-3.1	-1.5	2.2	7.3	0.9	-1.1	-2.5	0.1	2.2	-0.3	8.5	3.9	-1.1	7.9	3.4	-0.9
4	31	Dry	12.1	-5.5	-7.7	2.5	-2.6	-5.3	14.3	3.6	-3.7	10.1	-2.8	-3.0	10.5	1.0	-6.0	16.0	0.9	-4.1
4	23	Dry	14.2	-3.3	-6.3	6.1	1.1	0.5	16.2	5.1	-4.1	12.0	1.4	-1.8	14.1	7.6	-4.6	20.2	2.4	-4.0
4	21	Lub.	26.3	-2.5	-5.7	10.4	6.2	.1	17.5	12.5	-3.2	20.7	8.0	-7.4	24.1	10.6	-4.2	24.9	13.4	-1.8
8	31	Dry	51.4	23.4	-0.5	50.2	30.7	-1.0	59.0	35.1	0.7	58.6	27.9	-0.4	55.6	29.4	1.3	52.5	30.7	-4.4
8	16	Dry	53.2	46.2	3.3	48.8	26.4	7.2	59.9	37.4	4.7	40.6	26.4	3.7	58.3	32.5	3.0	57.2	20.3	2.8
8	4	Dry	88.6	30.9	4.4	64.0	31.9	9.6	63.2	37.7	2.9	61.9	25.8	3.4	64.8	29.9	3.8	61.1	30.3	2.7

Table 4: Angle-of-Attack of Each Axle of Test Locomotives For Eastbound Runs in Test #1

Degree of Curve	M.P.H.	Rail Flange Condition	Locomotive 5760 (Modified, Worn Wheels) Axle No.						Locomotive 5590 (Modified, Worn Wheels) Axle No.						Locomotive 5689 (Unmodified, New Wheels) Axle No.					
			1	2	3	4	5	6	1	2	3	4	5	6	1	2	3	4	5	6
2	33	Dry	0.5	0.9	0.6	0.4	4.9	20.6	-2.4	0.4	4.1	2.0	2.8	1.2	1.1	1.4	0.4	1.1	5.1	11.1
2	22	Dry	0.5	0.7	2.2	0.3	4.1	24.4	0.4	1.7	7.8	-2.1	3.7	2.7	3.9	0.7	2.4	1.9	4.7	8.6
4	31	Dry	5.0	14.6	23.0	7.0	10.0	20.5	2.5	10.4	24.4	4.6	11.3	17.0	3.6	9.6	20.4	4.4	9.7	27.3
4	22	Dry	4.1	11.5	25.2	8.1	15.2	24.1	4.5	10.2	27.1	5.0	15.3	17.1	4.2	12.0	22.0	4.7	19.0	28.7
8	31	Dry	-8.7	16.7	50.2	-3.8	26.3	52.5	-8.7	20.8	56.5	-8.4	22.2	40.7	-6.7	22.0	51.8	-8.6	33.4	52.6
8	19	Dry	-1.2	13.2	50.6	0.2	23.3	57.5	1.2	20.5	58.1	-0.5	27.7	47.7	-0.4	20.1	42.3	-2.8	33.7	52.9

Table 5: Angle of Attack of Each Axle For Westbound Runs of Test Locomotives in Test #2

Degree of Curve	M.P.H.	Rail Flange Condition	Locomotive 5760 (Unmodified, Worn Wheels) Axle No.						Locomotive 5590 (Modified, Worn Wheels) Axle No.						Locomotive 5689 (Modified, New Wheels) Axle No.					
			1	2	3	4	5	6	1	2	3	4	5	6	1	2	3	4	5	6
2	39	Dry	1.3	-.6	-1.7	-2.6	2.1	2.9	2.5	-1.5	-2.7	1.8	.7	.2	2.4	-.8	-1.1	7	-1.4	-1.9
2	22	Dry	3.5	1.3	-.2	-.2	3.6	4.1	6.4	-.3	.4	1	3	-1.6	5.5	2.2	-.6	7	.7	.7
4	30	Dry	15.6	-.7	-5.2	5.2	-.5	-3.2	16.9	3.7	-3.4	12.2	-.5	-2.3	13.3	4.5	-3.9	20.3	2.8	-2.4
4	20	Dry	14.8	2.1	-4.1	6.7	5	-3	19.2	8	-2.1	14.1	0	.4	15.4	8.6	-2.7	21.2	3	-.4
4	20	Lub.	18.5	4.9	-2.7	11.3	10.4	1	19.7	18.6	-1.9	21	6.9	-2.9	28.1	13.9	-3.1	26.8	14.4	0
8	29	Dry	54	21.7	-1.7	45.7	21.7	-1.7	57.1	26.1	.8	50.5	16	-2.2	53.3	23.1	1.7	60.9	16.1	1.7
8	16	Dry	53.4	23	-2.1	46.7	22.6	-3.7	58.1	29.5	1.3	49.4	14	1.5	49.8	24.1	1.1	56.8	19.8	2
8	16	Lub.	59.5	31.4	-2.2	49.9	24.1	-1.4	64.9	40.5	3	54.2	18.2	2.3	65	32.5	2.9	63.5	23.9	1.3

Table 6: Angle of Attack of Each Axle For Eastbound Runs of Test Locomotives in Test #2

Degree of Curve	M.P.H.	Rail Flange Condition	Locomotive 5760 (Unmodified, Worn Wheels) Axle No.						Locomotive 5590 (Modified, Worn Wheels) Axle No.						Locomotive 5689 (Modified, New Wheels) Axle No.					
			1	2	3	4	5	6	1	2	3	4	5	6	1	2	3	4	5	6
2	35	Dry	-2.3	-1.4	-1	-1.3	2.8	20.6	-1.5	1.8	4.1	-1	.8	-2.3	-.03	-.1	-3.1	-2.8	.1	8.6
2	19	Dry	.2	1.2	1.5	.1	4.4	25.3	1.1	1.3	5.1	.6	4.1	-1.1	1.2	.7	-1.6	-.4	2.5	6.7
4	30	Dry	5.2	11.7	20.4	5.3	6.7	35.9	1.7	6.8	23.7	3.9	9.2	16.9	.8	6	16	3.1	8.4	23.4
4	20	Dry	3	8.9	22.4	6.7	12.5	40.1	2.9	6.6	24.5	3	13.3	14.3	1.6	7.1	17.8	3.1	14	25.3
8	30	Dry	-11	11.4	49.7	-9.6	12.7	56.6	-9.2	14.7	56	-9.1	11.7	43.4	-9.7	12.9	47	-9.2	14.5	52.6
8	17	Dry	-7.8	15.2	49.8	-6.1	15.6	58.2	-3.3	18	54	-3.7	13.9	44.5	-5.3	16.2	46.3	-3.8	22.8	52.9
8	17	Lub.	-9.1	15.9	49.7	-6.5	19.5	58.3	-4.7	17.5	55.9	-4.2	31.3	47.7	-6.6	19.1	49	-5.8	40.3	56.1

Degree of Curve	M.P.H.	Rail Flange Condition	Locomotive 5760 Unmodified, Worn Wheels Lateral Force Leading Outer Wheel		Locomotive 5590 Modified, Worn Wheels Lateral Force Leading Outer Wheel		Locomotive 5689 Modified, New Wheels Lateral Force Leading Outer Wheel	
			1	2	1	2	1	2
2	39	Dry	.6	.1	2	-1.4	2.7	2.6
2	22	Dry	-1	1.4	-.7	-0.8	2.2	1.7
4	30	Dry	8.2	3.4	7.3	7.5	10.7	11.6
4	20	Dry	7.6	3.8	8.4	8.9	9.7	12.4
4	10	Dry	6.0	3.8	5.5	5.5	7.7	8.9
8	30	Dry	13	13	11.6	13.6	13	13.7
8	15	Dry	11.9	11.9	10.6	11.4	14.2	14
8	15	Lub.	13.6	13.4	6.5	10.2	15	14.6

Table 7: Lateral Force (Kips) on Leading Outer Wheels
For Each Locomotive Truck for Westbound Runs of Test #2

Degree of Curve	M.P.H.	Rail Flange Condition	Locomotive 5760 Unmodified, Worn Wheels Lateral Force Leading Outer Wheel		Locomotive 5590 Modified, Worn Wheels Lateral Force Leading Outer Wheel		Locomotive 5689 Modified, New Wheels Lateral Force Leading Outer Wheel	
			1	2	1	2	1	2
2	35	Dry	3.6	.8	-.6	-.6	-1.8	-.9
2	19	Dry	1.8	.3	-.5	-1	-2.6	-2.1
4	30	Dry	7.3	-.1	7.9	7.6	13.6	13.4
4	20	Dry	7.6	-1.6	7.1	8	12.3	14.2
8	30	Dry	11.6	5.6	11.5	15	16.8	16.9
8	15	Dry	10.6	2	10.3	10.2	15.5	13
8	15	Lub.	11	3.2	12.6	11.5	18.8	15.4

Table 8: Lateral Force (Kips) on Leading Outer Wheels For Each Locomotive Truck for Eastbound Runs of Test #2

TEST NUMBER	M.P.H.	LOCOMOTIVE 5760		LOCOMOTIVE 5590		LOCOMOTIVE 5689	
1	22	7.4	-.8	5.6	5.6	11	8
2	20	7.5	-1.7	7.5	7.6	12.6	13.9
1	31	8.5	1.5	7.4	6.6	11.2	9.9
2	30	7.3	-.1	7.8	7.7	13.6	13.5
1	35	7.4	.8	7.4	7	11	11.6
2	36	6.5	.1	8.3	9.6	13.3	14.9

TABLE 9: Average lateral force (Kips) on leading outer wheel of each locomotive truck in the Eastbound direction on 4 degree curve.

NOTE: Test 1 17/5/82

5760 : modified WW
5590 : reference, modified WW
5689 : unmodified NW

Test 2 12/6/82

5760 : unmodified WW
5590 : reference, modified WW
5689 : modified NW

WW - Worn Wheels

NW - New Wheels

TEST NUMBER	M.P.H.	LOCOMOTIVE 5760		LOCOMOTIVE 5590		LOCOMOTIVE 5689	
1	22	4	3.9	5.8	6.3	6.2	7.5
2	21	7.7	3.8	8	9	9.7	12.1
1	31	7	5.1	7.4	7.2	9.2	9.2
2	30	8.2	3.4	7.3	7.5	10.7	11.6
1	35	6.9	6.2	6.8	6.9	9.3	9.8
2	35	8.8	4.8	7.9	8.2	11.6	11.2

TABLE 10: Average lateral force (Kips) on leading outer wheel of each locomotive truck in the Westbound direction on 4 degree curve.

NOTE: Test 1 17/5/82

5760 : modified WW
5590 : reference, modified WW
5689 : unmodified NW

Test 2 12/6/82

5760 : unmodified WW
5590 : reference, modified WW
5689 : modified NW

WW - Worn Wheels

NW - New Wheels

TEST NUMBER	M.P.H.	LOCOMOTIVE 5760		LOCOMOTIVE 5590		LOCOMOTIVE 5689	
1	18.4	7.7	2.4	8.1	10.1	20.9	18.1
2	17.2	10.1	2.1	10.8	10.2	16.6	14.2
1	31.7	11.1	6.7	11.5	14.0	18.2	17.4
2	30.3	11.6	5.6	11.5	15.0	16.8	16.9
1	27.6	11.1	5.8	10.1	11.8	14.7	13.6
2	25	10.5	3.5	9.6	12.3	15.4	14.1

TABLE 11: Average lateral force (Kips) on leading outer wheel of each locomotive truck in the Eastbound direction on 8 degree curve.

NOTE:

Test 1 14/5/82

5760 : modified WW
5590 : reference, modified WW
5689 : unmodified NW

Test 2 13/6/82

5760 : unmodified WW
5590 : reference, modified WW
5689 : modified NW

WW - Worn Wheels
NW - New Wheels

TEST NUMBER	M.P.H.	LOCOMOTIVE 5760		LOCOMOTIVE 5590		LOCOMOTIVE 5689	
1	17.1	14.8	8.9	12.3	13.8	19.7	21.9
2	15.3	12.4	12.2	11.0	10.5	13.5	13.1
1	31	14.6	11.2	14.2	15.0	15.7	16.6
2	29	12.8	12.6	10.3	12.7	12.4	13.1
1	26	12.1	10.9	11.6	13.3	12.1	20.0
2	24.3	11.4	11.7	8.6	9.9	7.8	10.2

TABLE 12: Average lateral force (Kips) on leading outer wheel of each locomotive truck in the Westbound direction on 8 degree curve.

NOTE:

Test 1 14/5/82

5760 : modified WW
5590 : reference, modified WW
5689 : unmodified NW

Test 2 13/6/82

5760 : unmodified WW
5590 : reference, modified WW
5689 : modified NW

WW - Worn Wheels
NW - New Wheels

WHEELSET ANGLE-OF-ATTACK MEASUREMENT OF REGULAR TRAIN CONSISTS

Executive Summary

At the request of the Engineering Department of CP Rail, the Research Department conducted wheelset angle-of-attack measurements for regular freight traffic on an 11 degree curve at Mileage 96.8, Mountain Subdivision, Revelstoke Division.

The field test was performed concurrently with tests conducted by Portec at the same site to evaluate the performance of concrete tie fastenings. The objective of the tests carried out by the Research Department was to provide initial statistical information on the misalignment angle of axles in train consists during curving and to assess the possibility of identifying "bad performers".

The angle-of-attack equipment was installed in the fully developed section of the 11 degree curve to capture "steady-state" truck curving performance. Westbound traffic passed through a flange lubricator at curve entry. A total of six eastbound and westbound trains were monitored and the axle angle-of-attack data including curving speed was captured.

From the angle-of-attack data, it would seem possible to identify individual trucks which parallelogram excessively and "stuck trucks".

It is recommended that consideration be given to developing a semi-permanent wayside system capable of monitoring angle-of-attack and curving forces on medium and high curvature track. The information obtained might be used as a tool to provide data for regular maintenance, as well as to reduce derailment risks due to "bad performers" in the regular fleet.

Sommaire

A la demande des services techniques du CP Rail, le bureau de recherches de cette compagnie a mesuré les angles d'inscription des essieux des convois de marchandises réguliers abordant une courbe de 11 degrés, au droit du point milliaire 96,8, Subdivision Mountain, Division de Revelstoke.

Ces travaux ont eu lieu concurremment avec les essais faits par Portec, une compagnie américaine, sur cette même voie, et visant à évaluer la tenue des fixations de traverses en béton. Le but poursuivi par le bureau de recherches était l'obtention de renseignements statistiques préliminaires sur le désalignement angulaire des essieux à l'inscription dans une courbe, et l'étude d'une méthode permettant de dépister les essieux défectueux.

L'appareillage de mesure de l'angle d'inscription, placé là où le rayon de courbure est maximal, visait à déterminer le comportement des bogies en régime permanent d'inscription en courbe, les convois en direction ouest ayant eu les boudins de roue préalablement lubrifiés à l'entrée de la courbe. Des données sur les angles d'inscription et les vitesses en courbe ont été recueillies à l'égard de six convois en tout, en direction est et ouest.

Grâce à ces données, il serait possible de déceler tous les bogies qui se déforment excessivement ou qui grippent.

Le rapport recommande l'étude d'un système semi-permanent, à poser en bordure de voie, pour mesurer les angles et les forces d'inscription dans les courbes allant de moyennes à prononcées. Les données obtenues pourraient servir à établir la périodicité de l'entretien des bogies en plus de mener à la détection des bogies défectueux, réduisant ainsi les risques de déraillement.

Acknowledgements

The Research Department acknowledges the contribution of personnel from the following organizations.

- Chief Engineer's Office for assistance during the course of this test program.
- Transportation Development Centre, Transport Canada for financial support under contract #OSD81-00006.

Introduction

At the request of the Engineering Department of CP Rail, the Research Department conducted wheelset angle-of-attack measurements for regular freight traffic on an 11 degree curve at Mileage 96.8 on the Mountain Subdivision, Revelstoke Division, in April, 1982.

The field test was performed concurrently with track force and deflection measurements conducted by Portec at the same site to evaluate the performance of concrete tie restraints.

The objective of the study was to provide initial statistical information on the misalignment angle of axles in train consists during curving and to assess the possibility of identifying "bad performers".

Test Site Condition

The angle-of-attack equipment was installed in the fully developed section of the 11 degree curve to capture the "steady-state" curving performance of trucks. At curve entry, westbound traffic passed through a flange lubricator and the gauge face of the high rail was well lubricated throughout the duration of the test. The superelevation was 3 1/2 inches on the test curve and the corresponding equilibrium curving speed was 22 MPH.

Data Presentation Format

A total of six trains both eastbound and westbound were monitored and the axle angle-of-attack data including the curving speed of each car is presented from page 10 to page 29 inclusive (Appendix 1). In these tabulated results, each row presents complete information for one car using the following notation:

ID : L for Locomotives
C for Cars

OBS : Car number

SPED 1 : speed of the lead axle of the car (in MPH).

Angl 1-6 : angle-of-attack of axles (in minutes of arc)
1 - 6 for locomotives and
1 - 4 for freight cars with the lead axle of the leading truck as Angle 1.

The numbers for each locomotive and freight car can be readily traced from the consist sheets which are presented in Appendix 2.

At the end of each angle-of-attack tabulation for a complete consist, the statistical mean and standard deviation of all angle-of-attack measurements are presented for comparison with other train consists.

Figures 1 through 4 show the angle-of-attack distribution for each of Angles 1 and 3 for Eastbound and Westbound runs. These histograms depict the frequency of occurrence for a given angle-of-attack. The statistical mean and standard deviation are also presented for comparison.

The angle-of-attack data of a small number of axles were not successfully monitored due to various reasons. Some of these problems occurred with locomotive axles with a sandpipe installed too close to railhead which intercepted the laser beams and caused an erroneous reading. These data were left blank in the angle-of-attack tabulations.

A small alignment error is usually introduced in the angle-of-attack data due to the difficulty of aligning the lasers with the true radial line of the curve. This offset error, which was compensated for, is estimated to be less than 5 minutes of arc.

General Observations

1. Wheelbase Effect

In normal 3-piece freight car trucks, truck axles parallelogram on high curvature track (such as the present 11 degree curve), generating large positive angle-of-attack at the leading outer wheel. Since the axles of a 3-piece truck do not yaw relative to each other, the angle-of-attack of the trailing axle, on the average, is less than the leading axle by an amount equal to the wheelbase divided by curve radius, expressed in minutes.

It was established theoretically that a 70" wheelbase truck on an 11 degree curve (522 ft. radius), will experience a difference between its leading and trailing axle angle-of-attack of the magnitude of 38.4 minutes. This value generally corresponded to the calculated difference of the mean of the measured leading and trailing axle angle-of-attacks for both leading and trailing trucks of each car in the train consist.

2. Coupling Effect Between the Leading and Trailing truck of each Car

It is observed that on the average, the leading truck has higher angle-of-attack than trailing truck for each car, and the effect is particularly dominant for Eastbound traffic which consists mainly of empty cars. This "coupling effect" can be attributed to opposite body/truck rotation in a curve which generates opposite torque at the body-truck connections. The torque at the leading truck parallelograms the axles even further and the torque on trailing truck does the opposite.

Among empty Eastbound cars, a substantial number of cars have negative angles-of-attack at the trailing truck, indicating improper truck rotation with respect to the curve.

Conclusions and Recommendations

From the angle-of-attack tabulation and consist description sheets, one can readily identify individual trucks which parallelogram excessively and "stuck trucks". These undesirable curving characteristics can be attributed to various factors such as insufficient truck rotation on the centre plate during curve entry, excessively or asymmetrically worn wheels, excessive truck component wear etc. which could be examined carefully during scheduled maintenance.

From the angle-of-attack distribution charts one can observe that the mean value of Angle 1 is higher for Eastbound runs as compared to Westbound runs. The variance is also larger for Eastbound runs indicating more variability in values of Angle 1 in Eastbound runs as compared to the Westbound runs.

It is considered possible to obtain a complete data file of angle-of-attack profile together with curving force distribution for each individual locomotive truck and trucks for all unit coal cars at a convenient location on medium and high curvature tracks. Once initiated, this data file could be updated periodically to isolate trucks with less desirable curving performance and to compare individual truck performance before and after scheduled maintenance.

A semi-permanent wayside system capable of monitoring angle-of-attack and curving forces could be an invaluable tool to provide data for regular maintenance, as well as reducing derailment risks due to "bad performers" in the regular fleet.

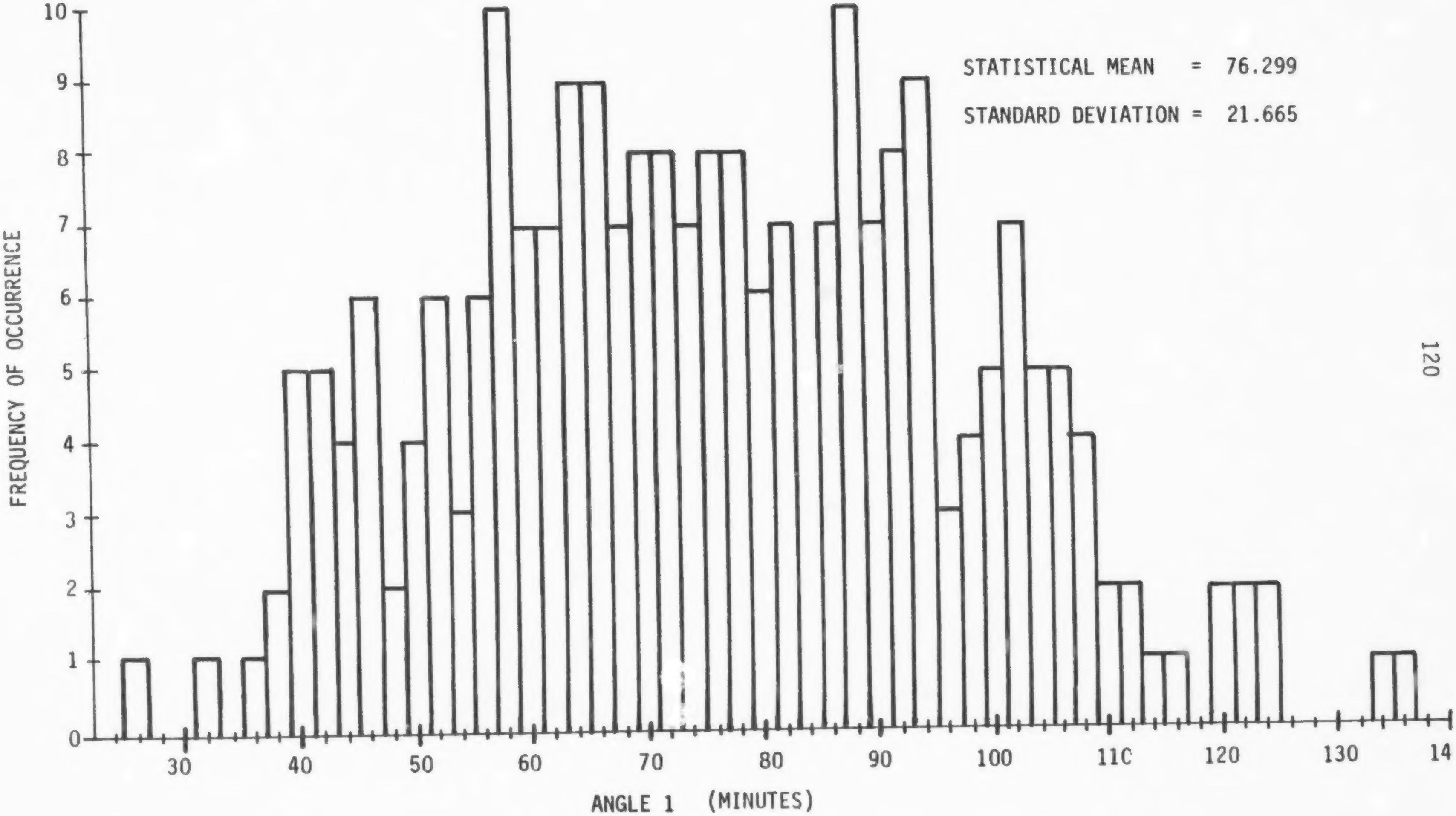

FIGURE 1: FREQUENCY BAR CHART FOR EASTBOUND RUNS (ANGLE 1)

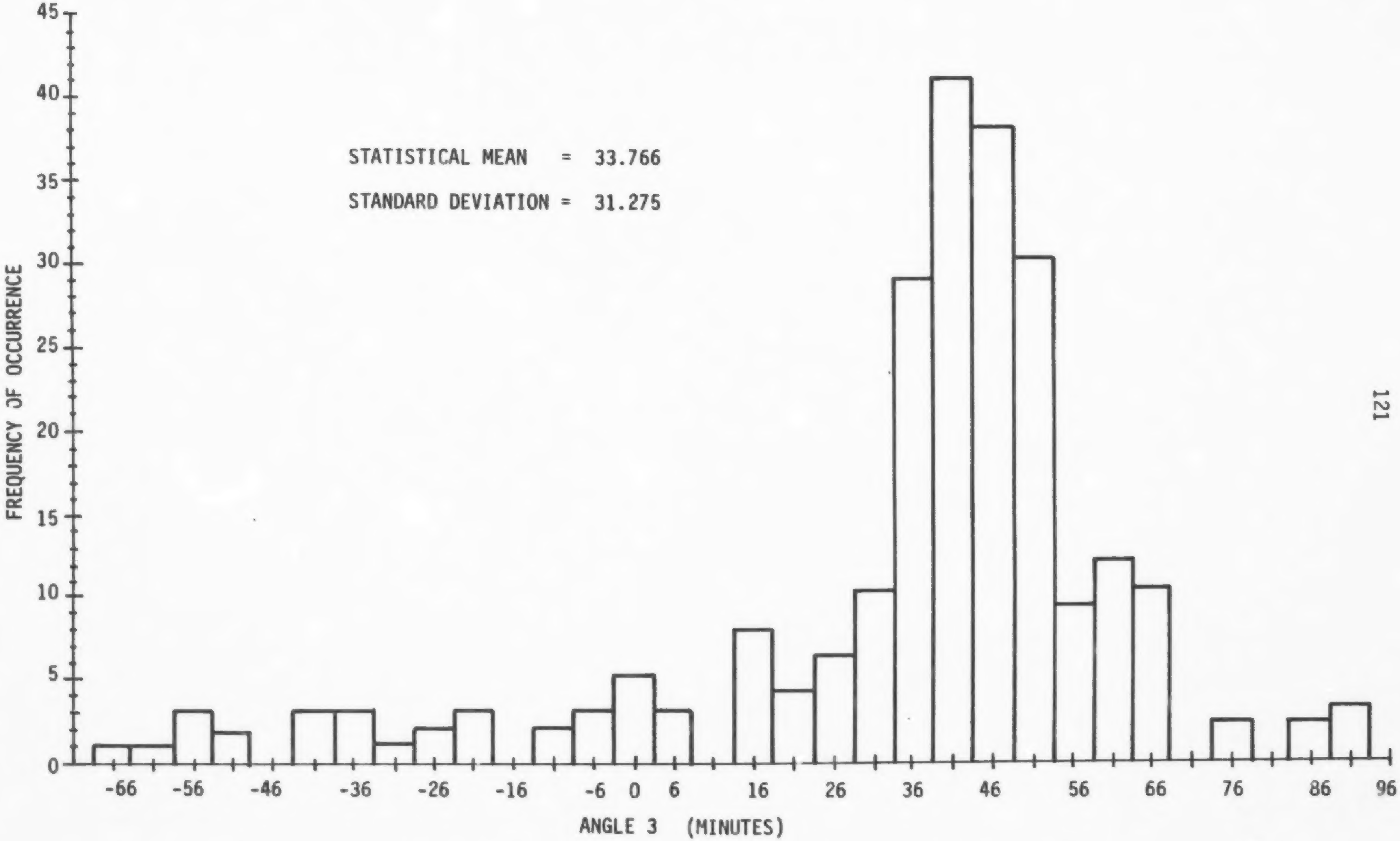

FIGURE 2: FREQUENCY BAR CHART FOR EASTBOUND RUNS (ANGLE 3)

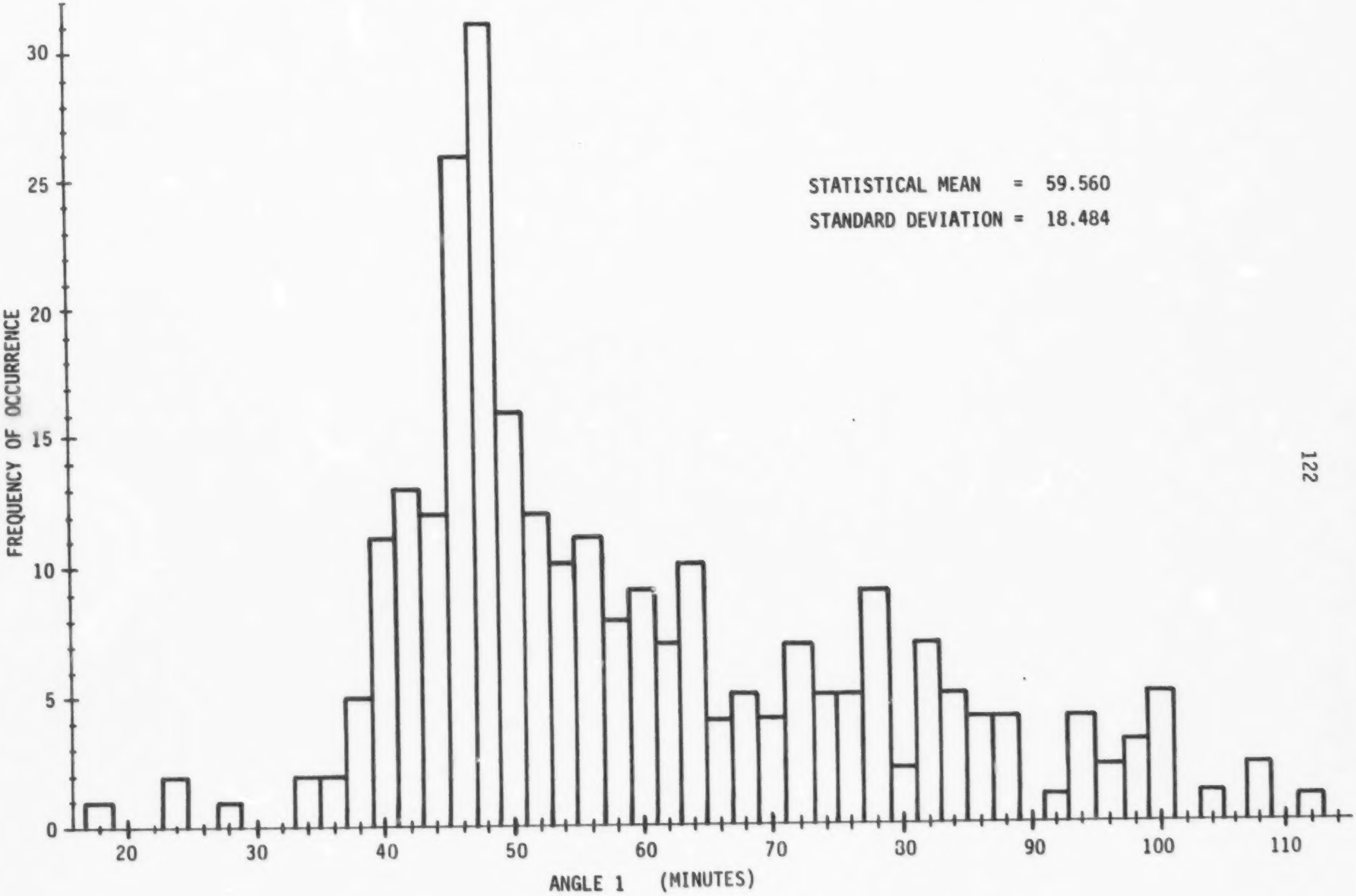

FIGURE 3: FREQUENCY BAR CHART FOR WESTBOUND RUNS (ANGLE 1)

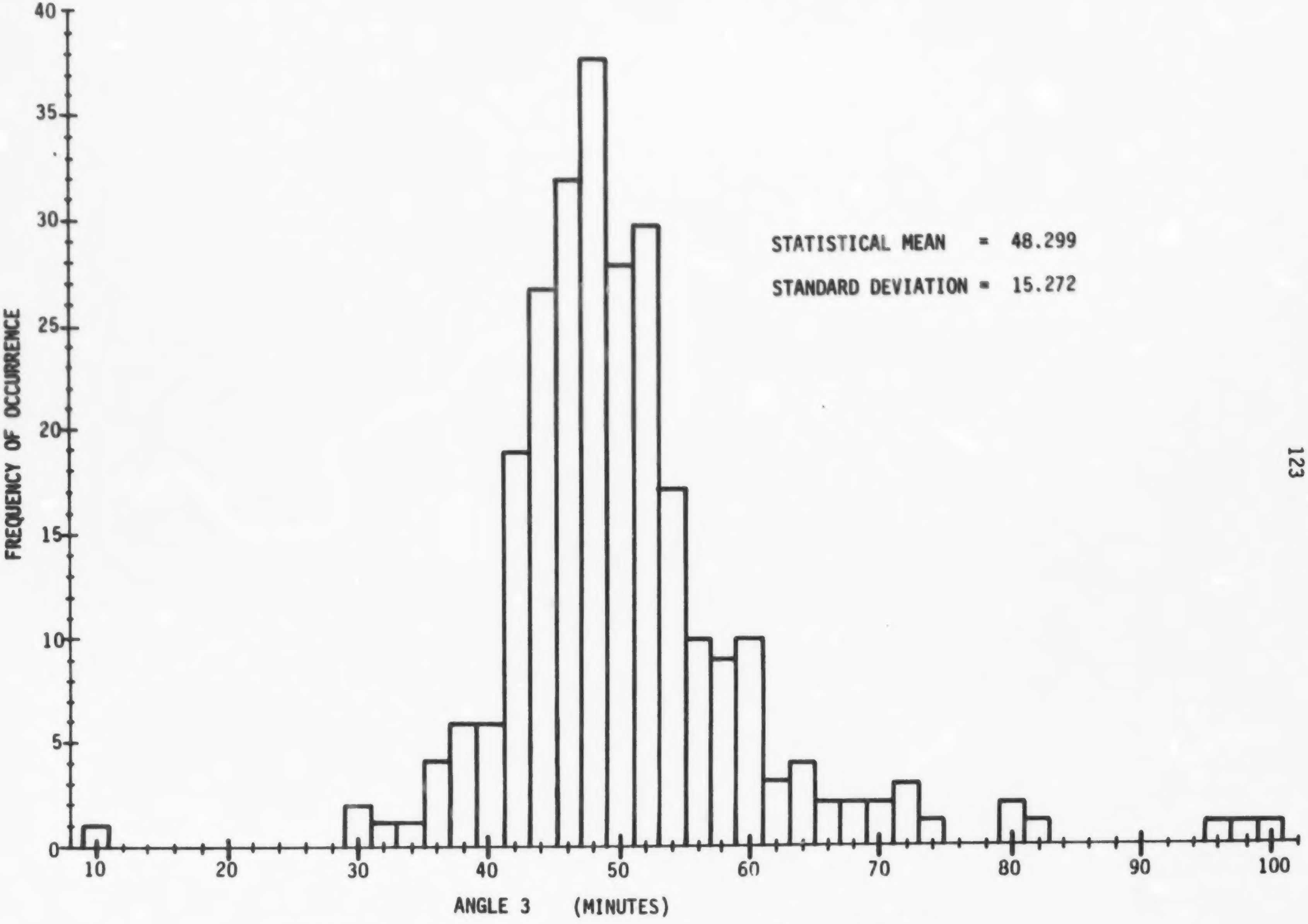

STATISTICAL MEAN = 48.299

STANDARD DEVIATION = 15.272

FIGURE 4: FREQUENCY BAR CHART FOR WESTBOUND RUNS (ANGLE 3)

ON THE PERFORMANCE OF THE EXPERIMENTAL BAINITIC CHROMIUM-MOLYBDENUM RAIL STEEL

I. Introduction

In 1973, the Research Department of Canadian Pacific initiated a study of rail metallurgy as part of its cost sharing track/train dynamics program with Transport Canada. The major objective of this study was to investigate routes that could lead to improvement in the operational life of rail steel in the Canadian traffic environment and conditions. To achieve this objective, many aspects related to the rail steel structure were explored in a preliminary work by Kalousek and Beynon (1). In this work it was concluded that rail life, all variables being constant, could be increased by refining both grain size and spacings between pearlite lamella - a conclusion that has been shared by several other authors (2-5). Several methods are known to achieve this type of refinement, such as heat treating the existing rail; alloying the rail steel with elements that control the grain size and lamella spacings; or, finally, by combining the heat treatment route with the alloying method. The different facets of each method were discussed in Ref (1) and for economic reasons the alloying method was selected as a practical route for Canadian Pacific to follow in its attempts to improve the rail steel structure. Commercially available alloyed rails, or those being experimentally investigated in the U.S., Europe, Japan and Australia at that time, 1975, were analyzed and compared (1). Out of these compositions, shown in Table 1, the chromium-molybdenum rail proposed by Climax Molybdenum Co. of Michigan appeared to be the most desirable for future premium alloyed rails.

Having selected the rail type, and in order to optimize the rail microstructure in gradual manner, it was suggested that three phases be followed in the refining of this microstructure: the first. is to obtain a rail with a subsurface structure having a hardness level of [illegible]0-360 BHN:

the second phase, to reach 360-380 BHN, while the last would aim for 380-450 BHN. To carry out the first phase, an ingot casting heat of Cr-Mo steel rolled into 132 lb/yd was produced by Algoma for Canadian Pacific in October 1975.

Realizing the difficulties associated with a new production, major problems were encountered due to an abnormal straightening pattern of the Cr-Mo rails during cooling on the hot bed. Some of the rails developed excessive curvature in the vertical or the lateral planes resulting in excessive camber or sweep limits. It was subsequently difficult to test this rail under field conditions due to the limited number of valid straight lengths from this heat. A series of laboratory tests was, however, carried out on this heat and its analysis was detailed in Ref. (6). A result of this analysis was that streaks of martensite and upper bainite, with different densities, were observed to be located at segregated regions in the center of the web of this rail. This form of streaks, shown in Figure 1a, could considerably reduce a fatigue crack initiation period in the segregated regions and thus effect the service life of the rail length.

In an effort to reduce such segregation and thus eliminate web streaks a second heat (9273B) of continuously cast Cr-Mo rail was made in early 1977. It was intended that this heat also fall into the phase I category; i.e. achieving a rail structure with a hardness level of 340-360 BHN. Metallurgical examinations of this heat showed, however, that the average head hardness of this heat was over 380 BHN. Furthermore, its microstructure was found to be dominantly bainitic*. Canadian Pacific, as well as many other railraods in the world, did not have previous experience with the use of bainitic steel in railways; therefore, the risk associated with testing such steel in the heavy haul line of the Pacific region, where a need for high hardness rail exists, could not be calculated. It was consequently decided that, in addition to laboratory testing, a field test using the track loop of the Facilitiy for Accelerated Service Testing (F.A.S.T.) in Pueblo, Colorado, should be carried out to estimate the wear and fatigue performance of the bainitic heat. A series of reports detailing the laboratory testing was published in 1979 and 1980, see Refs. (6 & 7). This report is a summarized description of the field test and its results.

---

*Bainite is a structure formed by relatively rapid cooling of austentite, consisting of needles of cementite and highly strained ferrite.

II. Field Tests on F.A.S.T.

II.1. Test Arrangements

In February 1978, 55 lengths of Cr-Mo(B)* arrived at the Transportation Test Center in Pueblo for the purpose of accelerated metallurgical service testing. To obtain preliminary data on the general performance of this bainitic rail two rails were placed on a tangent track of section 11 of the F.A.S.T. loop. During a period of 15 months the two rails accumulated 140 million growth tons (MGT) and were then removed in May 1979 due to bolt hole cracks in both and the occurrence of a transverse defect over one bolt hole in one of the rails. It was at that time suggested that the practice of rail-end-build-up, which was used with this rail alloy, was the reason for the rail end failures.

At the end of this test, the average head profile of the two rails was obtained and compared to the new rail. No evidence of surface wear was observed . This type of test, while not valid for estimating the performance of Cr-Mo(B) on curves, was regarded, however, as a basis for further testing of the rail on curved sections of the F.A.S.T. loop.

---

*Cr-Mo(B) will be used in the report to identify the Chromium-Molybdenum rail produced by Algoma as heat 9273B having a bainitic microstructure.

To install the remaining Cr-Mo(B) rails in the loop track, 53 rail lengths were welded at Burlington Northern welding plant in Pueblo. The welding cycle used in this operation is shown in Table 2 and compared to that established by Canadian Pacific by using the welding facilities of the Transcona welding plant. As a result of the welding process in Burlington Northern, high hardness measurements were found to exist at the top of the rail end surface. To avoid brittle steel characteristics at the weld regions, rail ends were tempered to modify this hardness level. Twenty of these rails, welded and tempered, were included in the third experimental metallurgy test which was underway in sections 3 and 17 of the F.A.S.T. loop.

The Cr-Mo(B) rails were placed in section 3 which has a 5° curvature, a 2% grade and a $\frac{1}{40}$ cant. Seven other different rail types, in addition to Cr-Mo(B), were to be tested in this section; all of these were 132 lb/yd. One of these rails was a chromium-molybdenum rail manufactured by CF&I and known as a weldable grade which requires no post heat cycles during welding; its chemistry is shown in Table 3 and is compared with Cr-Mo(B). Compositions of other rails tested in this experiment are also shown in the same Table. In section 3, the experimental test was designed so that rails of a given metallurgy were welded together while segments of different metallurgies were linked by mechanical joints. The layout of all test metallurgies in section 3 followed a tie number sequence as listed in Table 4.

In this experiment, which is detailed in an excellent paper by

R. Steele and R. Reiff (8), rails were subjected to programmed regimes of lubricated and dry conditions so that wear and metal flow in both regimes could be studied and compared. By early June 1980, the rails in section 3, including the 20 length of Cr-Mo(B), had accumulated 47 MGT during two cycles; one cycle (33 MGT) was carried out with unlubricated rails. At that time corrugations with random wave lengths were observed on the surface of some of some of the Cr-Mo(B) while others of the same rail had developed welded rail-end batter. To control this form of surface disturbance, rails were ground twice on a selective basis. In June 1981 the twenty lengths of Cr-Mo(B) were removed from the F.A.S.T. loop after an accumulation of 115 MGT, consisting of lubricated and dry cycles.

III. Wear Performance

The main parameter that was studied during the field tests of Cr-Mo(B) and other rails in F.A.S.T. was high rail curve wear (8). Wear measurement included gage face wear, head height and total head area loss. These measurements which were obtained using a "snap gage" of accuracy ±0.002 are illustrated in Fig. 1. For the Cr-Mo(B) these measurements were taken at intervals of approximately 2 months. Such measurements were compared each time with corresponding measurements taken on other rail metallurgies. These profile comparisons are shown in Figures 2 and 3. Furthermore, direct snap gage measurements vs. tonnage accumulations are shown in Figure 5 for Cr-Mo(B). From the aforementioned figures an average wear rate was calculated, and results are shown in Tables 5 and 6.

Hardness measurements of the running surface and gauge face of all tested rail for lubricated and dry regimes were obtained (8) and are shown in Table 7. Table 8 shows these hardness values as compared to those of

Cr-Mo(B). Furthermore, Figure 4 shows the gauge face wear rate in relation to the running surface hardness for rails tested in section 3.

From the analysis of wear data and hardness measurements of Cr-Mo(B), as summarized before, it could be concluded that Cr-Mo(B) rail performance in the dry regime was similar to most of the premium rails. However, in the lubricated regime, although its surface and gauge hardness were higher than all of the test rails with the exception of SiCr, its wear performance was virtually the same as the standard rail. Furthermore, when the wear rate was related to the gauge face hardness in both lubricated and dry conditions, the performance of Cr-Mo rail was the lowest among all premium rails.

IV. Welding Performance

As mentioned in the previous section, Cr-Mo(B) rails were welded at the Burlington Northern welding plant using what is described in Ref. (8) as a short delay practice and long delay practice. The difference in the two practices was the time delay introduced in the post heat cycles. The apparent difference between the two practices in the Heat Affected Zone (HAZ) of the Cr-Mo(B) rail was that the short delay practice can cause the distance between the HAZ boundaries at the running surface to be about twice as large as that produced by the long delay practice. Figure 5 shows the HAZ for a weld produced using the short delay practice. Surface hardness is obtained from the two practices as a function of distance from the weld bond line, shown in Figures 6 and 7.

When samples of this weld were metallurgically analyzed, their matrix structure was typical of that shown in Figures 6, 7 and 8 about which the following was concluded.

i) The microstructure of the head, mid-web and base included martinsite bands with a percentage of 20-40%.

ii) Knops hardness number of over 700 was measured on the martinsite bands which indicated the untempered martinsite.

In order to reduce the amount of martinsite and improve the high hardness values on the running surface of the weld, all Cr-Mo(B) welds were tempered, as mentioned before, by heating the rails to 1000°F for 20 minutes. In spite of this, some of the Cr-Mo(B) rails exhibited severe rail-end batter. A typical surface profile of the batter depth is shown in Figure 9. At 90 MGT the batter depth reached 0.09" and was expected to reach 0.15" by 150 MGT. To eliminate the effect of the surface batter, the Cr-Mo(B) was ground twice on a selective basis. Figure 10 shows the change in weld batter depth of Cr-Mo(B) from the first remedial grinding as compared to that of Cr.V rail in section 17 which was also ground twice. This indicates that no improvement had occurred in the rail end surface of Cr-Mo(B) after grinding, and the batter depth continued to increase as the amount of accumulated tonnage increased.

V. Conclusions

Data presented in this report, as detailed in Reference (8), concerning the performance of the bainitic chromium-molybdenum rail steel, with the specific composition shown in Table 1(b), indicates the following:

1. Under dry test conditions, wear characteristics of Cr-Mo(B) did not show any significant improvement when compared with different premium rails, a list of which is shown in Table 1(a)
2. Under lubricated conditions, wear characteristics of Cr-Mo(B) were comparable only to the standard carbon rail steel

3. Cr-Mo(B) requires a special flash butt welding cycle which involves long periods of preheat and postheat cycles. This makes the welding cycle longer and more expensive than any premium rail type. Furthermore, no success was achieved in obtaining a welding cycle for this rail that could be valid for service conditions.

The obvious conclusion is that the bainitic chromium-molybdenum steel (heat 9273B) cannot be viewed as a premium rail steel.

Last comment: Heat 9273B was intended to be a pearlitic rail steel with hardness values falling in the range of 340-360 BHN. It emerged, however, as a baintic rail with hardness values exceeding 400 BHN. This outcome indicates a less than adequate control of chemical composition and hardenability during the steel making process.

VI. References

1. Kalousek, J. and Beynon, G., "Rail Metallurgy", Canadian Pacific Report No. S497-75, July 1975.

2. Young, J.D., "The Manufacture of Improved Rail Steels", Iron and Steel Institute Meeting, London, November 23, 1972.

3. Heller, W., "The Development and Further Development of the Quality and Service Properties of Modern Rail Steels", ETR - Eisenbahntechnische Rundschau No. 1 and 2, 1971.

4. Manning, R.D., Reichhold, H.M., and Hodge. J.M., "A Peralite Hardenability Concept as a Bassis for Alloy Development." Transformation and Hardenability in Steels, Symposium, February, 1967.

5. Fowler, G.J. and Tetelman, A.S., "The Effect of Grain Boundary Ferrite on Fatigue Crack Propagation in Pearlitic Rail Steels", STP644, ASME, Philadelphia, 1978.

6. Ghonem, H. and Kalousek, J., "Development of High Strength Weldable Chromium-Molybdenum Rail", Canadian Pacific Report No. S571-78, 1978.

7. Kalousek, J., Parsons, D. and Ghonem, H., "Effects of Streaks on the Fracture Toughness of Chromium-Molybdenum Rail Steel", Canadian Pacific Report No. S651-80, 1980, Transport Canada Report No. TP2720.

8. Steele, R.K., "A Perspective Review of Rail Behaviour at the Facility for Accelerated Service Testing", FRA/TTC-81/07, June 1981. Also see Steele, R.K., and Reiff, R.P., "Rail: Its Behaviour and Relationship to Total System Wear", 1981.

MANUFACTURER	RAIL TYPE		U.T.S.		0.2% Y.S.		El	R.A.	HARDNESS
			ksi	MPa	ksi	MPa	%	%	BHN
	STANDARD AREA		134	924	74	510	11	30	255
BETHLEHEM STEEL	HEAT TREATED	FULLY HEAT TREATED	177	1,220	126	870	13	30	365
U.S. STEEL		HEAD HARDENED	183	1,260	132	910	12	33	380
NIPPON STEEL		HEAD HARDENED	165	1,140	120	830	17	50	360
NIPPON KOKAN		HEAD HARDENED	165	1,140	120	830	17	50	360
RUSSIAN		FULLY HEAT TREATED	181	1,250	119	820	14	40	380
CF&I	ALLOYED	Hi Si	142	980	75	520	11	14	285
BRITISH STEEL		Cr	164	1,130	100	690	11	17	325
ALGOMA		Cr	150	1,035	95	655	9	17	320
CF&I		Cr-Mo	181	1,250	124	855	12	20	365
KLOCKNER		Cr-Mo-V	166	1,145	102	703	12	20	325
SYDNEY		Mn-Cr-V	150	1,035	102	703	12	18	325
SYDNEY		Cr-Si-Nb	165	1,140	102	703	10	16	340
KRUPP		Cr-Si	165	1,140	98	676	12	20	315
THYSSEN		Cr-Si-V	164	1,130	99	683	12	20	320

Table: 1(a) Typical Tensile Properties and Hardness of Several Types of Rail

MANUFACTURER	RAIL TYPE		C	Mn	Si	Cr	Mo	V	Nb
	STANDARD AREA		.80	.90	.20	-	-	-	-
BETHLEHEM STEEL	HEAT TREATED	FULLY HEAT TREATED	.80	.90	.20	-	-	-	-
U.S. STEEL		HEAD HARDENED	.80	.90	.20	-	-	-	-
NIPPON STEEL		HEAD HARDENED	.65	.90	.20	-	-	-	-
NIPPON KOKAN		HEAD HARDENED	.65	.90	.20	-	-	-	-
RUSSIAN		FULLY HEAT TREATED	.75	.90	.30	-	-	-	-
CF&I	ALLOYED	Hi Si	.75	.80	.65	-	-	-	-
BRITISH STEEL		Cr	.75	1.25	.35	1.15	-	-	-
ALGOMA		Cr	.75	.65	.25	1.15	-	-	-
CF&I		Cr-Mo	.75	.90	.25	.8	.18	-	-
KLOCKNER		Cr-Mo-V	.65	.80	.30	1.00	.10	.10	-
SYDNEY		Mn-Cr-V	.70	1.65	.20	.30	-	.10	-
SYDNEY		Cr-Si-Nb	.70	1.10	.55	.80	-	-	.06
KRUPP		Cr-Si	.70	1.05	.75	1.00	-	-	-
AUG. THYSSEN		Cr-Si-V	.65	1.05	.60	1.15	-	.20	-

Table:1(b) Typical Chemical Composition of Several Types of Rails

A. Welding Cycle Performed at Burlington Northern Plant (December 1989 and February 1979)

Flash off
7 preheat cycles (7.5 seconds on, 2.5 seconds off)
Forging
10 postheat cycles (3 seconds on, 10 seconds off)
Shear

B. Welding Cycle Performed at Canadian Pacific's Transcona Welding Plant (March 1978)

Flash off
7 preheat cycles (2.5 seconds on, 1 second off)
Forging
10 postheat cycles (3 seconds on, 2 seconds off)
Shear

Table 2: Welding Cycles of Cr-Mo(B)

	Weight Percent Rail Type	C	Mn	P	S	Si	Cr	Mo	V
	Std	0.76	0.86	0.022	0.024	0.18	-	-	-
	FHT	0.81	0.93	0.018	0.041	0.20	-	-	-
	HH	0.77	0.83	0.021	0.030	0.17	-	-	-
	NHH	0.76	0.93	0.020	0.020	0.22	-	-	-
	SiCr(HH)	0.76	0.82	0.020	0.006	0.82	0.50	-	-
	SiMn(HH)	0.76	1.24	0.023	0.009	0.84	-	-	-
Different Manufacturer	1% Cr	0.71	0.73	0.014	0.021	0.27	1.16	-	-
	1% Cr	0.73	1.30	0.023	0.026	0.30	1.25	-	-
	1% Cr	0.75	0.88	0.030	0.027	0.23	0.95	-	-
	Cr V	0.67	1.15	0.009	0.013	0.34	1.11	-	0.110
	Cr V	0.72	1.72	0.014	0.030	0.22	1.04	-	0.087
	Cr-Mo(CF&I)	0.72	0.79	0.009	0.023	0.25	0.78	0.21	-
	Cr-Mo(B)	0.79	0.60	0.026	0.016	0.26	0.61	0.17	-

Table 3: Composition of Rails Tested in F.A.S.T. 3rd Metallurgical Experiment

Tie Position Rail Type	Outer Rail	Inner Rail
Std	→ 210	→ 220
HH	210-330	221-342
Cr-Mo(B)	330-450	342-464
Cr-Si	450-570	464-582
1% Cr(British)	572-724	582-734
Cr-Mo(CF&I)	724-843	734-855
HH	843-964	855-976
Std	964-1084	976-1096
FHT	1084-1205	1096-1216
HH	1205-1325	1216-1337
Std	1325-1446	1337-1457
Cr-Mo	1447-1567	1457-1577
Cr-Si	1567-1696	1578-1701
1% Cr(CF&I)	1696-1810	1701-1822
Cr-Mo(CF&I)	1810-1922	1822-1943
Std	1929-2049	1943-2063
HH	2064-2199	2063 →

Table 4: Rail Tested in Section 3 of F.A.S.T.
by Tie Number

	INCHES PER MGT			
SECTION 3	LUBRICATED	AVG	UNLUBRICATED	AVG
Standard				
Tie #110 to 200	0.0010	0.0010	0.0059	0.0066
Tie #977 to 1429	0.0009		0.0065	
Tie #1348 to 1429	0.0011		0.0069	
Tie #1955 to 2040	0.0011		0.0069	
Head Hardened (Std)				
Tie #220 to 314	0.0006	0.00075	0.0020	0.0023
Tie #865 to 954	0.0008		0.0024	
Tie #1217 to 1314	0.0007		0.0027	
Tie #2036 to 2177	0.0009		0.0021	
SiCr (HH)				
Tie #475 to 554	0.0007	0.00065	0.00160	0.0017
Tie #1591 to 1669	0.0006		0.00185	
1% Cr				
Tie #600 to 707	0.0006	0.00065	0.0027	0.0029
Tie #1716 to 1801	0.0007		0.0031	
CrMo (CF&I)				
Tie #751 to 830	0.0006	0.00065	0.0028	0.0029
Tie #1841 to 1919	0.0007		0.0031	
CrMo(B)				
Tie #354 to 428	0.0009	0.0009	0.0039	0.0036
Tie #1470 to 1544	0.0009		0.0036	
FHT				
Tie #1096 to 1190	0.0007		0.0031	

Table 5: Gauge Face Wear Rates of Rails in Section 3 of F.A.S.T. (8)

	Dry	Lubricated
Cr-Mo(B)	1.00	1.00
Std	1.1	1.83
HH	0.83	0.63
SiCr(HH)	0.72	0.47
1% Cr(BSC)	0.72	0.81
Cr-Mo(CF&I)	0.72	0.81
FHT	0.78	0.86

Table 6: Ratio of Rail Wear Rate to that of Cr-Mo(B) for All Tested Rails on Section 3 of F.A.S.T.

Metallurgy	Running Surface	Gage Face
Standard	324	314
Fully Heat Treated	366	386
Head Hardened (HH)	355	381
Silicon Chrome (SiCr(HH))	391	405
Cr-Mo(CF&I)	344	353
Cr-Mo(B)	383	398
Chrome Vanadium	372	365
1% Chrome (BSC)	348	353

Table 7: Hardness Measurements (BHN) on the Surface and the Gauge Face of Tested Rails

Metallurgy	Running Surface Ratio	Gage Face Ratio
Cr-Mo(B)	1.00	1.00
Standard	0.85	0.79
Fully Heat Treated	0.95	0.97
Head Hardened	0.93	0.96
Silicon Chrome	1.02	1.02
Cr-Mo(CF&I)	0.90	0.89
Chrome Vanadium	0.97	0.92
1% Cr	0.91	0.89

Table 8: Ratio of Hardness Measurements of Tested Rails to that of Cr-Mo(B)

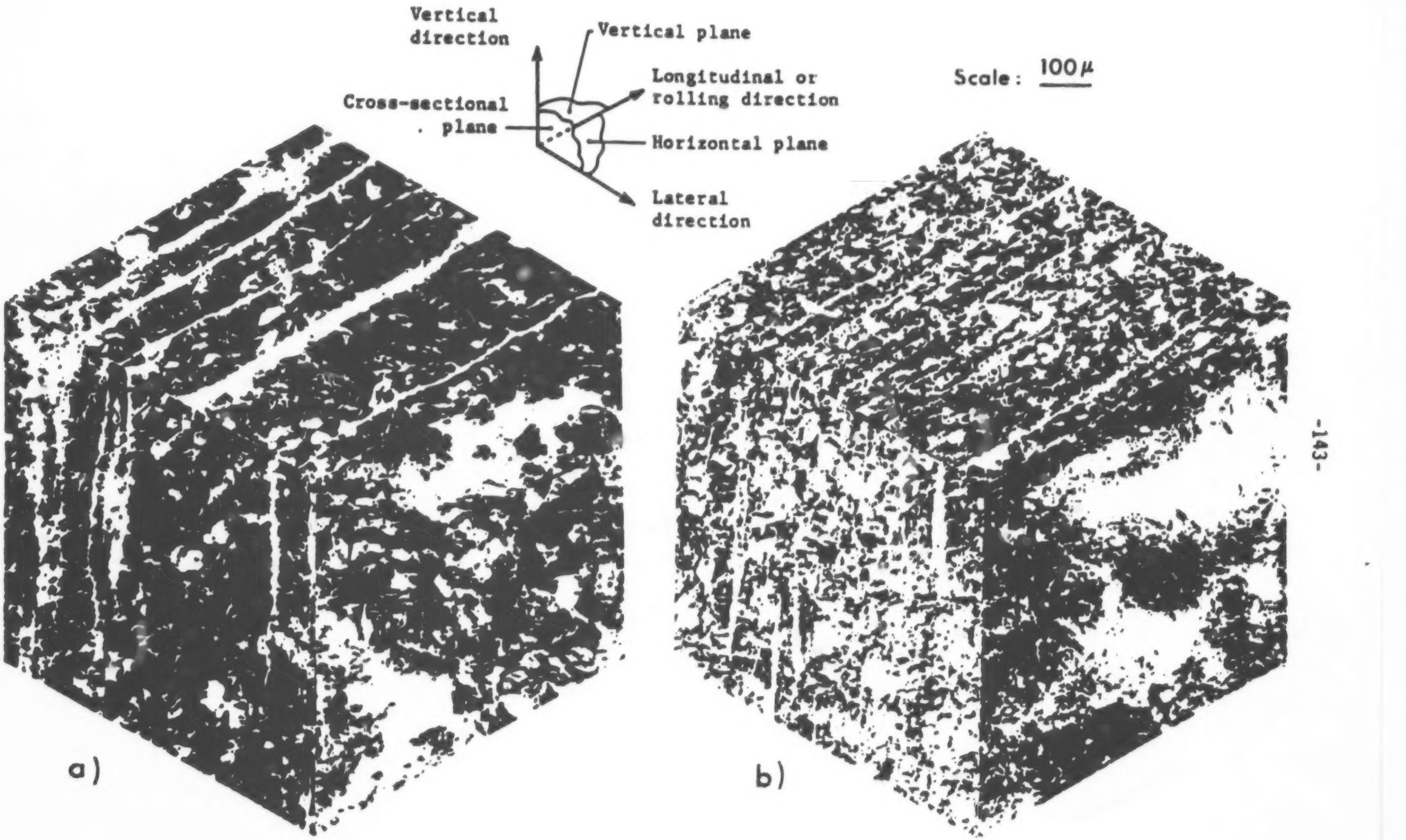
Vertical direction
Vertical plane
Longitudinal or rolling direction
Cross-sectional plane
Horizontal plane
Lateral direction
Scale: 100μ
a)
b)

Figure 1a: Microstructure of Cr-Mo Web Material, on the Three Processing Planes Depicting the Shape of 'Streaks' a) Cr-Mo I (C5599) b) Cr-Mo II (9237B)

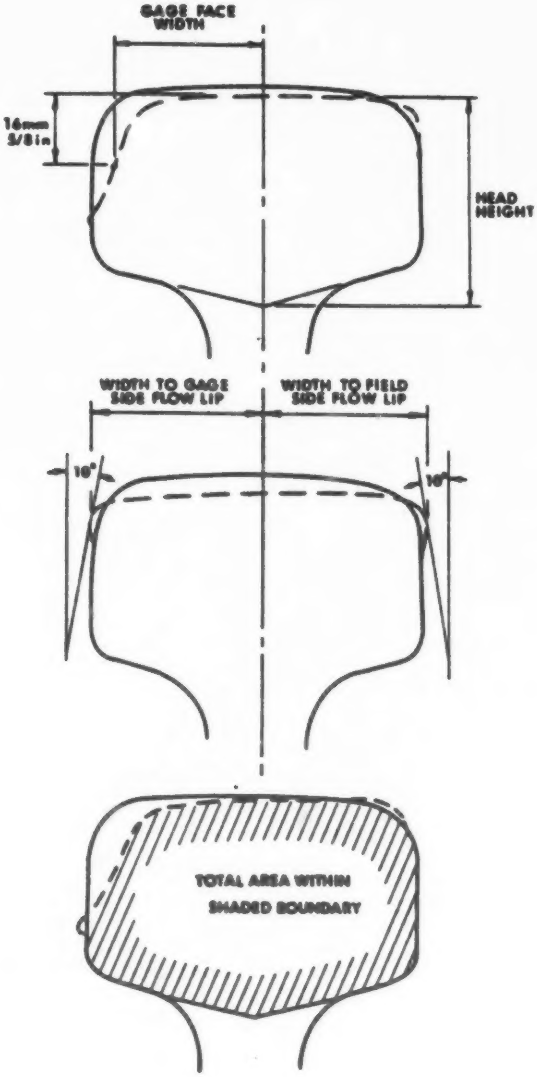
GAGE FACE WIDTH
16mm
5/8in
HEAD HEIGHT
WIDTH TO GAGE SIDE FLOW LIP
WIDTH TO FIELD SIDE FLOW LIP
10°
10°
TOTAL AREA WITHIN SHADED BOUNDARY

Figure 1: "Snap Gage" Measurements on the Rail Head (8)

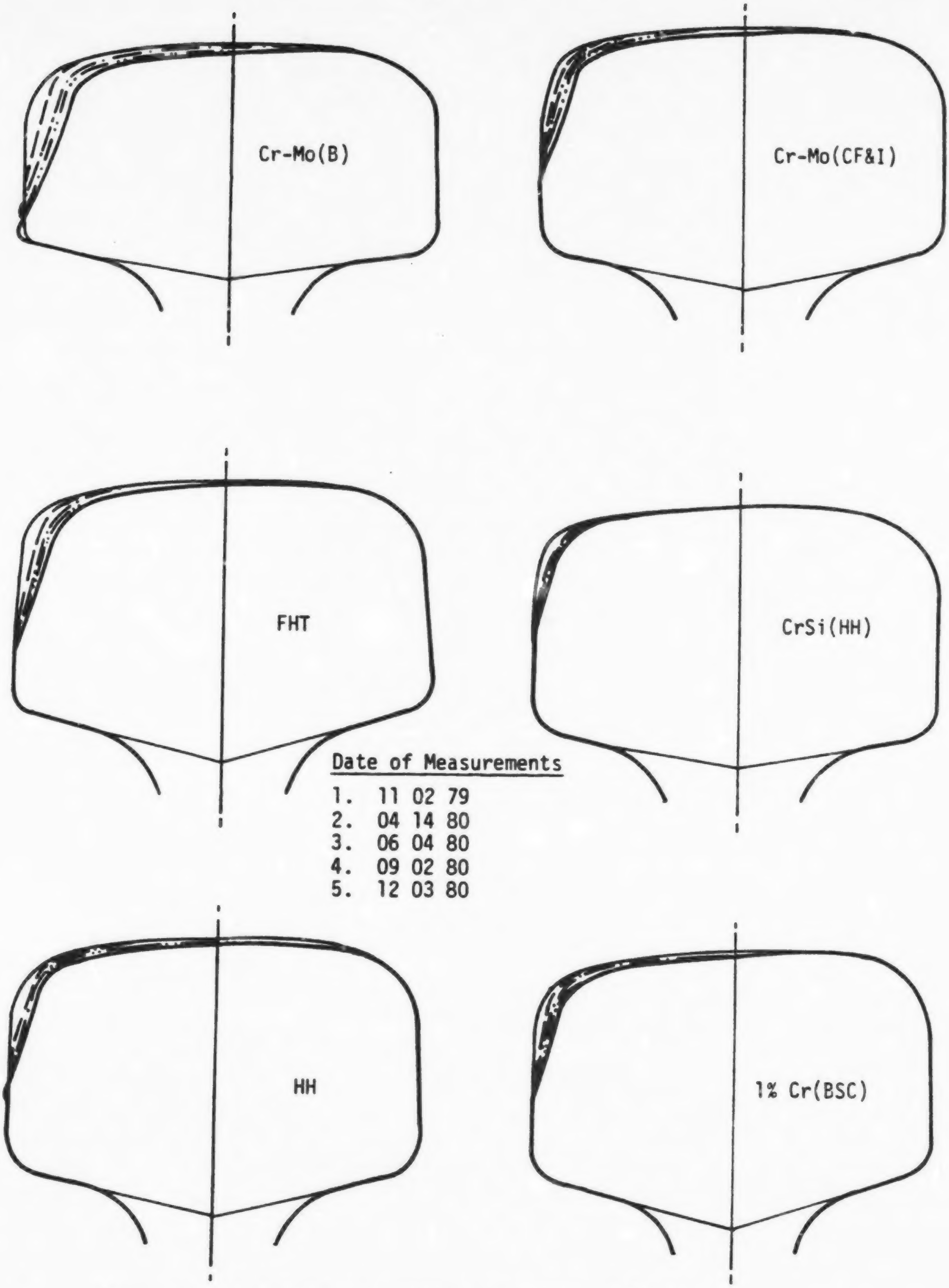
Cr-Mo(B)
Cr-Mo(CF&I)
FHT
CrSi(HH)
Date of Measurements
1. 11 02 79
2. 04 14 80
3. 06 04 80
4. 09 02 80
5. 12 03 80
HH
1% Cr(BSC)

Figure 2: Comparison of Tested Rails Head Profile

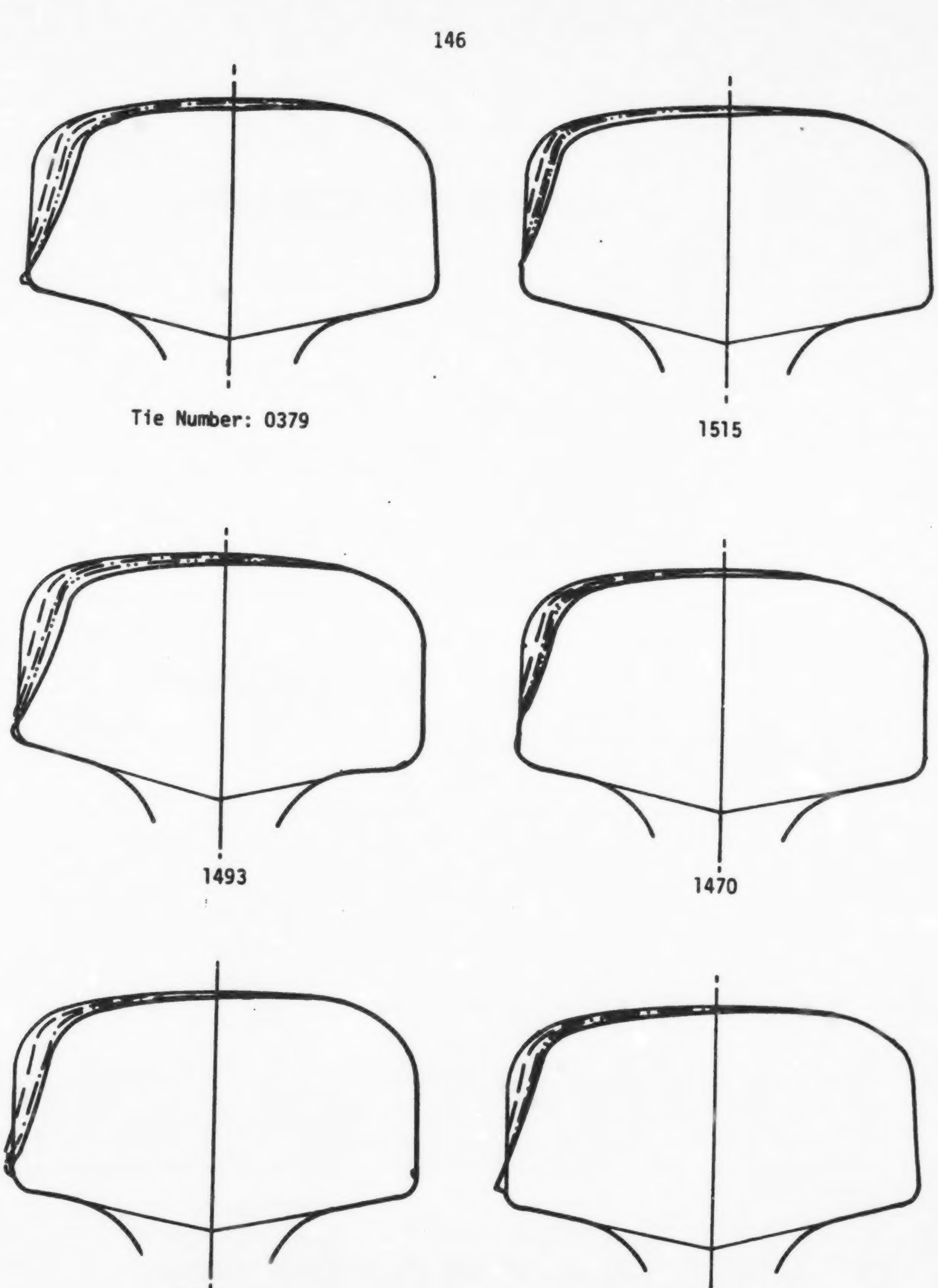

Tie Number: 0379

1515

1493

1470

0354

1538

Figure 3: Comparison of Cr-Mo(B) Rail Head Profile at Different Tie Positions on Section 3 of F.A.S.T.

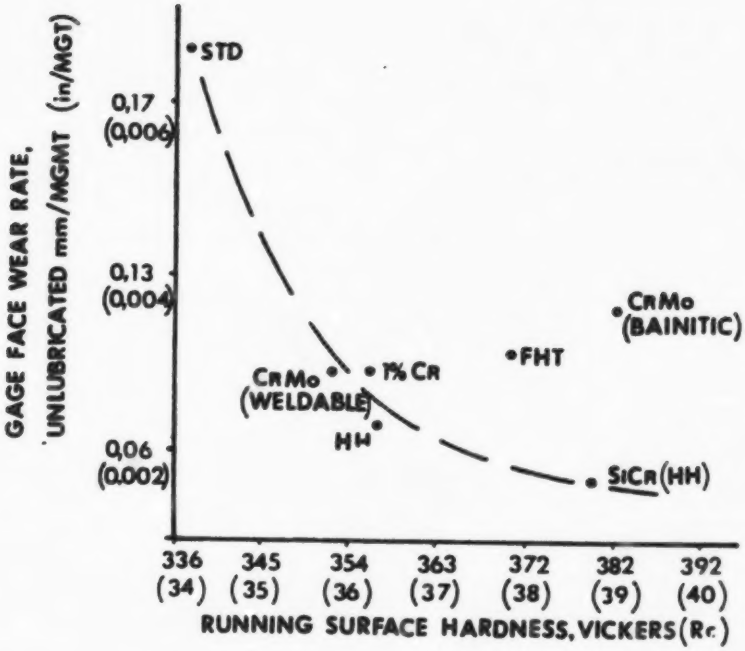

Figure 4: Gauge Face Wear Rate in Relation to the Running Surface Hardness

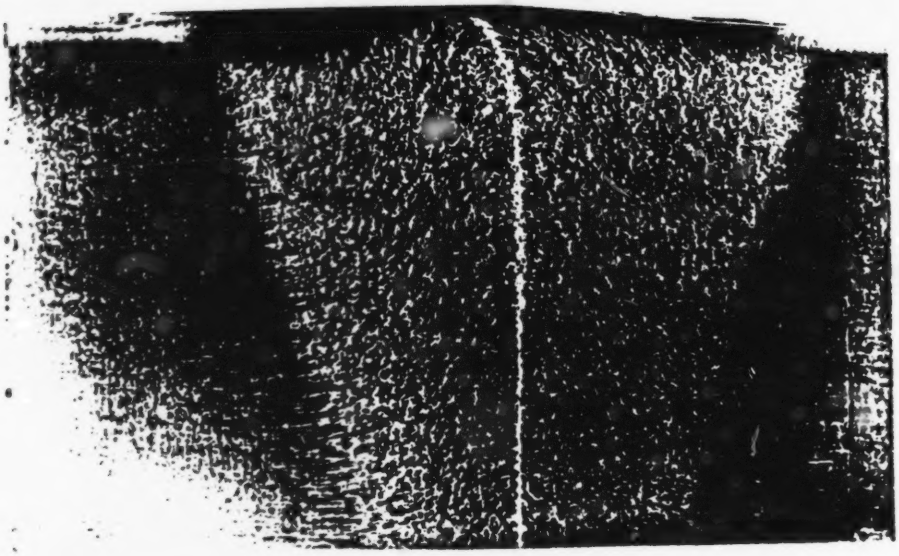

Fig. 5(a) Heat Affected Zone for Short Delay Welding Practice.

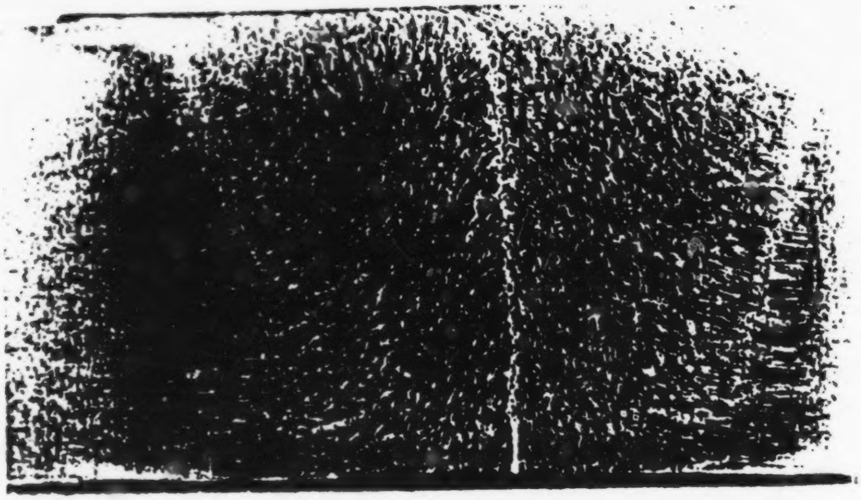

Fig. 5(b) Heat Affected Zone for Long Delay Welding Practice

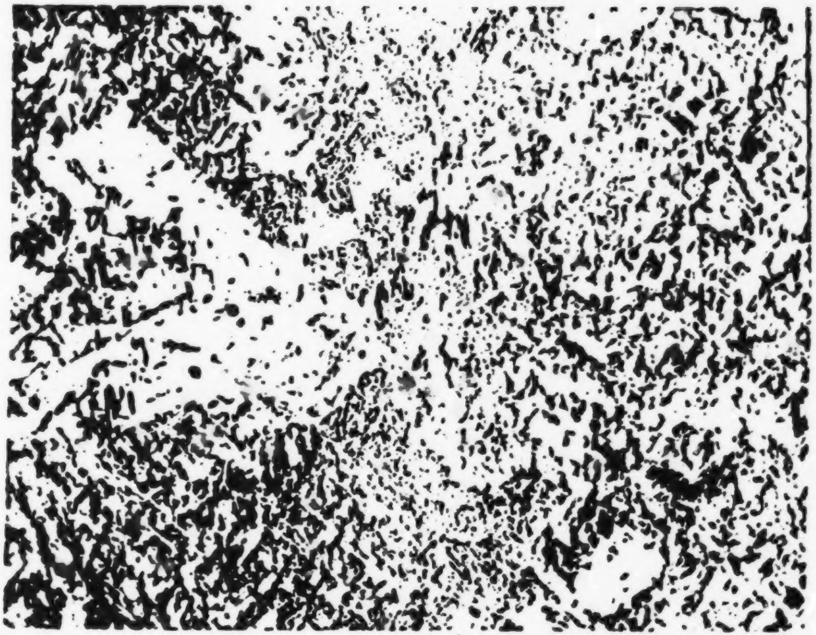

Figure 6: Microstructure of a Welded Base Section

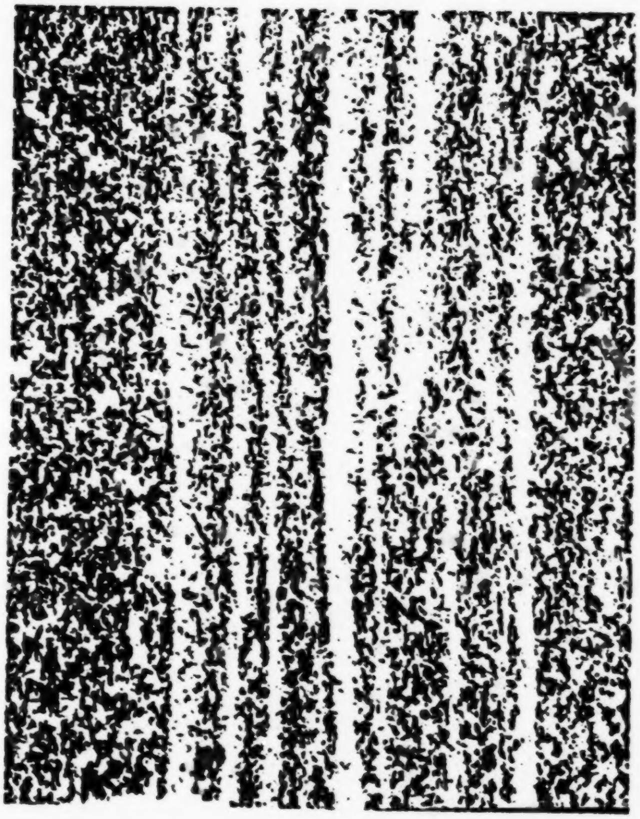

Figure 7: Microstructure of a Welded Head Section

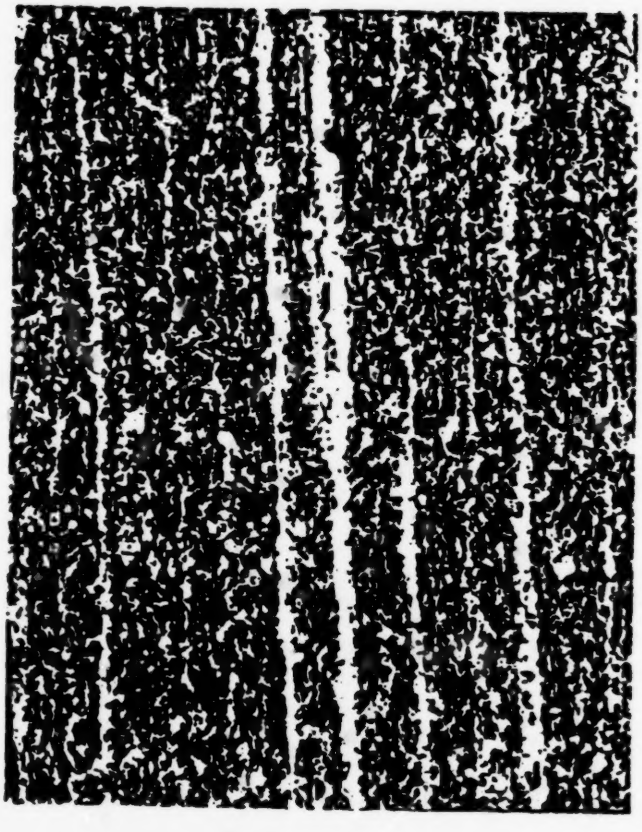

Figure 8: Microstructure of a
Welded Base Section

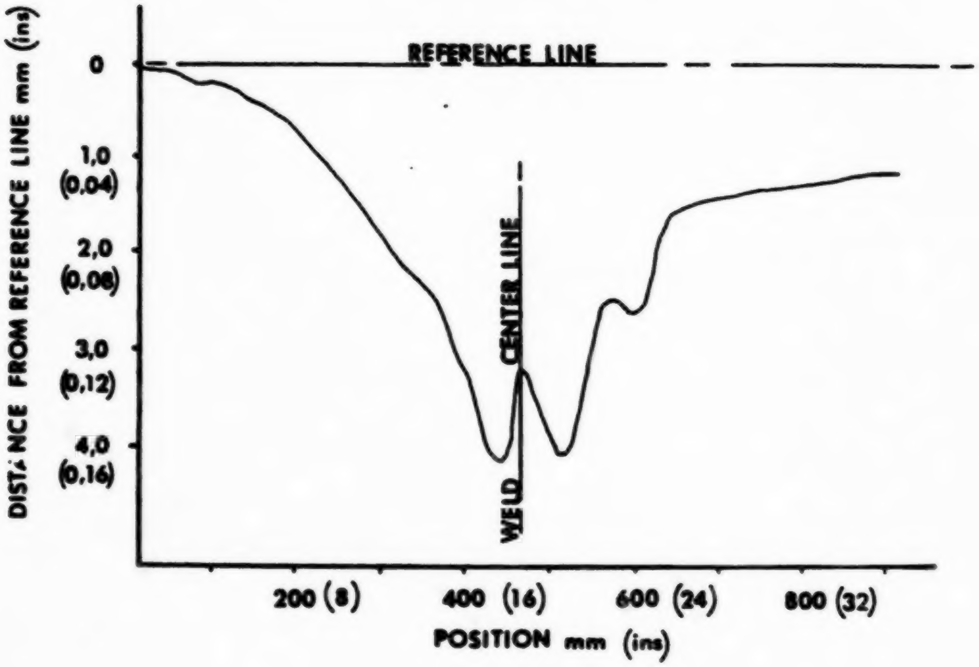

Figure 9: A Typical Surface Profile of the Batter Depth for Cr-Mo(B)

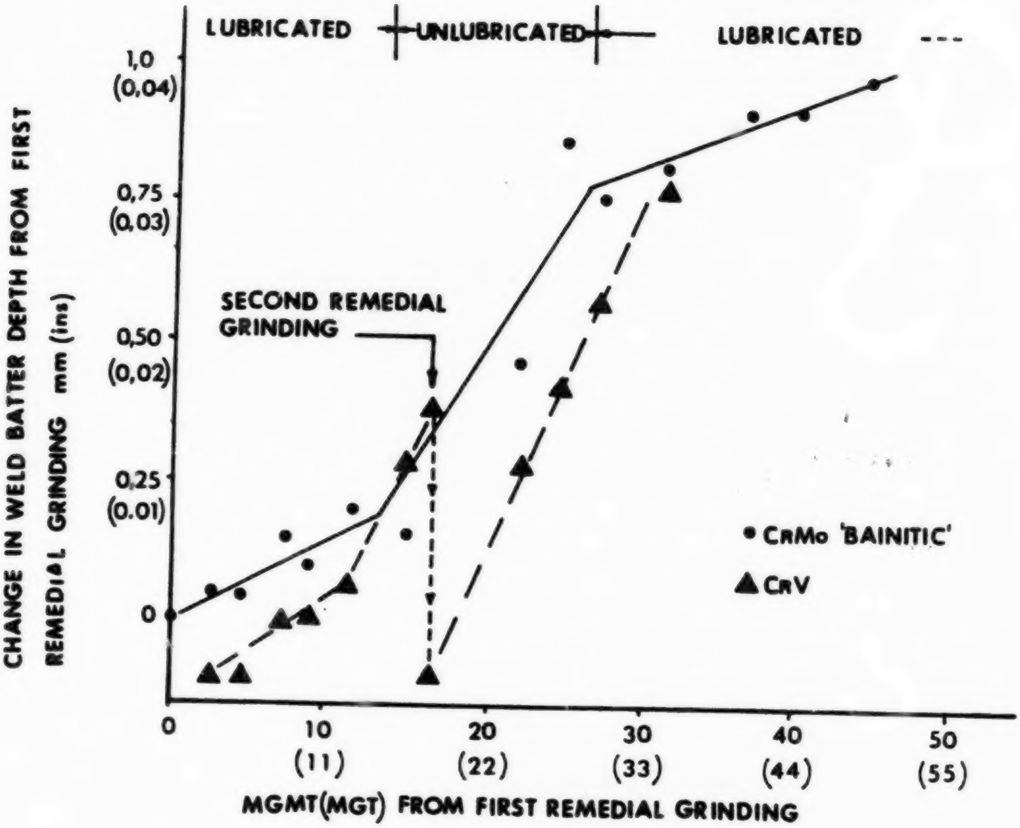

Figure 10: Changes in Weld Batter Depth of Cr-Mo(B) From the First Remedial Grinding as Compared to that of Cr-V Rail in Section 17 of F.A.S.T.

CONCEPT OF A PROFILOMETER FOR RAIL WEAR DETERMINATION

Abstract

The objective of this report is to document the development of a concept for a rail (wheel) profilometer capable of measuring a large number of profiles on-site, with sufficient precision to meet the requirements for accurate wear determination.

The "floating" profilometer concept proposed in the report uses contour features of the unworn regions of the rail (wheel) head profile as reference points to eliminate referencing concerns. Digitizing profile image measurements permits automatic processing of results. The most important element of the "floating" profilometer concept is a process whereby successive profiles are matched for wear determination. The investigation demonstrated that this process can be accomplished with no loss of accuracy. A supplementary software package analyzes the data and reports the results in a format convenient for further analysis.

Résumé

L'objectif de ce rapport consiste à rendre compte des travaux de recherche sur le concept d'un profilomètre de rails qui pourrait mesurer un grand nombre de profils de roues avec une précision suffisante pour rencontrer les exigences d'une détermination exacte de l'usure.

Le concept du profilomètre à montage souple, proposé dans le rapport, utilise les éléments du contour des profils non usés des rails comme points de références pour éliminer les problèmes de leur concordance. Les données par l'affichage numérique de l'exactitude des profils permettent le traitement automatique des calculs. L'élément le plus important du concept d'un profilomètre à montage souple est un procédé au moyen duquel les profils successifs sont comparés pour déterminer l'usure. Cette étude a démontré que ce concept peut être employé sous aucune perte d'exactitude. Un ensemble supplémentaire de logiciels analyse les données et donne un compte rendu des conclusions dans une présentation propice à des analyses ultérieures.

Acknowledgements

The authors would like to thank a colleague, W. Pak, for his insight and constructive contributions during the course of the work.

1. Introduction

Rail wear is a subject which is receiving much attention at the present time. Excessive rail wear results in frequent rail replacement and hence high costs. It is desired to obtain information about the characteristics of rail wear under different track conditions (heavy traffic, braking processes, curves, grades, etc.) for different rail steel materials. Therefore, there is a need for development of a rail profilometer capable of measuring rail head transverse profiles on-site, for a large number of samples, with precision conforming to the requirements of accurate rail wear determination.

For the collection of useful wear data, any measurement system in use must provide:

1. high accuracy, so that reliable wear results can be determined after a minimum amount of traffic;
2. ease and speed of measurements, so that many profiles can be gathered in reasonable time, thus making the sample size closer to the population size and improving the accuracy of the mean wear estimates;
3. flexibility, to allow measurements of various rail types and large amounts of wear;
4. weather resistance and robustness, for the proper operation of the profilometer in the field.

There are many methods which have been used in the past to measure the transverse profile of a rail head or wheel tread. Common to all profilometers which are used to collect rail/wheel wear data is the problem of referencing. Some sort of reference is needed so that profiles at the same location measured after different amounts of traffic, can be matched together and the corresponding wear compared. It is this reference which limits the overall accuracy of any profilometer.

Profile measurements with pantograph tracing machines (such as the French Geismar Rail Profile Plotting Device and the Japanese Yoshidaseiki Rail Section Gauge) use graphical profile images, whereby measured rail profiles are matched by eye. Therefore, the accuracy expected for wear detection cannot be achieved.

Another way of profile matching is to insure that the profilometer is mounted in exactly the same position with respect to the rail/wheel head when the measurements are being taken. This normally is done by using surfaces of the rail (wheel) not affected by wear as datum or reference surfaces. Experience with the wheel profilometer developed by CP Research which uses this type of mechanical reference system has shown that it is not wholly satisfactory for automatic processing of collected data. This is because the initial accuracy of the reference surface is less than the accuracy required to detect small amount of wear.

One way to improve the accuracy of both the graphical matching and mechanical reference systems mentioned thus far is to provide machined datum surfaces or witness grooves somewhere on the unworn surfaces. The Swedish YMS system uses machined notches for graphical matching. The CN profilometer uses machined witness grooves for alignment in a consistent position. Despite the advantages, machining reference features into a rail/wheel head is not desirable because it involves chaning the rail shape and introduces another factor into the wear process. Also, alignment of the profilometer against these references in the field usually consumes time and may create additional difficulties in operation.

Because of the questions concerning accuracy, speed, referencing, etc., none of the existing profilometers satisfies all the requirements of wear measurements.

This report presents a concept for a rail profilometer which uses an alternative approach for wear measurements. Also presented is a series of computer programs for data analysis, which demonstrate the viability of the profilometer concept.

2. Floating Profilometer Concept

The problem of referencing rail profiles to allow comparison is the main obstacle in the way of accurate wear determination. In order to help solve this problem, a so-called "floating profilometer" is proposed, which uses contour features of the unworn regions of the rail head profile itself as reference points. As the rail wears down, some regions of the profile remain unaffected - these stable features can be matched up to align the profiles together and in this way compare wear directly. Because referencing concerns are eliminated during the actual profile measurements, the alignment of the profilometer with respect to the rail head is not important, thus the term "floating" is used to describe the concept. In effect, this concept applies the manual graphical matching technique (used with the pantograph profile measurements) to an automated measurement system. This retains most of the advantages of the simple graphical method while increasing its speed and accuracy.

In order to test the viability of the floating profilometer concept, it was necessary to establish a theoretical model of the rail head/profilometer system. One initial consideration was the shape of the rail head profile. The rail head bottom or fillet region remains unworn, even after a large amount of traffic. The field side of the rail head, and to a lesser degree the gauge side, retain some of their original profile until the accumulative tonnage of traffic is large (see Figure 1). These above mentioned surfaces are therefore available for use as reference features for the profile matching and wear determination process. The profilometer must have the capability to measure the sides and bottom of the rail head in addition to the crown, if the reference features are to be used.

A possible profilometer configuration, and the one which was chosen for consideration in this report, consists of three straight slide carriage assemblies equipped with a stylus to trace the rail profile. Each slide

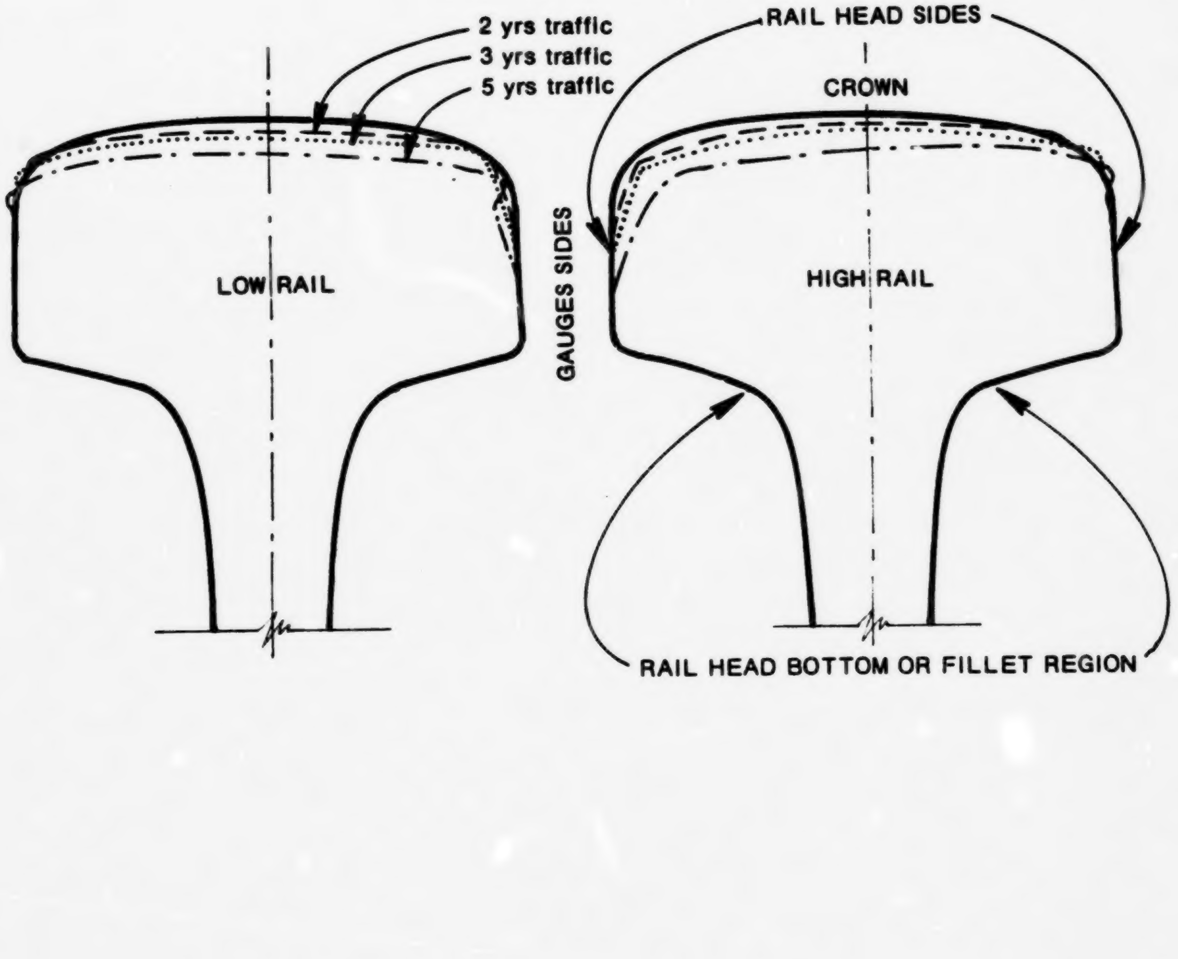
2 yrs traffic
3 yrs traffic
5 yrs traffic
LOW RAIL
GAUGES SIDES
RAIL HEAD SIDES
CROWN
HIGH RAIL
RAIL HEAD BOTTOM OR FILLET REGION

Figure 1. Typical Rail Wear Profiles

produces XY coordinate data of the profile in its own cartesian coordinate frame. The orientations of the slides must be chosen to maximize the resolution of the profile measurements by remaining as close to parallel with the rail profile contours as possible. At the same time, the profilometer must be allowed to slip on and off the rail head without disassembly. A profilometer of this sort produces three independent data sets for each rail profile, each data set consisting of the coordinate data from a single slide (see Figure 2).

In order for the profile data to be useful, it must be transformed such that all the coordinates refer to a single fixed cartesian frame of reference. Once this has been done, it is possible to "normalize" the profile. Normalizing the profile is the process whereby each profile is positioned in the same place in the fixed cartesian frame. The choice of this "normal position" with respect to the cartesian axes is arbitrary and a matter of convenience, as long as it is consistent for all profiles. This process of positioning the profiles accomplishes the matching required for wear determination (see Figure 3). The unworn reference features on the rail profile are needed to perform the normalization. By comparing the positions of the reference features on the measured profiles with the desired normal values, the translations and rotations necessary to normalize the profile can be deduced.

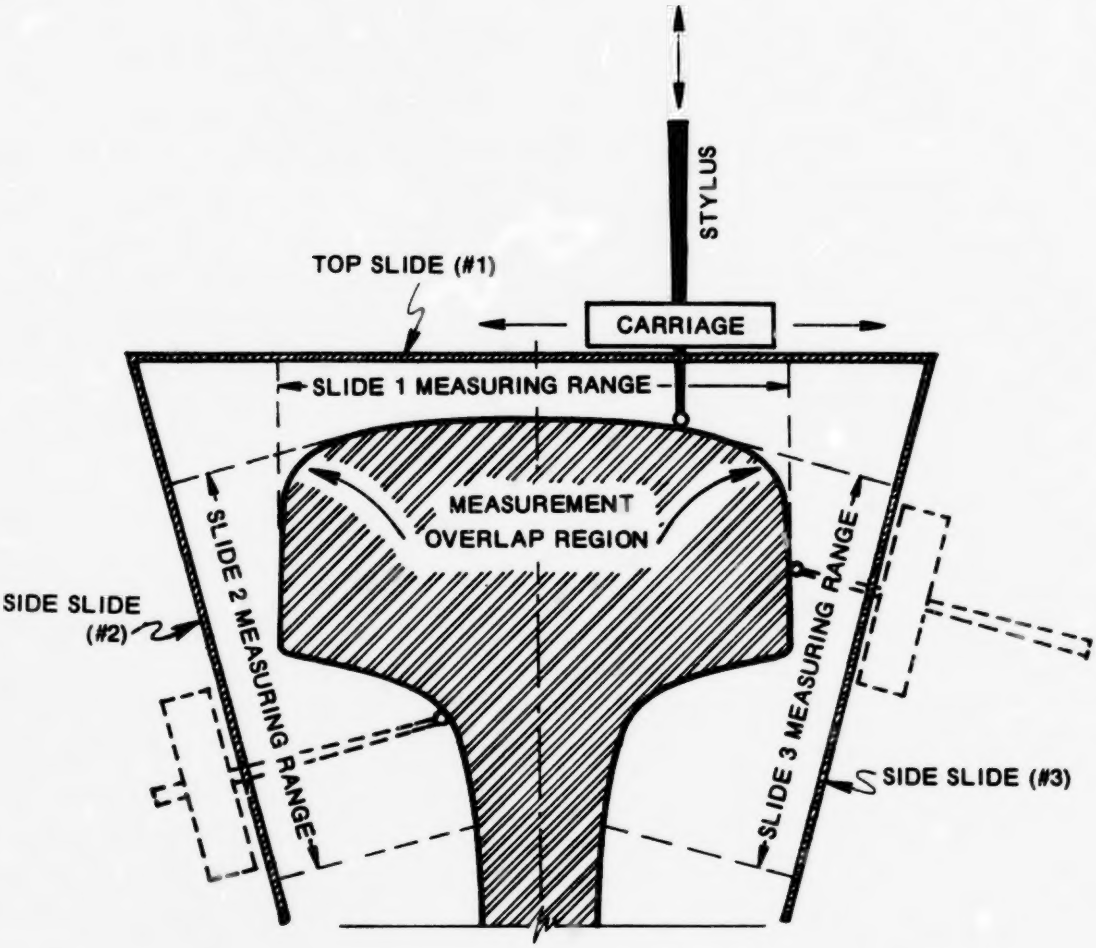
STYLUS
TOP SLIDE (#1)
CARRIAGE
SLIDE 1 MEASURING RANGE
MEASUREMENT OVERLAP REGION
SIDE SLIDE (#2)
SLIDE 2 MEASURING RANGE
SLIDE 3 MEASURING RANGE
SIDE SLIDE (#3)

Figure 2. Likely General Configuration of Profilometer

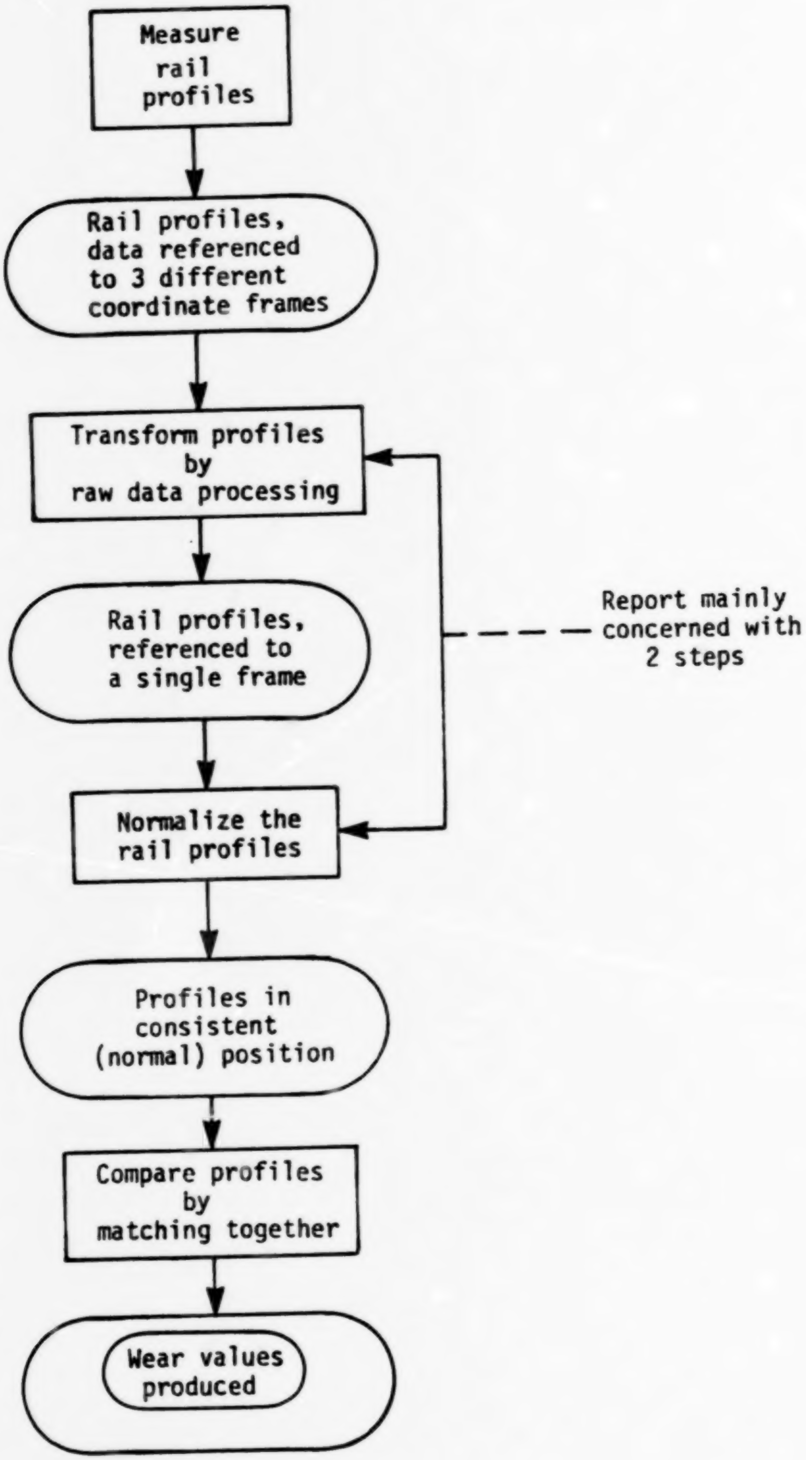
Measure rail profiles
Rail profiles, data referenced to 3 different coordinate frames
Transform profiles by raw data processing
Rail profiles, referenced to a single frame
Report mainly concerned with 2 steps
Normalize the rail profiles
Profiles in consistent (normal) position
Compare profiles by matching together
Wear values produced

Figure 3. General Strategy for Wear Determination

3. Data Analysis Algorithms

3.1 Test Data Generation

To test both the profilometer concept and the data analysis algorithms, some representative data was needed. The simplest way to generate this data was to measure it from a blue-print of the new 136 RE rail transverse profile. The chosen configuration of 3 slide axes was drawn around the rail, as if the profilometer was sitting on the rail head. Using a drafting table, the perpendicular distance from each slide axis to the profile was measured (Y distance), at even intervals along the slide axis (X direction). This produces 3 data sets for each profile, which simulates the output data from the proposed profilometer. It was found that X intervals of 1 mm. provided sufficient resolution to produce an adequate representation of the profile (see Figure 4).

Two profile data files were created: a "straight" profile, where the profilometer was centered and straight on the rail (normal); a "misaligned" profile, where the profilometer was deliberately offset and tilted from the normal position. When these two profiles are processed by a successful normalization algorithm, the straight profile will not be moved, because it is already in the normal position, but the misaligned profile will be moved to the normal position, and the 2 profiles will match exactly. This is a check on the viability of any normalization technique.

3.2 Raw Data Processing

The first data analysis task is to transform the rail profile raw data taken from the measurements, which is given in three separate slide coordinate frames, to a single common cartesian coordinate frame. This is simply a matter of using some trigonometric transformations which depend on the geometric configuration of the profilometer slides. If the coordinates XX and YY represent the single fixed coordinate system and the coordinates X and Y represent the local slide coordinate system, then the transformations are as follows:

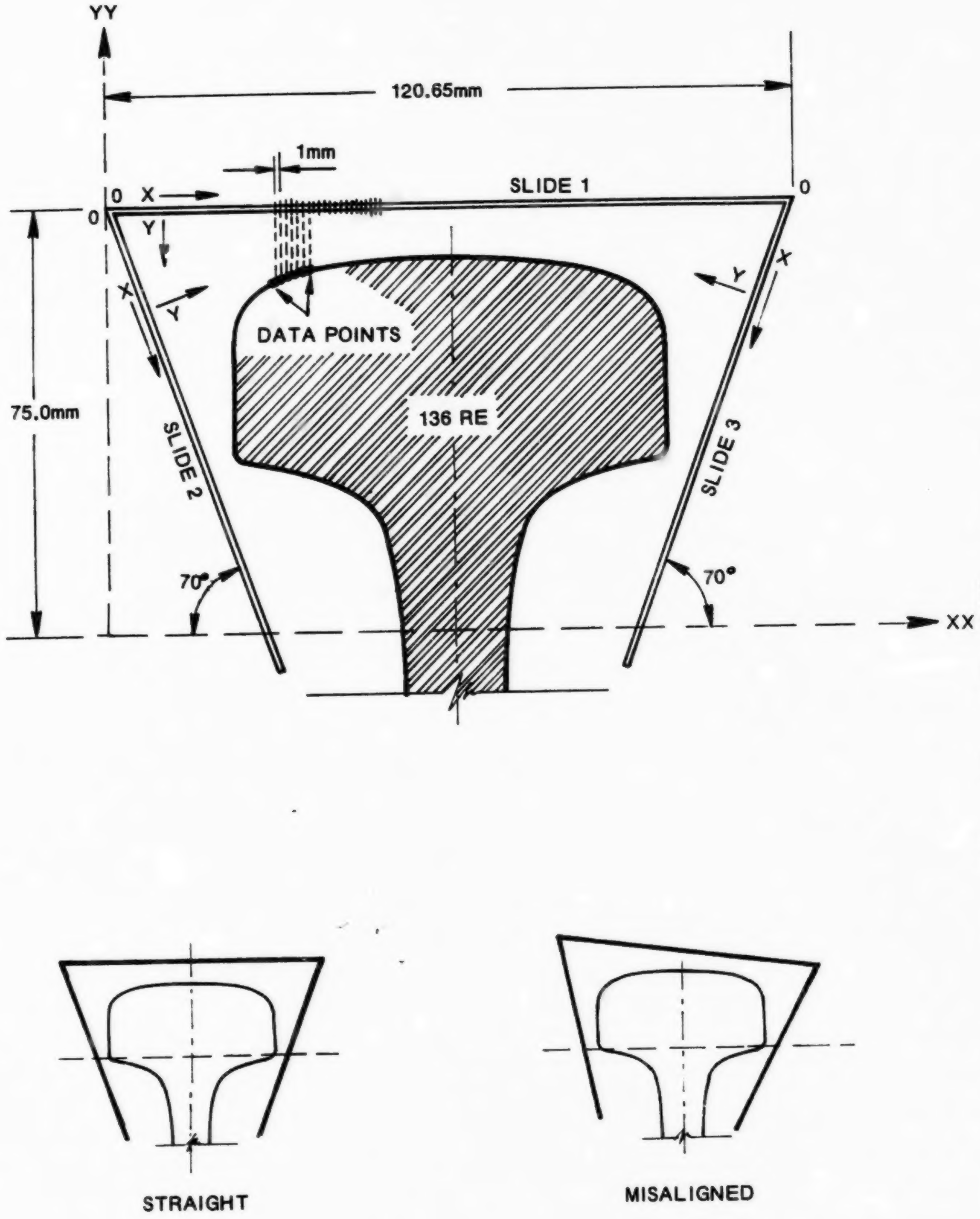
YY
120.65mm
1mm
0
X
SLIDE 1
0
0
Y
X
Y
DATA POINTS
Y
X
75.0mm
136 RE
SLIDE 2
SLIDE 3
70°
70°
XX
STRAIGHT
MISALIGNED

Figure 4. Test Data Generation Set Up

For slide 1 (top slide) XX = X
YY = YHGHT - Y
For slide 2 (side slide) XX = X · SIN (THETA2)+Y·COS(THETA2)+DX2
YY = YHGHT+Y·SIN(THETA2)-X·COS(THETA)+DY2
For slide 3 (side slide) XX = XLEN-X·SIN(THETA3)-Y·COS(THETA3)+DX3
YY = YHGHT+Y·SIN(THETA3)-X·COS(THETA3)+DY3

where YHGHT,XLEN,DX2,DY2,DX3,DY3,THETA2,THETA3 are physical parameters of the profilometer (see Figure 5).

During later data analysis it is useful to have the coordinates of the points on the profile closest to each of the three slides. Before the above-mentioned transformations are done, the Y values are searched to find the point of minimum Y for each slide (see Figure 6).

3.3 Normalization

When the profilometer is mounted on the rail head, there are six possible types of misalignment which would cause the measured profile to deviate from the normal position in the fixed cartesian frame (see Figure 7). The Z direction represents the location along the rail chosen for the profile measurements and does not have a normal position, therefore it does not concern the normalization process. The X and Y rotations (pitch and yaw) have their effect out of the plane of the transverse profile, thus affect the profile by projections of the rotation on the XY plane - these misalignments are of lesser importance and will be considered later in the report. The normalization process will be concerned mainly with X and Y offset, and Z rotation, because they exert the most powerful influence on the profile measurements.

The easiest reference features on the profile to recognize and use are points and straight lines, because of their simplicity of zero and one dimension respectively. The coordinates of a point can give information about X and Y offset, and the orientation of a line can supply rotation information. On the unworn portions of a rail head profile, four line segments and three points of their intersection are available for use (see Figure 8). Many different normalization algorithms are possible using different numbers of reference lines and points, and different ways of locating them.

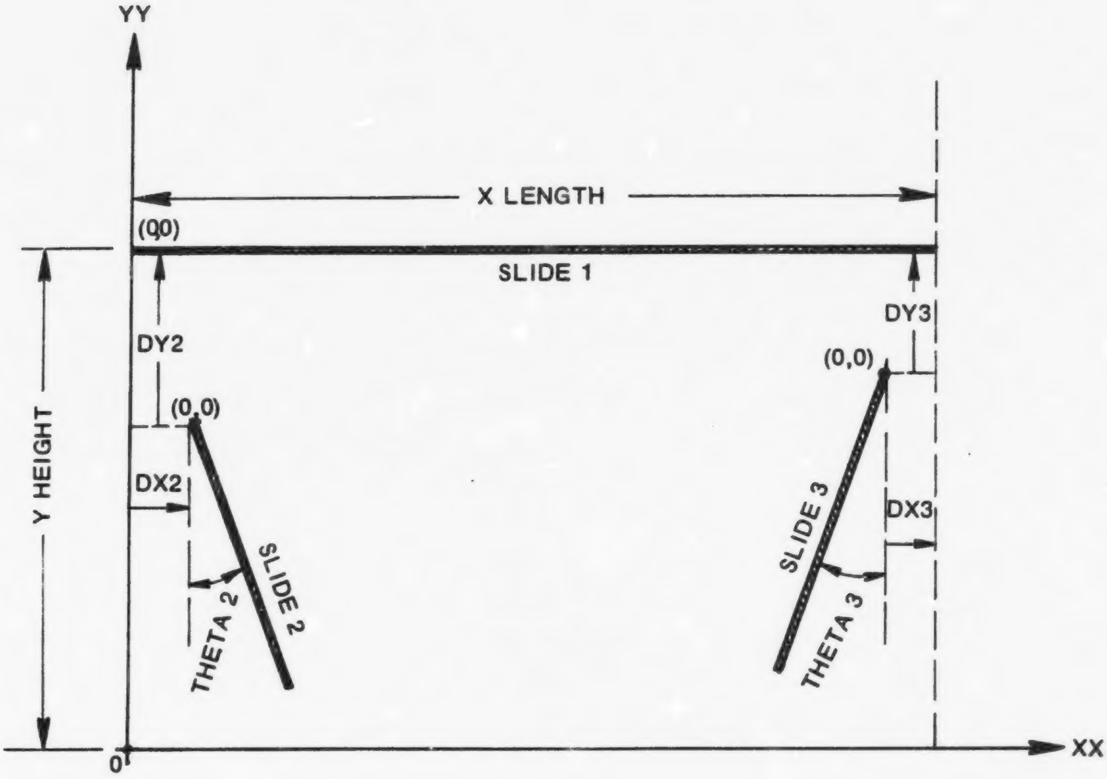
YY
X LENGTH
(0,0)
SLIDE 1
DY2
DY3
(0,0)
(0,0)
Y HEIGHT
DX2
DX3
SLIDE 2
THETA 2
SLIDE 3
THETA 3
0
XX

Figure 5. Physical Parameters of the Profilometer

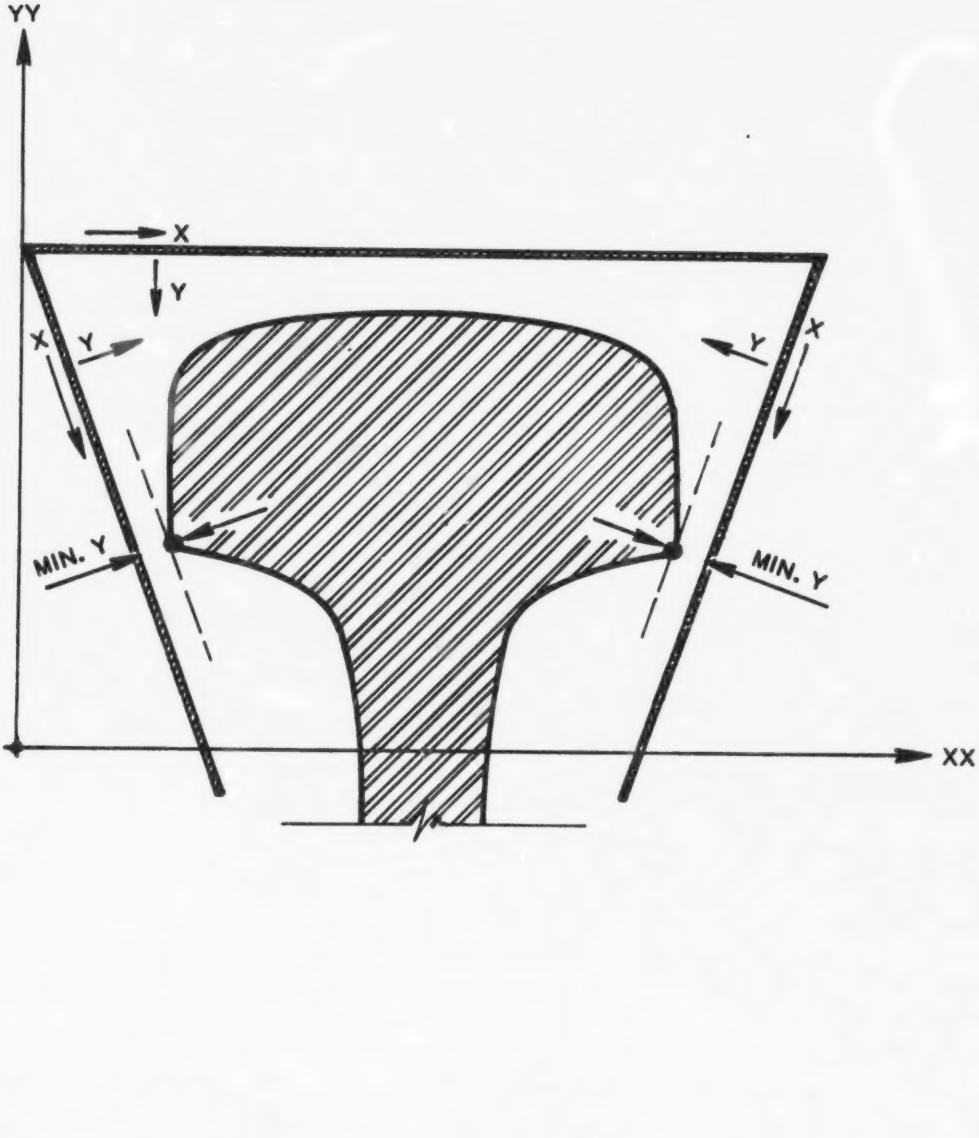
YY
X
Y
X
Y
Y
X
MIN. Y
MIN. Y
XX

Figure 6. Points of Minimum Y on Profile

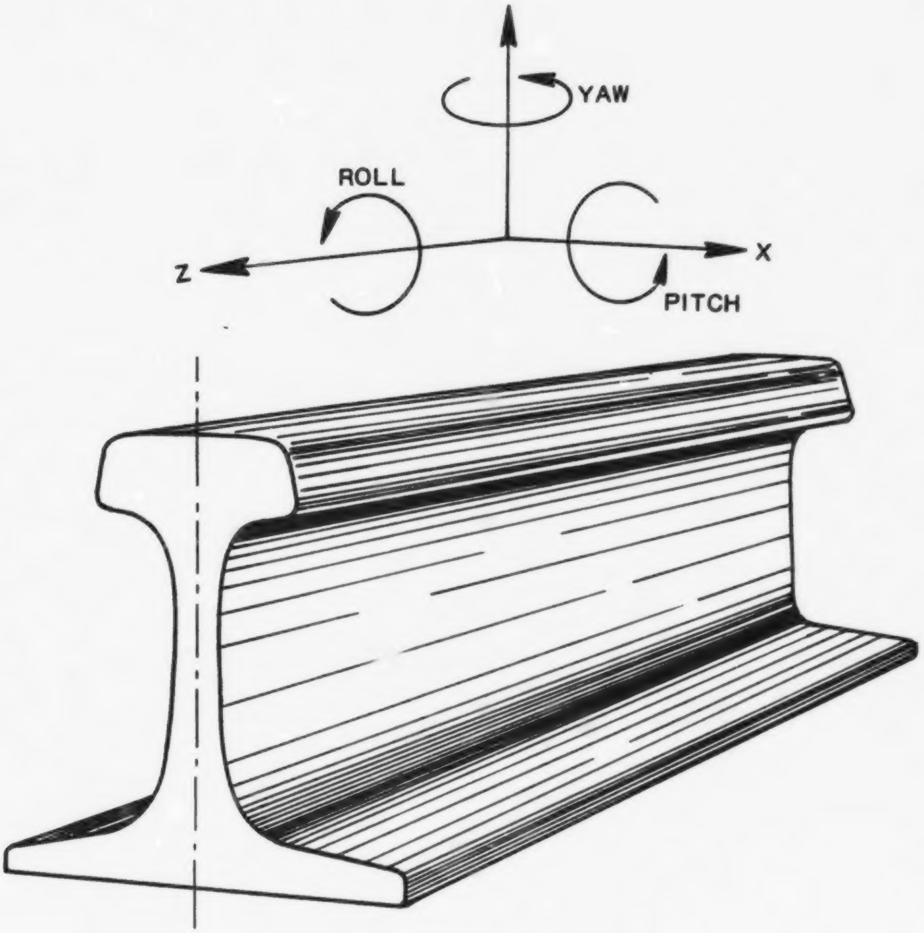
Y
YAW
ROLL
Z
X
PITCH

Figure 7. Directions and Rotations in Fixed Cartesian Frame

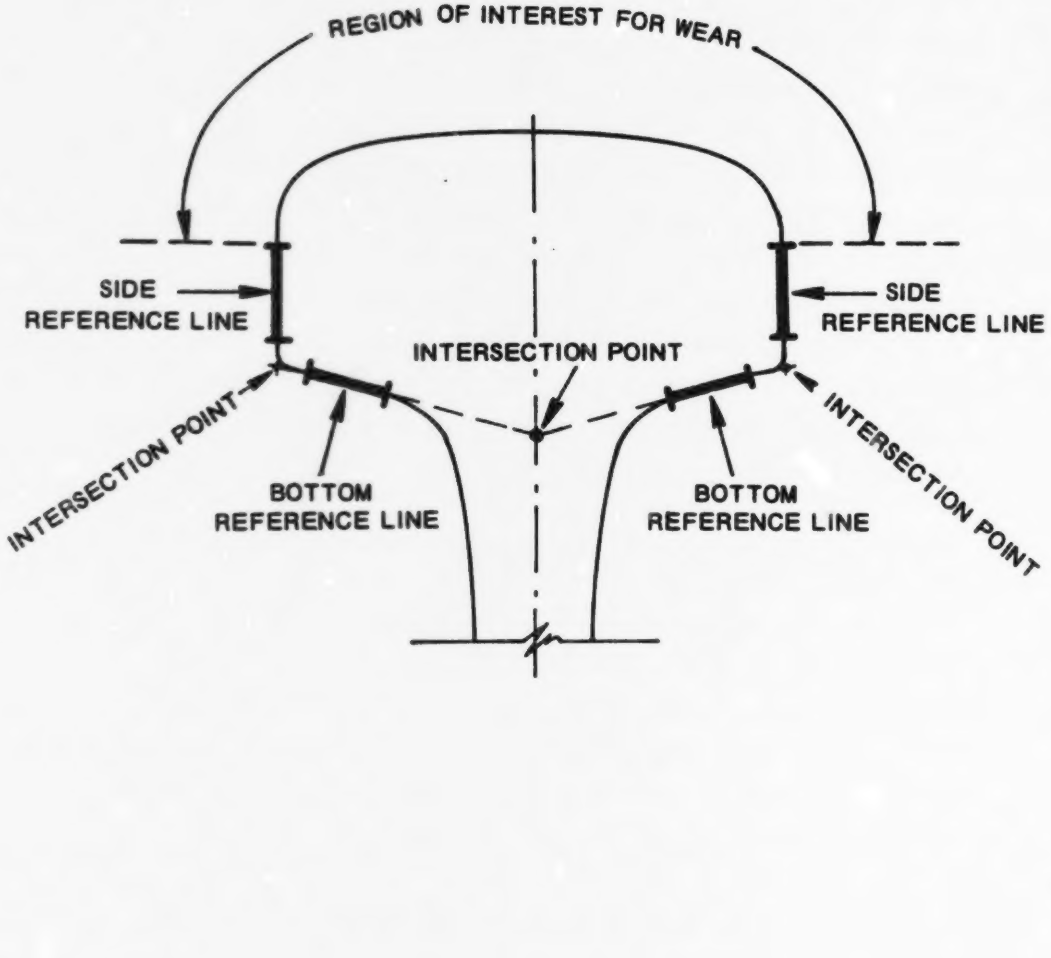
REGION OF INTEREST FOR WEAR
SIDE REFERENCE LINE
SIDE REFERENCE LINE
INTERSECTION POINT
INTERSECTION POINT
INTERSECTION POINT
BOTTOM REFERENCE LINE
BOTTOM REFERENCE LINE

Figure 8. Regions of Interest or Rail Profile

Several processes are common to all the normalization algorithms that were tried. One of these processes was the determination of the slope at any point on the profile. This was done by finding the slope between the data points on either side of the point of interest, as follows (see Figure 9):

Given points on the profile ...., (XA,YA),(XB,YB),(XC,YC), ...

At point (XB,YB), $\text{SLOPE} = \dfrac{\text{YA-YC}}{\text{XA-XC}}$.

Once the slope at each point along the profile is known, it is simple to locate a straight reference line, by looking for a region of the profile where the slope stabilizes at a constant value, within a certain tolerance. Once this region containing the straight line segment is known, the slope of the derived reference line can be found by averaging the slope at all the data points within the region. The reference line is fully defined by this average slope and a chosen data point in the region through which it passes. The intersection point, (X,Y), of two reference lines can be found once the two lines are defined by their slopes and contained data points, as follows (see Figure 9):

$$\text{X} = \frac{(\text{Y1-Y2-SLOPE1}\cdot\text{X1+SLOPE2}\cdot\text{X2})}{\text{SLOPE2-SLOPE1}}$$

$$\text{Y} = \text{Y2-SLOPE2}\cdot(\text{X2-X})$$

where (X1,Y1) = coordinates of a point on the 1st reference line
(X2,Y2) = coordinates of a point on the 2nd reference line
SLOPE1 = slope of 1st reference line
SLOPE2 = slope of 2nd reference line.

The simplest normalization algorithm uses only the two rail head bottom reference lines and their intersection point. Each reference line is located by searching for the point on the profile at which the absolute value of the slope is minimum. This indicates the approximate center of the bottom reference line (see Figure 8). Using this minimum slope as a

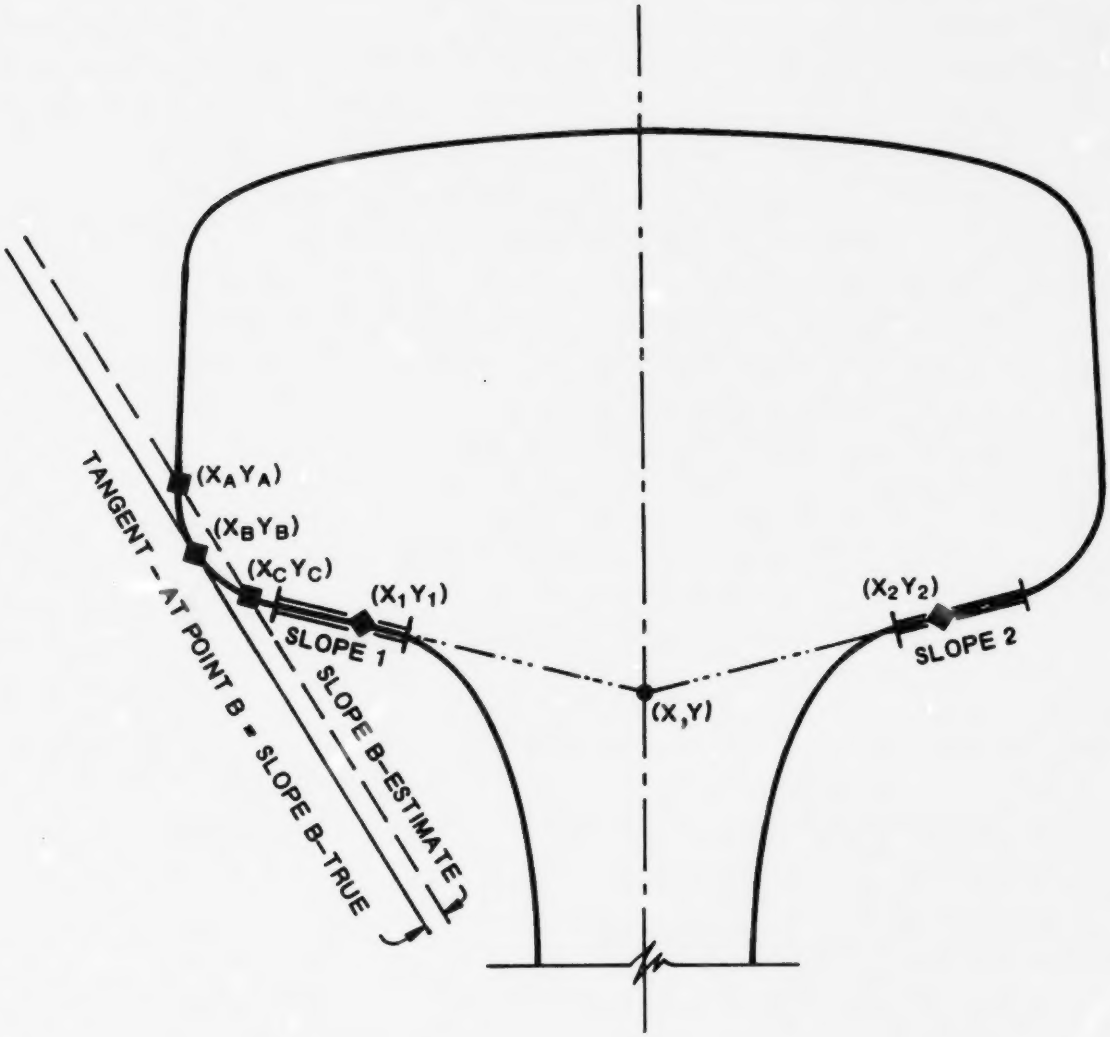
(X_A Y_A)
(X_B Y_B)
(X_C Y_C)
(X_1 Y_1)
(X_2 Y_2)
SLOPE 1
SLOPE 2
(X,Y)
TANGENT – AT POINT B = SLOPE B–TRUE
SLOPE B–ESTIMATE

Figure 9. Determination of Reference Line Slope & Intersection Points

base value, the region of the straight line is defined by searching for all the points on either side of the point of minimum slope which have slopes within a range around the base value. At this time, the reference lines and intersection point can be fully defined by the previously mentioned processes. The X and Y shift factors necessary to move the profile to the normal position are found by subtracting the coordinates of the intersection point from the normal values. These shift factors are added to the profile coordinates to translate the profile to the normal position. To find the rotation required for normalization, the reference line slopes are converted to angles, compared to the normal values, and the profile is rotated by the average deviation from the normal value of the two reference line angles. The profile is rotated around the coordinate system origin such that a data point with the coordinates (X,Y) is transformed to the coordinates (X*,Y*), by a rotation THETA, in the following way:

$$\begin{aligned} PHI &= THETA + ARCTAN\ (Y/X); \\ X^* &= \sqrt{}(X^2 + Y^2)\ .\ COS(PHI); \\ Y^* &= \sqrt{}(X^2 + Y^2)\ .\ SIN(PHI); \end{aligned}$$

The as-measured, i.e. not normalized, profiles for both the straight and misaligned profilometer are shown in Figure 10. The result of this normalization scheme, as shown in Figure 11, is not satisfactory. Both the translation and rotation are unsuccessful in matching the two profiles.

The next generation of normalization algorithm uses a side reference line as additional information. The two bottom reference lines are still used in the same way for rotation, but the intersection of the two bottom reference lines is not used. Instead, the intersection of the one side and the bottom reference line is used to get the X and Y shift factors. The side reference line is located by looking for a region with a particular, predefined slope (in this case, near-vertical i.e. large slope). The center of rotation is changed from the origin to

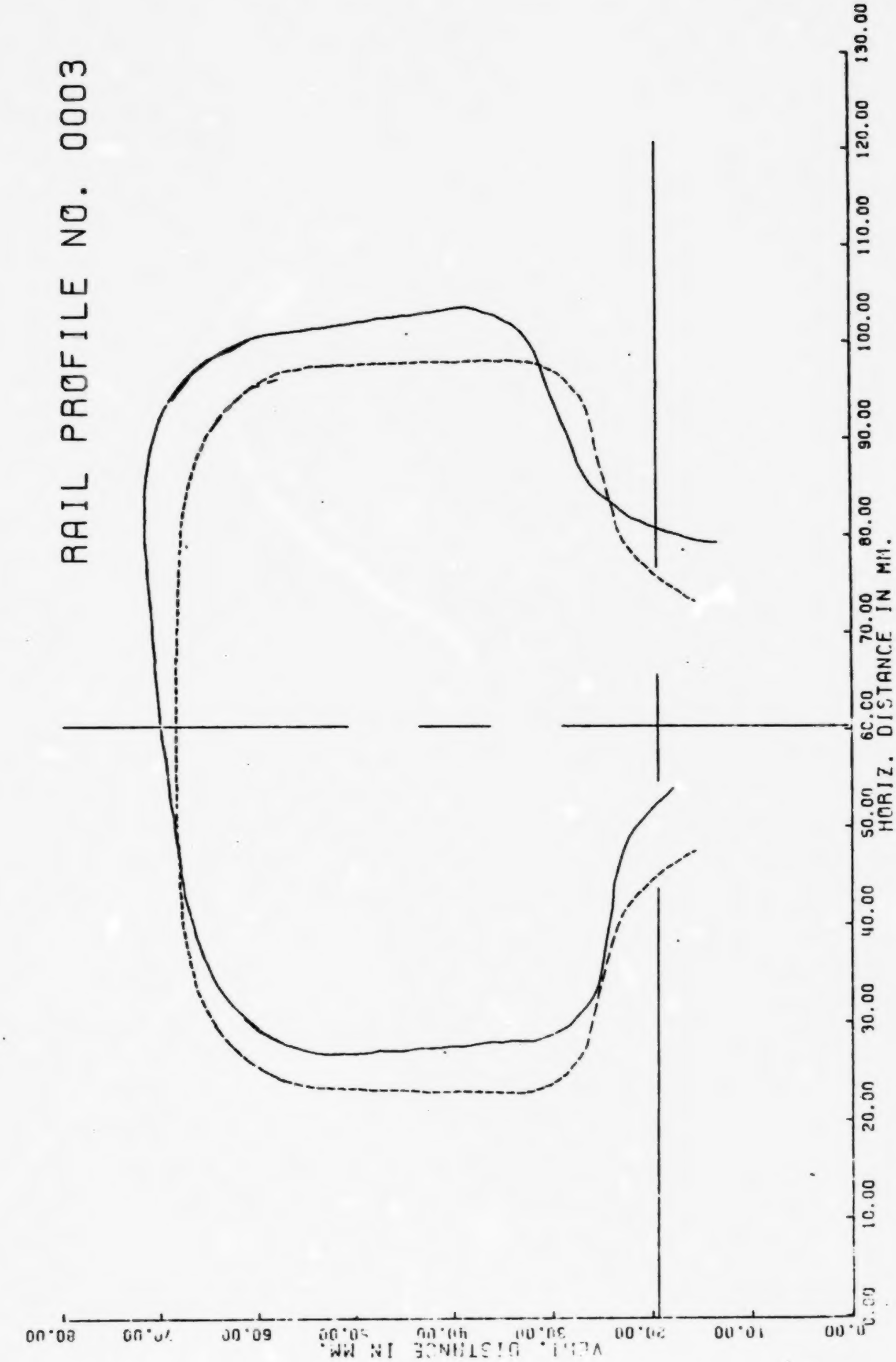
RAIL PROFILE NO. 0003
0.00
10.00
20.00
30.00
40.00
50.00
60.00
70.00
80.00
90.00
100.00
110.00
120.00
130.00
HORIZ. DISTANCE IN MM.
0.00
10.00
20.00
30.00
40.00
50.00
60.00
70.00
80.00
VERTL. DISTANCE IN MM.

Fig. 10

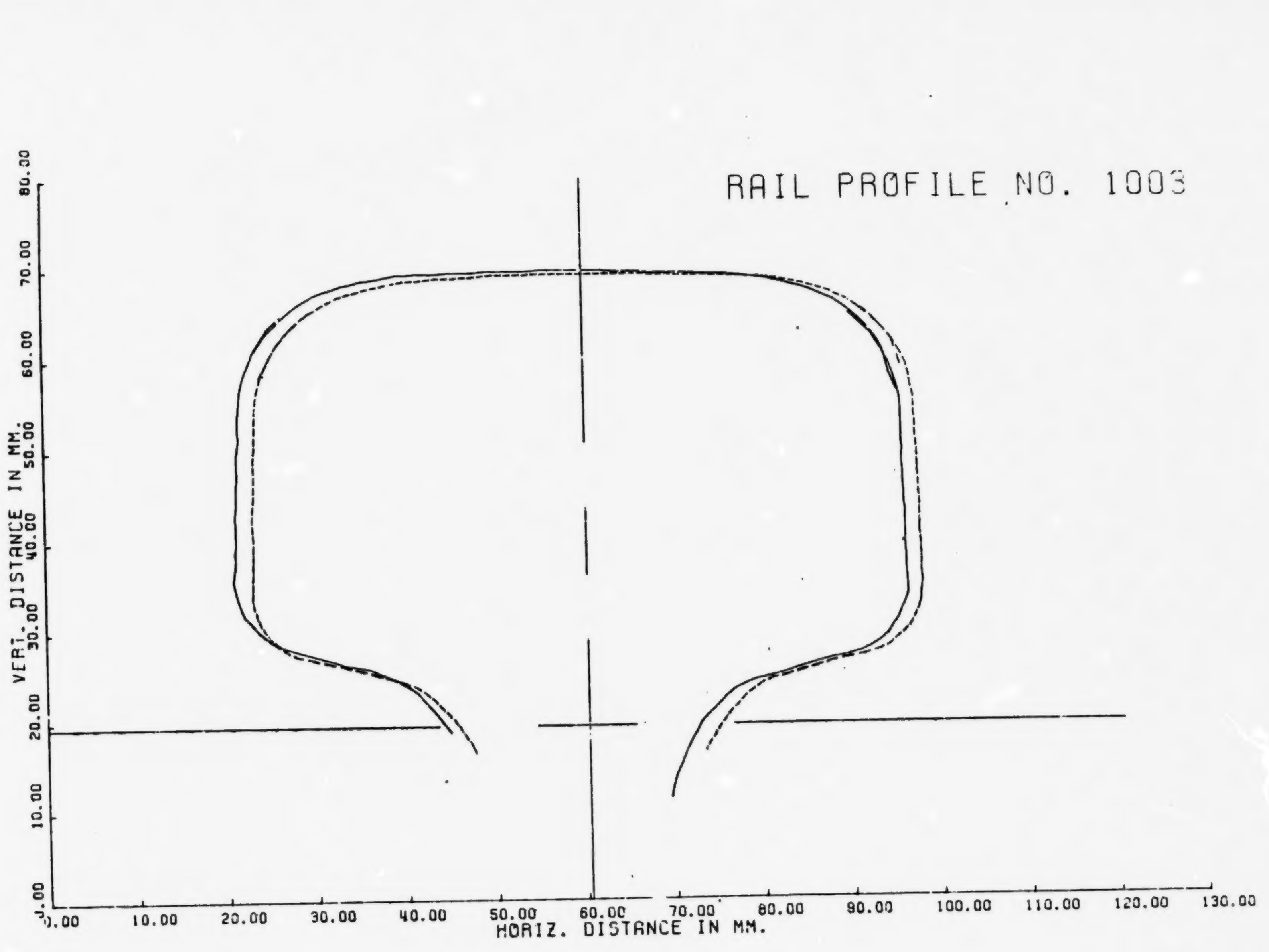
RAIL PROFILE NO. 1003
VERT. DISTANCE IN MM.
80.00
70.00
60.00
50.00
40.00
30.00
20.00
10.00
0.00
HORIZ. DISTANCE IN MM.
0.00
10.00
20.00
30.00
40.00
50.00
60.00
70.00
80.00
90.00
100.00
110.00
120.00
130.00

Fig. 11

the normal center of the rail, to reduce asymmetry of the rotation transformation, and the following relations are used:

$$\mathrm{PHI} = \mathrm{THETA} + \mathrm{ARCTAN}\ ((\mathrm{Y}-\mathrm{YREF})/(\mathrm{X}-\mathrm{XREF}))$$

$$\mathrm{X} = \surd((\mathrm{X}-\mathrm{XREF})^2 + (\mathrm{Y}-\mathrm{YREF})^2)* \mathrm{COS}(\mathrm{PHI}) + \mathrm{XREF}$$

$$\mathrm{Y} = \surd((\mathrm{X}-\mathrm{XREF})^2 + (\mathrm{Y}-\mathrm{YREF})^2)* \mathrm{SIN}(\mathrm{PHI}) + \mathrm{YREF}$$

where XREF,YREF = X and Y coordinates of normal rail center.

Figure 12 shows that the results of this algorithm are improved, but still not satisfactory.

All four of the available reference lines are used by the next algorithm. Before any further processing is done, the profile is rotated to a roughly normal orientation. Because of symmetry, this can be done by finding the angle of a line drawn between the two side slide local Y minimums (which were found by the raw data processing algorithm) and rotating the profile until this angle is zero. This rough rotation aids the process of side reference line location for this algorithm, but is not necessary for later algorithms. To find the exact required rotation, the slope of each reference line is calculated and converted to an angle. Since the rail head bottom is symmetrical, the average angle of all four reference lines should be 90° for a normalized profile. In other words, the central rail symmetry line is made to be perpendicular to the X-axis. The deviation of this calculated average angle from 90° is used to rotate the profile. The two intersections where each side and bottom line meet are used to find the shift factors. Again because of symmetry, the average X coordinate of the two points defines the rail centerline, and is used to find the X shift factor. The average Y coordinate of the two intersection points is compared to the normal position of these points, and the Y shift factor is found in this way.

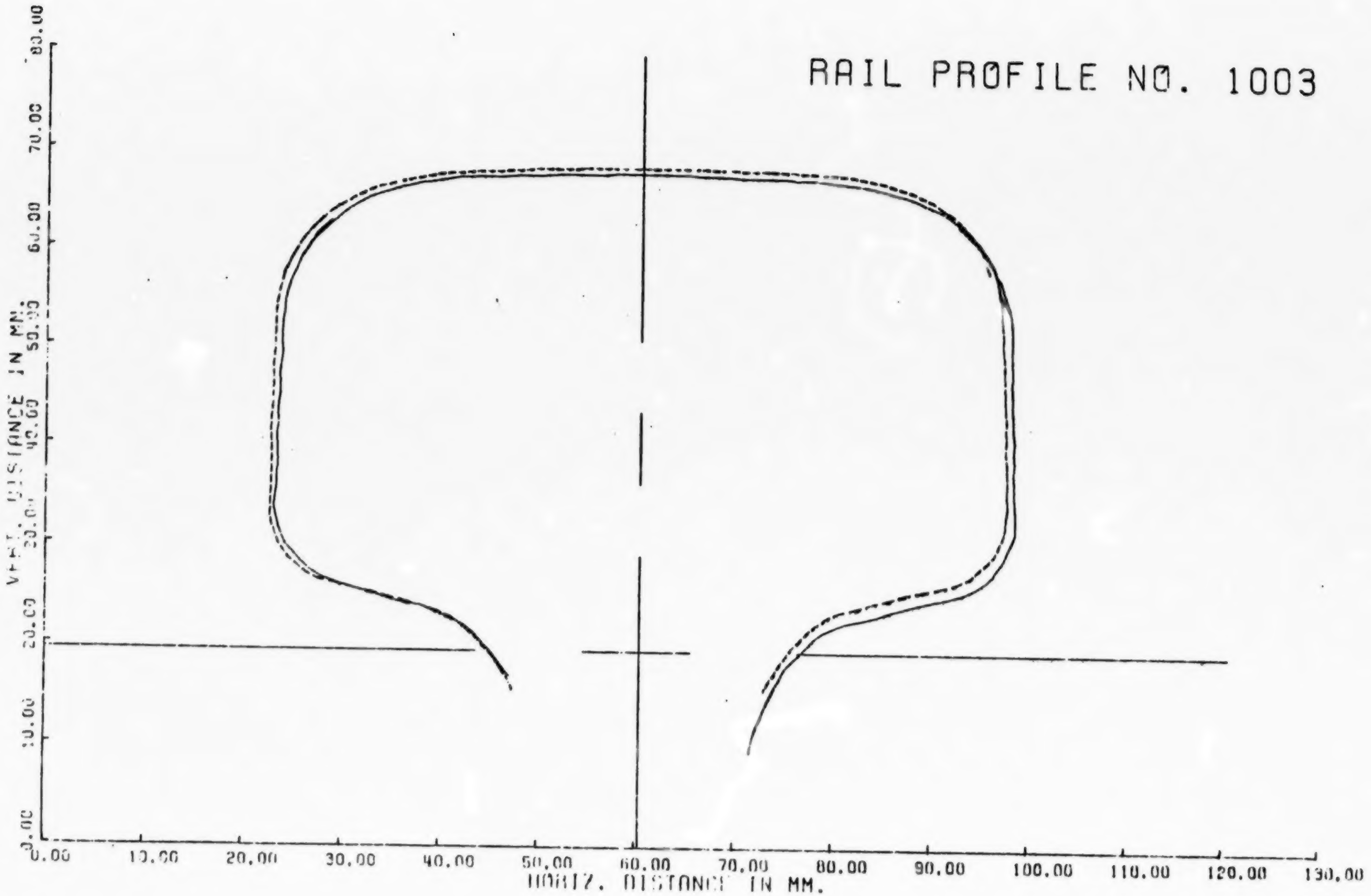
RAIL PROFILE NO. 1003
VERT. DISTANCE IN MM.
0.00
10.00
20.00
30.00
40.00
50.00
60.00
70.00
80.00
HORIZ. DISTANCE IN MM.
0.00
10.00
20.00
30.00
40.00
50.00
60.00
70.00
80.00
90.00
100.00
110.00
120.00
130.00

Fig. 12

Examination of Figure 13 shows that this normalization scheme is highly successful, and the matching obtained is as accurate as the measurements themselves (±.2mm).

An improvement of the previous algorithm can be made by generalizing the technique used to search for the side reference lines. Instead of looking for a particular range of slopes which would indicate the correct region of the profile for the side reference line, it is better to search for a region where the slope stabilizes (at any value), i.e. where the profile portion forms a straight line. This change in the algorithm makes it more easily adaptable to different rail shapes, while the normalization remains successful (see Figure 14).

An attempt was made to use the intersection of the two bottom reference lines for X and Y shift-factor determination since it is better defined on rail profile blue-prints, and hence easier to specify as a normal position. However, this scheme does not result in satisfactory normalization, so the convenience is not a gain (Fig. 15).

Although the out-of-plane rotational misalignments (X and Y rotation) are not as significant as the in-plane misalignments (X,Y offset, Z rotation), they can still affect the precise measurements involved in wear determination. This algorithm demonstrates a way of correcting for Y rotation (yaw) misalignment by comparing the measured width of the rail with the theoretical width from a blue-print - a disparity must be a result of yaw, and the profile is compressed accordingly (see Figure 16). The results of this rotation (Figure 17) show an imperfect match in the X-direction, because the determination of width depends on only two measurement points and is therefore not very reliable.

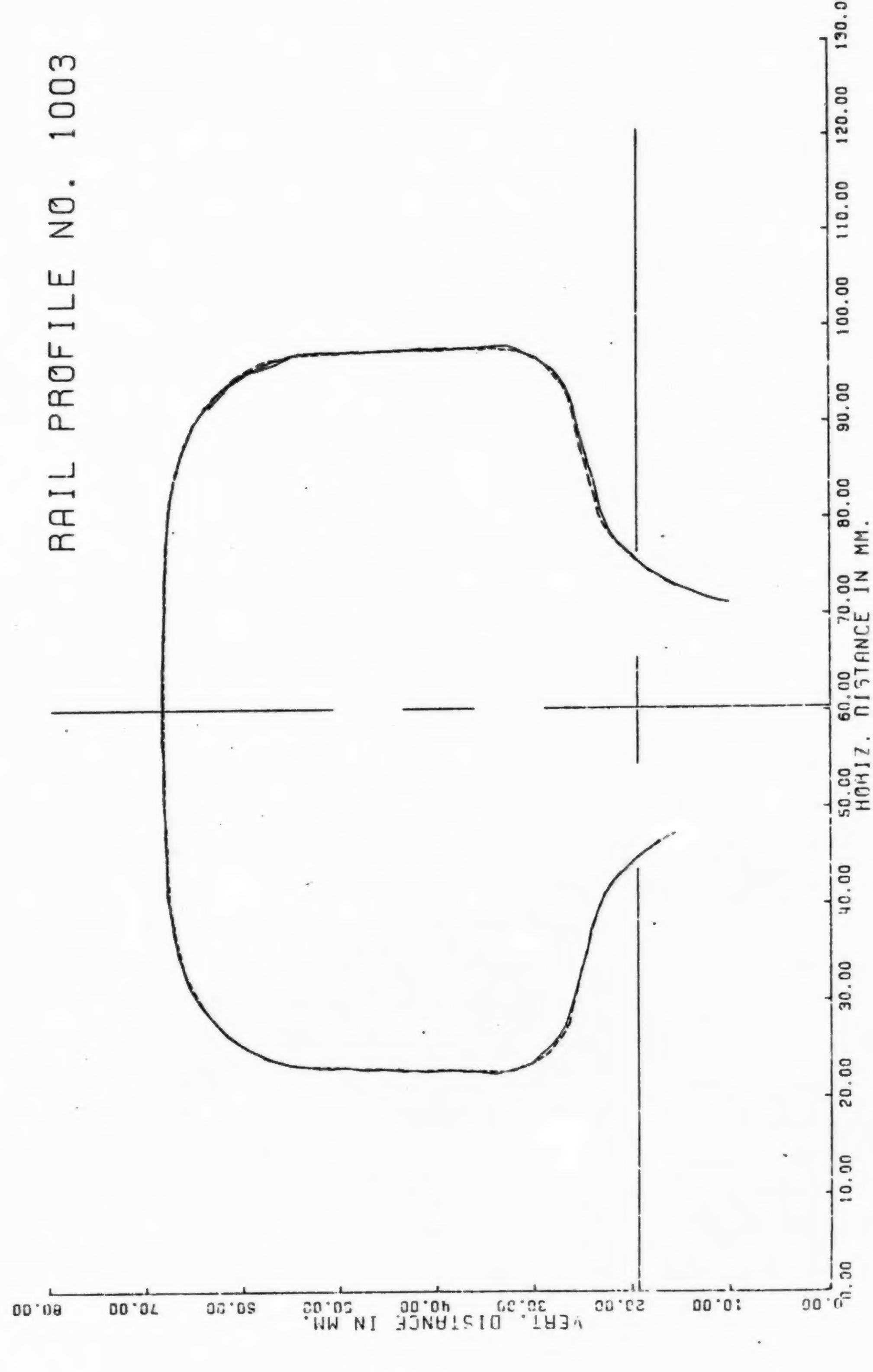
RAIL PROFILE NO. 1003
0.00
10.00
20.00
30.00
40.00
50.00
60.00
70.00
80.00
90.00
100.00
110.00
120.00
130.00
HORIZ. DISTANCE IN MM.
0.00
10.00
20.00
30.00
40.00
50.00
60.00
70.00
80.00
VERT. DISTANCE IN MM.

Fig. 13

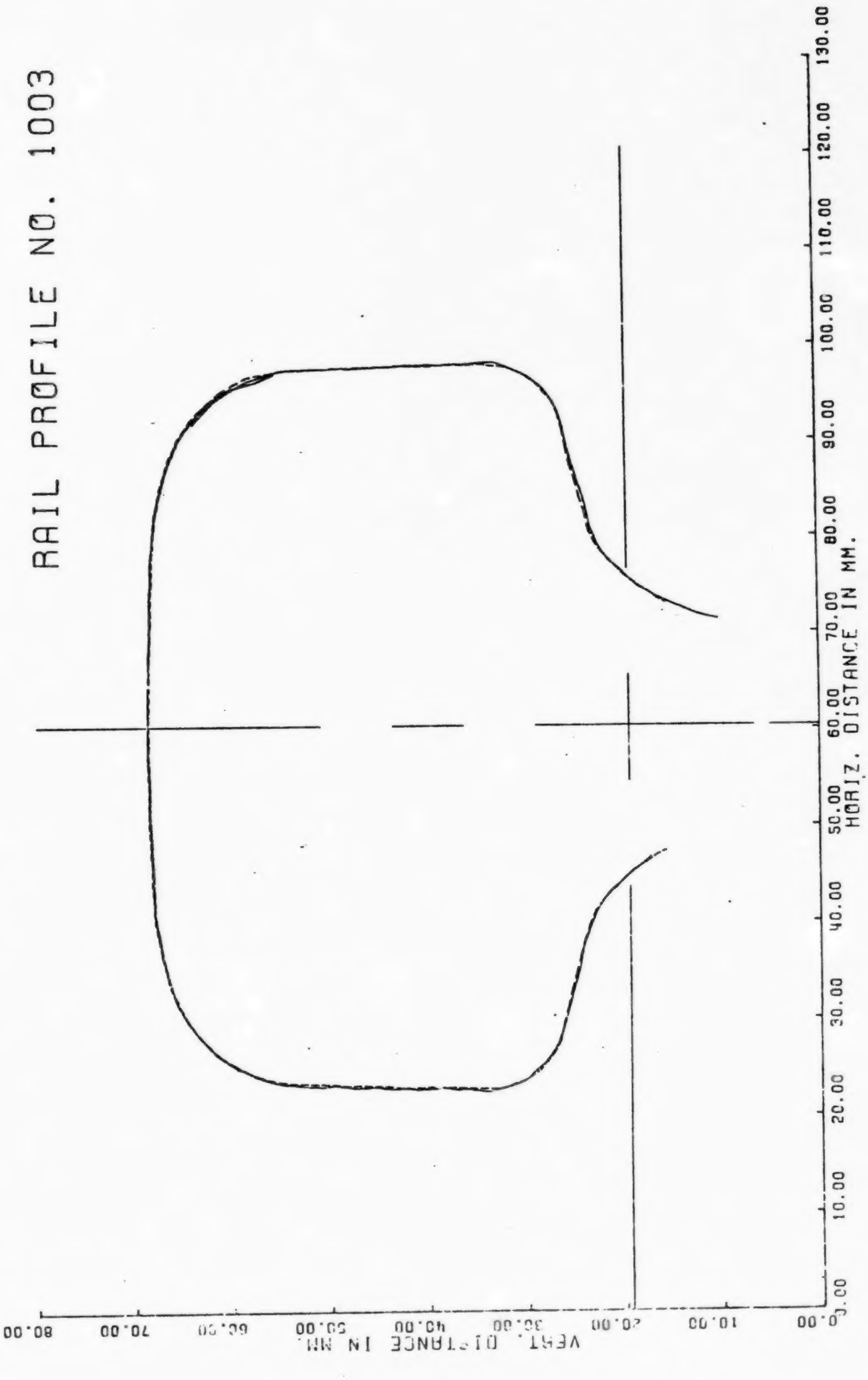
RAIL PROFILE NO. 1003
HORIZ. DISTANCE IN MM.
0.00
10.00
20.00
30.00
40.00
50.00
60.00
70.00
80.00
90.00
100.00
110.00
120.00
130.00
VERT. DISTANCE IN MM.
0.00
10.00
20.00
30.00
40.00
50.00
60.00
70.00
80.00

Fig. 14

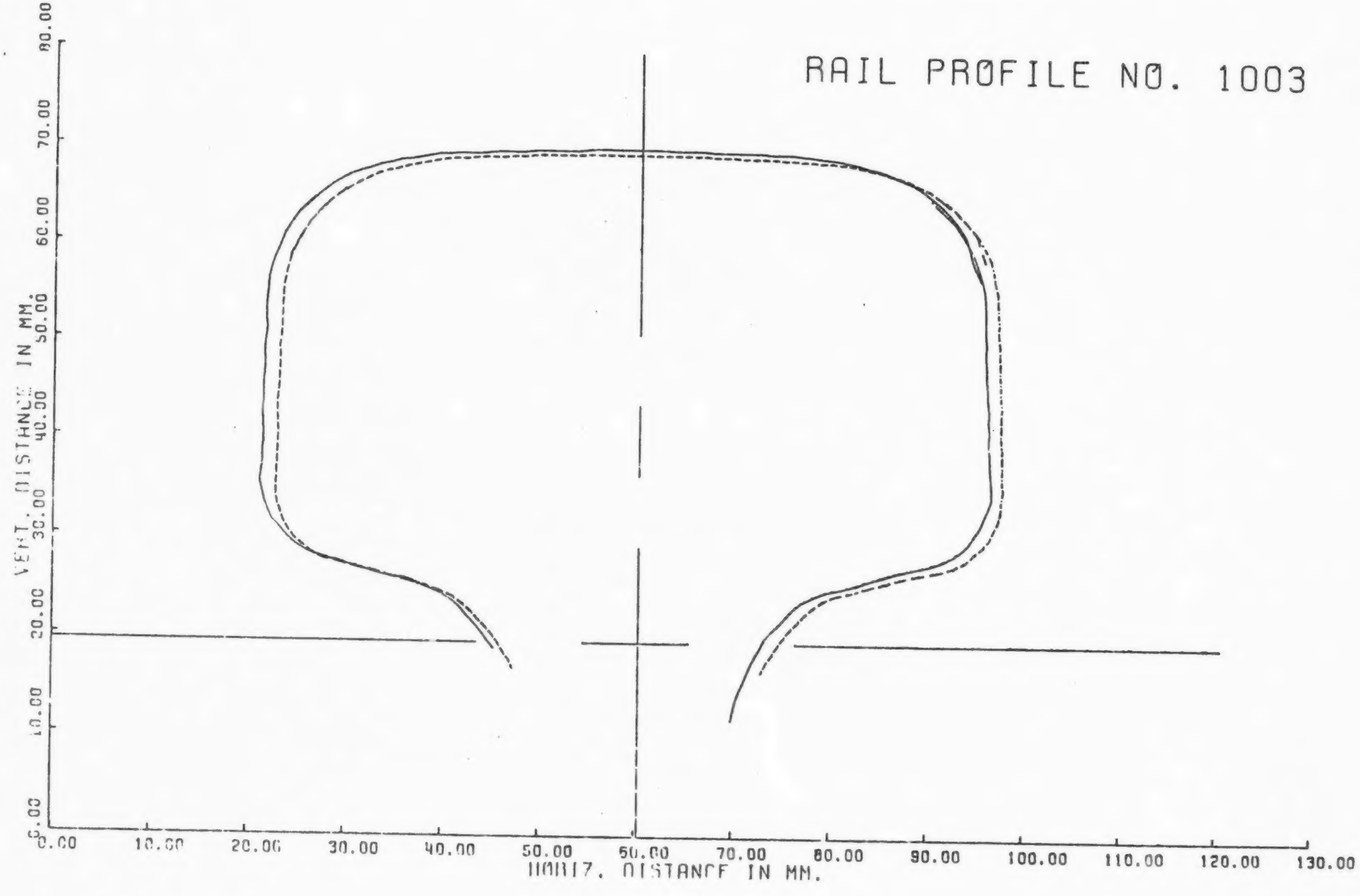
RAIL PROFILE NO. 1003
VERT. DISTANCE IN MM.
0.00
10.00
20.00
30.00
40.00
50.00
60.00
70.00
80.00
HORIZ. DISTANCE IN MM.
0.00
10.00
20.00
30.00
40.00
50.00
60.00
70.00
80.00
90.00
100.00
110.00
120.00
130.00

Fig. 15

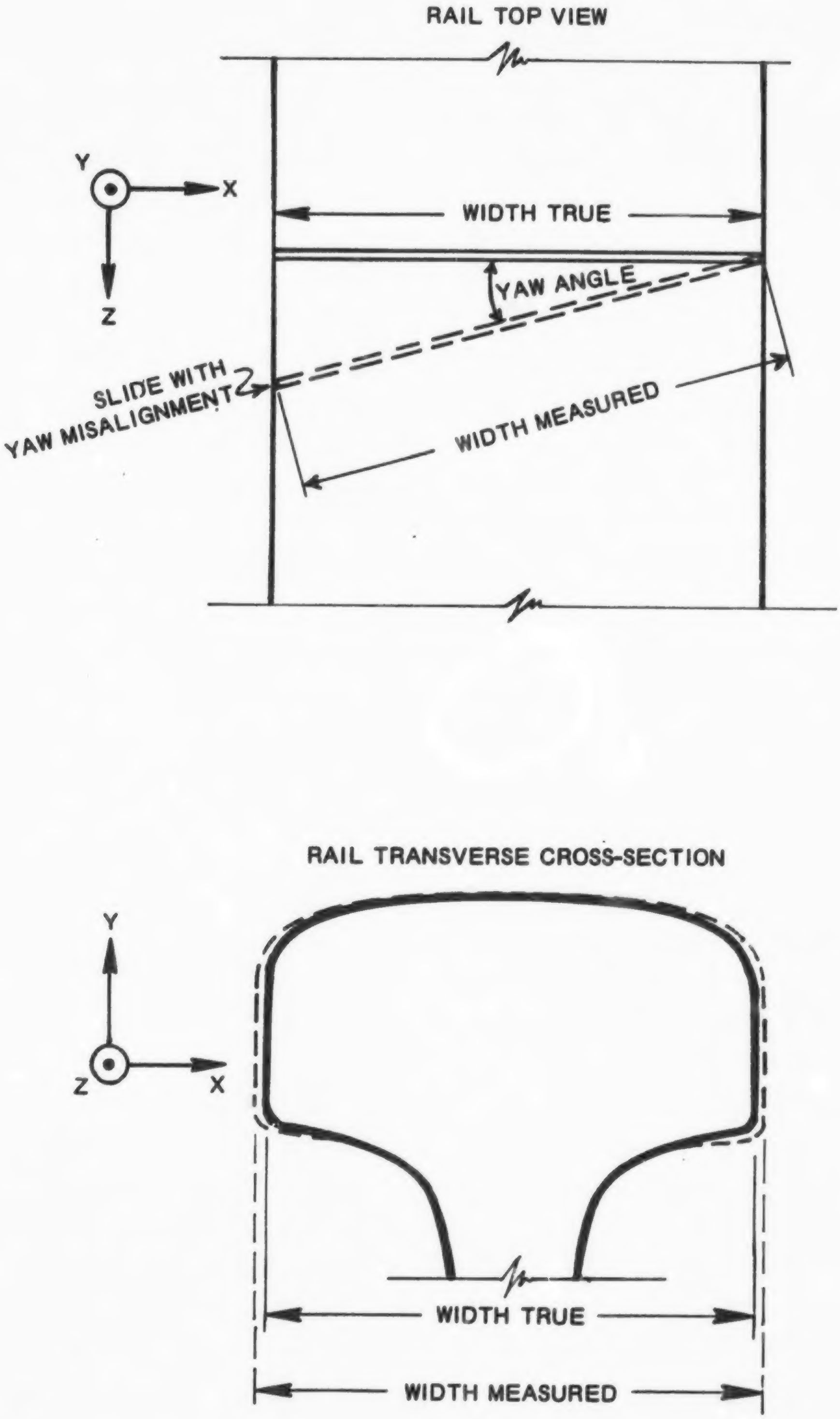
RAIL TOP VIEW
Y
X
Z
WIDTH TRUE
YAW ANGLE
SLIDE WITH
YAW MISALIGNMENT
WIDTH MEASURED
RAIL TRANSVERSE CROSS-SECTION
Y
Z
X
WIDTH TRUE
WIDTH MEASURED

Figure 16. Profilometer YAW Misalignment Connection

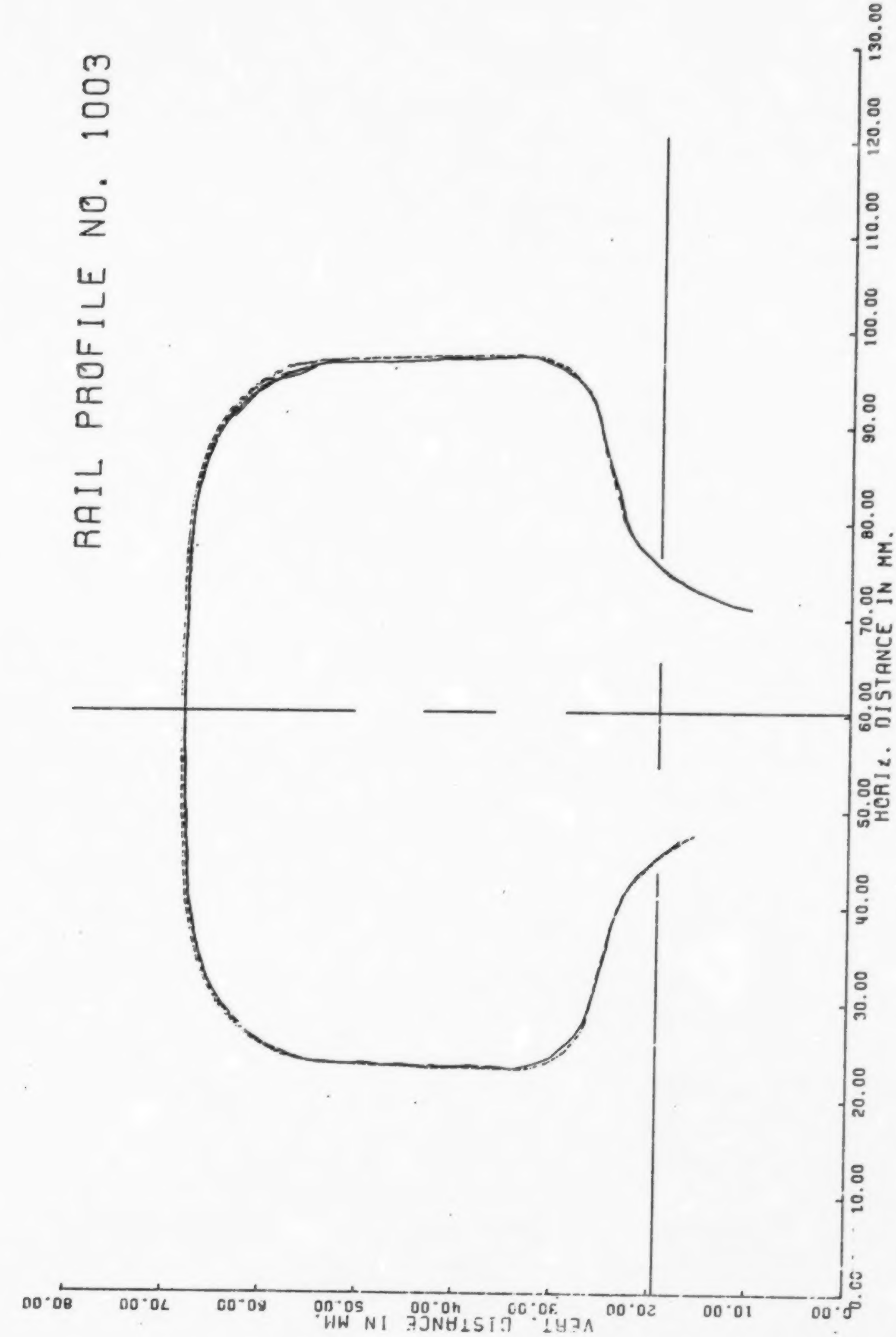
RAIL PROFILE NO. 1003
HORIZ. DISTANCE IN MM.
0.00
10.00
20.00
30.00
40.00
50.00
60.00
70.00
80.00
90.00
100.00
110.00
120.00
130.00
VERT. DISTANCE IN MM.
0.00
10.00
20.00
30.00
40.00
50.00
60.00
70.00
80.00

Fig. 17

4. Conclusions & Recommendations

1. The most important and challenging part of the Floating Profilometer Concept for rail profile measurement is the process whereby successive profiles are matched together for later wear determination, i.e., the normalization process. It has been demonstrated that this normalization can be accomplished with accuracy that is as good as the profile data measurements themselves. The best accuracy is obtained when the most reference surfaces are used for normalization purposes. The other data analysis tasks leading up to wear determination should not pose any major problems, as long as the normalization procedure is working.

2. Although the algorithms and computer programs presented in this report do not require very large amounts of computation, a certain gain in economy of computer time and storage space can be expected from further work on the programs. Also, switching from slope averaging to linear regression for the location of normalization reference lines is suggested if more accuracy is desired.

3. A rail profile measuring system is envisioned, incorporating the Floating Profilometer Concept, which would use a micro-computer as the data collection system. Profile data can be digitally recorded and processed in realtime, as the profile is measured.

4. The advantages of the type of system described above are many. The lack of any need for alignment of the profilometer on the rail head should greatly increase the speed and accuracy of wear determination. Also, because no alignment is necessary, many shapes of rail can be accommodated, with only small changes in the software. Because profile data can proceed directly from measurement to wear determination through computer processing, there are no intermediate manual steps (such as graphical matching) to introduce slowdowns and inaccuracies. The possibility of on-site data processing should also increase efficiency by locating faulty or unusual data before the measurements are completed.

5. Attention should be given to compensate for the possible yaw and pitch misalignment. This can be done by software improvement or by preventing misalignment with the special mounting frame design.
6. The limitation for this type of profilometer application, as it can be seen now, is a condition where the gauge side of a rail has noticeable plastic deformation.

Use of the Floating Profilometer Concept in automated data collection and processing system would result in a measurement system which would satisfy the requirements of high accuracy, ease and speed of measurement, and flexibility needed for rail wear determination.

5. References

1. Tage J. Anderson, YMS - Method for Measuring Small Amounts of Wheel Wear, Swedish State Railways.

2. J.D. Jackson, Wheel and Rail Profile Measurements for Urban Rail Transit Systems, Ontario Ministry of Transportation and Communications, 1980.

3. P. Marcotte, R. Mathewson, Wheel Profile Test on Luscar Coal Service Gondolas, Progress Report #1, CN Technical Research Memorandum: March 18, 1976.

4. R.J. Gostling, The Measurement of Real Wheel and Track Profiles, and Their Use in Finding Contact Conditions, Equivalent Conicity and Equilibrium, Rolling Line, British Railways Research Technical Note DA 22: February, 1971.

5. G. Izbinsky, W. Pak, Experimental and AAR Wheel Profile Measurements on a CP Unit Coal Train, CP Department of Research, Interim Report No. S-644-80, July, 1980, Transport Canada Report No. TP 2728.

ANALYTICAL STUDIES OF THE RAIL-WHEEL SYSTEM: AN OVERVIEW OF APPLICATIONS OF ROLLING CONTACT THEORY

Analytical Studies of the Rail-Wheel System: An Overview of Applications of Rolling Contact Theory

The wide range of problems associated with rail-wheel systems are best approached by balanced theoretical/experimental investigations. CP Research is very active in conducting field tests, examples of which are measurement of wheel and rail wear, vehicle lateral stability and curving performance. A series of programs has been undertaken to increase the contribution of simulation studies to these projects.

A thorough understanding of the nature of the contact between a wheel and rail is essential to theoretical investigations of the system. This paper outlines the approach to rail-wheel contact followed during the last year and how this related to other projects, both theoretical and experimental.

There are many parameters which must be considered to fully define all aspects of rail-wheel contact, ranging from geometry of the two surfaces prior to contact, to composition of the material existing between the surfaces within the contact zone. It is, of course, desirable to include all those parameters relevant to a particular application. It is also highly desirable to neglect those which influence the results minimally, in order to keep computational costs to a minimum.

One of the first steps in investigating rolling contact is to determine the undeformed geometry of the contacting surfaces. This can be done quite precisely by means of wheel and rail profilometers, described for example in reference (1)*. The profilometers developed by CP Research were intended initially as tools to assist in the evaluation of wheel and rail wear, and require minor modifications to more precisely yield profile data in the form required for geometry of contact calculations. Currently, approximate radii of curvature of the contacting surfaces are obtained.

---

* This report is contained within this volume on page 154.

To obtain information on the contact zone dimensions, a Hertzian contact program was written based on the formulation as presented in reference (2). There are several assumptions of Hertzian contact theory which are violated by rail-wheel rolling contact, the most obvious being that no frictional force exists between the surfaces. The conformity of the two surfaces is another area where this theory and the actual case may differ substantially. The most direct method of obtaining the contact zone shape and dimensions is by measurement (3), but this is very difficult to accomplish, particularly under field conditions. Theoretical work has been done on conformal contact (4), and this may prove to be very useful in studies where greater detail of the phenomena occurring within the contact zone itself are of interest, such as in wear studies.

Simulations conducted by the Research Department to date have assumed an elliptical contact zone, with the semi-axis dimensions obtained from Hertzian contact theory or by measurement. One objective of future work will be to assess the Hertzian approach for a variety of applications. The creepage forces for elliptical contact may be determined in many ways. Two of these are Kalker's Linear Theory and Johnston's method, which have been programmed from the theory presented in references (5) and (6). In addition, two programs were obtained from their authors: one written by Goree based on Kalker's Simplified Theory of Rolling Contact (7), (8), and another called Duvorol written by Kalker and based on his Exact Theory (9). The details of the theoretical bases and simplifying assumptions of each of these approaches are too lengthy to discuss here; it is sufficient to say that they are mentioned above in order of increasing complexity. There are other programs available which are worth consideration, most notable of which is Contact, again written by Kalker (10).

The selection of a creepage force program for a particular application is a difficult problem. It is known, for example, that under certain conditions the critical speed of a vehicle, at which hunting commences, is not particularly sensitive to the magnitudes of the creepage forces (11), and the Linear Theory may be sufficient. A vehicle dynamics program is currently under development by CP Research and consideration will be given to the selection of creepage-force relationships appropriate to the instantaneous values of the contact parameters. A steady state curving program recently developed by the department (12)* uses the Johnston formulation. Suspension and contact point equations are non-linear and the reduction in computational costs with the linear creepage theory were not substantial.

Of great concern to many railroads is the general deterioration of track structure and vehicle components which has become more severe, due in many cases, to the trend towards higher axle loads. One aspect of this problem which is particularly significant is the wear of wheels and rails. A recent paper which discussed the influence of lateral creepage and lubrication on wear in curves, approached this problem with a combination of laboratory experiments, theory and field observations (3). It was found that a rolling contact program such as Duvorol can provide useful information regarding the trajectories of points on the wheel and rail as they slip relative to one another. There are difficulties which must be overcome when using a theoretical approach such as this, an example being, determining the influence of wear particles present in the contact zone, but preliminary results indicate that continued work along this line is justified.

---

* This report is contained within this volume on page 24.

References

1. Izbinsky, G. and Warshaw, G., "Concept of a Profilometer for Rail Wear Determination", Department of Research, CP Ltd., 1981.

2. Seely, F.B. and Smith, J.O., "Advanced Mechanics of Materials", John Wiley and Sons, Inc., New York, 1932.

3. Kalousek, J., Rosval, G. and Ghonem, H., "Lateral Creepage and its Effect on Wear in Rail Wheel Interface", proceedings of the International Symposium on Contact Mechanics and Wear of Rail/Wheel Systems", Vancouver, B.C., 1982.

4. Hashemi, J. and Paul, B., "Contact Stresses on Bodies With Arbitrary Geometry, Applications to Wheels and Rails", FRA Report No. FRA-ORD-79/23, 1979.

5. Kalker, J.J., "Survey of Wheel-Rail Rolling Contact Theory", Vehicle Systems Dynamics 5 (1979), pp. 317-358.

6. Johnson, K.L., "Adhesion", Proc. Inst. Mech. Engrs., Vol. 178, part 3E (1964).

7. Goree, J.G. and Law, H.E., "User's Manual for Kalker's Simplified Nonlinear Creep Theory", FRA Report No. FRA/ORD-78/06, 1978.

8. Kalker, J.J., "Simplified Theory of Rolling Contact", Delft Progr. Rep., Series C: Mechanical and Aeronautical Engineering and Shipbuilding, 1 (1973), pp. 1-10.

9. Kalker, J.J., "The Computation of Three-Dimensional Rolling Contact With Dry Friction", International Journal for Numerical Methods in Engineering, Vol. 14, 1979.

10. Kalker, J.J., "Introduction to Duvorol and Contact for the Solution of 3-D Contact Problems", Report of the Dept. of Mathematics and Informatics, No. 82-29, Delft, 1982.

11. Wickens, A.H., "The Dynamics of Railway Vehicles on Straight Track: Fundamental Considerations of Lateral Stability", Proc. Inst. Mech. Engrs. 1965-66.

12. Pak, W. and Rosval, G., "Theoretical Curving Performance of Four Freight Car Trucks", Department of Research, CP Ltd., 1982.

POOR

QUALITY

ORIGINAL